

Molecular Switches. Edited by Ben L. Feringa
Copyright © 2001 Wiley-VCH Verlag GmbH
ISBNs: 3-527-29965-3 (Hardback); 3-527-60032-9 (Electronic)

Molecular Switches
Edited by Ben L. Feringa

Molecular Switches. Edited by Ben L. Feringa
Copyright © 2001 Wiley-VCH Verlag GmbH
ISBNs: 3-527-29965-3 (Hardback); 3-527-60032-9 (Electronic)

Molecular Switches

Edited by
Ben L. Feringa

 **WILEY-VCH**

Weinheim – New-York – Chichester – Brisbane – Singapore – Toronto

Molecular Switches. Edited by Ben L. Feringa
Copyright © 2001 Wiley-VCH Verlag GmbH
ISBNs: 3-527-29965-3 (Hardback); 3-527-60032-9 (Electronic)

Editor

Prof. Dr. Ben L. Feringa

Faculty of Mathematics and Natural Sciences
University of Groningen
Nijenborgh 4
9747 AG Groningen
The Netherlands

■ This book was carefully produced. Nevertheless, authors, editor, and publisher do not warrant the information contained therein to be free of errors. Readers are advised to keep in mind that statements, data, illustrations, procedural details or other items may inadvertently be inaccurate.

Library of Congress Card No.:
applied for

British Library Cataloguing-in-Publication Data
A catalogue record for this book is available from the British Library.

Die Deutsche Bibliothek – CIP Cataloguing-in-Publication Data
A catalogue record for this publication is available from Die Deutsche Bibliothek

© 2001 WILEY-VCH GmbH, Weinheim, Germany

All rights reserved (including those of translation in other languages). No part of this book may be reproduced in any form – by photoprinting, microfilm, or any other means – nor transmitted or translated into a machine language without written permission from the publisher. Registered names, trademarks, etc. used in this book, even when not specifically marked as such, are not to be considered unprotected by law.

Printed in the Federal Republic of Germany

Printed on acid-free paper

Composition Kühn & Weyh, Freiburg
Printing betz-druck GmbH, Darmstadt
Bookbinding Wilh. Osswald & Co.,
Neustadt (Weinstraße)

ISBN 3-527-29965-3

Contents

Preface XI

List of Contributors XIII

Abbreviations and Symbols XVII

1	Approaches to a Molecular Switch Using Photoinduced Electron and Energy Transfer	1
1.1	Introduction	1
1.2	Systems Consisting of Single Molecules	3
1.2.1	Two-level Systems	3
1.3	Systems Consisting of Multiple Chromophores	7
1.3.1	Intramolecular Electron Transfer	7
1.3.2	Intramolecular Energy Transfer	17
1.4	Conclusions and Future Prospects	30
2	Photoswitchable Molecular Systems Based on Diarylethenes	37
2.1	Introduction	37
2.2	Basic Diarylethene Photochromic Performance	38
2.2.1	Fatigue Resistance Characteristic	39
2.2.2	Thermal Irreversibility	43
2.2.3	Response Time	44
2.3	Host–Guest Interactions	47
2.4	Photoelectrochemical Switching	50
2.5	Liquid Crystalline Switches	54
2.6	Photooptical Switching – Refractive Index Change	55
2.7	Conclusion	60
3	Optoelectronic Molecular Switches Based on Dihydroazulene-Vinylheptafulvene (DHA-VHF)	63
3.1	Introduction	63
3.2	Photochromic Molecular Switches	67
3.2.1	Molecular Switches Based on Fulgides	68

3.2.2	Photochromic Switches Based on Dihydroindolizine	69
3.2.3	Multimode Molecular Switch Based on Flavylum Ion	69
3.2.4	Dihydroazulene-Vinylheptafulvene Photochromism (DHA-VHF Photochromism)	70
3.2.4.1	Molecular Switches Based on DHA-VHF	79
3.2.4.2	Multimode Photochromic Switches Based on DHA-VHF	87
3.3	Future Directions	103
3.4	Conclusions	104
4	Molecular Switches with Photochromic Fulgides	107
4.1	Introduction	107
4.1.1	Photochromism	107
4.1.2	Fulgides[2]	108
4.2	Switching of Photochromic Properties of Fulgides by Additives	109
4.3	Switching of Fluorescence in Fulgides	111
4.4	Switching of Non-linear Optical Properties through Fulgide Photochromism	113
4.5	Switching of Supramolecular Properties of Fulgides	114
4.6	Switching of Chiral and Chiroptical Properties of Fulgides	114
4.7	Switching of Liquid Crystalline Properties through Fulgide Photochromism	117
4.8	Switching of Biological Activities through Fulgide Photochromism	119
4.9	Future Perspectives	119
5	Chiroptical Molecular Switches	123
5.1	Introduction	123
5.2	Switching of Enantiomers	126
5.2.1	Overcrowded Alkenes	127
5.2.2	Axially Chiral Cycloalkanones	130
5.3	Switching of Diastereoisomers	132
5.3.1	Overcrowded Alkenes	132
5.3.2	Diarylethenes	139
5.3.3	Other Diastereoselective Switches	142
5.4	Multifunctional Chiral Switches	144
5.4.1	Gated Photoisomerization	144
5.4.2	Dual-mode Photoswitching of Luminescence	145
5.4.3	Chiral Molecular Recognition	146
5.4.4	Unidirectional Rotary Motion	147
5.5	Switching of Macromolecules and Supramolecular Organization	152
5.5.1	Photochromic Polymers	152
5.5.2	Reversible Gel Formation	154
5.5.3	Switching of Liquid Crystalline Phases	155
5.6	Conclusions	159

6	Photochemical Biomolecular Switches: The Route to Optobioelectronics	165
6.1	Introduction	165
6.1.1	Reversible Photochemical Switching of Biomaterial Functions	167
6.1.1.1	Photoswitchable Biomaterial Functions through Tethering of Photoisomerizable Units to Proteins	168
6.1.1.2	Photoswitchable Biomaterials by Integration of Biomaterials with Photoisomerizable Matrices and Microenvironments	178
6.2	Electronic Transduction of Photoswitchable Redox Functions of Biomaterials	185
6.2.1	Amperometric Transduction of Optical Signals Recorded by Photoisomerizable Enzyme Electrodes	187
6.2.2	Light-Switchable Activation of Redox Proteins by Means of Photoisomerizable “Command Interfaces” Associated with Electrodes	191
6.3	Electronic Transduction of Photoswitchable Antigen–Antibody Interactions at Solid Supports	197
6.4	Complex Photochemical Biomolecular Switches	204
6.5	Applications of Photoswitchable Biomaterials	208
6.6	Conclusions and Future Perspectives	213
7	Switchable Catenanes and Molecular Shuttles	219
7.1	Introduction	219
7.2	Catenanes and Rotaxanes Containing Transition Metals	220
7.3	Catenanes and Rotaxanes Containing -Electron-deficient and -Electron-rich Recognition Sites	226
7.4	Rotaxanes Containing Cyclodextrins	237
7.5	Molecule-based Logic Gates	239
7.6	Conclusions	243
8	Metallo-Rotaxanes and Catenanes as Redox Switches: Towards Molecular Machines and Motors	249
8.1	Introduction	249
8.1.1	Generalities Regarding Machines and Motors	249
8.1.2	Proteins Undergoing Folding–Defolding Processes	249
8.1.3	Biological Molecular Motors	250
8.1.4	Previously Described Synthetic Systems based on Purely Organic Components	252
8.1.5	Motion in Transition Metal-based Molecules	252
8.2	Rotaxanes Containing Transition Metals: From Electronic to Molecular Motion	254
8.2.1	Photoinduced Intramolecular Electron Transfer Within Porphyrinic Rotaxanes	254
8.2.2	Lateral Translation of a Ring on the Molecular String on which it is Threaded: Electrochemically-driven Motion	257

- 8.2.3 Towards Rotary Motors: Pirouetting of a Two-coordinate Ring on its Thread 264
- 8.2.3.1 Electrochemical Behavior of Chemically Isolated 16(4)+ and 16(5)2+ 268
- 8.3 Electrochemically Driven Ring Gliding Motion in Catenanes 271
- 8.3.1 A Twin-geometry Catenane 271
- 8.3.2 A Triplet-configuration Copper Catenane 273
- 8.4 Conclusion and Prospects 276

- 9 Switchable Molecular Receptors and Recognition Processes: From Photoresponsive Crown Ethers to Allosteric Sugar Sensing Systems 281**
- 9.1 Introduction: Why is the Switch Function Indispensable in Molecular Receptors? 281
- 9.2 The Origination of Photoresponsive Crown Ethers 283
- 9.3 Dynamic Actions of Calixarenes in Ion and Molecule Recognition 287
- 9.4 Artificial Sugar-sensing Systems utilizing Photoinduced Electron Transfer (PET) 291
- 9.5 Dynamic and Efficient Guest-binding Achieved through Allosteric Effects 297
- 9.5.1 Negative Heterotropic Systems 297
- 9.5.2 Positive Heterotropic Systems 299
- 9.5.3 Negative Homotropic Systems 301
- 9.5.4 Positive Homotropic Systems 302
- 9.6 Concluding Remarks 304

- 10 Multistate/Multifunctional Molecular-level Systems – Photochromic Flavylium Compounds 309**
- 10.1 Introduction 309
- 10.2 Multistate/Multifunctional Compounds 310
- 10.3 Natures of the Species involved in the Chemistry of Flavylium Compounds 312
- 10.4 Thermal Reactions of the 4'-Methoxyflavylium Ion 314
- 10.5 Photochemical Behavior of the 4'-Methoxyflavylium Ion 315
- 10.5.1 Continuous Irradiation 315
- 10.5.2 Pulsed Irradiation 317
- 10.6 Flavylium Ions with OH Substituents 318
- 10.7 Energy Level Diagrams 319
- 10.8 Chemical Process Networks 323
- 10.8.1 Write-lock-read-unlock-erase Cycles 323
- 10.8.2 Reading without Writing in a Write-lock-read-unlock-erase Cycle 325
- 10.8.3 Micelle Effect on the Write-lock-read-unlock-erase Cycle 327
- 10.8.4 Permanent and Temporary Memories 328
- 10.8.5 Oscillating Absorbance Patterns 329
- 10.8.6 Color-tap Effect 330

10.8.7	Logic Operations	330
10.8.8	Multiple Reaction Patterns	333
10.9	Conclusions	334
11	Molecular Logic Systems	339
11.1	Introduction	339
11.2	YES Logic	339
11.3	NOT Logic	341
11.4	AND Logic	343
11.5	NAND Logic	347
11.6	OR Logic	349
11.7	NOR Logic	351
11.8	XOR Logic	353
11.9	XNOR Logic	354
11.10	INHIBIT Logic	355
11.11	Enabled OR Logic	357
11.12	Conclusion	358
12	Liquid Crystal Photonics: Opto-photochemical Effects in Photoresponsive Liquid Crystals	363
12.1	Introduction	363
12.2	LC Alignment Change by Means of Photochemical Processes	364
12.2.1	Photochemical Phase Transitions in Guest/Host Systems	364
12.2.2	Photochemical Phase Transitions in Guest/Polymer LC Systems	365
12.3	Novel Approach to Alignment Change in LCs through Photochemical Processes	367
12.4	New Concept for Fast LC Response through the Agency of Photochemical Processes	371
12.5	Photochemical Control of LC Alignment by Linearly Polarized Light	378
12.6	Manipulation of LC Alignment through Photoactive Surface Layers	381
12.7	Modulation of Light Waves in Polymer/LC Composite Films	384
12.8	Holography as a Future Technology in Photonics	388
12.8.1	Distinct Image-recording and Image-displaying Techniques	388
12.8.2	LC Materials in Holography	390
13	Photoswitchable Polypeptides	399
13.1	Introduction	399
13.1.1	Photoresponsive Polymers	399
13.1.2	Structure and Conformation of Polypeptides	400
13.1.3	Chiroptical Properties of Polypeptide Structures	402
13.1.3.1	CD Spectrum of the α -Helix	402
13.1.3.2	CD spectrum of the β -Structure	403
13.1.3.3	CD Spectra of Random Coil Structures	403
13.1.3.4	CD Spectra of Polypeptides with Chromophoric Side Chains	403

13.2	Photomodulation of Polypeptide Macromolecular Structure	404
13.2.1	UV Light-induced Conformational Transitions in Azobenzene-containing Polypeptides	404
13.2.1.2	Azobenzene-containing Poly(L-glutamic acid)	405
13.2.1.3	Azobenzene-containing Poly(L-lysine)	410
13.2.1.4	Azo-Modified Polypeptide Analogues of Poly(L-lysine)	414
13.2.1.5	Photoinduced Helix-sense Reversal in Azobenzene-containing Poly(L-aspartate)s	415
13.2.1.6	Other Photochromic Polypeptide Systems	418
13.2.2	Sunlight-induced Conformational Transitions in Spiropyran-containing Polypeptides	419
13.2.2.1	Spiropyran-modified Poly(L-glutamate)s	
13.2.2.2	Photoresponsiveness of Poly(spiropyran-L-glutamate) under Acidic Conditions	421
13.2.2.3	Spiropyran-modified Poly(L-lysine)	423
13.2.3	Photostimulated Aggregation-disaggregation Effects	426
13.3	Photoeffects in Molecular and Thin Films	428
13.3.1	Photomechanical Effects in Monolayers	428
13.3.2	Photoresponsive LB and Thin Films	431
13.4	Photoresponsive Polypeptide Membranes	433
13.5	Summary and Future Prospects	437
	Index	443

Preface

Information technology has revolutionized daily life in the last decades and the continuously increasing amount of data to be stored and manipulated strongly stimulated the search for switching and memory elements as tiny as a single molecule. Molecular switches can be converted from one state to another by an external stimulus such as light, electricity or a chemical reaction. Like with their macroscopic counterparts, one is able to control numerous functions and properties of materials and devices.

Applications in computer chips, optical recording systems, holographic and liquid crystal display materials are close to reality. Some of the optical molecular switches emerged from well-known photochromic dyes, others are based on entirely new design principles. The use of molecular switches and trigger elements in biomedicine, for instance in drug delivery systems and biosensors, will open up entirely new horizons. In a broader context, the design of molecular switches present a formidable challenge on the road toward miniaturization in future nanotechnology.

Tremendous progress has been seen in recent years in the development of molecular switching, typically at the interface between chemistry and materials science. Emphasis so far has been on the mechanism of molecular switching and stability and reversibility. Important part of the research has been devoted to find means to address the molecular switches and to use these as trigger elements to control materials properties. Recent insight into the detailed functioning of “biological machinery” at the molecular level will, without doubt, be a new source of inspiration to design more advanced switches and a rapid expansion of this field of research into molecular biology can be expected.

Key questions ahead of us concern new concepts for addressing individual molecular switches and the construction of more complex systems which incorporate several switchable functions. Advances in scanning – probe techniques and single molecule spectroscopy as well as supramolecular chemistry will play an important role in this endeavor.

It is considered timely to provide a survey of a number of important developments in this field. The aim of this book is to discuss basic principles and different approaches that have been used and present applications of molecular switches in the control of functions and material properties. It is not the intention to be comprehensive, but a selection of topics is made that reflects the fascinating possibilities

offered by the synthesis and application of novel molecules designed as switches. This volume describes energy and electron transfer systems, molecular switches based on photoisomerization and reversible photocyclization, redox-based switches, rotaxanes and catenanes, chiroptical switches and systems that function by virtue of chemical reactions. Multifunctional switches, logic gates, biomolecular switches and switchable molecular receptors are examples of more complex systems discussed. The chapters on peptides and liquid crystals illustrate the use of molecular switches to control macromolecular and mesoscopic systems.

To cover the variety of topics in such an interdisciplinary area, the help of many colleagues and friends was needed. I am extremely grateful to the authors for their excellent contributions. I hope that this book will be a source of inspiration for many researchers and stimulate new developments in this challenging field of science.

January 2001

Ben L. Feringa, Groningen

List of Contributors

Ayyppanpillai Ajayaghosh

Photochemistry Research Unit
Regional Research Laboratory
CSIR
Trivandrum 695 019
India

Vincenzo Balzani

Dipartimento di Chimica „G. Ciamician“
Università di Bologna
I-40126 Bologna
Italy

Francesco Ciardelli

Dipartimento di Chimica e Chimica industriale
Università di Pisa
via Risorgimento, 35
I-56126 Pisa
Italy

Jean-Paul Collin

Laboratoire de Chimie Organo-Minérale
UMR 7513 du CNRS
Faculté de Chimie
Université Louis Pasteur
4, rue Blaise Pascal
F-67070 Strasbourg Cedex
France

Jörg Daub

Institut für Organische Chemie
Universität Regensburg
Universitätsstrasse 31
D-93040 Regensburg
Germany

Ben L. Feringa

Faculty of Mathematics and Natural Sciences
University of Groningen
Nijenborgh 4
NL-9747 AG Groningen
The Netherlands

Tomiki Ikeda

Research Laboratory of Resources Utilization
Tokyo Institute of Technology
4259 Nagatsuta, Midori-ku
J-Yokohama 226–8503
Japan

Masahiro Irie

Department of Chemistry and Biochemistry
Graduate School of Engineering
Kyushu University
Hokozaki 6–10–1
Higashi-ku
Fukuoka 812–8581
Japan

Akihiko Kanazawa

Research Laboratory of Resources Utilization
Tokyo Institute of Technology
4259 Nagatsuta, Midori-ku
J-Yokohama 226–8503
Japan

Jean-Marc Kern

Laboratoire de Chimie Organo-Minérale
UMR 7513 du CNRS
Faculté de Chimie
Université Louis Pasteur
4, rue Blaise Pascal
F-67070 Strasbourg Cedex
France

Aaron S. Lukas

Department of Chemistry
Northwestern University
Evanston
IL 60208–3113
USA

Mauro Maesri

Dipartimento di Chimica „G. Ciamician“
Università di Bologna
I-40126 Bologna
Italy

Nathan D. McClenaghan

School of Chemistry
Queen's University
Belfast BT9 5AG
Northern Ireland

Colin P. McCoy

School of Pharmacy
Queen's University
Belfast BT9 7BL
Northern Ireland

Thomas Mrozek

Institut für Organische Chemie
Universität Regensburg
Universitätsstrasse 31
D-93040 Regensburg
Germany

Oswaldo Pieroni

Department of Chemistry and Industrial Chemis-
try
CNR-Institute of Biophysics
University of Pisa
Via Risorgimento 35
I-56100 Pisa
Italy

Fernando Pina

Departamento de Química
Centro de Química Fina e Biotecnologia
Faculdade de Ciências e Tecnologia
Universidade Nova de Lisboa
P-2825 Monte de Caparica
Portugal

Laurence Raehm

Laboratoire de Chimie Organo-Minérale
UMR 7513 du CNRS
Faculté de Chimie
Université Louis Pasteur
4, rue Blaise Pascal
F-67070 Strasbourg Cedex
France

Françisco M. Raymo

Center for Supramolecular Science
Department of Chemistry
University of Miami
1301 Memorial Drive
Coral Gables, FL 33124-0431
USA

Jean-Pierre Sauvage

Laboratoire de Chimie Organo-Minérale
UMR 7513 du CNRS
Faculté de Chimie
Université Louis Pasteur
4, rue Blaise Pascal
F-67070 Strasbourg Cedex
France

Seiji Shinkai

Department of Organic Synthesis
Faculty of Engineering
Kyushu University
Fukuoka University
J-Fukuoka 812
Japan

Prasanna de Silva

School of Chemistry
Queen's University
Belfast BT9 5AG
Northern Ireland

J. Fraser Stoddart

Department of Chemistry and Biochemistry
University of California
Los Angeles
405 Hilgard Avenue
Los Angeles, CA 90095-1569
USA

Matthijs K. J. ter Wiel

Laboratory of Organic Chemistry
Strating Institute
University of Groningen
Nijenborgh 4
NL-9747 AG Groningen
The Netherlands

Richard A. van Delden

Laboratory of Organic Chemistry
Strating Institute
University of Groningen
Nijenborgh 4
NL-9747 AG Groningen
The Netherlands

Michael R. Wasielewski

Chemistry Division
Argonne National Laboratory
Argonne, IL 60439
USA

Bilha Willner

Institute of Chemistry and
The Farkas Center for Light-Induced Processes
The Hebrew University of Jerusalem
Jerusalem 91904
Israel

Itamar Willner

Institute of Chemistry and
The Farkas Center for Light-Induced Processes
The Hebrew University of Jerusalem
Jerusalem 91904
Israel

Yasushi Yokoyama

Dept. of Materials Chemistry
Faculty of Engineering
Yokohama National University
79-5, Tokiwadai, Hodogaya-ku
Yokohama 240-8501
Japan

Abbreviations and Symbols

Chapter 1

ANI	4-aminonaphthalene monoimide
BDPY	borondipyrromethene dye
EPR	electron paramagnetic resonance
$^{+1}E_{1/2}$	electrochemical oxidation potential
eV	electron volt
FBP	free base porphyrin
FBOAP	free base octaalkyl porphyrin
FB3PN	free base tri-pentylporphyrin
HOMO	highest occupied molecular orbital
LUMO	lowest unoccupied molecular orbital
MgP	magnesium porphyrin
mT	millitesla
NI	naphthalene-1,8:4,5-diimide
PDI	perylene-3,4:9,10-tetracarboxylicdiimide
PDP	phenyldimethylpyrromethene
PI	pyromellitimide
pyr-PMI	9-(N-pyrrolidiny)perylene-3,4-dicarboximide
RP-ISC	radical pair intersystem crossing
S-T ^o (or S-T ^{±1})	singlet-triplet mixing
SO-ISC	spin-orbit intersystem crossing
TB	through-bond
TS	through-space
TREPR	time-resolved electron paramagnetic resonance spectroscopy
TLS	two-level system
T _c	Curie temperature
ZnP	zinc porphyrin
Zn3PN	zinc-tripentylporphyrin
α-ZrP	Zr(HPO ₄) ₂ · H ₂ O
τ	lifetime (luminescence etc.)

Chapter 2

LB	Langmuir–Blodgett (films)
T _g	glass transition temperature

Chapter 3

DHA	dihydroazulene
DHI	dihydroindolizine
DTE	dithienylethene
EC	first step <u>e</u> lectron transfer, second step <u>c</u> hemical reaction
E_p	peak potential
I/E response	(current/potential) response
ITO	indium-tin-oxide
NLO	NLO activity
OTE	optically transparent working electrode
PET	photoinduced electron transfer
PMMA	poly(methyl methacrylate)
PYP	photoactive Yellow Protein
TBAHFP	tetrabutylammonium hexafluorophosphate
VHF	vinylheptafulvene

Chapter 4

C	“colored” form
5CB	4-cyano-4'-pentylbiphenyl
DC	direct current
M	minus (enantiomeric helicity)
P	plus (enantiomeric helicity)
PMMA	poly(methyl methacrylate)
PMMA–PMA	poly(methyl methacrylate)-polymethacrylate
pss	photostationary state
SHG	secondary harmonic generation

Chapter 5

e.e.	enantiomeric excess
g	Kuhn anisotropy factor
g_λ	anisotropy factor at wavelength λ
HTP	helical twisting power
l -CPL	left circularly polarized light
LC	liquid crystal
LPL	linearly polarized light
ORD	optical rotatory dispersion

p	macroscopic helical pitch
PMMA	poly(methyl methacrylate)
PS	polystyrene
p.s.s.	photostationary state
PVC	polyvinyl chloride
PVAC	polyvinylalcohol/polyvinylacetate
r -CPL	right circularly polarized light
T_g	gelation temperature
UPL	unpolarized light
β_m	helical twisting power

Chapter 6

Acm	acetamide
AlcDH	alcohol dehydrogenase
Amd	ϵ -amidinated
anti-DNP-Ab	anti-dinitrophenyl-antibody
ATP	adenosine triphosphate
Con.A	concanavalin A
cAMP	cyclic adenosine monophosphate
cGMP	cyclic guanosine monophosphate
COx	cytochrome oxidase
Cyt. C	cytochrome c
DCC	dicyclohexylcarboximide
DCIP	2,6-dichlorophenol-indophenol
DI	diaphorase
FAD	flavine adenine dinucleotide
HFP	hexafluoropropanol
Gox	glucose oxidase
HOSu	N-hydroxysuccinimide
NAD ⁺ and NADH	nicotine adenine dinucleotide
NSOM	near-field scanning optical microscope
QCM	microgravimetric quartz crystal microbalance
R_{et}	electron transfer resistance;
SPR	surface plasmon resonancespectroscopy
TFA	trifluoroacetic acid
X_{aa}	<i>trans</i> -azobenzene phenylalanine
$Z_{im}(\omega)$	imaginary impedance
$Z_{re}(\omega)$	real impedance
Z1HO1	a monoclonal antibody

Chapter 7

XNOR	exclusive NOR gate
XOR	exclusive OR gate

Chapter 8

bipy	2,2'-bipyridine
BPh	a bacteriopheophytin
CN	coordination number
CV	cyclic voltammetry
cyt c	cytochrome c
dap	2,9-di-p-anisyl-1,10-phenanthroline
dpp	2,9-diphenyl-1,10-phenanthroline
EC	electrochemical process in which an electron transfer is followed by an irreversible chemical reaction
ipa	intensity of anodic peaks
ipc	intensity of cathodic anodic peaks
MLCT	metal-to-ligand charge transfer
phen	1,10-phenanthroline
SP	dimer of bacteriochlorophylls called 'Special Pair'
terpy	2,2',6', 2''-terpyridine
$t_{1/2}$	half-life

Chapter 9

BOC	<i>tert</i> -butoxycarbonyl
CPK	Cory-Pauling-Koltun
<i>I</i>	fluorescence intensity
K_{ass}	association constants
<i>n</i>	the Hill coefficient
PET	photoinduced electron transfer

Chapter 10

CD-ROM	compact disk, read only memory
CTAB	cetyltrimethylammonium bromide
DNA	deoxyribonucleic acid
SDS	sodium dodecyl sulfate
Triton X-100	neutral polyoxyethylene(10)-isooctylphenylether
XNOR	eXclusive NOR
XOR	eXclusive OR

Chapter 11

ATP	adenosine triphosphate
CT	charge transfer
LMCT	ligand to metal charge transfer
NAND	not AND
SDS	sodium dodecyl sulfate

Chapter 12

8AB8	4,4'-dioctylazobenzene polyacrylate with strong donor-acceptor pairs in the azobenzene moiety ACB-ABA6
AFLC	antiferroelectric LC
BMAB	4-butyl-4'-methoxyazobenzene
5CB	4-pentyl-4'-cyanobiphenyl
Ch	cholesteric
f_c	threshold frequency in composites containing <i>trans</i> -azobenzene
f_{cs}	threshold frequency in composites with <i>cis</i> -azobenzene
FLC	ferroelectric LC
I	isotropic
LC	liquid crystal
LCD	LC display
LC-SLM	LC spatial light modulator
LMW	low-molecular-weight
N	nematic
NCAP	nematic curvilinear aligned phase
NLC	nematic LC
PDLC	polymer-dispersed liquid crystal
PI film	polyimide film
PLC	polymer liquid crystal
PNLC	polymer network liquid crystal
P_s	spontaneous polarization
PSLC	polymer-stabilized liquid crystal
SHG	second harmonic generation
Sm	smectic
SmC*	chiral smectic C
S/N	signal to noise (ratio)
T_g	glass transition temperature
TNI	N to I phase transition temperature
T-V	transmission-voltage (profile)

Chapter 13

CD	circular dichroism
D	Debye
DAC	dodecyl ammonium chloride
DCCI	dicyclohexylcarbodiimide
DCE	1,2-dichloroethane
FTIR	Fourier transform infrared
HFP	hexafluoro-2-propanol
HOBt	<i>N</i> -hydroxy-benzotriazole
LB	Langmuir–Blodgett (films)
ORD	optical rotatory dispersion
<i>Pfr</i>	far red absorbing phytochrome
<i>Pr</i>	red absorbing phytochrome

Subject Index

- a**
- absolute configuration 151
 - absorbance 411
 - absorption maxima,
 - dihydroazulene 75
 - vinylheptafulvene 75
 - absorption spectra 107, 221
 - poly(L-glutamic acid)
 - containing 85 %
spiropyran units 420
 - absorption spectroscopy 232
 - acid/base-controllable 236
 - acid-base equilibrium 110
 - activation energy 43, 115
 - affinity chromatography 210
 - affinity interactions,
 - photoisomerization control
by 169
 - aggregation-disaggregation
effects, photostimulated 426
 - alcohol dehydrogenase,
 - reversible
photostimulation 207
 - alkali metal 111
 - alkaline earth metal 114
 - 1,2-alternate 287
 - 1,3-alternate 287
 - AM1 115
 - amino-azobenzene-4'-sulfonic
acid 409
 - amorphous film 53
 - amorphous systems 57
 - amperometry,
 - photomodulated 80
 - amplification 153, 437
 - β -amylase, nitrospiropyran-
functionalized 176
 - AND logic 343
 - AND logic gate 98, 242
 - endo*-annulus orientation 289
 - antenna complexes 18
 - anthocyanins 312
 - anthracene 26
 - anthraquinone 88
 - anthraquinone derivative
 - dihydroazulene 87
 - vinylheptafulvene 87
 - anthraquinone radical anion 88
 - antibody
 - trans*-azobenzene 208
 - binding 206
 - binding affinity 173
 - selective association 212
 - antibody-antigen
 - binding 173
 - dissociation 173
 - anti-dinitrophenyl-antibody 205
 - sensing 200
 - antigen
 - dinitromerocyanine
 - monolayer 200
 - dinitrospiropyran
 - monolayer 200
 - monolayer 200
 - monolayer-functionalized 200
 - photochemical
 - isomerization 200
 - photoisomerisation 174
 - antigen-antibody
 - affinity interactions 199
 - photoswitchable binding 199
 - antigen-antibody affinity
complexes
 - amperometric
transduction 198
 - faradaic impedance
spectroscopy 198
 - microgravimetric Quartz
Crystal Microbalance 198
 - optical transduction 198
 - surface plasmon
resonance 198
 - antigen-antibody complex
 - at electrode surfaces 197
 - at electronic transducer 197
 - impedance spectrum 198
 - resonance frequency of a
piezoelectric crystal 198
 - antigen-monolayer electrode
electrical insulation 200
 - oxidation of glucose 200
 - apo-glucose oxidase 195
 - reconstitution 188
 - surface reconstitution 196
 - aromatic stabilization energy 43
 - artificial receptors 289
 - association constants 111
 - photoisomerizable
concanavalin A 171
 - atom economy 349
 - Au electrode,
 - photoisomerizable
monolayer 192
 - axially chiral 127
 - azobenzene 168, 237
 - cis*- 174
 - dipole moment 185

- trans*- 173 f, 283, 364, 399 ff
 azobenzene-LCs 372
 azobenzene poly(L-glutamic acid) 179
 α -helix structure 180
 photoisomerization 179
 azobenzene poly(L-lysine)
 α -helix 180
 β -sheet 180
 azobenzene-sulfonate 434
 groups 433
 azobenzoyl-L-lysine 410
 azobis(benzocrown ethers) 284
 azo chromophore 407
cis-azo-polypeptides 405
 azulenes,
 electropolymerization 97
- b**
- barbituric acid derivatives 290
 benzidine 232 f
 benzo-crown 48
 betaine 69
 biarylype rotor 147
 binaphthol 112, 116
 derivative 116
 1,1'-binaphthyl,
 dihydroazulene 86
 binary logic 124
 biocomputer 208
 bioimprinting 119
 biological activities 119
 biology
 ATP synthase 250 ff
 linear motor 250
 rotary motor 250
 biomaterial, photosensory 209
 biomolecular switches 165
 photochemical 204
 biosensor devices
 enzyme electrode 209
 photoswitchable enzyme 209
 biphenol 232
 biphotochromic compounds 102
 bisarylamine 85
 bistable species 309
 blood clotting, light-regulated 211
- boronic acids 48
 boronic acid-saccharide interactions 294
 brakes 147
 branched arrays 11
 bulk amorphous systems 57
 by-product 42 f
- c**
- caclic voltammetry 51
 calixarene 287
 calix[4]arene 299 f
 calix[4]aryl esters 289
 carboxyazobenzene
 trans-2 174
 trans-3 174
 trans-4 174
 carotenoid 15
 catenanes 219, 226, 241, 243
 electrochemistry 271 ff
 gliding 271 ff
 spectroscopy 271 ff
 spectroscopy EPR 272
 three-state 273
 CD spectra 116, 293
 dihydroazulene 86
 α -helix 402
 poly(L-glutamic acid)
 containing 85 mol %
 spiropyran units 421
 poly(L-glutamic acid)
 incorporating 85 mol %
 spiropyran units 422
 poly(L-lysine) containing
 46 mol % spiropyran
 units 424
 polypeptides with
 chromophoric side
 chains 403
 poly(N^e-*p*-phenylazo-
 benzenesulfonyl-L-
 lysine) 412
 random coil structure 403
 β -structure 403
 cellulose 74
 cerium(IV) bis(porphyrinate)
 double decker 302
 chalcone 26
 charge transfer (CT) 355
 charge-transfer band 240
 charge-transfer complex 239
 charge-transfer interactions
 228, 232
- chemical structure, spiropyran
 poly(L-lysine) 426
 chiral azobenzene dyes 437
 chiral dopant 118
 chiral HPLC 134
 chiral recognition of
 saccharides 296
 chiroptical molecular switch 123
 chiroptical properties 114
 chiroptical trigger 130
 o-chloroanil 229
 cholesteric 117
 cholesteric pitch 118
 cholesteric screw sense 156
 cholesteric sense 119
 cholesteric (twisted nematic) 155
 chiroptical properties
 polypeptide structures 402
 α -chymotrypsin 119, 182
 α -chymotrypsin 184
 circular dichroism (CD) 49,
 128, 238, 402
 circularly polarized light 125
 circumrotation 221, 227 f,
 231
 clearing point 118
 clockwise rotation 151
 Co(CN)₆³⁻ system 333
 co-conformational change 220, 231, 235
 coil- α -helix transition 412
 coloration – decoloration
 cycles 438
 color-tap effect 330
 complementary recognition
 sites 232
 complex formation 49
 compounds as azobenzene and
 spiropyran, photochromic 437
 concanavalin A 119
 nitrospiropyran-tethered 171
 photoisomerizable 169
 conducting films 97
 conducting polymers 79
 cone 287
 conformational transition
 spiropyran-containing 419
 UV light-induced 404

- conformation of polypeptides 400
 π -conjugation 51
 conrotatory ring-closure 140
 cooperative guest binding 302
 copolymers
 N-octadecyl-L-aspartate 417
 p-phenylazobenzyl-L-aspartate 417
 copolypeptide
 β -benzyl-L-aspartate 416
 para-phenylazo-L-aspartate 416
 coumarin 28, 112
 counter-clockwise rotation 151
 counterion exchange 231, 237
 cross-bar switching 59
 cross-talk ratio 59
 crown ether 47
 crystalline phase 46
 CT 355
 cyclic peptide, photochromic 418
 cyclic voltammetry 65, 82 ff, 225
 cyclic voltammogram 66, 88, 94
 [8+2] cycloaddition 70
 cyclodextrin 147, 237 f, 243
 cyclophane 226 ff, 232 f, 235
 cytochrome
 electron transfer mediator 192
 light-induced binding 192
 photoswitchable activation/deactivation 192
 cytochrome C, electron transfer communication 191
 cytochrome oxidase, reduction of oxygen 193
- d**
- data storage 130
 delayed emission 348
 demetallation 222, 231
 dendritic 22
 deprotonation 98
 detergent micelles 358
 devices 241, 243
 Dexter 17
 DHAs 75, 77
 furanyl-derivatized 76
 structurally fused photochromic system 99
 DHA-VHF 63
 2,6-diaminopyridine receptor 290
 dianion 66
 diarylethenes 37
 diastereomer ratio 116
 diastereomers 124
 diastereoselective 116
 diastereoselective photocyclization 141
 diastereoselectivity 116
 diazacrown ether 299
 diazo-thioketone coupling 133
 dibenzodioxin subunit, radical cation 94
 1'-dibenzodioxinyl 90
 6-O-[4-(1,1-dicyano-1,8a-dihydroazulen-2-yl)-benzoyl]-2,3-di-O-methylcellulose 76
 dielectric constant 118
 diethienylethenes 42
 difluoroboradiaza-s-indacenes 65
 dihydroazulene 70 ff
 absorption maxima 75
 anthraquinone derivative 87
 1,1'-binaphthyl 86
 CD spectra 86
 photochemistry of-chiral molecules 86
 synthesis 72
 dihydroazulene-vinylheptafulvene 63, 75
 dihydroazulene-vinylheptafulvene photochromism 68, 70
 fluorescence quantum yield 78
 information storage 92
 reaction profile 78
 singlet pathway 78
 thermal back reaction 78
 dihydroindolizine 69
 4,7-dihydroxyflavylium compound, energy level diagram 320
 μ -oxo dimer 301 f
 dimeric anthracene 290
 dimeric dication 95
 dimerization, radical cations 94, 97
 dimethylaminoindolylfulgide 111
 2'-dimethylphenazinyl 90
 dinitrospiropyran, antigen monolayer 200
 1,4-dioxybenzene 229
 disable signal 356
 disaccharides 293
 dithienylethene, structurally fused photochromic system 99
 dodecyl ammonium chloride (DAC) 409
 doping 54
 chiral nematic 55
 nematic 55
 doublet state 9
 dual-mode chiral response 142
 dual-mode stimulation 312
 dual-mode systems 311
 dual-mode transducers 345
 durability 39, 41
 dynamic NMR 148
 dynamic optical filtering 208
- e**
- EC-type mechanism 94
 effective volume viscosity 168
 elasticity constant 118
 elastin-like poly (pentapeptide) 418
 electrical contact, glucose oxidase 196
 electric fields, optical control 16
 electrochemical cell 84
 electrochemical oxidation 233
 electrocyclic reaction 108
 electrode
 antigen-antibody complex 198
 cytochrome 194
 cytochrome oxidase 194

- dinitrospiropyran
 monolayer 202
 monolayer 200
 nanoengineering 191
 photoisomerizable
 monolayer 193
 photoisomerizable redox
 enzyme 185
 electrolysis 223
 electron beam deposition
 242
 π -electron delocalization 50
 electronic circuits 243
 electronic coupling 8
 electronic transducer 186
 electronic transduction 186
 electron mediator 195
 electrostatic repulsion 196
 π -electrons 50
 electron transfer 26 f, 79,
 165
 cytochrome c 194
 cytochrome oxidase 194
 liquid triggered 80
 photoinduced (PET) 63
 electron transfer mediator
 188
 electrostatic interactions
 191
 electron transfer resistance
 197
 electropolymerization,
 azulenes 97
 electrostatic repulsion 228,
 231, 288
 enabled OR logic 357
 enabling/disabling input 357
 enantiomeric excess 126
 enantiomers 124
 energy acceptor 112
 energy donor 112
 energy gradient 22
 energy level diagram 319 ff,
 324, 326
 energy transfer 17, 27, 43
 stepwise 25
 TB mechanism 21
 TS mechanism 21
 enthalpy-entropy
 compensation relationship
 281
 enzyme
 light-active 209
 nitrospiropyran-FAD-
 reconstituted 190
 photoisomerization 190
 photoswitching direction
 191
 surface-reconstituted 195
 enzyme cascade 165
 enzyme electrode
 biocomputers 209
 photoisomerizable 187
 enzyme monolayer
 photoisomerizable 187
 photoisomerization 190
 EPR 14
 esterification 119
 esterified poly(L-glutamate)
 410
 exciplex 142
 exclusive NOR (XNOR) logic
 gates 240
- f**
- faradaic impedance
 spectroscopy 197
 far red absorbing
 phytochrome 428
 fatigue 125, 138, 406, 420,
 438
 process 42
 resistance 38 ff
 ferrocenecarboxylic acid
 206
 ferrocenedicarboxylic acid,
 diffusional electron transfer
 mediator 190
 ferrocene-dihydroazulene
 conjugate 85
 flash photolysis 313
 flavin 290
 flavylum compound 309 ff
 chemical process networks
 323
 chemistry 312
 structural transformations
 313
 thermodynamic and kinetic
 constants 319
 flavylum ion 69
 flavylum ions with OH
 substituents 318
 flavylum salts 346
 flow dialysis 185
 fluorescein 28
- fluorescence 43, 80, 111, 125,
 145, 239, 294, 312
 effect of pH 67
 „ON/OFF“-switching 68 f
 fluorescence-pH profile 294
 fluorescence switching 67
 metal ion-dependent 65
 fluorescence was efficiently
 quenched 288
 fluorescent monoboronic
 acids 292
 fluorescent sensor 294
 fluorophore 288
 Förster 17
 D -fructose 296
 fulgenate 108
 fulgide 68, 107, 400
 fulgide derivatives 168
 fulgimides 68, 108
 fullerene 15
 functional integration 351
 furan 74, 80
 furylfulgide 37 f, 108
- g**
- gated photoresponse 425
 gated response 144
 gel 125
 Gibbs free energy 303
 α -D-glucopyranose 170
 α -D-glucopyranose monolayer,
 binding of the lectin 171
 glucose 48 f
 oxidation 190
 photostimulated oxidation
 188
 D -glucose 292
 glucose oxidase 207
 dinitrospiropyran-
 functionalized 205
 electrical communication
 194
 electrostatic attraction
 194
 ferrocene-tethered 195
 nitrospiropyran-FAD-
 reconstituted 190
 oxidation of glucose 187
 photochemical activation
 194
 photoisomerizable 187
 photonic activation 194
 photoswitchable 187

protonated
 nitromerocyanine-FAD-
 reconstituted 190
 reconstitution 188
 gold electrode 52
 green's majority rule 154
 guests 239, 243

h

hairy rod structure 431
 half-adder 353
 half-life 43
 helical chirality 114
 helical pitch 155
 helical rods, amphiphilic 436
 helices
 left-handed 438
 right-handed 438
 helix 421
 α -helix 401
 helix inversion 135
 helix-sense reversal 415 ff
 Heller 108
 hemoprotein
 cytochrome 191
 electrical communication
 191
 1,3,5-hexatriene 108
 Hill coefficient 304
 ^1H NMR spectroscopy 229
 hole injection 52 f
 hole transport layer 52
 holographic data storage
 152
 holographic pattern
 recording 208
 host-guest interaction 47
 hosts 239, 243
 hybrid solid state devices 29
 hydraulics analogy 321 ff
 hydrogen bonds 237
 [C-H \cdots O] hydrogen bonds
 226
 hydrogen transfer 109
 hydroquinone 88
 N-(2-hydroxyethyl)-
 spiropyran 419
 4'-hydroxyflavylium compound
 AND logic behavior 330
 energy level diagram 321,
 326
 network of processes 334
 OR logic behavior 331

write-lock-read-unlock-erase
 cycle 325 ff
 7-hydroxyflavylium compound,
 energy level diagram 320
 4'-hydroxyflavylium ion 70
 write-lock-read-unlock-erase
 cycle 328

i

immunosensor 197, 199
 photoisomerizable 199
 photoisomerizable antigen
 200
 reusable 200
 reversible 199, 203
 impedance spectroscopy 197
 indolylfulgide 115
 information storage 67, 123,
 310
 dihydroazulene-
 vinylheptafulvene
 photochromism 92
 information storage device
 208
 inherently dissymmetric
 alkenes 132
 INHIBIT logic 355
 injection current 53
 input-output behavior 358
 [C-H $\cdots\pi$] interactions 226
 π - π interaction 348
 interlocked molecules 243
 intersystem crossing
 radical pair 12
 spin-orbit 14
 inverse temperature
 transition 418
 ion channel 165
 ionization potential 52
 ion sensors 79
 irreversible switches 242
 isomerization
cis-trans 429
E-Z 146
trans-cis 405 ff
Z/E 287
 isomerization thermal 179

j

job diagram 303

k

Kuhn anisotropy factor 126

l

Langmuir-Blodgett (LB) 431
 films 42, 430
 Langmuir-Blodgett technique
 241
 Langmuir trough 241
 laser photolysis
 femtosecond 45
 picosecond 45
 lateral translation 257
 LC display technology 155
 lectin 170
 ligand to metal charge transfer
 (LMCT) 352
 light-absorbing antenna 18
 light-controllable switching
 238
 light excitation 309, 312
 light-triggered electron
 transfer 80
 linearly polarized light 129
 liquid crystalline 125
 liquid crystalline phases
 130
 liquid crystalline properties
 117
 liquid crystals 54, 117, 363
 alignment 54
 chiral nematic 54
 induced cholesteric 54
 nematic 54
 liquid membrane 286
 LMCT 352
 lock-state 97
 logic gates 63, 239, 242, 310,
 339
 logic operations 239, 330
 luminescence 339
 „ON/OFF“-switching 66
 luminescent sensors 359
 lumophore-spacer-receptor
 systems 343
 lysine 119

m

Mach-Zehnder
 interferometers 58
 macrocyclic polyether 226,
 228, 231, 237
 magnetic interaction 54
 α -D-mannopyranose 170
 monolayer 172
 mechanical bonds 219

- D-(+)-melibiose 294
 - membrane photopigments
 - 410
 - membranes, photoresponsive
 - 434
 - merocyanine form 419
 - mesogen 117
 - metal ion 47
 - metalloporphyrins 18 f
 - metal picrate 47
 - 4'-methoxyflavylium, XOR
 - (exclusive OR) logic behavior 333
 - 4'-methoxyflavylium
 - compound
 - absorption spectra 314
 - energy level diagram 319, 321
 - molar fraction distribution as a function of pH 315
 - 4'-methoxyflavylium ion 313, 324
 - continuous irradiation 315
 - energy level diagram 324
 - fluorescence spectra 316
 - photochemical behavior 315
 - pulsed irradiation 317
 - spectral changes caused by continuous irradiation 316
 - thermal reaction 314
 - 8-methoxyheptafulvene 70
 - micelles 436
 - microgravimetric quartz
 - crystal microbalance (QCM) analysis 197
 - mixed monolayer, thiolated
 - nitrospiropyran and thiolated pyridine 192
 - molecular dynamics
 - simulation 421
 - molecular electronic devices 50
 - molecular functions 38
 - molecular-level devices 312
 - molecular-level switching
 - devices 309
 - molecular memory elements 159
 - molecular motors 147
 - molecular photoswitches 166
 - molecular recognition 125, 146
 - molecular scale arithmetic 353
 - molecular sensors 63
 - molecular shuttles 219
 - molecular switches 287, 399
 - optoelectronic 63
 - photochromic 67
 - photoresponsive 63 ff
 - three-way 97
 - molecular switching,
 - multimode 99
 - molecular turnstiels 147
 - molecular type wire 141
 - molecular wire 52, 141
 - molecule-based logic gates 239
 - molecules, mechanically
 - interlocked 219
 - monoclonal antibody 173
 - monolayer 241 f
 - antigen 200
 - antigen-antibody complex 200
 - azobenzene 181
 - azobenzene-containing poly(L-glutamate)s 429
 - azobenzene (poly-L-lysine) 181
 - binding of DNP-Ab 202
 - cyclic amperometric 201
 - cyclic microgravimetric sensing 203
 - dinitrospiropyran 202
 - DNP-Ab sensing 201
 - faradaic impedance transduction 201
 - glucose oxidase 190
 - nitrospiropyran 196
 - photoisomerizable 201
 - photoisomerizable
 - dinitrospiropyran 203
 - photoisomerization 181, 192, 194, 202
 - protonated
 - dinitromerocyanine 201 f
 - protonated
 - nitromerocyanine 196
 - pyridine-protonated-nitromerocyanine 193
 - surface pressure 181
 - thiolated nitrospiropyran 194
 - monolayer-functionalized
 - electrode
 - dinitrospiropyran-modified 200
 - electron transfer resistance 200
 - impedance spectrum 200
 - isomerization 200
 - protonated
 - dinitromerocyanine 200
 - monosaccharides 292
 - monolayer 171
 - motion 125
 - multimode photochromic switches 87
 - multiple reaction patterns 333
 - multistate/multifunctional
 - molecular-level systems 309 ff
- n**
- NAND logic 347
 - nanotechnology 159
 - naphthalene diimide 9
 - naphthalene monoimide 9
 - negative heterotropic systems 297
 - negative homotropic systems 301
 - nematic 117, 155
 - neuron-like networks 310
 - new sensory system for sugar molecules 293
 - nitrophenyl- α -D-
 - mannopyranose 170
 - nitrospiropyran 168, 170, 179
 - NLO-active 79
 - noncovalent bonding
 - interactions 226
 - noncovalent bonds 243
 - nondestructive read-out 109, 125
 - nonlinear optical properties 113, 310
 - nonlinear optics 152
 - nonselective receptors 349
 - NOR logic 351
 - NOT logic 341

- o**
- octaalkyl porphyrin 15
 - ON, Dimmed, and OFF states 146
 - “ON/OFF” photoswitch 283
 - optical fiber 60
 - optical image storage 376
 - optical memory 143, 208
 - optical nonlinearity 80
 - optical resolution 115
 - optical rotation 116, 433
 - optical rotatory dispersion (ORD) 405
 - optical switches 55
 - optical waveguide 55
 - optobioelectronics 165, 185, 213
 - optobioelectronic switch 205
 - optoelectronic, molecular switches 63
 - optoelectronic devices 310
 - optoelectronic gate 24
 - order – disorder
 - conformational changes 437
 - organic photoconductors 53
 - organogel 154
 - OR logic 349
 - OR logic gates 242
 - oscillating absorbance patterns 329
 - overcrowded alkenes 127
 - oxidation potential 65
- p**
- papain
 - azobenzene-functionalized 175
 - azobenzene-modified 174
 - trans*-4-carboxyazobenzene-tethered 175
 - photoregulated hydrolytic activities 175
 - partial-cone 287
 - patterning, dinitrospiropyran 212
 - permanent and temporary memories 328
 - permeability 168
 - permeability changes 435
 - perylene 16
 - perylene diimide 17
 - PET 339
 - switching principle 341
 - phase change 54 f
 - phase shifters 55
 - phenanthroline ligands 220 f, 223, 225
 - 3'-phenothiazinyl 90
 - 4'-phenoxathiinyl 90
 - 3'-phenoxazinyl 90
 - para*-phenylazo-L-aspartyl residues 416
 - N^ε-*p*-phenylazobenzene-sulfonyl-L-lysine 410
 - p*-phenylazobenzyl/*p*-benzyl-L-aspartate 435
 - p*-phenylazo-L-phenylalanine 404, 407
 - phenylfulgide 114
 - pH jump 313
 - phosphorescence 345
 - photoactive dopants 155
 - photoactive yellow protein (PYP) 69
 - photobiocatalytic 190
 - photobioelectrocatalytic switch 190
 - photobiological switches
 - multicycle photobiological switches 166
 - reversible artificial photobiological switches 166
 - single-cycle photobiological switches 166
 - photobistable 123
 - photochemical activation, bioelectrocatalytic functions 195
 - photochemical activation – deactivation, enzymes 176
 - photochemical
 - bioswitches 204
 - biphasic 204
 - glucose oxidase 204
 - photochemical flip of polarization of FLC 369
 - photochemical isomerization 207
 - trans*-azobenzene modified NAD⁺-cofactor 208
 - cis*-azobenzene NAD⁺-cofactor 208
 - protonated
 - dinitromerocyanine 201
 - photochemical patterning 212
 - photochemical phase transitions 364
 - chiral dopant 370
 - dynamic gratings 391
 - isotropic glass 377
 - phase-type holograms 391
 - reflection-mode system 375
 - photochemical switching 167
 - biocatalytic redox functions 185
 - bioelectrocatalytic properties 194
 - glucose oxidase 194
 - photochemistry of chiral molecules, dihydroazulene 86
 - photochromic 123, 345
 - performance 38
 - photochromic chromophores 37
 - photochromic compounds 364, 399
 - applications 309
 - computer memory elements 310
 - photochromic dopant 117
 - photochromic polymers 152, 433
 - photochromic polypeptides 432
 - photochromic protein 428
 - photochromic reactions, spiropyrans 422
 - photochromic switching, multifold 74
 - photochromism 37, 67, 107, 309
 - electrochemical triggering 85
 - photoreactions 75
 - quantum yields 75
 - photocyclization 38, 139
 - photocycloreversion 38
 - photodestruction 126
 - photodevices 291
 - photodimerization of anthracene 284

- photoeffects, molecular and thin films 428
- photoelectrochemical switching 50
- photoexcitation 141
- photoinduced electron transfer (PET) 291, 294, 339
- photoinduced *E/Z* isomerization 283
- photo-induced spectral hole burning
poly(methyl methacrylate) 5
- tetrabenzoporphyrin 5
- photoinduced swelling 435
- photoisomer
dinitrospiropyran 207
- protonated
dinitromerocyanine 207
- photoisomerizable
assemblies 179
- association 205
- azobenzene-functionalized peptide 181
- azobenzene-modified
NAD⁺ 207
- trans*-azobenzene modified
NAD⁺-cofactor 208
- cis*-azobenzene NAD⁺-cofactor 208
- command interfaces 191
- dinitrospiropyran 205, 211
- dinitrospiropyran monolayer 201
- electrodes 191
- FAD cofactor 188 f
- immobilized enzyme 182
- inhibitors 167, 213
- liposomes 178
- macromolecules 179
- matrices 167, 178
- microenvironments 178
- photoregulation of
biomaterials 182
- polypeptide 180
- redox proteins 204
- photoisomerizable antigen
173, 213
- coenzymes 208
- enzyme activation
deactivation 208
- inhibitors 208
- photoisomerizable cofactor
167
- nitrospiropyran-FAD 189
- photoisomerizable
components 168
- photoisomerizable enzyme
electrodes 187
- glucose oxidase 187
- layered electrode 190
- oxidation of glucose 187
- photoisomerizable interface
186
- photoisomerizable lectin,
kinetics of association
171
- photoisomerizable membrane-mimetic assemblies 178
- liposomes 168
- monolayers 168
- polymers 168
- photoisomerizable
monolayer 178, 193
- thiolatednitrospiropyran
194
- photoisomerizable peptide,
NMR studies 181
- photoisomerizable polymer
179
- acrylamide-copolymers
184
- nitrospiropyran-acrylamide 183
- nitrospiropyran-modified-poly(*t*-glutamic acid)
179
- photoisomerizable protein
170
- directed functionalization
176
- mutant 176
- phospholipase A 176
- photoisomerizable substrate,
photoswitchable binding
199
- photoisomerizable units
167 f, 170
- photoisomerization 38, 55, 145, 165
- biocatalyst 175
- cis-trans* 98, 132
- cofactor 168, 208
- dinitromerocyanine 203
- dinitrospiropyran 203
- dinitrospiropyran
monolayer 200
- enzyme monolayer 205
- inhibitor 168
- nitrospiropyran 192
- protonated
dinitromerocyanine
state 200
- protonated
nitromerocyanine 192
- reversible 205
- trans-cis* 399, 415
- photoisomerization antigen
patterning of antibodies
211
- patterning of surfaces 211
- photomechanical effects,
monolayers 428
- photomodulated
amperometry 80, 82
- photomodulation 85
- photomodulation
amperometry 90
- photomorphogenesis 165
- photonic materials 124, 159
- photonics
all-optically controllable
polymer/LC composite
films 387
- amplitude-type hologram
389
- anisotropic rearrangement
379
- antiferroelectric LCs 369
- azobenzene LCs 372
- 4-butyl-4'-methoxyazo-
benzene 365
- crosslinked PLC networks
377
- 4,4'-dioctylazobenzene 372
- donor-acceptor
azobenzenes 374
- ferroelectric LCs 367
- glasstransition
temperature 372
- guest/host systems 364
- guest/polymer LC systems
365
- highly fatigue-resistant
optical switching 376
- holography 388
- information processing
363

- LC alignment by linearly polarized light 378
 LC alignment change 364
 LC materials in holography 390
 new concept for fast LC response 371
 nonlinear optical effect 388
 nonrubbing alignment 383
 novel approach to alignment change in LCs 367
 optical dichroism 379
 out-of-plane alignment 381
 PDLC-SLM 385
 4-pentyl-4'-cyanobiphenyl 365
 phase-type hologram 389
 photoactive surface layers 381
 photoalignment techniques 383
 photochemical phase transition 364
 photochromism-based grating formation 390
 photoinduced alignment behavior 379
 polyimide (PI) film 382
 polymerazobenzene LCs 373
 polymer/LC composite films 384
 polymer liquid crystals 365
 thioindigo 371
 photonic signals amplified amperometric transduction 193
 electrical transduction 191
 photonic triggering 185
 photon-mode 109
 photooptical switching devices 58
 photoracemization 128
 photoreaction photochromism 75
 quantum yields 77
 photoreceptor 165
 photoredox switches 64
 photoregulated ion binding 290
 photoregulated matrix 168
 photoregulation azobenzene-modified poly(L-glutamic acid) 179
 electrode interfaces 185
 electron transfer reactions 185
 membrane permeability 437
 polypeptide 179
 photoresolution 128, 131
 photoresponse, gated 413
 photoresponsive, liquid crystals 363
 photoresponsive crown ethers 283
 photoresponsive guest 156
 photoresponsive LB and thin films 431
 photoresponsive polypeptide 182
 photoresponsive waveguides 431
 photosensitive biomaterial, encoded information 185
 photosensor 165, 213
 photosolubility effects 426
 photosolubilization 427
 photostationary equilibrium 174
 photostationary state (p.s.s.) 40, 108, 126, 411
 photostimulated electron transfer 81
 photoswitchable antigen-antibody 208, 210
 antigen-antibody interactions 197
 azobenzene-tethered papain 175
 binding 170
 binding interactions 213
 biochips 210
 bioelectrocatalysis 189
 bioelectrocatalytic function 187
 bioelectrocatalytic properties 188
 bioelectrocatalyzed oxidation of glucose 197
 biosensor arrays 210
 cofactor-enzyme 210
 electrocatalytic functions 204
 enzyme electrode 209
 functions 213
 hydrolytic functions 175
 redox biomaterials 185 ff
 redox enzymes 210
 substrate-protein 210
 photoswitchable biomaterial 178, 208, 210 f, 213
 amplification 210
 antigens/antibodies 209
 biochips 210
 biocomputers 210
 bioelectronics 210
 biosensor 210
 biosensor arrays 210
 cofactors 209
 DNA 209
 enzymes 209
 hormones 209
 inhibitors 209
 multisensor arrays 210
 optical information 210
 photoelectrochemical systems 210
 photonic amplifiers 210
 receptors 209
 photoswitchable devices 437
 photoswitchable enzymes 211
 biotransformations 210
 blood clotting 210
 therapeutic enzymes 210
 photoswitchable hydrolysis 184
 photoswitchable polypeptides 399 ff
 photoswitching bioelectrocatalytic functions 196
 enzyme electrode 196
 photoswitching molecular systems 38
 piperazine 26
 pitch 158
 PMMA matrix 76
 poly(L-alanine) 402
 poly(L-aspartate)s 415
 containing azobenzene units 415
 poly(β -benzyl-L-aspartate) 415
 poly(γ -benzyl-L-glutamate) 404
 poly(butyl methacrylate) 435

- poly(N^{ϵ} -carbobenzoxy-L-lysine) 404
 poly(L- α , α -diaminobutanoic acid) 414
 poly(L- α , β -diaminopropanoic acid) 414, 427
 poly(L-glutamate)s,
 photochromic Langmuir-Blodgett films, hairy rod 430
 spiropyran-modified 419
 poly(L-glutamic acid)
 azobenzene-containing 405
 carbocyanine 431
 containing 85 mol %
 azobenzene units, change in solubility 427
 containing leucocyanide (triphenylmethyl cyanide) groups 435
 spiropyran 431
 poly(hydroxyethyl methacrylate) 435
 poly(L-lysine) 403, 410
 azobenzene-containing 410
 monolayer 429
 photochromic reactions of
 spiropyran-modified 423
 spiropyran-modified 423
 polymer 7, 125
 dendritic 23
 fluorophores 23
 light-harvesting 23
 polymer azobenzene LCs 373
 all-optical switching materials 374
 dynamic holographic materials 374
 polymer claddings 59
 polymer liquid crystals 365
 polymer matrix 152
 polymer membranes,
 transport 185
 polymers
 azobenzene-acrylamidecopolymer 182
 bis-dimethylamino triphenyl carbinol-acrylamide copolymer 182
 nitrospiropyran-acrylamide copolymer 182
 photoresponsive 399 ff
 poly(methacrylate)s 432
 poly(methyl methacrylate) 74
 poly(L-ornithine) 414
 polypeptide IV, cross-linked 434
 polypeptide membranes,
 photoresponsive 433
 polypeptides 419
 amphiphilic structures 436
 photochromic 418
 photoswitchable 399 ff
 poly(N^{ϵ} -*p*-phenylazobenzene-sulfonyl-L-lysine) 410
 poly(N^{ϵ} -*p*-phenylazobenzoyl-L-lysine) 410
 poly(phenyleneethynylene) 23
 polystyrene 53
 poly(L-tryptophan) 403
 polyvinyl/polypeptide graft copolymers 435
 porphinatoiron(III) 301
 porphyrin 24, 28
 positive exciton coupling 293
 positive heterotropic systems 299
 positive homotropic systems 302
 positive or negative
 allosterism 297
 precipitation-dissolution cycles 427
 promoter, pyridine units 191
 protein 249
 photonic information 209
 protein G, activation 194
 protein modification with photoisomerizable groups 176
 protein shrinkage, dynamic 173
 protonated dinitromerocyanine monolayer, faradaic impedance spectra 202
 protonation-deprotonation 87, 98
 proton transfer 63, 79
 pseudomacrocycles 286
 pseudorotaxane 239 ff, 353
 P-type chromophores 37
 pyranose 119
 pyromellitimide 9
- q**
- quantum efficiency 126
 quantum yields 39
 photochromism 75
 quartz crystal mass 199
 quartz crystal microbalance,
 binding interactions 201
 quencher 288
 quinone, benzodifuran 64
- r**
- racemization 115, 125
 racemization barriers 135
 radical anion 66, 82
 radical cation 95
 dibenzodioxin subunit 94
 dimerization 94, 97
 radical pair, intersystem crossing 12
 ratchets 147
 ratiometric fluorescent sensors 350
 reaction center, synthetic 94
 recognition sites 225 f, 235, 237, 240
 reconstituted enzyme 190
 red absorbing phytochrome 428
 redox active 79
 redox-active photochromic compound 88
 redox behavior 93
 redox biomaterial, switching 186
 redox-controllable switching 222, 224 f, 227, 229, 234
 redox-controllable XNOR gate 240
 redox enzymes,
 photoswitchable activation 209
 redox potentials 80
 redox proteins
 electrical contact 191
 light-switchable activation 191
 reversible light-induced activation 209
 redox switch, luminescent 64
 reduction 233

- reflectivity 58
 refractive index 55 f, 58
 repeatable cycle number 41
 response time 44, 125
 reversible demetallation 221
 reversible immunosensors 210
 photoisomerizable antigens 211
 reversible irradiation 103
 room temperature phosphorescence 356
 rotaxanes 219, 226, 237, 241 ff
 copper 255 ff, 264 ff, 271 ff
 electrochemistry 260 ff, 268 ff
 kinetic 270
 kinetic constant 270
 phenanthroline 254, 260 ff, 266 ff
 photoinduced intramolecular electron transfer 254 ff
 pirouetting 264 ff
 porphyrine 254 ff
 rotary motors 264 ff
 terpyridine 259 ff, 266 ff
 translation 257
 [2]rotaxanes, chemically and electrochemically controllable 232
- s**
- saccharide 48, 344
 1:2 sandwich complexes 298
 secondary harmonic generation 113
 self-accelerating 302
 self-assembly 237
 sensing system 282
 sensory devices 185
 sergeants and soldiers effect 153
 shuttling 220, 225, 233
 silica glass cladding 59
 single crystal
 electron transfer 15
 magnetic field 15
 single molecule limit 339
 sodium dodecyl sulfate 415
 sol-gel materials 57
 sol-gel phase transition 155
 sol-gel transitions 168
 solid state 228
 solvated helix 421
 solvent extraction 47
 specific rotation 116
 spectroelectrochemical measurements 65
 spectroelectrochemistry 82
 spin 12
 spincoated films 432
 spirobenzopyran 43
 spiropyran 399 ff
 spiropyran form 419
 [$\pi \cdots \pi$] stacking 226, 231
 steric strain 133
 stilbenes 294
 stimulus 289
 Stobbe 108
 structurally fused photochromic system DHA 99
 dithienylethene 99
 β -structure 401
 succinic anhydride 108
 sugar-sensing systems 291
 sugar tweezer 301
 supramolecular 123
 supramolecular arrays
 dendrimers 28
 membranes 28
 polymers 28
 zeolites 28
 supramolecular chemistry 219
 supramolecular properties 114
 surface plasmon resonance 197, 204
 surface plasmon resonance spectroscopy 199
 antigen monolayer 204
 photoisomerizable monolayer 204
 reversible binding 204
 surfactant effect 409
 switch 242
 switch function 281
 switching 220, 281
 switch-on factor 296
- t**
- temperature jump 313
 template-directed strategy 221
 template-directed synthesis 219, 221 ff, 241
 terpyridine ligand 223
 tetrathiafulvalene 227 ff
 tetrathiafulvalene unit 240
 thermal cycloreversion 43
 thermal irreversibility 109
 thermal relaxation 103
 thermal stability 43
 thermochromism 43
 1'-thianthrenyl 90
 thienylfulgide 118
 thin films 28
 thin layer cyclovoltammogram 94
 thiophene fulgide 170
 photoisomerizable 169
 threading/unthreading processes 353
 three-dimensional switching 101
 three-position optical switch 157
 three-way, molecular switch 97
 threshold device 332
 time-resolved fluorescence 146
 time-resolved light scattering 173
 time-resolved observation 357
 TLS
 phthalocyanine 4
 poly(methyl methacrylate) 4
 transistors 243
 γ - γ transition 406
 transition, coil \rightarrow α -helix 412
 transition metals 220
 transition state 115
 translational isomers 226 f, 229, 232
 transport system 286
 trigger elements 124
 triptenylporphyrin 16 f
 triphenylmethane 400
 triplet-triplet annihilations 356

- T-type chromophores 37
- β -turn structure 418
- twisting power 55
- two-level system (TLS)
 - pentacene 3
 - perylene 3
 - terrylene 3
- two memory levels 328

- u**
- unidirectional rotation 151
- unpolarized light (UPL) 129
- unsubstituted flavylum
 - compound, energy level diagram 322
- unsubstituted flavylum ion,
 - write-lock-read-unlock-erase cycle 327

- v**
- variable attenuators 55
- variable frequency filter 55

- vectorial electron flow 52
- vectorial electron transport 52
- VHFs 75
- vibrational loss mechanism 352
- vinylheptafulvene 70 ff
 - absorption maxima 75
 - anthraquinone derivative 87
 - s-trans*, *s-cis* forms 73
 - synthesis 72
 - thermal electrocyclization 70 ff
 - X-ray structure 77

- w**
- wettability 168
- wires 242
- wiring problem 347
- Woodward-Hoffmann rules 108

- write-lock-read-unlock-erase cycle 144, 311 ff, 323, 325 ff
 - micelle effect 327
 - two memory levels 328

- x**
- XNOR logic 354
- XOR gate 239
- XOR (eXclusive OR) logic 333, 353
- X-ray crystallographic analysis 42, 227

- y**
- YES logic 339

1

Approaches to a Molecular Switch Using Photoinduced Electron and Energy Transfer

Aaron S. Lukas and Michael R. Wasielewski

1.1

Introduction

We are poised at an interesting time in the history of chemistry, as our fundamental understanding of complex processes such as photosynthesis and gene replication has reached the molecular level. Advances in these areas would not be possible without the development of many new physical techniques. Ultrafast photonics and single molecule science were fields yet to be discovered a mere thirty years ago. In the coming decade, researchers hope to synthesize concepts gleaned from research in these fields and develop a computer, the operation of which is based on the interactions of individual molecules with one another. This computer has the potential to be orders of magnitude smaller, faster, and more efficient than those based on semiconductor technology.^[1-3] Massive size reductions using molecular switches will most probably be limited by quantum statistical considerations (see, however, comments on quantum computation in Section 1.4), if reasonable data error rates are to be maintained.^[4] Nevertheless, molecular devices that use visible light for addressing and control purposes have a realizable data density of approximately 2×10^9 bits cm^{-2} merely through diffraction-limited spot size considerations alone. Recent results suggest that three-dimensional addressing,^[5] the use of excitonic waveguides,^[6,7] and near field optical techniques^[8,9] can greatly increase this resolution. Furthermore, since energy and electron transfer processes can occur on a subpicosecond timescale, it is possible to produce devices that respond with equal rapidity. Employment of fast, photo-driven processes of high quantum efficiency should also reduce the heat load produced by present-day computing devices, resulting in a more energy efficient system, and conceivably in economically viable molecular electronic devices.

Nonetheless, a working device has yet to be achieved. Successful examples of molecular systems capable of rectification,^[10,11] wiring,^[12-42] memory storage,^[5,43-47] and switching^[48-55] have been demonstrated; however, integration of these various components has proved difficult.

The development of a set of underlying principles to guide this undertaking is an active area of research.^[56,57] One promising approach is to base such a device on the interaction of light with these various components.^[58-62] There are several advantages to performing switching operations by means of optical inputs and outputs.

Electronic absorption is an extremely rapid process, and it should be possible to create switching devices that respond equally as rapidly. The excited states of molecules can fluoresce, undergo electron and energy transfer, and cause bond making and bond breaking. Each of these processes can be used for switching and storing data. Variable addressing of molecular states can be achieved by modulating the wavelengths, intensities,^[63] polarizations, and temporal and spatial properties of laser pulses. Information can be read from these systems by means of fluorescence, spectral bleaching,^[64–73] circular dichroism,^[74–76] readout of electronic spin states, and other methods.

Switching systems based on photochromic behavior,^[29,43,45,77–100] optical control of chirality,^[75,76,101] fluorescence,^[102–108] intersystem crossing,^[109–113] electrochemically and photochemically induced changes in liquid crystals,^[114–119] thin films,^[70,120–129] and membranes,^[130,131] and photoinduced electron and energy transfer^[132–150] have been synthesized and studied. The fastest of these processes are intramolecular and intermolecular electron and energy transfer. This chapter details research in the development and applications of molecular switches based on these processes.

Theoretical work strongly supports the idea that an electron transfer reaction can form the basis for a molecular switch.^[11,46,151–153] Yet the field has been slow to develop, because the optimal use of electron transfer processes requires careful control of molecular structure, electronic coupling, and thermodynamics in a complex array of donors and acceptors. Experimental work has focused mainly on approaches to molecular switches that make use of photochemical and electrochemical conformational changes within molecules. The general class of molecules to be discussed has several distinguishing properties. It is any molecule or array of molecules capable of absorbing a photon at a first wavelength, λ_1 , which induces a change in its electronic and/or nuclear structure. This structural change does two things; it attenuates the absorption of a second photon at λ_1 , and introduces a new absorption at a second wavelength, λ_2 . The switch has been turned “on”. Turning the switch “off” can be done in one of several ways. We will examine systems the lifetime of which is modulated thermally, magnetically, and also by absorption of a photon either at this second wavelength, λ_2 , or at some other part of the spectrum. The lifetime of the “on” state determines the turnover time and also the potential applications of a switch. Molecules with very long state lifetimes are no longer switches, but are considered memory devices.

The operation of any optically controlled device is critically dependent upon the efficiency of light absorption by the input chromophore, and its ability to undergo electron transfer. Three characteristics make an excellent input chromophore: a large ground state extinction coefficient, long-lived excited state (several nanoseconds), and high fluorescent quantum yield. The most commonly used chromophores for light absorption are fused polycyclic aromatic hydrocarbons, metallated and free base porphyrins, and derivatives of other light absorbers found in nature.

Reading the electronic state of the switch is often performed by use of optical transient absorption and fluorescence emission spectroscopy. Fluorescence is a much more sensitive technique, and can be done even at the single molecule level.

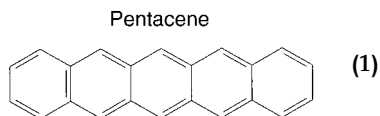
It also requires a much smaller density of photons to provide a stable signal; however, very few charge-separated ion pair states exhibit radiative charge recombination. In these cases, transient absorption is often used, because it allows direct non-destructive observation of a molecule's electronic configuration. Problems with this technique include photodegradation of more sensitive biological systems. Also, transient absorption is difficult to perform on monolayers or in the solid state, in which absorption cross sections are much lower than in solution. For this reason, monolayers and thin film assemblies are generally characterized using fluorescence emission or other more sensitive techniques.

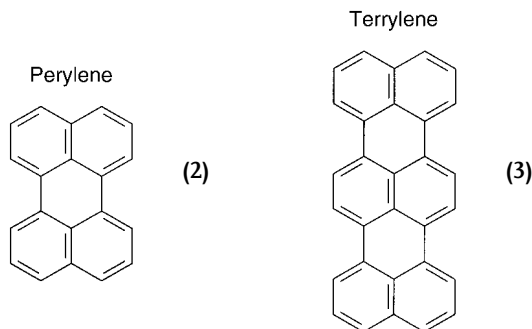
1.2 Systems Consisting of Single Molecules

Perhaps the simplest optically controlled switches are single molecules embedded in a solid host matrix. These systems consist of an amorphous, polycrystalline, or crystalline film doped with dilute concentrations of impurity molecules. The most commonly used dopant molecules are fused polycyclic aromatic hydrocarbons and porphyrins. In addition to facile sample preparation, these planar molecules absorb in the visible to near IR regions of the spectrum, possess large extinction coefficients in both the ground and excited states, and have high fluorescence quantum yields.

1.2.1 Two-level Systems

Theoretically, the simplest molecular switch is a two-level system (TLS) consisting of a double well potential in which two near degenerate states are separated by a potential barrier.^[154] Single molecules embedded in solid media demonstrate TLS properties, and the study of these systems for optically controlled molecular switching is an active area of research.^[155–161] The most commonly studied impurity molecules are pentacene (**1**), perylene (**2**), and terylene (**3**). The coupling of single or multiple neighboring TLSs results in spectral diffusion in the emission spectra from these single molecules. The TLS behavior may arise from structural relaxation within the single molecule, or more probably from small rearrangements of the surrounding medium. Structural fluctuations in the medium are probably coupled to phonon excitations in the impurity molecule. While initial work on TLS suggested this effect should only be observed in amorphous solids, it has also been observed in polycrystalline matrices^[157] and crystalline^[161] solids.





The switching lifetime of the resonance frequency has been observed to exhibit an exponential dependence on the intensity of irradiation.^[157] The intensities of the emission lines from each state are proportional to the probability of the TLS population in that site. This ratio is given by

$$\exp(-\Delta E/kT) \quad (1)$$

where ΔE is the energy separation between sites. When many TLSs are coupled to a single molecule, multiple resonance frequencies are observed.^[157]

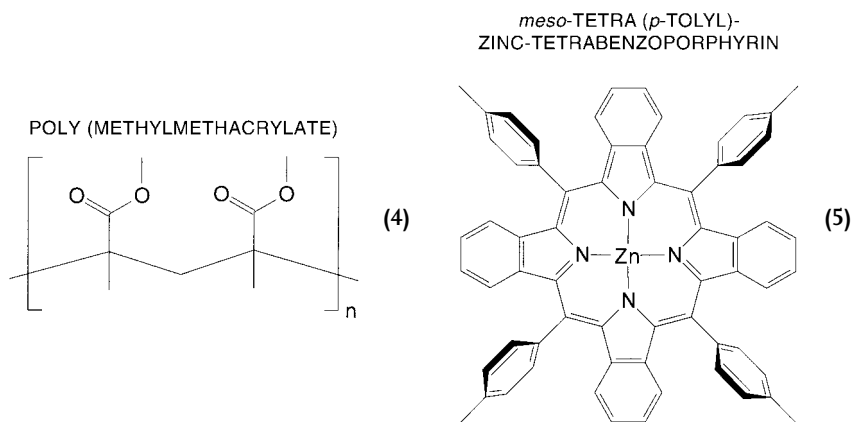
Investigation of the microscopic origin of these TLSs has demonstrated the feasibility of modulating resonance shifts in a single molecule by interrogation of neighboring solvent molecules coupled to the system.^[158] In poly(methyl methacrylate) doped with free base phthalocyanine and small amounts of water, it has been shown that reorientation of nearby water molecules is the source of spectral diffusion observed in the phthalocyanine.

These systems demonstrate the possibility that an optical switch might be based on photochemical manipulation of a single molecule's electronic state and local environment. However, these systems also possess several limitations:

- 1) These switching phenomena are observed only at liquid helium temperatures.
- 2) These systems suffer from photo-bleaching at relatively low photon densities.
- 3) Single molecules do not allow for broad spectral coverage. While perylene, terylene, and porphyrins all have large extinction coefficients, their absorption bands are only 20 to 50 nm wide. In some cases, it may be desirable to incorporate light-absorbing antenna complexes to enhance this spectral coverage. By selecting molecules on the basis of their spectral and electrochemical properties, it should be possible to cover any region of the visible spectrum. This should also improve the lifetime of these systems, because a single molecule need not absorb photons during each clock cycle, which can lead to photodegradation.
- 4) Switching events based on a TLS are on the order of seconds to minutes, and probably have greater application to optical data storage.

- 5) It will not be possible to take full advantage of the gains in data storage density provided by such systems unless improvements are made in our ability to address single molecules. These experiments are performed in dilute solid solutions, in which single impurity molecules can easily be addressed without interference from neighboring molecules. This technology has yet to be applied to arrays of molecules in close contact with one another. This leap must be made before consideration can be given to devising high-density data storage systems based on TLS switching.

Photo-induced spectral hole burning^[64–73] uses small fluctuations in local environment to store bundles of information in a single molecule. In these systems, the presence (or absence) of a spectral hole at a particular frequency is utilized to encode numerous bits of digital information within a single, focused laser spot. In some systems, the absorption of two photons encodes the data, while the readout is performed with a one-photon process.^[68] These systems have the advantage of greatly increased readout speeds, allowing for fast switching in small laser spots.



Carter and co-workers demonstrated spectral hole burning by means of an intermolecular electron transfer mechanism. In this experiment, poly(methyl methacrylate) (4) films were doped with zinc tetrabenzoporphyrin (5) electron donors and chloroform (CHCl_3) electron acceptors. The formation of gated holes occurred when both the singlet-singlet and triplet-triplet absorptions were excited, as seen in the Jablonski diagram in Figure 1. Excitation of the ground state with 627 nm light (λ_1) resulted in a triplet population, with a quantum yield of 0.8. The lifetime of the triplet state is $\tau = 39$ ms. If a second photon arrives before this state decays, then triplet-triplet transitions can occur. This excited state readily donates electrons to nearby acceptors, chloroform molecules in this case. The color of the second photon need not be specific, although the highest yield for electron transfer occurred with $\lambda_2 = 488$ nm. Electron transfer from two-photon absorption results in hole formation in the singlet manifold, and the observed photobleaching. The energy of the reduced CHCl_3 was not determined, but this system is likely to work with other electron acceptor groups. It is unclear whether the free electrons can migrate between

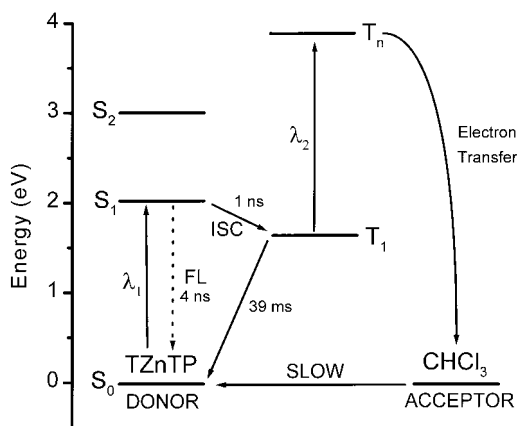


Fig. 1: Energy level diagram for the zinc tetrabenzoporphyrin donor/chloroform acceptor system.

chloroform molecules, adding to the stability of the system; however, this is likely in view of the high concentrations of CHCl₃ used. Optimal electron transfer was observed when chloroform was used in a molar excess of 10⁵:1. Furthermore, a weak electron acceptor such as chloroform makes the charge recombination a highly Marcus-inverted process.

In their current form, these systems offer far greater applicability to the construction of high-density optical memory devices. Several fundamental issues remain unresolved before single molecules can be widely used. Presently these switching effects are observed only at liquid nitrogen temperatures or below. It should be possible to observe the same effects under ambient conditions. Additionally, cross-talk between molecules is likely to occur as the concentration of the dopant molecules increases and nearest neighbor interactions become important. But this may not be a problem, as the density of states should also increase in this situation, making possible even greater gains in the data storage capacity. It is clear, though, that many of these questions will not be answered until the experiments are performed. Work on the single molecule level can also lend insight into covalently bound systems consisting of multiple subunits. We now examine such systems.

1.3 Systems Consisting of Multiple Chromophores

1.3.1 Intramolecular Electron Transfer

Covalently linked arrays of electron donors and acceptors can be used to perform switching operations. In addition, systems can be designed to store and transport digital information. It is possible to tune both the optical and electrochemical properties of a multicomponent system by selecting the appropriate electron donors and acceptors. These systems are inherently more complex, yet allow for a wider range of applications than devices based on single molecules. Generally, these systems consist of an input chromophore, a bridging group, and an output chromophore. Absorption of a photon results in one of two processes: stepwise photoinduced electron transfer, resulting in a charge-separated state, or energy transfer followed by fluorescence.

An early hypothesis for a molecular switch based on stepwise photoinduced electron transfer appeared in 1988.^[46] The design comprises a polymer consisting of a $[D-A_1-A_2]_n$ monomer unit, in which D is an electron donor moiety and A_1 and A_2 are primary and secondary electron acceptors, respectively. The system is designed to form a rigid photoactive chemical bridge, capable of storing and transferring digital information between two electrodes. This is done by means of synchronization of two processes: oxidation/reduction of the termini at an electrode and photoexcitation of the electron donor within the polymer.

The clock cycle for the switching process begins with photoexcitation of every electron donor in the polymer, forming the $[^1D-A_1-A_2]_n$ state. There are three potential deactivation pathways from this state to consider: fluorescence back to the ground state (dot), forward electron transfer to A_1 (solid), or backward electron transfer to A_2 in the adjacent monomer unit (dash-dot). A HOMO / LUMO scheme for these processes in the first three units of such a polymer is shown in Figure 2a. The donor-terminated end of the polymer can decay only by the first two paths. It should be relatively simple to enhance the coupling between 1D and A_1 such that forward electron transfer is the preferential process. Spontaneous thermal electron transfer, resulting in the state $[D^+-A_1-A_2^-]_n$ (Figure 2b), follows this initial charge separation step. This places free electrons and holes on neighboring monomers adjacent to one another. The basis for switching in this system is that electron tunneling between monomer units in this state (solid), resulting in charge recombination, is kinetically preferred over charge recombination to the ground state within a single $[D-A_1-A_2]$ monomer (dash-dot). If the electronic coupling can be controlled, to favor charge recombination across the unit, this leaves a single hole on the donor adjacent to the cathode. The next phase in the clock cycle is the data writing process, which is done electrochemically. If cathodic current flows and returns the donor to its ground state electronic configuration, then photoinduced electron transfer can occur from this donor site during the next clock cycle. However, if no reduction occurs, the hole will propagate along the polymer during the next clock cycle, leav-

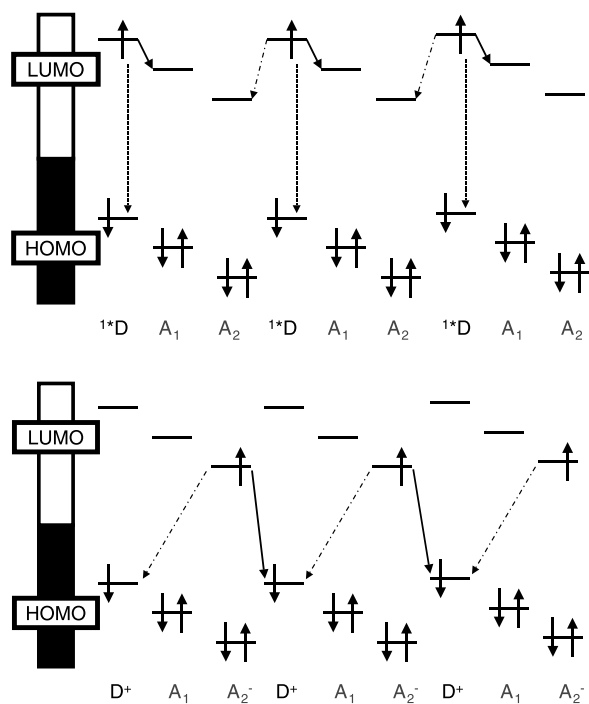


Fig. 2: HOMO / LUMO scheme for operation of a proposed molecular shift register.^[46] The clock cycle is initiated by photoexcitation of the donor moiety, resulting in the electronic configuration shown in (a). Decay pathways from this excited state are forward electron transfer within the same monomer unit (solid), back

electron transfer to the adjacent monomer unit (dash-dot), and fluorescence (dot). Successive forward electron transfer steps results in the electronic configuration shown in (b). The charge-separated state $[D^+-A_1-A_2]_n$ can charge-recombine within a single monomer unit (dot-dash) or with the adjacent monomer unit (solid).

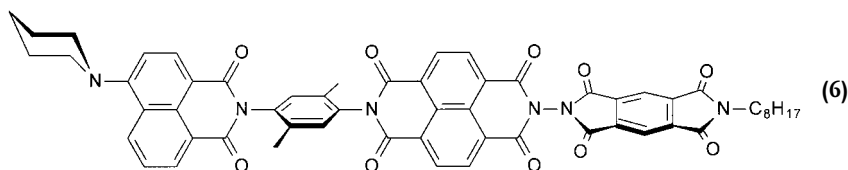
ing positive charge on the first two electron donors in the system. The holes are read out at the anode as zeros. The system must register n cycles before data entered at the cathode is read at the anode.

The authors discuss several parameters related to optimizing the efficiency of such a device. Firstly, the chromophore that is photoexcited must possess a distinct absorption band with a large extinction coefficient. Other chromophores in the polymer should not absorb in this spectral region. The second concern is the ability for charge recombination to occur between monomer units. This process must be favored over charge recombination within a single monomer, or a switching error occurs. The free energy for each process is identical, and thus preference for one path over the other is based exclusively on the electronic coupling between the various sites. There are many examples of molecules with long-lived charge-separated states that would be appropriate for such a system. Even if tunneling through the barrier separating monomer units were slow, of the order of hundreds of nanoseconds, this could still be much faster than charge recombination within the $[D-A_1-A_2]$ monomer. Bottlenecks can be avoided by encoding data to the polymer only on alter-

nate clock cycles. This also improves the yield for charge shift between monomers. Thus, if tunneling had a quantum efficiency of 0.95, this would improve after two clock cycles to 0.99 for transfer from a single monomer to the next. However, even a device with 99 % efficiency is not sufficient for a polymer with more than several repeat units. For a polymer of 100 repeat units, the yield of transmission for a single bit through the polymer drops to 36 %. Many systems have been designed which undergo highly efficient, long-lived charge separation appropriate for such a device,^[132,162,163] but as of yet no working system has been constructed.

In the proposed device, the transport of holes is the basis for data transmission; however, polymeric and oligomeric systems capable of soliton propagation have also been synthesized and studied.^[14,16,31,32,34,35,37,39,42] Further examination shows that one could operate this system to transport negative charge along the polymer. In this scheme, the clock cycle begins with the electrochemical encoding of data into the polymer. Reduction (or lack of reduction) of the ground electronic state of the donor adjacent to the electrode places a free electron into its LUMO. This reduced species undergoes spontaneous stepwise thermal electron transfer until the negative charge is localized on the last acceptor group in the first monomer (Figure 3a). Radical anions of many organic chromophores have distinct spectral signatures with large extinction coefficients. Selective photoexcitation of the $[D-A_1-A_2]$ state gives an excited doublet state, with the electronic configuration as shown in Figure 3b. Optical switching is achieved by preferential charge shift from this excited state to the LUMO of the donor in the next monomer unit. Competitive charge shift to the adjacent acceptor will result in switching errors.

While such a device has yet to be constructed, Debreczeny and co-workers have synthesized and studied a linear $D-A_1-A_2$ triad suitable for implementation in such a device.^[164] In this system, compound **6**, a 4-aminonaphthalene monoimide (ANI) electron donor is excited selectively with 400 nm laser pulses. Electron transfer from the excited state of ANI to A_1 , naphthalene-1,8:4,5-diimide (NI), occurs across a 2,5-dimethylphenyl bridge with $\tau = 420$ ps and a quantum yield of 0.95. The dynamics of charge separation and recombination in these systems have been well characterized.^[165] Spontaneous charge shift to A_2 , pyromellitimide (PI), is thermodynamically uphill and does not occur. The mechanism for switching makes use of the large absorption cross-section of the NI^- anion radical at 480 nm, ($\epsilon = 28,300$). A second laser pulse at 480 nm can selectively excite this chromophore and provide the necessary energy to move the electron from NI^- to PI. These systems do not rely on electrochemical oxidation-reduction reactions at an electrode. Thus, switching occurs on a subpicosecond time scale.



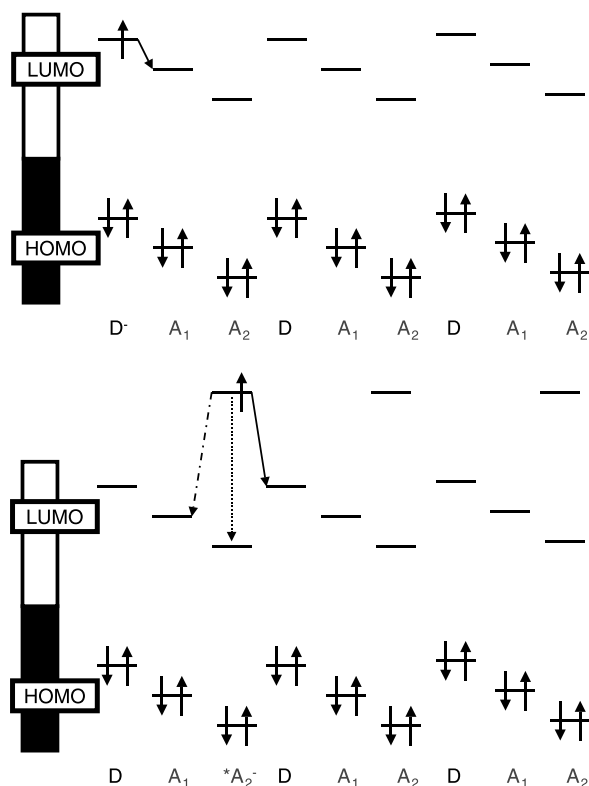
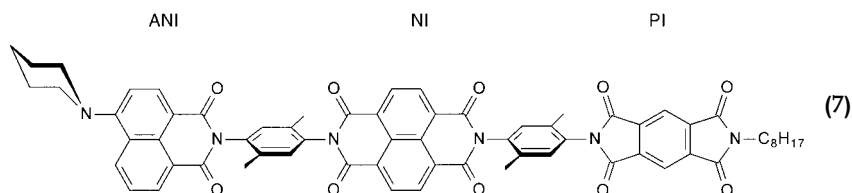


Fig. 3: HOMO / LUMO scheme for a modified molecular shift register in which bits are encoded and propagate as free electrons instead of the system based on hole transfer described in Figure 2. Data is encoded by electrochemical reduction of the donor moiety adjacent to the cathode, resulting in the electronic configuration shown in (a). Subsequent stepwise thermal electron transfer

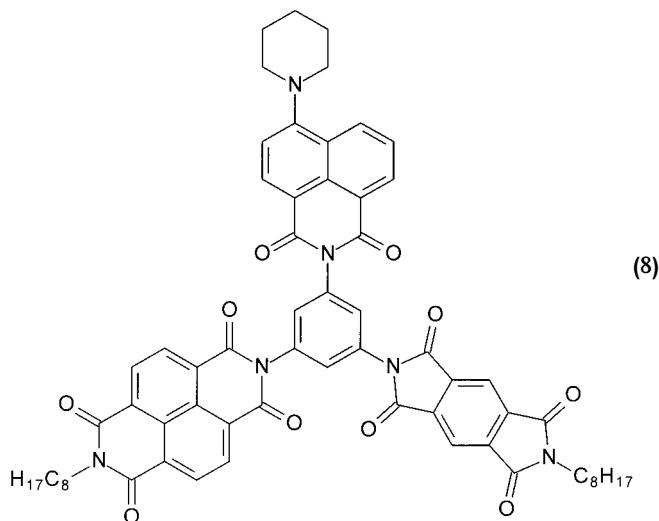
localizes the free electron on A_2 . Photoexcitation of this species results in an excited doublet state, (b), which can decay by forward electron transfer (solid), back electron transfer (dash-dot), or internal relaxation processes (dot). Tuning of the energetics and electronic coupling to favor the forward electron transfer pathway propagates the charge to the next monomer unit.

Excitation of the NI^- anion radical within ANI^+-NI^- -PI with a 480 nm laser pulse rapidly forms the $\text{ANI}^+-^*\text{NI}^-$ -PI excited doublet state. Its electronic configuration is analogous to that in Figure 3b. There are two pathways for decay from this excited state: charge recombination back to yield the 1^*ANI excited state or charge shift to PI. The driving force for each of these paths is nearly identical, and thus the yield for each process is determined by electronic coupling. The electronic coupling between NI and PI is much greater than that between NI and ANI, because no phenyl bridge separates them. As expected, this is the preferential path for deactivation, and can be observed directly by monitoring the formation of PI^- at 720 nm. Charge shift to PI occurs with $\tau = 300$ fs and a quantum yield of 0.88. The overall yield for the switching process is 0.84.

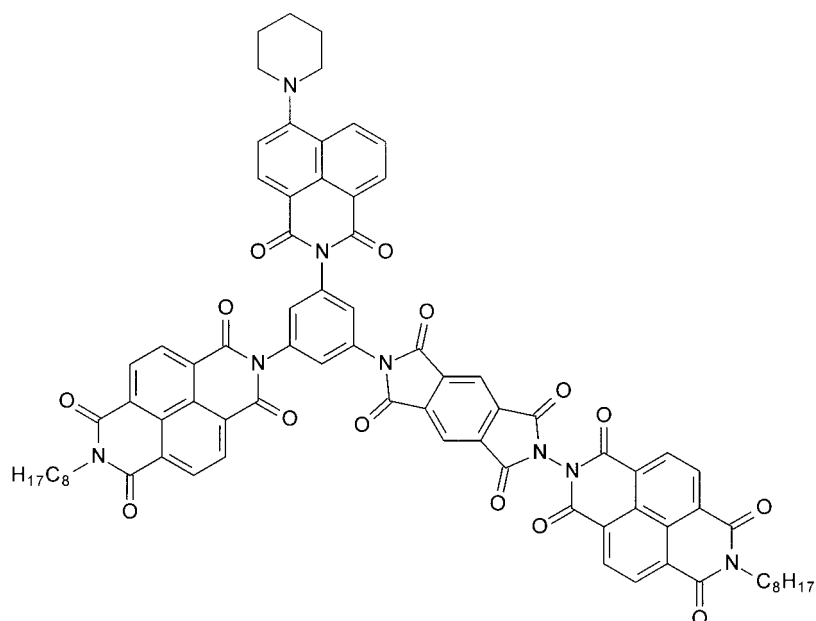
The electronic coupling can be changed by the insertion of a phenyl bridge between the NI and PI, resulting in compound 7. Identical excitation of the NI⁻ with 480 nm laser pulses results in a much slower charge shift to PI, $\tau = 4$ ps, and a quantum yield of only 33 %.^[166] It is clear that, as hypothesized, the ability to control electronic coupling between various sites is the determining factor in realizing the construction of a working device. However, enhancing the electronic coupling to favor the charge shift reaction from NI⁻ to PI also increases the rate for back electron transfer from PI⁻ to NI. The PI⁻ state undergoes back electron transfer to NI with $\tau = 600$ fs in 6 and $\tau = 312$ ps in 7. It is likely that the addition of a third electron acceptor attached to PI could provide a lower energy electronic state into which the system could relax, thereby reducing back electron transfer to NI. This would be more analogous to the polymeric systems described earlier.



Recent work has investigated the potential for controlling the partitioning of charge in branched arrays.^[167] This has many potential applications to the development of photoactive networks and dendritic systems capable of electron transfer. Compounds 8 and 9 employ 1,3,5-triaminobenzene as the central branch point. In each molecule, ANI is attached to the 1-position and serves as the electron donor. The electron acceptors again are NI and PI, and are attached to the 3- and 5-positions, respectively, in compound 8. Excitation of ANI with 400 nm laser pulses results exclusively in electron transfer to the NI branch. This is due to the 0.3 V difference in reduction potentials between NI and PI. Excitation of NI⁻ within NI⁻-ANI⁺-PI with 480 nm laser pulses 2 ns after formation of this initial ion pair results in formation of an excited doublet state. This excited state can decay by charge recombination back to ANI, or by charge shift to PI. The 720 nm absorption band of PI⁻ appears with $\tau = 600$ fs, and a quantum yield of 0.44. Competitive charge recombination to the ^{1*}ANI excited state also occurs quite rapidly ($\tau = 500$ fs), and is the reason for the observed yield. The NI-ANI⁺-PI⁻ state is 0.3 eV above that of the NI⁻-ANI⁺-PI state, and 2.7 eV above the ground state. Charge recombination to the ground state is a Marcus-inverted process, and so charge shift back to the initial charge-separated state ($\tau = 400$ ps) is the exclusive decay path. The lifetime of the electron on the second branch of the system was significantly enhanced by the addition of a lower energy acceptor on the end of PI, in this case a second NI moiety. In compound 9 the rate of switching from branch 2 back to branch 1 is $\tau = 2$ ns; however, the yield for the initial switching between branches decreases to 0.36.



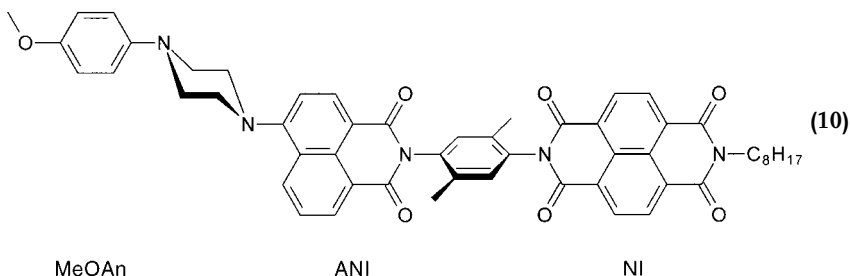
(8)



(9)

The spin properties of charge-separated ion pairs can also be exploited for the purposes of all optical switching. Radical pair intersystem crossing (RP-ISC) of the form $^1[D^+-A^-] \leftrightarrow ^3[D^+-A^-]$ to yield the spin-correlated triplet state is observed in the photosynthetic reaction center, but is seen rarely in synthetic systems. The reason for this observation is that the spin-spin interactions are generally strong even in systems which undergo charge separation over large distances. However, the time for charge recombination in the triplet manifold is usually greatly different to

that in the singlet state. An all-optical switch based on this property can be devised by controlling the rate, and thus the yield, of the intersystem crossing.



Wasielowski et al.^[110] developed the first multi-step donor(1)-donor(2)-acceptor molecule – MeOAn-ANI-NI, compound **10** – that mimics all of the primary spin-dependent charge separation and recombination dynamics of the photosynthetic reaction center. This makes it possible to use the same strategy as an entry point to a molecular switch based on photocontrollable spin dynamics. Transient absorption spectroscopy carried out on **10** in toluene determined the nature of the intermediates and the rate constants for intramolecular electron transfer between the electronic states in the energy level diagram displayed in Figure 4. At 295 K, excitation with 420 nm, 130 fs laser pulses selectively excites the ANI chromophore within MeOAn-ANI-NI. The lowest excited singlet state of ANI accepts an electron from MeOAn with $\tau = 8$ ps. A subsequent dark electron transfer step with $\tau = 430$ ps forms the final radical ion pair, $^1[\text{MeOAn}^{\bullet+}-\text{ANI}-\text{NI}^{\bullet-}]$, with a lifetime of 310 ns. Photoexcitation of **10** oriented in a solid liquid crystal matrix results in the two broad electron paramagnetic resonance (EPR) spectra shown at two orientations in Figure 5, with

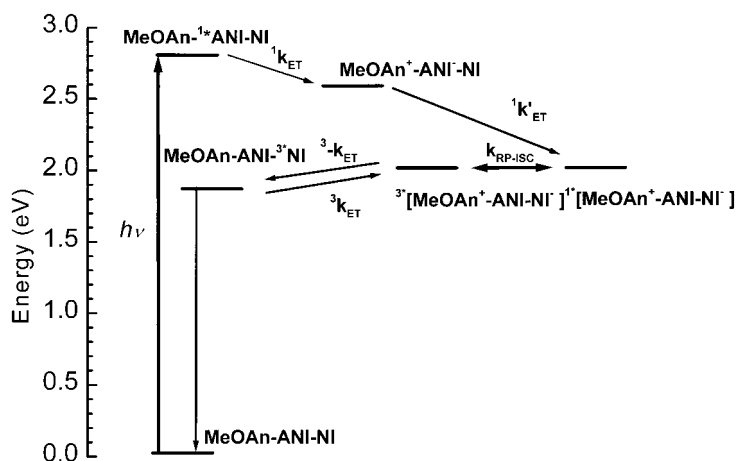


Fig. 4: Energy level scheme for **10**. Internal conversion occurs in the fully charge-separated state to give the triplet. Charge recombination gives the T_1 state localized on the NI chromophore.

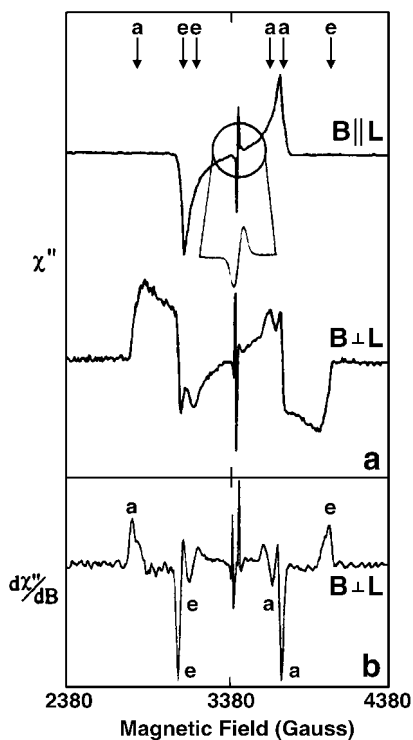
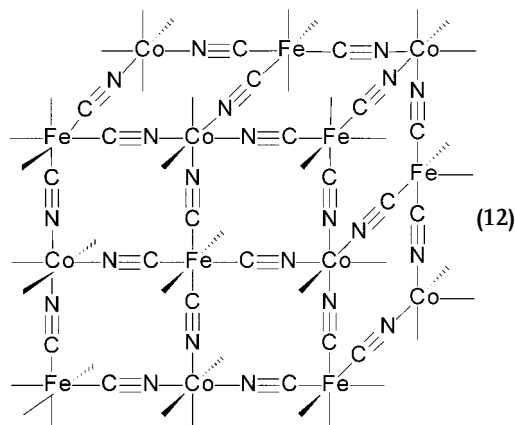
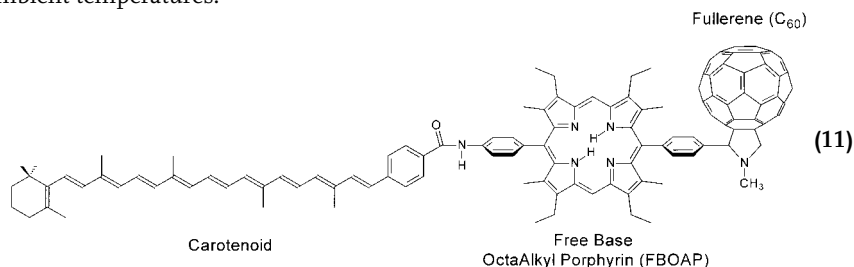


Fig. 5: (a) Direct detection TREPR spectra of MeOAn-ANI-³*NI in the nematic liquid crystal mixture E-7 (Merck) at two orientations of the liquid crystal director, L, taken 700 ns after a 420 nm laser pulse at 150 K. The narrow signal is an expansion of the radical pair signal. (b) Numerical differentiation of the $B \perp L$ spectrum.

additional narrow lines superimposed at the center of the spectra. The broad spectra are due to a triplet state.

In all the covalent electron donor-acceptor systems produced earlier, triplet states observed by EPR were formed via a spin-orbit intersystem crossing (SO-ISC) mechanism. Another possible mechanism of triplet formation is RP-ISC, mentioned above, which results from radical ion pair recombination, and which had been observed previously, by time-resolved electron paramagnetic resonance spectroscopy (TREPR), only in bacterial reaction centers and in the green plant reaction centers Photosystems I and II. These two mechanisms can be differentiated by the polarization pattern of the six EPR transitions at the canonical orientations. In SO-ISC, the three zero-field levels are selectively populated and this selectivity is carried over to the high-field energy levels. RP-ISC is also selective, but acts directly on the high-field triplet sublevels via singlet-triplet mixing $S-T^0$ (or $S-T^{\pm 1}$). Thus, SO-ISC results in mixed absorption (a) and emission (e) lines within a particular EPR transition, i.e., $T^i \leftrightarrow T^0$ ($i = \pm 1$), while in RP-ISC a mixed polarization pattern is impossible. Inspection of the triplet spectra (Figure 5) in the $B \perp L$ and $B \parallel L$ orientations shows that the polarization pattern of a,e,e,a,a,e can only be attributed to a RP-ISC mechanism, as found for reaction center proteins. This unique triplet state is localized on C, and exhibits zero-field splitting parameters identical to those obtained by direct observation of C itself.

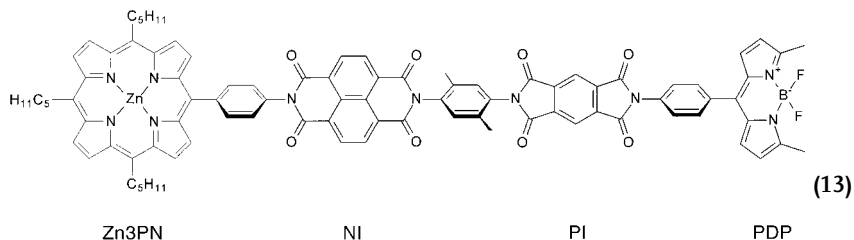
In a subsequent study, Gust and co-workers synthesized and studied compound **11**, consisting of carotenoid (C) and free base octaalkyl porphyrin (FBOAP) electron donors, and a fullerene (C_{60}) electron acceptor.^[168] In the fully charge-separated state, this molecule decays exclusively to the triplet. The lifetime of the excited triplet state can be modulated by applying an external magnetic field at 77 K.^[111] Excitation of the FBP with 416 nm laser pulses resulted in electron transfer to form the $C-P^+-C_{60}^-$ charge-separated state with $\tau = 10$ ps, and unity quantum efficiency. Hole transfer from the FBP to C competes with charge recombination and occurs with $\tau = 270$ ps and a yield of 0.14. In the absence of a magnetic field, this final charge-separated state decays exclusively to the carotenoid triplet state, ${}^3C-P-C_{60}$ with $\tau = 1.3$ μ s. Application of a relatively weak magnetic field, $B = 4.1$ mT, resulted in a 50 % increase in the lifetime of the triplet state to $\tau = 2.0$ μ s. No effect was observed at ambient temperatures.



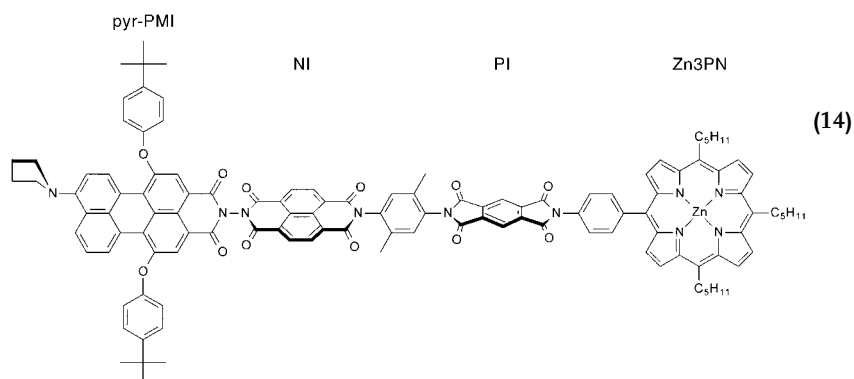
Sato and co-workers reported the first example of the ability to change the magnetic field in a single crystal by optical means. While the magnetic field is a macroscopic property, the principle behind the switching mechanism is photoinduced electron transfer within the crystalline lattice. Sato and co-workers employed a Prussian Blue complex of stoichiometry $K_{0.2}Co_{1.4}[Fe(CN)_6] \cdot 6.9 H_2O$, which formed the rock salt crystalline lattice depicted in **12**. The Curie temperature (T_c), below which long range ordering of the electron spins results in the creation of a magnetic material, was 14 K. Illumination with 660 nm flashes of light raised this temperature to

19 K. The mechanism for this switching of the magnetic properties is photoinduced electron transfer from the diamagnetic low-spin complex $\text{Fe}^{\text{II}}\text{-CN-Co}^{\text{III}}$ to the high-spin electronic configuration $\text{Fe}^{\text{III}}\text{-CN-Co}^{\text{II}}$. At 5 K this results in a doubling of the magnetic field strength. Furthermore, the lattice can be switched back to the low-spin diamagnetic state by the application of a second laser pulse at 450 nm. While the overall time for both switching processes is of the order of several seconds, this result is an important example of the capability to control macroscopic properties by switching on a molecular level. One can also envision the integration of switches based on spin control with this technology, to yield an all optical magnetic device.

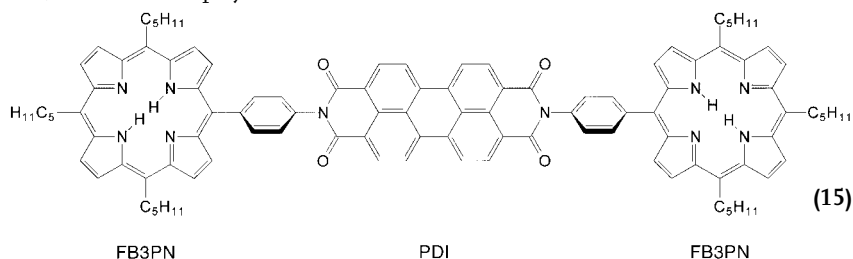
The systems examined thus far have all been based on the propagation of positive or negative charge using consecutive laser pulses. Alternatively, it should be possible to base optical switches on the application of consecutive laser pulses to cause charge recombination. Electric fields can also have a profound effect on the lifetimes of charge-separated states. Debreczeny and co-workers demonstrated the all-optical control of an ion pair lifetime by means of the large, anisotropic, local electric field generated by a second ion pair.^[169] The molecular tetrad **13** consists of zinc-tripentylporphyrin (Zn3PN) and phenyldimethylpyrromethene (PDP) electron donors and NI and PI electron acceptor groups. Selective excitation of PDP with 513 nm laser pulses resulted in electron transfer to form the $\text{Zn3PN-NI-PI}^-\text{-PDP}^+$ charge-separated state with $\tau = 700$ ps and unity quantum yield. The lifetime of this charge-separated state is $\tau = 1.3$ ns. However, if a 416 nm laser pulse excited the tetrad 700 ps after the formation of the ion pair, its decay to ground state was accelerated by an order of magnitude.



Further work used a similar system to inhibit the formation of a second ion pair completely, using the electric field of an initial ion pair. In compound **14**, Zn3PN and 9-(*N*-pyrrolidinyl)perylene-3,4-dicarboximide (pyr-PMI) are the electron donors, while NI and PI are once again electron acceptors.^[170] Photoinduced electron transfer from Zn3PN to PI with 416 nm laser pulses occurs with $\tau = 27$ ps; however, if a 645 nm laser pulse is used to excite pyr-PMI first, this event is completely inhibited.



Photoinduced electronic switching may also be performed by modulating the intensity, as well as the wavelength and timing, of laser pulses. This was demonstrated by O'Neil and co-workers, using a molecule (**15**) consisting of two free base tri-pentylporphyrin (FB3PN) electron donors covalently bound to either end of a perylene-3,4,9,10-tetracarboxylicdiimide (PDI) electron acceptor **15**.^[63] Excitation of the FBP with 585 nm laser pulses resulted in single electron transfer to PDI, forming the state $\text{FB3PN}^+ - \text{PDI}^- - \text{FB3PN}$. When the intensity of the laser pulse was increased, both FBP moieties were excited, resulting in double electron transfer to PDI, forming the state $\text{FB3PN}^+ - \text{PDI}^{2-} - \text{FB3PN}^+$. This effect is detectable because the PDI anion absorbs at 713 nm, while the dianion absorbs at 546 nm. Thus, by modulating the laser intensity, one can reduce the perylene acceptor either singly or doubly. This is possible because only 0.2 V separates the one- and two-electron reductions of PDI. Other molecules, with closely spaced reduction potentials, such as terrylene, quaterrylene, and many metal complexes, should also display this behavior.



1.3.2

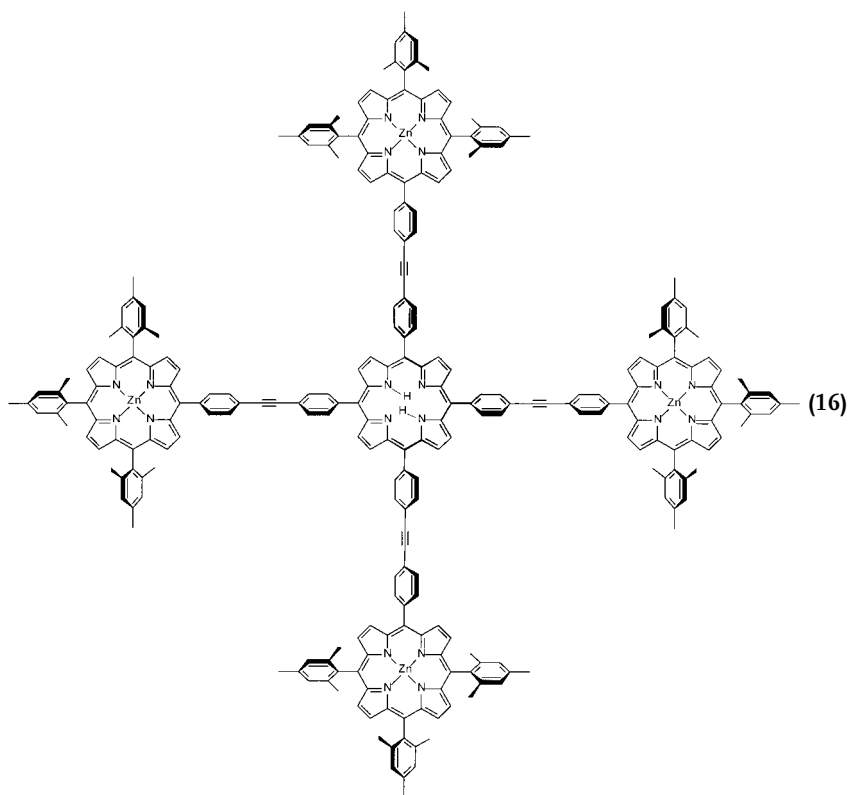
Intramolecular Energy Transfer

While electron transfer reactions that occur through a superexchange mechanism depend exponentially on the distance between electron donor and acceptor, Förster type, through-space (TS) energy transfer has a distance dependence of $1/r^6$. Thus, it is known to occur efficiently over much larger distances. Energy transfer is also known to occur by means of a Dexter, through-bond (TB), mechanism. For most of the rigidly linked systems described here, in which site-to-site distances are less than 20 Å, the Dexter mechanism is predominant. Within an antenna of mixed chromophores, energy transfer proceeds downhill in a site-to-site fashion until energy is localized on the chromophore with the lowest excited state energy. One advantage of using an antenna is that excitation is not site-specific, and absorption of a photon by any chromophore results in energy transfer to the same low-energy site. Fluorescence, non-radiative decay, electron transfer, or a combination of these processes follows energy transfer. Thus, employing light absorbers with large extinction coefficients allows versatility in the choice of electron donors or fluorophores. Designing systems for efficient light absorption across the visible spectrum that can transfer this energy to chromophores capable of converting the energy to chemical

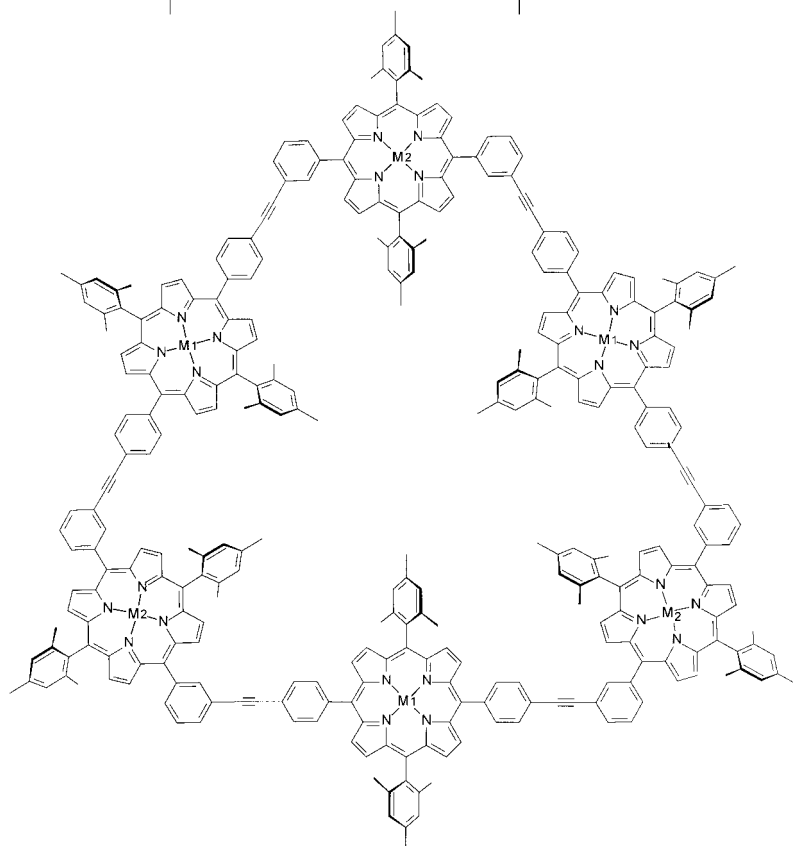
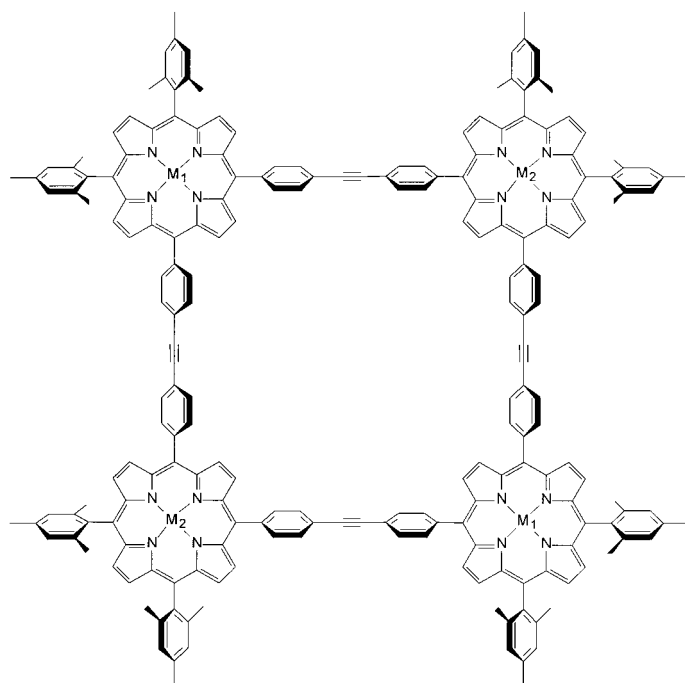
potential is an active area of research.^[132,171,172] It also has applications for the design of efficient optical switching devices.

Many of the molecules discussed in the previous section are not very robust and photodegrade rapidly under intense visible irradiation. However, switching errors are more likely to occur at low photon densities. A simple solution to this problem is to use a light-absorbing antenna that can efficiently transfer energy to the input chromophore. This greatly increases the lifetime of the devices and, in addition, makes it possible to design an antenna that absorbs either at specific wavelengths, or across the entire visible spectrum. By judicious choice of chromophores, energy transfer can alleviate many of the problems inherent in devising efficient, robust all-optical switches employing electron transfer reactions. Many antenna complexes based on mixed metalloporphyrins have been studied.^[137,138,141–143,146–148,150,173] Porphyrins are often used because their electrochemical and spectral properties can be tuned by substitution of appropriate metals.

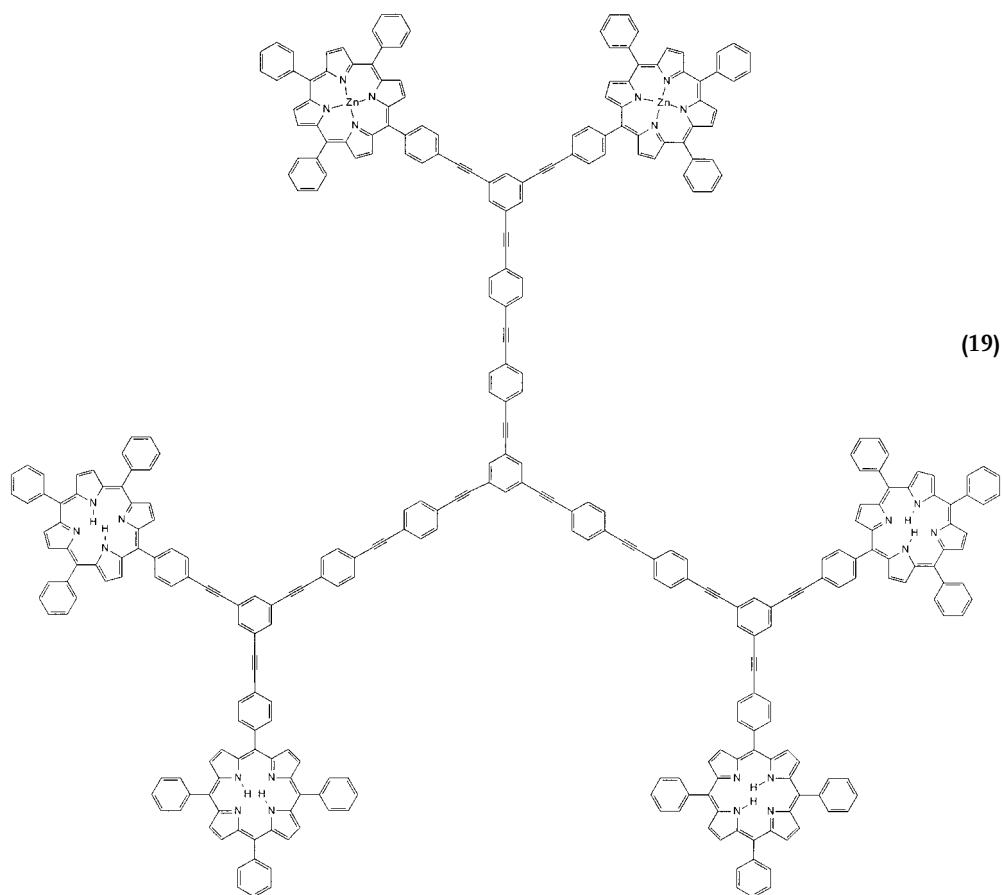
A synthetic system should meet several requirements in order for researchers to learn useful information about the transfer of energy among the chromophores. It should be structurally rigid, soluble in organic solvents, and incorporate controlled metallation sites including free base and metalloporphyrins. Even so, there is no limit to the variety of architectures that can be constructed from arrays of covalently linked chromophores. Porphyrins are natural candidates for the creation of arrays with fourfold symmetry. Lindsey and co-workers synthesized pentamer **16**, consisting of four ZnPs surrounding a central FBP.^[134] This system undergoes energy transfer from the ZnP \rightarrow FBP with a quantum yield of approximately 90 % based on quenching of the ZnP emission. Further work from his laboratory has enabled the placement of eight light-harvesting chromophores about the periphery of a single free base or zinc porphyrin.^[144] The phenyl rings of the porphyrin are substituted at the 3- and 5-positions with ethynyl groups linked to boron-dipyrromethene dye molecules.

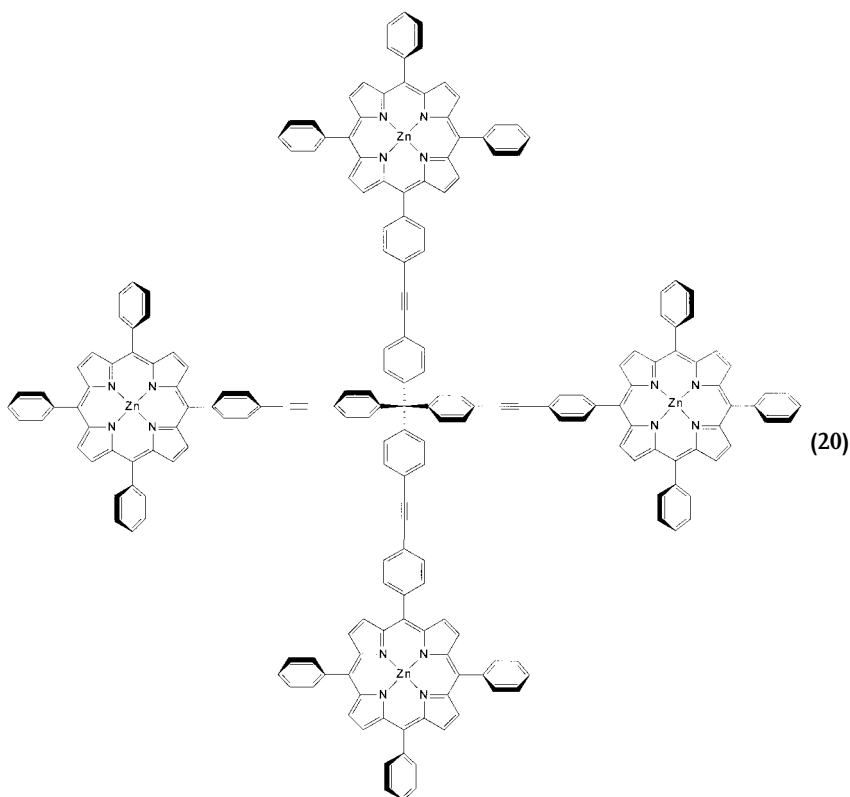


Lindsey and co-workers also constructed macrocyclic square (17) and hexagonal (18) structures in which alternating metalloporphyrins and free base porphyrins formed the subunits.^[143,150] The all-free-base and the zinc- and magnesium-substituted arrays ($M_1 = M_2$) were synthesized as reference systems. In each system, the dominant electronic mechanism was TB energy transfer; however, the rate decreased by 50 % between the square ($\tau_{TB} = 12$ ps) and hexagonal architectures ($\tau_{TB} = 17$ ps). This occurred despite there being one chemical bond fewer and a slight decrease in the center-to-center distance separating the chromophores. This effect was attributed to the change in substitution pattern from a *para* to *meta* linker. Thus, energy transfer in these architectures occurs via mediation of the conjugated linker groups, and not through the σ -bonded framework. Although these competitive rates are quite similar, due to the proximity of the two chromophores, it should be possible to control energy transfer over greater distances on the basis of this effect.

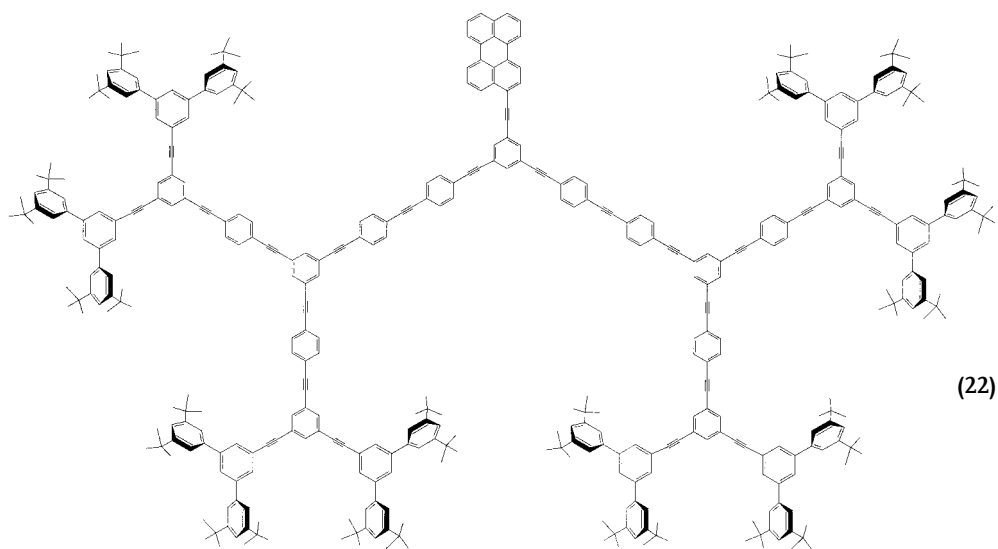
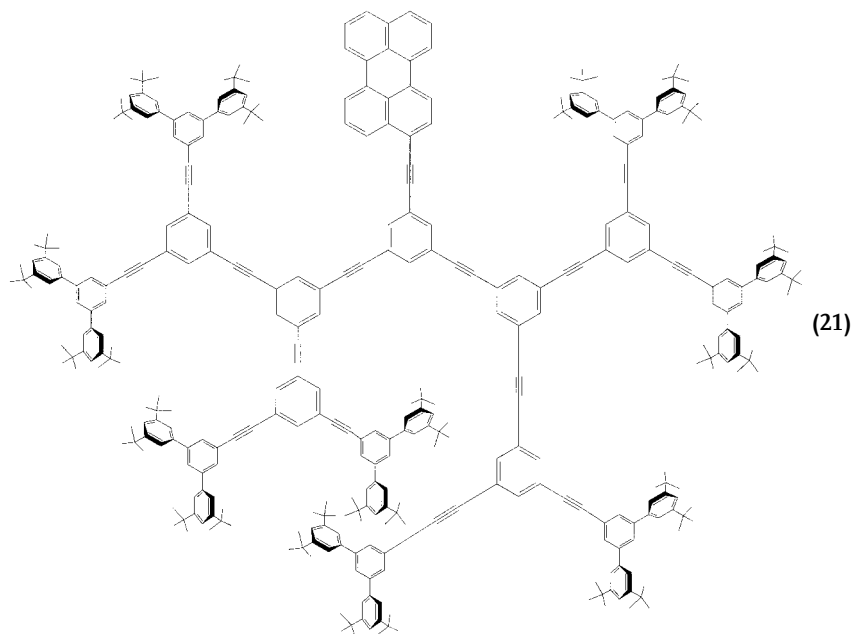


The trigonal and tetrahedral macromolecules **19** and **20**, synthesized by Vauthey and co-workers,^[147] are systems in which these ideas might be applied. Interestingly, these systems show significant contributions both from TB and from TS energy transfer mechanisms. In **19**, the ZnP to FBP distance is 35.5 Å along the shortest line, and 67.5 Å via the bonded pathway. The rate of ZnP → FBP energy transfer is $\tau = 62$ ps, and occurs primarily via a TS mechanism. Only when the bonded pathway became smaller (< 45 Å) did the authors observe a shift to the TB mechanism. However, in compound **20**, in which the interchromophore distance is 27 Å through space and 32 Å through the bonded pathway, the TS mechanism is still dominant. The TB mechanism is disrupted by the sp^3 -hybridized central carbon. This again demonstrates the need to give significant consideration to the electronic structure of the medium through which electronic communication must occur. The conjugation of the linker is especially important when energy and electron transfer events occur across large distances.



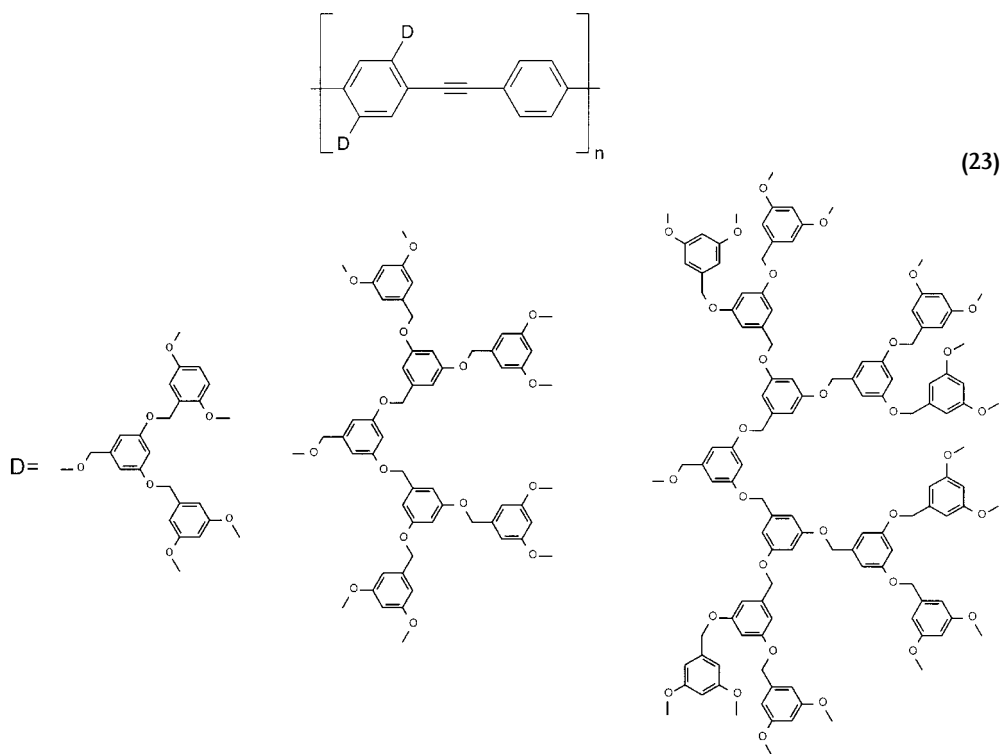


In **19**, the array of chromophores is beginning to take on a dendritic type architecture, with the termini capped with light-harvesting antennae. Recent work has demonstrated not only the construction of dendritic antenna complexes, but also the construction of systems in which the dendrimer itself is the light harvester.^[136,139,149] The great advantage of using dendritic architectures is that the number of light-harvesting chromophores increases as 2^n for each additional generation. Unfortunately, this increase in photon absorption efficiency is countered by a decrease in energy transfer efficiency. The dendritic compounds **21** and **22**, synthesized by Moore and co-workers, again demonstrated the requirements for constructing efficient energy transfer dendrons. Once more, the electronic structure of the intervening medium is crucial in designing an efficient system. While **21** and **22** each contain sixteen light-absorbing groups, the linking groups between absorber and collector are different. Compound **21** is a dendrimer with a simple fan-out macromolecular structure, while **22** contains localized regions of π -conjugation between the absorber and collector. This creates an energy gradient, which results in a directional energy flow and is reflected in the rates of energy transfer. Energy transfer occurs with $\tau = 311$ ps in **21**, while despite the greater inter-chromophore distance the rate of energy transfer in **22** increases by almost two orders of magnitude to $\tau = 5.3$ ps, with a yield of 98 %.

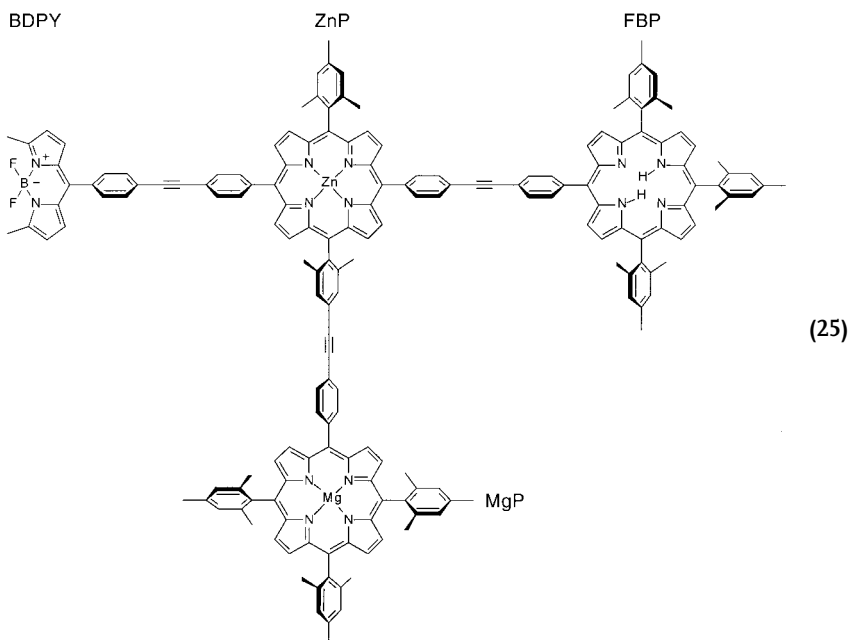
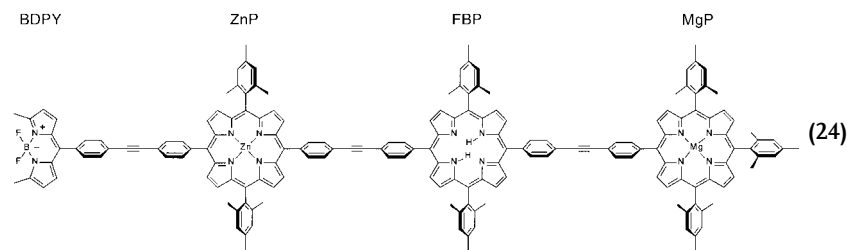


It is also possible to incorporate dendritic design motifs into polymeric systems. Recent work by Sato and co-workers has demonstrated the feasibility of constructing light-harvesting, dendritic side chains on polymer chains of fluorophores.^[149] The repeat units of the dendrimer are 1,3,5-poly(benzyl ether) moieties. Polymers with dendritic side chains ranging between two and four generations were synthesized (23). The attachment of these groups to the poly(phenyleneethynylene) polymer

introduces a large absorption band at 278 nm in the ultraviolet region of the spectrum. Excitation in this region results in energy transfer to the polymer backbone with unity quantum efficiency, and is observed as a fluorescence at 454 nm. In addition to acting as light absorbers, the dendritic side chains act as solubilizing groups and also increase the fluorescent quantum yield in solution by preventing interchain collisional deactivation. Similar types of dendrimers are readily applicable to polymers of the $[-D-A_1-A_n-]_n$ monomer type,^[174] both to improve solubility and to act as light-harvesting antennae.



Thus far we have examined systems designed for the absorption of energy by one chromophore, transfer of this excitation, and final dissipation of this energy by emission in some other chromophore. It is also possible to modulate this emission and create a molecular switch based on competing routes of energy transfer, one of which is non-radiative. An example of such a switch employing energy transfer in porphyrin arrays is an optoelectronic gate synthesized by Lindsey and co-workers.^[148] This consisted of three porphyrins and a light-absorbing dye in a linear (24) or branched (25) arrangement; their operation is identical, however. The branched design 25 consists of a trisubstituted zinc porphyrin (ZnP) with a borondipyrromethene dye (BDPY) and magnesium and free base porphyrins (MgP and FBP, respectively) on its periphery.



The FBP *para* to the BDPY has the lowest-energy excited state, and is highly fluorescent. A HOMO / LUMO scheme for this array is shown in Figure 6. Excitation of the BDPY with 485 nm light initiates a stepwise energy transfer. The energy becomes localized on the FBP and is dissipated radiatively as fluorescence centered at 650 nm. The quantum yield for the total process is approximately 0.8 for both the linear and the branched architectures. Activation of a non-radiative decay pathway within the system can modulate this emission. The MgP has the lowest oxidation potential (${}^+{}^1E_{1/2} = 0.34$ V vs. SCE) and a vacancy in its HOMO can be easily created by electrochemical or chemical oxidation. For this experiment, iron perchlorate ($\text{Fe}^{\text{III}}(\text{ClO}_4)_3$) was used as the chemical oxidant. Once oxidized, energy is transferred to the MgP^+ , which has low-lying absorptions indicative of a variety of low energy singlet-singlet transitions. These are non-radiative, and thus no emission is observed from the monocationic species. Furthermore, the fluorescence signal was fully restored by returning to the neutral species by addition of triethylamine or electro-

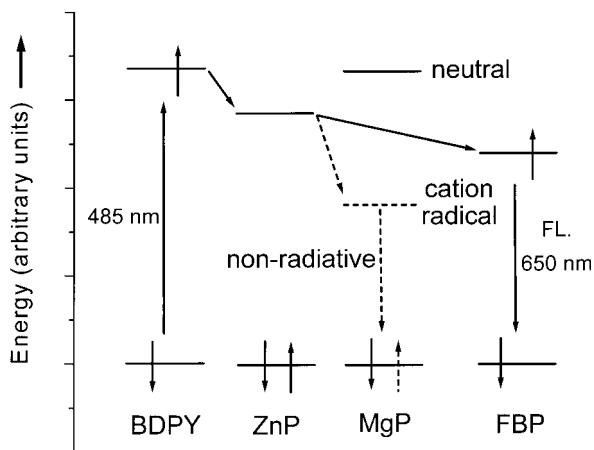
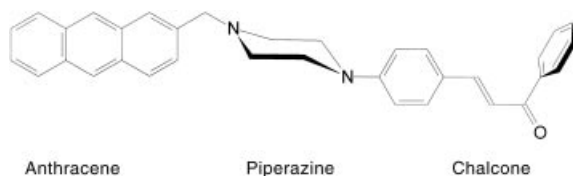


Fig. 6: Energy level scheme for compounds **24** and **25**. Excitation with 485 nm light initiates a series of energy transfers, which localizes the excitation onto the chromophore with the lowest-

energy excited state. In the neutral state (solid), this is the FBP. Electrochemical oxidation of MgP lowers its excited state energy (dash) and activates a non-radiative decay pathway.

chemical reduction. This system demonstrates an ability to modulate energy transfer in large arrays; however, the “ON/OFF” switching of fluorescence is limited by diffusional processes, which are relatively slow compared to the energy transfer events.^[92]

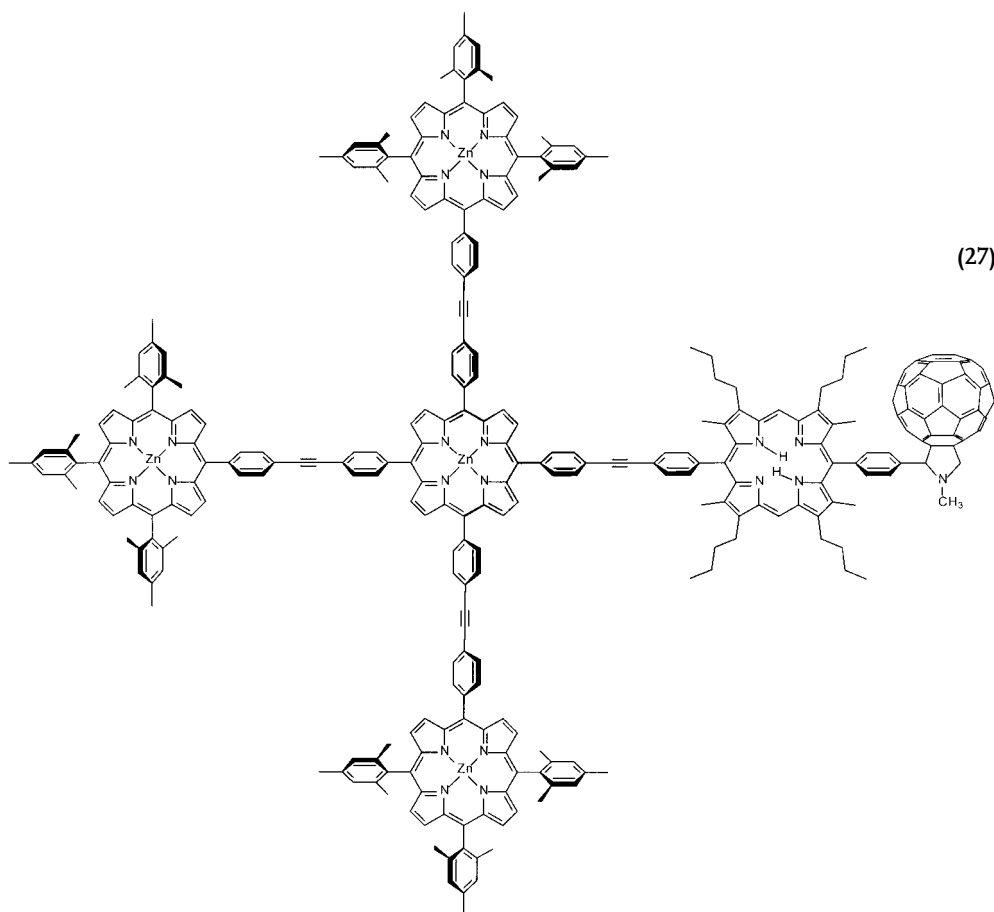
A trichromophoric system (**26**) studied by Wang and Wu switches between energy and electron transfer pathways in a single molecule by proton binding.^[105] In **26**, absorption of near ultraviolet light by the anthracene results in quenching by electron transfer from a nearby piperazine. Bound to the other side of the piperazine is a chalcone moiety, an α,β -unsaturated carbonyl group, which has a lower excited state energy than the anthracene. When H^+ ions are added to solution, electron transfer is quenched by H^+ binding at the piperazine site, and energy transfer can proceed from the anthracene to the chalcone. Again, while this system is highly efficient, it relies upon diffusion and binding of ions in solution and would not be feasible in the solid state.



(26)

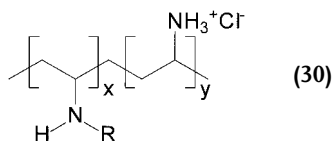
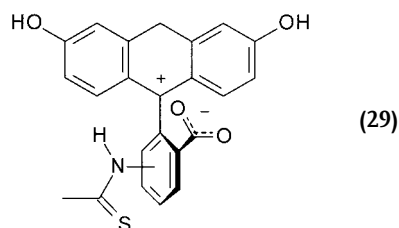
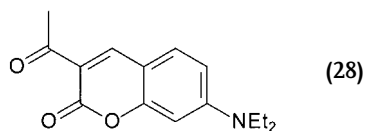
Gust and co-workers designed a synthetic antenna reaction center capable of undergoing energy transfer followed by electron transfer.^[146] Four ZnP chromophores are covalently linked to a FBP electron donor, forming a cross, and the FBP is in turn attached to a C_{60} electron acceptor (compound **27**). Excitation of a ZnP

results in energy transfer, $\tau = 240$ ps, to the FBP, with a quantum yield of 0.69. The excited state of the FBP decays exclusively by electron transfer, $\tau = 3$ ps, giving rise to the charge-separated $\text{ZnP}_4\text{-FBP}^+\text{-C}_{60}^-$ state, which has a lifetime of $\tau = 1$ ns. The authors discussed several parameters that determine the efficiency of energy transfer in light-harvesting antennas. The choice of metal for substitution in the porphyrin is key in determining the rate and yield of energy transfer, because the metal exercises control both over the electrochemical properties and over the excited state lifetime. As stated previously, a through-bond energy transfer mechanism is dominant for most antenna complexes, and the choice of linkage is thus critical in determining electronic coupling between sites. This includes factors such as substitution site and steric hindrance, in addition to site-to-site distance and bond type. Several small, fast, and highly efficient energy transfer steps are likely to be much more efficient than a single, one-step energy transfer.

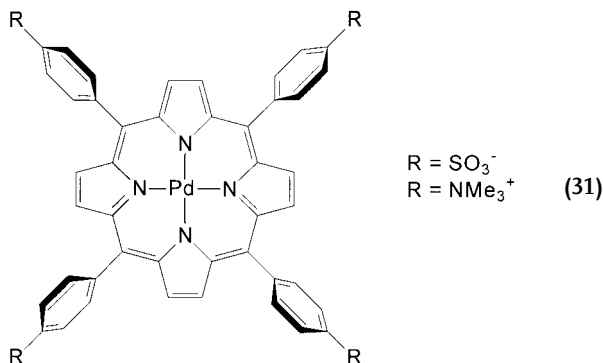


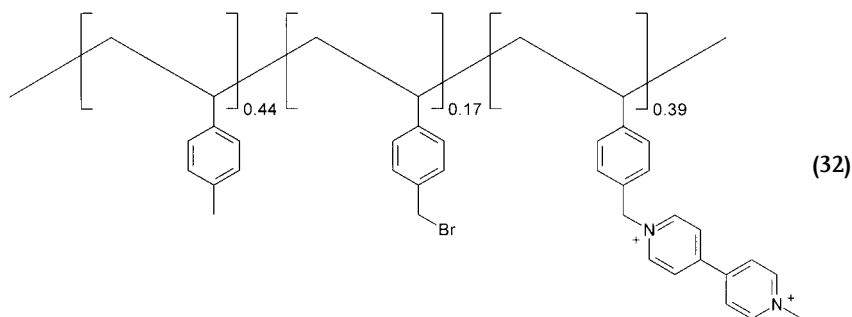
One of the greatest concerns in this field is the leap to be made from studying isolated complexes to the synthesis of large assemblies that will retain the character-

istics of single molecules. The synthesis of large, covalently linked light-harvesting and switching assemblies becomes increasingly complex as more chromophores and redox-active units are added. It is clear that many of the design considerations that apply to the single molecule level are not suitable for the synthesis of macromolecules. Thus, it is desirable to construct architectures by means of self assembly,^[175–182] or other techniques^[183] which have exceedingly high yields and produce arrangements with a minimum of defect sites. Dendrimers,^[184–190] polymers,^[191–194] membranes,^[195–199] and zeolites^[200–208] have been employed as supports for the construction of well defined supramolecular arrays. However, it may be unnecessary to construct entire arrays in which the local environment of each subunit is rigorously controlled.



Recent work has demonstrated the deposition of consecutive thin films (nanometers thick) of light-harvesting and redox-active molecular subunits, creating a layered structure capable of stepwise energy and electron transfer.^[209] The light-harvesting chromophores coumarin (28) and fluorescein (29) are incorporated into ionic polymers of poly(allylamine hydrochloride) (30; R = H). Deposited sequentially, they absorb light across a large portion of the visible spectrum and funnel it to a palladium(II)tetrakis(4-sulfonatophenyl) porphyrin 31. This chromophore has a long-lived excited triplet state, and can transfer an electron to an acceptor in the next layer. In this case the electron acceptor is viologen-substituted polyvinyl toluene 32.





A key aspect of this system is the insertion of semiconductor layers between the layers of chromophores. Local control is exerted over the network of covalent bonds, but there is no rigorous control over the local environment during film formation. The inorganic spacers ensure that each layer maintains a homogeneous distribution of chromophores, and that there is no interlayer migration. No covalent bonds link any of the redox-active chromophores. The semiconductors both increase the yield and rate of electron transfer from the excited state of the donor and inhibit the back electron transfer reaction from the acceptor. These layers consist of anionic $\text{Zr}(\text{HPO}_4)_2 \cdot \text{H}_2\text{O}$ (α -ZrP) or HTiNbO_5 sheets. Figure 7 shows the scheme for this assembly. Energy and electron transfer occurred with quantum yields of 0.47 and 0.61 in the α -ZrP and HTiNbO_5 spaced assemblies, respectively.

The rate of energy and electron transfer in any of these systems is an ensemble average of all sites within the layered assembly, and thus there is no single rate for any of the processes in the assemblies. Nonetheless, in addition to the increased quantum yield, assemblies constructed with the HTiNbO_5 spacer exhibit a long-lived charge-separated state component not observed in the α -ZrP spaced assemblies, of $\tau = 900 \mu\text{s}$. While there is still much to be learned from the study of multi-chromophore arrays, this synthetic approach appears to hold much promise for the creation of organic-inorganic hybrid solid state devices.

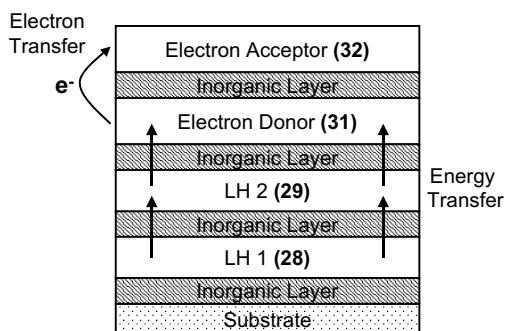


Fig. 7: Schematic representation of the organic-inorganic solid state hybrid synthesized by Mallouk and co-workers.^[209] Absorption of a photon by any of the organic layers results in energy transfer to the electron donor layer. This initiates an intermolecular electron transfer reaction. Interestingly, both the yield of energy and electron transfer can be modulated by changing the electronic characteristics of the inorganic semiconductor material.

1.4

Conclusions and Future Prospects

There are still many hurdles to cross before optical molecular switches are integrated with other components to build all-optical computing devices. The synthesis of large arrays of molecule-sized switches into a network capable of processing information is a major challenge. While covalent attachment schemes can be used to test a variety of switch concepts, ultimately a molecular self-assembly strategy is necessary to carry out organization of these elementary units into large, working arrays. The use of such switches must be implemented in a solid, organized matrix. Surface attachment and/or three-dimensional order induced by incorporation into a crystalline matrix may be necessary to achieve full functionality for such systems. Addressing molecular switches remains a problem as well. The use of diffraction-limited focused light pulses provides a useful start, but sub-diffraction optical techniques need to be improved and implemented for transfer of information into and out of these molecular arrays. Present day near-field optical techniques are relatively slow, so that although they provide better spatial resolution, the speed of information access is somewhat limited. Finally, the fundamental quantum mechanical challenges of using molecules themselves to store and process information needs to be more fully explored. While the fundamental limitations dictated by the Heisenberg uncertainty principle place stringent criteria on such information processing, the intrinsic properties of quantum systems may be exploited for molecule-based computation. The ability of quantum systems to function as coherent superpositions of states may make it possible to design molecules that take advantage of these properties to implement quantum computation schemes. The future of this area is quite promising, especially when one considers the vast possibilities provided by molecular design and synthesis coupled with utilization of the numerous photophysical properties of molecules.

Acknowledgment

The authors wish to thank the National Science Foundation for support of this work (CHE-9732840).

References

- 1 J.S. Millner, *Adv. Mater.* **1990**, *8*, 378–9.
- 2 J.S. Miller, *Adv. Mater.* **1990**, *10*, 495–7.
- 3 J.S. Miller, *Adv. Mater.* **1990**, *12*, 601–3.
- 4 R.C. Haddon, A. A. Lamola, *Proc. Natl. Acad. Sci. USA* **1985**, *82*, 1874–1878.
- 5 D. A. Parthenopoulos, P. M. Rentzepis, *Science* **1989**, *245*, 843–845.
- 6 K. Lieberman, S. Harush, A. Lewis, R. Kopelman, *Science* **1990**, *247*, 59.
- 7 L. Thylen, Karlsson, G. Nilsson, O. *IEEE Commun. Mag.* **1996**, *February*, 106–113.
- 8 M. J. Feldstein, P. Vohringer, W. Wang, N. F. Scherer, *J. Phys. Chem.* **1996**, *100*, 4739–4748.
- 9 D. A. Higgins, D. A. Vanden Bout, J. Kerimo, P. F. Barbara, *J. Phys. Chem.* **1996**, *100*, 13794–13803.
- 10 J. M. Tour, J. S. Schumm, *J. Am. Chem. Soc.* **1991**, *113*, 7064–7066.
- 11 D. H. Waldeck, D. N. Beratan, *Science* **1993**, *261*, 576–577.
- 12 A. O. Patil, A. J. Heeger, F. Wudl, *Chem. Rev.* **1988**, *88*, 183.
- 13 M. R. Wasielewski, D. G. Johnson, W. A. Svec, K. M. Kersey, D. E. Cragg, D. W. Minsek, *Long-distance photoinitiated electron transfer through polyene molecular wires* Ed. J. R. Norris, Elsevier, New York, NY: Chem. Div., Argonne Natl. Lab., Argonne, IL, 60439, USA, 1989, pp 135–47.
- 14 M. Sundram, S. A. Chalmers, P. F. Hopkins, A. C. Gossard, *Science* **1991**, *254*, 1326–1335.
- 15 M. Blanchard-Desce, T. S. Arrhenius, M. Dvořáček, S. I. Kugimiya, T. Lazrak, J. M. Lehn, *AIP Conf. Proc.* **1992**, *262*, 48–57.
- 16 L. M. Tolbert, *Acc. Chem. Res.* **1992**, *25*, 561–8.
- 17 R. W. Wagner, J. S. Lindsey, *J. Am. Chem. Soc.* **1994**, *116*, 9759–9760.
- 18 M. Kemp, V. Mujica, M. A. Ratner, *J. Chem. Phys.* **1994**, *101*, 5172–8.
- 19 J. S. Schumm, D. L. Pearson, J. M. Tour, *Angew. Chem.* **1994**, *106*, 1445–8.
- 20 J. R. Reimers, J. S. Craw, G. B. Bacskay, N. S. Hush, *BioSystems* **1995**, *35*, 107–11.
- 21 L. M. Tolbert, X. Zhao, Y. Ding, L. A. Bottomley, *J. Am. Chem. Soc.* **1995**, *117*, 12891–2.
- 22 T. Shimidzu, H. Segawa, F. Wu, N. Nakayama, *J. Photochem. Photobiol. A* **1995**, *92*, 121–127.
- 23 T. Shimidzu, *Synth. Met.* **1996**, *81*, 235–241.
- 24 M. Kemp, A. Roitberg, V. Mujica, T. Wanta, M. A. Ratner, *J. Phys. Chem.* **1996**, *100*, 8349–55.
- 25 A. Harriman, R. Ziessel, *Chem. Commun.* **1996**, 1707–1716.
- 26 L. A. Bumm, J. J. Arnold, M. T. Cygan, T. D. Dunbar, T. P. Burgin, L. Jones, II D. L. Allara, J. M. Tour, P. S. Weiss, *Science* **1996**, *271*, 1705–07.
- 27 J. R. Reimers, T. X. Lu, M. J. Crossley, N. H. Hush, *Chem. Phys. Lett.* **1996**, *256*, 353–359.
- 28 L. Jones, II J. S. Schumm, J. M. Tour, *J. Org. Chem.* **1997**, *62*, 1388–1410.
- 29 G. M. Tsivgoulis, J. M. Lehn, *Adv. Mater.* **1997**, *9*, 39–42.
- 30 D. L. Pearson, J. M. Tour, *J. Org. Chem.* **1997**, *62*, 1376–1387.
- 31 G. M. de Silva, *Synth. Met.* **1997**, *86*, 2245–2246.
- 32 G. M. de Silva, P. H. Acioli, *Synth. Met.* **1997**, *87*, 249–256.
- 33 S. J. Tans, M. H. Devoret, H. Dai, A. Thess, R. E. Smalley, L. J. Geerligs, C. Dekker, *Nature* **1997**, *386*, 474–477.
- 34 S. Frank, P. Poncharal, Z. L. Wang, W. A. de Heer, *Science* **1998**, *280*, 1744–1746.
- 35 W. B. Davis, W. A. Svec, M. A. Ratner, M. R. Wasielewski, *Nature* **1998**, *396*, 60–63.
- 36 J. Hu, T. W. Odom, C. M. Lieber, *Acc. Chem. Res.* **1999**, *32*, 435–445.
- 37 B. Schlicke, P. Belsler, L. De Cola, E. Sabbioni, V. Balzani, *J. Am. Chem. Soc.* **1999**, *121*, 4207–4214.
- 38 E. C. Constable, C. E. Housecroft, E. R. Schofield, S. Encinas, N. Armaroli, F. Barigelletti, L. Flamigni, E. Figgemeier, J. G. Vos, *Chem. Commun.* **1999**, 869–870.
- 39 S. Creager, C. J. Yu, C. Bamdad, S. O'Connor, T. MacLean, E. Lam, Y. Chong, G. T. Olsen, J. Luo, M. Gozin, J. F. Kayyem, *J. Am. Chem. Soc.* **1999**, *121*, 1059–1064.
- 40 H. L. Anderson, *Chem. Commun.* **1999**, 2323–2330.
- 41 F. A. Cotton, L. M. Daniels, C. A. Murillo, X. Wang, *Chem. Commun.* **1999**, 2461–2462.
- 42 H. Ness, A. J. Fisher, *Phys. Rev. Lett.* **1999**, *83*, 452–455.
- 43 Z. F. Liu, K. Hashimoto, A. Fujishima, *Nature* **1990**, *347*, 658–660.
- 44 S. Hunter, F. Kiamilev, S. Esener, D. A. Parthenopoulos, P. M. Rentzepis, *Appl. Opt.* **1990**, *29*, 2058–66.
- 45 B. L. Feringa, W. F. Jager, B. de Lange, *Tetrahedron* **1993**, *49*, 8267–8310.

- 46 J. J. Hopfield, J. N. Onuchic, D. N. Beratan, *Science* **1988**, *241*, 817–819.
- 47 A. S. Dvornikov, C. M. Taylor, Y. C. Liang, P. M. Rentzepis, *J. Photochem. Photobiol. A* **1998**, *112*, 39–46.
- 48 A. Aviram, *J. Am. Chem. Soc.* **1988**, *110*, 5687–5692.
- 49 J.-M. Lehn, *Angew. Chem. Int. Ed. Engl.* **1988**, *27*, 89–112.
- 50 J.-M. Lehn, *Angew. Chem. Int. Ed. Engl.* **1990**, *29*, 1304–1319.
- 51 T. W. Ebbesen, *New J. Chem.* **1991**, *15*, 191–197.
- 52 C. A. Mirkin, M. A. Ratner, *Molecular Electronics Annual Reviews Inc.*, 1992 Vol. 43.
- 53 P. Ball, L. Garwin, *Nature* **1992**, *355*, 761–766.
- 54 D. Gust, T. A. Moore, A. L. Moore, *IEEE Eng. Med. Biol.* **1994**, *94*, 58–66.
- 55 I. Willner, B. Willner, *J. Mater. Chem.* **1998**, *8*, 2543–2556.
- 56 J. R. Heath, P. J. Kuekes, G. S. Snider, R. S. Williams, *Science* **1998**, *280*, 1716–1721.
- 57 J. M. Tour, M. Kozaki, J. M. Seminario, *J. Am. Chem. Soc.* **1998**, *120*, 8486–8493.
- 58 J. A. Neff, *Opt. Eng.* **1987**, *26*, 2–9.
- 59 M. T. Shirikawa, T. Ohtsubo, *Opt. Commun.* **1996**, *124*, 333–344.
- 60 B. S. Wherrett, *Synth. Met.* **1996**, *76*, 3–9.
- 61 T. Bjornholm, *Isr. J. Chem.* **1996**, *36*, 349–356.
- 62 T. Yatagai, S. Kawai, H. Huang, *IEEE Proc.* **1996**, *84*, 828–852.
- 63 M. P. O'Neil, M. P. Niemczyk, W. A. Svec, D. Gosztola, G. L. Gaines, III, M. R. Wasielewski, *Science* **1992**, *257*, 63–5.
- 64 F. A. Burkhalter, G. W. Suter, U. P. Wild, *Chem. Phys. Lett.* **1983**, *94*, 483–487.
- 65 U. P. Wild, S. E. Bucher, F. A. Burkhalter, *Appl. Opt.* **1985**, *24*, 1526–1530.
- 66 A. Winnacker, R. M. Shelby, R. M. Macfarlane, *Opt. Lett.* **1985**, *10*, 350–352.
- 67 H. W. H. Lee, M. Gehrtz, E. E. Marinero, W. E. Moerner, *Chem. Phys. Lett.* **1985**, *118*, 611–616.
- 68 W. E. Moerner, T. P. Carter, C. Brauchle, *Appl. Phys. Lett.* **1987**, *50*, 430–432.
- 69 T. P. Carter, C. Brauchle, V. Y. Lee, M. Manavi, W. E. Moerner, *Opt. Lett.* **1987**, *12*, 370–2.
- 70 U. P. Wild, S. Bernet, B. Kohler, A. Renn, *Pure & Appl. Chem.* **1992**, *64*, 1335–1342.
- 71 B. Kohler, S. Bernet, A. Renn, U. P. Wild, *Opt. Lett.* **1993**, *18*, 2144–2146.
- 72 E. S. Maniloff, S. B. Altner, S. Bernet, F. R. Graf, A. Renn, U. P. Wild, *Appl. Opt.* **1995**, *34*, 4140–8.
- 73 X. A. Shen, A.-D. Nguyen, J. W. Perry, D. L. Huestis, R. Kachru, *Science* **1997**, *278*, 96–100.
- 74 W. F. Jager, J. C. de Jong, B. de Lange, N. P. M. Huck, A. Meetsma, B. L. Feringa, *Angew. Chem., Int. Ed. Engl.* **1995**, *34*, 348–50.
- 75 N. P. Huck, W. F. Jager, B. de Lange, B. L. Feringa, *Science* **1996**, *273*, 1686–1688.
- 76 S. Zahn, J. W. Canary, *Angew. Chem. Int. Ed. Engl.* **1998**, *37*, 305–307.
- 77 H. Bouas-Laurent, A. Castellan, J.-P. Desvergne, *Pure and Appl. Chem.* **1980**, *52*, 2633–2648.
- 78 T. Nagamura, K. Sakai, T. Ogawa, *J. Chem. Soc., Chem. Commun.* **1988**, 1035–1037.
- 79 G. J. Ashwell, *Nature* **1990**, *347*, 617.
- 80 S. Hunter, F. Kiamilev, S. Esener, D. A. Parthenopoulos, P. M. Rentzepis, *Appl. Opt.* **1990**, *29*, 2058–2066.
- 81 S. Nespurek, M. Schwartz, S. Bohm, J. Kuthan, *J. Photochem. Photobiol. A* **1991**, *60*, 345–353.
- 82 S. Nespurek, W. Schnabel, *J. Photochem. Photobiol. A* **1991**, *62*, 151–159.
- 83 J. Achatz, C. Rischer, J. Salbeck, J. Daub, *J. Chem. Soc., Chem. Commun.* **1991**, 504–507.
- 84 P. Sebek, S. Nespurek, R. Hrabal, M. Adamec, J. Kuthan, *J. Chem. Soc. Perkin Trans. 2* **1992**, 1301–1308.
- 85 M. Jorgensen, K. Lerstrup, P. Frederiksen, T. Bjornholm, P. Sommer-Larsen, K. Schaumburg, K. Brunfeldt, K. Bechgaard, *J. Org. Chem.* **1993**, *58*, 2785–2790.
- 86 J. Walz, K. Ulrich, H. Port, H. C. Wolf, J. Wonner, F. Effenberger, *Chem. Phys. Lett.* **1993**, *213*, 321–324.
- 87 S. Nespurek, J. Sworakowski, *IEEE Eng. Med. Biol.* **1994**, *94*, 45–57.
- 88 S. H. Kawai, S. L. Gilat, J.-M. Lehn, B. Ganem, *Chemtracts: Org. Chem.* **1994**, *7*, 273–5.
- 89 S. H. Kawai, S. L. Gilat, J. M. Lehn, *J. Chem. Soc., Chem. Commun.* **1994**, 1011–13.
- 90 S. H. Kawai, S. L. Gilat, R. Ponsinet, J.-M. Lehn, *Chem.–Eur. J.* **1995**, *1*, 285–93.
- 91 A. DelMedico, S. S. Fielder, A. B. P. Lever, W. J. Pietro, *Inorg. Chem.* **1995**, *34*, 1507–13.
- 92 J. Daub, M. Beck, A. Knorr, H. Spreitzer, *J. Pure Appl. Chem.* **1996**, *68*, 1399–1404.
- 93 J. Otsuki, M. Tsujino, T. Iizaki, K. Araki, M. Seno, K. Takater, T. Watanabe, *J. Am. Chem. Soc.* **1997**, *119*, 7895–7896.
- 94 M. Seibold, M. Handschuh, H. Port, H. C. Wolf, *J. Lumin.* **1997**, *72–74*, 454–456.

- 95 C. Weber, F. Rustemeyer, H. Durr, *Adv. Mater.* **1998**, *10*, 1348–1351.
- 96 A. Archut, F. Vogtle, L. De Cola, G. C. Azzellini, V. Balzani, P. S. Ramanujam, R. H. Berg, *Chem.–Eur. J.* **1998**, *4*, 699–706.
- 97 R. H. Mitchell, T. R. Ward, Y. Wang, P. W. Dibble, *J. Am. Chem. Soc.* **1999**, *121*, 2601–2602.
- 98 L. Gobbi, P. Seiler, F. Diedrich, *Angew. Chem. Int. Ed. Engl.* **1999**, *35*, 674–678.
- 99 S. H. Kawai, S. L. Gilat, J.-M. Lehn, *Eur. J. Org. Chem.* **1999**, 2359–2366.
- 100 S. Benard, P. Yu, *Adv. Mater.* **2000**, *12*, 48–50.
- 101 C. Westermeier, H.-C. Gallmeier, M. Komma, J. Daub, *Chem. Commun.* **1999**, 2427–2428.
- 102 L. Fabbrizzi, A. Poggi, *Chem. Soc. Rev.* **1995**, 197–202.
- 103 A. P. de Silva, H. Q. N. Gunaratne, T. Gunnlaugsson, A. J. M. Huxley, C. P. McCoy, J. T. Radmacher, T. E. Rice, *Chem. Rev.* **1997**, *97*, 1515–1566.
- 104 K. A. Mitchell, R. G. Brown, D. Yuan, S.-C. Chang, R. E. Utecht, D. E. Lewis, *J. Photochem. Photobiol. A* **1998**, *115*, 157–161.
- 105 P. Wang, S. Wu, *J. Photochem. Photobiol. A* **1998**, *118*, 7–9.
- 106 E. Kimura, T. Koike, *Chem. Soc. Rev.* **1998**, *27*, 179–184.
- 107 S. Arounaguirri, B. G. Maiya, *Inorg. Chem.* **1999**, *38*, 842–843.
- 108 H. Kijima, M. Takeuchi, A. Robertson, S. Shinkai, C. Cooper, T. D. James, *Chem. Commun.* **1999**, 2011–2012.
- 109 Z.-Z. Wu, H. Morrison, *J. Am. Chem. Soc.* **1989**, *111*, 9267–9269.
- 110 K. Hasharoni, H. Levanon, S. R. Greenfield, D. J. Gosztola, W. A. Svec, M. R. Wasielewski, *J. Am. Chem. Soc.* **1995**, *117*, 8055–8056.
- 111 D. Kuciauskas, P. A. Liddell, A. L. Moore, T. A. Moore, D. Gust, *J. Am. Chem. Soc.* **1998**, *120*, 10880–10886.
- 112 T. Klumpp, M. Linsenmann, S. L. Larson, B. R. Limoges, D. Burssner, E. B. Krissinel, C. M. Elliott, U. E. Steiner, *J. Am. Chem. Soc.* **1999**, *121*, 1076–1087.
- 113 G. P. Wiederrecht, W. A. Svec, M. R. Wasielewski, *J. Am. Chem. Soc.* **1999**, *121*, 7726–7727.
- 114 K. Kondo, H. Takezoe, A. Fukuda, E. Kuze, *Jpn. J. Appl. Phys., Part 2* **1983**, *22*, 85–7.
- 115 S. S. Bawa, A. M. Biradar, K. Saxena, S. Chandra, *Jpn. J. Appl. Phys., Part 1* **1987**, *26*, 1952–8.
- 116 T. Ikeda, O. Tsutsumi, T. Sasaki, *Synth. Met.* **1996**, *81*, 289–296.
- 117 A. Shishido, O. Tsutsumi, A. Kanazawa, T. Shiono, T. Ikeda, N. Tamai, *J. Am. Chem. Soc.* **1997**, *119*, 7791–7796.
- 118 S. Kurihara, A. Sakamoto, T. Nonaka, *Macromolecules* **1998**, *31*, 4648–4650.
- 119 Y. Wu, J.-I. Mamiya, A. Kanazawa, T. Shiono, T. Ikeda, Q. Zhang, *Macromol.* **1999**, *32*, 8829–8835.
- 120 C. Chiang, *Appl. Phys. Lett.* **1997**, *31*, 553–555.
- 121 S. Kawamura, T. Tsutsui, S. Saito, Y. Murao, K. Kina, *J. Am. Chem. Soc.* **1988**, *110*, 509–511.
- 122 U. P. Wild, A. Rebane, A. Renn, *Adv. Mater.* **1991**, *3*, 453–456.
- 123 M. Iwamoto, Y. Majima, H. Naruse, T. Noguchi, H. Fuwa, *J. Chem. Phys.* **1991**, *95*, 8561–7.
- 124 M. Iwamoto, T. Noguchi, H. Fuwa, Y. Majima, *Jpn. J. Appl. Phys., Part 1* **1991**, *30*, 1020–3.
- 125 M. Iwamoto, K. Ohnishi, X. Xu, *Jpn. J. Appl. Phys., Part 1* **1995**, *34*, 3814–19.
- 126 L. A. Vermeulen, M. E. Thompson, *Nature* **1992**, *358*, 656–658.
- 127 M. L. C. M. Oosterling, A. M. Schoevaars, H. J. Haitjema, B. L. Feringa, *Isr. J. Chem.* **1996**, *36*, 341–348.
- 128 J. C. Owrutsky, H. H. Nelson, A. P. Baranavski, O.-K. Kim, G. M. Tsvigoulis, S. L. Gilat, J.-M. Lehn, *Chem. Phys. Lett.* **1998**, *293*, 555–563.
- 129 I. Willner, A. Doron, E. Katz, *J. Phys. Org. Chem.* **1998**, *11*, 546–560.
- 130 K. Kano, Y. Tanaka, T. Ogawa, M. Shimomura, Y. Okahata, T. Kunitake, *Chem. Lett.* **1980**, 421–424.
- 131 P. S. Cremer, J. T. Groves, L. A. Kung, S. G. Boxer, *Langmuir* **1999**, *15*, 3893–3896.
- 132 D. Gust, T. A. Moore, A. L. Moore, *Acc. Chem. Res.* **1993**, *26*, 198–205.
- 133 B. Alpha, J.-M. Lehn, G. Mathis, *Angew. Chem. Int. Ed. Engl.* **1987**, *26*, 266–267.
- 134 S. Prathapan, T. E. Johnson, J. S. Lindsey, *J. Am. Chem. Soc.* **1993**, *115*, 7519–7520.
- 135 N. Holl, H. Port, H. C. Wolf, H. Strobel, F. Effenberger, *J. Chem. Phys.* **1993**, *176*, 15–220.
- 136 F. Vogtle, M. Frank, M. Vieger, P. Belsler, A. von Zelewski, V. Balzani, F. Barigelli, L. De Cola, L. Flamigni, *Angew. Chem., Int. Ed. Engl.* **1993**, *32*, 1643–1645.
- 137 J. Seth, V. Palaniappan, T. E. Johnson, S. Prathapan, J. S. Lindsey, D. F. Bocian, *J. Am. Chem. Soc.* **1994**, *116*, 10578–92.

- 138 R. W. Wagner, T. E. Johnson, J. S. Lindsey, *J. Am. Chem. Soc.* **1996**, *118*, 11166–11180.
- 139 C. Devadoss, P. Bharathi, J. S. Moore, *J. Am. Chem. Soc.* **1996**, *118*, 9635–9644.
- 140 D. Gust, *Nature* **1997**, *386*, 21–22.
- 141 P. G. Van Patten, A. P. Shreve, J. S. Lindsey, R. J. Donohoe, *J. Phys. Chem. B* **1998**, *102*, 4209–4216.
- 142 S. I. Yang, R. K. Lammi, J. Seth, J. A. Riggs, T. Arai, D. Kim, D. F. Bocian, D. Holten, J. S. Lindsey, *J. Phys. Chem. B* **1998**, *102*, 9426–9436.
- 143 R. W. Wagner, J. Seth, S. I. Yang, D. Kim, D. F. Bocian, D. Holten, J. S. Lindsey, *J. Org. Chem.* **1998**, *63*, 5042–5049.
- 144 F. Li, S. I. Yang, Y. Ciringh, J. Seth, C. H. Martin III, D. L. Singh, D. Kim, R. R. Birge, D. F. Bocian, D. Holten, J. S. Lindsey, *J. Am. Chem. Soc.* **1998**, *120*, 10001–10017.
- 145 D. Gust, T. A. Moore, A. L. Moore, D. Kuciauskas, P. A. Liddell, B. D. Halbert, *J. Photochem. Photobiol. B* **1998**, *43*, 209–216.
- 146 D. Kuciauskas, P. A. Liddell, S. Lin, T. E. Johnson, S. J. Weghorn, J. S. Lindsey, A. L. Moore, T. A. Moore, D. Gust, *J. Am. Chem. Soc.* **1999**, *121*, 8604–8614.
- 147 P. Brodard, S. Matzinger, E. Vauthey, O. C., P. Mongin, A. Gossauer, *J. Phys. Chem. A* **1999**, *103*, 5858–5870.
- 148 R. W. Wagner, J. S. Lindsey, J. Seth, V. Palaniappan, D. F. Bocian, *J. Am. Chem. Soc.* **1996**, *118*, 3996–3997.
- 149 T. J. Sato, D.-L. Jiang, T. Aida, *J. Am. Chem. Soc.* **1999**, *121*, 10658–10659.
- 150 J. Li, A. Ambrose, S. I. Yang, J. R. Diers, J. Seth, C. R. Wack, D. F. Bocian, D. Holten, J. S. Lindsey, *J. Am. Chem. Soc.* **1999**, *121*, 8927–8940.
- 151 A. Aviram, M. A. Ratner, *Chem. Phys. Lett.* **1974**, *29*, 277–283.
- 152 R. M. Metzger, C. A. Panetta, N. E. Heimer, A. M. Bhatti, E. Torres, G. F. Blackburn, S. K. Tripathy, L. A. Samuelson, *J. Mol. Electron.* **1986**, *2*.
- 153 R. M. Metzger, *Adv. Chem. Ser.* **1994**, *240*, 81–129.
- 154 W. A. Phillips, *J. Low Temp. Phys.* **1972**, *7*, 351–360.
- 155 T. Basche, W. E. Moerner, *Nature* **1992**, *355*, 335–337.
- 156 L. Fleury, A. Zumbusch, M. Orrit, R. Brown, J. Bernard, *J. Lumin.* **1993**, *56*, 15–28.
- 157 W. E. Moener, T. Plakhotnik, T. Irngartinger, M. Croci, V. Palm, U. P. Wild, *J. Phys. Chem.* **1994**, *98*, 7382–7389.
- 158 K. Barth, W. Richter, *J. Lumin.* **1995**, *64*, 63–67.
- 159 S. Kummer, T. Basche, C. Brauchle, *Chem. Phys. Lett.* **1994**, *229*, 309–316.
- 160 T. Basche, S. Kummer, C. Brauchle, *Nature* **1995**, *373*, 132–134.
- 161 F. Kulzer, S. Kummer, R. Matzke, C. Brauchle, T. Basche, *Nature* **1997**, *387*, 688–691.
- 162 M. R. Wasielewski, G. L. Gaines, III, D. Gosztola, M. P. Niemczyk, W. A. Svec, *Supramolecular structures modeling photosynthetic reaction center function* Ed. N. Murata, Kluwer, Dordrecht, Neth, 1992 Vol. 2, pp 795–800.
- 163 H. Kurreck, M. Huber, *Angew. Chem., Int. Ed. Engl.* **1995**, *34*, 849–66.
- 164 M. P. Debreczeny, W. A. Svec, E. M. Marsh, M. R. Wasielewski, *J. Am. Chem. Soc.* **1996**, *118*, 8174–8175.
- 165 S. R. Greenfield, W. A. Svec, D. Gosztola, M. R. Wasielewski, *J. Am. Chem. Soc.* **1996**, *118*, 6767–6777.
- 166 M. P. Debreczeny, W. Svec, M. R. Wasielewski, *Unpublished Results*.
- 167 A. S. Lukas, S. E. Miller, M. R. Wasielewski, *J. Phys. Chem. A* **2000**, *104*, 6545–6551.
- 168 D. Carbonera, M. Di Valentin, C. Corvaja, G. Agostini, G. Giacometti, P. A. Liddell, D. Kuciauskas, A. L. Moore, T. A. Moore, D. Gust, *J. Am. Chem. Soc.* **1998**, *120*, 4398–4405.
- 169 M. P. Debreczeny, W. A. Svec, M. R. Wasielewski, *Science* **1996**, *274*, 584–587.
- 170 D. Gosztola, M. P. Niemczyk, M. R. Wasielewski, *J. Am. Chem. Soc.* **1998**, *120*, 5118–5119.
- 171 M. R. Wasielewski, *Chem. Rev.* **1992**, *92*, 435–61.
- 172 G. Steinberg-Yfrach, P. A. Liddell, S.-C. Hung, A. L. Moore, D. Gust, T. A. Moore, *Nature* **1997**, *385*, 239–241.
- 173 L. Feirong, S. I. Yang, Y. Ciringh, J. Seth, C. H. Martin III, D. L. Singh, D. Kim, R. R. Birge, D. F. Bocian, D. Holten, J. S. Lindsey, *J. Am. Chem. Soc.* **1998**, *120*, 10001–10017.
- 174 Q. T. Zhang, J. M. Tour, *J. Am. Chem. Soc.* **1998**, *120*, 5355–5362.
- 175 S. I. Stupp, V. LeBonheur, K. Walker, L. S. Li, K. E. Huggins, M. Kesser, A. Amstutz, *Science* **1997**, *276*, 384–389.
- 176 S. H. Gellman, *Acc. Chem. Res.* **1998**, *31*, 173–180.

- 177 S. Valiyaveetil, K. Mullen, *New J. Chem.* **1998**, *22*, 89–95.
- 178 W. T. S. Huck, A. Rohrer, A. T. Anikumar, R. H. Fokkens, N. M. M. Nibbering, F. C. J. M. van Veggel, D. N. Reinhoudt, *New J. Chem.* **1998**, *22*, 165–168.
- 179 K. Kishikawa, S. Tsubokura, S. Kohmoto, M. Yamamoto, *J. Org. Chem.* **1999**, *64*, 7568–7578.
- 180 F. S. Schoonbeek, J. H. van Esch, B. Wegewijs, D. B. A. Rep, M. P. de Haas, T. M. Klapwijk, R. M. Kellogg, B. L. Feringa, *Angew. Chem. Int. Ed.* **1999**, *38*, 1393–1397.
- 181 B. Gong, Y. Yan, H. Zeng, E. Skrzypczak-Jan-kunn, Y. W. Kim, J. Zhu, H. Ickes, *J. Amer. Chem. Soc.* **1999**, *121*, 5607–5608.
- 182 L. Giribabu, T. A. Rao, B. G. Maiya, *Inorg. Chem.* **1999**, *38*, 4971–4980.
- 183 J. M. Tour, *Chem. Rev.* **1996**, *96*, 537–553.
- 184 S. Serroni, A. Juris, M. Venturi, S. Campagna, I. R. Resino, G. Denti, A. Credi, V. Balzani, *J. Mater. Chem.* **1997**, *7*, 1227.
- 185 J. Issberner, F. Voegtle, L. De Cola, V. Balzani, *Chem. – Eur. J.* **1997**, *3*, 706.
- 186 A. Archut, F. Vogtle, L. De Cola, G. C. Azzellini, V. Balzani, *Chem. – Eur. J.* **1998**, *4*, 699.
- 187 S. Serroni, S. Campagna, G. Denti, A. Juris, M. Venture, V. Balzani, *Adv. Dendritic Macromol.* **1996**, *3*, 61.
- 188 V. Balzani, S. Campagna, G. Denti, A. Juris, S. Serroni, M. Venturi, *Acc. Chem. Res.* **1998**, *31*, 26–34.
- 189 E. C. Constable, C. E. Housecroft, M. Cattalini, D. Phillips, *New J. Chem.* **1999**, *22*, 193–200.
- 190 D. Felder, J.-L. Gallani, D. Guillon, B. Heinrich, J.-F. Nicoud, J.-F. Neirengarten, *Angew. Chem. Int. Ed.* **2000**, *39*, 201–204.
- 191 C. A. Slate, D. R. Striplin, J. A. Moss, P. Chen, B. W. Erickson, T. J. Meyer, *J. Am. Chem. Soc.* **1998**, *120*, 4885.
- 192 R. E. Sassoan, S. Gershuni, J. Rabani, *J. Phys. Chem.* **1992**, *96*, 4692.
- 193 D. M. Watkins, M. A. Fox, *J. Am. Chem. Soc.* **1996**, *118*, 4344.
- 194 R. D. Fossum, M. A. Fox, *J. Am. Chem. Soc.* **1997**, *119*, 1197.
- 195 J. Rebek Jr., *Acc. Chem. Res.* **1999**, *32*, 278–286.
- 196 P.-A. Brugger, M. Gratzel, *J. Am. Chem. Soc.* **1980**, *102*, 2461.
- 197 Y. S. Kang, H. J. D. McManus, K. Liang, L. Kevan, *J. Phys. Chem.* **1994**, *98*, 1044.
- 198 R. Humphry-Baker, D. H. Thompson, Y. Lei, M. J. Hope, J. K. Hurst, *Langmuir* **1991**, *7*, 2592.
- 199 B. C. Patterson, D. H. Thompson, J. K. Hurst, *J. Am. Chem. Soc.* **1988**, *110*, 3656.
- 200 P. K. Dutta, J. A. Incavo, *J. Phys. Chem.* **1987**, *91*, 4443.
- 201 J. A. Incavo, P. K. Dutta, *J. Phys. Chem.* **1990**, *94*, 3075.
- 202 P. K. Dutta, W. Turbeville, *J. Phys. Chem.* **1992**, *96*, 5024.
- 203 S. Sankaraman, K. B. Yoon, T. Yake, J. Kochi, *J. Am. Chem. Soc.* **1991**, *113*, 1419.
- 204 X. Liu, K.-K. Liu, J. Thomas, *J. Phys. Chem.* **1989**, *93*, 4120.
- 205 M. Borja, P. K. Dutta, *Nature* **1993**, *362*, 43.
- 206 K. Maruszewski, D. P. Strommen, J. R. Kincaid, *J. Am. Chem. Soc.* **1993**, *115*, 8345.
- 207 M. Ledney, P. K. Dutta, *J. Am. Chem. Soc.* **1995**, *117*, 7687.
- 208 Y. I. Kim, T. E. Mallouk, *J. Phys. Chem.* **1992**, *96*, 2879.
- 209 D. M. Kaschak, J. T. Lean, C. C. Waraksa, G. B. Saupe, H. Usami, T. E. Mallouk, *J. Am. Chem. Soc.* **1999**, *121*, 3435–3445.

2

Photoswitchable Molecular Systems Based on Diarylethenes

Masahiro Irie

2.1

Introduction

The term “photochromism” can be defined as a light-driven reversible transformation between two isomers possessing different absorption spectra.^[1,2] The two isomers differ from one another not only in their absorption spectra, but also in their geometrical structures, oxidation/reduction potentials, refractive indices, and dielectric constants. When such photochromic chromophores are incorporated into functional molecules, such as polymers, host molecules, conductive molecular wires, or liquid crystals, the functions can be switched by photoirradiation.^[3–6] Photostimulated reversible changes in refractive index can also be applied to optical waveguide switching.^[7] This chapter reviews applications of photochromic chromophores, especially diarylethene derivatives, in various photoswitching molecular systems.

The photochromic chromophores can be classified into two categories, depending on the thermal stability of the photogenerated isomers. When photogenerated isomers are unstable and revert thermally to their initial isomer state in the dark, the chromophores are classified as T-type (thermally reversible type). Most photochromic chromophores belong to this type. The photogenerated blue color of 6-nitro-1',3',3'-trimethylspiro-[2*H*-1-benzopyran-2,2'-indoline], for example, disappears in less than half an hour even in high T_g polymer matrices.^[8] Such thermally unstable photochromic chromophores cannot be applied in photoswitchable molecular systems, because the switched states are unstable. For those applications, the characteristic of persistence, or in other words thermal irreversibility, is indispensable.

Such thermally irreversible photochromic chromophores represent the other class, classified as P-type (photochemically reversible type). Although many photochromic compounds have been so far reported, P-type chromophores are very rare. Only two families, furylfulgide derivatives and diarylethene derivatives, exhibit this reactivity.^[9,10] The photogenerated isomers of these derivatives are thermally stable and never revert to their initial isomers even at elevated temperatures (~100 °C). The thermally stable photochromic compounds offer potential for various applications in photoswitching and memory devices.

The primary difference, for our purposes, between furylfulgide derivatives and diarylethene derivatives is fatigue resistance. Diarylethenes have high durability; col-

oration/decoloration cycles can be repeated more than 10^4 times while maintaining satisfactory photochromic performance, whereas in most cases the corresponding cycles for furylfulgide derivatives are limited to less than 100.^[11] Another advantage of diarylethenes is that the synthetic routes to them are fairly short in comparison with those to furylfulgide derivatives. Section 2.2 describes photochromic performance of diarylethenes which belong to the P-type category.

Properties which change concomitantly with diarylethene derivative photoisomerization are: geometrical structures, electronic structures, refractive indices, and chiral properties (when the molecules have chiral substituents). Table 1 shows how the above property changes are applied to various photoswitching molecular systems. Details of these photoswitching functions are described in Sections 2.3 to 2.6.

Tab 1: Photoswitching of diarylethenes.

Photoreversible Property Changes	Molecular Functions
Geometrical Structures	Host–Guest Interactions
Electronic Structures	Absorption Spectra
	Fluorescence Intensities
	Electrochemical Properties
	(Oxidation/Reduction Potentials)
	Electron Flow in Molecular Wires
	Magnetic Interactions
Refractive Indices	Optical Waveguide Switches
Chiral Properties	Liquid Crystalline Phases

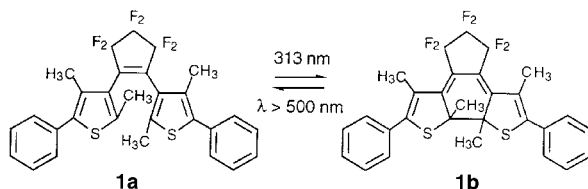
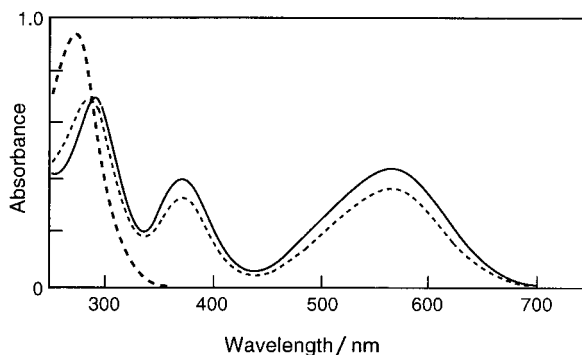
2.2

Basic Diarylethene Photochromic Performance

Figure 1 shows a typical diarylethene derivative absorption spectral change.^[12] Upon irradiation with 313 nm light, a colorless hexane solution of 1,2-bis(2,4-dimethyl-5-phenylthiophen-3-yl)perfluorocyclopentene **1a** turned blue, in which an absorption maximum was observed at 562 nm.

The blue color was disappeared by irradiation with visible ($\lambda > 500$ nm) light. In the dark, however, the blue color remained stable and at room temperature never reverted to the colorless form. In toluene, the colored isomer was found to be stable even at 100 °C. The stable, colored isomer was isolated by HPLC and its molecular structure was analyzed by NMR and X-ray crystallography. Both indicated that the blue colored isomer was the closed-ring form. Therefore, the photochromism of the diarylethene derivative was ascribed to the following photocyclization and cycloreversion reactions.

Fig. 1: Absorption spectra of hexane solutions of (—) **1a** and (—) **1b**, and (- - -) in the photostationary state under irradiation with 313 nm light.



Hereafter, **a** and **b** indicate the closed- and open-ring form isomers, respectively. The photocyclization and cycloreversion quantum yields were determined to be 0.46 and 0.015, respectively.^[12] In the absence of oxygen, the coloration/decoloration cycle could be repeated more than 2000 times.^[13] The basic performance of diarylethenes is described below.

2.2.1

Fatigue Resistance Character

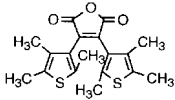
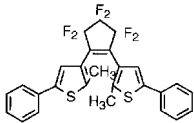
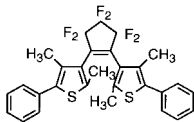
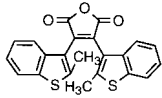
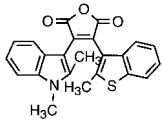
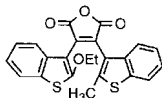
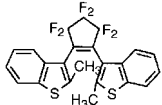
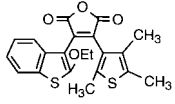
A fatigue resistance character is an indispensable property for applying photochromic compounds in photoswitching devices. Photochromic reactions are always attended by rearrangement of chemical bonds. During this bond rearrangement, undesirable side reactions take place to some extent, limiting the durability of the photochromic compounds. The difficulty inherent in obtaining fatigue resistant photochromic compounds can easily be understood by the following reaction sequence, in which a side reaction to product **B'** is involved in the forward process.



Even if the side reaction quantum yield, Φ_S , is as small as 0.001 and **B** converts perfectly into **A** ($\Phi_{\text{B} \rightarrow \text{A}} = 1$), 63 % of the initial concentration of **A** will decompose after 1000 coloration/decoloration cycles. Thus, if the cycle is to be repeated more than 10,000 times, the quantum yield of by-product formation has to be less than 0.0001.

The fatigue resistance character of several diarylethene derivatives has been measured as follows.^[14] A benzene solution containing a diarylethene ($\sim 10^{-4}$ mol/L) is irradiated with UV light of wavelength λ_1 , capable of exciting the open-ring isomer, until the absorbance of the closed-ring isomer corresponds to 90 % of the photostationary state. The colored, closed-ring isomer is then completely bleached by irradiation with visible

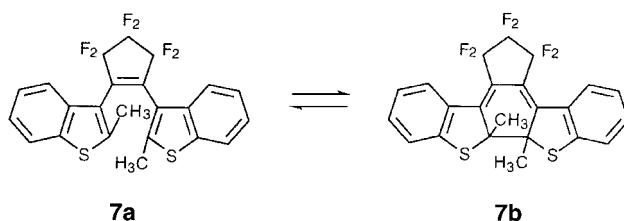
Tab. 2: Fatigue resistance properties of diarylethenes in benzene.

Compounds	Repeatable Cycle Number ^{a)}		
	in air	under vacuum	
	2a	70	480
	3a	80 (in hexane)	200 (in hexane) > 10 ⁴ (in crystal)
	1a	200 (in hexane) (n _{1/2} = 500)	> 2000 (in hexane)
	4a	3.7 × 10 ³	1.0 × 10 ⁴
	5a	–	> 1.1 × 10 ⁴
	6a	> 1.1 × 10 ⁴	–
	7a	> 1.3 × 10 ⁴ (in methylcyclohexane)	–
	8a	3.0 × 10 ⁴ (in polystyrene)	7.0 × 10 ⁴ in polystyrene protected with PVA in the presence of singlet oxygen quenchers

a) The number of photochromic cycles at which the absorption of the open-ring isomer has decreased to 80 % of the value at the first cycle. n_{1/2} is the number of cycles after which half of the open-ring isomers have decomposed.

light of wavelength λ_2 . This operation is repeated many times, and after each 100 cycles the absorbance of the open-ring isomer (or the closed-ring isomer) is measured. The repeatable cycle number can be defined as the number of photochromic cycles after which the absorption of the open-ring isomer (or the colored closed-ring isomer) has decreased to 80 % of the value at the first cycle.

Table 2 summarizes the result of repeatable cycle numbers in benzene.^[13,15–19] In the presence of air, 1,2-di(2,3,5-trimethylthiophen-3-yl)maleic anhydride **2a** and 1,2-di(2-methyl-5-phenylthiophen-3-yl)perfluorocyclopentene **3a** decomposed in fewer than 80 cycles. The low durability is due to endoperoxide formation,^[19] the endoperoxide possibly being produced by reaction with photogenerated singlet oxygen. When the thiophene rings were replaced with benzothiophene rings, the number increased remarkably;^[16] benzothiophene has a much lower reactivity to singlet oxygen. For 1,2-bis(2-methyl-1-benzothiophen-3-yl)perfluorocyclopentene **7a** in hexane, the photocyclization/cycloreversion reactions could be repeated over more than 13,000 cycles, even in the presence of oxygen.^[16]



It is worth noting the difference in the fatigue resistance characteristics of **1** and **3**.^[13] Compound **1a** has methyl groups at the 4- and 4'-positions of the thiophene rings, while compound **3a** has no methyl groups at these positions. Figure 2 shows the cycle number dependence of absorbances of the bleached samples.

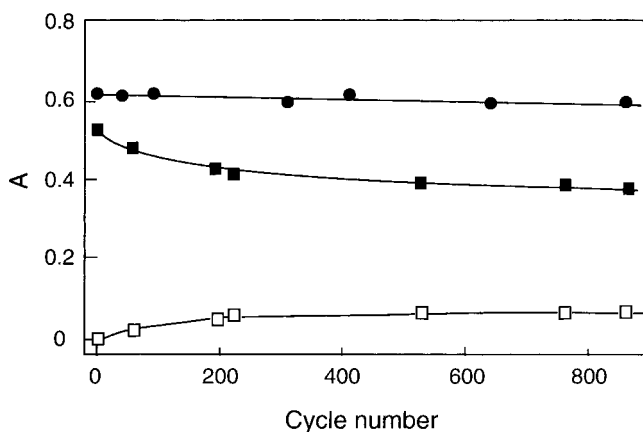


Fig. 2: Fatigue resistance properties of **1** and **3** in deaerated hexane upon alternate irradiation with 313 nm and $\lambda > 440$ nm light. Absorbances of **1a** (●) and **3a** (■) were plotted

after irradiation with visible light. The visible absorbance at 547 nm (□), which still remained after visible irradiation of a hexane solution containing **3**, was also plotted.

The absorbance of **1a** remained almost constant even after 850 cycles, while the absorbance of **3a** gradually declined. At the same time, a photostable, violet product with an absorption maximum at 547 nm was formed. The photostable by-product could be isolated by HPLC, and was found by elemental analysis and molecular mass determination to be isomeric with compound **3a**. Its molecular structure was determined by X-ray crystallographic analysis to be a six-membered condensed ring structure **9**, as shown in Figure 3. The by-product was produced from the closed-ring form more efficiently by UV irradiation.

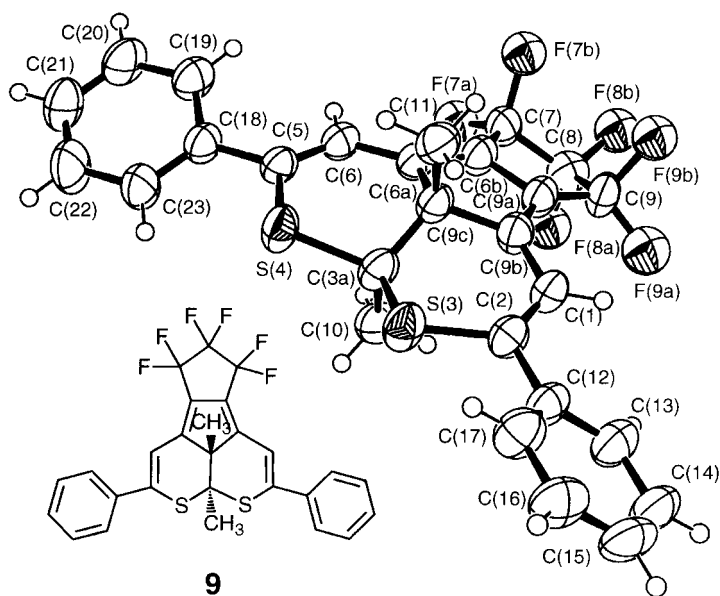
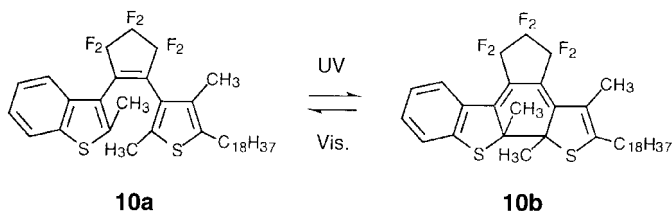


Fig. 3: ORTEP view of by-product **9** showing 50 % probability displacement ellipsoids and its chemical structure.

Such by-product formation is the main fatigue process, in the absence of oxygen, of dithienylethenes with no methyl groups at the 4- and 4'-positions of the thiophene rings. The methyl substituents at the 4- and 4'-positions are considered to block rearrangement of the thiophene rings to the six-membered condensed ring. The blocking of such rearrangements improved the fatigue resistance characteristics of benzothienylethene derivatives **4**, **5**, **6**, **7**, and **8**.

The fatigue resistance character of the following diarylethene was also examined in LB films.^[17]



To measure the character, the excitation energy transfer method was employed, using an LB double layer film consisting of an acceptor monolayer containing photochromic chromophores and a monolayer containing fluorescent oxacarbocyanine. This method is highly sensitive for detecting fluorescence from the donor monolayer and useful to detect photochromic reactions in the acceptor monolayer. The fluorescence intensity is modulated by the photochromic reactions in the acceptor layer. Upon irradiation with UV light, the spirobenzopyran LB film underwent prompt bleaching to half of the initial fluorescence intensity change at 1500 s, while the fluorescence intensity change in the diarylethene-containing LB films remained constant for 10,000 s. The quantum yield of by-product formation was estimated to be less than 0.25×10^{-5} . This value suggests that the cycle can be repeated more than 10^5 times. Diarylethenes possessing benzothiophene aryl groups have durability applicable to practical photoswitching molecular systems.

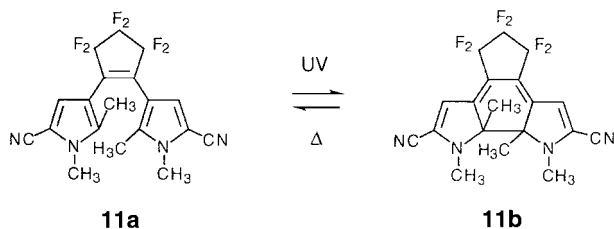
2.2.2

Thermal Irreversibility

Thermal stability of both isomers is an indispensable character for application to photoswitching molecular systems, as described in the introduction. None of the diarylethenes so far reported exhibit thermochromism;^[10] the open-ring isomers are thermally stable. The thermal stability of the closed-ring isomers is dependent on the nature of the aryl groups.^[20] When the aryl groups are furan, thiophene, or thiazole rings, which have low aromatic stabilization energy, the closed-ring isomers are thermally stable and do not revert to the open-ring isomers at room temperature.

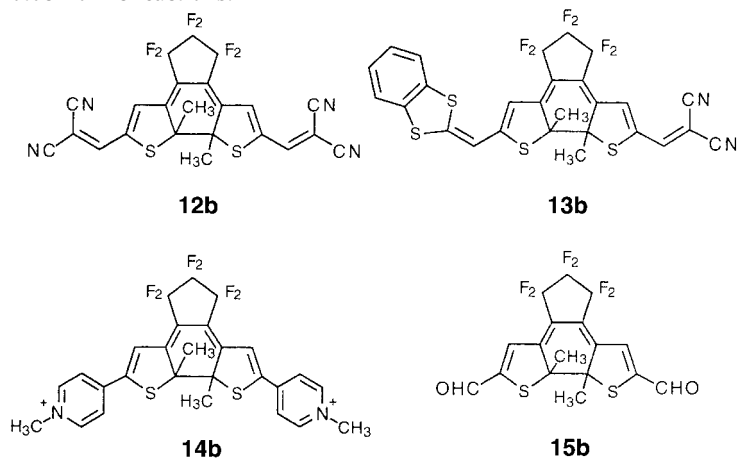
The thermal stability of **3a** above 150 °C was measured in crystalline and melt states.^[21] Its half-life at 150 °C was determined to be 3.3 h. The activation energy was determined as 139 kJ mol⁻¹ from the temperature-dependence of the thermal cycloreversion rates. This value suggests that the half-life of the closed-ring isomer is 1900 years at 30 °C. The closed-ring isomer is stable enough for practical application.

On the other hand, photogenerated closed-ring isomers of diarylethenes with pyrrole, indole, or phenyl rings, which have rather high aromatic stabilization energy, are thermally unstable.^[22] The photogenerated, blue, closed-ring isomer of 1,2-bis(2-cyano-1,5-dimethyl-4-pyrrolyl)perfluorocyclopentene **11a** disappeared in 37 s ($= \tau_{1/2}$) at 25 °C.



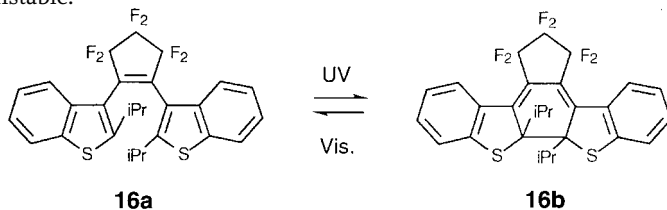
Regarding the closed-ring isomers, the difference in behavior between those diarylethenes with furan, thiophene, or thiazole rings and those with pyrrole, indole, or phenyl rings agrees well with the theoretical prediction that the thermal stability depends on the aromatic stabilization energy of the aryl group.^[20]

Some diarylethene derivatives that possess strongly electron-withdrawing substituents deviate from the general rule.^[5,23] The closed-ring isomers of **12b** and **13b**, possessing dicyanoethylene substituents, reverted to the open-ring isomers in 3.3 min and 186 min, respectively, at 60 °C. The dithienylethenes **14b**, with pyridinium ion substituents, and **15b**, with formyl residues, also underwent thermally reversible photochromic reactions.



The thermal instability of these closed-ring isomers is ascribed to the fact that the photogenerated central carbon–carbon bonds in the closed-ring isomers are weakened by the electron-withdrawing substituents.

When bulky substituents are introduced at the 2-positions of the benzothiophene rings, as in **16a**, the red closed-ring isomers were found to become thermally unstable.^[24]



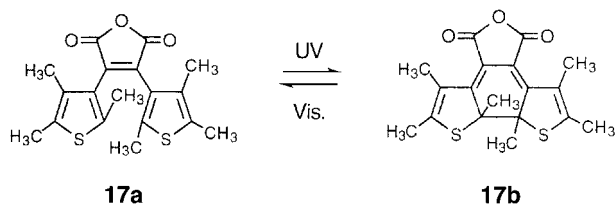
The red color disappeared in 20 h at 70 °C, while no such instability was observed for the closed-ring isomer **7b**, with methyl groups at its 2-positions. It is considered that the bulky substituents at the reactive carbons also weaken the photogenerated central carbon–carbon bond.

2.2.3

Response Time

Although photochemical reactions in general take place very rapidly, for application to switching devices it is essential to know the response times. The photoinduced coloration and decoloration rates of diarylethenes have been measured by using

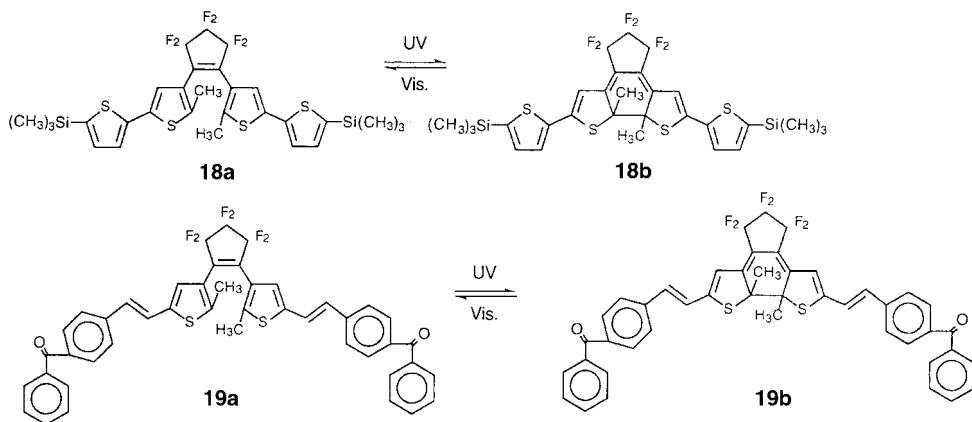
picosecond and femtosecond laser photolysis methods in solution, as well as in crystals. Both the coloration and the decoloration rates (“ON” and “OFF” rates) were determined for the following compound **17** in hexane.^[25]



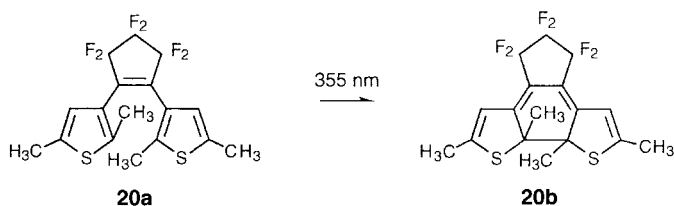
The open-ring isomer was excited with a 355 nm laser pulse (fwhm: 22 ps) and the formation of the closed-ring isomer was followed at 560 nm in hexane. A rapid spectral evolution in a few tens of picoseconds was observed, and attributed to the photocyclization reaction. The rise curve was reproduced by taking into account the pulse duration and the time constant of formation ($\tau = 8$ ps). Taking the rather long pulse duration into account, it was concluded that the switching time is shorter than 10 ps.

The decoloration process was also measured, by exciting the closed-ring isomer **17b** with a 532 nm laser pulse. Immediately after the excitation, the depletion was observed in the absorption around 560 nm, together with an increase in absorption around 600–750 nm. The increase in absorption is ascribed to S1–S_n transition. The bleached signal partly recovered and reached a constant value. A time constant of 2–3 ps reproduced the recovery of the decreased absorption, indicating that switching from the closed-ring to the open-ring isomers took place within 2–3 ps.

The above experiment is only one example in which both “ON” and “OFF” processes were measured in the same molecular system. However, the pulse duration used was longer than the switching rates. To know switching rates precisely, it is necessary to use a shorter pulse. Using a femtosecond laser pulse, the photocoloration rate of **18a**^[26] and the photodecoloration rate of **19b**^[27] were measured.



The coloration rate of **18a** was determined to be 1.1 ps, while the decoloration rate of **19b** was 2.1 ps. Both coloration/decoloration reactions take place in less than a few picoseconds in solution.



The photocoloration rate of **20a** was measured in the crystalline phase, as shown in Figure 4. The time evolution of the absorption at 505 nm indicated that the appearance of the colored isomer **20b** is very rapid even in the crystalline phase. The time profile of the absorbance at 505 nm immediately after the excitation is shown in Figure 4b. The solid lines in the figure are simulation curves, taking into account the duration of the excitation and monitoring laser pulses and the time constants of

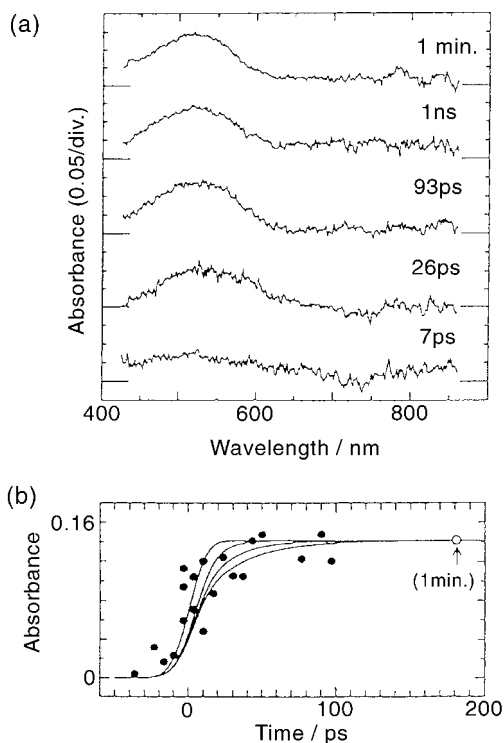


Fig. 4: (a) Time-resolved transient absorption spectra of microcrystalline **20a** excited with a picosecond 355 nm laser pulse. (b) Time profile of transient absorbance at 505 nm for

microcrystalline **20a** excited with a picosecond 355 nm laser pulse. Solid lines are simulation curves calculated on the basis of pulse widths of pump and probe light and time constant.

the absorbance change. Although the S/N ratio of the time profile is rather poor, it is clearly shown that the coloration reaction took place within 10 ps. In addition, no spectral evolution was observed at and after several tens of picosecond following the excitation. The switching time in the crystal was similar to that in solution, indicating that there is no appreciable difference in switching rates between the solution and the solid phases.

The following section describes various photoswitching molecular systems employing diarylethenes as the switching units.

2.3

Host–Guest Interactions

Switching of host–guest interactions by means of photoirradiation may potentially enable us to carry out active transportation of guest molecules. Photochromic compounds such as thioindigo,^[28] azobenzene,^[4,29] and anthracene^[30] have been widely used as switching moieties. Diarylethenes can also be used as switching units after introduction of two crown units, as shown in Figure 5.^[31–33] In the open-ring isomer, two crown ether moieties in a parallel conformation can cooperatively bind with a large metal ion, while in the photogenerated closed-ring isomer, the crown ether moieties are separated from each other and cannot capture the metal ion. Two-phase solvent extractions of alkali metal picrates were carried out: with the open-ring isomers and with their photostationary states under irradiation with 313 nm light. The decrease in the aqueous phase absorption due to the picrates was used to estimate the extraction capability of the compounds.^[31,32]

In the case of dithienylethene **22a**, with benzo-15-crown-5 ether residues, the solution of the open-ring isomer extracted KPic and RbPic into the organic phase to an extent as high as 50 %. Upon irradiation with 313 nm light, the extraction capability was dramatically decreased to 10–20 %, similar to the extraction capability of a single benzo-crown model compound. The open-ring form captures the large

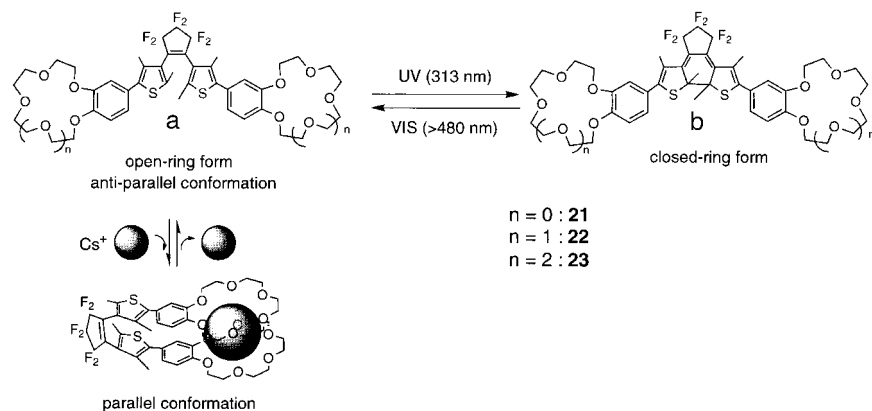


Fig. 5: Concept for photoswitchable ion tweezers possessing a diarylethene switching unit.

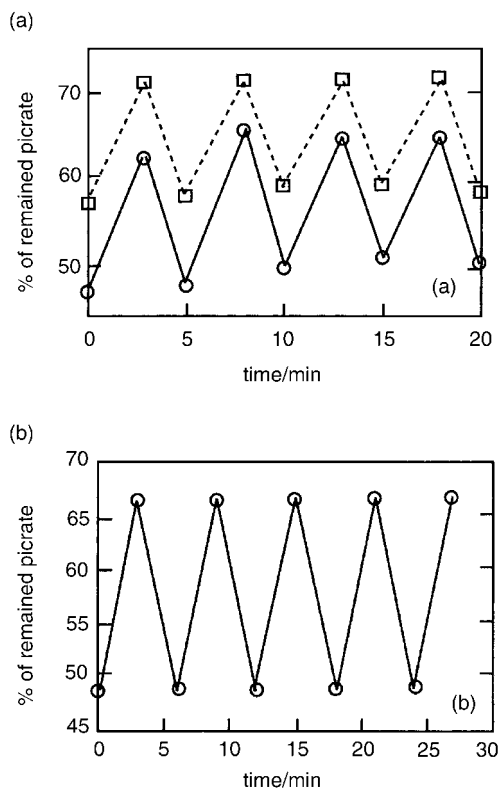


Fig. 6: Control of aqueous phase concentrations of (a) KPic (solid line) and RbPic (dotted line), using **22** in CH₂Cl₂, and (b) CsPic with **23**. Alternating irradiation with 330 ± 70 nm and > 480 nm light.

metal ions in a tweezer-like manner. When the dithienylethene **23a**, with benzo-18-crown-6 ether residues, was used, photostimulated extraction capability enhancement was observed only for CsPic. In the case of **21a**, the extraction capability was very small and the photoeffect was unremarkable. Figure 6 shows the switching behavior of metal ion capture upon alternate irradiation with UV (330 ± 70 nm) and visible (> 480 nm) light. Good reversibility without photodestruction was observed in all cases.

Not only metal ions but also glucoses can be reversibly captured by a diarylethene possessing boronic acid groups upon photoirradiation, as shown in Figure 7.^[34] Boronic acids are widely used for recognition of saccharides, as saccharides have many hydroxyl groups that can form esters with them. The open-ring isomer **24a** is expected to form a 1:1 complex with a saccharide through ester formation between two facing boronic acids and four hydroxy groups. In the closed-ring isomer the boronic acid groups are separated from each other and cannot form the complex.

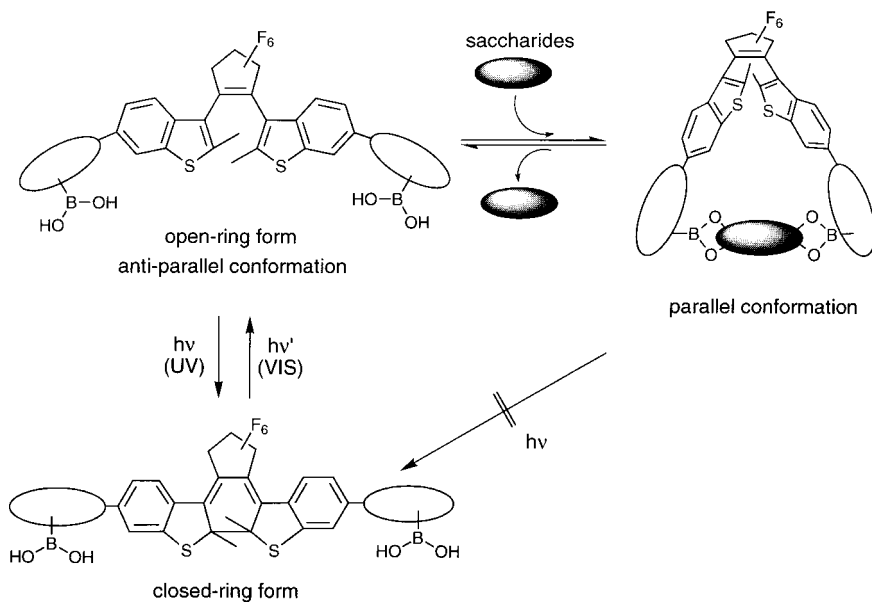
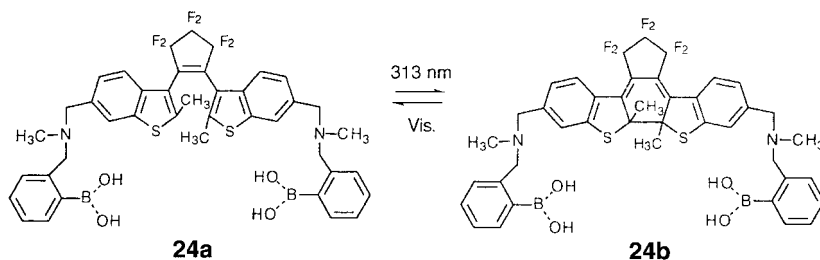


Fig. 7: Concept for photoswitchable saccharide tweezers possessing a diarylethene unit.



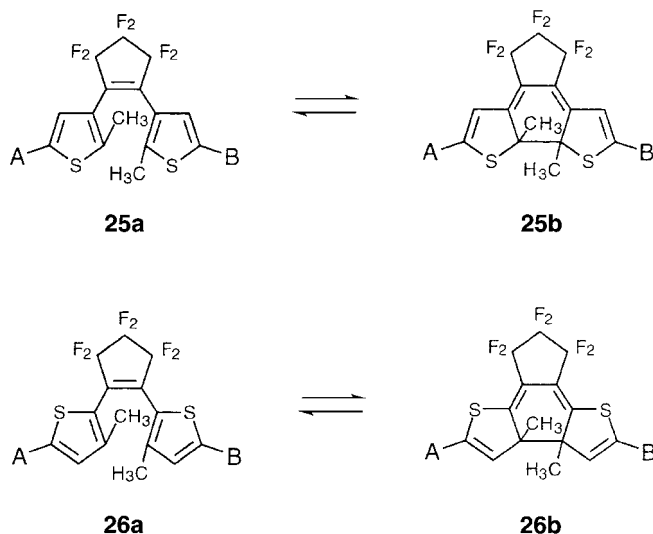
When D-glucose was added to EtOH-tris-HCl buffer solution (pH 7.8) containing **24a**, a circular dichroism (CD) spectrum appeared and its intensity increased with increasing D-glucose content. This indicates that D-glucose reacts with **24a** to produce a complex. Upon irradiation with 313 nm light, the $\Delta\epsilon$ value decreased to 40 % of the previous one, the degree of conversion in the photostationary state under irradiation with 313 nm light being 60 %. This indicates that the closed-ring isomer scarcely reacts with D-glucose. Upon irradiation with visible light, the $\Delta\epsilon$ value returned once more to that prior to UV irradiation. Complex formation could be switched upon alternate irradiation with UV and visible light.

2.4

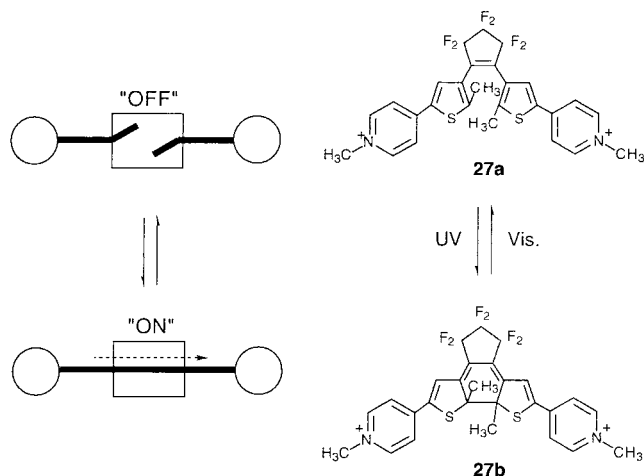
Photoelectrochemical Switching

Photoirradiation-controllable reversible switching of electrochemical properties is of fundamental importance for the development of molecular electronic devices. It is possible to introduce such functionality into a molecule through incorporation of a diarylethene unit.

π -Electron delocalization in diarylethene derivatives with thiophene aryl groups depends on the position at which the thiophene rings are linked to the ethylene moiety.^[35] When the thiophene rings are attached to the ethylene moiety through their 3-positions, as in **25a**, π -electrons are delocalized throughout the molecule when it is in the closed-ring isomer state **25b**, whereas in the open-ring isomer **25a** they are localized in the thiophene rings. Therefore, in the closed-ring isomer, the A and B substituents can interact with each other through the conjugated double bonds. In the open-ring isomer, however, there is no interaction in between A and B. The former may be referred to as the “ON” state and the latter as the “OFF” state. On the other hand, when the thiophene rings are attached through their 2-positions, as in **26a**, π -electrons are delocalized in the open-ring isomer **26a**, and A and B can interact with each other. In the closed-ring isomer **26b**, π -electrons are localized in the central cyclohexadiene structure, and A and B may only interact very weakly.



Incorporation of such dithienylethene units capable of reversibly interrupting conjugation into a polyene molecular wire permits reversible switching of conductive properties by photoirradiation.^[5,23] A typical example is shown below.



In the open-ring isomer, two pyridinium ion groups are electronically separated from each other and there is no appreciable interaction between them. This is the "OFF" state. In the photogenerated closed-ring isomer, on the other hand, π -conjugation results in delocalization between the two pyridinium ion groups, and the absorption spectrum shifts to a longer wavelength: from 352 to 662 nm. This is the "ON" state. Cyclic voltammetry indicated that, whereas no electrochemical process occurred for the open-ring isomer in the region from +0.6 to -0.6 V, a clear, reversible, and monoelectronic reduction wave was observed for the closed-ring isomer: at a potential $E_{1/2} = -230$ mV versus a standard calomel electrode, as shown in Figure 8. The compound repre-

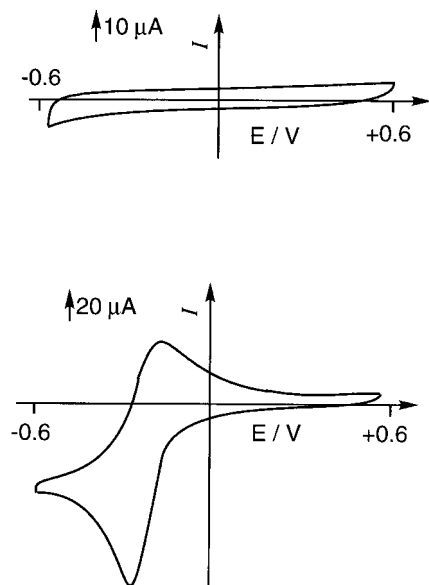
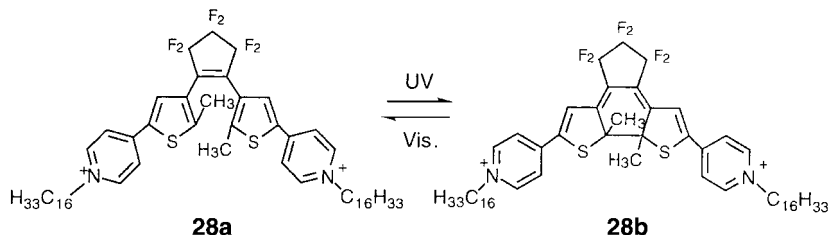


Fig. 8: Cyclic voltammograms for the open-ring (top) and the closed-ring (bottom) forms of **27** in acetonitrile (supporting electrolyte NBu_4BF_4).

sents a prototype switching molecular wire, in which electron flow can be reversibly switched by photoirradiation. A similar switching response was also observed for diarylethene **18**, with oligothiophene aryl groups.^[36]

When such photoswitching chromophores are immobilized on an electrode, vectorial electron flow from the electrode to electroactive species in solution can be controlled by photoirradiation.^[37,38] Using an *n*-octadecanethiol-modified gold electrode incorporated with diarylethene **28a**, it was possible to switch vectorial electron transport from the electrode to hexacyanoferrate(III) in solution by photoirradiation.



Hole injection efficiency from a metal electrode to an organic film can be controlled by inserting a thin film of diarylethene derivatives between the metal electrode and an Au or organic hole transport layer, as shown in Figure 9.^[39] As described above, the π -conjugation distance of diarylethene derivatives changes upon photoisomerization. This means that ionization potentials also depend on the isomers. A film of diarylethene **18** was prepared and the ionization potentials of the open-ring and closed-ring forms were measured. From the oxidation potential changes of the compound in an acetonitrile solution (1.57 V for the open-ring isomer and 0.63 V for the closed-ring isomer), the ionization potential of the closed-ring isomer was determined to be 5.82 eV, and that of the open-ring isomer was estimated to be 6.8 eV. The two isomers thus display a very large difference in ionization potentials.

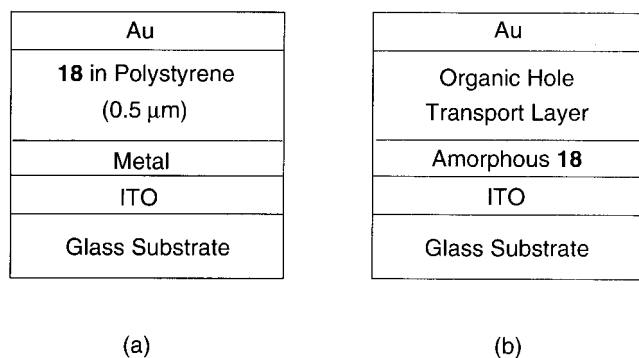


Fig. 9: Structure of sandwich cells for measurement of photo-switching of hole injection. (a) metal-diarylethene-Au, (b) ITO-diarylethene-organic hole transport layer.

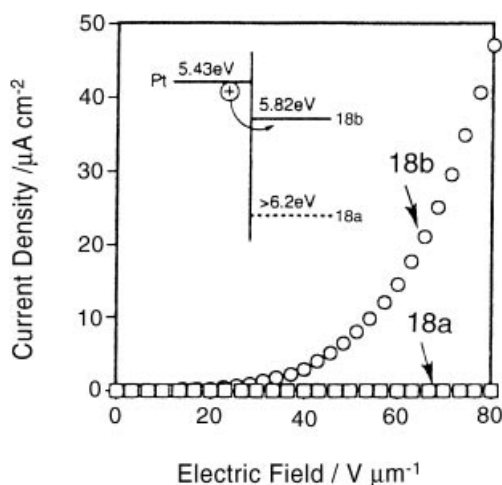


Fig. 10: Electric field dependence of current density for **18a** and **18b** dispersed in polystyrene film (40 wt%). Positive electrode: Pt.

Photoswitching of hole injection from a metal electrode to an organic layer was carried out using a sandwich type cell, in which polystyrene thin film (0.5 μm) containing **18** (40 wt%) was inserted between metal and Au electrodes. When Pt, which has a working function of 5.43 eV, was used as the positive electrode, efficient hole injection was observed when the closed-ring isomer **18b** was used, as shown in Figure 10. The injection was not observed for the polystyrene film containing **18a**. The closed-ring isomer has a low ionization potential and holes can be transferred from the Pt electrode, but the open-ring isomer can not accept the holes because of the large energy differences (as shown in the inset of Figure 10).

Fig. 11 shows the photoswitching of the injection current. Upon UV irradiation, the hole injection current increased, while decreasing to zero on irradiation with visible light. Very thin amorphous diarylethene film as thin as 0.2 μm could also control the hole injection to the organic hole transport layer (Fig. 9b). These results are potentially applicable to optical memory-type organic photoconductors.

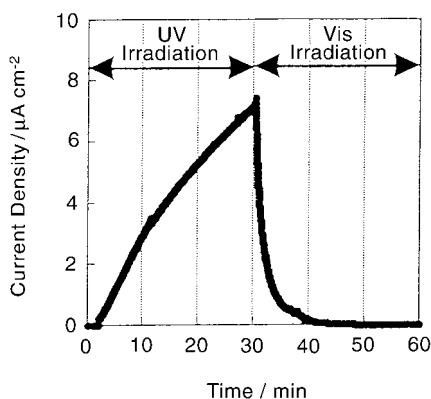
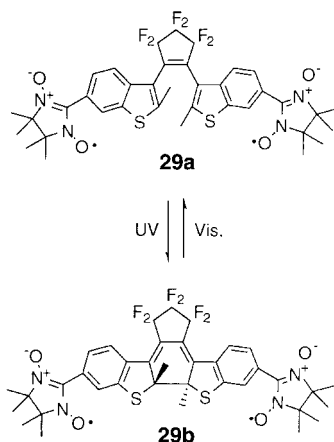


Fig. 11: Photoswitching of the injection current for diarylethene **18** dispersed in polystyrene film (40 wt%) under a constant electric field of 60 V/ μm .

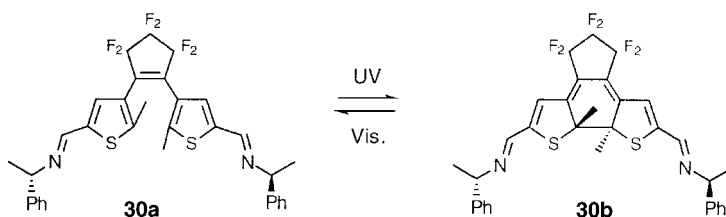
This concept of controlling conjugate interaction in a terminally functionalized polyene can also be applied to magnetic interaction.^[40] A diarylethene **29a**, incorporating two nitronyl nitroxide radicals, was prepared and intramolecular magnetic interaction was compared in the open-ring and closed-ring isomers. Appreciable interaction difference was observed between the open-ring ($2J/k_B = -2.2$ K) and the closed-ring ($2J/k_B = -11.6$ K) isomers.



2.5

Liquid Crystalline Switches

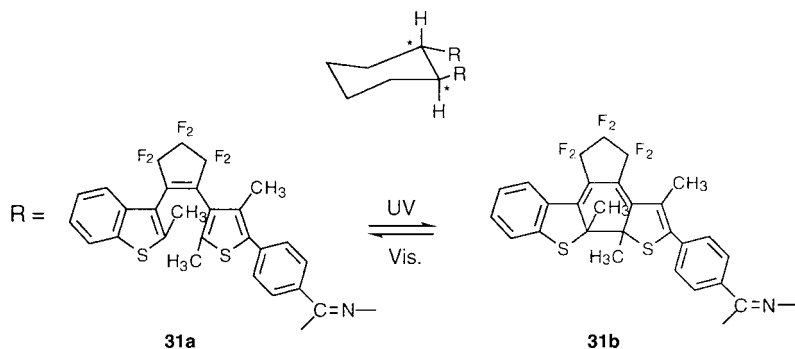
Photoirradiation-based control of optical properties of liquid crystals is a major challenge in the development of molecular devices. So far, various attempts have been made to control liquid crystal alignment, as well as phase, by using photochromic chromophores, almost exclusively involving azobenzene derivatives.^[41,42] It is well known that nematic liquid crystals can be converted into chiral nematic (induced cholesteric) liquid crystals using chiral dopants.^[43] The phase change is highly significant for display technology, because these two phases display a distinct optical property change. In a few cases, reversible switching between these phases has been reported.^[44–46] The phase changes can be induced by using diarylethene **30**, with chiral substituents.^[47]



Doping of nematic liquid crystal materials ZLI-389 and K₁₅ with **30a** resulted in stable cholesteric phases. The cholesteric phase was induced by the addition of 0.7 wt% **30a** to ZLI-389 at 51–54 °C, and the phase was stable for many hours. When

the mixture was irradiated for 50 s with UV light of 300 nm, the chiral nematic phase disappeared and a nematic phase texture was observed. Irradiation of the sample with visible light for 30 s resulted in the reappearance of the cholesteric fingerprint texture. The switching could be repeated six times without deterioration of the liquid crystal phase. The result indicates that the twisting power of the closed-ring isomer is smaller than that of the open-ring isomer.

When the twisting power of the closed-ring isomer is larger than that of the open-ring isomer, it is expected that UV irradiation should induce the phase change from the nematic to chiral nematic phases.^[48] A diarylethene **31a**, with two diarylethene units in a chiral cyclohexane, was incorporated into K₁₅ and the phase change concomitant with photoisomerization was measured.



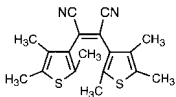
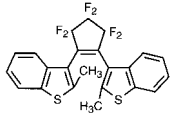
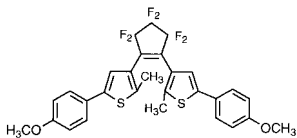
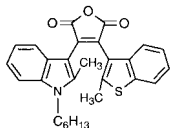
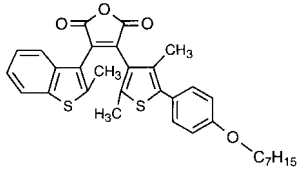
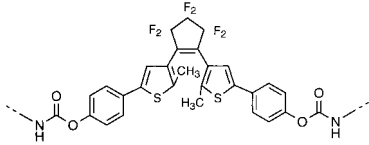
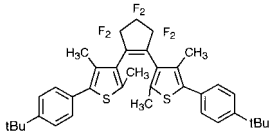
In this case, photocyclization induced the phase change from nematic to chiral nematic, and cycloreversion returned the phase to the nematic state.

2.6 Photooptical Switching – Refractive Index Change

Photochromic compounds that alter their refractive indices in a near infrared region are very useful for optical waveguide components, such as optical switches, variable frequency filters, variable attenuators, and phase shifters. With such applications in mind, several research groups have examined refractive index changes of diarylethenes.^[7,49–57] Table 3 summarizes their values and measuring conditions. For the dye/polymer systems, the maximum refractive index change was 3.9×10^{-3} at 1300 nm. The relatively small refractive index change is due to low conversion in polymer matrices. The quantity of a diarylethene that can be dissolved in a polymer matrix is limited to less than 30–50 wt%, and open-ring to closed-ring photoisomerization conversion is suppressed. Taking the degree of conversion into account, the relationship between the weight fraction (*f*) of photoisomerized compound and the refractive index change (Δn) at 633 nm is expressed for **7** in PMMA as follows.^[50]

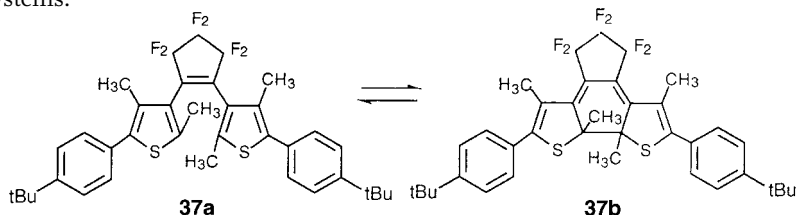
$$\Delta n = 0.128 f \quad (2)$$

Tab. 3: Refractive index changes concomitant with photoisomerization.

Compounds	Δn
	<p>32</p> <p>1.5×10^{-3} (633 nm, 3 wt% conversion in amorphous polyolefin)</p>
	<p>18</p> <p>2.8×10^{-3} (633 nm, 2 wt% conversion in PMMA)</p> <p>1.5×10^{-3} (633 nm, 3 wt% conversion in amorphous polyolefin)</p> <p>5×10^{-4} (1300 nm; in polyfluoroethyl methacrylate containing 10 wt% dye after UV irradiation)</p>
	<p>33</p> <p>3.5×10^{-3} (633 nm, after UV irradiation in sol-gel film)</p> <p>3.0×10^{-3} (785 nm, after UV irradiation in sol-gel film)</p>
	<p>34</p> <p>1.8×10^{-3} (1300 nm, in PMMA film containing 50 wt% dye after UV irradiation)</p>
	<p>35</p> <p>3.9×10^{-3} (1300 nm, in PMMA film containing 50 wt% dye after UV irradiation)</p>
	<p>36</p> <p>4.0×10^{-2} (785 nm, in sol-gel film. see the text)</p>
	<p>37</p> <p>3.8×10^{-2} (817 nm, in bulk amorphous film)</p>

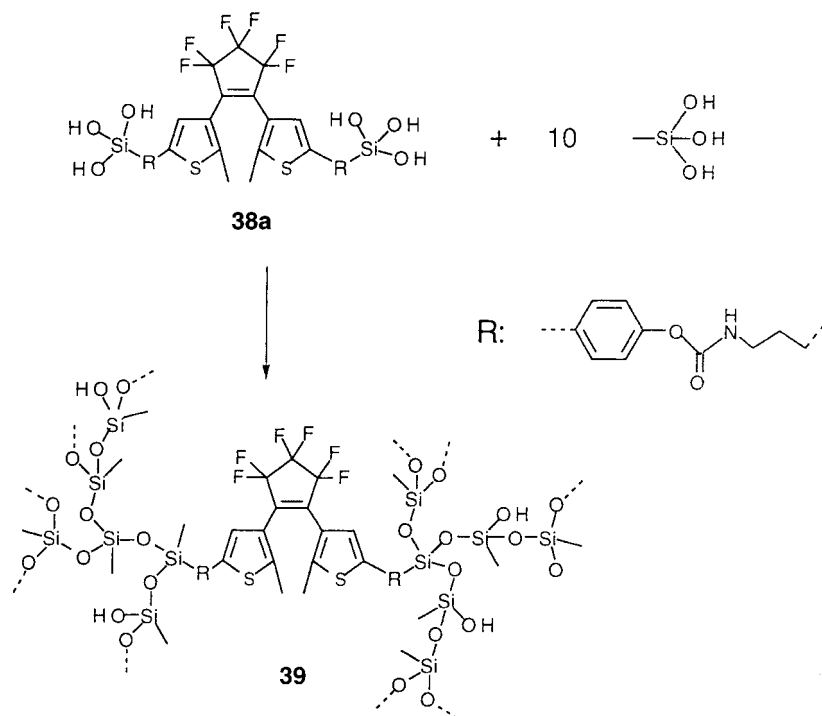
This relationship means that the refractive index change could be greater in bulk amorphous photochromic systems or in solid matrices containing high concentrations of diarylethenes.

The following diarylethene undergoes photochromism even in bulk amorphous systems.^[56]



The T_g was measured as 67 °C. The closed-ring isomer was isolated by HPLC and coated on a glass substrate by a dip-coating method, using hexane as a solvent. The refractive index was measured at 817 nm before and after irradiation with visible ($\lambda > 500$ nm) light. The initial refractive index of 1.589 changed after visible light irradiation to 1.551; the photoinduced refractive index change was as large as 3.8×10^{-2} . The refractive index increased again after irradiation with UV ($\lambda = 366$ nm) light; recovery was around 80 %. After the first cycle, the refractive index could be changed reversibly from 1.55 to 1.58 by alternate irradiation with visible and UV light.

A sol-gel technique was used to prepare hybrid organic-inorganic xerogels containing high concentrations of dithienylethenes. The sol-gel materials were prepared by a method based on co-condensation between the hydrolyzed species of the diarylethene derivative **38a** and of methyltrihydroxysilane precursors as shown below.



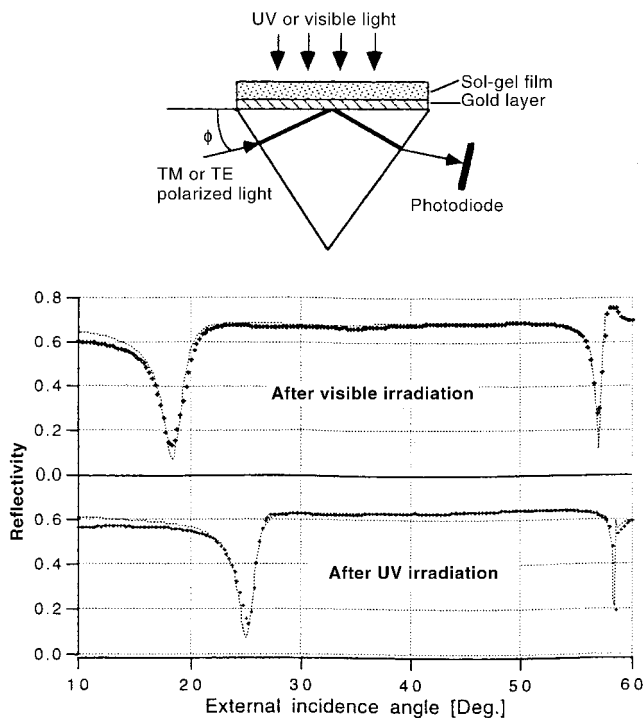


Fig. 12: Reflectivity recorded as a function of the external incidence angle (Φ of the measuring device above) for TM polarized light at 785 nm wavelength, after visible irradiation and after UV irradiation. The crosses represent experimental data and the dotted lines are the theoretical curves obtained from the fitting procedure.

Absorption measurement indicated that the degree of photostationary state conversion from the open-ring to the closed-ring forms upon irradiation with 313 nm light was as large as 95 %, even in the gel matrix. The refractive index was measured at 785 nm. Figure 12 shows the experimental reflectivity curve for the gel film. The reflectivity was first recorded when the photostationary state was reached under UV irradiation and then after powerful illumination at 633 nm. A large angular shift of the reflectivity dip was observed. The angular dependence indicated that the colorless, open-ring isomer had a refractive index of $n=1.533$, while this increased to $n=1.573$ after irradiation with UV light. The refractive index change was as large as 4×10^{-2} . This large Δn value is promising for photooptical applications. The film thickness of the sample, deduced from the above experiment, was $0.65 \mu\text{m}$. Several optical components, such as gratings and waveguides (directional couplers and Mach–Zehnder interferometers), have been designed and fabricated using gels containing dithienylethenes.

For the dye/polymer systems, the refractive index changes are rather low, as shown in Table 3. Even so, the refractive index change can be applied to photooptical switching devices. A self-holding and optical-optical 2×2 photochromic switch using a Mach–Zehnder interferometer has been constructed. The device was fabricated using a silica-based integrated optic Mach–Zehnder interferometer with a clad-

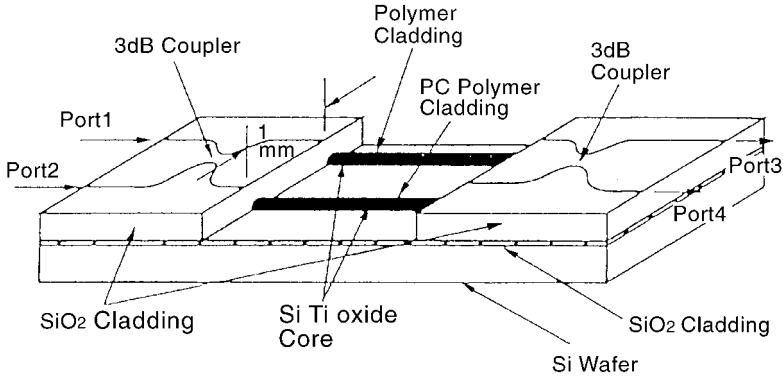


Fig. 13: Optical switch. Schematic view.

ding polymer containing diarylethenes, as shown in Figure 13. The refractive indices of the two polymer claddings were adjusted to that of the silica glass cladding by changing the copolymerization ratio of poly(trifluoroethyl methacrylate-co-methyl methacrylate). One polymer cladding contained 7.

Cross-bar switching was achieved by alternate irradiation with ultraviolet (313 nm) and visible ($\lambda > 500$ nm) light, as shown in Figure 14. The switching was self-holding and the cross-talk ratio of the switching was -12 dB at $1.55 \mu\text{m}$. At the material level, self-maintaining at 80°C was confirmed. According to calculation, a refractive index change as large as 0.00014 is required for full switching. The observed refractive index change was approximately 0.0003: enough for full switching operation. The switching time of the system was 20–30 s. This new optical switch can be applied for repairing the route of an optical fiber.

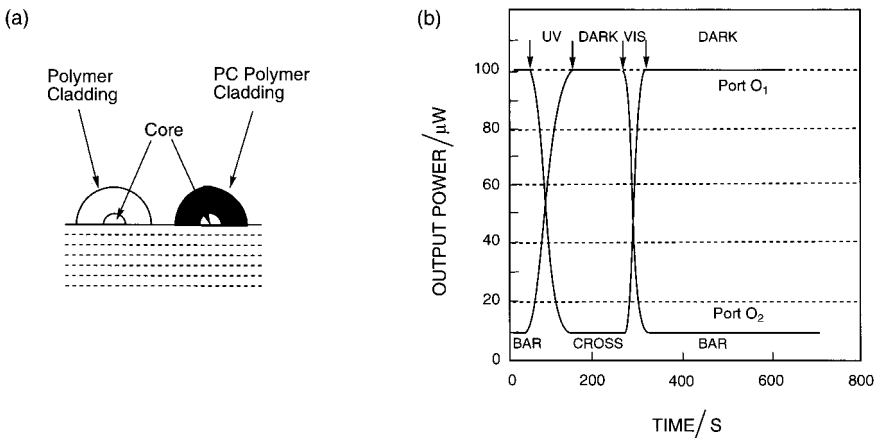


Fig. 14: (a) Schematic view of a photooptical switching device, (b) relationship between output power and irradiation time. Alternating irradiation by UV and visible light.

2.7

Conclusion

Various types of molecular photoswitching systems using diarylethene derivatives as the switching unit have been reviewed. Concomitantly with their photochromic reactions, diarylethene derivatives change such of their properties as their geometrical structures, electronic structures, refractive indices, and chiral properties. These property changes have successfully been applied to construction of molecular photoswitching systems, such as host-guest complexes, molecular wires, organic photoconductors, molecular magnets, liquid crystals, and optical waveguides.

References

- 1 G. H. Brown, Ed., *Photochromism*, Wiley Interscience: New York, 1971.
- 2 H. Dürr, H. Bouas-Laurent, Eds, *Photochromism, Molecules and Systems*, Elsevier: Amsterdam, 1990.
- 3 M. Irie, *Adv. Polym. Sci.* **1990**, 94, 27.
- 4 S. Shinkai, O. Manabe, *Top. Curr. Chem.* **1984**, 121, 67.
- 5 S. L. Gilat, S. H. Kawai, J.-M. Lehn, *Chem. Eur. J.* **1995**, 1, 275.
- 6 E. Sackmann, *J. Am. Chem. Soc.* **1971**, 93, 7088.
- 7 F. Ebisawa, M. Hoshino, K. Sukegawa, *Appl. Phys. Lett.* **1994**, 65, 2919.
- 8 G. Smets, *Adv. Polym. Sci.* **1983**, 50, 17.
- 9 H. G. Heller, S. A. Harris, S. N. Oliver, *J. Chem. Soc. Perkin 1*, **1991**, 3258.
- 10 M. Irie, K. Uchida, *Bull. Chem. Soc. Jpn.* **1998**, 71, 985.
- 11 A. Kaneko, A. Tomoda, M. Ishizuka, H. Suzuki, R. Matsushima, *Bull. Chem. Soc. Jpn.* **1988**, 61, 3569.
- 12 M. Irie, K. Sakemura, M. Okinaka, K. Uchida, *J. Org. Chem.* **1995**, 60, 8305.
- 13 M. Irie, T. Lifka, K. Uchida, S. Kobatake, Y. Shindo, *Chem. Commun.* **1999**, 747.
- 14 M. Irie, in *Organic Photochromic and Thermochromic Compounds*, Vol. 1, Crano, J.C., Guglielmetti, R. Eds.; Plenum Press: New York, **1999**, p 207.
- 15 M. Irie, M. Mohri, *J. Org. Chem.* **1988**, 53, 803.
- 16 M. Hanazawa, R. Sumiya, Y. Horikawa, M. Irie, *J. Chem. Soc., Chem. Commun.* **1992**, 206.
- 17 S. Abe, K. Uchida, I. Yamazaki, M. Irie, *Langmuir* **1997**, 13, 5504.
- 18 K. Uchida, Y. Nakayama, M. Irie, *Bull. Chem. Soc. Jpn.* **1990**, 63, 1311.
- 19 H. Taniguchi, A. Shinpo, T. Okazaki, F. Matsui, M. Irie, *Nippon Kagaku Kaishi*, **1990**, 1138.
- 20 S. Nakamura, M. Irie, *J. Org. Chem.* **1988**, 53, 6136.
- 21 M. Irie, T. Lifka, S. Kobatake, N. Kato, unpublished result.
- 22 K. Uchida, T. Matsuoka, K. Sayo, M. Iwamoto, S. Hayashi, M. Irie, *Chem. Lett.* **1999**, 835.
- 23 S. L. Gilat, S. H. Kawai, J.-M. Lehn, *J. Chem. Soc. Chem. Commun.* **1993**, 1439.
- 24 K. Uchida, E. Tsuchida, Y. Aoi, S. Nakamura, M. Irie, *Chem. Lett.* **1999**, 63.
- 25 H. Miyasaka, S. Arai, A. Tabata, T. Nobuto, N. Mataga, M. Irie, *Chem. Phys. Lett.* **1994**, 230, 249.
- 26 N. Tamai, T. Saika, T. Shimidzu, M. Irie, *J. Phys. Chem.* **1996**, 100, 4689.
- 27 J. Ern, A. T. Bens, A. Bock, H.-D. Martin, C. Kryschi, *J. Luminescence* **1998**, 76&77, 90.
- 28 M. Irie, M. Kato, *J. Am. Chem. Soc.* **1985**, 107, 1024.
- 29 H. G. Löhr, F. Vögtle, *Acc. Chem. Res.* **1985**, 18, 65.
- 30 H. Bouas-Laurent, J.-P. Desvergne, *Pure Appl. Chem.* **1980**, 52, 2633.
- 31 M. Takeshita, M. Irie, *Tetrahedron Lett.* **1998**, 39, 613.
- 32 M. Takeshita, M. Irie, *J. Org. Chem.* **1998**, 63, 6643.
- 33 S. H. Kawai, *Tetrahedron Lett.* **1998**, 39, 4445.
- 34 M. Takeshita, M. Irie, *J. Chem. Soc., Chem. Commun.* **1996**, 1807.
- 35 K. Uchida, M. Irie, *Chem. Lett.* **1995**, 969.
- 36 T. Saika, M. Irie, T. Shimidzu, *J. Chem. Soc., Chem. Commun.* **1994**, 2123.
- 37 N. Nakashima, Y. Deguchi, T. Nakanishi, K. Uchida, M. Irie, *Chem. Lett.* **1996**, 817.
- 38 N. Nakashima, T. Nakanishi, A. Nakatani, Y. Deguchi, M. Murakami, T. Sagara, M. Irie, *Chem. Lett.* **1997**, 591.
- 39 T. Honma, M. Yokoyama, *Densi Shashin Gakkaishi* **1997**, 36, 5.
- 40 K. Matsuda, M. Irie, *J. Am. Chem. Soc.* **2000**, 122, 7195, 8309.
- 41 K. Ichimura, *Supramolecular Sci.* **1996**, 3, 67.
- 42 T. Ikeda, O. Tsutsumi, *Science* **1995**, 268, 268.
- 43 G. Solladie, R. G. Zimmerman, *Angew. Chem. Int. Ed. Engl.* **1984**, 23, 348.
- 44 S. Z. Janicki, G. B. Schuster, *J. Am. Chem. Soc.* **1995**, 117, 8524.
- 45 T. Yokoyama, S. Toshiya, *Chem. Lett.* **1997**, 687.
- 46 N. P. M. Huck, W. F. Jager, B. Lange, B. L. Feringa, *Science* **1996**, 273, 1986.
- 47 C. Denekamp, B. L. Feringa, *Adv. Mater.* **1998**, 10, 1080.
- 48 T. Yamaguchi, T. Inagawa, H. Nakazumi, S. Irie, M. Irie, *Chem. Mater.* **2000**, 12, 869.
- 49 N. Tanio, M. Irie, *Jpn. J. Appl. Phys.* **1994**, 33, 1550.
- 50 N. Tanio, M. Irie, *Jpn. J. Appl. Phys.* **1994**, 33, 3942.

- 51 T. Yoshida, K. Arishima, F. Ebisawa, M. Hoshino, K. Sukegawa, Y. Horikawa, *J. Photochem. Photobio. A: Chem.* **1996**, *95*, 265.
- 52 T. Yoshida, K. Arishima, M. Hoshino, F. Ebisawa, K. Sukegawa, A. Ishikawa, T. Kobayashi, M. Hanazawa, Y. Horikawa, *Polym. Mater. Sci. Eng.* **1996**, *75*, 368.
- 53 M. Hoshino, F. Ebisawa, T. Yoshida, K. Sukegawa, *J. Photochem. Photobio. A: Chem.* **1997**, *105*, 75.
- 54 J. Biteau, G. M. Tsivgoulis, F. Chaput, J.-P. Boilot, S. Gilat, S. Kawai, J.-M. Lehn, B. Darracq, F. Martin, Y. Lévy, *Mol. Cryst. Liq. Cryst.* **1997**, *297*, 65.
- 55 J. Biteau, F. Chaput, K. Lahlil, J.-P. Boilot, G. M. Tsivgoulis, J.-M. Lehn, B. Darracq, C. Marois, Y. Lévy, *Chem. Mater.* **1998**, *10*, 1945.
- 56 T. Kawai, N. Fukuda, D. Mayer, S. Kobatake, M. Irie, *Jpn. J. Appl. Phys.* **1999**, *38*, 1194.
- 57 K. Eunkyong, H. C. Kyong, B. R. Suh, *Macromolecules*, **1998**, *31*, 5726.

3

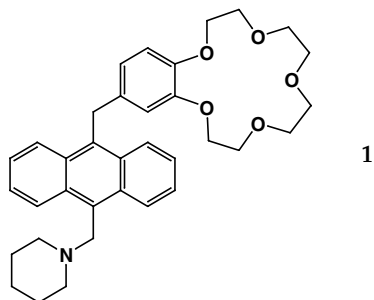
Optoelectronic Molecular Switches Based on Dihydroazulene-Vinylheptafulvene (DHA-VHF)

Thomas Mrozek, Joerg Daub, and Ayyappanpillai Ajayaghosh

3.1

Introduction

Molecular switches are the active components of molecular electronic devices capable of inducing chemical and physical changes in response to external stimuli such as electrical current, light, and biological impulses.^[1] Switching needs selective and fast activation processes, making photons, electrons, phonons, or protons the best means for the supply of energy. An optoelectronic molecular switch is a molecular system possessing electronic properties that can be triggered or controlled with the aid of stimuli such as light or application of electrochemical potential. The most amazing natural process assisted by a photonic switch is the phenomenon of vision in living systems. It is now reasonably well known that rhodopsin undergoes changes in geometry upon optical excitation, altering from the *cis* to the *trans* conformation on a subpicosecond time scale, and that this is responsible for the various switching processes in vision. Over recent years there have been several attempts to design molecular switches with the goal of developing molecular electronic devices, expected to be a key technology of the future.^[2] Photoresponsive molecular switches in particular are of great interest, since use of light as an external stimulus allows for rapid and clean interconversions of distinctly different states.^[3] Several classes of photoresponsive molecular switches are known, operating through such various processes as reversible bond formation and breaking, *cis-trans* isomerization, photo-induced electron transfer (PET), and proton transfer. PET is one of the most interesting rapid switching mechanisms, allowing for regulation of properties such as luminescence behavior. Fluorescence emission is perhaps the most widely exploited property in the design of PET molecular switches, since it is extremely sensitive to various perturbations: such as solvent polarity, donor-acceptor interactions, and the presence of metal ions. Several such systems have also been used in the design of AND logic gates (Compound 1) and molecular sensors.^[4]



1

Photoredox switches (**P**: photoactive subunit; **R**: redox active subunit) are another important class of molecular switches.^[5] Reversible redox interconversion between two different states can result in the switching on and off of luminescence in a two-component system **P-R**. In such a system, switching is achieved when the oxidized or reduced form of **R** induces an electron transfer or energy transfer process to or from the photoexcited subunit **P***; a schematic representation is given in Figure 1. A luminescent redox switch reported by Lehn and co-workers is based on a quinone/hydroquinone moiety attached to a luminescent $(\text{Ru}^{\text{II}}(\text{bpy})_3)^{2+}$ fragment (Structure 2).^[6] The electron transfer process from the bipyridyl fragment in its excited state to the adjacent quinone moiety quenches luminescence, while reversion to the reduced hydroquinone form results in the restoration of emission (Figure 2/top).

Another example of a photoredox molecular switch is based on a ferrocene-ruthenium trisbipyridyl conjugate, in which the luminescent form **4** switches to the non-luminescent form **5** upon electrochemical oxidation (Figure 2/bottom)^[7]. Biological systems exploit the interplay of redox and molecular recognition to regulate a wide variety of processes and transformations. In an attempt to mimic such redox systems, Deans et al. have reported a three-component, two-pole molecular switch, in which noncovalent molecular recognition can be controlled electrochemically.^[8] Willner et al. have reported on their research activities in developing novel means to achieve reversible photostimulation of the activities of biomaterials (see Chapter 6).^[9] Recently, we have shown that it is possible to switch the luminescence in benzodifuran quinone **6** electrochemically.^[10] The reduction in THF of the quinone moiety

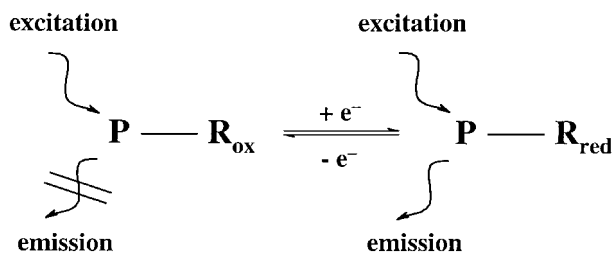


Fig. 1: Schematic representation of photoredox switching; Luminescence quenched in the oxidized state of **R** (R_{ox}).

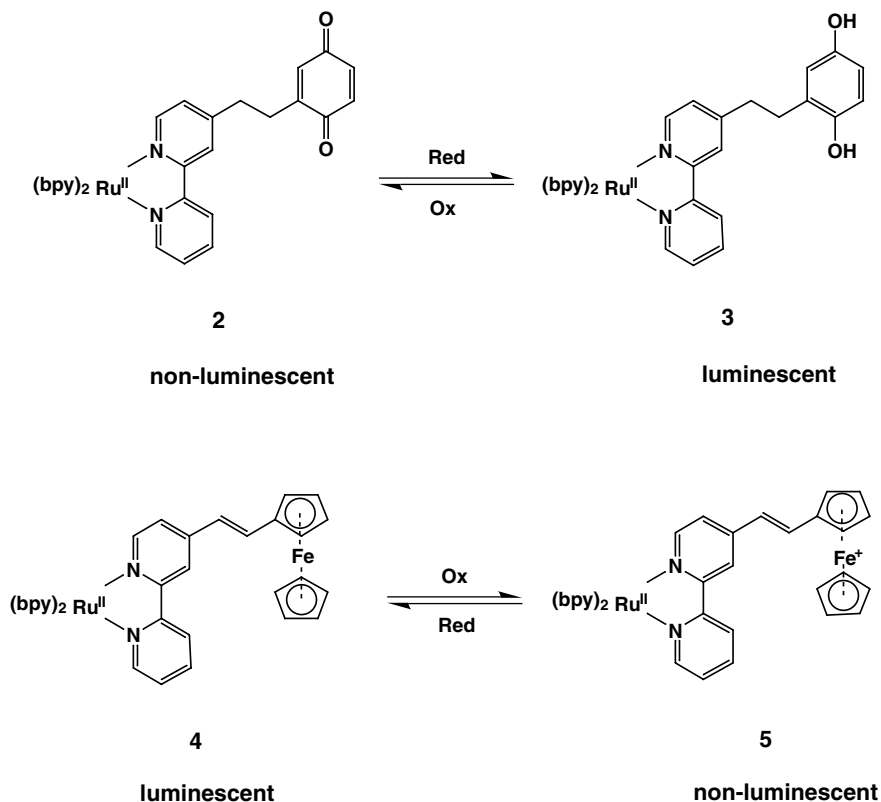


Fig. 2: Redox luminescence switching in trisbipyridyl metal complexes.

to the hydroquinone dianion occurs in a reversible, two-step process at $E_{1/2} = -1223$ mV and -1913 mV. The spectra obtained for the radical anion forms by UV/Vis/NIR spectroelectrochemical measurements agree with the quinone structure, illustrating that the two reversible redox processes are largely localized at the benzodifuran unit (Figure 3/top). The fluorescence spectrum of **6**, which is weak at the beginning of the electrochemical reduction, becomes stronger during the reduction to 6^{2-} , as shown in Figure 3/bottom.

Functionalized difluoroboradiaza-s-indacenes have recently been shown to undergo proton-dependent and metal ion-dependent fluorescence switching.^[11] For example, compound **7** initially displays a very low fluorescence quantum yield, but, as shown in Figure 4, this is enhanced significantly upon addition of aqueous HCl.^[11b] Cyclic voltammetry on **7** indicated that the oxidation of the dimethylamino group, appearing between the oxidation and the reduction of the indacene framework, disappeared upon protonation.^[11a] The increase in oxidation potential of the protonated **7** makes the nonradiative deactivation process less efficient, thereby enhancing the efficiency of the fluorescence quantum yield.

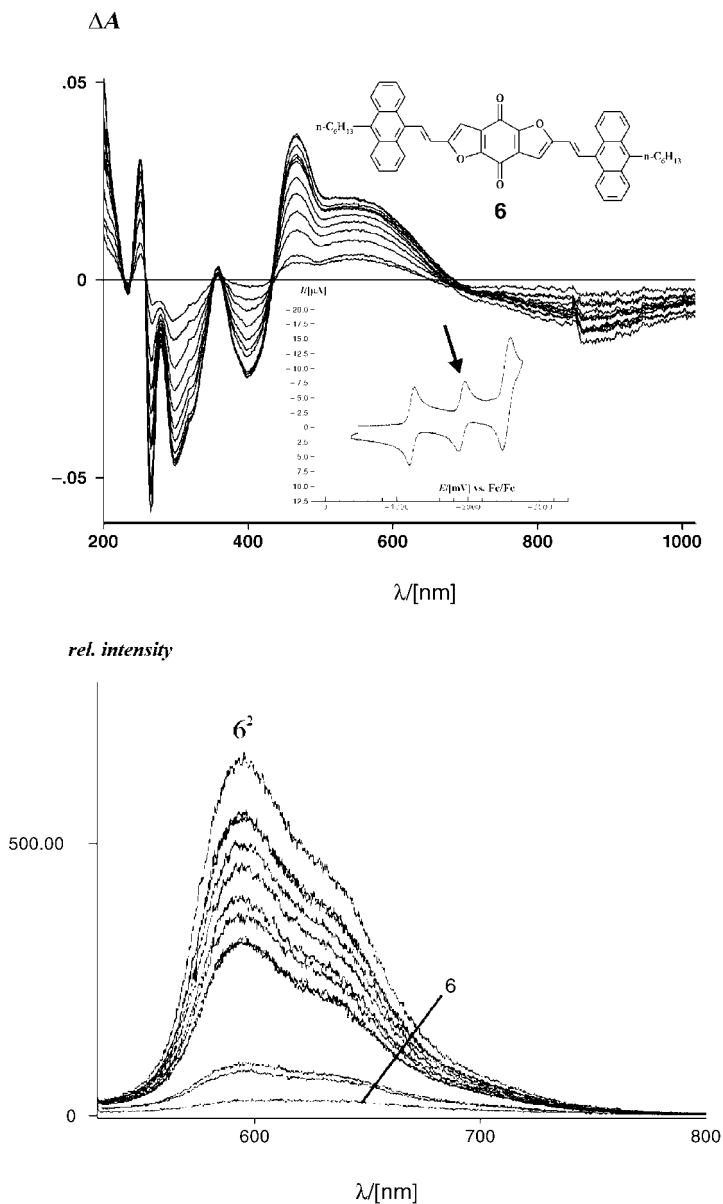


Fig. 3: Top: Difference spectra (referenced to the spectrum of the radical anion $6^{\bullet-}$) showing the formation of the dianion 6^{2-} from $6^{\bullet-}$. The cyclic voltammogram is shown in the inset. The applied potential is indicated by the arrow. Bottom: "ON/OFF"-switching of luminescence during reduction of **6**.

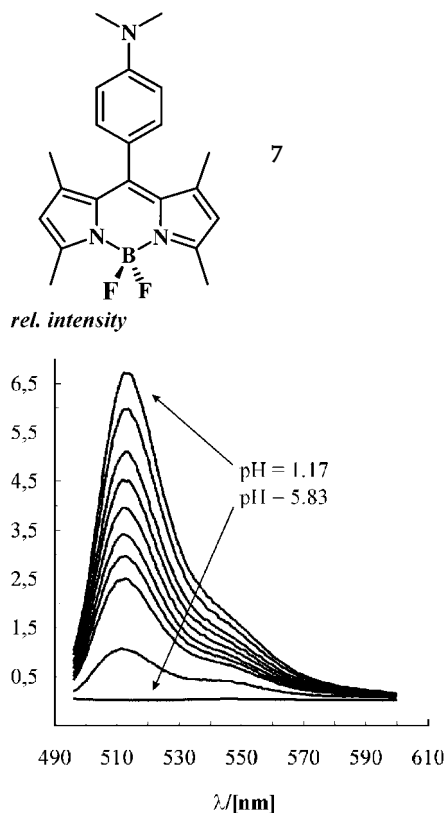


Fig. 4: Effect of pH on the fluorescence switching of compound **7** in a methanol–water mixture (volume fraction [$\phi = 0.5$]). The pH values (in order of decreasing fluorescence intensity) are: 1.17, 2.10, 2.51, 2.65, 3.07, 3.24, 3.37, 3.53, 3.81, and 5.83.

3.2 Photochromic Molecular Switches

Information storage at the molecular level, using switchable molecular devices, is expected to revolutionize information processing and communication systems. Photochromic groups are known to have the potential to reversibly alter the molecular structure, electronic properties, and/or physical characteristics of a substrate attached to them.^[3] Therefore, the photochromic behavior of organic molecules can be used to trigger the switching of a required property, which in turn can be exploited in the designing of materials useful for molecular electronic and photonic devices. Because of this, an ever increasing effort is being directed towards designing and studying dynamic molecular systems for utilization as switching devices that can undergo reversible changes between different states. Judicious manipulation of the molecular structures of such systems permits tuning and optimization of the switching behavior for specific applications.

Photochromism is the phenomenon whereby a molecule can exist reversibly in two or more different forms with distinctly different physical or chemical properties, and can be induced to change between them by photochemical means. It may be

due to simple isomerization of a substituted ethylenic double bond, or it may be the result of ring-closure and ring-opening in the presence of light energy of different wavelengths. Several examples of such systems are known in the literature. For example, the well known *cis-trans* isomerization of azobenzene and its derivatives has been extensively studied,^[12] while other photochromic systems studied at length include fulgides^[13] and diarylethenes^[14]. Many of these systems have been exploited for the designing of molecular level switching devices, with the goal of developing viable information storage systems. Before going into the details of dihydroazulene-vinylheptafulvene photochromism and its use in molecular switches, it is appropriate to take a brief look at some of the other known photochromic systems.

3.2.1

Molecular Switches Based on Fulgides

Fulgides and fulgimides are promising candidates for designing photochromic switches (see Chapter 10 for an extensive discussion). It is known that they undergo reversible ring-closure and ring-opening upon irradiation with UV light and visible light respectively, giving rise to the corresponding **closed (C)** and **open (O)** forms (8/9) (Figure 5).^[13] Walz et al. have successfully utilized this photochromic system to

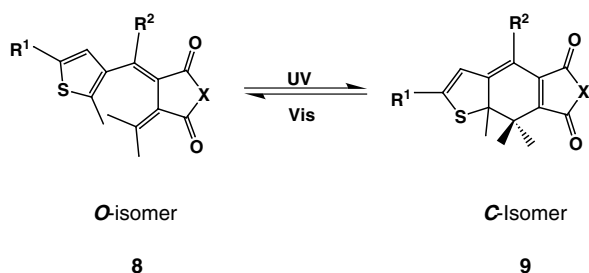


Fig. 5: Photochromism in fulgide (X=O) and fulgimide (X=NR³)-type systems.

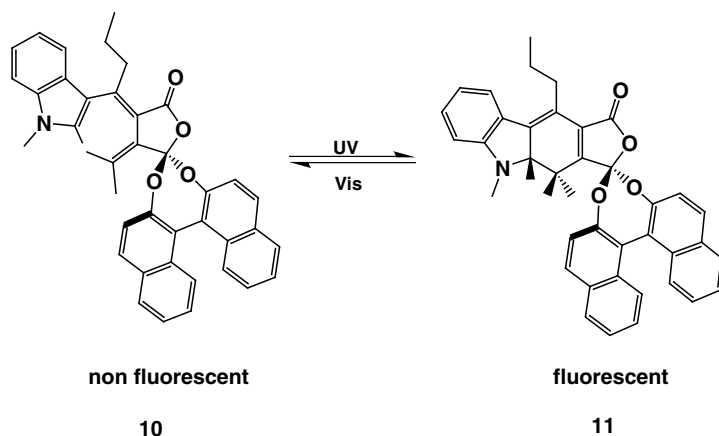


Fig. 6: “ON/OFF”-switching of fluorescence in a fulgide-type system.

design molecular switches consisting of a donor-fulgide-acceptor triad^[15]. The switching “on” and “off” of the fluorescence of an attached fluorophore depends upon the energy transfer process between a donor and an acceptor, and this in turn depends upon the geometric configuration of the photochromic fulgide, as shown in Figure 5. Inada et al. have reported perfect on-off switching of fluorescence emission in a fulgide photochromic system with an attached binaphthol substituent.^[16] While the colorless form of the propyl-substituted binaphthol-condensed indolylfulgide **10** did not display fluorescence, its colored form **11**, obtained on irradiation with UV light, exhibited fluorescence in toluene at room temperature (Figure 6).

3.2.2

Photochromic Switches Based on Dihydroindolizine

Recently, Weber et al. have reported a dual mode molecular switching device with nondestructive readout capability, based on a photochromic dihydroindolizine (DHI).^[17] The write-lock-read-erase mechanism, as shown in Figure 7, is based on irradiation of **12** to form the colored betaine **13** and its subsequent protonation to **14**. This in turn can undergo deprotonation back to **13** and, finally, thermal reversion to **12**. However, the absorption ranges of the ring-closed **12** and the ring-opened betaine **14** are not optimal, and its use as a data storage system is limited accordingly.

3.2.3

Multimode Molecular Switch Based on Flavylium Ion

The photochromic system constituted by the 4'-hydroxyflavylium ion **15a**, reported by the groups of Pina, Maestri, and Balzani,^[18a,b] is an interesting system, being a multistable, multifunctional molecular switch reminiscent in its photoactive *trans*-2,4'-dihydroxychalcone form (**15d**) of Photoactive Yellow Protein (PYP), a sensory protein in nature (see also Chapter 10).^[18c,d] System **15** (Figure 8) has been found suitable as an optical memory device with multiple storage capability at different memory levels and nondestructive readout capacity through a write-lock-read-unlock-erase cycle. All the observed processes are fully reversible, and are accompanied by large changes in absorption and emission properties.

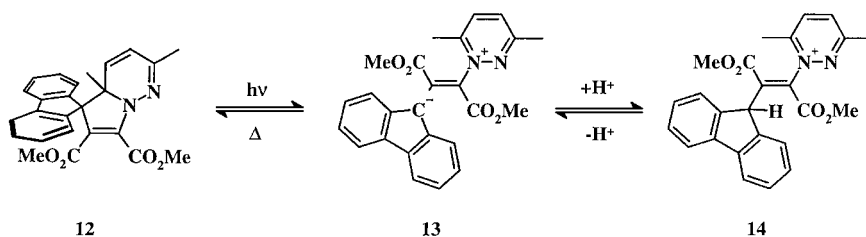


Fig. 7: Light-driven switch represented by dihydroindolizine **12**, betaine **13**, and protonated betaine **14** (Δ = thermal activation).

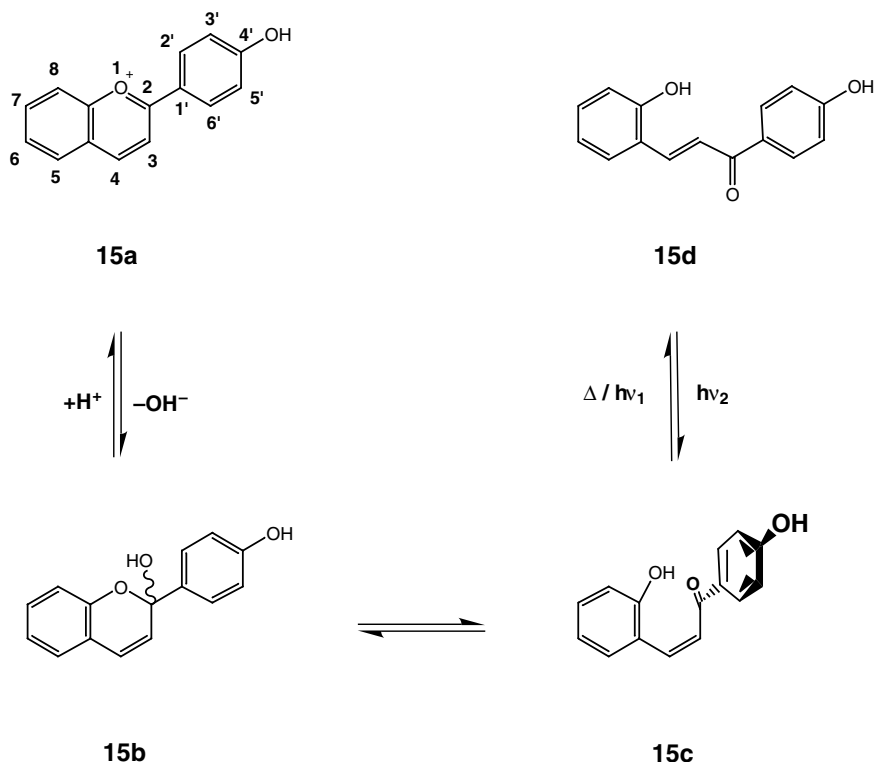


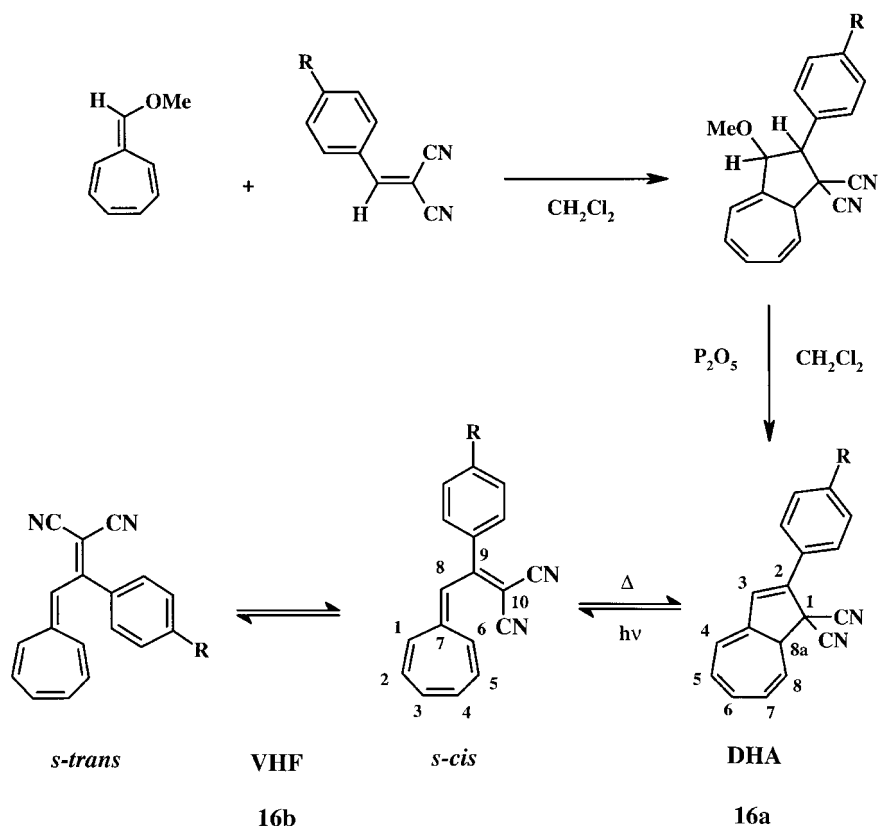
Fig. 8: Structural transformations of the 4'-hydroxyflavylium ion 15a. Only the important forms are shown.

3.2.4

Dihydroazulene-Vinylheptafulvene Photochromism (DHA-VHF Photochromism)

Dihydroazulenes are alternant π -tetraenic systems, that can be obtained directly by the [8+2] cycloaddition of 8-methoxyheptafulvene with dicyanoethylenes, followed by elimination of methanol (Scheme 1a). An alternative means of preparation is by C–C bond formation between a cycloheptatrienylium cation and an appropriate dicyanoethylene derivative, followed by dehydrogenation to afford the nonalternant π -pentaenic vinylheptafulvenes, which immediately rearrange thermally to the corresponding DHAs (Scheme 1b). A variation on this route can also be accomplished using the corresponding carbonyl compounds, as depicted in Scheme 1b. The latter synthetic route (Scheme 1b) provides DHAs featuring more complex substitution patterns – 2,3-disubstituted DHA derivatives – while the former (Scheme 1a) gives DHAs substituted solely at the 2-position.

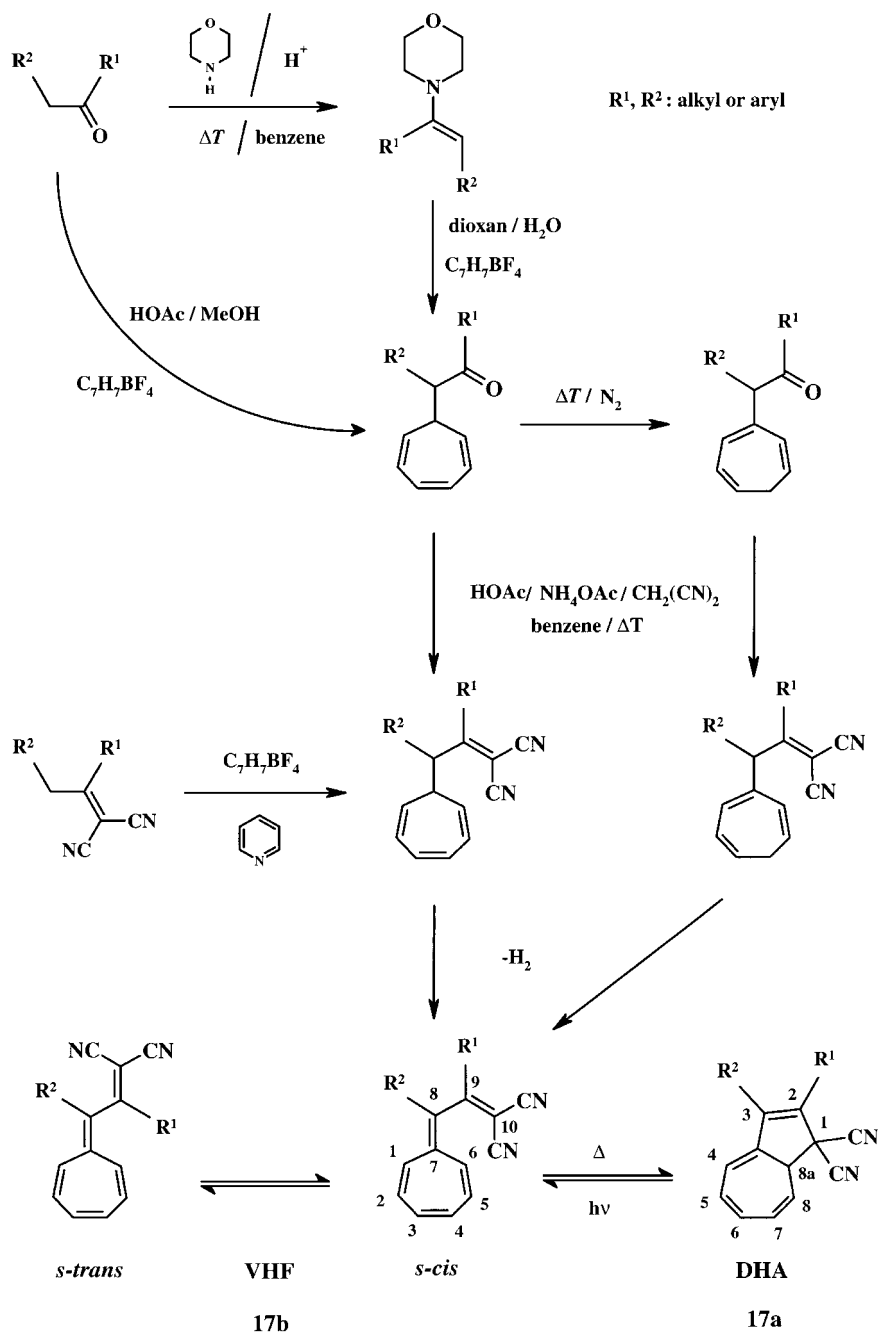
The DHAs undergo an interesting photoinduced rearrangement to the corresponding VHF, and this is accompanied by a change of color from, in the case of the phenyl derivative 18a (Scheme 2), yellow to dark red.^[3a,19] In this case, it was

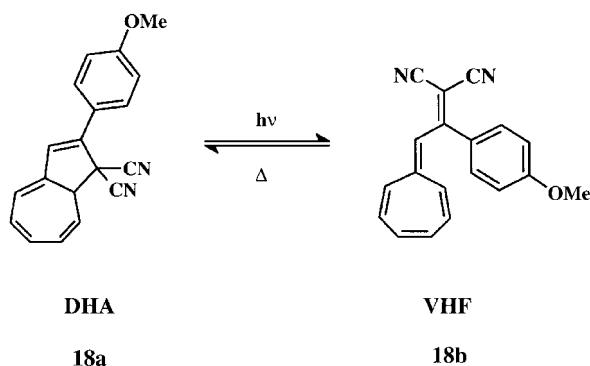


Scheme 1a: 'Direct' pathway for the synthesis of dihydroazulenes.

observed that upon irradiation (in acetonitrile) the intensity of the absorption band at 350 nm decreased while a new, long wavelength absorption at 468 nm was formed through four isosbestic points (Figure 9). The **VHF 18b** underwent quantitative thermal reversion to the **DHA 18a** within 70 h at 25 °C. The quantitative conversions of the photochemical forward reaction and the thermal back reaction could be followed by ^1H NMR spectral studies. The photoreaction occurs from the excited singlet state; the quantum yield of the reaction was 0.55. The rate constant for the thermal back reaction at 25 °C was found to be $7 \times 10^{-5} \text{ s}^{-1}$.

The photochromic properties of **DHA** systems depend strongly upon the substituents on the five-membered ring, the reaction media, and the temperature. For example,^[20] to obtain a steady state equilibrium mixture of **22a** and **22b** (Scheme 3), the 2,4-dinitrophenyl derivative of the **DHA 22a** had to be irradiated (in acetonitrile, 366 nm irradiation wavelength) at low temperature (200 K). In contrast to this, arene derivatives **21a** and **23a**, on irradiation at 250 K, were quantitatively converted to the corresponding **VHFs 21b** and **23b**, respectively. In the case of the **DHA 24a**, a stationary equilibrium between **24a** and **24b** could be observed at room temperature. Thus, in general, it was observed that the presence of electron-withdrawing substitu-

Scheme 1b: Synthesis of dihydroazulenes via corresponding vinylheptafulvenes; ΔT = reflux.



Scheme 2: Photochromic isomerization between **18a** and **18b**.

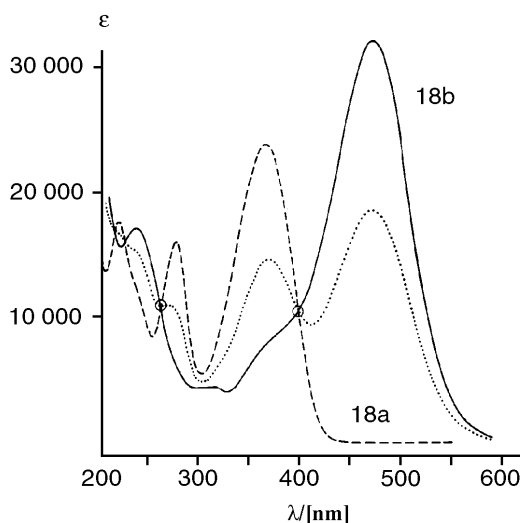


Fig. 9: Photochemistry of **18a** in acetonitrile ($c = 4.9 \times 10^{-5} \text{ mol dm}^{-3}$), irradiation by sunlight. (---) start; (•••) after 1 min, (—) after 7 min.

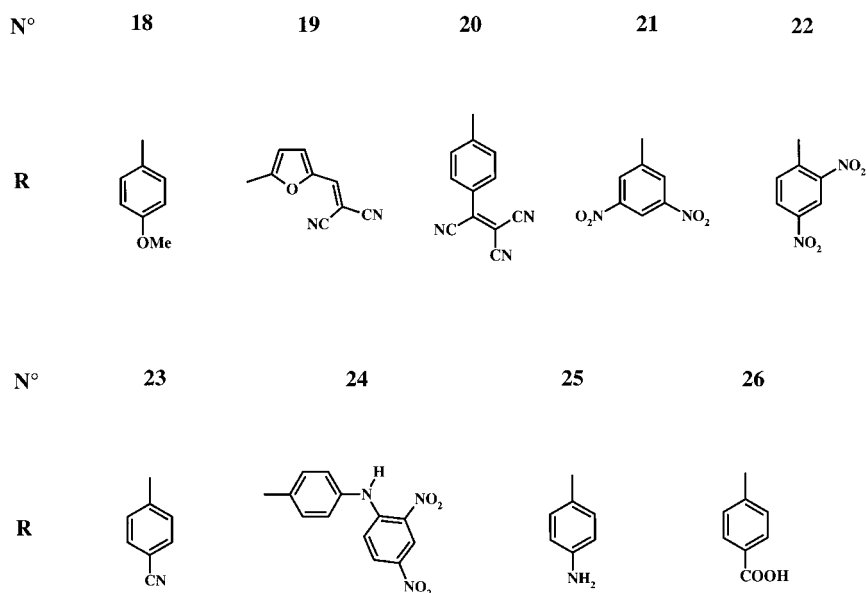
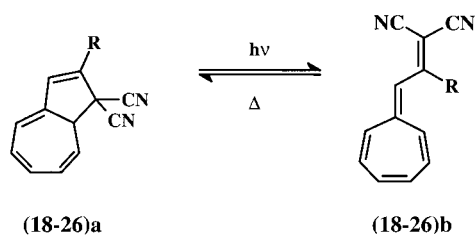
ents such as nitro and cyano groups facilitate the thermal back reaction. On the other hand, electron-donating substituents such as amino groups have the opposite effect.

The effect of substitution patterns on the long wavelength absorptions of various **DHAs** and **VHFs** are clear from Table 1.^[21] The tricyanovinyl-substituted system **20a**/**20b** differs significantly (Figure 10), **DHA 20a** absorbing at 450 nm (in DMSO) and **VHF 20b** at 610 nm. This can be explained by charge transfer transitions due to the strong acceptor group. In addition, the shoulder on the absorption band of **20b** is aberrant. We explain this by the presence of both *s-trans* and *s-cis* forms in solution.^[21c]

A furan substituent at the C-2 position in a DHA has a significant effect on the kinetics of the photochemical and thermal reactions, as illustrated for the case of the DHA **19a** (Scheme 4). In this case, to observe the photochemical formation of the VHF **19b**, the system must be cooled down to $-50\text{ }^{\circ}\text{C}$, due to the fast thermal back reaction.

Another significant observation is that the photochemical ring-opening of the DHA **18a** to the corresponding VHF is blocked in the crystalline state; this is probably due to the crystal packing. Irradiation of DHA **18a** in poly(methyl methacrylate) film, however, results in the formation of VHF **18b** (Figure 11). On heating at $80\text{ }^{\circ}\text{C}$, it reverts quantitatively to **18a**. This observation reinforces speculation that crystal packing plays a major role in the photochromic behavior of DHA **18a**.

Attachment of DHA **26a** to cellulose, as a biopolymer representative, provides another way to test the feasibility of multifold photochromic switching within a



Scheme 3: Various DHA-VHF couple substitution patterns.

Tab. 1: Absorption maxima of DHAs and VHF and quantum yields $\Phi_{\text{DHA} \rightarrow \text{VHF}}$ of DHA \rightarrow VHF photoreactions in nondegassed solutions at 24 °C, $\lambda_{\text{irr}} = 366$ nm. (a) At -50 °C, $\lambda_{\text{irr}} = 420\text{--}480$ nm; (b) At 25 °C; absorption at 608 nm assigned to *s-trans*-VHF; absorption at 680 nm assigned to *s-cis*-VHF; (c) Same value in argon-saturated solution; (d) Limiting value due to thermal back conversion.

Compound	Solvent	λ_{DHA} [nm] (a)	λ_{VHF} [nm](b)	$\Phi_{\text{DHA} \rightarrow \text{VHF}}$
2-Phenyl-DHA	methylcyclohexane	349	440	0.35
	toluene	354	459	0.6
	ethanol	348	468	0.5
	acetonitrile	350	468	0.55
18	acetonitrile	360	465	0.4
19	ethanol ^[a]	440	548	
20	DMSO	449	608, 680 (sh) ^[b]	
21	methylcyclohexane	362	464	0.55
	toluene	368	482	0.45 ^[c]
	ethanol	364	492	0.09
	acetonitrile	364	490	0.002 ^[c]
22	toluene	310	480	0.005
	ethanol	315	470	≤ 0.008 ^[d]
	acetonitrile	320	488	≤ 0.0004 ^[d]
23	methylcyclohexane	361	452	0.4
	toluene	368	470	0.65
	ethanol	362	474	0.35
	acetonitrile	362	474	0.6
24	acetonitrile	386	468	
25	methylcyclohexane	376	440	0.4
	toluene	382	448	0.3
	acetonitrile	381	450	0.15
26	methylenechloride	361	474	

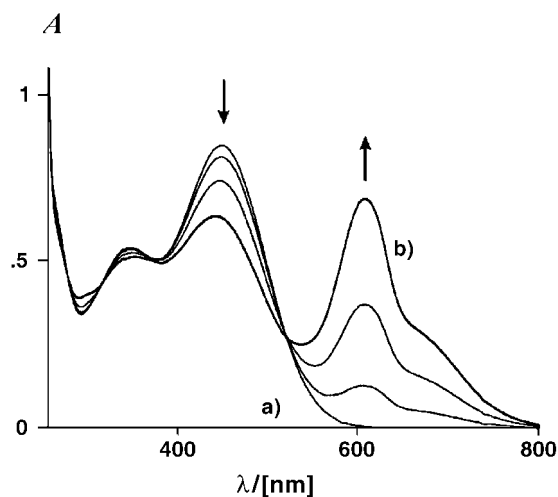
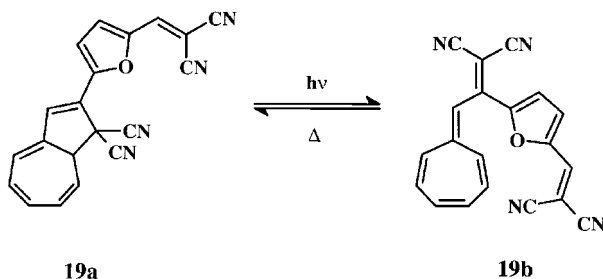


Fig. 10: Photochromism of **20a/20b** in DMSO (25 °C); irradiation with 366 nm light after 0 (a), 1, 5, 10 (b) seconds.



Scheme 4: Photochromism of the furanyl-derivatized **DHA** derivative.

macromolecular architecture, as well as affording the opportunity to investigate the influence of the conformation of the polymeric network on photoswitching behavior.^[22] Scheme 5 shows the photochemical conversion of the 6-*O*-[4-(1,1-dicyano-1,8a-dihydroazulen-2-yl)-benzoyl]-2,3-di-*O*-methylcellulose **27a** (degree of substitution of the photochromic subunit equals 0.25). Irradiation of a solution of **27a** in THF caused the characteristic **DHA** absorption band at 365 nm to decrease, while, on the other hand, the formation of the **VHF** derivative was verified by an increase in absorbance at 474 nm (Figure 12). After thermal relaxation, the original spectrum was restored. Note the blurred isobestic point at 400 nm, which we attribute to the structurally nonequivalent photochromic subunits.

Taking account of data from photophysical and photochemical investigations of the switching behavior of various **DHA/VHF** derivatives,^[21,23] we assume a qualitative energetic profile of the **DHA/VHF** couple as depicted in Figure 13.

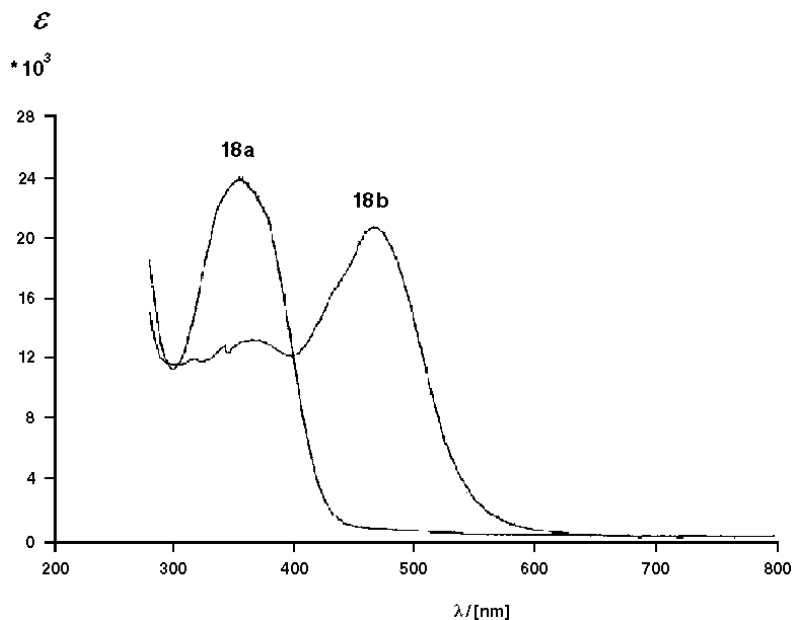
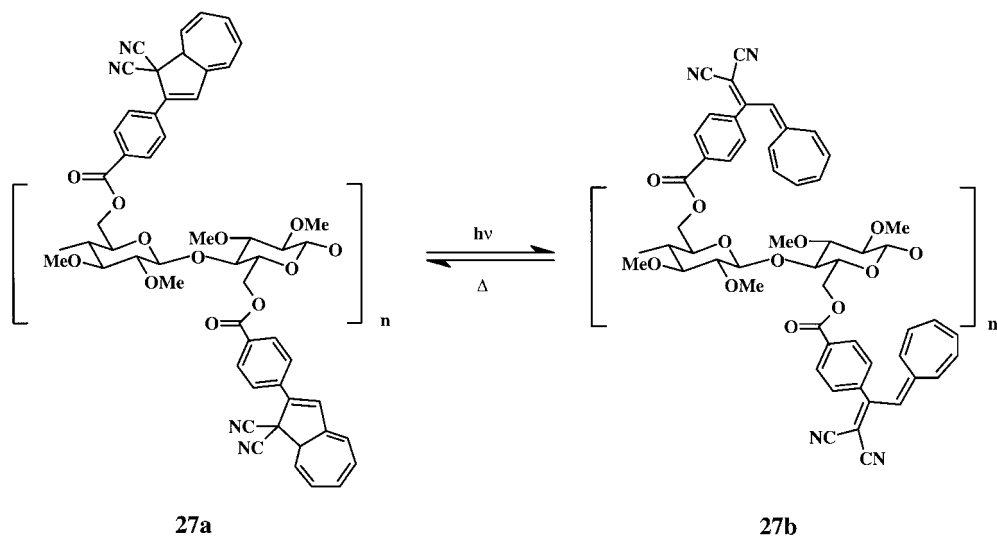


Fig. 11: Photochromism of the **DHA/VHF** couple **18a/18b** in a PMMA matrix.



Scheme 5: Photochromism of **27a**.

DHAs undergo an efficient photoreaction to the corresponding VHF; the quantum yields at room temperature ($\Phi_{\text{DHA} \rightarrow \text{VHF}}$) range from very small values (≤ 0.0004) to a respectable 0.6 (Table 1). The VHFs are non-emitting and photochemically inactive. X-ray analytical investigations of crystallized photoproducts have revealed the exclusive formation in the crystalline phase of the *s-trans* VHF isomer.^[19a] In solution, where a thermal equilibrium exists between the *s-trans* and *s-cis* isomers, we assume a high concentration of the thermodynamically favorable *s-trans*

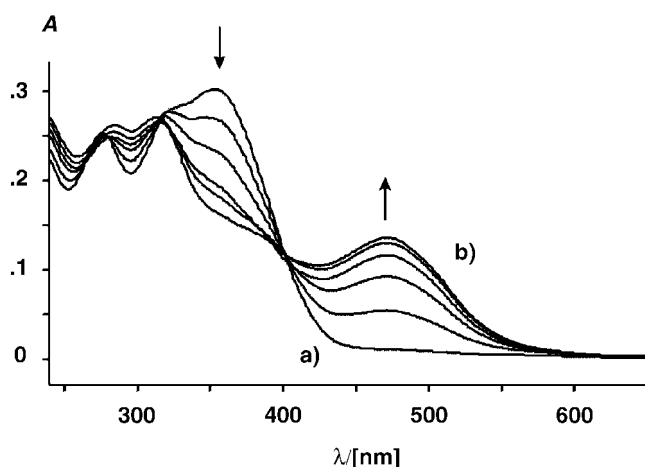


Fig. 12: Spectral developments on irradiation of **27a** in THF with an Osram 500 W lamp: 0 s (a), 200 s (b).

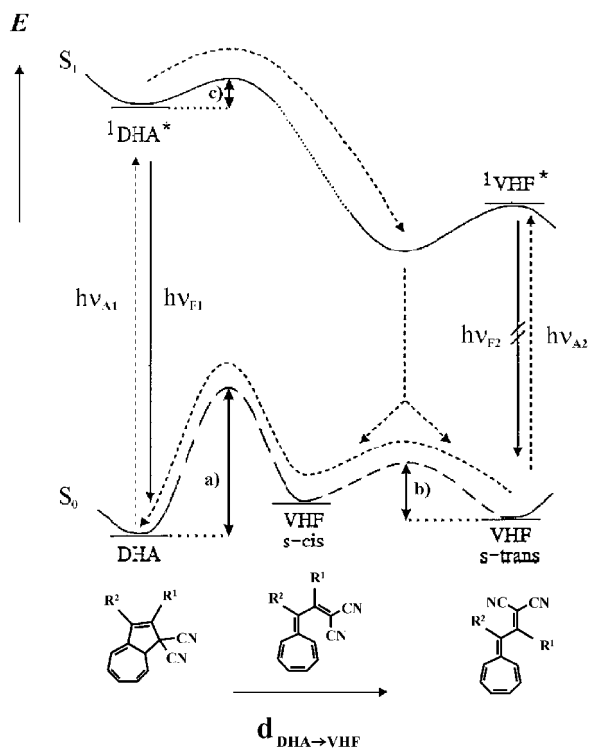


Fig. 13: Schematic representation of the reaction profiles of the photochemical pathway **DHA→VHF** and the thermal pathway **VHF→DHA**. Thermal barriers a), b), and c) are dependent on solvent parameters and substitution pattern. Absorption: $h\nu_{A1}$, $h\nu_{A2}$. Fluorescence: $h\nu_{F1}$, $h\nu_{F2}$ ($h\nu_{F2}$ is not detected).

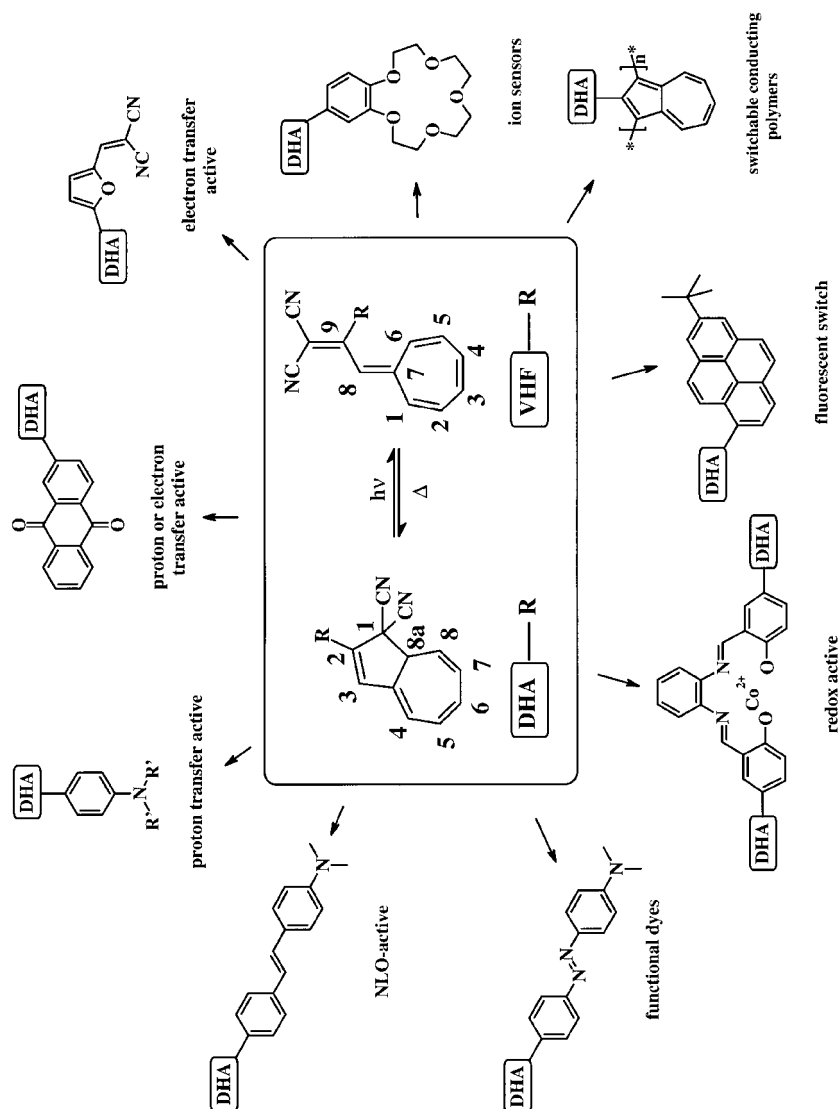
form (see, however, compound **20b**, Figure 10). This assumption is also supported by semiempirical quantum chemical calculations.^[24] The activation barrier between the *s-trans* and *s-cis* forms is believed to depend mainly on the R^1 and R^2 substitution pattern: that is, the bulkier the substituents, the higher the activation barrier. The VHF's undergo thermal rearrangement to the corresponding DHAs. The activation barrier for this back reaction (*s-cis*-VHF→DHA) is 75–110 kJ mol⁻¹, corresponding to half-lives ranging from a few seconds to several hours. It, too, depends on the substitution pattern (R^1 , R^2) and, significantly, on the solvent polarity: the more polar the solvent, the faster the thermal rearrangement, which indicates that the transition state must be more polar than the ground state.

The photoproduct is formed by a singlet pathway ${}^1\text{DHA}^* \rightarrow \text{VHF}$; triplet states are not involved in this reaction. Fluorescence is observed, weakly in fluid solution and with greatest efficiency in glasses at low temperature (also see above, for crystal packing effects). The increase in ϕ_F at low temperature is accompanied by a notably retarded DHA→VHF process, indicating competition between the photochemical

step ($\phi_{\text{DHA} \rightarrow \text{VHF}}$) and photophysical dissipation of energy (ϕ_{p}), due to an activation barrier ($< 21 \text{ kJ mol}^{-1}$) along the $^1\text{DHA}^* \rightarrow \text{VHF}$ pathway.

3.2.4.1 Molecular Switches Based on DHA-VHF

The photochemical ring-opening reaction of a **DHA**, leading to the colored **VHF**, brings about considerable changes in the electronic structure of the π -system. The alternant conjugated π -system in **DHA** is converted to a nonalternant topology in **VHF**. During this process, the cyano groups of the **DHA** come into conjugation with



Scheme 6: Examples of optoelectronic molecular switching systems based on **DHA/VHF**-photochromism.

the π -system of the VHF, which strongly influences the electronic properties of the substituent at C-9. This versatile photochromic rearrangement can therefore allow photoswitching of electronic properties such as fluorescence, redox potentials, and optical nonlinearity, leading to a variety of optoelectronic molecular switching systems,^[25] as illustrated in Scheme 6.

The furan-derived DHA **19a** is an interesting photochromic system from the point of view of molecular switch development.^[26] This system consists of a photochromic DHA structure and an electron transfer active dicyanovinylfuryl group. Since the electron acceptor strength of the dicyanovinylfuran is increased upon the photochemical rearrangement of the DHA **19a** to the VHF **19b**, the electrochemical reduction of the latter must occur at a lower negative reduction potential. This is clear from photomodulation amperometric studies of DHA **19a** and VHF **19b**, which demonstrate a structure dependency in current/time (I/t)-plots. Figure 14 gives a schematic representation of the molecular process involved during photomodulation amperometry. It is important to note that the electrode potential first has to be adjusted so that no response is observed when light is excluded. In the first step, DHA **19a** rearranges to the VHF **19b** upon irradiation, resulting in the appearance of electric current, due to the production of an electroactive species. In darkness, this current flow gradually decays, while on further illumination the current intensity increases again. Several repetitions of such an operation are shown in Figure 15. These observations can be explained qualitatively by simple molecular orbital considerations, as depicted in Figure 16. The occupied energy level representing the

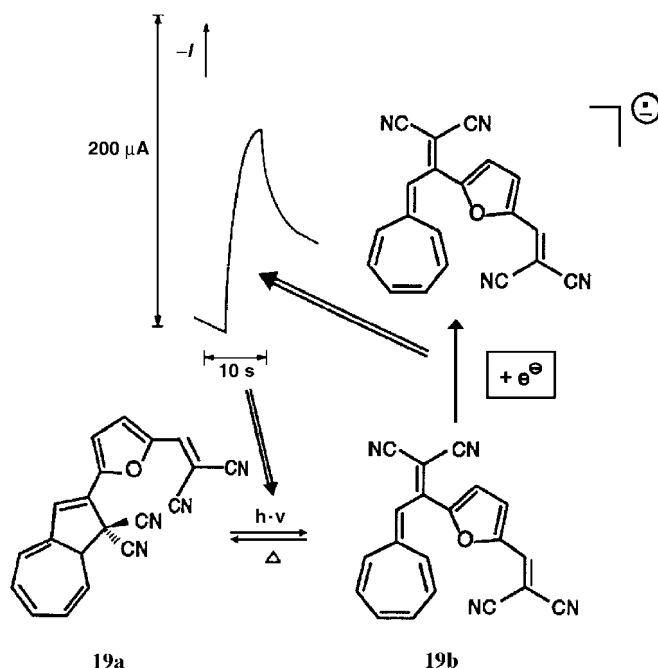


Fig. 14: Light-triggered electron transfer, monitored by photomodulated amperometry.

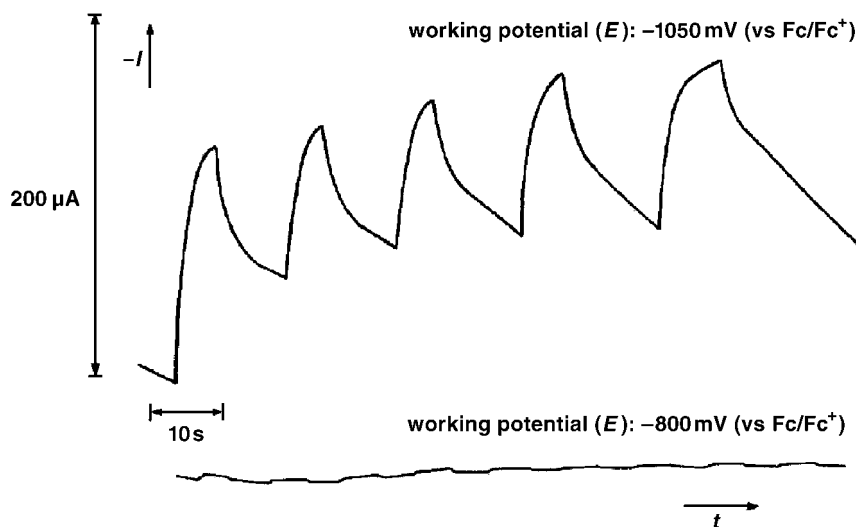


Fig. 15: Upper plot: Photostimulated electron transfer activation induced by irradiation of **DHA 19a** in acetonitrile ($c = 10^{-3} \text{ mol dm}^{-3}$) at working potential -1050 mV vs. Fc/Fc^+ . Lower plot: No switching occurred at working potential -800 mV vs. Fc/Fc^+ .

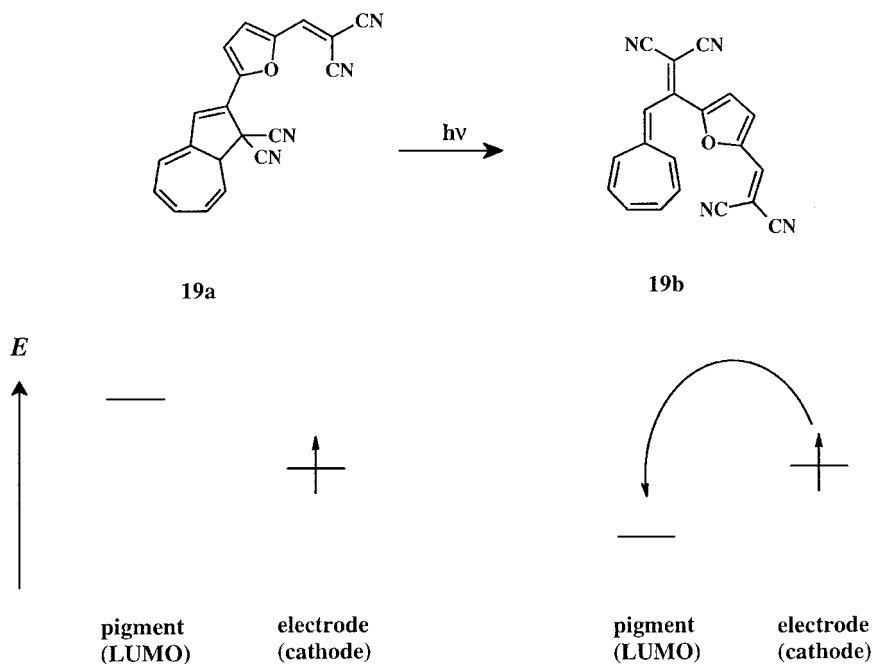


Fig. 16: Schematic representation of electronic changes due to photostimulated electron transfer.

cathodic electrode potential is maintained constant under this approximation, while the energies of the lowest unoccupied orbitals (LUMO) of the **DHA** and **VHF** are structure-dependent. For example, during the photoconversion of the **DHA 19a** to **VHF 19b**, the energy of the LUMO decreases and electron transfer becomes thermodynamically favorable, as shown in Figure 16. This process of switching allows light pulse inputs to be translated into electrical signal outputs at a molecular level.

The cyclic voltammetry, UV/Vis spectroelectrochemistry, and photomodulated amperometry characteristics of the **DHAs (21–24)a** and **VHFs (21–24)b** (Scheme 3) are quite interesting.^[20] Reversible reduction waves were noticed for the radical anion formation of **21a**, **22a**, and **24a**, with **21a** and **22a** undergoing reduction at comparatively negative potentials (–1165 mV, –1130 mV). The reduction waves of **24a**, however, occurred at a slightly higher negative potential, due to the presence of the amino group. The dianion formation turned out to be chemically irreversible in the case of **22a**, but supported a partially reversible **21a**, indicating **EC** (first step electron transfer, second step chemical reaction) behavior. Absorption spectra obtained during electrochemical reduction confirmed the reversibility of the formation of **21a^{•–}** (492 nm) from **21a** (Figure 17) and **22a^{•–}** (559 nm) from **22a**, observations consistent with dinitrophenyl radical anions. Cyclic voltammograms measured after stepwise “off-line” irradiation of **23a** in homogeneous solution are shown in

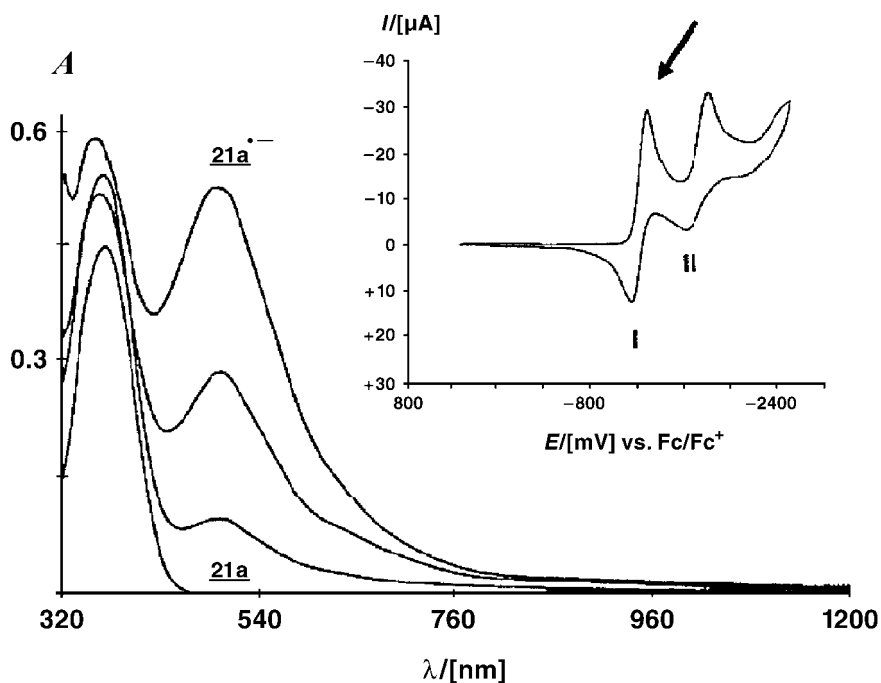


Fig. 17: Spectroelectrochemistry of **21a**, formation of the radical anion **21a^{•–}** on application of –900 mV (vs. Ag/AgCl). Inset: Cyclic voltammogram of **21a** in acetonitrile with 0.1 mol dm^{–3} TBAHFP, at a Pt electrode vs. Fc/Fc⁺ and a scan rate of 50 mV s^{–1}.

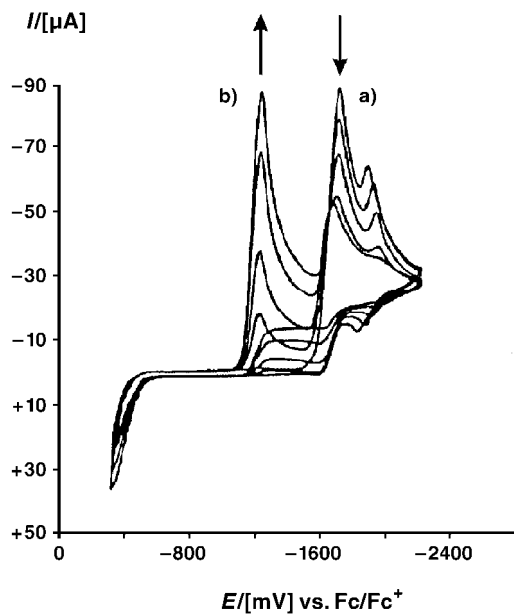


Fig. 18: Cyclic voltammogram of **23a** after irradiation (under nitrogen); irradiation time (in min): 0 (a), 2, 4, 8, 12 (b). Irradiation was performed using an Osram HWLS 500 W lamp as the light source.

Figure 18. On irradiation, a new peak appears, indicating the formation of a new species with a less negative reduction potential. After irradiation for 16 min, **23a** showed a distinctly different I/E trace, as shown in Figure 19. This observation indicates that the VHF form **23b** is reduced at a less negative potential, due to its π -acceptor dicyanovinyl substituent.

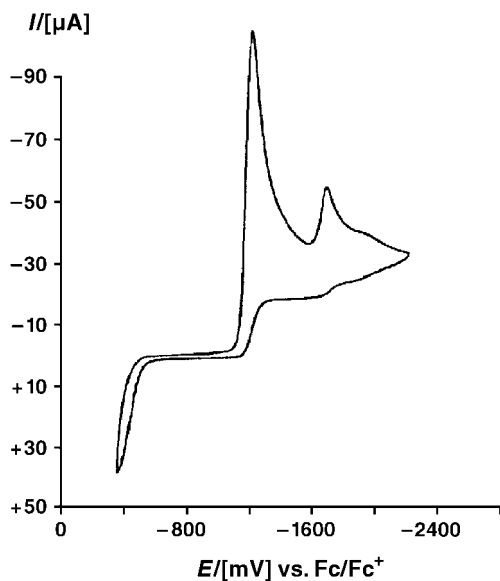


Fig. 19: Cyclic voltammetry of **23a** after irradiation for 16 min. Same conditions as Figure 18.

Photomodulation amperometry of the DHAs (**21–24**)**a** is shown in Figure 20. Because of the increased acceptor strength in **22b**, the 2,4-dinitrophenyl derivative **22a** exhibits oscillating behavior at an electrode potential less negative than that required for the constitutional isomer **21a** (Figure 20: **21a**, **22a**). On the other hand, the 4-cyanophenyl derivative **23a** displays increased sensitivity, which seems to be the result of the higher quantum yield of the photoreaction from **23a** to **23b** (Figure

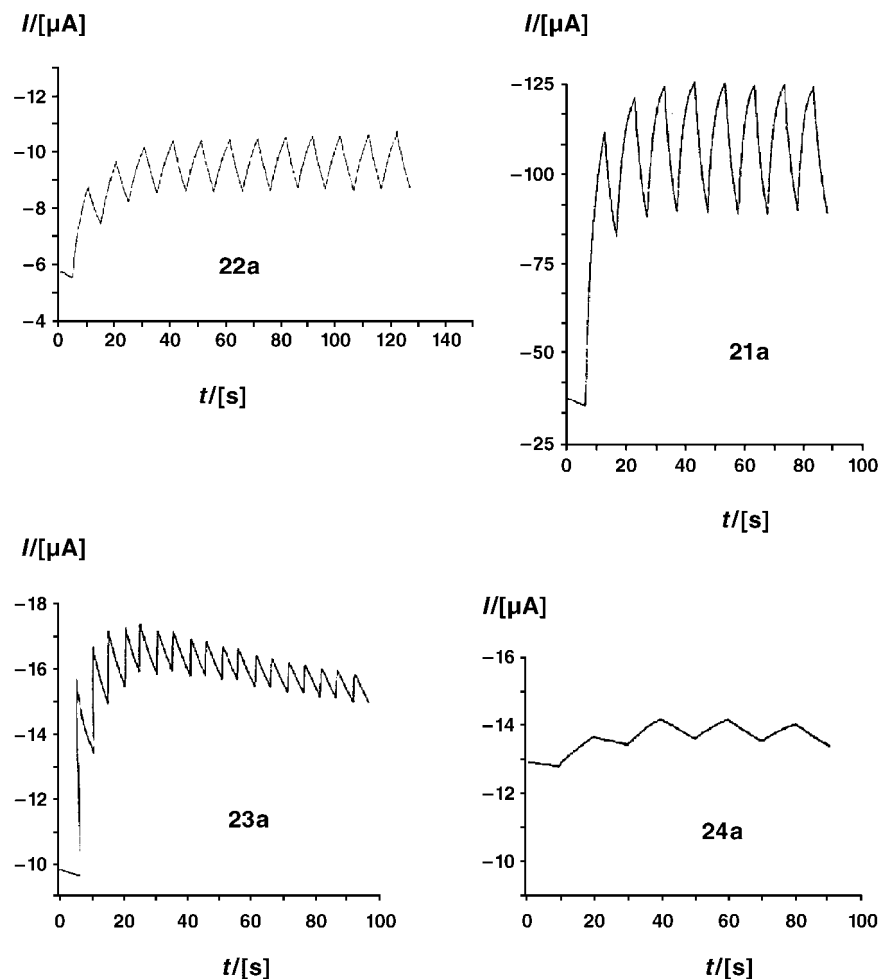


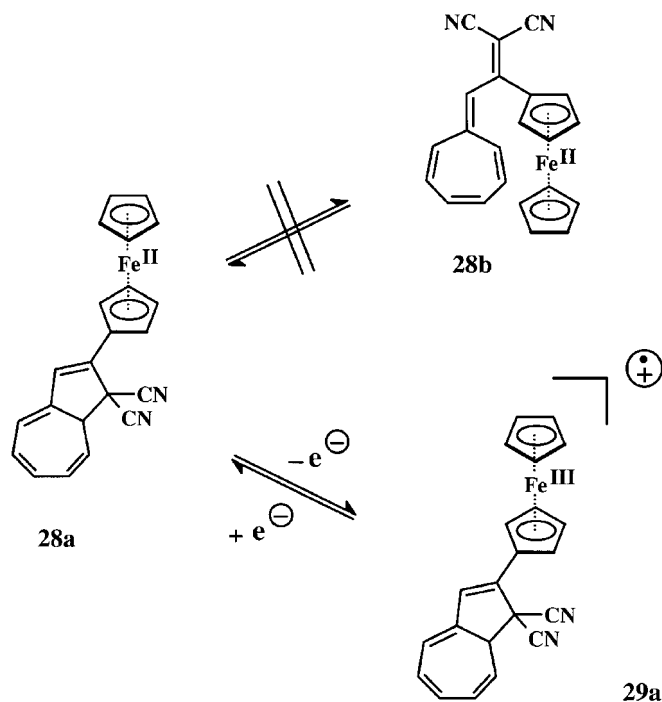
Fig. 20: Current changes produced by **21a**, **22a**, **23a**, and **24a**, respectively, upon irradiation in acetonitrile ($c = 5.9 \times 10^{-4} \text{ mol dm}^{-3}$ (**21a**), $9.9 \times 10^{-4} \text{ mol dm}^{-3}$ (**22a**), $8.9 \times 10^{-4} \text{ mol dm}^{-3}$ (**23a**), $8.8 \times 10^{-4} \text{ mol dm}^{-3}$ (**24a**)). The “ON/OFF” switching times, in seconds, are: **21a**, 5/5; **22a**, 5/5; **23a**, 0.25/5, and **24a**, 10/10 at working potentials of -700 mV ,

-500 mV , -900 mV , and -500 mV , respectively. Undivided electrochemical cell with optically transparent working electrode (OTE) [indium oxide/tin oxide (ITO) on glass] also serving as the window for irradiation; counter electrode glassy carbon, quasi-reference electrode Ag/AgCl; light source 1000 W Xenon-Mercury arc lamp LXM 1000-1 (Conrad-Hanovia).

20: **23a**). Finally, the effect of π -conjugation is demonstrated by bisarylamine **24a**, the poor sensitivity (Figure 20: **24a**) of which is presumed to result from the decreased perturbation of the redox-active subunit by the photochemically induced valence isomerization. This results in a smaller difference between the reduction potentials of **24a** and **24b**.

Aryl-substituted DHAs (**21–24a**) are able to produce electric current flow as a consequence of photomodulation by means of a light pulse sequence. To be of practical use, the peak potential E_p of (**21–24b**) must be less negative than the E_p of (**21–24a**). It has been demonstrated that various factors can improve the sensitivity of the oscillating behavior. For example, high photochemical reaction quantum yields, reduction at less negative electrode potential, and a strong interaction between the acceptor subunit and the VHF moiety (leading to enhanced stability of the radical anions of (**21–24b**)) all exert significant influence on the oscillatory behavior. Photomodulation of these compounds enables an electric current to be triggered by light pulses.

The photochromic properties of the ferrocene-dihydroazulene conjugate **28a** are dependent on the oxidation state, making the compound a novel, redox-active photochromic molecular switching unit.^[27] It is interesting to note that irradiation of compound **28a** with visible light at room temperature did not show any evidence for its ring-opening to the VHF **28b** (Scheme 7). This could be the result of the fast thermal back reaction, or may be due to quenching by the auxiliary ferrocene moiety. On the



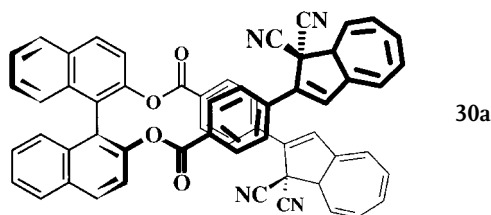
Scheme 7: Electrochemical triggering of photochromism.

other hand, the oxidized form **29a**, when irradiated with visible light, showed the long wavelength absorption corresponding to the vinylheptafulvene moiety ($\lambda_{\text{max}} = 470 \text{ nm}$), while the absorption due to the dihydroazulene chromophore at 362 nm decreased significantly.

Photochemical reactions influenced by chiral auxiliaries represent another interesting aspect of molecular switches and optical data storage systems.^[16,28] For purposes of manipulating photochemical reactions in a desired stereochemical sense, it is necessary to consider two different cases:^[29] *asymmetric photochemistry* and the *photochemistry of chiral molecules*. The latter refers simply to the photochemistry of pure enantiomers, with no relationship to asymmetric induction. The former term, however, signifies photochemically induced transfer of optical information (by circular polarized light, for example) to a racemic substrate. This may be accomplished through the CD effect, which produces a difference in sensitivities between the enantiomers of a compound to left-polarized and right-polarized light. Consequently, it might be the case that only one enantiomer would be excited by light carrying specific chiral information. A fruitful combination of a photochromic compound with a distinct optically active moiety would give rise to an information storage system capable of storing twice as much information as one without a chiral attachment.

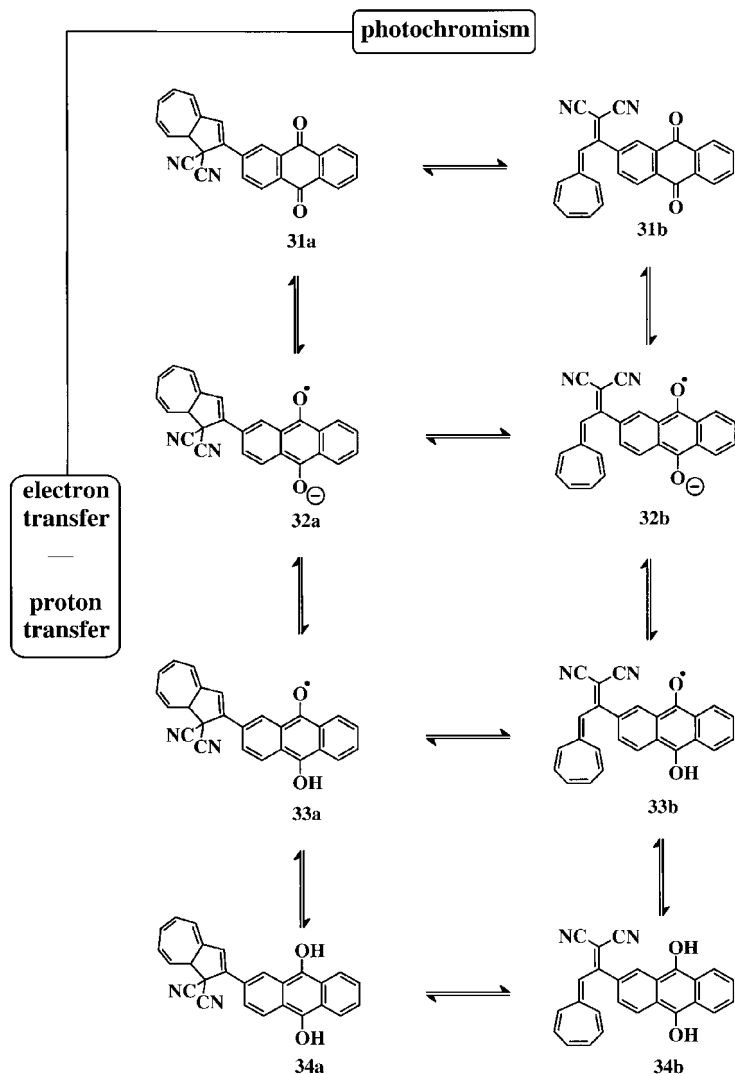
The chiral information intrinsic to the **DHA** system is vested in the asymmetric **C-8a**. In the case of the **DHA/VHF** couple, this information would be destroyed by the photochemical transformation into the prochiral **VHF**, since the thermal recyclization would, in the absence of a chiral 'flag', produce the racemate.^[30] In the presence of a chiral auxiliary, however, the prochiral **VHF** might be expected to turn back into the **DHA**, with the same chiral information as before. Thus, in a racemic mixture consisting of molecules designed according to such a system, information could be read out by application of circular polarized light, which would trigger 50 % of the substrate (first information output). Scanning with light of the opposite polarity would give the second information output stored in the racemic mixture.

One approach towards such a system was accomplished by the synthesis and examination of (*S*)-1,1'-binaphthyl-2,2'-diyl bis[4-(1,1-dicyano-1,8a-dihydro-(8*S*)-azulen-2-yl)]-benzoate (**30a**), monitoring its photochromic behavior by UV/Vis and CD spectroscopy. After irradiation of a solution of **30a** in acetonitrile for 15.5 min, fundamentally altering its spectral properties, subsequent thermal relaxation in the dark for 12h resulted in complete restoration of the UV/Vis and CD spectra. This is a first step towards a powerful **DHA/VHF**-based information storage system controlled by asymmetric induction. Further investigations are underway.



3.2.4.2 Multimode Photochromic Switches Based on DHA-VHF

When covalently attached to electron transfer active subunits, the **DHA-VHF** couple can facilitate chemical and physical switching of electronic properties, as a result of photochemically induced rearrangement accompanied by a change in the redox potential. An interesting example of such a switching system is the compound containing a dihydroazulene component and a covalently attached anthraquinone moiety.^[31] This system is able to act as a multimode switch, assisted by various processes such as photochromism, reversible electron transfer, and protonation-deprotonation reactions (Scheme 8).



Scheme 8: Light-driven multimode molecular switching of the electron transfer active dihydroazulene **31a**.

The redox-active photochromic compound **31a** is reversibly reduced to the quinone radical anion ($E_{1/2} = -780$ mV vs. Ag/AgCl) at a potential slightly less negative than that required for 9,10-anthraquinone ($E_{1/2} = -925$ mV vs. Ag/AgCl) under the same conditions. The cyclic voltammogram of the anthraquinone DHA conjugate **31a** is shown in Figure 21. Further reduction of the radical anion to the dianion occurs irreversibly at $E_{1/2} = -1295$ mV vs. Ag/AgCl at a scan rate of 250 mV, with the formation of a new species identified by an oxidation peak at $E_p = +90$ mV vs. Ag/AgCl. The reduction of **31a** depends upon the solvent and pH. In tetramethylammonium acetate-acetic acid buffer, cyclic voltammetry of compound **31a** revealed a complex electron and proton transfer mechanism, with EC characteristics originating from two one-electron transfer steps, accompanied by fast protonation, leading through the intermediate semiquinone **33a** to the hydroquinone **34a**. This spectroelectrochemical study of compound **31a** reiterates the reversibility of the individual processes observed in the cyclic voltammograms. Under neutral conditions (Figure 22: top), the formation of the radical anion **32a** is indicated by the long wavelength absorption originating from the anthraquinone radical anion. On the other hand, the spectra obtained by multisweep voltammetry of **31a** at pH 5.6 showed two new absorption bands with λ_{max} at around 363 and 465 nm, with the formation of two isobestic points at 400 and 437 nm, indicating the formation of the hydroquinone **34a** (Figure 22/bottom).

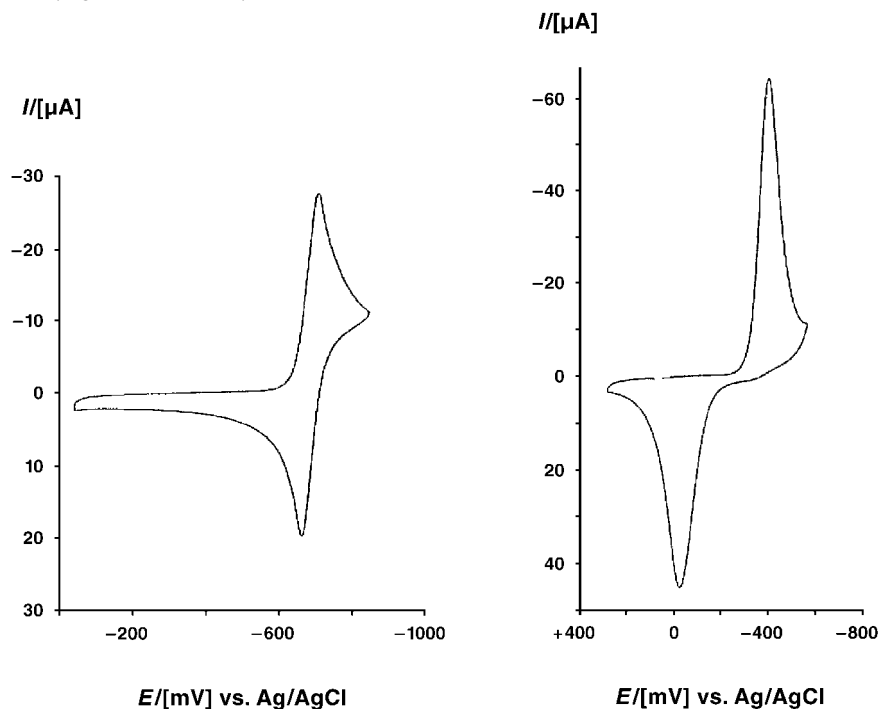


Fig. 21: Cyclic voltammetry of **31a** in acetonitrile as a function of pH. Left: under neutral conditions. Right: at pH 5.6 (ammonium acetate-acetic acid).

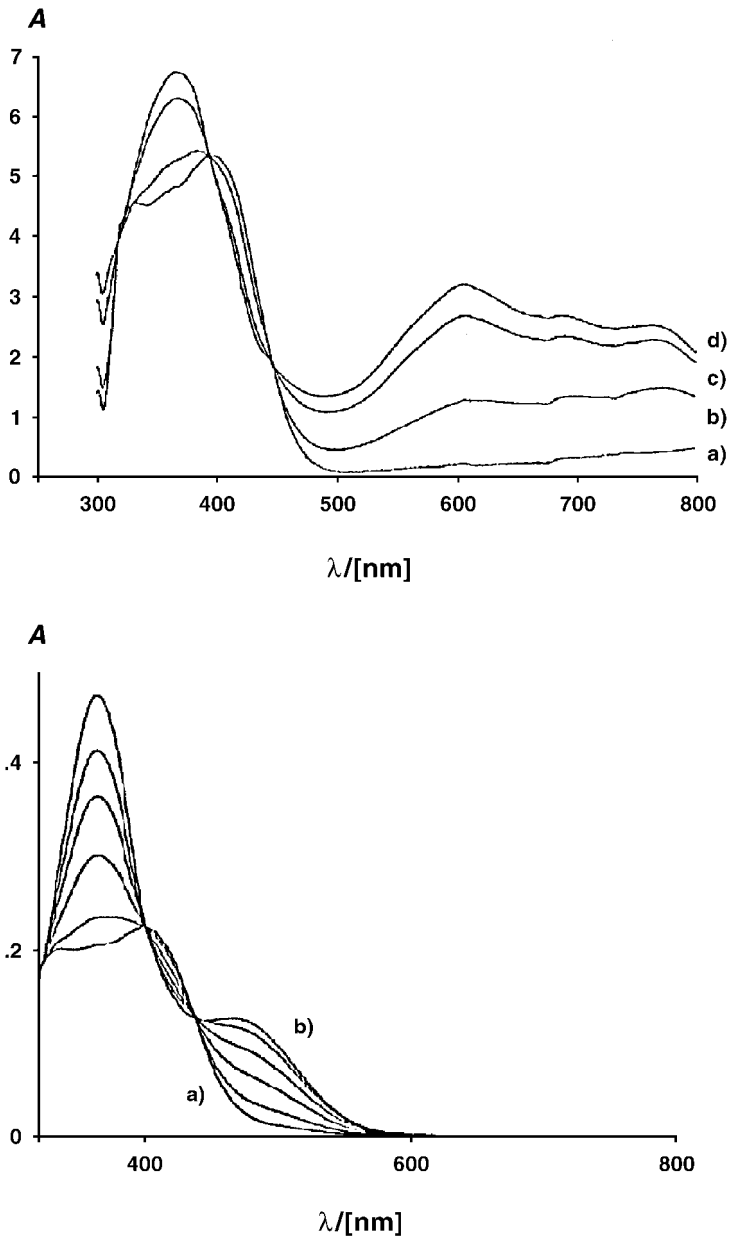


Fig. 22: Spectra obtained by multisweep voltammetry of **31a** as a function of pH. Top: in acetonitrile: (a) 0 mV, (b) -800 mV, (c) -900 mV, (d) -950 mV (vs. Ag/AgCl). Bottom: in acetonitrile at pH 5.6 (trimethylammonium acetate-acetic acid buffer): (a) 0 mV, (b) 700 mV (vs. Ag/AgCl).

It is interesting to note that the photochromic behavior of **31a** depends upon the solvent and the pH used during the irradiation. In dichloromethane and chloroform, the photochemical rearrangement of **31a** and its thermal back reaction is clear (Figure 23: top), whereas in acetonitrile the photochemical rearrangement could not be observed. Interestingly, the hydroquinone **34a** obtained by the electrochemical reduction of **31a** at pH 4–5 showed only a minor change in the absorption spectrum even after prolonged irradiation, as shown in Figure 23 (bottom). The switching signals obtained by photomodulation amperometry of a homogeneous solution of the anthraquinone **31a** are shown in Figure 24. During light-induced rearrangement of **31a** into **31b**, the reduction potential decreases and a fast electron transfer takes place, reducing **31b** to the corresponding radical anion and causing a cathodic current which retreats after interruption of the light source. Obviously, because of the fast electron transfer, even a small amount of the photochemically generated VHF-anthraquinone conjugate **31b** is sufficient to create the photomodulation pattern as shown in Figure 24.

Heteroaryl-functionalized DHA-VHF photochromic systems are another interesting class of multimode photochromic switches.^[32] Electron-rich heteroaromatic subunits such as 1'-dibenzodioxinyl, 1'-thianthrenyl, 4'-phenoxathiinyl, 3'-phenothiazinyl, 3'-phenoxazinyl, and 2'-dimethylphenazinyl, when attached to the dihydroazulene chromophore, are found to be potential candidate multimode switches for information data storage^[33]. The multimode redox switching and photochemical switching of electronic properties of such systems are depicted in Figure 25. In order to verify the viability of the multimode switching processes shown in Figure 25, a series of compounds consisting of the DHA system linked to those heteroaromatic subunits mentioned have been synthesized and subjected to detailed photochromic, redox, and spectroelectrochemical investigation.

The structures of the systems under investigation and the various processes involved in their photochemical and electrochemical switching are illustrated in Scheme 9.

Except for DHA **40a**, all DHA derivatives exhibit photochromic behavior at ambient temperature, with the formation of the characteristic long wavelength absorption band of the corresponding VHF (**35–39b**). As a representative case, the change in the absorption spectrum of the DHA **37a** is shown in Figure 26. The long wavelength absorption bands of the DHAs were found to be considerably influenced by the donor strength and the substitution pattern of the attached heteroaromatic system, as we had noticed in earlier studies. For example, the DHA derivatives (**38–40a**), which are less sterically hindered because of their C-2-C-3' {2'} linkages, exhibited bathochromic shifts in the absorption maxima with increasing donor strength of the heteroaromatic subunit. On the other hand, DHAs such as the thianthrene derivative **36a**, in which the heteroaromatic subunits are joined in the C-2-C-1' {4'}-fashion, showed significant hypsochromic shifts. Nevertheless, the absorption spectra of the corresponding VHFs are less dependent on the substituents at C-9.

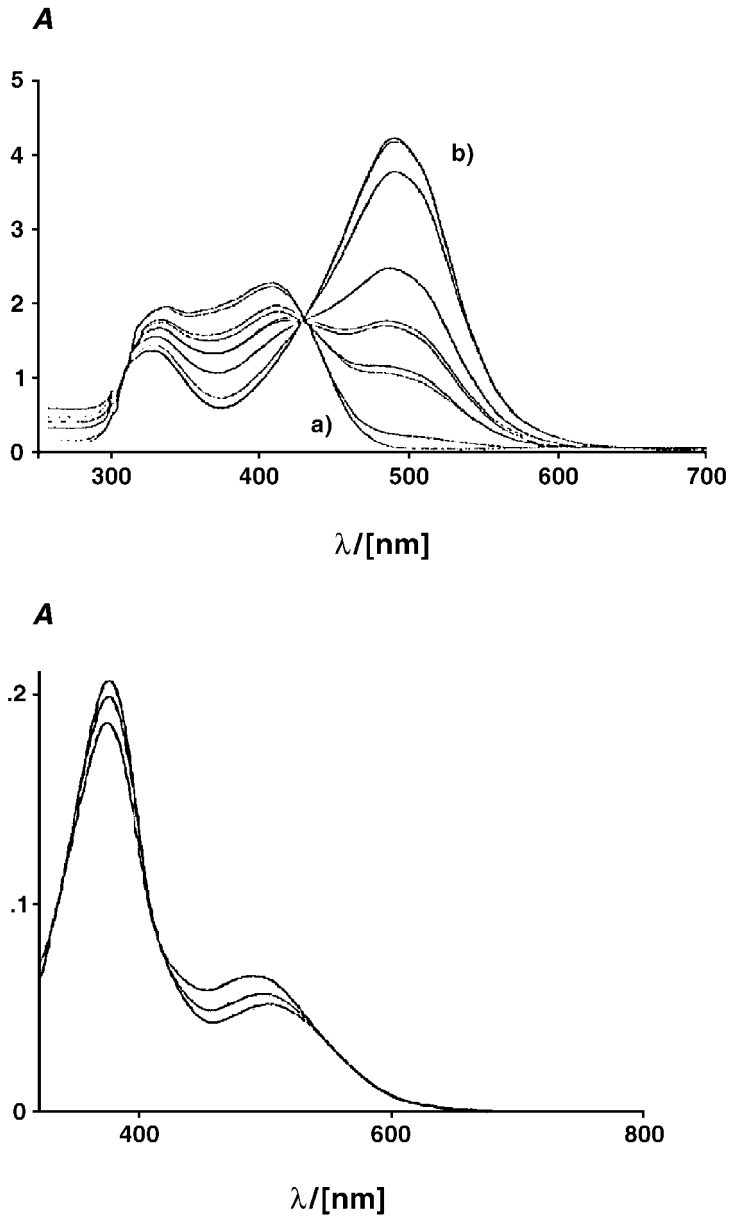


Fig. 23: Spectral changes upon irradiation of **31a**. Top: in dichloromethane, (a) before irradiation, (b) after 1 min irradiation with an Osram HWLS 500 W lamp. Bottom: in dichloromethane at pH 4–5, irradiation with a daylight lamp after reduction to hydroquinone **34a**.

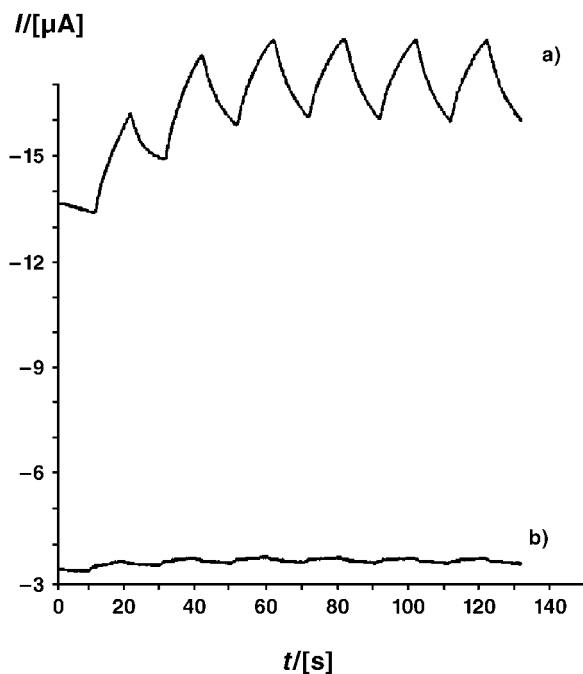


Fig. 24: Pulsed irradiation of a homogenous solution of anthraquinone **31a**, in acetonitrile ($c = 8.9 \times 10^{-4} \text{ mol dm}^{-3}$), at room temperature. Working potential: (a) -800 mV , (b) -700 mV (vs. Ag/AgCl). Switching sequence – light on: 10s, light off: 10s.

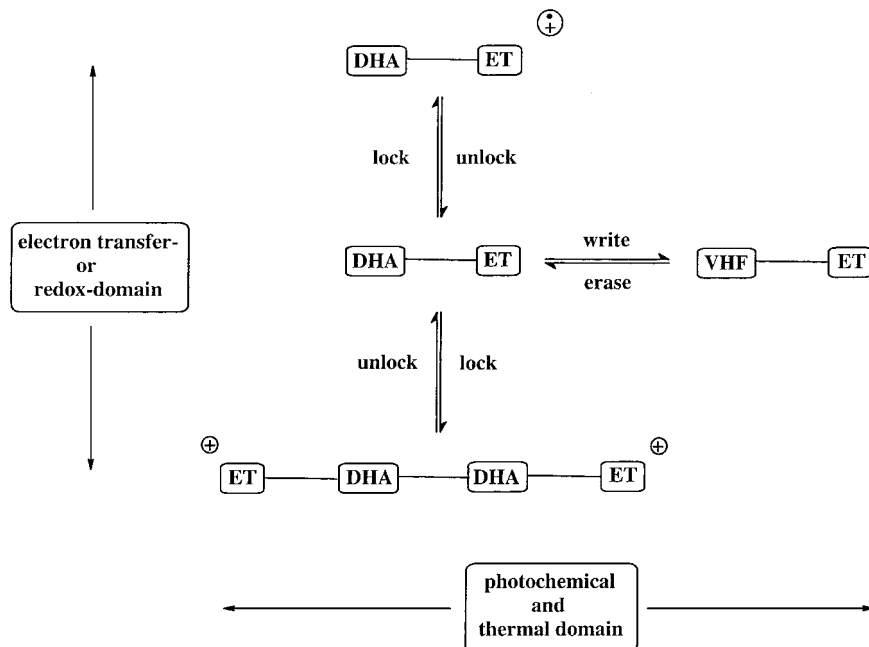
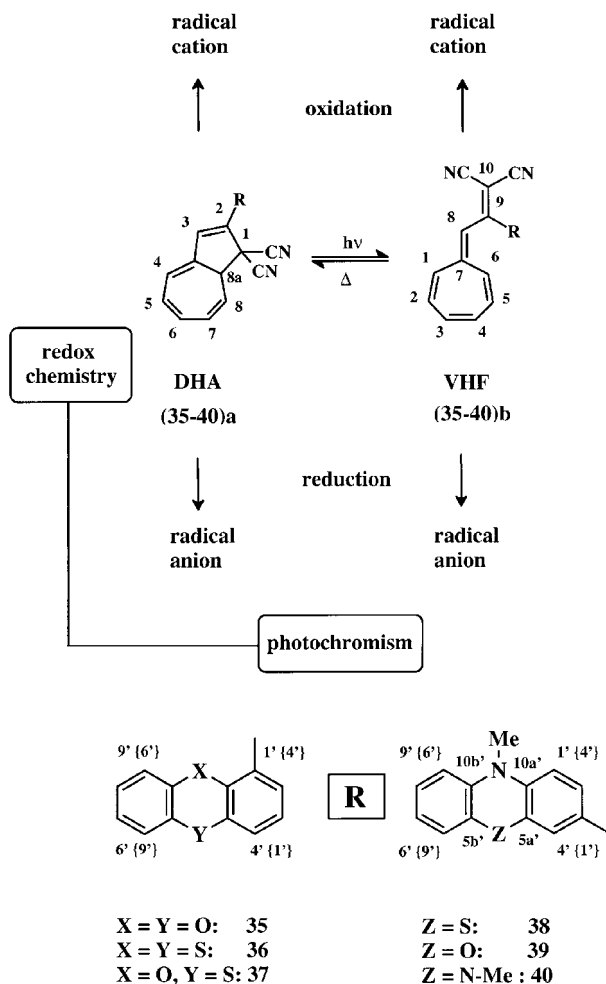


Fig. 25: Information storage in dihydroazulene/vinylheptafulvene systems attached to heteroaromatic groups.



Scheme 9: Photochromic and redox behavior of the **DHA/VHF** subunit, and the various heteroatomic groups used as substituents at C-2 of the five-membered ring.

Switching of the redox properties of (35–40)a has been examined by means of cyclic voltammetry and UV/Vis/NIR spectroelectrochemistry. For all **DHA-VHF** couples, we have observed three different *I/E* (current/potential) responses:

- 1) a reversible anodic wave ($E_{1/2}$ (het-ox)) for the oxidation of the heterocyclic structures of the **DHA** and **VHF** forms;
- 2) the waves (E_{pa} (ring-ox)/ E_{pc} (ring-ox)), which signify the electrochemical oxidation (quasireversible or irreversible electrode process) of the dihydroazulene and vinylheptafulvene subunits, respectively;
- 3) the irreversible cathodic waves (E_{pc} (ring-red)) due to the reduction of the **DHA-VHF** subunits.

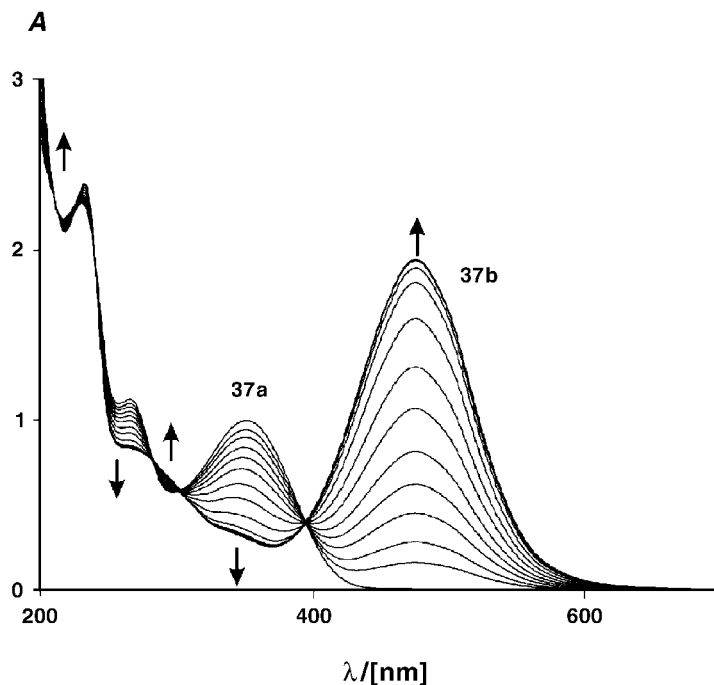


Fig. 26: Appearance of the long wavelength absorption of VHF 37b upon irradiation of DHA 37a in acetonitrile (20 °C, λ_{irr} : 260–390 nm).

The typical cyclic voltammograms of DHA 35a, before (unbroken line) and after (dashed line) irradiation (15 min) in daylight in acetonitrile, are shown in Figure 27. The broken line is assigned to the photoisomer VHF 35b, and is significantly different from that of the corresponding DHA 35a.

The thin layer cyclovoltammogram of 35a showed two independent oxidation processes: (i) an irreversible wave at $E_{pa} = 1034$ mV (vs. Fc/Fc⁺) ($E_{pc} = -232$ mV (vs. Fc/Fc⁺)) and (ii) a reversible wave ($E_{1/2}$ (het-ox)), which corresponds to the formation of the radical cation of the dibenzodioxin subunit (Figure 28). The irreversible wave represents a two-step process involving a one-electron oxidation of the DHA subunit followed by a chemical step (EC-type mechanism) leading to a significant change in the molecular structure. Since polyenic radical cations have a preference for dimerization,^[34] it is reasonable to speculate on the formation of the dimeric dication species as shown in structure 41. The chemical reversibility of this EC-type process was confirmed by multisweep thin layer experiments.

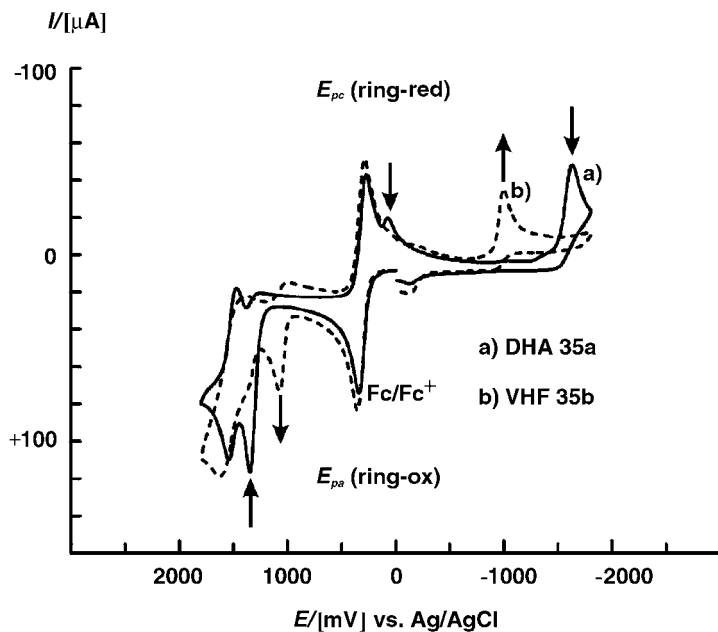
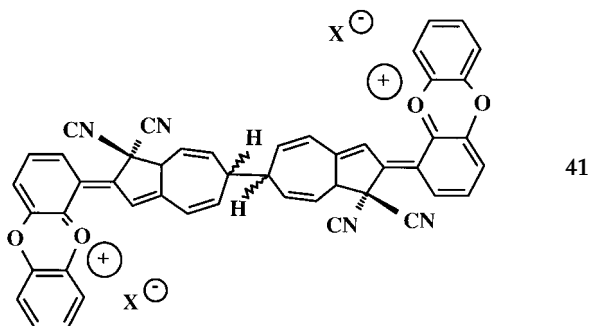


Fig. 27: Cyclic voltammogram of **DHA 35a** before (a) and after (b) irradiation (15 min) with daylight. Solvent: acetonitrile; $\nu = 250 \text{ mV s}^{-1}$.



This interpretation of the irreversible oxidation wave (E_{pa} (ring-ox)) as being caused by the formation of the dimeric dication species **41** can be further substantiated by spectroelectrochemical studies. Figures 29 and 30 display spectroelectrograms for the first oxidation waves of the **DHAs 35a** and **39a**. As foreseeable from the significantly different oxidation potentials, the features of the spectra are completely different, indicating varying regiochemistry in the oxidation processes. On electrochemical oxidation of the **DHA 35a**, the absorption of the neutral form at 353 nm decreases, while a strong band, too short to be attributable to the radical cation of **DHA 35a**, appears at 438 nm (Figure 29). In the case of **DHA 39a**, on the other hand, the long wavelength absorptions at 545 and 860 nm can be assigned to the

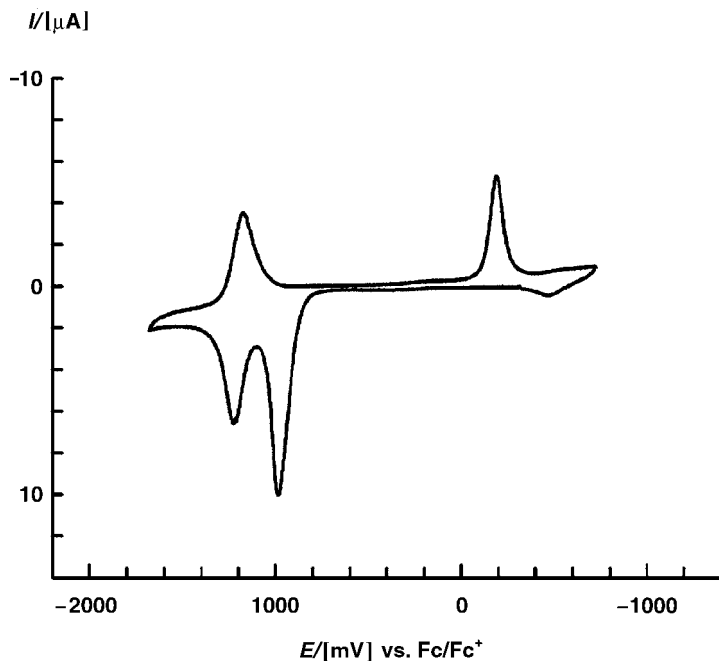


Fig. 28: Thin layer cyclic voltammogram of DHA 35a in acetonitrile; $\nu = 25 \text{ mV s}^{-1}$.

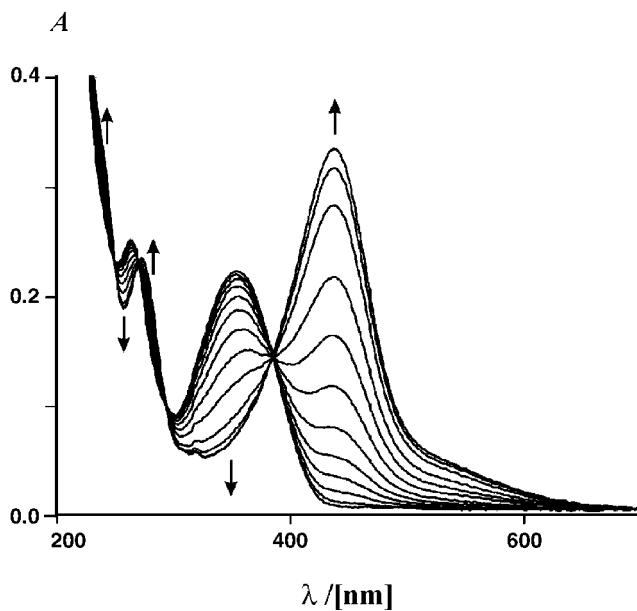


Fig. 29: Spectroelectrogram obtained on oxidation of DHA 35a to the dimeric dication 41 (solvent: acetonitrile).

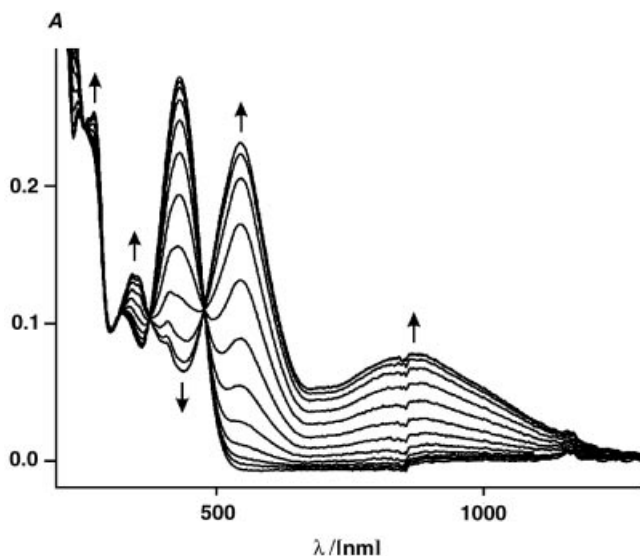


Fig. 30: Spectroelectrogram obtained on oxidation of **DHA 39a** to the radical cation **DHA 39a⁺** (solvent: acetonitrile).

radical cation (Figure 30). Thus, **DHAs** with weak donor substituents (**DHA (35–37)a**) undergo oxidative dimerization ('lock'-state), and such systems satisfy the requirements for application in information storage.

A strategy to enable multifold switching in macromolecular systems is briefly described below. On the basis of previous work, which showed that switchable and conducting films can be obtained by electropolymerization of 1,3-unsubstituted azulenes (Figure 31),^[35] investigations were carried out on **DHA/azulene** derivatives.^[36]

It was found that azulene derivative **42a** is non-photochromic at room temperature. The same was true for derivative **43a**. Obviously, if **DHA** and azulene subunits are strongly coupled, as in **42a** and **43a**, then photophysical deactivation processes must quench photochemical ring-opening. By careful screening of spacer-linked azulene/**DHA** conjugates, however, we found that amide-linked derivative **44a** clearly gave rise to ring-opening under photochemical conditions (Figure 32).

Monomer **44a** was also found to electropolymerize on indium-tin-oxide (ITO) under potential-sweep conditions (Figure 33). The resulting film (*poly-44a*) can be electrically doped by oxidation, as was demonstrated by UV/Vis spectroelectrochemistry (oxidative dotation leads to a broad absorption band beyond 1000 nm). We found that on irradiation with a 500 W incandescent lamp the pristine film (at 0 mV vs. Ag/AgCl) gave rise to the formation of the **VHF** form (*poly-44b*). Under thermal conditions, the **DHA** spectrum could be restored (Figure 34).

Recently, Diederich and co-workers have made use of the **DHA-VHF** system for designing a three-way chromophoric molecular switch, which can be controlled by pH, light, and heat.^[37] The system is based on a molecule with three addressable subunits, that can undergo individual, reversible switching cycles. These processes

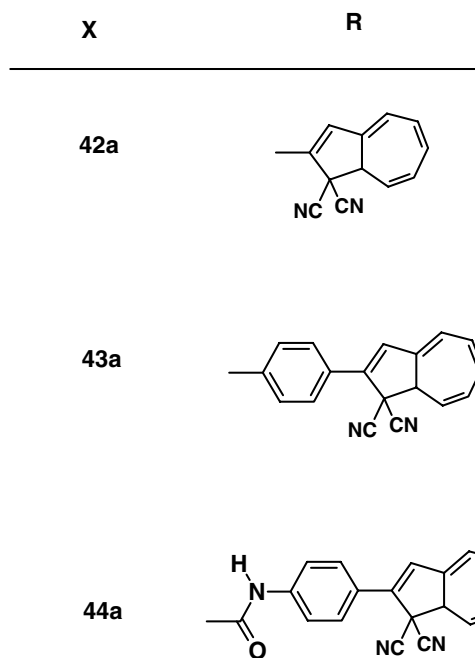
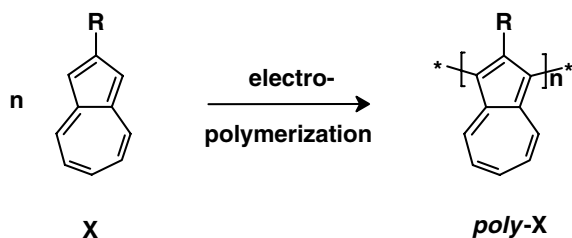


Fig. 31: DHA/azulene conjugates.

are illustrated in Scheme 10. With three possible switching processes, the molecule 45 can theoretically adopt eight interconvertible states, of which six states can be detected. Interestingly, the reversible conversions of *trans*-45a to *trans*-45a⁺ and to *trans*-45b⁺ function like an AND logic gate; the *trans*-45b⁺ state can be obtained only in the presence of protons and light. In addition, three write/erase processes are also possible in system 45: these are the reversible *cis*–*trans* photoisomerization between *trans*-45a and *cis*-45a, and the two reversible protonation/deprotonation processes of the *trans*-45a/*cis*-45a and *trans*-45a⁺/*cis*-45a⁺ couples. Since the fluorescence enhancement after deprotonation of 45a⁺ amounts to a factor of about 300, a very efficient, nondestructive information readout is available in the shape of the *cis*-45a/

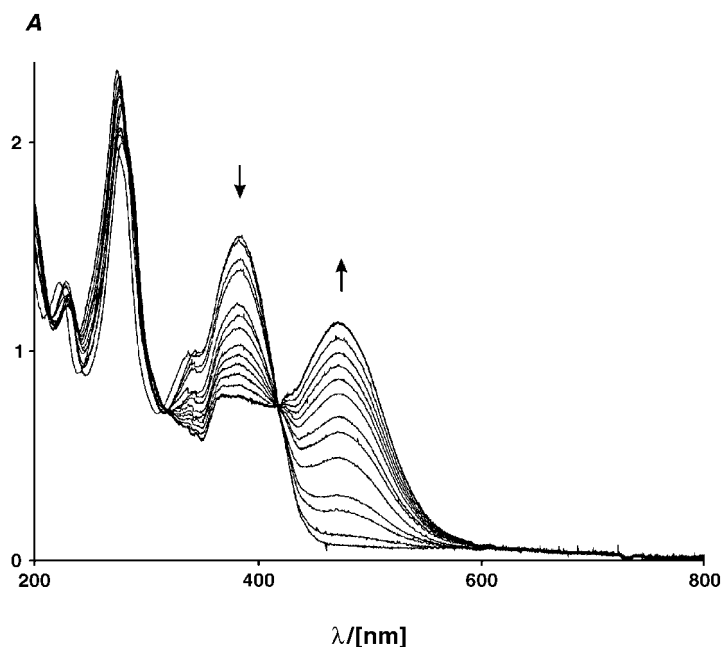


Fig. 32: Spectral changes on irradiation of **44a** (Hg/Xe lamp, Schott filter UG11, transmittance 250–390 nm) in acetonitrile ($c = 4.6 \times 10^{-5} \text{ mol dm}^{-3}$). Time of irradiation (seconds): 0, 5, 15, 25, 35, 45, 55, 75, 95, 110, 140, 200, 355.

45a⁺ and *trans*-**45a**/**45a**⁺ couples, at $\lambda_{\text{emission/45a}} = 606 \text{ nm}$, by using excitation light of 396 nm for the *cis* isomer and 464 nm for the *trans* isomer.

In a recent development, the concept of multimode molecular switching in a cyclic four-stage process has been introduced in the form of a structurally fused photochromic system comprising a **DHA** component and a dithienylethene (**DTE**) moiety (Scheme 11)^[38]. The open/open **47** and the closed/closed **48** are rapidly formed on irradiating the open/closed **46**. The open/open **47** rearranges thermally to **46**, whereas **48** can be made to revert to **46** photochemically. Figure 35 shows the spectral properties associated with these interconversions. This is the first attempt towards an electronically strongly coupled molecular switch, combining the **DHA-VHF** photochromic system with the well known dithienylethene system. In principle, this can give rise to four different switchable states: **46**, **47**, **48**, and **49**. However, the closed/open form **49** has not yet been observed in this system for the substitution pattern $R^1=R^2=\text{CH}_3$. It is expected that appropriate donor and acceptor groups at the dithienylethene moiety may facilitate its formation, and this is under investigation.

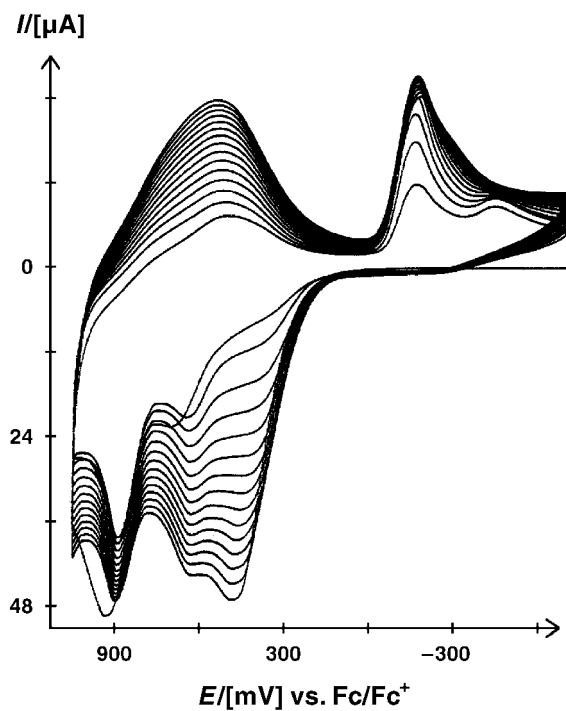


Fig. 33: Multisweep cyclic voltammogram of **44a** in acetonitrile (0.1 mol dm^{-3} TBAHFP, Pt electrode, $\nu = 250 \text{ mV s}^{-1}$): Synthesis of *poly-44a* is shown.

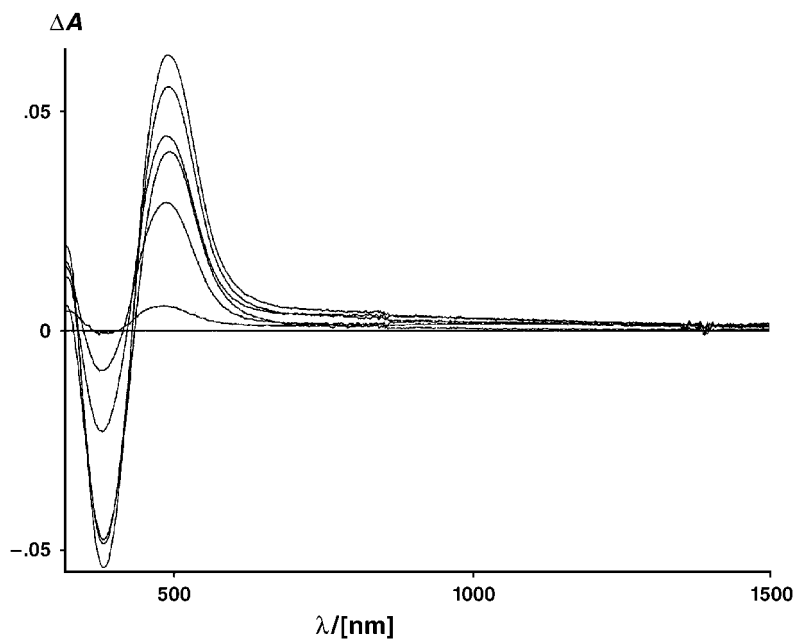
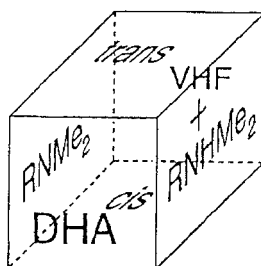
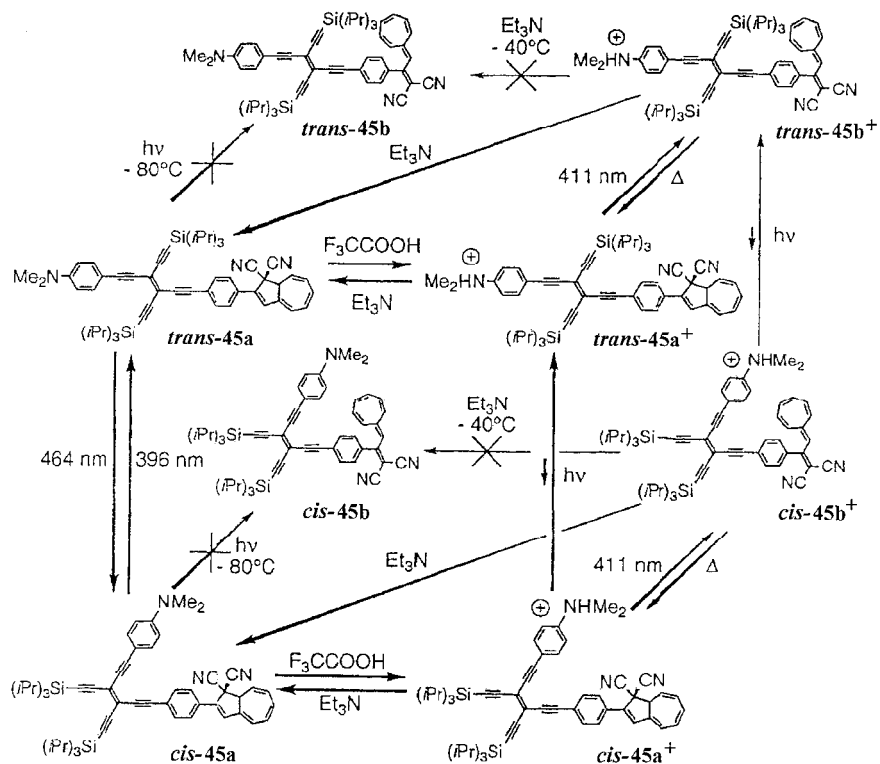
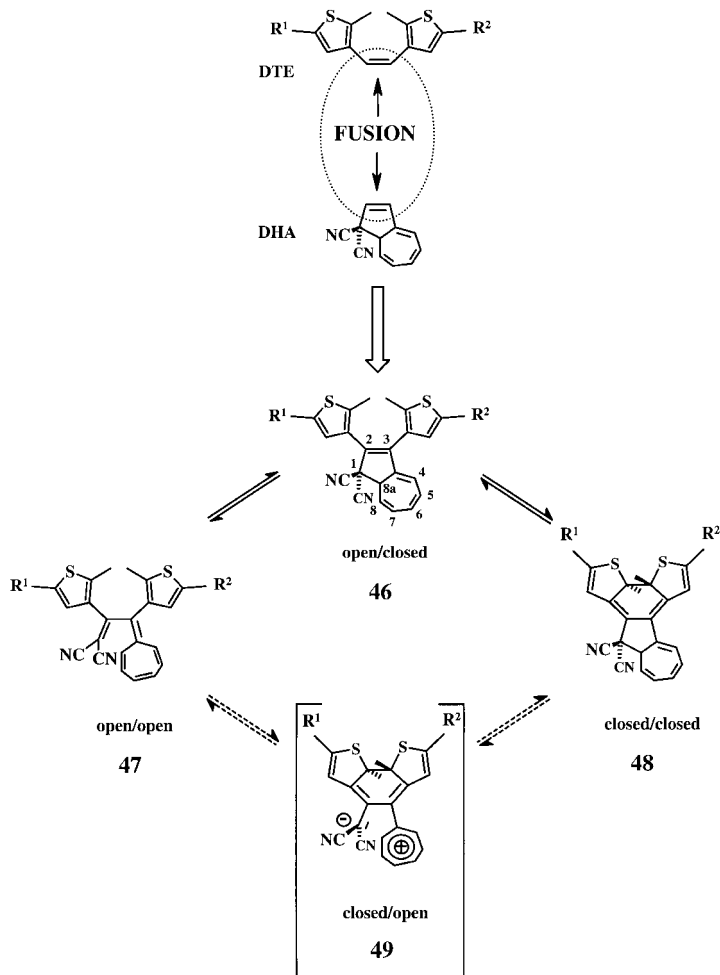


Fig. 34: UV/Vis/NIR difference spectra on irradiation of *poly-44a*. Irradiation times (min): 0, 4, 5, 7, 11, 16, 21.



Scheme 10: Three-dimensional switching diagram of compound 45. The eight possible states are shown as the corners of a cube.



Scheme 11: Conception for a four-step cyclic process with biphotocromic compounds. The notation 'open/closed' for isomer **46** refers to the dithienyl moiety in its 'open' constitution and the dihydroazulene moiety in its 'closed' one. This notation applies equally to **47**, **48**, and **49**.

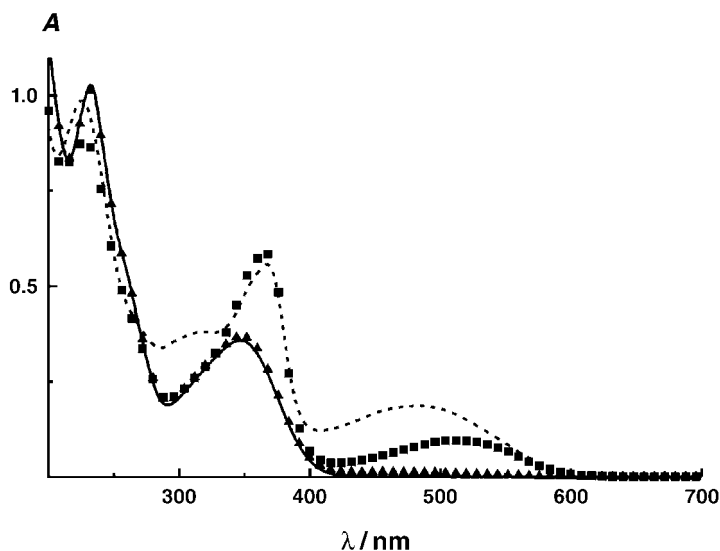


Fig. 35: Reversible irradiation of **46** in cyclohexane (4.4×10^{-5} mol dm $^{-3}$) at room temperature: **46** prior to (—) and after irradiation at 254 nm (- -), after thermal relaxation (■), and after subsequent irradiation with visible light (≥ 450 nm), in which **46** is restored (▲).

3.3 Future Directions

It has been predicted that what electrons did for the twentieth century, photons may do for the twenty-first. The reason is that photons can effect switching of properties in a shorter time scale and can carry information much more quickly, more efficiently, and over longer distances than electrons can. Therefore, considerable efforts have been directed in recent years toward the design of photoactive organic molecules, the physical properties of which can be manipulated by means of light. However, the major problems inherent in such molecules are their difficulties associated with device fabrication, due to a lack of processability and stability at various device operating conditions. On the other hand, polymers are more adaptable to structural manipulation and device fabrication and hence play a key role in the designing of advanced materials for optoelectronic and photonic devices. As a result, during the past decade, organic and polymer chemists have joined the quest to develop novel materials for various advanced technological applications. Even though there exist several studies pertaining to the use of photoswitchable organic molecules as photonic devices in combination with solid matrices such as polymers and sol-gels, their use as integral components of conjugated macromolecular systems to control the optoelectronic properties of the latter has not received adequate attention.^[39] Processable and stable polymers possessing optoelectronic properties that can be controlled by photoswitches may well emerge as novel materials for optoelectronic

applications. In this context, the integration of photochromic systems such as dihydroazulenes and diarylethenes with appropriate conjugated polymers would be of great interest, particularly from the viewpoint of device fabrication. Although these areas imply technological applications, the state of the art is at a stage that requires considerable basic research input to build a solid foundation for the development of future technologies. Our future activities will be oriented towards designing macromolecular systems, based on **DHA-VHF** photochromism, possessing switchable optoelectronic properties such as electrical conductivity, light emitting properties, and NLO activity.

3.4

Conclusions

Recent studies of **DHA-VHF** photochromism have demonstrated that this all-carbon system can be used as an active component of a molecular switch. Photoinduced ring-opening of **DHAs** to the corresponding **VHFs** brings the electron-withdrawing cyano groups into conjugation with the π -system, thus engendering strong perturbations in electronic properties. Incorporation of appropriate functional moieties, possessing strong fluorescence and donor-acceptor interaction capabilities, into the **DHA-VHF** photochromic system can therefore lead to novel organic materials with switchable fluorescence, light emitting properties, and NLO activity. Nevertheless, the substitution and structure patterns currently in use do not allow for reversion of **VHFs** back into their corresponding **DHAs** on application of light of a different wavelength. Further molecular engineering studies to overcome this handicap will have to be performed in the future.

References

- 1 a) *Molecular Electronics: Some Directions* (Eds.: J. Jortner, M. Ratner), Blackwell, Oxford, UK, **1997**; b) *Molecular Electronics: Science and Technology* (Eds.: A. Aviram, M. Ratner), The New York Academy of Sciences, New York, **1998**.
c) *Molecular Electronics, Biosensors and Biocomputers* (Ed.: F. T. Houg), Plenum Press, New York, **1989**.
- 2 a) J.-M. Lehn, *Supramolecular Chemistry*, VCH, Weinheim, **1995**, pp. 124–138; b) M. P. Debreczeny, W. A. Svec, M. R. Wasielewski, *Science* **1996**, *274*, 584–587; c) V. Balzani, M. Gomez-Lopez, J. F. Stoddart, *Acc. Chem. Res.* **1998**, *31*, 305–414; d) W. A. Reinerth, L. Jones II, T. P. Burgin, C. Zhou, C. J. Muller, M. R. Deshpande, M. A. Reed, J. M. Tour, *Nanotechnology*, **1998**, *9*, 246–250; e) J.R. Sheats, P.F. Barbara, *Acc. Chem. Res.* **1999**, *32*, 191–192.
- 3 a) J. Daub, T. Knöchel, A. Mannschreck, *Angew. Chem.* **1984**, *96*, 980–981; *Angew. Chem., Int. Ed. Engl.* **1984**, *23*, 960–961; b) V. Balzani, F. Scandola in *Comprehensive Supramolecular Chemistry, Vol. 5* (Ed.: D. N. Reinhoudt), Pergamon-Elsevier, Oxford, **1996**, pp. 687–746; c) B. L. Feringa, W. F. Jager, B. de Lange, *Tetrahedron* **1993**, *49*, 8267–8310; d) *Photochromism, Molecules and Systems* (Eds.: H. Dürr, H. Bouas-Laurent), Elsevier, Amsterdam, **1990**; e) *Organic Photochromic and Thermochromic Compounds* (Eds.: J. C. Crano, R. J. Guglielmetti), Vol. 1 and Vol. 2, Plenum Press, New York, **1999**; f) M. Grätzel, *Coord. Chem. Rev.* **1998**, *171*, 245–250.
- 4 a) A. P. de Silva, H. Q. N. Gunaratne, C. P. McCoy, *J. Am. Chem. Soc.* **1997**, *119*, 7891–7892; b) A. P. de Silva, H. Q. N. Gunaratne, T. Gunnlaugsson, A. J. M. Huxley, C. P. McCoy, J. T. Rademacher, T. E. Rice, *Chem. Rev.* **1997**, *97*, 1515–1566; c) K. Rurack, M. Kollmannsberger, U. Resch-Genger, J. Daub, *J. Am. Chem. Soc.* **2000**, *122*, 968–969.
- 5 a) R. Bergonzi, L. Fabbrizzi, M. Licchelli, C. Mangano, *Coord. Chem. Rev.* **1998**, *170*, 31–46; b) J. Otsuki, K. Harada, K. Araki, *Chem. Lett.* **1999**, 269–270.
- 6 V. Goulle, A. Harriman, J.-M. Lehn, *J. Chem. Soc., Chem. Commun.* **1993**, 1034–1036.
- 7 K. Schaumburg in *Nanostructures Based on Molecular Materials* (Ed.: W. Göpel, C. Ziegler), VCH, Weinheim, **1992**, 153–173.
- 8 R. Deans, A. Niemz, E. C. Breinlinger, V. M. Rotello, *J. Am. Chem. Soc.* **1997**, *119*, 10863–10864.
- 9 I. Willner, *Acc. Chem. Res.* **1997**, *30*, 347–356.
- 10 J. Daub, M. Beck, A. Knorr, H. Spreitzer, *Pure Appl. Chem.* **1996**, *68*, 1399–1404.
- 11 a) M. Kollmannsberger, T. Gareis, S. Heinel, J. Breu, J. Daub, *Angew. Chem.* **1997**, *109*, 1391–1393; *Angew. Chem., Int. Ed. Engl.* **1997**, *36*, 1333–1335; b) T. Werner, Ch. Huber, S. Heinel, M. Kollmannsberger, J. Daub, O. S. Wolfbeis, *Fresenius J. Anal. Chem.* **1997**, *359*, 150–154; c) M. Kollmannsberger, K. Rurack, U. Resch-Genger, J. Daub, *J. Phys. Chem. A.* **1998**, *102*, 10211–10220.
- 12 Z. Sekkat, W. Knoll, *Proc. SPIE-Int. Soc. Opt. Eng.* **1997**, *2998*, 164–184.
- 13 a) J. Whittall in *Photochromism: Molecules and Systems*, (Ed.: H. Dürr, H. Bouas-Laurent), Elsevier, Amsterdam, **1990**, 467–492; b) Y. C. Liang, A. S. Dvornikov, P. M. Rentzepis, *Res. Chem. Intermed.* **1998**, *24*, 905–914; c) P. J. Darcy, H. G. Heller, P. J. Strydom, J. Whittall, *J. Chem. Soc., Perkin Trans. I* **1981**, 202–205.
- 14 a) M. Irie, K. Uchida, *Bull. Chem. Soc. Jpn.* **1998**, *71*, 985–996; b) A. T. Bens, D. Frewert, K. Kodatis, C. Krysch, H.-D. Martin, H. P. Trommsdorff, *Eur. J. Org. Chem.* **1998**, 2333–2338; c) M. Irie in *Lit. 3e*, Vol. 1, 207–222.
- 15 J. Walz, K. Ulrich, H. Port, H. C. Wolf, J. Wonner, F. Effenberger, *Chem. Phys. Lett.* **1993**, *213*, 321–324.
- 16 a) T. Inada, S. Uchida, Y. Yokoyama, *Chem. Lett.* **1997**, 321–322; b) Y. Yokoyama, S. Uchida, Y. Yokoyama, Y. Sugawara, Y. Kurita, *J. Am. Chem. Soc.* **1996**, *118*, 3100–3107.
- 17 a) C. Weber, F. Rustemeyer, H. Dürr, *Adv. Mater.* **1998**, *10*, 1348–1351.
- 18 a) F. Pina, A. Roque, M. J. Melo, M. Maestri, L. Belladelli, V. Balzani, *Chem. Eur. J.* **1998**, *4*, 1184–1191; b) F. Pina, M. Maestri, V. Balzani, *Chem. Commun.* **1999**, 107–114; c) G. K. Faber, *Nat. Struct. Biol.* **1998**, *5*, 415–417; d) J. Vanhanen, V. P. Leppanen, T. Jaaskelainen, S. Parkkinen, J. P. S. Parkkinen, *Opt. Commun.* **1998**, *153*, 289–294.

- 19 a) J. Daub, S. Gierisch, U. Klement, T. Knöchel, G. Mass, U. Seitz, *Chem. Ber.* **1986**, *119*, 2631–2646; b) S. Gierisch, J. Daub, *Chem. Ber.* **1989**, *122*, 69–75; c) S. Gierisch, W. Bauer, T. Burgemeister, J. Daub, *Chem. Ber.* **1989**, *122*, 2341–2349; d) J. Daub, T. Mrozek, A. Ajayaghosh, *Mol. Cryst. Liq. Cryst.* **2000**, *344*, 41–50.
- 20 J. Daub, C. Fischer, J. Salbeck, K. Ulrich, *Adv. Mater.* **1990**, *2*, 366–369.
- 21 a) H. Görner, C. Fischer, S. Gierisch, J. Daub, *J. Phys. Chem.* **1993**, *97*, 4110–4117; b) H. Görner, C. Fischer, J. Daub, *J. Photochem. Photobiol. A: Chem.* **1995**, *85*, 217–224; c) H. Mrozek, *PhD Thesis*, University of Regensburg, **1993**; d) M. Komma, *Diplomathesis*, University of Regensburg, **1996**.
- 22 a) O. Köthe, *PhD Thesis*, University of Regensburg, **1999**.
- 23 H. Spreitzer, J. Daub, *Liebigs. Ann.* **1995**, 1637–1641.
- 24 a) T. Mrozek, *PhD Thesis*, University of Regensburg, **2000**; b) A. Knorr, *Diploma Thesis*, University of Regensburg, **1992**; c) For recent results using femtosecond-resolved transient absorption spectroscopy, see: J. Ern, M. Petermann, T. Mrozek, J. Daub, K. Kuldova, C. Krysch, *Chem. Phys.* **2000**, *259*, 331–337.
- 25 a) J. Daub, C. Fischer, S. Gierisch, J. Sixt, *Mol. Cryst. Liq. Cryst.* **1992**, *217*, 177–185; b) C. Fischer, J. Daub, *Chem. Ber.* **1993**, *126*, 1631–1634.
- 26 a) J. Daub, J. Salbeck, T. Knöchel, C. Fischer, H. Kunkely, K. M. Rapp, *Angew. Chem.* **1989**, *101*, 1541–1542; *Angew. Chem., Int. Ed. Engl.* **1989**, *28*, 1494–1496; b) J. Daub, K. M. Rapp, J. Salbeck, U. Schöberl in *Carbohydrates as Organic Raw Materials* (Ed.: F. W. Lichtenthaler), VCH, Weinheim, **1991**, pp.323–350.
- 27 J. Daub, S. Gierisch, J. Salbeck, *Tetrahedron Lett.* **1990**, *31*, 3113–3116.
- 28 a) M. Sisido in *Photo-React. Mater. Ultrahigh Density Opt. Mem.* (Ed.: M. Irie), Elsevier, Amsterdam, **1994**; b) N. P. M. Huck, W. F. Jager, B. de Lange, B. L. Feringa, *Science* **1996**, *273*, 1686–1688; c) L. Eggers, V. Buss, *Angew. Chem.* **1997**, *107*, 885–887; *Angew. Chem., Int. Ed. Engl.* **1997**, *36*, 881–883; d) K. S. Burnham, G. B. Schuster, *J. Am. Chem. Soc.* **1998**, *120*, 12619–12625; e) Y. Yokoyama, S. Uchida, Y. Yokoyama, T. Sagisaka; Y. Uchida, T. Inada, *Enantiomer* **1998**, *3*, 123–132; f) A. Manschreck, K. Lorenz and M. Schinabeck in Lit. 3b), Vol. 2, 261–295.
- 29 a) H. Rau, *Chem. Rev.* **1983**, *83*, 535–547; b) Y. Inoue, *Chem. Rev.* **1992**, *92*, 741–770; c) M. Sakamoto, M. Takahashi, T. Arai, M. Shimizu, T. Mino, S. Watanabe, T. Fujita, K. Yamaguchi, *J. Chem. Soc., Chem. Commun.* **1998**, 2315–2316; d) N. Koumura, N. Harada, *Chem. Lett.* **1998**, 1151–1152.
- 30 a) P. A. Bross, *PhD Thesis*, University of Regensburg, **1992**; b) G. Beer, *PhD Thesis*, University of Regensburg, **2001**.
- 31 J. Achatz, C. Fischer, J. Salbeck, J. Daub, *J. Chem. Soc., Chem. Commun.* **1991**, 504–507.
- 32 H. Spreitzer, J. Daub, *Chem. Eur. J.* **1996**, *2*, 1150–1158.
- 33 a) A. P. de Silva, C. P. McCoy, *Chem. Ind.* **1994**, 992–996; b) L. F. Lindon, *Nature (London)* **1993**, *364*, 17–18; c) A. Aviram, *J. Am. Chem. Soc.* **1988**, *110*, 5687–5692.
- 34 a) J. Bindl, P. Seitz, U. Seitz, E. Salbeck, J. Salbeck, J. Daub, *Chem. Ber.* **1987**, *120*, 1747–1756; b) M. Baumgarten, K. Müllen, *Top. Curr. Chem.* **1994**, *169*, 1–103.
- 35 a) J. Daub, M. Feuerer, E. Mirlach, J. Salbeck, *Synthetic Metals*, **1991**, *41–43*, 1551–1555; b) A. Mirlach, M. Feuerer, J. Daub, *Adv. Mater.* **1993**, *5*, 450–453; c) W. Schuhmann, J. Huber, A. Mirlach, J. Daub, *Adv. Mater.* **1993**, *5*, 124–126; d) M. Porsch, G. Sigl-Seifert, J. Daub, *Adv. Mater.* **1997**, *9*, 635–639; e) F. X. Redl, O. Köthe, K. Röckl, W. Bauer, J. Daub, *Macromol. Chem. Phys.* **2000**, *201*, 2091–2100.
- 36 P. A. Bross, A. Mirlach, J. Salbeck, J. Daub, *Dechema-Monographien* **1990**, *121*, 375–382.
- 37 L. Gobbi, P. Seiler, F. Diederich, *Angew. Chem.* **1999**, *111*, 737–740; *Angew. Chem., Int. Ed. Engl.* **1999**, *38*, 674–677.
- 38 a) T. Mrozek, H. Görner, J. Daub, *Chem. Commun.* **1999**, 1487–1488; b) T. Mrozek, H. Görner, J. Daub, *Chem. Eur. J.* **2001**, *7*, no. 5, 1028–1040.
- 39 Y. Atassi, J. Chauvin, J. A. Delaire, J.-F. Delouis, I. Fanton-Maltesy, K. Nakatani, *Pure Appl. Chem.* **1998**, *70*, 2157–2166.

4

Molecular Switches with Photochromic Fulgides

Y. Yokoyama

4.1

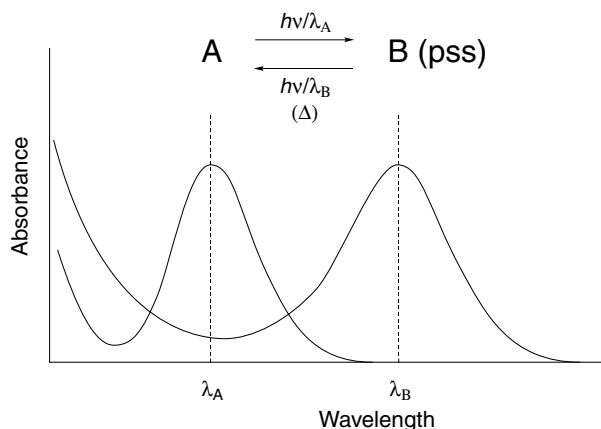
Introduction

4.1.1

Photochromism

“Photochromism” may be defined as the “reversible transformation of a single chemical species, being induced in one or both directions by electromagnetic radiation between two states having different distinguishable absorption spectra.”^[1] Therefore, photochromism itself has the nature of a “switch” inherent in it: photochromic substances change their structures as a result of the action of light, and the changes in structure cause switching of physical and chemical properties, as well as switching of interaction with molecular environments. Alterations in absorption spectra are one such property change (Scheme 1).

The reason why the change in absorption spectrum is important is that, when the absorption bands of individual species undergoing irradiation are widely separated, the relative proportions of the species involved can usually be altered markedly. In these cases, the associated properties can be “switched”, rather than merely “changed”.

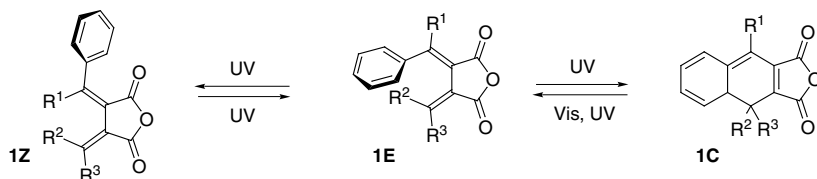


Scheme 1: Photochromism.

4.1.2

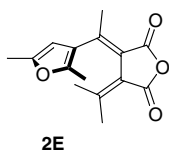
Fulgides^[2]

Fulgides, the common name for bismethylenesuccinic anhydrides possessing at least one aromatic ring on the methylene carbon atoms, such as **1**, were first, and extensively, synthesized by Stobbe early in the 20th century.^[3]



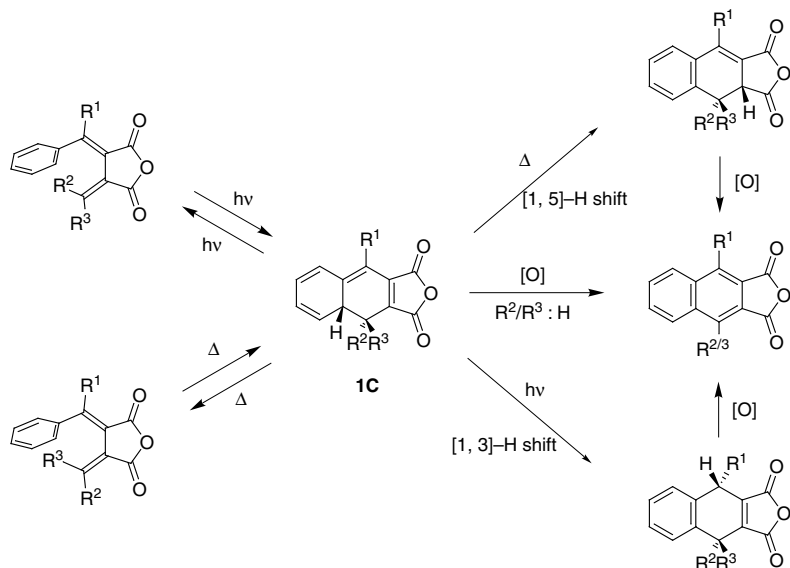
Upon UV irradiation, the colorless (or faintly colored) isomer of a fulgide (E form, **1E**), incorporating a 1,3,5-hexatriene moiety, changes through electrocyclic reaction into a deeply colored isomer (C, or “colored”, form). The process obeys the Woodward–Hoffmann rules (i.e., the photochemical rearrangement occurs in conrotatory fashion).^[4] During UV irradiation, the E form also converts into another colorless form (Z form) as the result of simple photochemical *E*–*Z* double bond isomerization. As the C form and Z form also absorb UV light, interconversions between E and Z forms, and between E and C forms, continue until a photostationary state (pss) is reached. On the other hand, because only the C form absorbs visible light, irradiation of the C form (or the photostationary state) by visible light induces only the transformation from the C form to the E form, until the C form disappears completely. Since change in absorption is the requirement for photochromism, the transformation between E and C forms is usually termed fulgide photochromism.

Thanks to the fulgides’ succinic anhydride moiety, modification to obtain more sophisticated photochromic molecules has been easy. This chapter deals with imides (fulgimides), diesters (fulgenates), and some other derivatives, as well as fulgides themselves.



Since 1981, when Heller and co-workers synthesized a furylfulgide **2**,^[4] fulgides have included representatives of thermally irreversible photochromic compounds among their number. Fulgides known until then had been thermally reversible. Three major modifications were made to the fulgide structure:

- the introduction of a methyl group on the ring-forming carbon atom of the aromatic ring,
- the use of a heteroaromatic ring such as furyl or thienyl instead of phenyl, and



Scheme 2: Possible photochemical and thermal reactions of phenylfulgides.

- the use of an isopropylidene (or similar alkylidene) group as the other methylene unit.

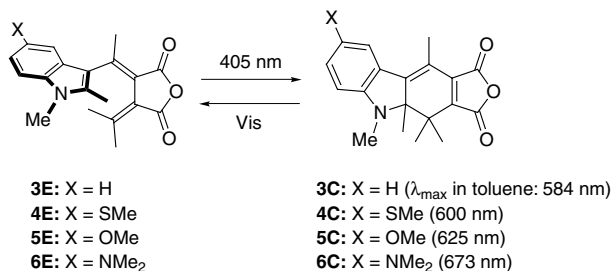
These measures blocked all side reactions, such as oxidative aromatization, hydrogen transfer, and thermal disrotatory back reaction, as well as increasing the proportion of the C form at the UV irradiation pss.

The great merit of thermal irreversibility is the permanent nature of the states. Therefore, fulgides have long been viewed as potential candidates for photon–mode optical recording materials. In addition, fulgides have been used as prototypes to demonstrate their potential applicability as photoswitchable functional materials. Those switch models that had appeared up until the end of 1999 are described in this chapter.

4.2

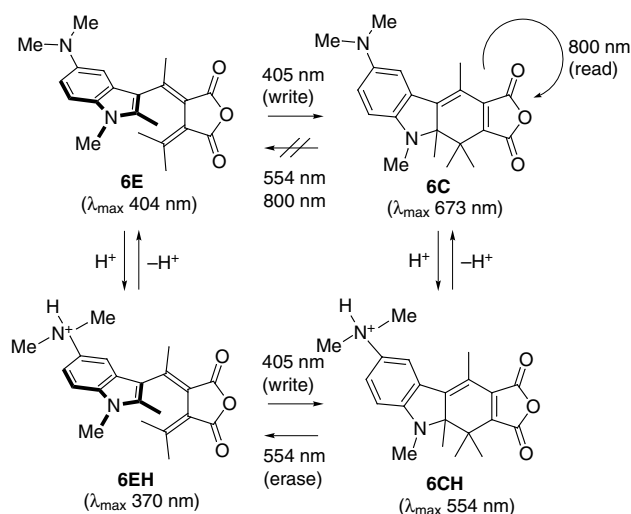
Switching of Photochromic Properties of Fulgides by Additives

Application of a thermally irreversible photochromic compound in an optical memory medium requires that several conditions should be satisfied. Among them, the development of a non-destructive readout method is a difficult problem. Exposure to light that might be absorbed should be avoided, because it causes destruction of memory.



Yokoyama et al. found that introduction of electron-donating groups at the 5-positions of the indole rings of compounds **3** resulted in bathochromic shifts of absorption in the C forms.^[5] Among these, **6C** had an absorption maximum at 673 nm in toluene. Surprisingly, the quantum yield of decoloration by visible light irradiation ($\Phi_{\text{CE}}^{\text{Vis}}$) was practically zero. Upon addition of trichloroacetic acid, however, $\Phi_{\text{CE}}^{\text{Vis}}$ became large, while a pronounced shift of absorption towards shorter wavelength was also unexpectedly observed. When a small amount of acid was present in this system during photoirradiation, an acid–base equilibrium was set up. This system was developed into a non-destructive memory media readout method, using three different light sources (Scheme 3).

At 800 nm, only **6C** absorbed light, but no photoreaction occurred. Light of this wavelength could therefore be used as the readout light. At 550 nm, both **6C** and **6CH** absorbed light, but only **6CH** changed to **6EH**, with perturbation of the acid–base equilibrium. To restore equilibrium, **6C** would be protonated to be **6CH**, which then changed to **6EH** under the 550 nm light irradiation. This could serve as the method for erasure. Irradiation of a mixture of **6E** and **6EH** with light of wavelength 405 nm or less generated a mixture of **6C** and **6CH**, which represents the writing



Scheme 3: Nondestructive readout method using **6**/ H^+ .

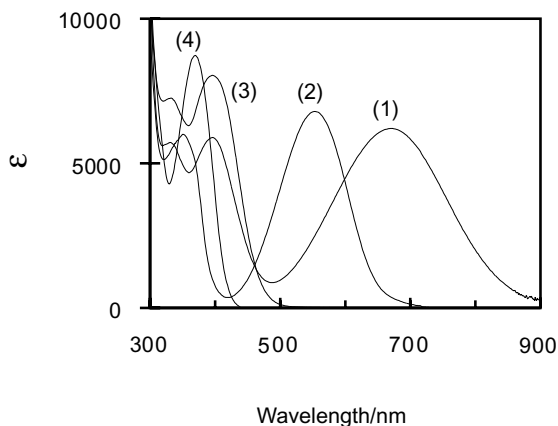
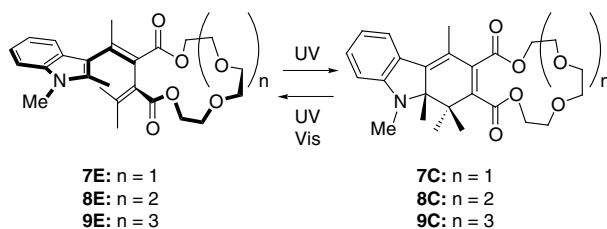


Fig. 1: Absorption spectra of dimethylaminoindolylfulgide **6** in toluene in the absence and in the presence of acid. (1) **6C**; (2) **6CH**; (3) **6E**; (4) **6EH**.

procedure.^[6] The same phenomena were also observed when the system was adapted as a PMMA film containing trichloroacetic acid or in a copolymer of PMMA–PMA.^[7]

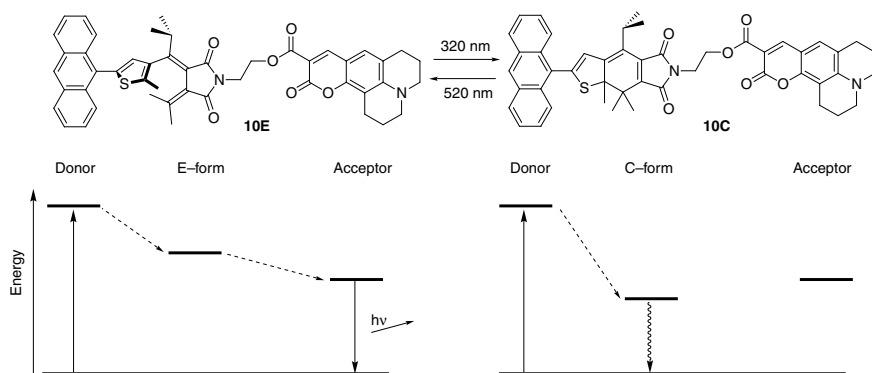
Yokoyama et al. also synthesized cyclic diesters (fulgenates) **7–9**.^[8] Because of their greater flexibility, their association constants with alkali metal cations were larger for the E and the Z forms than for the C forms. No cyclization was observed for combinations of **8E** and Na⁺ and of **9E** and K⁺ upon irradiation with UV light, because of changes in ground state conformations.



4.3

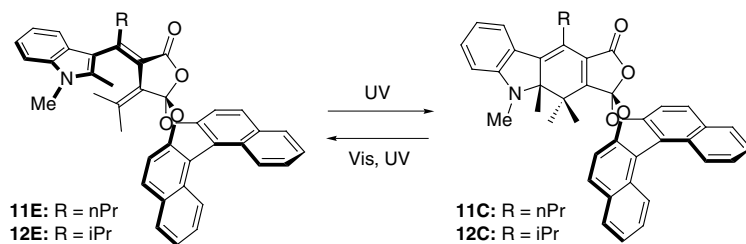
Switching of Fluorescence in Fulgides

While E form fulgides rarely emit fluorescence unless they have fluorescent substituents, C forms often fluoresce at lower temperatures.^[9]



Scheme 4: Switching of luminescence of fulgide **10**.

Port et al. synthesized a fulgimide (**10**) possessing an anthracene ring as a light antenna (energy donor: D) on the thiophene ring, and an aminocoumarin ester as a luminescent moiety (energy acceptor: A) on the fulgimide nitrogen.^[10] When the fulgimide component was in the E form, excitation of the anthracene moiety with light of wavelength 400 nm resulted in emission of fluorescence from the coumarin constituent. The energy transfer from anthracene to the coumarin had taken place through the E form fulgimide core. On the other hand, after irradiation by 320 nm light to cyclize **10E** and produce the photostationary state, the fluorescence intensity decreased. Because the energy level of the excited state of the C form core of fulgimide **10C** was lower than that of the coumarin, it worked as an energy trap between D and A. Radiationless deactivation then followed to produce the ground state **10C**. The intensity of fluorescence could be changed repeatedly between “strong” and “weak” by means of photochromism.



Yokoyama et al. reported that the fluorescence properties of (*R*)-binaphthol–condensed fulgide **11** were changed by photochromism (Figure 2).^[11,12] While **11E** was not fluorescent in toluene, **11C** was fluorescent. After visible light irradiation, fluorescent **11C** was no longer present, and so this represents the first example of complete “ON/OFF” fluorescence. Compound **12** behaved similarly, although its fluorescence intensity was only about one tenth that of **11**.

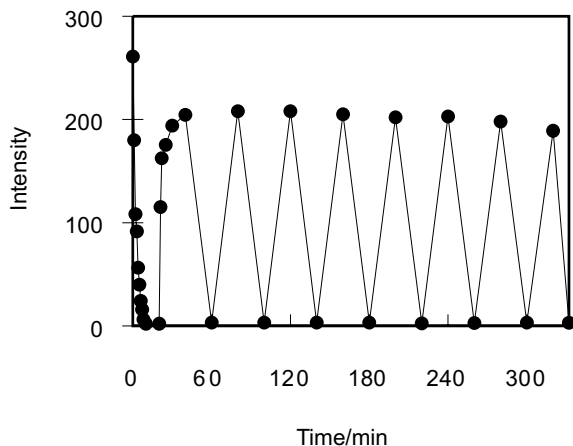
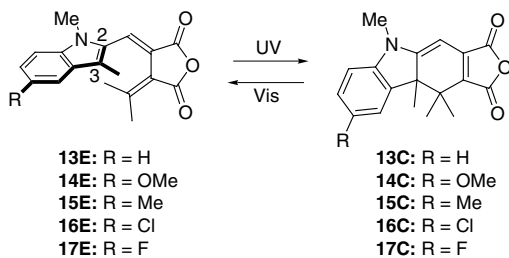


Fig. 2: Change in fluorescence intensity of **11** in toluene upon photoirradiation. Starting from **11C**. One cycle of irradiation; irradiation with >470 nm light for 20 min, then irradiation with 366 nm light for 20 min. Excitation wavelength: 470 nm. Detection wavelength: 610 nm.

Rentzepis et al. found a similar phenomena for compounds **13**–**17**. The indole rings in these cases were connected through the 2-positions, rather than the more usual 3-positions.^[13] The C forms of these compounds were fluorescent at room temperature, while the E and Z forms were not.^[14]



4.4

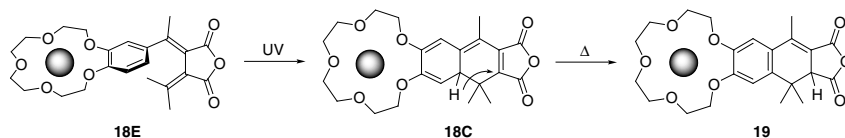
Switching of Non-linear Optical Properties through Fulgide Photochromism

Delaire et al. demonstrated photochemical control of secondary harmonic generation (SHG) properties of fulgide-doped PMMA films. When PMMA film doped with the E form of furylfulgide (**2**) was irradiated with UV light in a DC electric field, the molecules arranged in such a way that the transition moment of the C form molecule was pointing in the direction of the DC field. While the SHG signal ($I_{2\omega}$) was then observed at 1064 nm (Nd-YAG laser), it disappeared after visible light irradiation. This cycle was repeatable on alternative irradiation with UV and with visible light, although the orientation of molecules gradually became disordered.^[15]

4.5

Switching of Supramolecular Properties of Fulgides

Guo et al. prepared a phenylfulgide (**18**) possessing a benzo-15-crown-5 moiety, and examined its photochromic properties in the presence and absence of metal cations.^[16] The absorption both of the colored and of the colorless forms shifted hypsochromically by 28 nm in the presence of sodium cation, while shifting only 12 nm in the presence of potassium cation. Hypsochromic shifts greater than 40 nm were observed for alkaline earth metal cations. Addition of sodium cation also inhibited the thermal 1,5-sigmatropic rearrangement of the colored form to the nonphotochromic species **19**.

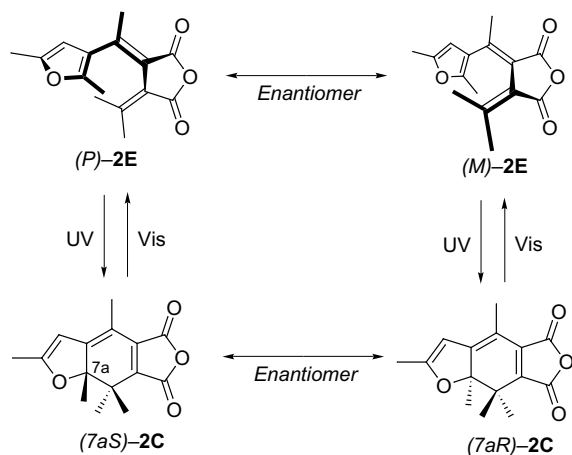


The photochromism of fulgide-related diesters (fulgenates) **7–9**, possessing crown-ether moieties, is described in Section 4.2. The most notable feature was that photochromic coloration did not occur when a host-specific alkali metal salt was added.^[8]

4.6

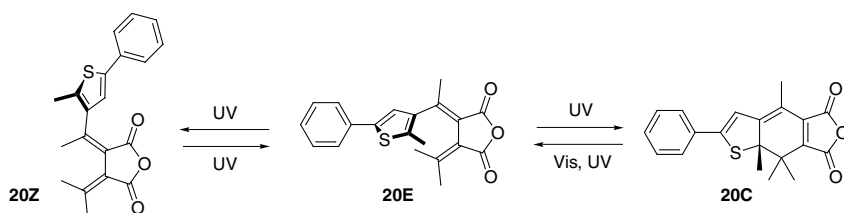
Switching of Chiral and Chiroptical Properties of Fulgides

Because the overcrowded nature of the structure of the E form of fulgides forces them to adopt the helical configuration of the photoreactive 1,3,5-hexatriene moiety, it generates helical chirality (Scheme 5). The two enantiomeric helicities are abbre-

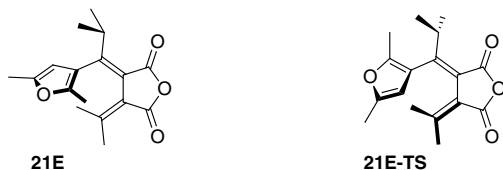
Scheme 5: Chirality in fulgide **2**.

viated as *P* for plus and *M* for minus, representing right-handed screw-like orientation and left-handed screw-like orientation, respectively. Upon UV irradiation, this helical chirality is stereospecifically translated through a 6π -electrocyclic reaction into a stereogenic quaternary carbon atom in the C form (for **2**, for example, *S* from *P* and *R* from *M*) in accordance with the Woodward–Hoffmann rules.^[4] The change in chiral nature associated with the photochromic absorption spectral change can induce some interesting switching of chiroptical properties.

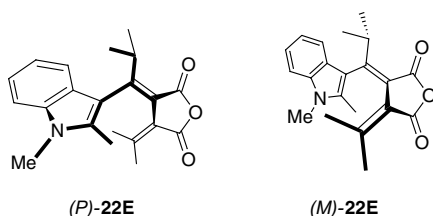
Kaftory performed X-ray crystallographic analyses of **20E**, **20Z**, and **20C**, and found that crystals of **20E** and **20Z** were composed of single enantiomers of helical chirality, while crystals of **20C** comprised a racemic mixture of enantiomers about the quaternary chiral carbon atom.^[17] Irradiation of a crystal of **20E** with UV light to induce photocoloration in the crystalline state resulted in the coloration only of the surface of the crystal.



Using ^1H NMR, Yokoyama et al. observed the racemization of helicity of an E form fulgide in solution for the case of **21E**.^[18] The ΔH^\ddagger value of racemization of **21E** obtained experimentally was compared with those for the possible racemization pathways calculated by AM1 semiempirical MO calculations, and the racemization process was deemed to occur by way of the highly strained transition state **21E-TS**.



Yokoyama et al. also succeeded in the optical resolution of an isopropyl-substituted indolylfulgide **22E** (Figure 3).^[19] The enantiomers displayed a change in their CD spectra on photochromic reaction. Upon heating or prolonged irradiation of UV light, however, gradual racemization occurred. The activation energy of thermal racemization, determined experimentally, was 107 kJ mol^{-1} .



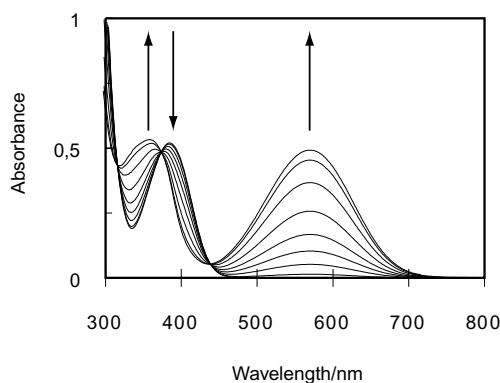
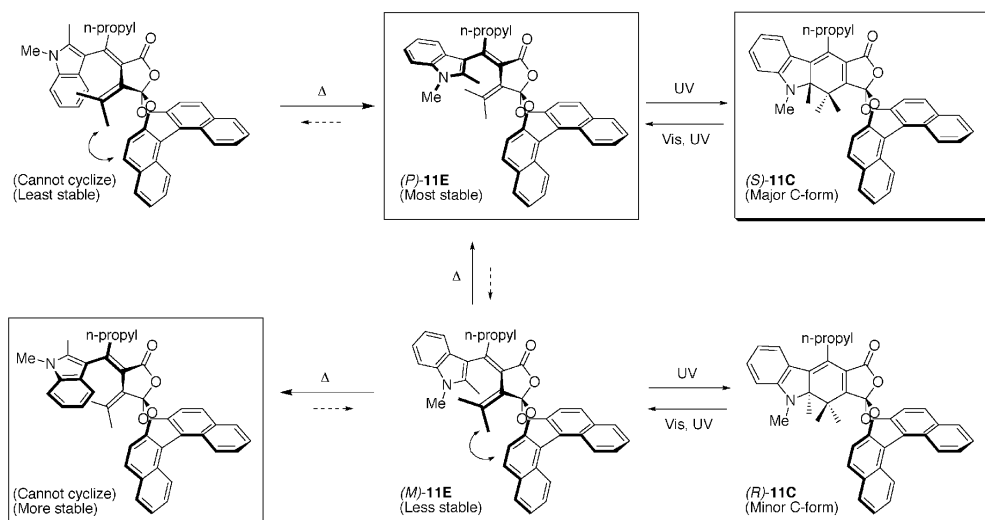


Fig. 3: Change in absorption spectrum of **22** in toluene on irradiation with 405 nm light. Starting from **22E**. Concentration (mol dm^{-3}): 8.42×10^{-5} . Irradiation time (min): 0, 0.5, 2, 4.2, 7.4, 13, 23, 42, 71 (photostationary state).

Yokoyama et al. reported as well a highly diastereoselective photochromic system in the shape of compound **11**, which has already appeared in Section 4.3. Introduction of (*R*)-binaphthol onto the succinic anhydride ring of the corresponding fulgide in an acetal-like fashion produced an unexpected result.^[20] Because of steric repulsion between one of the binaphthol naphthalene rings and an isopropylidene methyl group pointing away from the molecule, the hexatriene moiety of **11E** was forced to adopt *P* helicity (Scheme 6). Consequently, the diastereomer ratio in the C form (**11C**) generated by UV irradiation was 95/5 (90 % de), with the *S* diastereomer predominant.^[11,21]



Scheme 6: High diastereoselectivity in photochromic cyclization of **11**.

The specific rotation values of **11E** and its UV pss at the sodium D-line (589 nm; $[\alpha]_D$) in toluene were -572° and -186° , respectively: hence markedly different. This phenomenon was reproduced in PMMA films. Because irradiation at the sodium D-line wavelength does not induce photochromic reactions, measurement of optical

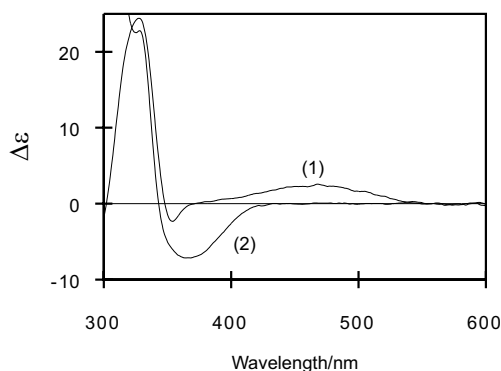


Fig. 4: Change in CD spectrum of **11** in toluene on photoirradiation. (1) **11C**; (2) **11E**.

rotation values at this wavelength or longer might in principle be a method of non-destructive readout for optical memory. CD spectra also differed between **11E** and **11C** (Figure 4).

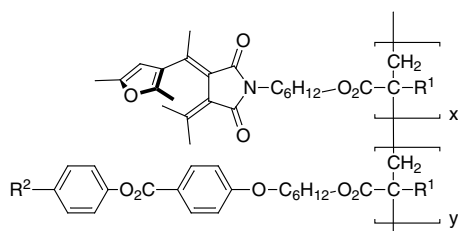
Similar results were observed for a benzofuryl derivative.^[22]

4.7

Switching of Liquid Crystalline Properties through Fulgide Photochromism

Photochromic compounds can reversibly change their degree of interaction with their environments by means of photochemical changes in their structures. When a photochromic compound is added to a liquid crystalline compound that adopts the stable, ordered orientation, the photochromic compound acts as a perturbing factor on the ordered molecular orientation. The degree of perturbation of the ordered structure of the liquid crystal can be reversibly changed by structural alteration in the photochromic dopant. Although this may occur for any liquid crystals with fulgide derivatives, it has so far only been reported for nematic and cholesteric types.

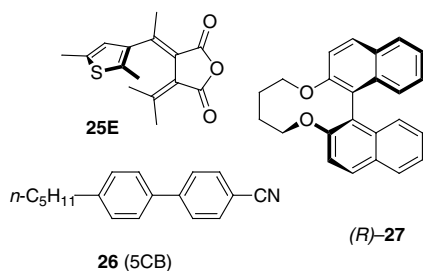
Ringsdorf et al. prepared liquid crystalline methacrylic and acrylic copolymers **23** and **24** from monomers possessing a fulgimide unit and monomers possessing a phenyl benzoate mesogen unit.^[23] Their photochromic properties were preserved in polymer films. Irradiation with UV light to change the E forms to C forms resulted in higher clearing temperatures. They reported that the optically stored image of a photomask was observed under a polarizing microscope.



23: $R^1 = H$, $R^2 = CN$

24: $R^1 = Me$, $R^2 = OMe$

Gleeson et al. added a furylfulgide (**2**) or a thienylfulgide (**25**) (less than 2 % w/w) to a nematic liquid crystal (E7, Merck: composed of several biphenyl derivatives).^[24] Although a large change of clearing point due to photochromism had been expected, only a subtle change was observed. They also studied changes in dielectric constants^[25] and elasticity constants arising from photochromism of **25** in E7.^[26] Although some differences were observed, they originated mostly from the changes in clearing points, and no significant change was observed when they were compared on the basis of “reduced temperature”, their deviation from the clearing points.



Schuster et al. reported that the photochromism of a fulgide could change the helical pitch length of a cholesteric liquid crystal.^[27] They added an indolylfulgide **3** (5.2 % w/w) to a cholesteric liquid crystal composed of 4-cyano-4'-pentylbiphenyl **26** (5CB) and 1.35 % (w/w) of a chiral cyclic ether (*R*)-**27**, prepared from (*R*)-binaphthol. The cholesteric pitch length could be changed reversibly between 30 and 42 μm , after UV and visible light irradiation, respectively.

Yokoyama et al. showed that the binaphthol derivatives of indolylfulgides **11** and **12** functioned as chiral dopants to generate cholesteric phases on addition to nematic liquid crystal **26**. Photoirradiation induced dramatic changes in cholesteric

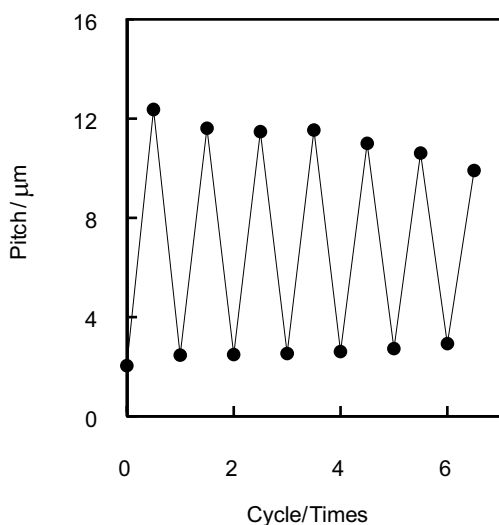


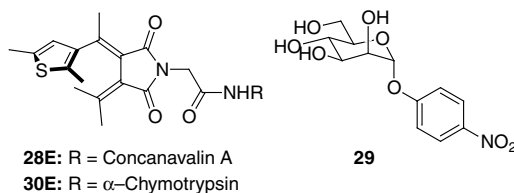
Fig. 5: Change in cholesteric pitch of a mixture of 5CB (**26**) and **11** on photoirradiation. Concentration of **11** in **26** (mol dm^{-3}): 1.22×10^{-2} . Starting from **11C**. One cycle of irradiation: irradiation with >450 nm light for 5 min, then irradiation of 366 nm light for 60 min. Pitch values were determined by Cano's method.^[28, 29]

pitch.^[28,12] Thus, addition of 1.1 mol% of **12** resulted in changes of pitch length of 15.8 and 2.6 μm , respectively, for the E form and the photostationary state of UV irradiation. Interestingly, the resolved indolylfulgide (*P*)-**22** produced much smaller changes in pitch than **11** and **12**, and the cholesteric sense of (*P*)-**22** was different from **11** and **12**, although the helicity of the fulgide core part was the same.^[29]

4.8

Switching of Biological Activities through Fulgide Photochromism

Willner et al. prepared a fulgimide **28**, attached to a lysine nitrogen of concanavalin A. Concanavalin A is a protein that can form complexes with α -D-mannopyranoside and some related pyranoses. Photoirradiation resulted in a structural change in the fulgimide, which in turn induced a change in the association constant with 4-nitrophenyl- α -D-mannopyranoside **29**. The largest change in association constant was observed when nine fulgimide molecules were linked to a protein molecule. The association constant changed from $0.78 \times 10^4 \text{ M}^{-1}$ when colorless to $1.21 \times 10^4 \text{ M}^{-1}$ when colored.^[30]



Willner et al. also prepared fulgimide-modified (through lysine nitrogen) α -chymotrypsin **30**, with nine fulgimide molecules in one protein.^[31] The modified protein was active towards esterification of *N*-acetylphenylalanine in cyclohexane. Together with the bioimprinting technique of the substrate, the rate of esterification could be accelerated by irradiation with UV light.

4.9

Future Perspectives

The history of research into fulgides began quietly at the beginning of the 20th century. In the 1980s, when fulgides endowed with thermal irreversibility became available, this family of compounds, exhibiting photochromism based on 6π -electrocyclization, attracted a number of researchers. Together with the discovery of new thermally irreversible diarylethenes,^[32] electrocyclization-based, thermally irreversible photochromic compounds are likely to be investigated more intensely than ever in the 21st century. A variety of materials which act as photochemically controllable molecular switches will surely be produced from research efforts into these compounds.

References

- 1 H. Dürr in *Photochromism: Molecules and Systems*; (Eds.: H. Dürr, H. Bouas-Laurent), Elsevier, Amsterdam, **1990**, pp. 1–14.
- 2 For reviews dealing with fulgides: a) J. Whittall in *Photochromism: Molecules and Systems*; (Eds.: H. Dürr, H. Bouas-Laurent), Elsevier, Amsterdam, **1990**, pp. 467–492; b) J. D. Margerum, L. J. Miller in *Techniques of Chemistry, Vol. III, Photochromism* (Ed.: G. H. Brown), John Wiley and Sons, New York, **1971**, pp. 557–632; c) H. G. Heller, *Spec. Publ., R. Soc. Chem., Fine Chem. Electron. Ind.* **1986**, *60*, 120–135; d) J. Whittall in *Applied Photochromic Polymer Systems* (Ed.: C. B. McArdle), Blackie, Glasgow, **1992**, pp. 80–120; e) M. Fan, L. Yu, W. Zhao, in *Organic Photochromic and Thermochromic Compounds, Vol. 1, Main Photochromic Families* (Eds.: J. C. Crano, R. Guglielmetti), Plenum Publishers, New York, **1999**, pp. 141–206; f) Y. Yokoyama, *Chem. Rev.*, **2000**, *100*, 1717–1739.
- 3 a) H. Stobbe, *Ber.* **1905**, *38*, 3673–3682; b) H. Stobbe, *Ann.* **1911**, *380*, 1–129; c) H. Stobbe, *Ber.* **1905**, *40*, 3372–3382.
- 4 P. J. Darcy, H. G. Heller, P. J. Strydom, J. Whittall, *J. Chem. Soc., Perkin Trans. 1* **1981**, 202–205.
- 5 a) Y. Yokoyama, T. Tanaka, T. Yamane, Y. Kurita, *Chem. Lett.* **1991**, 1125–1128; b) Y. Yokoyama, Y. Kurita, *Mol. Cryst. Liq. Cryst. Sect. A* **1994**, *246*, 87–94.
- 6 Y. Yokoyama, T. Yamane, Y. Kurita, *J. Chem. Soc., Chem. Commun.* **1991**, 1722–1724.
- 7 Y. Yokoyama, T. Yamane, Y. Kurita in *Chemistry of Functional Dyes, Vol. 2* (Eds.: Z. Yoshida, Y. Shirota), Mita Press: Tokyo, **1993**, pp. 383–387.
- 8 a) Y. Yokoyama, T. Ohmori, Y. Yokoyama, T. Okuyama, S. Uchida, *Abstracts of 7th International Kyoto Conference on New Aspects of Organic Chemistry*; Kyoto, 1997, p. 351; b) Y. Yokoyama, T. Ohmori, T. Okuyama, Y. Yokoyama, S. Uchida, *Mol. Cryst. Liq. Cryst.*, **2000**, *344*, 265–270.
- 9 a) A. Santiago, R. S. Becker, *J. Am. Chem. Soc.* **1968**, *52*, 3654–3658; b) J. Takeda, N. Nakayama, N. Nagase, T. Tayu, K. Kainuma, S. Kurita, Y. Yokoyama, Y. Kurita, *Chem. Phys. Lett.* **1992**, *198*, 609–614; c) J. Takeda, T. Tayu, S. Kurita, Y. Yokoyama, Y. Kurita, T. Kuga, M. Matsuoka, *Chem. Phys. Lett.* **1994**, *220*, 443–447.
- 10 a) J. Walz, K. Ulrich, H. Port, H. C. Wolf, J. Wonner, F. Effenberger, *Chem. Phys. Lett.* **1993**, *213*, 321–324; b) M. Seibold, H. Port, H. C. Wolf, *Mol. Cryst. Liq. Cryst.* **1996**, *283*, 75–80.
- 11 a) T. Inada, S. Uchida, Y. Yokoyama, *Chem. Lett.* **1997**, 321–322; b) T. Inada, S. Uchida, Y. Yokoyama, *Chem. Lett.* **1997**, 961.
- 12 Y. Yokoyama, S. Uchida, Y. Yokoyama, T. Sagisaka, Y. Uchida, T. Inada, *Enantiomer* **1998**, *3*, 123–132.
- 13 I. Y. Grishin, N. M. Przhivalgovskaya, Y. M. Chunaev, V. F. Mandzhikov, L. N. Kurkovskaya, N. N. Suvorov, *Khim. Geterotsikl. Soedin.* **1989**, 907–910.
- 14 a) Y. C. Liang, A. S. Dvornikov, P. M. Rentzepis, *Res. Chem. Intermed.* **1998**, *24*, 905–914; b) Y. Liang, A. S. Dvornikov, P. M. Rentzepis, *Tetrahedron Lett.*, **1999**, *40*, 8067–8069.
- 15 K. Nakatani, Y. Atassi, J. A. Delaire, *Nonlinear Optics* **1996**, *15*, 351–358.
- 16 Z. Guo, G. Wang, Y. Tang, X. Song, *Lieb. Ann.* **1997**, 941–942.
- 17 M. Kaftory, *Acta Cryst.* **1984**, *40*, 1015–1019.
- 18 a) Y. Yokoyama, T. Iwai, Y. Yokoyama, Y. Kurita, *Chem. Lett.* **1994**, 225–226; b) Y. Yokoyama, K. Ogawa, T. Iwai, K. Shimazaki, Y. Kajihara, T. Goto, Y. Yokoyama, Y. Kurita, *Bull. Chem. Soc. Jpn.* **1996**, *69*, 1605–1612.
- 19 Y. Yokoyama, Y. Shimizu, S. Uchida, Y. Yokoyama, *J. Chem. Soc., Chem. Commun.* **1995**, 785–786.
- 20 Y. Yokoyama, S. Uchida, Y. Yokoyama, Y. Sugawara, Y. Kurita, *J. Am. Chem. Soc.* **1996**, *118*, 3100–3107.
- 21 Y. Yokoyama, S. Uchida, Y. Shimizu, Y. Yokoyama, *Mol. Cryst. Liq. Cryst. Sect. A* **1997**, *297*, 85–91.
- 22 Y. Yokoyama, Y. Kurosaki, T. Sagisaka, H. Azami, *Mol. Cryst. Liq. Cryst.* **2000**, *344*, 223–228.
- 23 I. Cabrera, A. Dittich, H. Ringsdorf, *Angew. Chem. Int. Ed. Engl.* **1991**, *30*, 76–78.
- 24 H. Allinson, H. F. Gleeson, *Liq. Crystals* **1993**, *14*, 1469–1478.
- 25 H. Allinson, H. F. Gleeson, *Liq. Crystals* **1995**, *19*, 421–425.

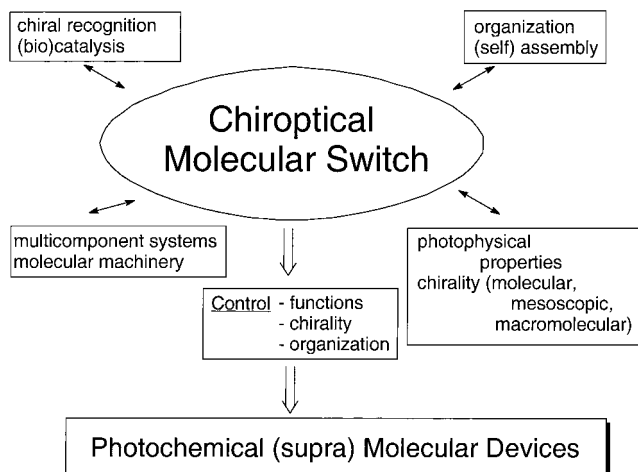
- 26 H. Allinson, H. F. Gleeson, *J. Mater. Chem.* **1995**, *5*, 2139–2144.
- 27 S. Z. Janicki, G. B. Schuster, *J. Am. Chem. Soc.* **1995**, *117*, 8524–8527.
- 28 Y. Yokoyama, T. Sagisaka, *Chem. Lett.* **1997**, 687–688.
- 29 T. Sagisaka, Y. Yokoyama, *Bull. Chem. Soc. Jpn.* **2000**, *73*, 191–196.
- 30 I. Willner, S. Rubin, J. Wonner, F. Effenberger, P. Bäuerle, *J. Am. Chem. Soc.* **1992**, *114*, 3150–3151.
- 31 I. Willner, M. Lion-Digan, S. Rubin, J. Wonner, F. Effenberger, P. Bäuerle, *Photochem. Photobiol.* **1994**, *59*, 491–496.
- 32 M. Irie, K. Uchida, *Bull. Chem. Soc. Jpn.* **1998**, *71*, 985–996.

5 Chiroptical Molecular Switches

Ben L. Feringa, Richard A. van Delden, and Matthijs K. J. ter Wiel

5.1 Introduction

Chiral photobistable molecules^[1] comprise a particularly attractive class of photochromic compounds^[2], as the reversible photochemical transformation between two forms can lead simultaneously to a chirality change in the system.^[3] In addition to the conventional absorption spectrum change associated with photochromic materials,^[1,2] and the possibility of modulating other physicochemical properties such as dipole moment or redox potential,^[4] it is also possible to exploit the unique properties associated with the different stereoisomers of such chiral photoresponsive molecules. It is important to realize that an intrinsic feature of living organisms is the precise control, in many essential components, of chirality at the molecular, supra-molecular, and macromolecular levels.^[5] In biosystems, molecular recognition, transport, information storage and processing, structure and assembly of materials, catalysis, and replication are all intimately controlled by chirality.^[6]



Scheme 1: Potential applications of a chiral optical (chiroptical) molecular switch.

Various types of chiral switches based on photochromic molecules, as discussed in this chapter, are schematically summarized in Scheme 2.

- A) Switching of enantiomers:
Unless chiral light is used, irradiation of either enantiomer of a chiral photochromic molecule (*R/S* or *P/M*) will, irrespective of the wavelength used, always lead to a racemic mixture, due to the identical absorption characteristics of the two enantiomers. In these systems, therefore, the enantiomers are interconverted at a single wavelength by employing left or right circularly polarized light (*l*- or *r*-CPL). Enantioselective switching in either direction is in principle possible.
- B) Switching of diastereomers:
The compound consists of two diastereomeric photobistable forms: for instance, **P** (right-handed) and **M'** (left-handed) helices, which can undergo photoisomerization at two different wavelengths: λ_1 and λ_2 . Alternatively, a chiral auxiliary (X^*) and a photochromic unit (**A**) (either chiral or achiral) may be present in systems **A**- X^* , with the auxiliary X^* controlling the change in chirality during the switching event.
- C) Functional chiral switches.
Because of the multifunctional nature of these photochromic systems, the change in chirality simultaneously triggers the modulation of some particular function, such as fluorescence, molecular recognition, or motion. In most cases, this is the result of a change in the geometry or the electronic properties of the system.
- D) Switching of macromolecules or supramolecular organization
Photobistable molecules (chiral or achiral) may be covalently attached to, for example, a polymer or be part of a host-guest system. The photoisomerization process induces changes in some property such as the helical structure of a chiral polymer or the organization of the surrounding matrix: the chiral phase of a liquid crystalline material or a gel, for example. The photochemical event is recorded by means of the chiral response of the structure, organization, or other property of the macromolecule or the larger ensemble.

Photochemical bistability is a *conditio sine qua non*, but a number of other requirements are essential for application of chiral switches in photonic materials or optical devices:^[1,4,10]

- Thermal stability; there should be a large temperature range in which no interconversion of the isomers takes place. This includes stability towards racemization.
- Low fatigue; numerous switching cycles should be possible without any change in performance.
- Fast response times, high sensitivity, and detectability; switching should be fast and easy, both forms should be readily detectable.
- Nondestructive read-out; the detection method should not erase the stored information.

- The photochemical and other properties must be retained when the chiral molecular switch is incorporated in a polymer or acts as a part of a multicomponent assembly.

In most photochromic systems, absorption or emission spectroscopy, monitoring near the switching wavelengths, is used for read-out. This often leads to partial reversal of the photochemical process used to store information.^[1,2,7,11] Chiroptical techniques allow the change in chirality of the photochromic system to be measured, and so a major advantage of chiroptical switches, compared to other photochromic systems, is the possibility of non-destructive read-out by monitoring the optical rotation at wavelengths remote from the wavelengths used for switching (information storage). The sensitivity towards changes in organization and chirality in larger ensembles such as gels and liquid crystals, together with the conformational changes in polymers, and concomitant change in physical properties associated with these events, offer other attractive possibilities for avoiding destructive read-out.^[3]

5.2

Switching of Enantiomers

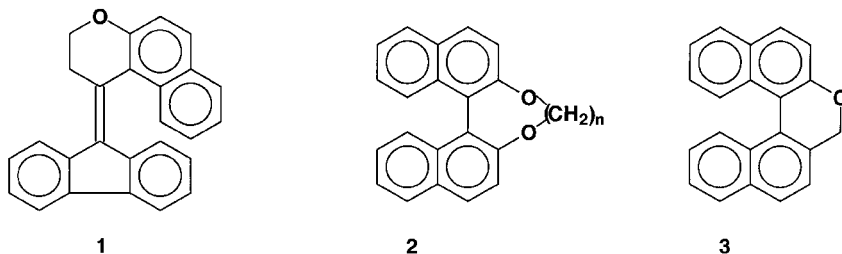
Dynamic control of molecular chirality through the use of circularly polarized light (CPL) is feasible, provided that the enantiomers of the photochromic compound are thermally stable but at the same time display bistability upon irradiation. Photochemical conversions using circularly polarized light are usually referred to as absolute asymmetric syntheses.^[12,13] Three pathways to generating optically active materials through CPL irradiation can be envisaged: photodestruction, photoresolution, and photochemical synthesis. Several enantiodifferentiating photochemical conversions using CPL have been reported,^[12,13] but only a very few meet the basic requirement of bistability. The enantioselectivity of a CPL irradiation-based molecular switch is governed by the Kuhn anisotropy factor g .^[12,13] The enantiomeric excess in the photostationary state (p.s.s.) can be obtained from equation 1.

$$e.e._{p.s.s.} = \frac{g}{2} = \frac{\Delta\varepsilon}{2\varepsilon} \quad (1)$$

As g seldom exceeds 0.01, except for some chiral ketones (vide infra), the enantiomeric excess (e.e.) that can be expected is usually below 0.5%.^[14] Large g -values are usually associated with forbidden transitions. Decisive factors for a successful molecular switch based on enantiomer interconversion are:

- irradiation with CPL light should cause the interconversion of enantiomers without any photodestruction;
- the enantiomers should have sufficiently high g -values;
- the enantiomers should be thermally stable ($\Delta G_{rac} > 21 \text{ kcal mol}^{-1}$);
- the quantum efficiency for photoracemization should be high, as the rate of photoresolution is exponentially related to this quantity.^[15]

Previous, unsuccessful attempts to demonstrate the principle of a molecular switch based on CPL irradiation include inherently dissymmetric fluorene derivative **1**,^[16] atropisomeric bridged binaphthyls **2**,^[17] and 1,1'-binaphthylpyran **3**.^[18] Inefficient photoracemization, low *g*-values, and insufficient sensitivity for detection were some of the problems encountered.



Successful photoresolution and switching of enantiomers has been accomplished with two types of systems: helical overcrowded alkenes and axially chiral cycloalkanones.

5.2.1

Overcrowded Alkenes

Figure 2 shows the structures of four classes of so-called overcrowded alkenes (see Section 5.3.1), designed as molecular components for a chiroptical switch based on CPL irradiation.^[19] Thanks to unfavorable steric interactions around the central olefinic bond, the molecules are forced to adopt a helical shape. The chirality in these inherently dissymmetric alkenes – denoted **M** and **P** for left-handed and right-handed helices, respectively – therefore originates from distortion of the molecular

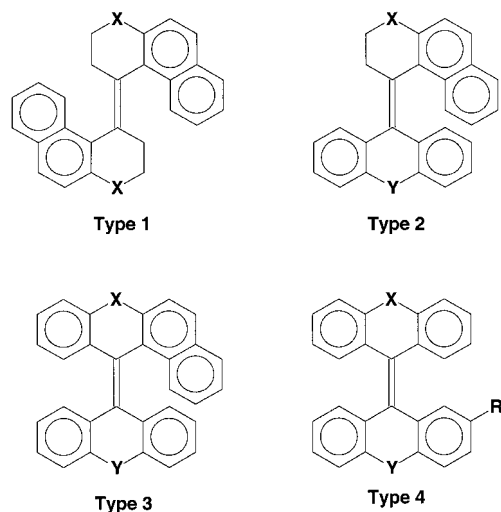


Fig. 2: Inherently dissymmetric overcrowded alkenes.

Tab. 1: Anisotropy factors of different types of inherently dissymmetric alkenes.

Compound	X	Y	λ ($\Delta\epsilon_{\max}$, $g^{\pm}\cdot 10^3$) ^a		
4 (Type 1)	CH ₂	CH ₂	224 (-281.3, -4.1)	240 (222.2, 6.1)	257 (-80.1, 8.0)
			283 (11.9, 1.7)	338 (-14.8, -2.8)	
5 (Type 2)	O	-	241 (41.2, 1.4)	261 (-41.7, -2.1)	273 (-37.7, -3.1)
			333 (-22.7, -3.9)	382 (10.7, 0.9)	
6 (Type 2)	CH ₂	O	225 (186.5, 2.6)	243 (-54.8, -2.0)	270 (-43.0, -5.9)
7 (Type 2)	CH ₂	S	212 (-40.9, -0.7)	228 (212.4, 2.9)	259 (-67.8, -4.1)
			327 (8.4, 0.6)		
8 (Type 3)	O	S	236 (128.6, 2.8)	314 (-51.3, -6.4)	356 (5.0, 0.4)
9 (Type 4)	S	S	225 (-13.7, -0.5)	244 (-13.7, 0.4)	282 (-10.6, -0.8)
			303 (9.0, 0.8)		

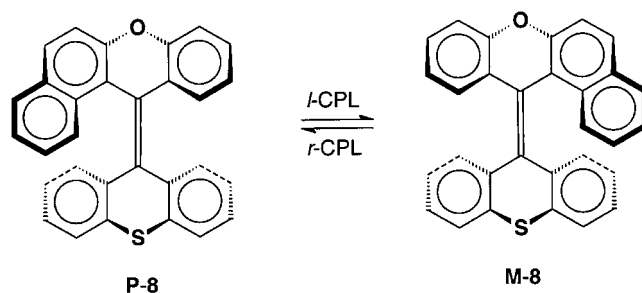
a: g -values calculated for the wavelengths where $\Delta\epsilon$ reaches a maximum. This need not be g_{\max} .

framework. The synthesis of these type of molecules is similar to that of the sterically overcrowded alkenes discussed in Section 5.3.1.

Since the anisotropy value g is decisive for the selectivity of a CPL-based switching process between enantiomers, representative examples of inherently dissymmetric alkenes and their corresponding g -values are given in Table 1. Only type 2 and type 3 alkenes exhibit significantly large g -values at wavelengths above 300 nm, which are considered useful for practical applications. From the data given, it can be seen that g -values above 0.01 % are not observed and that, under ideal conditions, an e.e. of 0.3 % might be achieved with **8**, while for **5** an e.e. of 0.2 % is the upper limit.

Of the large number of sterically overcrowded alkenes that have been synthesized, resolved, and their chiroptical properties examined, compound **8** satisfies the requirements given above (Scheme 3).

The enantiomers of **8** are stable at ambient temperatures ($\Delta G_{\text{rac}} = 25.9 \text{ kcal mol}^{-1}$) and fatigue resistant. Upon irradiation at 313 nm, a stereospecific photochemical isomerization process occurs, which converts **P-8** into **M-8** and vice versa. A fairly efficient, rapid, and selective photoracemization was observed when using unpolarized light ($\Phi_{\text{rac}} = 0.40$; *n*-hexane). Large circular dichroism (CD) absorptions and



Scheme 3: Photoresolution and photochemical interconversion of **P-8** and **M-8** upon irradiation at 313 nm with *l*- or *r*-CPL.

optical rotations ($[\alpha]_{436}^{20} = 900^\circ$) essential for detection of small e.e.s were found, as well as a sufficiently large g -value ($g = -6.4 \times 10^{-3}$ at 314 nm).

There are three switching steps involved in a CPL-based switch:

- 1) irradiation of a racemate (**MP**) with circularly polarized light results in an excess of one of the enantiomers (**P** or **M**);
- 2) irradiation at a single wavelength with alternating *r*- or *l*-CPL results in modulation between right-handed and left-handed helices; i.e., switching between **P-8** and **M-8** (Scheme 3);
- 3) the racemate is obtained again after irradiation with linearly polarized light (LPL).

Irradiation of racemic **P,M-8** with *l*-CPL at 313 nm resulted in deracemization and spectral features (CD) indicating the formation of an excess of **M-8**. Using *r*-CPL, a slight excess of **P-8** was found, together with a mirror image CD. Switching of **P,M-8** could indeed be accomplished by alternate irradiation with CPL at 313 nm.^[20] Figure 3 illustrates the modulation of the CD absorption upon successive irradiation with *l*- and *r*-CPL. Switching occurred between photostationary states with e.e.s of 0.07 % and -0.07 % (for **P** and **M** helices, respectively).^[21] Using LPL at the same wavelength, racemic **8** was obtained. The rather long irradiation time required to reach the photostationary state (approx. 30 min) and the low g -value are limitations of the CPL switch based on **8**.

Scheme 4 illustrates the principle of a potential data storage system based on **8**, or any other enantiomeric switching system. Irradiation of a racemate (**MP**) using *r*-CPL or *l*-CPL generates **P**-enriched or **M**-enriched regions, respectively. Detection of these is possible by measuring optical rotatory dispersion (ORD) in reflection or transmission outside the absorption band, with LPL. Written information can be erased by unpolarized light (UPL) or LPL at the original wavelength, generating **MP** again. In principle, this system constitutes a three-position switch of racemic, **P**-

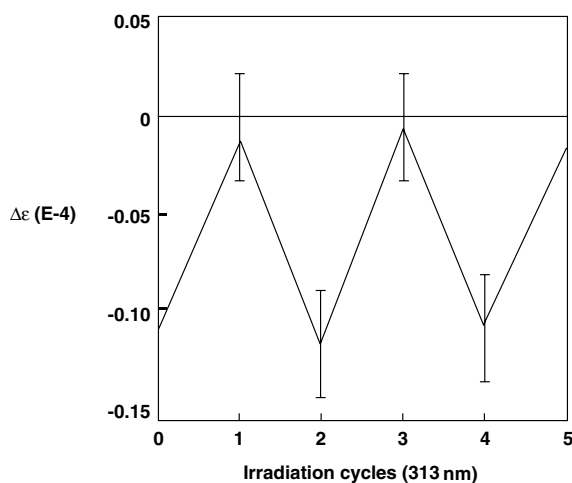
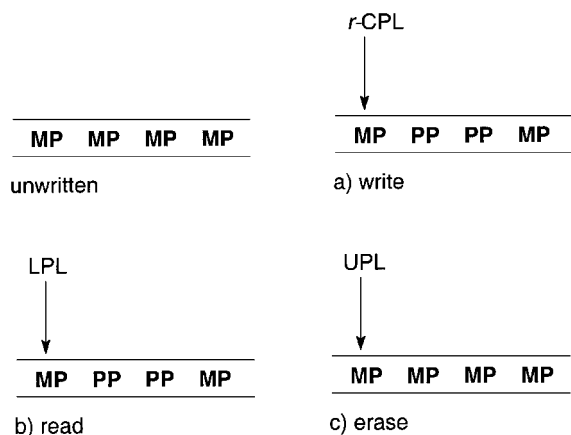


Fig. 3: The difference in CD absorption at 313 and 400 nm ($\Delta\epsilon_{313} - \Delta\epsilon_{400}$) for a solution of **8** (9×10^{-5} mol liter⁻¹) in *n*-hexane upon alternating irradiation with *l*- and *r*-CPL ($\Delta\epsilon_{400}$ is used as an internal reference value to enhance accuracy).



Scheme 4: Proposed optical data storage system based on optical switching of enantiomers. a) Writing with circularly polarized light (CPL), b) reading with linear polarized light (LPL) and erasing with unpolarized light (UPL).

enriched and **M**-enriched **8**. A distinct advantage is that all the processes can be performed at a single wavelength merely by changing the chirality of the light.

5.2.2

Axially Chiral Cycloalkanones

The optically active aryl-methylene cycloalkanes and related compounds, shown in Figure 4, were designed by Schuster et al. as chiral, photobistable materials to be used in particular as chiroptical triggers for the control of liquid crystalline phases (see Section 5.5).^[22]

These compounds exhibit axial chirality, and irradiation induces isomerization of the styrene moiety, which results in simultaneous racemization of the molecule. Irradiation of methyl ester **10** ($R = \text{OMe}$) at 251 nm indeed gave rise to a fast and selective racemization process. However, a very low anisotropy factor ($g_{254} = 7.5 \times 10^{-5}$) was found for methyl ester **10** ($R = \text{OMe}$). The magnitude of g was increased

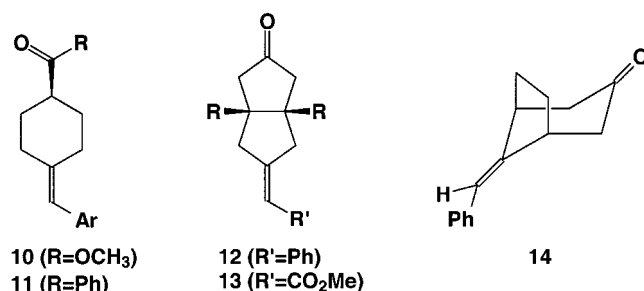
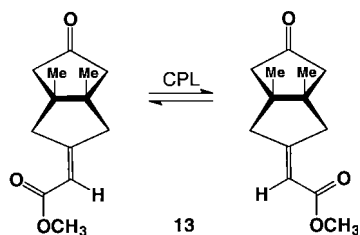


Fig. 4: Alkylidenecycloalkanone phototriggers.



Scheme 5: Photoresolution and interconversion of axial chiral **13** by CPL irradiation at 305 nm.

by a few orders of magnitude in the corresponding arylketones **11** and ketones **12**; this can be attributed to exciton coupling between the two chromophores present in these molecules. Unfortunately, photoisomerization and photodecomposition were found to be competing processes in these systems. Particularly instructive are the improvements achieved with the chiral bicyclo[3,3,0]octan-3-one (**12** and **13**) and bicyclo[3,2,1]octan-3-one (**14**) structures. The incorporation of the ketone chromophore into a rigid structure prevents any decrease in $\Delta\epsilon$ due to averaging effects of conformational isomers with opposing CD absorptions.^[23] Large CD effects have previously been observed with inherently dissymmetric ketones.^[24] Furthermore, the ketone $n\text{-}\pi^*$ transition is forbidden, which often results in small extinction coefficients and large anisotropy factors, and thus high g values.

Accordingly, compound **13** displayed a relatively high g -value of 10.5×10^{-3} . Moreover, a selective and efficient photoracemization of **13**, with a high quantum yield of 0.45 (max $\Phi_{\text{rac}} = 0.50$) and fatigue resistance after 12.5 h of irradiation, was observed upon irradiation at $\lambda > 305$ nm.

These favorable chiroptical and photochemical properties were essential for the successful demonstration of partial photoresolution of **13** by irradiation with circularly polarized light (Scheme 5).^[25] The photostationary state was reached after 400 min of irradiation, and an e.e. of 0.4 % was measured. The enantioselectivity in this process fitted with the e.e. calculated on the basis of g_{λ} . Successful switching between enantiomeric forms was also evident from the mirror CD spectrum obtained when the handedness of the CPL was changed. For bicyclic ketone **14**, an even higher anisotropy factor ($g_{313} = 0.0502$) was found.^[26] CPL irradiation of racemic **14** at 313 nm resulted in photoresolution and CD spectroscopy revealed an exceptionally high e.e. of 1.6 %. The photoresolution, however, was a rather slow process (47h irradiation to reach the p.s.s.) and, despite the highly favorable g -factor, considerable improvement in the response time is still needed.

5.3

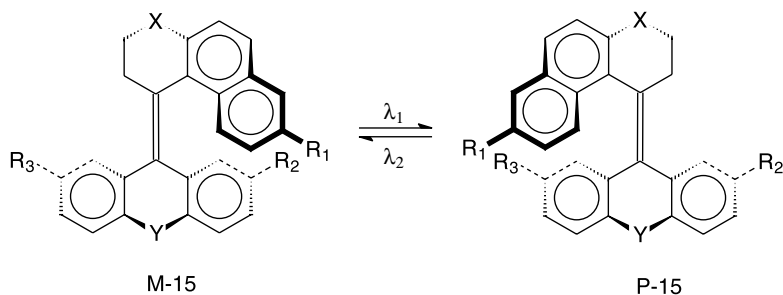
Switching of Diastereoisomers

5.3.1

Overcrowded Alkenes

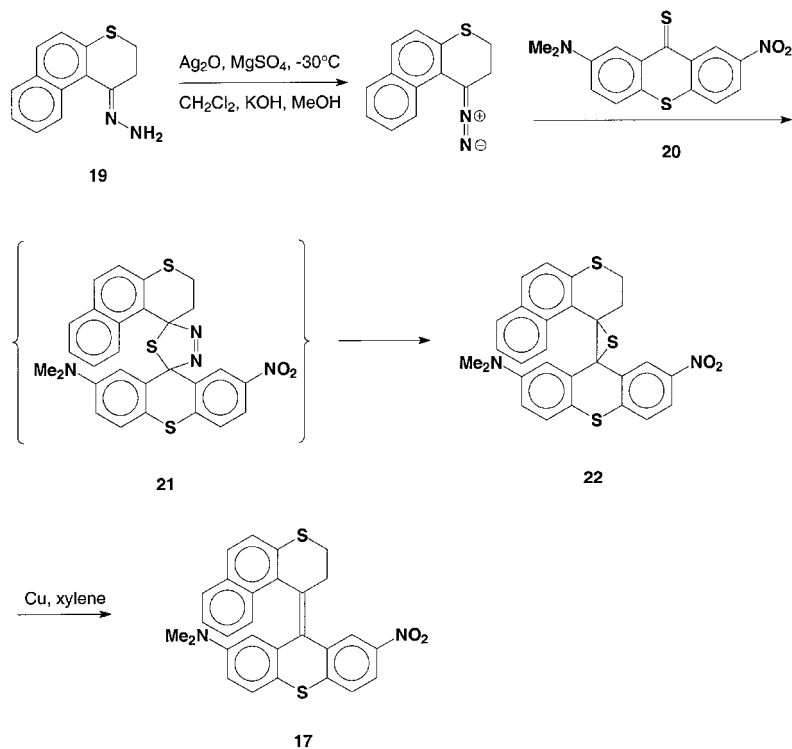
The sterically overcrowded alkenes shown in Scheme 6 have been exploited in our group since, from the perspective of molecular switches design, they combine a number of attractive structural features. Steric interactions between the groups attached to the central olefinic bond force these molecules to adopt a non-planar helical shape. The chirality of these so-called inherently dissymmetric alkenes^[3,27] is therefore the result of distortion of the entire molecular structure. Beside the helix-like geometry, both a *cis*- and a *trans*-stilbene chromophore are present in the same molecule.

These compounds, upon irradiation at the appropriate wavelength, undergo a stilbene-like *cis-trans* photoisomerization.^[28] The unique feature of these systems is that *cis-trans* isomerization simultaneously results in helix reversal, such as that, for example, of **M-15** (R_1, R_2, cis) to **P-15** ($R_1, R_2, trans$). Furthermore, the molecular architecture prevents stilbene-like photocyclization, which would result in fatigue during switching. The structure of these molecules consists of an asymmetric tetrahydrophenanthrene or 2,3-dihydronaphtho(thio)pyran upper half and a symmetric (except for the substituents) (thio)xanthene lower half. Routes developed to the overcrowded alkenes **15–18** were based on the synthesis of the ketones corresponding to the upper and lower halves, followed by formation of the sterically demanding central olefinic bond in the final stage. A variety of methods for preparing alkenes, including Wittig, Petersen, and McMurry olefination methods, were unsuccessful because



	R ₁	R ₂	R ₃	X	Y
15	H	OMe	NO ₂	S	S
16	Me	OMe	H	CH ₂	S
17	H	NO ₂	NMe ₂	S	S
18	NMe ₂	NO ₂	H	S	S

Scheme 6: Photochemical switches based on overcrowded alkenes.



Scheme 7: Synthesis of donor–acceptor substituted overcrowded alkene **17**.

of steric strain, low yields, or problems with functional group compatibility. The method of choice is diazo-thioetone coupling,^[29] illustrated in scheme 7 for the preparation of **17**. The hydrazone **19** of the upper part is oxidized in situ to the corresponding diazo compound and connected to the thioetone **20** of the lower part. The coupling involves a 1,3-dipolar cycloaddition to form a five-membered thiadiazoline intermediate **21**, followed by nitrogen elimination to provide the stable three-membered episulfide **22**. Subsequent sulfur extrusion affords the alkene **17**. Through this sequence, the steric strain is introduced into the system gradually.

Figure 5 shows the molecular structures of *cis*-2-nitro-7-(dimethylamino)-9-(2',3'-dihydro-1'*H*-naphtho[2,1-*b*]thiopyran-1'-ylidene)-9*H*-thioxanthene ((*P*)-*cis*-**17**) and *trans*-dimethyl-[1-(2-nitro-thioxanthene-9-ylidene)-2,3-dihydro-1*H*-benzo[*f*]thiochromen-8-yl]amine ((*P*)-*trans*-**18**). Anti-folded helical structures, in which the top and bottom parts are respectively tilted up and down relative to the plane of the central olefinic bond, are clearly observed. The extent of folding and twisting in these and related overcrowded alkenes can vary considerably. It should be emphasized that only minor deviation from planarity occurs at the central double bond (dihedral angles 5.4° (**17**) and 6.8° (**18**)), while normal bond lengths are found (1.353 Å (**17**) and 1.338 Å (**18**)).^[30,31]

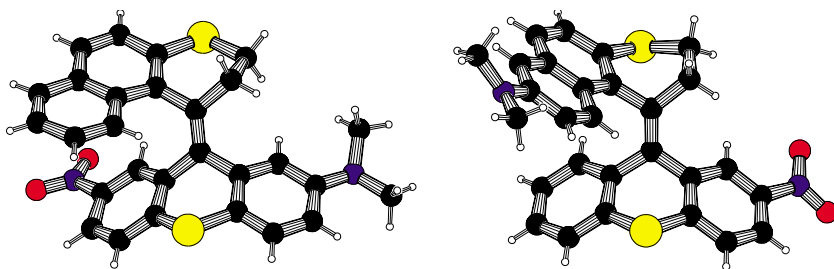
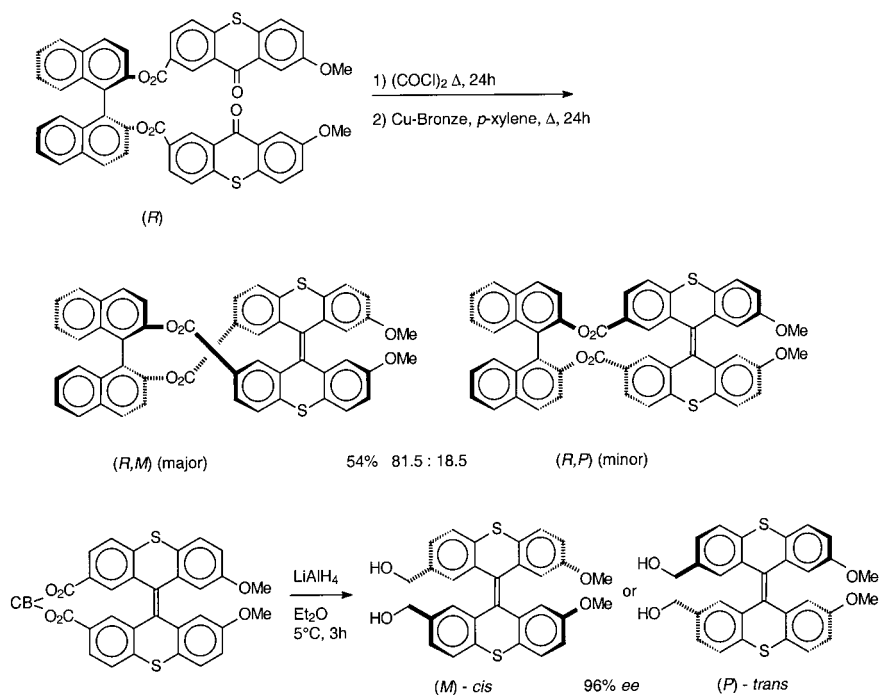


Fig. 5: Pluto diagrams of the crystal structures of *P-cis*-17 and *P-trans*-18.

The geometrical isomers and enantiomers of the overcrowded alkenes 15–18 can readily be separated using chiral HPLC. Recently, an asymmetric synthesis of overcrowded alkenes has been developed, involving chirality transfer from an axial single bond to an axial double bond (Scheme 8).³² This methodology is particularly attractive for preparation of larger quantities of enantiomerically pure chiral switches based on overcrowded alkenes. The orientation of the two xanthylidene moieties is dictated by a binaphthol template. After a coupling step and separation of the diastereomers, the bi-xanthylidene is obtained with 96 % e.e. after removal of the template.



Scheme 8: Asymmetric synthesis route to optically active overcrowded alkenes (CB = Chiral bridging unit).

Tab. 2: Racemization barriers in overcrowded alkenes **23** with different bridging moieties X and Y.

X	Y	Racemization barrier (kcal mol^{-1})	C ₂ -C ₁₁ distance (Å)
O	O	24.9 ± 0.3	2.34
CH ₂	O	27.4 ± 0.2	2.48
S	O	28.0 ± 0.2	2.75
S	S	28.9 ± 0.1	2.75
S	CHCH	29.0 ± 0.3	3.10

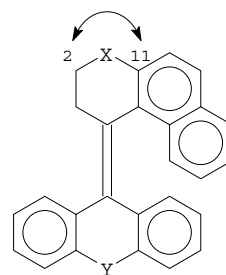
**23**

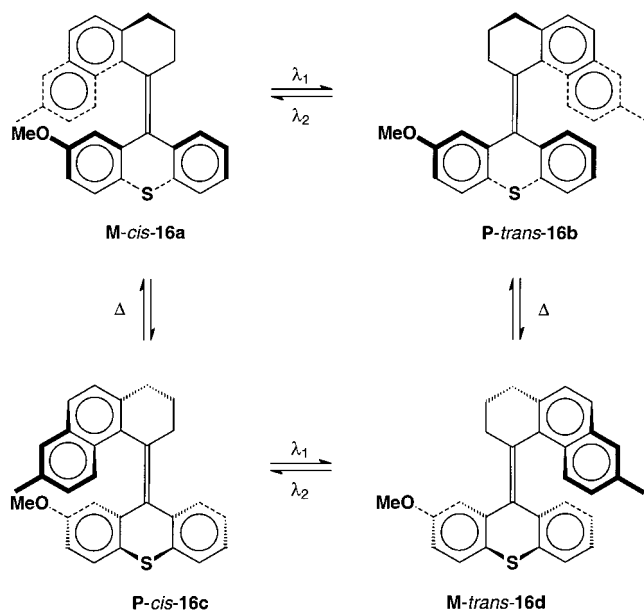
Table 2 summarizes the racemization barriers in unsubstituted chiral alkenes **23** with different bridging moieties in their upper and lower halves. As is evident from these data, the tetrahydrophenanthrene-type upper part is large enough to prevent fast racemization by movement of the aromatic moieties of upper and lower halves through the mean plane of the molecule. On the other hand, there is enough conformational flexibility in the molecules to prevent excessive distortion of the central olefinic bond (leading to ground state destabilization), which would lower the racemization barrier.

By modification of the bridging units X and Y in the upper and lower halves in **23**, it is possible to tune the racemization barriers. Similar structural effects have been found for other overcrowded alkenes. In particular, the effect of the (hetero)-atom X on the magnitude of the racemization barrier of xanthenes (Y = O) is very pronounced. The Gibbs energy of activation increases gradually from 24.9 (X = O) to 28.0 kcal mol^{-1} (X = S), with a concomitant increase in the C₂-C₁₁ interatomic distance from 2.34 Å to 2.75 Å. The growth in the racemization barriers is attributed to the increased steric hindrance in the so-called fjord region of the molecules as the naphthalene unit of the upper half and the (thio)xanthene lower part are pushed towards each other.^[33]

In these molecular switches, there is a delicate balance between ground state distortion and ease of helix inversion, leading to racemization. It should be emphasized that the possibility of tuning the barriers for thermal and photochemical isomerization processes is important for the construction of, for example, stable molecular switches and rotors.

The thermal and photochemical isomerization processes of the first chiroptical switch **16**, based on the principles described here, are shown in Scheme 9.^[34]

Upon heating a solution of enantiomerically pure **M-cis-16a** in *p*-xylene, racemization was observed, with **P-cis-16c** being produced ($\Delta G = +26.4 \text{ kcal mol}^{-1}$). No *cis*-*trans* isomerization (**16a** → **16b**) was evident. Irradiation of **M-cis-16a** at 300 nm gave a mixture of 64 % **M-cis-16a** and 36 % **P-trans-16b**, as determined by chiral HPLC, NMR, and CD spectroscopy. Irradiation at 250 nm resulted in a photostationary state containing 68 % **M-cis-16a** and 32 % **P-trans-16b**. Alternating irradiation at 250 and 300 nm resulted in a modulated CD (and ORD) signal which could readily be



Scheme 9: Thermal and photochemical switching behavior of the first chiroptical switch **16**.

detected at 262 nm. In this switching process a stereospecific interconversion of **M** and **P** helices had indeed been achieved, although 10 % racemization was observed after 20 switching cycles.^[34]

Structural modifications were introduced in order to improve stability towards racemization, to enhance the stereoselectivity of the process, and to shift the wavelengths for photoisomerization into the visible region.^[30,35] Compound **17** (Scheme 10), with a benzo[a]thioxanthylidene upper half, has a considerably higher racemization barrier ($\Delta G_{rac} = 29.2 \text{ kcal mol}^{-1}$). The presence of donor and acceptor substituents in the lower half result in large bathochromic shifts in the UV/Vis spectra and, compared to **16**, relatively large differences in absorption spectra between **M-cis-17a** and **P-trans-17b**. The first feature permits photoisomerization at wavelengths close to the visible region of the spectrum. The CD spectra of **M-cis-17a** and **P-trans-17b** are near mirror images (Figure 6a), illustrating the pseudoenantiomeric nature of both stereoisomers. In **M-cis-17**, the naphthalene chromophore faces the nitroarene acceptor moiety, whereas in **P-trans-17b** it faces the dimethylaminoarene donor moiety, leading to subtle differences in the UV/Vis spectra of the two forms. The extremes in the UV/Vis difference spectrum determine the optimal irradiation wavelength.

Irradiation of enantiomerically pure **M-cis-17a** (or **P-trans-17b**) at 365 nm and 435 nm in *n*-hexane resulted in photostationary states with **M-cis-17a** / **P-trans-17b** ratios of 30:70 and 90:10, respectively (Scheme 10).^[30,35]

Alternating irradiation at 435 and 365 nm resulted in switching between two states with either **M** or **P** helices in excess, as illustrated in Figure 6b. As well as the

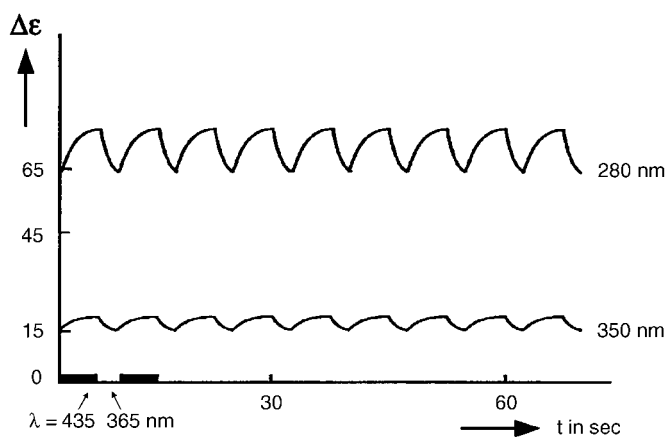
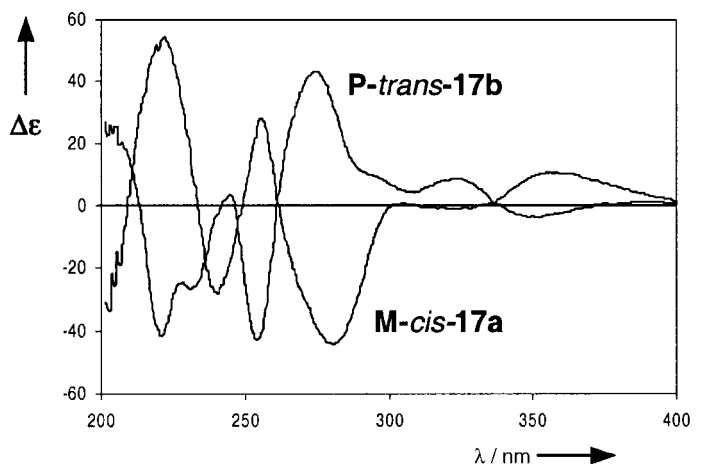
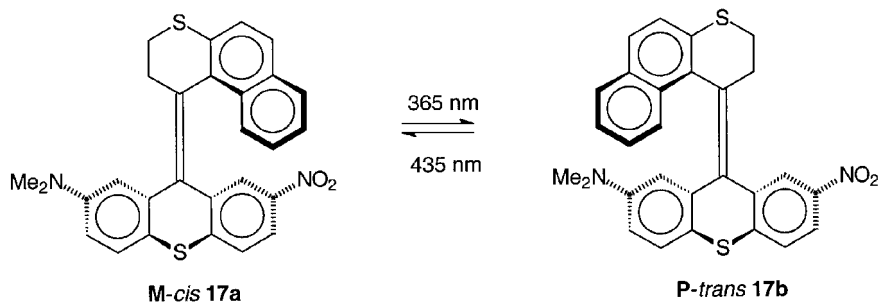


Fig. 6: (a) CD-spectra of *M-cis-17* and *P-trans-17*; (b) Plots of $\Delta\epsilon$ at 280 nm and 350 nm versus irradiation time for the *M-cis-17* \rightleftharpoons *P-trans-17* isomerization with alternating irradiation at $\lambda = 435$ nm and $\lambda = 365$ nm.



Scheme 10: Stereoselective photoisomerization of donor-acceptor-substituted molecular switch 17.

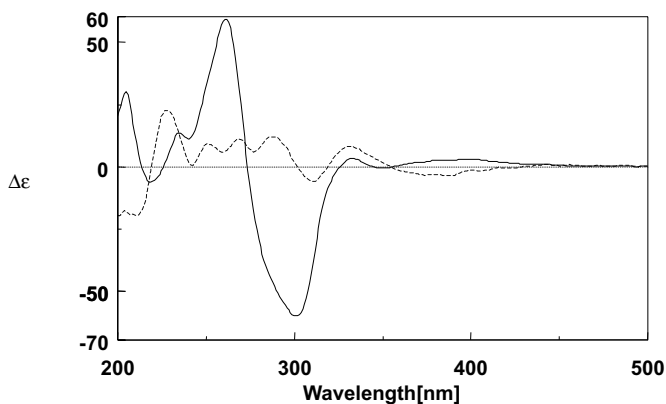


Fig. 7: CD spectra of **M-cis-18a** (continuous) and **P-trans-18b** (dashed).

efficient helix reversal and an improvement in photostationary state difference from 4 % (switch **16**) to 60 % (switch **17**), it was also possible to perform 80 cycles without fatigue or racemization.

The nature of the substituents is a critical factor in these chiroptical switches. Replacing the dimethylamino group in **17** by the weaker methoxy donor moiety, as in **15**, resulted in low stereoselectivity in the photoisomerization process.^[36] Introduction of the dimethylamino donor group in the upper part, as in structure **18** (Scheme 6), resulted in entirely different CD spectra for the **M-cis-18a** and **P-trans-18b** isomers (Figure 7). Although these isomers have opposite helicities, they can no longer be considered pseudoenantiomers, as a large difference in donor–acceptor interaction is present between the two isomers. Alternating irradiation at 340 and 435 nm in *n*-hexane resulted in photostationary states with **M-cis-18a** / **P-trans-18b** ratios of 76:24 and 94:6, respectively, and a modulated CD signal.

Upon irradiation at 435 nm in toluene, an extremely high stereoselectivity was observed, with a ratio of **M-cis-18a** to **P-trans-18b** of 99:1. Compared to chiroptical switch **17**, with a donor and acceptor moiety in the lower half, compound **18** suffers from poor reversibility, which can be attributed to the favorable donor–acceptor interaction in **M-cis-18a**. In view of the potential of gated response switching systems (see Section 5.4.1), it is noteworthy that the preference for the *cis*-form helicity can only be changed to a preference for the *trans*-form if the favorable donor–acceptor interaction is eliminated. This feature implies that it is possible to lock photochemically written information and that it then, irrespective of the wavelengths used, cannot be unlocked except by affecting the donor–acceptor interaction.

It should be noted that the photoisomerization process and the composition of the photostationary states in the chiroptical switches described here are strongly dependent on the irradiation wavelength and the medium. For instance, no stable photostationary states were reached with **15** in ethanol and chloroform, in contrast to its behavior in *n*-hexane. Compound **P-trans-18b** gave a photostationary state after 2 min irradiation at 435 nm in *n*-hexane, while in 1,4-dioxane under otherwise identical conditions this state had not been reached after 4h irradiation. Similar observa-

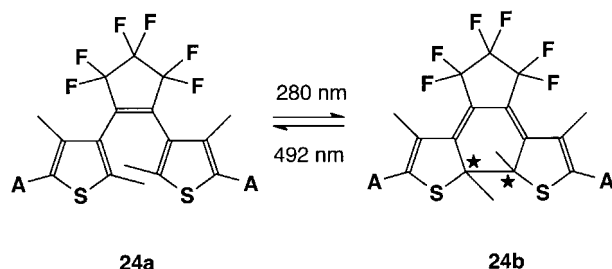
tions have recently been made in photoisomerization studies of other donor-acceptor substituted alkenes.^[31]

5.3.2

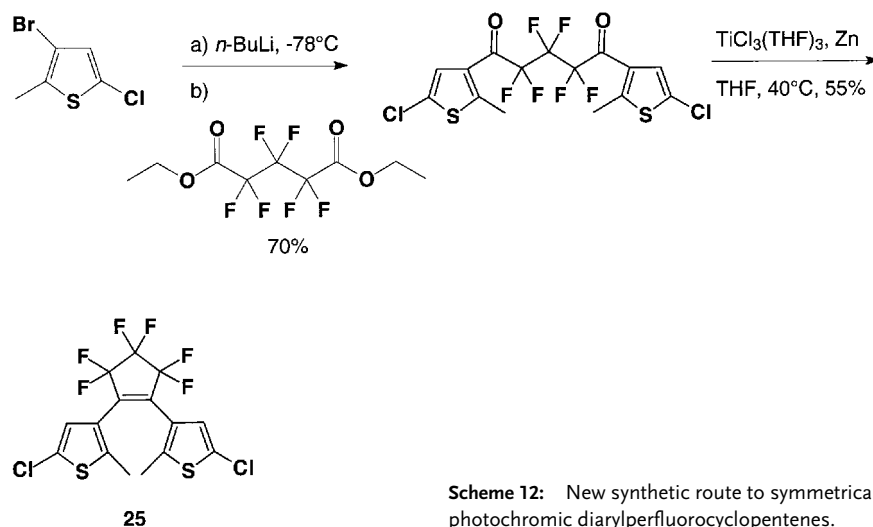
Diarylethenes

A reversible photocyclization forms the basis for molecular switches with the diarylethene structure (Scheme 11).^[37] Irradiation of the colorless, nonconjugated, open form **24a** with UV light results in ring-closure to the colored, conjugated form **24b**. With visible light, the process can be reversed.

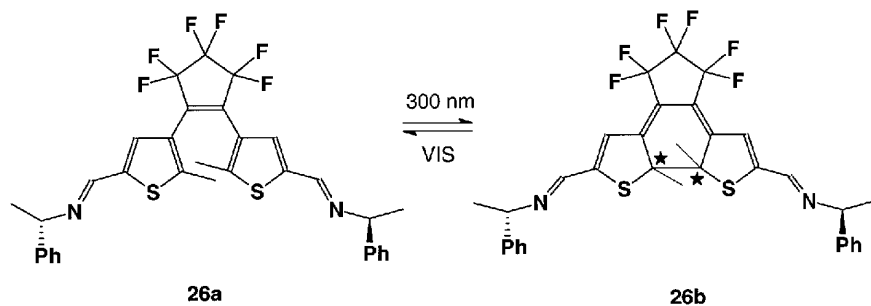
The introduction of the perfluorocyclopentene moiety, as present in the perfluorocyclopentenebisthien-3-yl systems **24**, has resulted in excellent thermal and chemical stability and often in high fatigue resistance, allowing many switching cycles. The common synthetic route involves double substitution of perfluorocyclopentene with the appropriate aryllithium, but low yields are often encountered. Recently an alternative route, based on an intramolecular McMurry coupling to produce **25**, has been developed (Scheme 12).^[38]



Scheme 11: Photochemical switching of diarylethene **24** (* denotes stereogenic center).



Scheme 12: New synthetic route to symmetrical photochromic diarylperfluorocyclopentenes.



Scheme 13: Chiroptical switch based on diarylethylene bis-imine **26**.

The groups of Irie and Lehn have developed a variety of diarylethenes, covering the whole visible spectrum.^[37] A detailed discussion is given in Chapter 2.

The open forms of diarylethenes consist of a dynamic system of helical conformers. Conrotatory ring-closure upon irradiation of a symmetric diarylethene **24** generates the enantiomers of the C_2 -symmetric ring-closed forms (*S,S*)-**24b** and (*R,R*)-**24b**. The resolution by chiral HPLC of a number of these closed forms was successful, but the stereogenic centers are lost upon ring-opening (Scheme 11).^[39] When chiral auxiliary groups are present, however, both the open and the closed forms are chiral, and ring-closure results in the formation of diastereomers. Particularly illustrative is the switching process of bisimine modified diarylethene **26**, containing

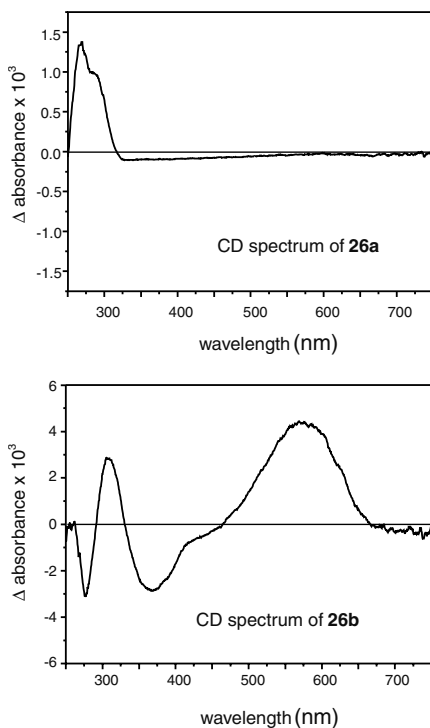


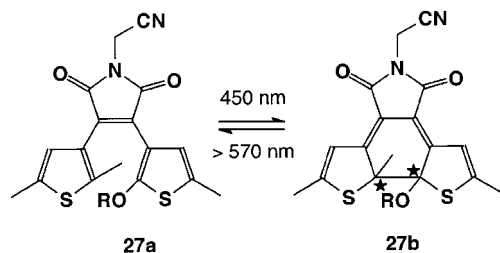
Fig. 8: CD spectra of the open form **26a** and closed form **26b** of the chiroptical switch based on diarylethylene bis-imine.

two (*S*)- α -phenylethylamine residues as chiral auxiliary groups (Scheme 13). In the open form, no CD absorptions above 325 nm are present (Figure 8a), despite the fact that the molecule adopts a helical structure, as is clear from the X-ray structure of the open form **26a**. After ring-closure (300 nm irradiation), a distinctive CD band is found at 575 nm (Figure 8b). It should be noted that, despite the fact that only low diastereoselectivity (approx. 10 % diastereomeric excess (d.e.)) was observed in the ring-closure of (*S,S*)-**26a**, the two states in this switching process can be readily detected due to the large differences in their chiroptical properties.

It is clear that the most prominent feature of diarylethene switches is the potential to interrupt conjugation in a molecular type wire in which the switches are incorporated. In the open state, electronic interaction between the groups A (Scheme 11) at the periphery is blocked, whereas in the closed form electron delocalization is restored.

Irie succeeded in a diastereoselective photocyclization using a diarylmaleimide-based switch **27**, in which a *d*- or *l*-menthyl moiety was present at the 2-position of one of the thiophene rings (Scheme 14).^[39] Irradiation of **27a** at 450 nm in toluene at 40 °C gave **27b** with a d.e. of 86.6 %.

Like in other chiroptical switches (Section 5.3.1), solvent polarity was found to play an important role. Diastereoselective cyclization was observed in THF and toluene, but not in nonpolar solvents such as *n*-hexane. Upon photoexcitation, diarylethenes **24** (Scheme 11) can adopt a planar and a twisted conformation, and photocyclization only proceeds through the planar conformation. In the case of chiral diarylethene **27a**, there are two diastereomeric planar conformations leading to the diastereomers of the cyclic product **27b**. The stereoselectivity in the photocyclization process is enhanced because of a decrease in the excited state energy of the unreactive twisted form, providing a relaxation pathway for the less favorable planar diastereoisomer in more polar solvents. Chiral photochromic diarylethenes are among the most prominent photoswitches known today, featuring nondestructive read-out, excellent reversibility, and the potential for construction of switchable molecular wires and modulation of liquid crystalline phases (see Section 5.5.3).^[40,41]



R = *d*-menthyl or *l*-menthyl

Scheme 14: Diastereoselective photocyclization of chiral diarylethene derivative **27**.

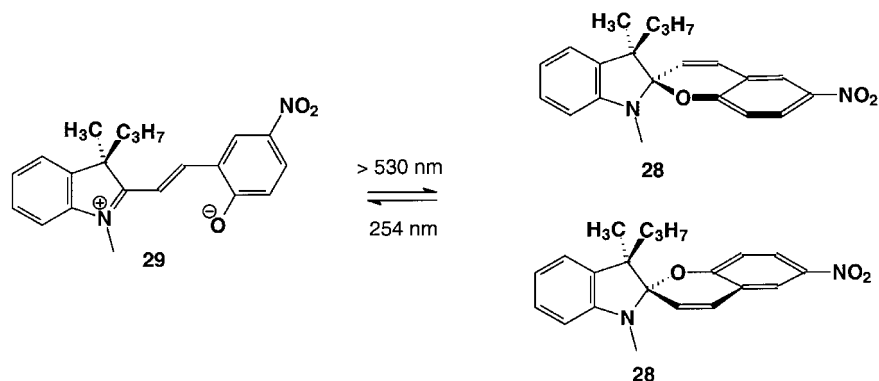
5.3.3

Other Diastereoselective Switches

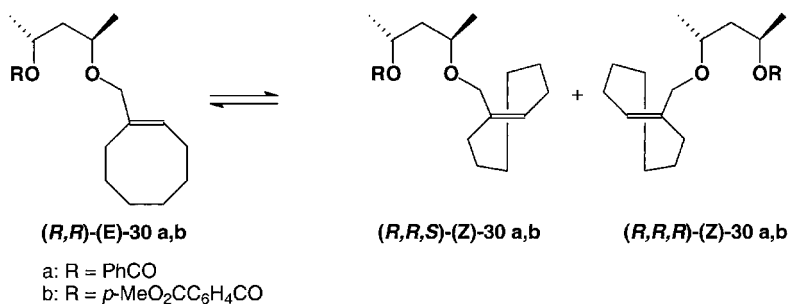
Following the pioneering work of Hirshberg,^[42] the photochromism of spiropyrans has been extensively studied.^[43] The photochromic and thermochromic behavior of this class of compounds is due to the interconversion of the closed spiropyran form to the open merocyanine form (Scheme 15). UV irradiation of the closed form **28** results in ring-opening to the zwitterionic form **29**, which reverts to the closed form either thermally or on irradiation with visible light.

The spiro carbon is a stereogenic center in spiropyrans, but because of the achiral structure of the open merocyanine form, the photochromic process will always lead to racemization unless additional chiral moieties are present. When a chiral substituent was introduced, remote from the spiro center, it was possible to isolate diastereoisomers of the spiropyrans, but rapid epimerization at the spiro center occurred.^[44] Diastereoselective switching was successful with **28**, in which a stereogenic center was present close to the spiro carbon (Scheme 15).^[45] Distinct changes in CD absorption at 250 nm were monitored upon irradiation with UV (250 nm) and with visible light (>530 nm) and a diastereomeric ratio of 1.6:1.0 was calculated for the closed form **28**. Furthermore, a temperature-dependent CD effect was observed with this system; it was attributed to an inversion of the diastereomeric composition at low temperatures. It might be possible to exploit such effects in dual-mode chiral response systems. A diastereoselective ring-closure was also recently observed in a photochromic N6-spirobenzopyran tricarbonyl chromium complex.^[45b]

Diastereoselective photoisomerization was also observed with chiral cyclooctenes **30** (Scheme 16). Extensive studies by Inoue^[46] on the enantioselective *E-Z* photoisomerization of cyclooctene in the presence of chiral sensitizers revealed that the geometry of the involved singlet exciplexes determine the stereochemical course of the process to a large extent. In **30**, the cyclooctene and the arylcarboxylate sensitizers are covalently connected through a chiral (2*R*,4*R*)-2,4-pentanediol tether, which might dictate a preferred exciplex geometry resulting in enhanced stereocontrol. Irradiation of benzoate **30a** gave a photostationary state with a *Z/E* ratio of 8/10 and



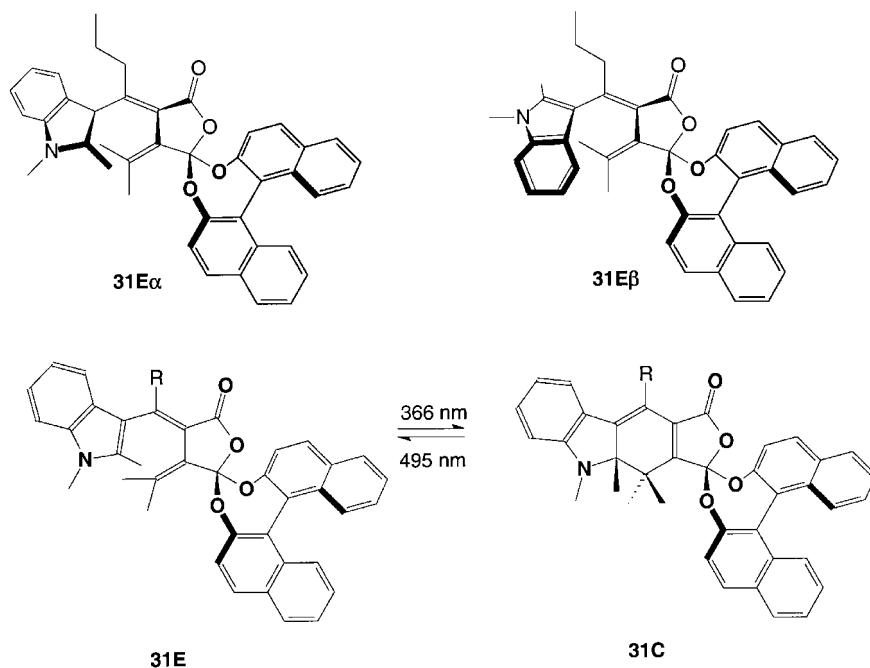
Scheme 15: Diastereoselective photochromism of spiropyran **28**.



Scheme 16: Diastereoselective photoisomerization of cyclo-octene **30** by intramolecular sensitization.

a d.e. of 19 % for the *Z* form. In contrast to the forward *E* to *Z* photoisomerization, no stereoselectivity was observed in the reverse reaction; the *Z* to *E* isomerization. This was attributed to very fast intramolecular quenching due to the high strain in the *Z* isomer. The highest diastereoselectivity in the *E*-*Z* photoisomerization was found with terephthalate derivative **30b** (d.e. = 44 %).

Fulgides have been extensively investigated as erasable and rewritable optical memory systems (see Chapter 4) and these photochromic molecules are attractive candidates for chiroptical switch development.^[47] Their bistability is based on the



Scheme 17: Diastereoselective photochromism of a binaphthol-based indolylfulgide **31**.

reversible conrotatory photochemical cyclization of a 1,3,5-hexatriene moiety. One promising chiroptical switch is based on fulgide **31**, containing a binaphthol chiral auxiliary moiety (Scheme 17).^[48] Photochemical switching is observed, involving the open (P)-**31E** form and the closed (9aS)-**31C** form.

Upon irradiation at 366 nm, a diastereomeric ratio of 95/5 for the closed form is reached, while subsequent irradiation at 495 nm regenerates the open form (as a mixture of conformers (P)-**31E** α /(P)-**31E** β = 57/43). From Scheme 17 it can be seen that only (P)-**31E** α adopts the right geometry for the hexatriene component to undergo photocyclization

5.4

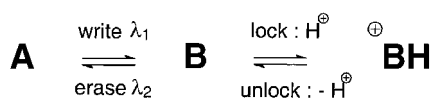
Multifunctional Chiral Switches

5.4.1

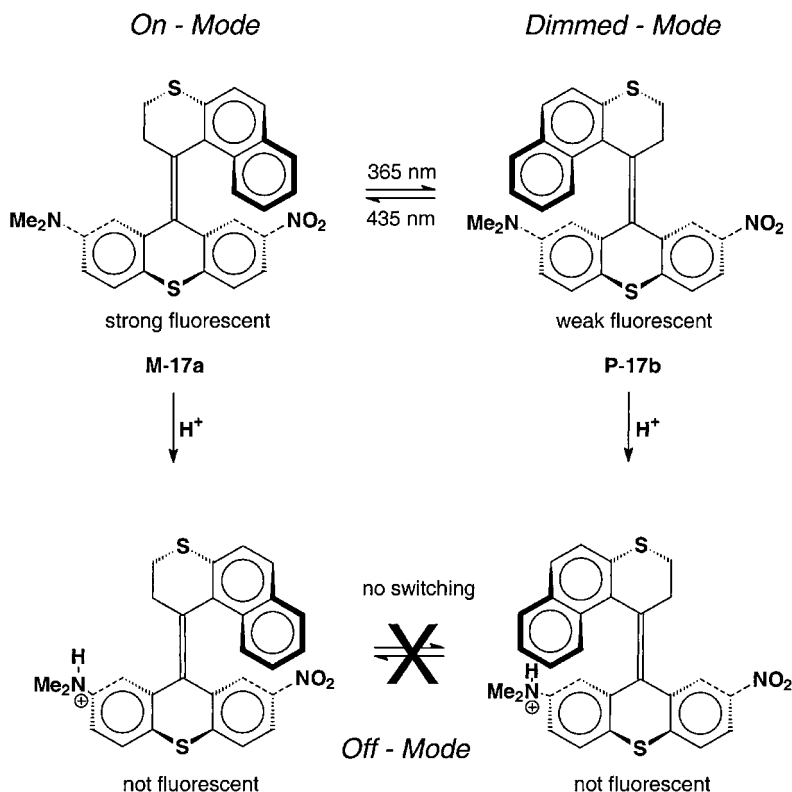
Gated Photoisomerization

A highly desirable property in information storage systems based on molecular switches is gated response.^[49] Gated photochemical reactivity implies that no change occurs upon irradiation unless another external stimulus, either physical or chemical, is applied to the system. Scheme 18 shows a typical write-lock-unlock-erase cycle involving photoisomerization and protonation.

A major advantage is the potential to lock (and protect) written information in the photobistable material. A number of chemical gated systems involving mutual regulation of the photochromic event and, for instance, fluorescence, ion binding, or electrochemical properties have been reported.^[50] Scheme 19 illustrates a chiral gated response system based on donor-acceptor substituted alkene **17**.^[51] The photochemical isomerization process of both the *M-cis* and the *P-trans* form was effectively blocked by the addition of trifluoroacetic acid. Protonation of the dimethylamine donor unit of *M-cis*-**17a** and *P-trans*-**17b** resulted in an ineffective acceptor-acceptor (nitro and ammonium) substituted thioxanthene lower half. Since the stereoselective photoisomerization of **17** relies on the presence of both a donor and acceptor unit, photochemical switching could be restored by deprotonation by the addition of triethylamine.



Scheme 18: Write – lock – unlock – erase cycle based upon a photoisomerization process and a protonation process.



Scheme 19: Dual-mode photoswitching of fluorescence.

5.4.2

Dual-mode Photoswitching of Luminescence

As well as the change in chirality, it is also possible that a second property might be modulated upon photoisomerization, thus constituting a dual-mode response system. Modulation of fluorescence is particularly attractive, as fluorescence provides a sensitive read-out method and can be used to probe medium and excited state effects. Large changes in fluorescence intensity between the two forms have been observed in a number of photochromic systems. Lehn and co-workers,^[50a] for example, found strong emission in the open form of a diarylethene-based switch, whereas the closed form showed only very weak fluorescence. In the case of sterically overcrowded alkene **17** (Scheme 19), excitation of *P-trans-17b* and *M-cis-17a* at 300 nm resulted in fluorescence at $\lambda_{\text{max}} = 531$ and 528 nm, respectively, with different intensities (Figure 9).^[51] An integrated fluorescence quantum yield (400–600 nm; ethanol) of 0.153 was measured for *P-trans-17b*, and of 0.137 for *M-cis-17a*. The fluorescence emission is attributed to intramolecular charge transfer of dimethylamine donor moiety and is dependent on the helicity. Photomodulation of the emission is shown in the inset of Figure 9.

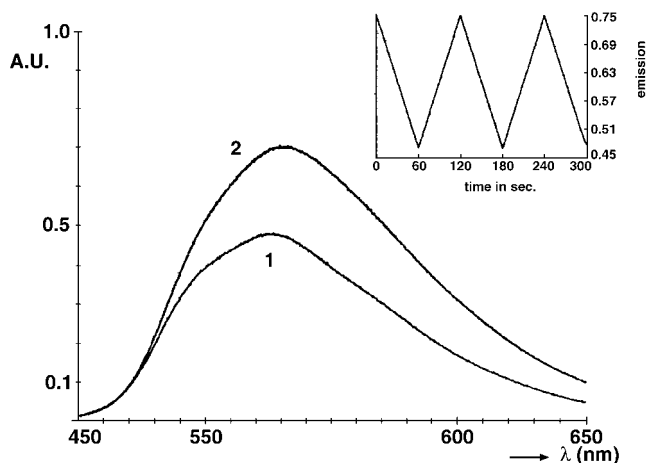


Fig. 9: Fluorescence emission spectra (*n*-hexane) of photo-stationary states of *cis*-**17a** and *trans*-**17b** in 90:10 and 30:70 ratios (A.U. = arbitrary units, relative intensities). Inset: modulated emission signal during alternating irradiation at 365 and 435 nm (excitation 300 nm, irradiation time 60s).

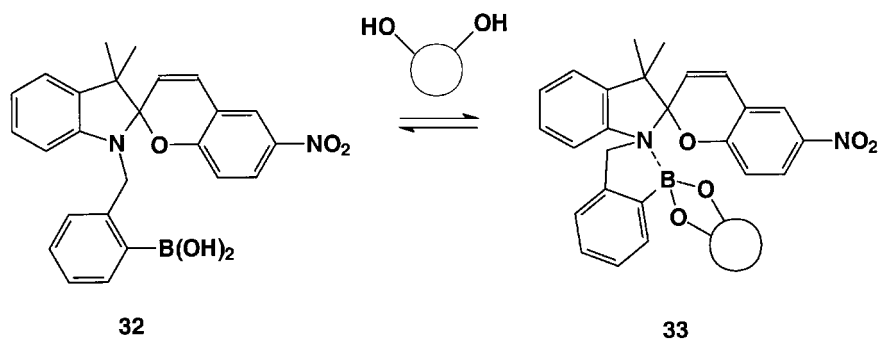
The emission of both **M-cis-17a** and **P-trans-17b** is quenched when trifluoroacetic acid is added. Addition of triethylamine fully restores it. This gated molecular switching system allows pH-dependent photomodulation of chirality and fluorescence. Three distinctive states can be addressed; the “ON”, “Dimmed”, and “OFF” states (Scheme 19). The **P** and **M** forms, with their different fluorescence intensities, can be considered the “ON” and “Dimmed” states. Upon protonation, both switching and emission are in the “OFF” mode, which constitutes a locking system. The photoswitching and fluorescence is switched “ON” again after deprotonation. On the basis of time-resolved fluorescence spectroscopy and circularly polarized luminescence measurements, it has recently been found that the chirality of the fluorescent excited states is a fourth parameter that can be modulated in this system.^[52] In this context it is worth mentioning that circularly polarized chemiluminescence was recently observed during photochemical isomerization of a chiral camphanic acid modified paracyclophane.^[53]

Yokoyama et al.^[54] found a complete “ON/OFF” switching of fluorescence with the binaphthol-derivatized fulgide **31** (Scheme 17). The closed form showed a weak emission ($\lambda_{max} = 610\text{nm}$, $\Phi = 0.01$) upon excitation at 470 nm in toluene, while the open form did not show any fluorescence.

5.4.3

Chiral Molecular Recognition

Photoresponsive host-guest systems based on azobenzene-substituted crown ethers have been shown to be particularly effective in the control of molecular recognition by light, due to their large geometrical changes upon *E-Z* isomerization.^[55] A num-



Scheme 20: Boronic acid-modified spiropyran **32** for reversible sugar binding.

ber of photoactive receptor systems have been developed in recent years. These include a diarylethene photoswitchable group functionalized with two arylboronic acid moieties for saccharide binding and photochromic nitro-spiroprans bearing arylboronic acid groups (**32/33**) that enable photochemical control of the binding of sugars and diols.^[56] An attractive feature of the latter system, shown in Scheme 20, is visual detection of guest binding through the observation of a color change. Willner et al.^[57] reported photochemically induced changes in association constants with an α -D-mannopyranoside using a photobistable fulgimide modified with the pyranoside binding protein concanavalin A.

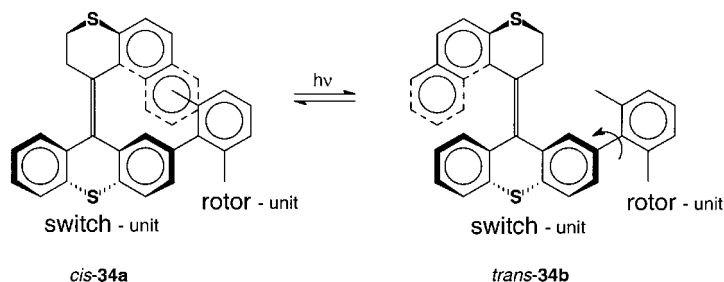
The *E*-*Z* isomerization of an azobenzene unit was employed in an approach towards photocontrol of the chiral recognition event in a membrane.^[58] To this end, {4-(phenyl-azo)phenyl}carbamate residues were attached to carbamate-protected glucose units of cellulose and amylose. The photomodulation of the chiral recognition was explained by a change in the ordering of the polymer, leading to a change in solubility.

The inclusion complexation of spiropyrans in cyclodextrins has also been explored as a means to control photochromic reactions.^[59] Distinct differences in complexation of sulfonic acid-modified spiropyrans to various cyclodextrins were observed and the closed spiropyran form bound to β -cyclodextrin was stable towards photochemical ring-opening.

5.4.4

Unidirectional Rotary Motion

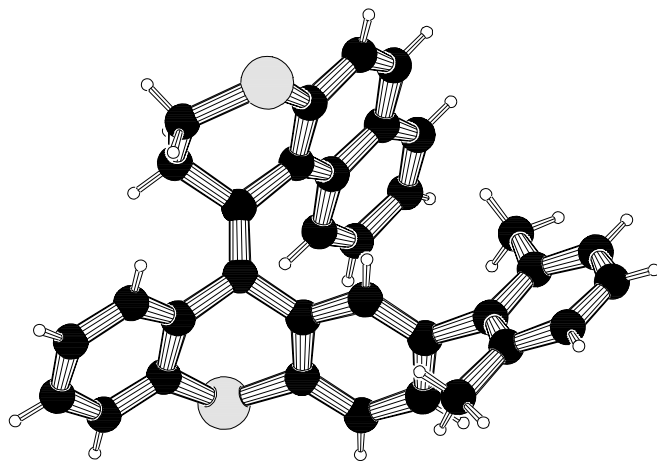
The fascinating molecular motors discovered in various biological systems in recent years offer the great challenge of controlling translational and rotary motion at the molecular level.^[60] With this goal in mind, a number of interlocked systems such as catenanes and rotaxanes have been designed. They undergo controlled movements triggered by chemical, electrochemical, or photochemical events^[61] (see Chapters 7 and 8). Molecular turnstiles, ratchets, brakes, and several metal complexes, in which redox switching is accompanied by large geometrical changes in the ligands, have been reported.^[62,63] The combination of a photoswitchable overcrowded alkene and a biaryl-type rotor has been used in an approach to controlling rotary motion around a biaryl-



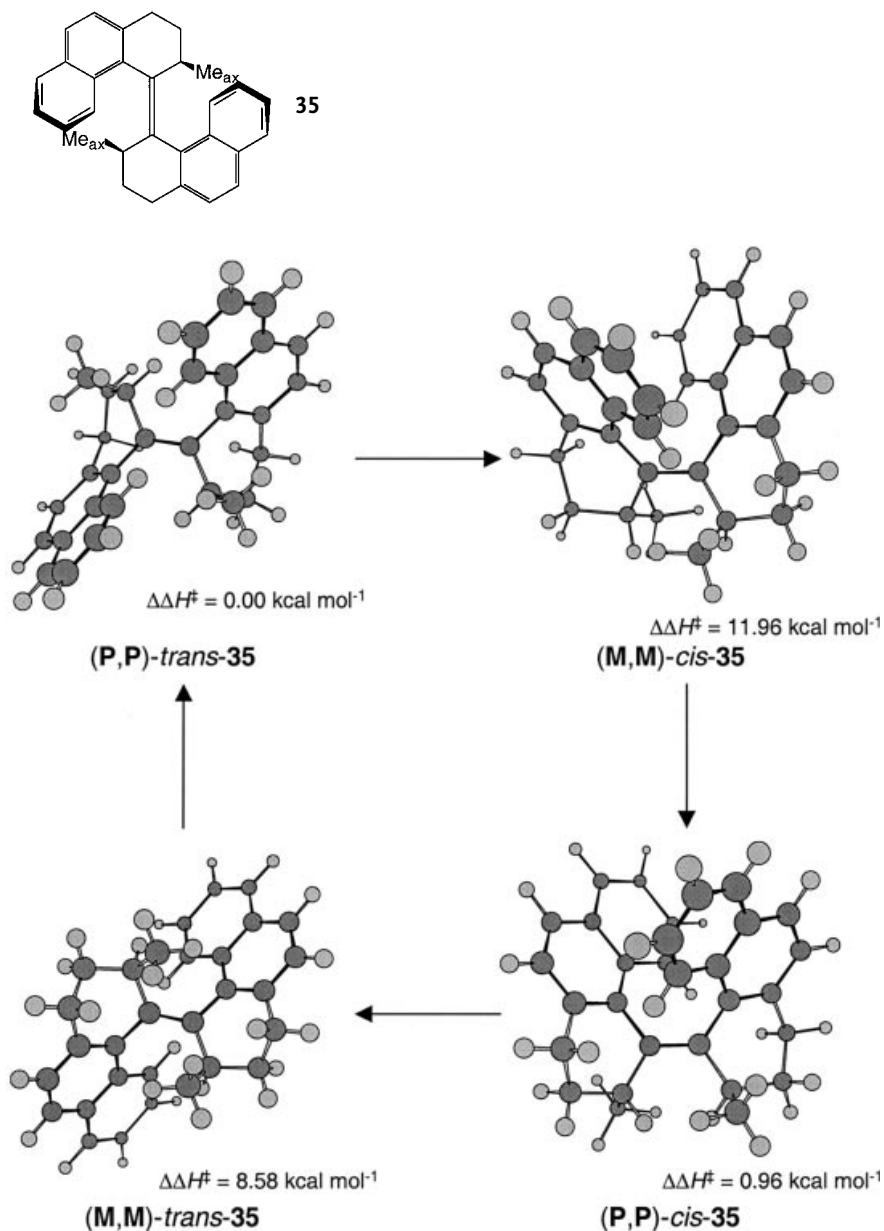
Scheme 21: Switchable molecular rotor.

single bond.^[64] As illustrated in Scheme 21, photoisomerization between the *cis* form **34a** and the *trans* form **34b** will cause a distinct difference in the interaction of the upper naphthalene component with the xylyl rotor moiety attached to the lower part. As the xylyl moiety faces the naphthalene in the case of *cis*-**34**, it might be possible to block the rotation. The X-ray structure of **34a** supports this notion (Figure 10).

In this system, three processes can be distinguished: photochemical isomerization of *cis*-**34a** to *trans*-**34b** with simultaneous helix inversion, thermal inversion of *P*-*cis*-**34a** into *M*-*cis*-**34a** (the barrier of 29 kcal mol⁻¹ blocks this pathway), and biaryl rotation. Dynamic NMR studies revealed barriers to biaryl rotation of $\Delta G = +19.0$ and 19.7 kcal mol⁻¹ for *cis*-**34a** and *trans*-**34b**, respectively.^[64] Surprisingly, the barrier for the *trans* isomer is higher than that for the *cis* isomer. Semiempirical calculations showed distinct differences in chiral conformations and steric effects associated with the folding of the *cis* and *trans* forms. In particular, the *o*-methyl groups of the xylyl rotor become entangled during rotary motion with the CH₂ groups of the upper half in *trans*-**34b**. In *cis*-**34a**, however, the nearly planar naphthalene moiety is bent away, leaving enough space for faster rotation (Figure 10). In this switchable rotor, the energy differences are still rather small and photoswitching is not very

Fig. 10: X-ray structure of **34a**.

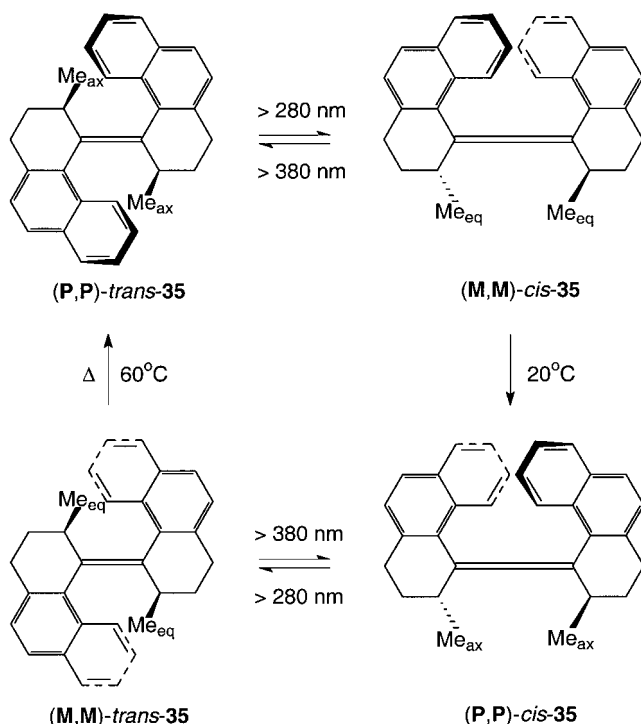
efficient. Furthermore as in other rotors and ratchets,^[62] there is no control over the direction of rotation, a *conditio sine qua non* for a molecular motor. The design of the light-driven monodirectional rotor **35**^[65] followed from an extensive investigation into the thermal and photochemical isomerization processes of bis-phenanthrylidenes.^[66]



Scheme 22: MOPAC93-AM1 calculations for the conformations of the molecular rotor **35**.

This compound ((3*R*,3'*R*)-(**P,P**)-*trans*-1,1',2,2',3,3',4,4'-octahydro-3,3'-dimethyl-4,4'-biphenanthrylidene, (**P,P**)-*trans*-35) was prepared by McMurry coupling of (*R*)-3-methyl-4-keto-1,2,3,4-tetrahydrophenanthrene, which in turn was obtained through resolution or asymmetric alkylation methods.^[67] X-ray analysis showed that (**P,P**)-*trans*-35 adopts a double helical structure, with the two methyl substituents in a pseudo-axial orientation. Calculations confirmed this preferred conformation for (**P,P**)-*trans*-35, and showed that (**M,M**)-*trans*-35, with both methyl groups in pseudo-equatorial orientations, was 8.6 kcal mol⁻¹ less stable (Scheme 22). For the *cis* isomer, the same features were observed, with (**M,M**)-*cis*-35 (diequatorial Me-substituents) less stable than (**P,P**)-*cis*-35 by 11.9 kcal mol⁻¹.

Irradiation ($\lambda > 280$ nm) of (**P,P**)-*trans*-35 at room temperature unexpectedly yielded (**P,P**)-*cis*-35, with the same helicity as the starting material and both methyl groups in axial orientations (Scheme 23). Low temperature irradiation (-55 °C), however, gave the expected helix inversion to provide (**M,M**)-*cis*-35 (*trans*-*cis* ratio 95:5). Upon heating to 20 °C, the less stable (**M,M**)-*cis*-35 converted into (**P,P**)-*cis*-35 in an irreversible helix inversion step. Continued irradiation at $\lambda > 280$ nm resulted in photoisomerization of (**P,P**)-*cis*-35 into (**M,M**)-*trans*-35 (*cis*-*trans* ratio 10:90), with simultaneous helix inversion. Subsequent heating at 60 °C produced a thermal isomerization of (**M,M**)-*trans*-35 into the starting compound (**P,P**)-*trans*-35. The combination of the



Scheme 23: Light-driven unidirectional molecular rotor 35.

two photochemical steps and two thermal steps adds up to a full 360° rotation of the upper half of the molecule relative to the lower half.

The unidirectionality of the rotary motion was established by CD spectroscopy. Figure 11 shows CD spectra for each stage of the four-step switching cycle and the modulation of the CD signal at 217 nm over 3 consecutive full cycles.

The controlling elements that govern the unidirectional rotation are: the helicity of the overcrowded alkene, the absolute configuration of the stereogenic centers, the conformational flexibility of the rings flanking the central olefinic bond, the photochemical *cis*–*trans* isomerization, and the thermal helix inversion. The entire process involves two photochemical – energetically uphill – steps and two thermal downhill steps. The unidirectionality is due to the interconversion of the less stable forms, with diequatorial Me substituents, to the more stable forms, with diaxial Me substituents. Depending on the absolute configuration, either clockwise or counter-clockwise rotation can be achieved. Kelly et al.,^[63] using a triptycene-based system, showed that unidirectional rotary motion through sequential chemical conversions is also possible. In the context of the development of multimode molecular switches, it should be emphasized that Scheme 23 comprises four different, addressable switching states.^[65]

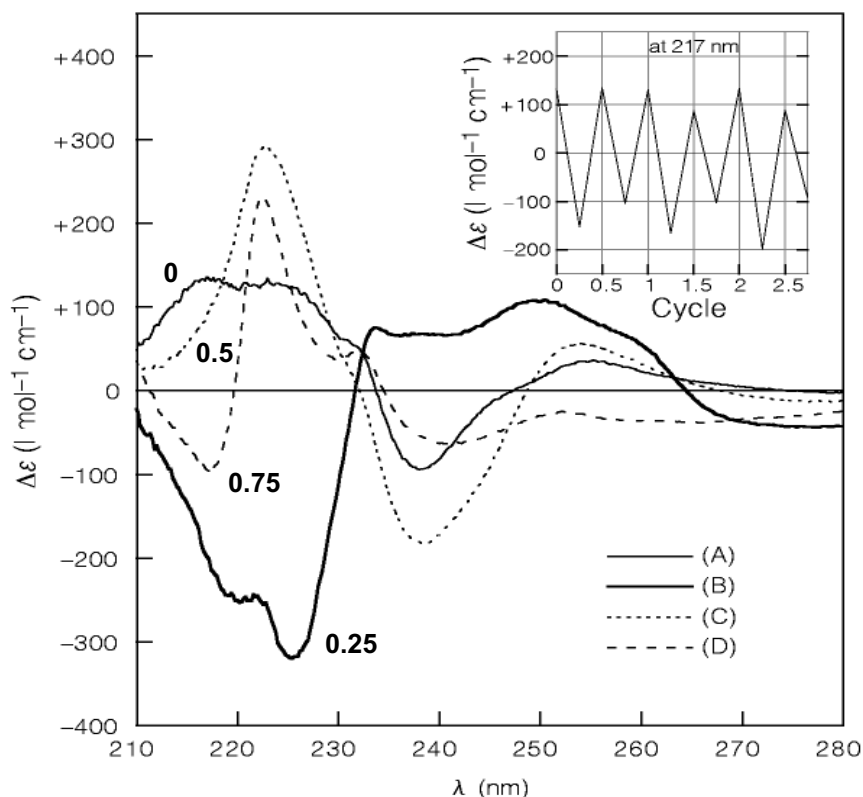


Fig. 11: CD spectra of the four stages of switching of the light-driven molecular rotor.

5.5

Switching of Macromolecules and Supramolecular Organization

5.5.1

Photochromic Polymers

Polymer-based photochromic systems have been studied extensively and are attractive in terms of practical applications because of their advantages of stability and processability. A number of reviews and articles dealing with various aspects of photochromic polymers and photoactive biomaterials have been published.^[68] Chiral photochromic peptides are discussed in Chapter 13, and photochromic liquid crystals and polymers for holographic data storage and nonlinear optics have been reviewed.^[69] Specific stereochemical effects in chiral photoresponsive polymers include:

- chiral matrix effects on an achiral photochromic unit,
- switching inducing a change in the conformation or organization of a chiral macromolecule,
- modulation of the chirality of the polymer by a chiroptical switch.

Here we will exclusively discuss polymer-based systems in which the switching unit itself is chiral.^[70]

The chiral, polymer-based molecular switch **36** was prepared by copolymerization of methyl methacrylate and methacrylates to which an optically active thioxanthene switching unit was connected through different spacers.^[71] Polymers with spacers of 2 to 6 carbons and incorporating up to 4.7 % photoactive units were synthesized (Figure 12). Irradiation of thin films of these chiral, photochromic polymers resulted in distinct changes in their CD spectra. In comparison with thin polymer films of polymethyl methacrylate doped with chiral switch **17**, the covalently bound system **36** suffers from low diastereoselectivity in the switching process. Furthermore, longer irradiation times are required to reach the photostationary states. Photochemical switching of *P-cis-17* doped in a number of polymers, including PMMA, PVC, PS, and PVAC, showed that the thermal and photochemical stability of the donor-acceptor substituted switch was retained in the polymer matrix.^[36] Kinetic studies, dielectric thermal analysis, and dynamic mechanical analysis showed that the isomerization processes critically depend on mobility in the matrix.

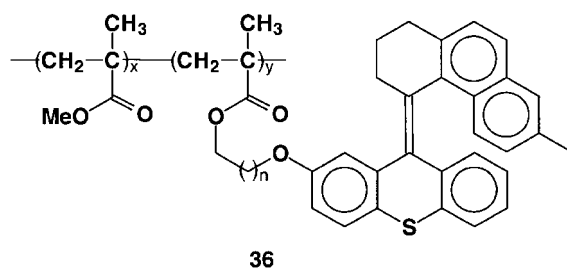
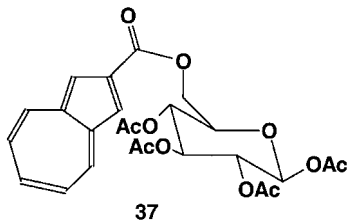


Fig. 12: Methacrylate co-polymer modified with chiroptical switch **36**.

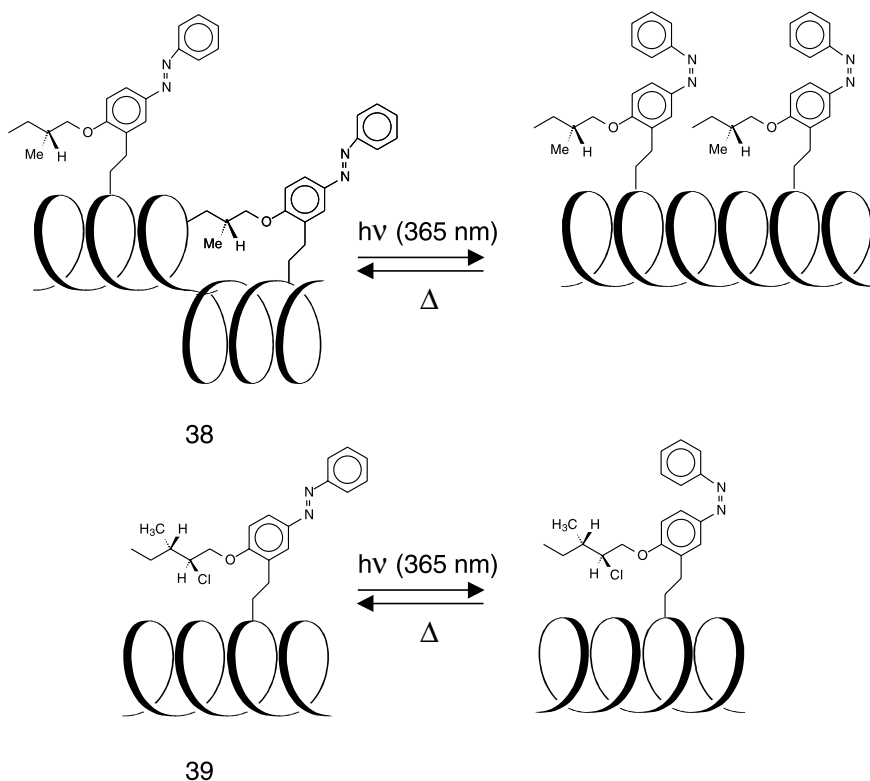
Molecular switches based on the dihydroazulene-vinylheptafulvene system are discussed in Chapter 3. Chiroptical switching was achieved with a carbohydrate-modified chiral polyazulene.^[72]



A conducting polymer film on a transparent ITO electrode was obtained by oxidative polymerization of 6-O-(2-azulenecarbonyl)- β -D-glucopyranose-1,2,3,4-tetraacetate **37**. A negative couplet (λ_{\max} 367 and 404 nm) in the CD spectrum was attributed to a twisted biazulene subunit with *R* configuration. Electrochemical oxidation resulted in the disappearance of the CD absorption, while reduction to the neutral form reestablished the CD band. The modulation of the chirality can be explained by interconversion between a neutral, twisted form of the polyazulene and a more planar, conducting form.

Photochemical control of chirality and organization of dynamic helical polymers, well known from peptides (see Chapter 13), has also been demonstrated with chiral polyisocyanates. Polyisocyanates, obtained from achiral monomers such as hexylisocyanate, are racemic mixtures of *P* and *M* helices or are composed of opposite helical segments in a long polymer chain.^[73] In the presence of chiral side groups, the polyisocyanide chains become diastereomeric and a strong preference for one helical twist sense can already be observed when a small number of chiral side groups is incorporated into copolymers. The high degree of cooperation, which results in strong amplification of chirality, has been termed the “sergeants and soldiers” effect by Green et al.^[74] Zentel et al.^[75] have prepared polyisocyanates with chiral azobenzene side groups containing one (**38**) or two (**39**) stereogenic centers in the switching unit (Scheme 24). Irradiation of **38** at 365 nm results in *E*–*Z* photoisomerization and a change in CD and ORD spectra. In this case, the population of helical segments changes but the preferred helical sense is the same in both states (Scheme 24). The same switching experiment with **39** resulted in an inversion of the helical twist sense in the polymer chain (Scheme 24).^[76]

The photoisomerization of several copolymers was studied, in order to determine the effects of the structure and switching of the chiral side chain on the helicity of the main chain. A delicate balance of parameters was found, including separation and nature of the stereocenters, solvent, and concentration of azobenzene moieties.^[77] Stereoselectivity was often greatly enhanced if the chiral moieties were closer to each other. Accordingly, it was found that the incorporation of the stereocenter into a short, two-carbon spacer resulted in much more pronounced helical preference, as well as CD effects at lower chiral chromophore concentrations. The greater helical twist and improved thermal stability of the *cis* form (half-life 40h at RT) are notable features.^[77] It was also found that the relationship between the *trans*–*cis*



Scheme 24: Chiral photoswitchable polyisocyanates: A) schematic representation of the shift in equilibrium between **P** and **M** helices upon irradiation. B) illustration of **P** to **M** helix transition in polyisocyanates upon photoisomerization of the azobenzene unit (adapted from references 75–78).

ratio of the azobenzene chromophore and the helical preference of the polyisocyanide could be linear or nonlinear. A linear relationship is observed at low concentration or with lower chiral induction by the side groups.^[78]

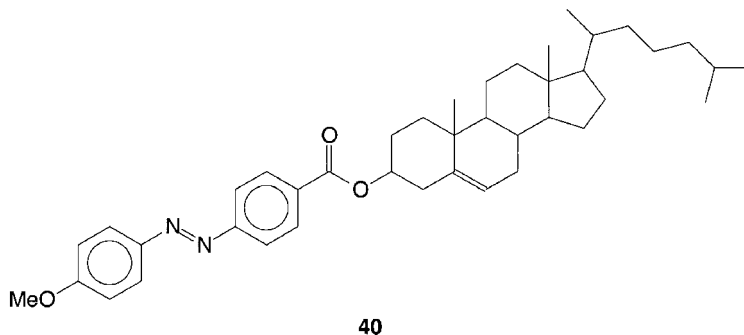
In these dynamic switchable systems, Green's majority rule is followed, with the group present at higher concentration or the isomer with the stronger chiral inductive effect controlling the helical conformation of the polymer.^[79]

5.5.2

Reversible Gel Formation

Control of the aggregation state in an organogel offers other attractive means for modulation of materials' properties and nondestructive read-out. A photoactive gelator (**40**) was obtained by Shinkai et al.^[80] by connecting 4-methoxyazobenzene through an ester linkage to cholesterol. The *trans*-isomer **40** formed a stable gel with

n-butanol, with $T_g = 15\text{ }^\circ\text{C}$. Irradiation ($330 < \lambda < 380\text{ nm}$) afforded a photostationary state with 38 % *cis* isomer and a decrease of the gelation temperature $T_g = 2\text{ }^\circ\text{C}$.



Irradiation at $\lambda > 460\text{ nm}$ gave a fast *cis*–*trans* isomerization, with a concomitant increase in T_g . The sol–gel phase transition could be controlled in this way by light, while read-out of the states could be performed by measuring the modulation of the transmission or CD. For instance, the *trans*-azobenzene gelators displayed a CD effect, presumably due to the formation of helical aggregates, whereas the *cis*-isomers did not.

5.5.3

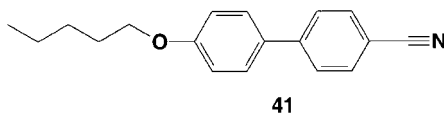
Switching of Liquid Crystalline Phases

Reversibly controlling the anisotropic properties of LC materials offers an attractive way to amplify the effects of molecular optical switches, with the additional benefit of nondestructive read-out. Electronic modulation of LC phases forms the basis of current LC display technology.^[81] Photochemical switching of LC phases might provide materials with potential advantages for all-optical devices, enhanced speed of data processing, and the possibility of modulating reflection and transmission with light. A variety of photochromic polymer liquid crystals for the construction of photoactive LC devices or optical data storage systems have been described (see Chapter 12 and refs^[82,83]). These are based on doping polymer liquid crystals with photochromic guest molecules^[84] or by covalently attaching photochromic side chain units.^[85] Discussion here is restricted to chiral photoactive dopants for the control of non-polymer-based LC phases.

The addition of small amounts of optically active guest molecules to a nematic liquid crystalline host can induce a cholesteric (twisted nematic) phase.^[86] Apart from the type of LC material, the resulting cholesteric phase depends strongly on the helical twisting power (HTP) and the structural compatibility of the chiral dopant.^[87] Photochemically induced changes in the structure or stereochemistry of the chiral dopant can therefore lead to significant changes in the organization of the LC phase. Irreversible light-induced conversion of cholesteric to nematic phases has been achieved by photodecomposition of a chiral guest or by photoracemization.^[17,88] Modulation of the helical pitch of a cholesteric liquid crystal phase was

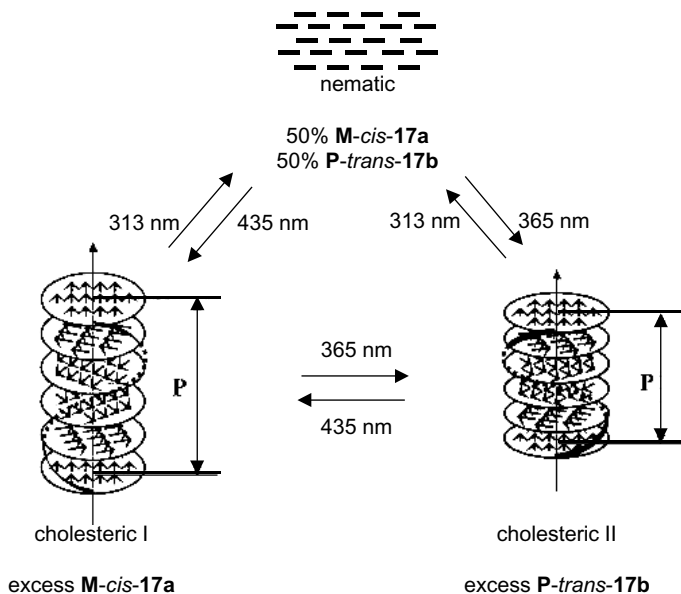
achieved with a combination of two dopants, including a photostable chiral binaphthyl dopant and a photochromic indole fulgide.^[89,90] An LC switch based on an optically active binaphthyl-modified indolylfulgide is discussed in Chapter 4.^[91]

Photochemical modulation of the helical screw sense and pitch of a cholesteric phase was achieved with the combination of a nematic liquid crystalline host and an optically active photoresponsive guest as illustrated in Scheme 25.^[92] Doping of 4'-(pentyloxy)-4-biphenylcarbonitrile **41** with **P-trans-17b** (1 wt%) converts the nematic phase into a cholesteric phase.



Irradiation of a thin film of this cholesteric phase at 365 nm or 435 nm resulted in photostationary states with an excess either of **M-cis-17a** or of **P-trans-17b** (Scheme 25) and two cholesteric phases with a distinct difference in pitch (12.29 μm for cholesteric I and 5.31 μm for cholesteric II). Modulation of the pitch occurred on alternating irradiation at 345 and 435 nm and the LC system was stable over 8 cycles.

The cholesteric screw sense was measured by the Grandjean-Cano method, which showed that **M-cis-17a** and **P-trans-17b** give cholesteric phases with opposite handedness. Observations of the switching behavior of **17** in a large number of LC materials,



Scheme 25: Photochemical switching processes of LC-phase **41** and chiral dopants **M-cis-17a** and **P-trans-17b**, representing a three position switch.

with good compatibility between liquid crystal and chiral switch, revealed nearly the same stability and selectivity in those photostationary states composed of **M-cis-17a** and **P-trans-17b** in the LC phases and solution phases. The switching times increased approximately three times in the LC phases, compared to in solution. Irradiation at 313 nm, near the isobestic point of the system, resulted in a nematic phase, while the cholesteric phases could be restored by subsequent irradiation at 435 nm or 365 nm. The formation of a compensated nematic phase is due to a photostationary state (near 50:50 ratio) of the guest molecule, in which the effects of opposite helices cancel (a pseudo-racemic state). This doped LC system functions as a three-position optical switch, since the distinct states can be addressed by a change in the wavelength of the light. However, it should be emphasized that the irradiation time is a fourth parameter controlling the ratio of **M-cis-17** and **P-trans-17** (and hence the cholesteric pitch) in the photostationary states. Therefore, **17** in principle represents a multistate system. The gradual change of a cholesteric pitch with irradiation time in LC (K15 and ZLI-389) systems doped with a chiral switch was indeed demonstrated (Figure 13).^[41, 93]

Optically active bis-imine-functionalized diarylethene (2–4 %) (Scheme 13) was used as a chiral, photoresponsive dopant in the nematic LC materials K15 and ZLI-389, resulting in stable cholesteric phases. For the open form of **26a**, β_m values of $11 \mu\text{m}^{-1}$ (K15) and $13 \mu\text{m}^{-1}$ (ZLI-389) were measured, while the closed form **26b** did not show any helical twisting power. Irradiation at 300 nm (30–50 s) resulted in the closed form and disappearance of the cholesteric phase. Irradiation with visible light restored the cholesteric phase. The gradual decrease in pitch, representing a multi-

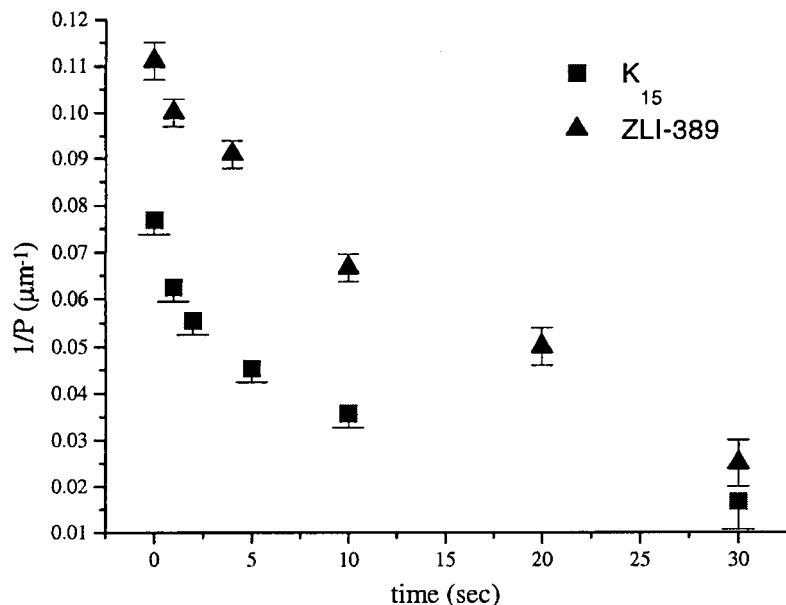


Fig. 13: The change of the reciprocal of the pitch value with irradiation time: 2.0 wt% of **26** in ZLI-389 at 52 °C and in K₁₅ at 32 °C (irradiation with 300 nm light), representing a multimode switch.

state system, is illustrated in Figure 13. Recently, using a chiral bis-diarylethene switch, the reverse behavior was observed, when a nematic LC phase was converted into a cholesteric phase upon ring-closure.^[41]

A particularly elegant way to address different LC states is by irradiating at a single wavelength and merely changing the chirality of the light.^[94] The basic requirements for this switching system are: i) an LC material with excellent compatibility with the switch and for which the pitch and twist sense of the cholesteric phase are highly sensitive to the chirality of the dopant; and ii) photoresolution by CPL irradiation of a racemic photobistable dopant, generating a sufficiently large β_m value. The macroscopic helical pitch p of a cholesteric liquid crystal generated by CPL is determined by the concentration C of the chiral dopant, the helical twisting power β_m and the enantiomeric excess $[e.e.]_{\text{pps}}$ in the photostationary state. The pitch is inversely related to $[e.e.]_{\text{pps}}$ according to

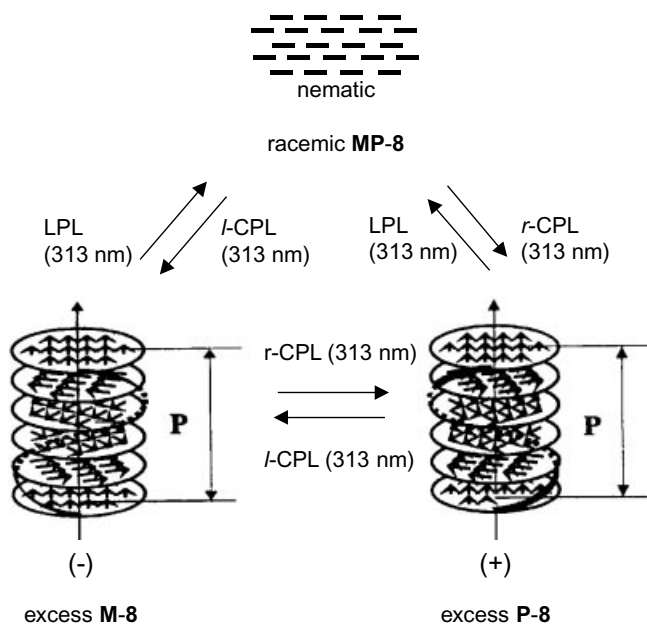
$$p = 1/C \cdot \beta_m \cdot [e.e.]_{\text{pps}}$$

As $[e.e.]_{\text{pps}}$ is related to the anisotropy factor g_x ($[e.e.]_{\text{pps}} = g_x/2$), both β_m and g_x must be sufficiently large to enable detection of a cholesteric phase.^[94]

Schuster et al.^[13g,89,95] have described several approaches towards CPL-based phototriggers for LC phases using optically active (arylmethylene)-cycloalkenes. Cholesteric phases were indeed obtained upon doping in K15 and ZLI-467, and photoracemization caused cholesteric to nematic phase transition. The reverse process was not observed, however, presumably due either to insufficient helical twisting power or to low g -values for these photobistable dopants. Bicyclo[3,3,0]octan-3-one **13** has a high g -value, but photoresolution of this compound doped in the nematic LC material *trans-n*-heptyl-4-(*p*-cyano)-phenylhexane did not result in a cholesteric phase, due to a low β_m ($5.5 \mu\text{m}^{-1}$). In contrast, for photobistable, mesogenic, axially chiral 1-benzylidene-4-[4'-((*p*-alkylphenyl)ethynylphenyl)-cyclohexane, the g -value and hence the enantiomeric excess on photoresolution were too small.

The discovery of a successful photoresolution of racemic overcrowded alkene (Scheme 3) led to the achievement of a liquid crystal switch based on CPL irradiation (Scheme 26).

Irradiation of a 50 μm film of nematic 4'-(pentyloxy)-4-biphenylcarbonitrile **41**, doped with racemic **M,P-8**, with *l*-CPL at 313 nm for 90 min resulted in a cholesteric phase.^[20] Irradiation of **M,P-8** with *r*-CPL also produced a cholesteric phase, but with opposite screw sense. The amount of dopant needed to obtain a chiral LC phase was relatively high, as only a very small e.e. (0.07 %) was obtained and as a consequence the pitch of the cholesteric phase was too large for direct determination. Irradiation of the cholesteric film with linearly polarized light at 313 nm gave the nematic LC film once more. As is illustrated in Scheme 26, switching between three states at a single wavelength is possible, being entirely controlled by the chirality of the light: changing between *l*-CPL and *r*-CPL modulates the chirality of the cholesteric phases. The use of LPL or CPL controls the switching between nematic and cholesteric phases.



Scheme 26: Switching between three different liquid crystalline states after irradiation at one wavelength. Nematic liquid crystal 41 and dopant **8** were used.

5.6

Conclusions

Reversible switching between two (or more) chiral states has been demonstrated with a number of photoactive organic materials. Both diastereomeric and enantiomeric photobistable compounds have been successfully employed. Chiral molecular switches offer the distinctive possibility of exploiting modulation in chiroptical properties, for nondestructive read-out, for instance, and of using the large changes in geometry associated with the interconversion of stereoisomers to control other functions. A sequence of four switching events with a single enantiomer of a propeller type system, for example, has allowed the demonstration of unidirectional rotary motion. Particularly attractive for future applications of chiral molecular switches is the possibility of controlling aggregation, polymer conformations, and liquid crystalline phases in a reversible manner. The systems discussed in this chapter show that material properties can be effectively modulated using light, and that amplification of the change in chirality upon photoswitching in polymers or LC materials is readily achieved. It should be emphasized that, for practical applications in photonic materials, molecular memory elements and retrieval systems, and as components for future nanotechnology, improvements with respect to stability, numbers of cycles, and switching rates are required for many of these chiroptical switches. However, the future of chiral switches and trigger elements for the bottom-up construction of complex molecular systems looks bright if one takes into account the role of chirality in nearly all essential molecules and processes in nature.

References

- 1 Feringa, B. L.; Jager, W. F.; de Lange, B. *Tetrahedron* **1993**, *49*, 8267.
- 2 (a) *Photochromism, Molecules and Systems in Studies in Organic Chemistry 40*; Dürr, H.; Bouas, H.; Laurent, H.; Eds, Elsevier: Amsterdam, 1990; (b) *Organic Photochromes*; El'tsov, A. V. Ed.; Plenum Press: New York, 1990; (c) *Photochromism in Techniques of Chemistry*; Brown, G. H. Ed.; Wiley-Interscience: New York, 1971, vol. 3.
- 3 Feringa, B. L.; Huck, N. P. M.; Schoevaars, A. M. *Adv. Mater.* **1996**, *8*, 681.
- 4 (a) *Photoreactive Materials for Ultrahigh Density Optical Memory*, Irie, M. Ed.; Elsevier, Amsterdam, 1994; (b) Willner, I.; Rubin, S. *Angew. Chem., Int. Ed. Engl.* **1996**, *35*, 367; (c) Gómez-López, M.; Stoddart, J. F. *Bull. Chim. Soc. Belg.* **1997**, *106*, 491; (d) Balzani, V.; Scandola, F. *Supramolecular Photochemistry*; Ellis Horwood: New York, 1991.
- 5 Gardner, M. *The Ambidextrous Universe*, Penguin, 1974.
- 6 Crick, F. *Life Itself*, McDonald & Co., London, 1981.
- 7 Feringa, B. L., van Delden, R. A., Koumura, N., Geertsema, E. M. *Chem. Rev.* **2000**, *100*, 1789.
- 8 (a) Feynman, R. P. in *Miniaturization*; Gilbert, H. D. Ed.; Reinhold: New York, 1961; p. 282; (b) Feynman, R. P. *Eng. Sci.* **1960**, *23*, 22; (c) Drexler, K. E. *Unbounding the Future: the Nanotechnology Revolution; Morrow: New York, 1991*; (d) Drexler, K. E. *Nanosystems: Molecular Machinery, Manufacturing and Computation*; Wiley: New York, 1992; (e) Kawai, S.; Gilat, S. L.; Lehn, J.-M. *J. Chem. Soc., Chem. Commun.* **1994**, 1011; (f) Gómez-López, M.; Preece, J. A.; Stoddart, J. F. *Nanotechnology* **1996**, *7*, 183; (g) *Nanofabrication and biosystems, integrated materials science, engineering and biology*; Hoch, H. C.; Jelinshi, L. W.; Craighead, H. G. eds., Cambridge University Press, Cambridge, 1996.
- 9 For stereochemical definitions, see: Eliel, E. L.; Wilen, S. H. *Stereochemistry of Organic Compounds*, Wiley, New York, 1994, see also: Cahn, R.S.; Ingold, C. K.; Prelog, V. *Angew. Chem., Int. Ed. Engl.* **1966**, *5*, 385.
- 10 Emmelius, M.; Pawlowski, G.; Vollmann, H. W. *Angew. Chem., Int. Ed. Engl.* **1989**, *28*, 1445.
- 11 Dürr, H. *Angew. Chem., Int. Ed. Engl.* **1989**, *28*, 413.
- 12 Feringa, B. L.; van Delden, R. A. *Angew. Chem. Int.* **1999**, *38*, 3419.
- 13 (a) Kuhn, W.; Braun, E. *Naturwissenschaften* **1929**, *17*, 227; (b) Kuhn, W.; Knopf, E. *Z. Phys. Chem., abt. B* **1930**, *7*, 292; (c) Stevenson, K. L.; Verdieck, J. F. *J. Am. Chem. Soc.* **1968**, *90*, 2974; (d) Moradpour, A.; Nicoud, J. F.; Balaivoine, G.; Kagan, H.; Tsoucaris, G. *J. Am. Chem. Soc.* **1971**, *93*, 2353; (e) Udayakumar, B. S.; Schuster, G. B. *J. Org. Chem.* **1992**, *57*, 348; (f) Udayakumar, B. S.; Devadoss, C.; Schuster, G. B. *J. Phys. Chem.* **1993**, *97*, 8713; (g) Suarez, M.; Devadoss, C.; Schuster, G. B. *J. Phys. Chem.* **1993**, *97*, 9299; (h) Udayakumar, B. S.; Schuster, G. B. *J. Org. Chem.* **1993**, *58*, 4165; (i) Izumi, Y.; Tai, A. *Stereo-Differentiating Reactions, the Nature of Asymmetric Reactions*, Academic Press, New York, 1977; (j) Inoue, Y.; *Chem. Rev.* **1992**, *92*, 741.
- 14 Rau, H. *Chem. Rev.* **1983**, *83*, 535.
- 15 Stevenson, K. L.; Verdieck, J. F. *Mol. Photochem.* **1969**, *1*, 271.
- 16 Jager, W. F., PhD Thesis, University of Groningen, 1994.
- 17 Zhang, M.; Schuster, G. B. *J. Phys. Chem.* **1992**, *96*, 3063.
- 18 Burnham, K. S.; Schuster, G. B. *J. Am. Chem. Soc.* **1998**, *120*, 12619.
- 19 de Lange, B. PhD thesis, University of Groningen, 1993.
- 20 Huck, N. P. M.; Jager, W. F.; de Lange, B.; Feringa, B. L. *Science* **1996**, *273*, 1686.
- 21 Because of bandwidth effects and incomplete polarization of the CPL light, the theoretical value was not reached.
- 22 Lemieux, R. P.; Schuster, G. B. *J. Org. Chem.* **1993**, *58*, 100.
- 23 Snatzke, G. *Proc. Roy. Soc., Ser. A* **1967**, *297*, 43.
- 24 (a) Emeis, C. A.; Oosterhoff, L.; de Vries, G. *Proc. R. Soc. London, Ser. A* **1967**, *297*, 54; (b) Windhorst, J. C. A. *J. Chem. Soc., Chem. Commun.* **1976**, 331; (c) Nicoud, J. F.; Eskenazi, C.; Kagan, H. B. *J. Org. Chem.* **1977**, *42*, 4270.
- 25 Suarez, M.; Schuster, G. B. *J. Am. Chem. Soc.* **1995**, *117*, 6732.
- 26 Zhang, Y.; Schuster, G. B. *J. Org. Chem.* **1995**, *60*, 7192.

- 27 Sandstrom, J. In *Topics in Stereochemistry*, Allinger, N.L.; Eliel, E.L.; Wilen, S.H. Eds.; Wiley: New York, 1983, vol 14, 160.
- 28 *Modern Molecular Photochemistry*, Turro, N. L.; University Science Books, Mill Valley, California.
- 29 (a) Barton, D. H. R.; Willis, B. J. *J. Chem. Soc., Chem. Commun.* **1970**, 1225; (b) Kellogg, R. M.; Buter, J.; Wassenaar, S. *J. Org. Chem.* **1972**, *37*, 4045.
- 30 Jager, W. F.; de Jong, J. C.; de Lange, B.; Huck, N. P. M.; Meetsma, A.; Feringa, B. L. *Angew. Chem., Int. Ed. Engl.* **1995**, *34*, 348.
- 31 van Delden, R. A.; Schoevaars, A. M.; Feringa, B. L.; unpublished results
- 32 Geertsema, E. M.; Meetsma, A.; Feringa, B. L. *Angew. Chem. Int. Ed.* **1999**, *38*, 2738.
- 33 Feringa, B. L.; Jager, W. F.; de Lange, B. *Tetrahedron Lett.* **1992**, *33*, 2887.
- 34 Feringa, B. L.; Jager, W. F.; de Lange, B.; Meijer, E. W. *J. Am. Chem. Soc.* **1991**, *113*, 5468.
- 35 Feringa, B. L.; Jager, W. F.; de Lange, B. *J. Chem. Soc., Chem. Commun.* **1993**, 288.
- 36 (a) Schoevaars, A. M. PhD thesis, University of Groningen, 1998; (b) Schoevaars, A. M.; van Delden, R. A.; Feringa, B. L. *Mol. Cryst. Liq. Cryst.*, in press.
- 37 (a) Irie, M. *Chem. Rev.* **2000**, *100*, 1685; (b) Gilat, S. L.; Kawai, S. H.; Lehn, J.-M. *J. Chem. Soc., Chem. Commun.* **1993**, 1439; (c) Irie, M.; Nakamura, S. *J. Org. Chem.* **1988**, *53*, 6136.
- 38 (a) Lucas, L. N.; van Esch, J.; Kellogg, R. M.; Feringa, B. L. *J. Chem. Soc., Chem. Commun.* **1998**, 2313; (b) Huang, Z. N.; Xu, B. A.; Jin, S.; Fan, M. G. *Synthesis* **1988**, 1092; (c) Lucas, L. N.; van Esch, J.; Kellogg, R. M.; Feringa, B. L. *Tetrahedron Lett.* **1999**, *40*, 1775.
- 39 Yamaguchi, T.; Uchida, K.; Irie, M. *J. Am. Chem. Soc.* **1997**, *119*, 6066.
- 40 Denekamp, C.; Schoevaars, A. M. *J. Chem. Soc. Perkin I*, in press.
- 41 Denekamp, C.; Feringa, B. L. *Adv. Mater.* **1998**, *10*, 1081.
- 42 (a) Hirshberg, Y. *J. Am. Chem. Soc.* **1956**, *78*, 2304; (b) Hirshberg, Y.; *New Scientist* **1960**, *7*, 1243.
- 43 Bertelson, R.C. in *Photochromism in Techniques in Chemistry*, Brown, G. H. Ed., Wiley-Interscience, New York, 1971, vol 3, chapter 3.
- 44 Miyashita, A. EP 0640605 A1 [Chem. Abstr. **1995**, *122*, 1660490a].
- 45 (a) Eggers, L.; Bush, V. *Angew. Chem., Int. Ed. Engl.* **1997**, *36*, 881; (b) Miyashita, A.; Iwamoto, A.; Kuwayama, T.; Shitara, H.; Aoki, Y.; Hirano, M.; Nohira, H. *Chem. Lett.* **1997**, 965.
- 46 (a) Inoue, Y.; Yokoyama, T.; Yamasaki, N.; Tai, A. *J. Am. Chem. Soc.* **1989**, *111*, 6480; (b) Inoue, Y.; Yamasaki, N.; Yokoyama, T.; Tai, A. *J. Org. Chem.* **1992**, *57*, 1332; (c) Inoue, Y.; Yamasaki, N.; Yokoyama, T.; Tai, A. *J. Org. Chem.* **1993**, *58*, 1011; (d) Inoue, Y.; Dong, F.; Yamamoto, K.; Tong, L.-H.; Tsuneishi, T.; Hakushi, T.; Tai, A. *J. Am. Chem. Soc.* **1995**, *117*, 11033; (e) Sugimura, T.; Shimizu, H.; Umemoto, S.; Tsuneishi, H.; Hakushi, T.; Inoue, Y.; Tai, A. *Chem. Lett.* **1998**, 323.
- 47 (a) Heller, H. G. *Chem. & Ind.* **1978**, 193; (b) Heller, H. G.; Oliver, S. J. *Chem. Soc., Perkin Tr. I* **1981**, 197; (c) Kurita, Y.; Goto, T.; Inoue, T.; Yokoyama, M.; Yokoyama, Y. *Chem. Lett.* **1988**, 1049; (d) Yokoyama, Y.; Shimizu, Y.; Uchida, S.; Yokoyama, Y. *J. Chem. Soc., Chem. Commun.* **1995**, 785.
- 48 Yokoyama, Y.; Uchida, S.; Yokoyama, Y.; Sugawara, Y.; Kurita, Y. *J. Am. Chem. Soc.* **1996**, *118*, 3100.
- 49 (a) Liu, Z. F.; Fujishima, A.; Hashimoto, A. *Nature* **1990**, *347*, 658; (b) Shimidzu, T.; Honda, K.; Iyoda, T.; Saika, T. *Tetrahedron Lett.* **1989**, *30*, 5429; (c) Gobbi, L.; Seiler, P.; Diederich, F. *Angew. Chem., Int. Ed. Engl.* **1999**, *38*, 674; (d) Spreitzer, H.; Daub, J. *Chem. Eur. J.* **1996**, *2*, 1150.
- 50 (a) Kawai, S. H.; Gilat, S. L.; Lehn, J. M. *J. Chem. Soc. Chem. Commun.*, **1994**, 1011; (b) Spreitzer, H.; Daub, J. *Liebigs Ann.* **1995**, 1637; (c) Görner, H.; Fischer, C.; Daub, J. *J. Photochem. Photobiol., A. Chem.* **1995**, *85*, 217; (d) Irie, M.; Miyatake, O.; Uchida, K. *J. Am. Chem. Soc.* **1992**, *114*, 8715.
- 51 Huck, N. P. M.; Feringa, B. L. *J. Chem. Soc., Chem. Commun.* **1995**, 1095.
- 52 van Delden, R. A.; Huck, N. M. P.; Warman, S. J. J.; Meskers, J. M.; Dekkers, S. C. J.; Feringa, B. L. *J. Am. Chem. Soc.*, submitted for publication.
- 53 Okamoto, H.; Dekkers, H.P.J.M.; Satake, K.; Kimura, M. *Chem. Commun.* **1998**, 1049.
- 54 Inada, T.; Uchida, S.; Yokoyama, Y. *Chem. Lett.* **1997**, 321.
- 55 (a) Shinkai, S.; Manabe, O.; Nakaji, T.; Nishida, Y.; Ogawa, T. *J. Am. Chem. Soc.* **1980**, *102*, 5860; (b) Shinkai, S.; Kusano, Y.; Manabe, O.; Nakaji, T.; Ogawa, T. *Tetrahedron Lett.* **1979**, *20*, 4569; (c) Willner, I.; Willner, B in *Bioorganic Photochemistry*, Vol 2: Biological

- Applications of Photochemical Switches*, ed.; Morrison, H.; Wiley, New York, 1993, p. 1–110.
- 56 (a) Takeshita, M.; Uchida, K.; Irie, M. *J. Chem. Soc., Chem. Commun.* **1996**, 1807; (b) Shinmori, H.; Takeuchi, M.; Shinkai, S. *J. Chem. Soc., Perkin Trans.* **2** **1996**, 1.
- 57 Willner, I.; Rubin, S.; Wonner, J.; Effenberger, F.; Bäuerle, P. *J. Am. Chem. Soc.* **1992**, 114, 3150.
- 58 (a) Yashima, E.; Noguchi, J.; Okamoto, Y. *Macromolecules* **1995**, 28, 8368; (b) Okamoto, Y.; Sakamoto, H.; Hatada, K.; Irie, M. *Chem. Lett.* **1986**, 983.
- 59 (a) Hamada, F.; Iti, I.; Suzuki, I.; Ota, T.; Ueno, A. *Macromol. Rapid Commun.* **1994**, 15, 531; (b) Hamada, F.; Hoshi, K.; Higuchi, Y.; Murai, K.; Akagami, Y.; Ueno, A. *J. Chem. Soc., Perkin Trans.* **2** **1996**, 2567.
- 60 Noji, H.; Yasuda, R.; Yashida, M.; Kinoshita, M. *Jr Nature*, **1997**, 386, 299.
- 61 (a) Sauvage, J.-P. *Acc. Chem. Res.* **1998**, 31, 611; (b) Balzani, V.; Gómez-López, M.; Stoddart, J. F. *Acc. Chem. Res.* **1998**, 31, 405.
- 62 Kelly, T. R.; Tellitu, I.; Sestelo, J. P. *Angew. Chem. Int. Ed. Engl.* **1997**, 36, 1866.
- 63 Kelly, T. R.; De Silva, H.; Silva, R. A. *Nature* **1999**, 401, 150.
- 64 Schoevaars, A. M.; Kruizinga, W.; Zijlstra, R. W. J.; Veldman, N.; Spek, A. L.; Feringa, B. L. *J. Org. Chem.* **1997**, 62, 4943.
- 65 Koumura, N.; Zijlstra, R. W. J.; van Delden, R. A. van, Harada, N.; Feringa, B. L. *Nature*, **1999**, 401, 152.
- 66 (a) Harada, N.; Saito, A.; Koumura, N.; Uda, H.; de Lange, B.; Jager, W. F.; Wynberg, H.; Feringa, B. L. *J. Am. Chem. Soc.* **1997**, 119, 7241; (b) Harada, N.; Saito, A.; Koumura, N.; Roe, D. C.; Jager, W. F.; Zijlstra, R. W. J.; de Lange, B.; Feringa, B. L. *J. Am. Chem. Soc.* **1997**, 119, 7249; (c) Harada, N.; Koumura, N.; Feringa, B. L. *J. Am. Chem. Soc.* **1997**, 119, 7256; (d) Zijlstra, R. W. J.; Jager, W. F.; de Lange, B.; van Duijnen, P. T.; Feringa, B. L.; Goto, H.; Saito, A.; Koumura, N.; Harada, N. *J. Org. Chem.* **1999**, 64, 1667.
- 67 ter Wiel, M. K. J.; Koumura, N.; van Delden, R. A.; Harada, N.; Feringa, B. L. *Chirality*, **2000**, 12, 734.
- 68 (a) Pieroni, O.; Fissi, A.; Popova, G. *Prog. Polym. Sci.* **1998**, 23, 81; (b) Ciardelli, F.; Pieroni, O.; Fissi, A.; Carlini, C.; Altomare, A. *Br. Polym. J.* **1989**, 21, 97; (c) Irie, M. *Adv. Polym. Sci.* **1990**, 94, 27; (d) *Applied Photochromic Polymer Systems*; McArdle C. B., Ed.; Blackie: Glasgow, UK, 1992; (e) Ciardelli, F.; Pieroni, O.; Fissi, A.; Houben, J. L. *Biopolymers* **1984**, 23, 1423; (f) Pieroni, O.; Ciardelli, F. *Trends in Polym. Sci.* **1995**, 3, 282; (g) Kinoshita, T. *Prog. Polym. Sci.* **1995**, 20, 527; (h) see ref 4b; (i) Willner, I. *Acc. Chem. Res.* **1997**, 30, 347.
- 69 Delaire, J. A.; Nakatani, K. *Chem. Rev.* **2000**, 100, 1817.
- 70 For other applications, see Chapter 13 and ref. 7.
- 71 Oosterling, M. L. C. M.; Schoevaars, A. M.; Haitjema, H. J.; Feringa, B. L. *Isr. J. Chem.* **1996**, 36, 341.
- 72 a) Schuhmann, W.; Huber, J.; Mirlach, A.; Daub, J. *Adv. Mater.* **1993**, 5, 124; (b) Nitta, M.; Takayasu, T. *J. Chem. Soc., Perkin Tr.* **1** **1998**, 1325; (c) Porsch, M.; Sigh-Seifert, G.; Daub, J. *Adv. Mater.* **1997**, 9, 635.
- 73 Lifson, S.; Green, M. M.; Andreola, C.; Peterson, N. C. *J. Am. Chem. Soc.* **1989**, 111, 8850.
- 74 Green, M. M.; Peterson, N. C.; Sato, T.; Teramoto, A.; Cook, R.; Lifson, S. *Science* **1995**, 268, 1860.
- 75 Müller, M.; Zentel, R. *Macromolecules* **1994**, 27, 4404.
- 76 Maxein, G.; Zentel, R. *Macromolecules* **1995**, 28, 8438.
- 77 (a) Müller, M.; Zentel, R. *Macromolecules* **1996**, 29, 1609; (b) Meyer, S.; Zentel, R. *Macromol. Chem. Phys.* **1998**, 199, 1675.
- 78 Mayer, S.; Maxein, G.; Zentel, R. *Macromolecules* **1998**, 31, 8522.
- 79 Green, M. M.; Garetz, B. A.; Munoz, B.; Chang, H.; Hoke, S.; Cooks, G. *J. Am. Chem. Soc.* **1995**, 117, 4181.
- 80 Murata, K.; Aoki, M.; Nishi, T.; Ikeda, A.; Shinkai, S. *J. Chem. Soc., Chem. Commun.* **1991**, 1715.
- 81 Kreysig, D.; Stumpe, J. in *Selected Topics in Liquid Crystalline Research*, Koswig, H. D., Ed. VCH, Weinheim, 1990; (b) Freemantle, M. *Chem. Eng. News* **1996**, 74 (50), 33; (c) De Gennes, P. G. *Angew. Chem., Int. Ed. Engl.* **1992**, 31, 842; (d) *Liquid Crystals: Applications and Uses*, Vol. I-III, Bahadur, B. Ed. World Scientific, Singapore, 1991; Gibbons, W. M.; Shannon, P. J.; Sun, S.-T.; Swetlin, B. *J. Nature* **1991**, 351, 49.
- 82 Ichimura, K. *Chem. Rev.* **2000**, 100, 1847.
- 83 (a) Ikeda, T.; Tsutsumi, O. *Science* **1995**, 268, 1873; (b) Hvilsted, S.; Andruzzi, F.; Kulinna, C.; Siesler, H. W.; Ramanujam, P. S. *Macro-*

- molecules **1995**, 28, 2172; (c) Tsutsumi, O.; Kitsuunai, T.; Kanazawa, A.; Shiono, T.; Ikeda, T. *Macromolecules* **1998**, 31, 355; (d) Tsutsumi, O.; Demachi, Y.; Kanazawa, A.; Shiono, T.; Ikeda, T.; Nagasa, Y. *J. Phys. Chem. B* **1998**, 102, 2869; (e) Shishido, A.; Tsutsumi, O.; Kanazawa, A.; Shiono, T.; Ikeda, T.; Tamai, N. *J. Am. Chem. Soc.* **1997**, 119, 7791; (f) Wu, Y.; Demachi, Y.; Tsutsumi, O.; Kanazawa, A.; Shiono, T.; Ikeda, T. *Macromolecules* **1998**, 31, 1104; (g) Tokuhisa, H.; Yokoyama, M.; Kimura, K. *J. Mater. Chem.* **1998**, 8, 889; (h) Bobrovski, A. Y.; Boiko, N. I.; Shibaev, V. P. *Adv. Mater.* **1999**, 11, 1025.
- 84** (a) Negishi, M.; Tsutsumi, O.; Ikeda, T.; Hiyama, T.; Kawamura, J.; Aizawa, M.; Takehara, S. *Chem. Lett.* **1996**, 319; (b) Negishi, M.; Kanie, K.; Ikeda, T.; Hiyama, T. *Chem. Lett.* **1996**, 583; (c) Ichimura, K.; Hosoki, A.; Ozawa, K.; Suzuki, Y. *Polym. Bull.* **1987**, 17, 285; (d) Ikeda, T.; Sasaki, T.; Ichimura, K. *Nature* **1993**, 361, 42; (e) Kusumoto, T.; Sato, K.; Ogino, K.; Hiyama, T.; Takehara, S.; Osawa, M.; Nakamura, K. *Mol. Cryst. Liq. Cryst.* **1993**, 14, 727.
- 85** (a) Schmidt, H. W. *Adv. Mater.* **1989**, 1, 940; (b) Gibbons, W. M.; Kosa, T.; Palffy-Muhoray, P.; Shannon, P. J.; Sun, S. T. *Nature* **1995**, 377, 43; (c) Anderle, K.; Wendorff, J. H. *Mol. Cryst. Liq. Cryst.* **1994**, 243, 51; (d) Andrews, S. R.; Williams, G.; Läsker, L.; Stumpe, J. *Macromolecules* **1995**, 28, 8463; (e) Akiyama, H.; Momose, M.; Ichimura, K.; Yamamura, S. *Macromolecules* **1995**, 28, 288; (f) Tazuke, S.; Horiuchi, S.; Ikeda, T.; Karanjit, D. B.; Kurihara, S. *Chem. Lett.* **1988**, 1679; (g) Tazuke, S.; Ikeda, T.; Yamaguchi, H. *Chem. Lett.* **1988**, 539; (h) Tazuke, S.; Ikeda, T.; Kurihara, S. *Chem. Lett.* **1987**, 911; (i) Wendorff, J. H.; Eich, M.; Reck, B.; Ringsdorf, H. *Macromol. Chem., Rapid Commun.* **1987**, 8, 59; (j) Wendorff, J. H.; Eich, M. *Macromol. Chem., Rapid Commun.* **1987**, 8, 467; (k) Ringsdorf, H.; Cabrera, I.; Dittrich, A. *Angew. Chem., Int. Ed. Engl.* **1991**, 30, 76; (l) Öge, T.; Zentel, R. *Macromol. Chem. Phys.* **1996**, 197, 1805.
- 86** Solladié, G.; Zimmermann, R. G. *Angew. Chem., Int. Ed. Engl.* **1984**, 23, 348.
- 87** (a) Gottarelli, G.; Spada, G. P.; Bartsch, R.; Solladié, G.; Zimmermann, R. G. *J. Org. Chem.* **1986**, 51, 589; (b) Gottarelli, G.; Osipov, M. A.; Spada, G. P. *J. Phys. Chem.* **1991**, 95, 3879.
- 88** (a) Lemieux, R. P.; Schuster, G. B. *J. Org. Chem.* **1993**, 58, 100; (b) Mioskowski, C.; Bourguignon, J.; Candau, S.; Solladié, G. *Chem. Phys. Lett.* **1976**, 38, 456.
- 89** Zhang, M.; Schuster, G. B. *J. Am. Chem. Soc.* **1994**, 116, 4852.
- 90** Janicki, S. Z.; Schuster, G. B. *J. Am. Chem. Soc.* **1995**, 117, 8524.
- 91** Yokoyama, Y.; Sagisaka, T. *Chem. Lett.* **1997**, 687.
- 92** Feringa, B. L.; Huck, N. P. M.; van Doren, H. A. *J. Am. Chem. Soc.* **1995**, 117, 9929.
- 93** Feringa, B. L.; Huck, N. P. M.; Schoevaars, A. M. *Adv. Mater.* **1996**, 8, 681.
- 94** (a) Baessler, H.; Laronge, T. M.; Labes, M. M. *J. Chem. Phys.* **1969**, 51, 3213; (b) Nakagiri, T.; Kodama, H.; Kobayashi, K. K. *Phys. Rev. Lett.* **1971**, 27, 564.
- 95** (a) Zhang, M.; Schuster, G. B. *J. Phys. Chem.* **1992**, 96, 3063; (b) Zhang, Y.; Schuster, G. B. *J. Org. Chem.* **1994**, 59, 1855.

6 Photochemical Biomolecular Switches: The Route to Optobioelectronics

Itamar Willner and Bilha Willner

6.1 Introduction

Different biological processes are triggered by light signals. Photosynthesis and the vision process are the most fundamental light-activated biological mechanisms in plants and animal systems, respectively. Other processes, such as photoinduced movement at various biological levels (movement of motile organisms, dynamics of plant tissues), photomorphogenesis (seed germination, induction of flowering, chlorophyll synthesis), and conversion of light energy into chemical energy (ATP synthesis, proton pumps, and ion transport), are important biological events which are activated by photonic signals.

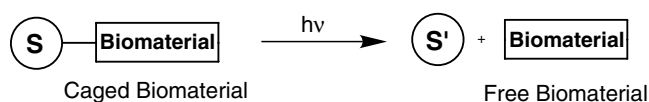
Several common features can be defined for the different light-activated biotransformations:

- All of the systems include a chromophore (photosensor or photoreceptor) that absorbs the light. The excitation of the photoreceptor is followed by a chemical reaction such as electron transfer, photoisomerization, ion channel formation, etc.
- The photoreceptor operates in a reversible and cyclic manner. After excitation and activation of the secondary chemical process, the photoreceptor relaxes to its original ground state configuration. This blocks the chemical transformation, which is switched off.
- The photochemical process usually includes self-regulating processes. These include mechanisms that control the light doses to which the biomaterial is exposed, pathways for light-harvesting in the biomaterial photoprocess, such as the antenna function in the photosynthetic reaction center, or mechanical movements for controlling light absorption, such as photomorphogenesis, as well as repair functions in damaged photoreceptors.
- The photoinduced chemical transformation that follows the excitation process often activates an enzyme cascade or opens an ion channel. These secondary reactions amplify the primary event of light absorption. In some mechanisms, translocation of electrons (photosynthesis, for example) or of

ions (such as in proton pumps or ion pumps) generates potential gradients or an electrical field.

Recent research efforts have been directed towards the development of semisynthetic photobiological switches^[1,2]. An artificial biological photochemical switch is defined as a biological material or environment that is chemically functionalized by photoresponsive units, enabling the photonic activation of the innate functions of the respective biological matrices. Within this broad definition one may define two subclasses of photobiological switches:

- 1) Single-cycle photobiological switches are biomaterials that are chemically modified by a photoactive group to yield a blocked, biologically inactive, compound. Upon photonic excitation of the modified material (Scheme 1), the deactivating group is removed and the active biomaterial is released.^[3,4] Activation of enzymes,^[5,6] photoinduced formation of specific ion-chelators,^[7,8] light-triggered formation of important biological messengers such as cAMP,^[9] cGMP,^[10] ATP,^[11] or InP_3 ^[12] are photonically generated by this manner. Usually, photoprotective chemical functionalities have been applied to cage the biomaterial and to temporarily deactivate its innate properties. Several review articles^[3,4] summarize the topic of single-cycle photoswitches and discuss the potential applications of such systems.
- 2) Multicycle photobiological switches are chemically engineered biomaterials that permit reversible switching of biological functions between a mute inactive state and an active “ON” configuration. The biomaterial is activated by an external photonic signal and it is “switched off” to the original inactive state by another photonic stimulus, which may be a thermal, electrical, or pH signal. Several review articles summarize advances in tailoring reversible artificial photobiological switches.^[1,2] It is the aim of this chapter to address progress in the area of reversible photobiological switches, and, in particular, to emphasize the relationship of this class of materials to the development of the scientific field of optobioelectronics. It is our aim to highlight the fact that photobiological switches are an important class of photonic switches that broaden the concepts of molecular photoswitches^[13,14] and macromolecular photoswitches^[15,16] to include photoactive assemblies that use materials of biological origin as their light-triggered functionalities.

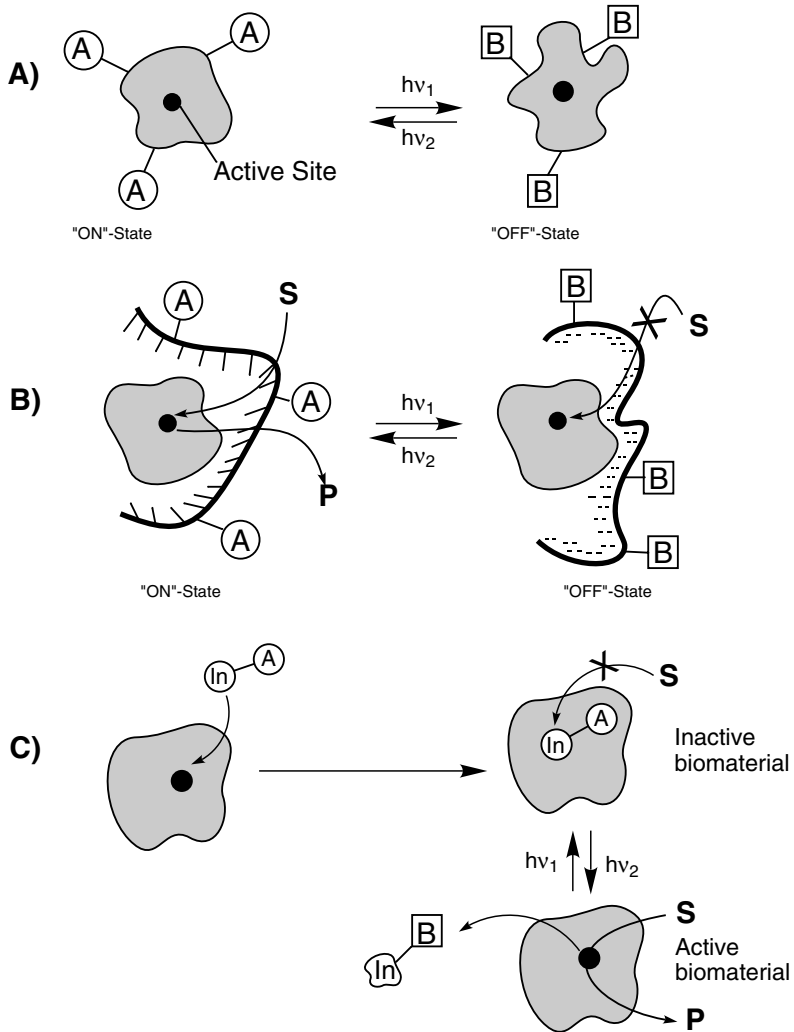


Scheme 1: Photochemical activation of a biomaterial by light-induced cleavage of a photoprotective group.

6.1.1

Reversible Photochemical Switching of Biomaterial Functions

Three general methodologies for photoregulating such activities of biomaterials as catalytic, binding, or recognition functions have been suggested (Scheme 2). One method involves the tethering of photoisomerizable units to a protein (Scheme 2(A)). In one photoisomer state, state A, the tertiary structure of the protein is



Scheme 2: Methods for the reversible photoactivation/deactivation of biomaterials by: (A) tethering of photoisomerizable groups onto the biomaterial, (B) immobilization of the biomaterial in a photoisomerizable matrix, (C) the application of a photoisomerizable inhibitor (or photoisomerizable cofactor).

retained, and the biomaterial is hence activated to perform its function. Photoisomerization of the light-active group, producing state B, distorts the tertiary structure of the protein and perturbs its active site function. This perturbation might originate from structural distortion of the active site, blocking its catalytic function and/or the binding of the substrate. Alternatively, distortion of the protein might lead to non-competitive inhibition of the active center, by remote deactivation of the active site microenvironment. By exploiting reversible photoisomerization of the photoactive groups, the biomaterial functions may be cycled between switched “ON” and switched “OFF” states. Different photoisomerizable components such as azobenzene,^[17] nitrospiropyran,^[18] or fulgide derivatives^[19] may be used for photoregulating catalytic functions of enzymes or binding characteristics of receptor proteins.

The second approach to photoregulating the functions of biomaterials involves the integration of the biomaterial within a photosensitive environment (Scheme 2(B)). Physicochemical properties of photoisomerizable membrane-mimetic assemblies such as polymers,^[20,21] monolayers,^[22,23] or liposomes^[24] are controlled by light. The wettability,^[25] sol-gel transitions,^[26] effective volume viscosity,^[27] or permeability^[28] of such matrices are regulated by light. Accordingly, immobilization of the biomaterial in a photoregulated matrix could control the permeability or transport characteristics of the substrate towards the entrapped biomaterial, resulting in switchability of interactions between the substrate and the immobilized biomaterial.

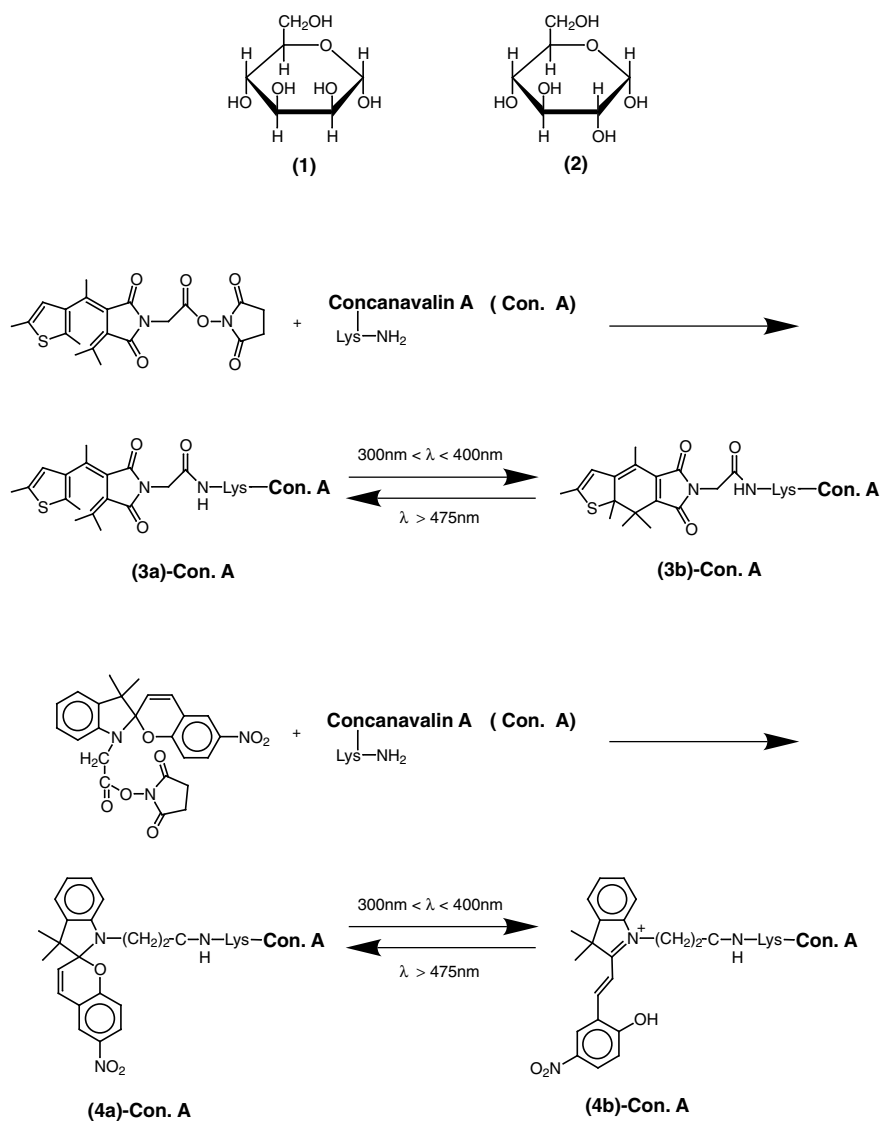
A further means to reversibly photoregulate the functions of biomaterials involves the application of photoisomerizable, low molecular weight, components that are recognized by the biological material (Scheme 2(C)). Inhibitors or cofactors act respectively as low molecular weight deactivators or activators of proteins. Thus, blocking of the protein-active center by an inhibitor in one photoisomer state – state A – may block the biological function of the biomaterial. Photoisomerization of the inhibitor to a configuration that lacks affinity for the binding site – state B – results in its release from the active site, and in the activation of the biomaterial. Similarly, photoisomerization of a cofactor may lead to active or inactive cofactor configurations for cyclic light-induced activation or deactivation of proteins.

6.1.1.1 Photoswitchable Biomaterial Functions through Tethering of Photoisomerizable Units to Proteins

Intermolecular recognition is the most fundamental feature of biomaterial functions. Biochemical transformations in which intermolecular recognition and binding events play a central role include:

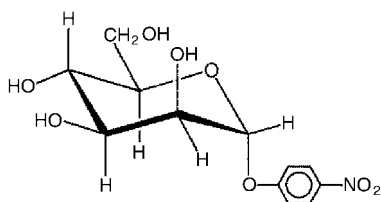
- the formation of substrate–enzyme or cofactor–enzyme complexes giving rise to enzyme biocatalytic functions,
- the antigen–antibody affinity interactions that are the fundamental phenomenon in the immune system,
- the complementary DNA interactions and polymerase replication of DNA, and
- the specific recognition of substrates by receptor units or ion channels, resulting in specific transport and storage of materials.

Chemical modification of the biomaterial with photoisomerizable units represents one approach to controlling intermolecular affinity interactions (Scheme 2(A)). In one photoisomer state of the biomaterial, its tertiary, biologically active structure is retained and the formation of the intermolecular complex is facilitated. In the complementary photoisomer state, the bioactive binding site is distorted and the formation of the intermolecular recognition complex is switched off. The bind-



Scheme 3: Synthesis of photoisomerizable Concanavalin A by the chemical linkage of photoisomerizable thiophene fulgide or nitrospiropyran residues to the protein.

ing properties of the lectin concanavalin A (Con.A) for binding to α -D-mannopyranose and α -D-glucopyranose have been controlled by chemical tethering of photoactive units to the protein.^[29] Con.A is a globular protein, consisting of four subunits ($M \approx 26$ kDa). Each of these subunits includes binding sites for Mn^{2+} and Ca^{2+} , which act cooperatively when associating with α -D-mannopyranose (**1**) or α -D-glucopyranose (**2**). The lectin was chemically modified by tethering photoisomerizable thiophene fulgide^[29] or nitrospiropyran^[30] components to it (Scheme 3). Con.A modified with thiophene fulgide – (**3a**)-Con.A – exhibited reversible photoisomerizable properties, and upon irradiation ($\lambda = 300\text{--}400$ nm) the photoactive units underwent electrocyclization to give (**3b**)-Con.A. Irradiation of the (**3b**)-Con.A state with visible light ($\lambda > 475$ nm) caused it to revert to the (**3a**)-Con.A state. Con.A functionalized with spiropyran – (**4a**)-Con.A – displayed similar reversible photoisomerizable features, and upon irradiation with filtered light ($300\text{ nm} < \lambda < 400$ nm) the merocyanine-tethered lectin (**4b**)-Con.A was formed. Further illumination of (**4b**)-Con.A with visible light ($\lambda > 475$ nm) regenerated the electrocycliced state (**4a**)-Con.A. The ring-cyclized photoisomer state (**3b**)-Con.A exhibited a higher affinity than (**3a**)-Con.A for α -D-mannopyranose, whereas the nitrospiropyran-functionalized protein (**4a**)-Con.A, displayed improved binding interactions with the substrate.



(5)

Table 1 summarizes the binding constants between the host substrate, nitrophenyl- α -D-mannopyranose (**5**) and Con.A tethered with different degrees of loading of the photoisomerizable units. The difference in the photostimulated binding affinities is strongly influenced by the degree of loading and, as the loading increases, the switching efficiency for binding the substrate is enhanced. This result is attributed to the enhanced structural perturbation of the protein upon photoisomerization of the photoactive groups at high degrees of loading. Loading of the protein with the synthetic photoisomerizable units is accompanied, however, by a decrease in the affinity interactions between the lectin and **5**, relative to the native protein. Thus, to attain optimal photoswitchable binding features of the protein, and to retain the association features of the lectin, an appropriate balance of the degree of loading is important. The higher binding constants of the electrocycliced isomer states (**3b**)-Con.A and (**4a**)-Con.A, were attributed to the lower steric volumes of these isomer states, resulting in less pronounced structural perturbation of the protein and its active site environment. The different affinities of the photoisomerizable protein for **5** make it possible for substrate **5** to bind to, and dissociate from, the protein in cyclic, light-induced fashion (Figure 1).

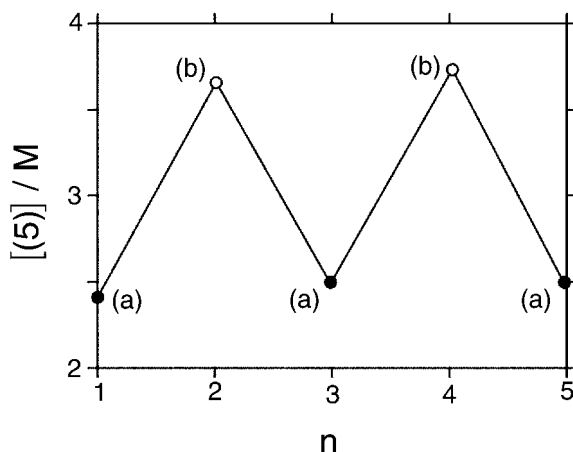


Fig. 1: Cyclic photoregulated association of 5 to 3b-Con.A (a) and dissociation of 5 from 3a-Con.A (b).

Tab. 1: Association constants of 5 to the photoisomerizable Concanavalin A systems (3)-Con.A and (4)-Con.A, as a function of the degree of loading.

Degree of Loading	$K_a (M^{-1})$ (3a)	$K_a (M^{-1})$ (3b)	$K_a (M^{-1})$ (4a)	$K_a (M^{-1})$ (4b)
0	22000 ± 300		24000	
3			23000	23000
6	16400	20000	18000	12000
8			10000	7300
9	7800	12100		
12	6400	6400		

The kinetics of association of the photoisomerizable lectin to the substrate is also controllable by light. The kinetics of the binding of the nitrospiropyran-tethered Con.A ((4a)-Con.A) and the complementary nitromerocyanine isomer state (4b)-Con.A were examined electrochemically.^[31] A monosaccharide monolayer consisting of α -D-mannopyranose (1) or α -D-glucopyranose (2) was assembled on an Au electrode (Figure 2(A)). Binding of the lectin to the monolayer insulated the electrode support from electrical interaction with the $Fe(CN)_6^{3-}/Fe(CN)_6^{4-}$ redox label solubilized in the electrolyte solution. As a result, the time-dependent decrease in the electrical response of the electrode corresponded to the kinetics of association of the lectin to the functionalized electrode (Figure 2(B)). While the association of native Con.A with the electrode was fast, the binding of the photoisomerizable protein was perturbed by the tethered synthetic units. The nitrospiropyran-Con.A – (4a)-Con.A – which displayed a high affinity for α -D-mannopyranose, bound to the monosaccharide monolayer more quickly than (4b)-Con.A did.

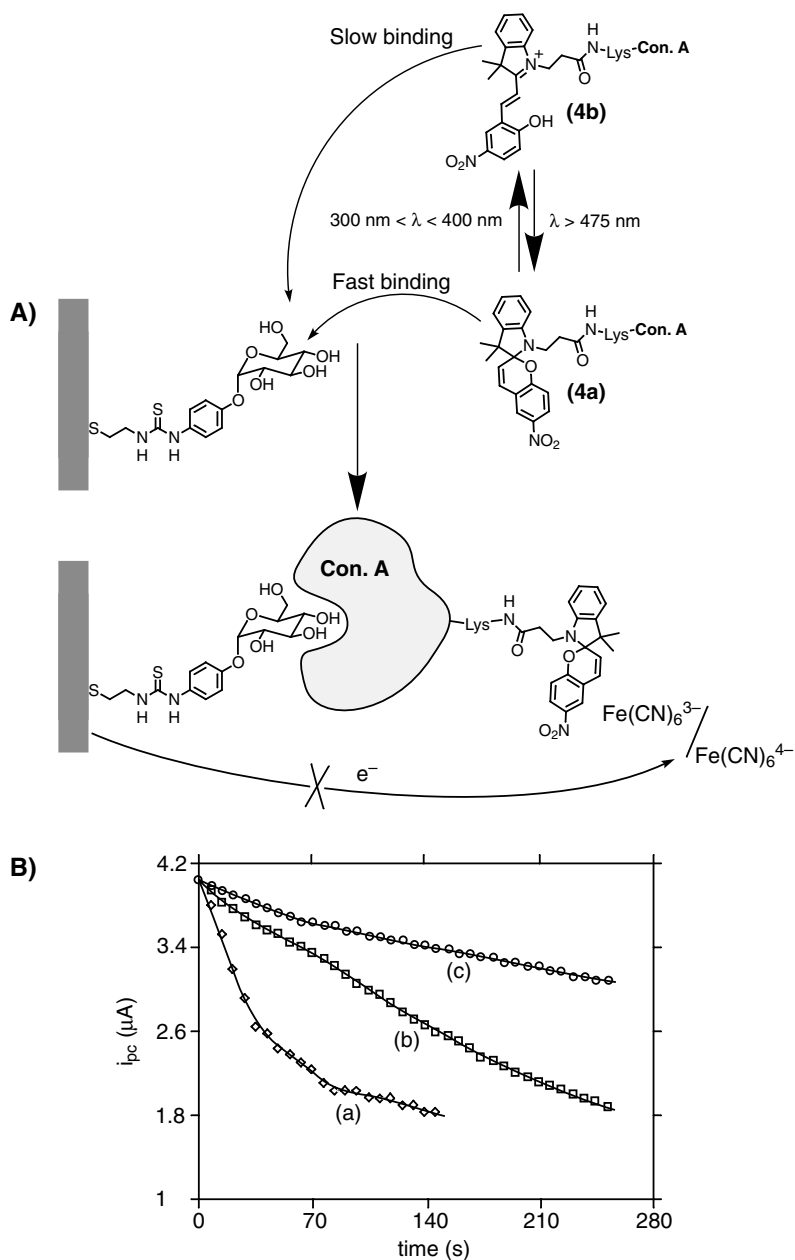


Fig. 2: (A) Assembly of an α -D-mannopyranose monolayer on an Au electrode and association of the photoisomerizable **4-Con.A** onto the monolayer. Binding of the protein to the interface is determined by following the degree of insulation of the electrode towards a redox

label $\text{Fe}(\text{CN})_6^{3-}/\text{Fe}(\text{CN})_6^{4-}$ solubilized in the electrolyte solution. (B) (a) Dynamics of association of native Con.A to the monosaccharide monolayer. (b) Kinetics of binding of **4a-Con.A** to the monolayer. (c) Kinetics of binding of **4b-Con.A** to the monolayer interface.

Evidence for the structural distortion of the protein upon the photoisomerization of the tethered synthetic groups, together with information related to the dynamics associated with the photoinduced perturbation of the protein structure, was found in time-resolved light scattering experiments.^[32] Photoisomerization of (4a)-Con.A to (4b)-Con.A, using the second harmonic Nd-Yag laser pulse signal ($\lambda = 355$ nm), was accompanied by a transient increase in the light-scattering signal of the protein, implying protein shrinkage upon formation of (4b)-Con.A, the protein state with lower affinity for the respective monosaccharides. The dynamics of the protein structural condensation was reflected by the time constant of the scattered light intensity. For the protein loaded with six nitrospiropyran units, the protein matrix shrank within 60 μ s.

Controlled photochemical binding and dissociation of an antibody-antigen complex was accomplished^[33] in the presence of the photoisomerizable antigen Glu-(*trans*-azobenzene Ala)-Gly₂ (6a) (Figure 3). A monoclonal antibody (Z1HO1) was elicited for the *trans*-azobenzene unit. Accordingly, the hapten (6a) exhibited high binding affinity to the antibody ($K_a = 5 \times 10^7$ M⁻¹), whereas the *cis*-azobenzene pep-

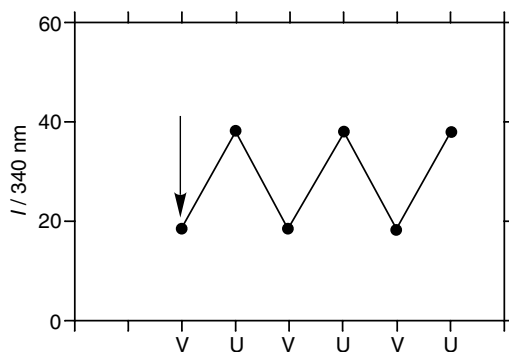
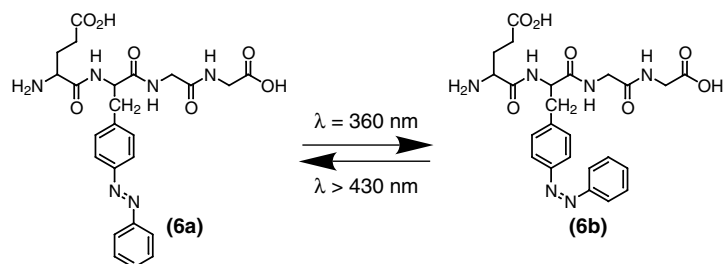
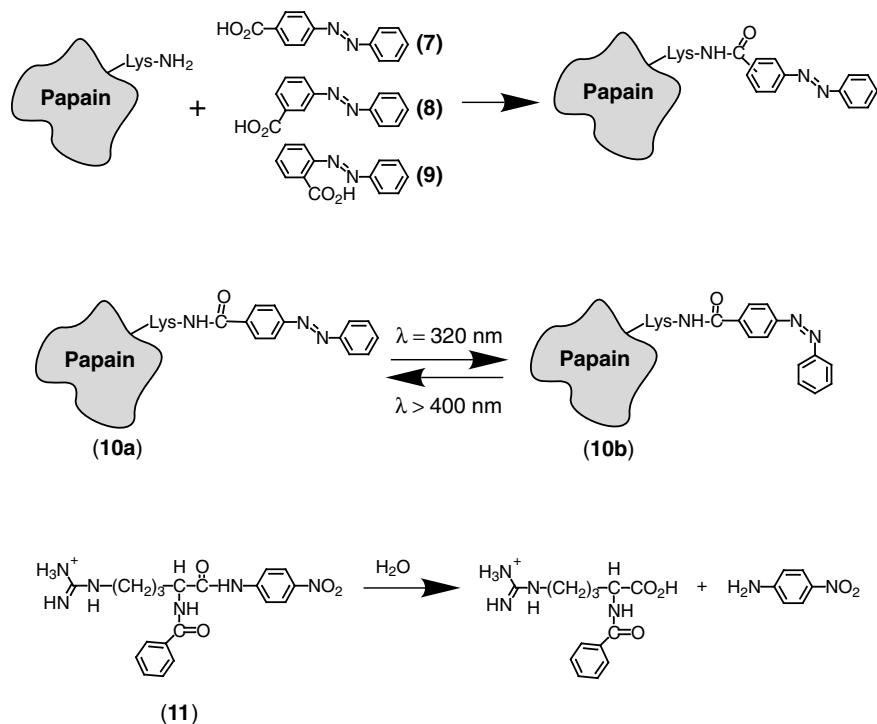


Fig. 3: Reversible photostimulated binding and dissociation of the photoisomerizable hapten **6** to and from the Z1HO1 monoclonal antibody, respectively. V and U indicate irradiation with visible and UV light, respectively. Visible

light generates **6a**, whereas UV irradiation yields **6b**. The binding of the hapten to the antibody is determined by following the fluorescence intensity I of the system at $\lambda = 340$ nm.

tide photoisomer lacked affinity for the antibody. The binding of (**6a**) to the antibody was studied by following the fluorescence quenching of the antibody through energy transfer to the associated *trans*-azobenzene antigen. Photoisomerization of the antigen to the *cis*-state (**6b**) ($\lambda = 360$ nm) was accompanied by the dissociation of the antigen–antibody complex, and the regeneration of the antibody fluorescence. Further photoisomerization of **6b** to **6a** ($\lambda > 430$ nm) regenerated the antigen–antibody complex. As a result of the cyclic photoisomerization of the antigen between the *trans*-(**6a**) state and the *cis*-(**6b**) configuration, the antibody is switched between a complexed configuration and a free state, respectively. The antibody fluorescence is quenched only to a lower level even upon irradiation of the system to the *cis*-peptide (**6b**), which lacks affinity for the antibody. This incomplete photoswitching of the dissociation of the antigen–antibody complex is attributed to the fact that photoisomerization of *trans*-azobenzene derivatives to the *cis*-azobenzene state always generates a photostationary equilibrium. This residual *trans*-antigen leads to the formation of the antigen–antibody complex and to the observed fluorescence quenching.

Tethering of photoisomerizable groups to enzymes has been used to photostimulate the biocatalytic functions of proteins.^[34,35] Papain was modified by the covalent coupling of the photoisomerizable units *trans*-4-carboxyazobenzene (**7**), *trans*-3-carboxyazobenzene (**8**), or *trans*-2-carboxyazobenzene (**9**) to the protein's lysine residues (Scheme 4). The new azobenzene-modified papains underwent reversible *trans* \rightleftharpoons *cis*



Scheme 4: Synthesis and photoisomerizable properties of azobenzene-functionalized papain.

photoisomerization. The most pronounced “ON”-“OFF” photostimulated activities were found for the *trans*-4-carboxyazobenzene-tethered papain (**10a**), which retained 86 % of its native biocatalyst activity. The photoregulated hydrolytic activities of the photoactive papain were demonstrated by the hydrolysis of N-benzyl-D,L-arginine nitroanilate (**11**) (Scheme 4 and Figure 4).^[35a] With an enzyme that incorporated an average loading of five photoactive units per protein, the *trans*-azobenzene-functionalized papain **10a** was about 2.75 times more active than the *cis*-azobenzene-modified biocatalyst **10b**. Irradiation of the biocatalyst with filtered UV light ($\lambda = 320$ nm) yielded the *cis* state of the biocatalyst (**10b**). This enzyme initiated the slow hydrolysis of the substrate **11**, and upon photoisomerization ($\lambda > 400$ nm) of the enzyme to the *trans* state **10a**, a significant enhancement of the hydrolysis rate was observed (Figure 4(A)). The direction of the hydrolytic enzyme switch could be reversed, and an initial fast hydrolysis of **11** was observed with **10a** (Figure 4(B)). Photoisomerization ($\lambda = 320$ nm) of the biocatalyst to the *cis* configuration retarded the hydrolytic process. In order to examine the origin of the photoswitchable hydrolytic functions of the azobenzene-tethered papain, the kinetic parameters of the enzyme in the two photoisomer states (**10a** and **10b**) were elucidated. The two enzyme states exhibited

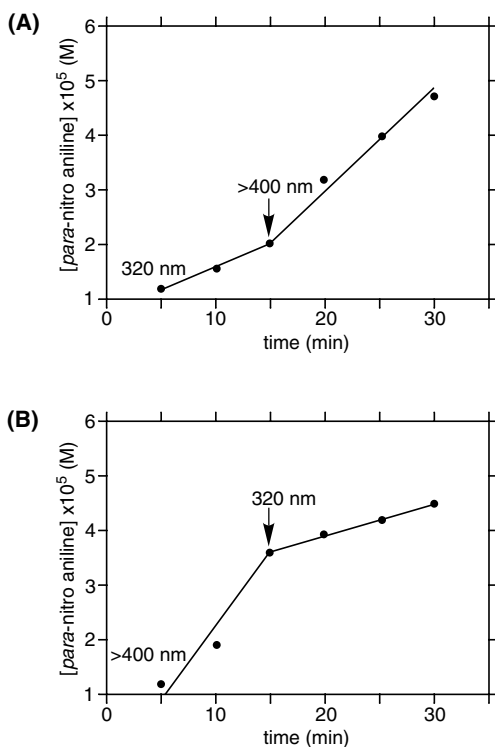


Fig. 4: Photoswitchable hydrolytic activities of 4-carboxyazobenzene-tethered papain (**10**):

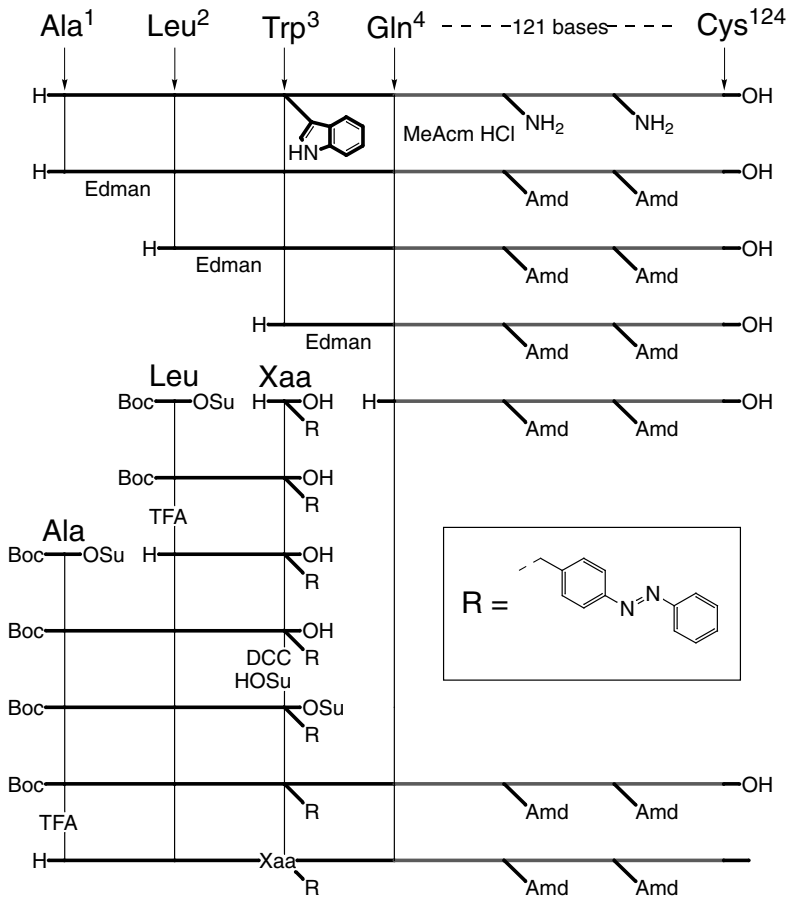
(A) Hydrolysis of **11** is initiated with **10b** and switched on by visible light irradiation of the

system ($\lambda > 400$ nm), which yields **10a**. (B)

Hydrolysis of **11** is initiated with **10a** and switched off by irradiation ($\lambda = 320$ nm), which yields **10b**.

similar V_{\max} values (1.9 ± 0.2 nM/min⁻¹), but differed in their K_m values ($K_m = (2.2 \pm 0.2)$ nM for **10a**, and $K_m = (6.5 \pm 0.6)$ nM for **10b**). This suggests that the binding of the substrate **11** to the enzyme active site was inhibited in biocatalyst **10b**, but that the catalytic functions of the active center were not influenced by the photoisomerization process. That is, the photoisomerization of the biocatalyst to the **10b** state had structurally perturbed the binding features of the substrate, and consequently the enzyme functions were switched off. Closely related reversible photochemical activation/deactivation of enzymes was reported for the covalent tethering of nitrospiropyran to different biocatalysts.^[34a] For example, a nitrospiropyran-functionalized β -amylase exhibited a 10-fold higher activity than the nitromerocyanine-functionalized biocatalyst.

The chemical modification of enzymes with photoisomerizable units led, however, to incompletely photoswitchable “ON/OFF” activities, and the switched-off state revealed residual activity. This is attributable to the non-optimized structural perturbation of the protein upon photoisomerization. Tethering of the photoisomerizable units to the protein by the synthetic methodologies so far described involves a random substitution pathway. The photoactive units are not coupled to those protein residues that are expected to yield maximum steric perturbation on the active site environment. Site-specific modification of proteins with photoisomerizable groups, and directed functionalization of the active site environment of proteins by the photoactive groups might be accomplished by genetic engineering or site-directed mutagenesis. Preliminary studies^[36] have used this approach for the semisynthetic preparation of a photoisomerizable mutant of phospholipase A₂. The lipolytic enzyme cleaves 2-acyl bonds in phosphoglycerides, and it exhibits enhanced activity towards substrates that are associated with aggregated interfaces, such as micelles or vesicles. It was suggested that the N-terminus of phospholipase A₂, composed of Ala-1, Leu-2, Trp-3, Arg-6, Leu-15, Met-20, Leu-31, and Try-69, adopts an α -helical conformation that creates a recognition site at the aggregated interface. This site facilitates the association of the enzyme at the lipid-water interfaces, and thereby enhances the hydrolysis of the respective substrates at these microheterogeneous boundaries. Thus, it was anticipated that covalent attachment of photoisomerizable units to amino acid residues associated with the recognition site domain for the aggregated interfaces would make photocontrol over enzyme activity possible. A photoisomerizable phospholipase A₂ mutant was prepared by the semisynthetic approach outlined in Scheme 5. The ϵ -amidinated enzyme was subjected to three consecutive Edman degradations, cleaving the terminal amino acids Ala-1, Leu-2, and Trp-3. The protein was then reconstituted by the stepwise synthesis of the tripeptide Boc-Ala-Leu-(*trans*-azobenzene-Phe) ($X_{aa} = \textit{trans}$ -azobenzene phenylalanine), followed by coupling of this tripeptide to the 121-mer obtained upon cleavage in the first step. This procedure had specifically substituted the Trp-3 residue with the photoisomerizable azobenzene-Phe unit. Assays were made of the activities of the photoisomerizable phospholipase A₂ mutants towards hydrolysis of lipids associated with palmitoyl phosphatidylcholine vesicles. Radiolabeled lipids, or vesicles that encapsulated fluorescence probes, were used to monitor the hydrolyses of the lipid matrices. The mutant in the *trans*-azobenzene-Phe configuration was inactive



Scheme 5: Semisynthetic method for the cleavage of phospholipase A₂ and the reconstitution of azobenzene-modified phospholipase A₂. Acm = acetamide, Amd = ϵ -amidated, DCC = dicyclohexylcarbodiimide, HOSu = N-hydroxysuccinimide, TFA = trifluoroacetic acid, Xaa = *trans*-azobenzene phenylalanine.

towards lipid hydrolysis. Photoisomerization of the mutant to the *cis*-azobenzene-Phe state, however, activated biocatalytic lipid hydrolysis, and the protein in the *cis*-azobenzene-Phe configuration displayed 10 % of the native activity of phospholipase A₂. CD spectroscopy revealed that the *cis*-azobenzene-Phe mutant included a substantially higher α -helical conformation content, compared to the *trans*-azobenzene-Phe mutant. This observation is in agreement with the known fact that an α -helical conformation in the active site environment is important for the biocatalytic hydrolysis of the lipids.

6.1.1.2 Photoswitchable Biomaterials by Integration of Biomaterials with Photoisomerizable Matrices and Microenvironments

The physical and chemical properties of photoisomerizable molecular films or photoisomerizable polymers are controlled by light. Photochemical control of the formation of liquid crystal phases, or sol-gel transitions,^[37,38] of polymers containing photoisomerizable components demonstrates signal regulation of the structure and properties of microscopic and macroscopic phases. Physicochemical properties of photoisomerizable membrane-mimetic assemblies such as liposomes,^[24] mono-

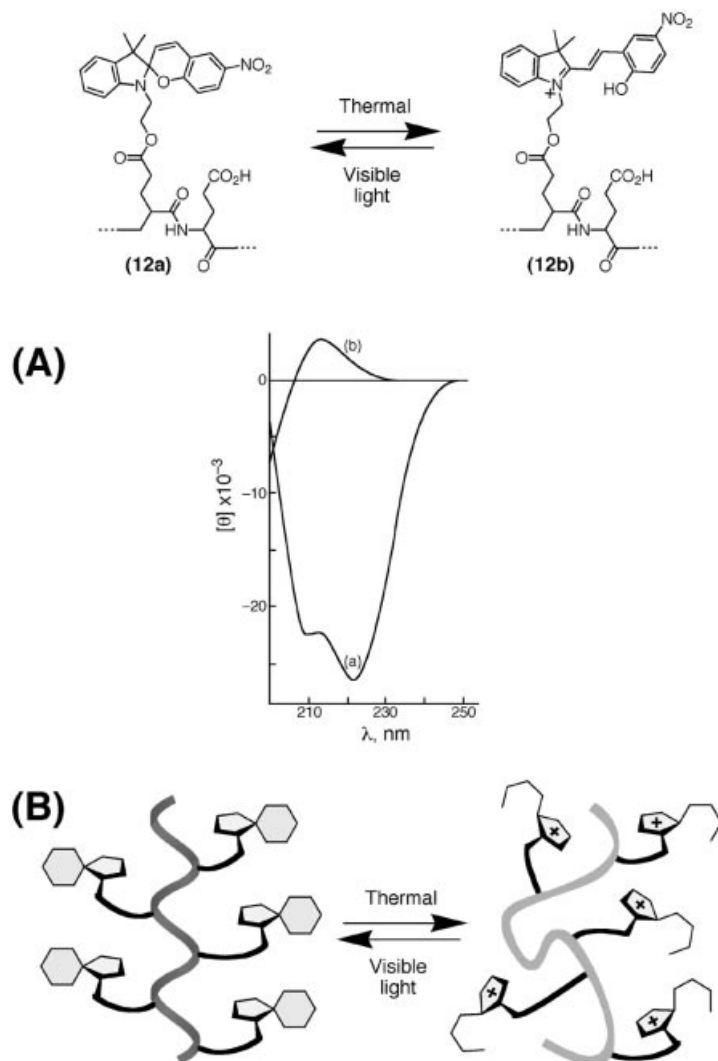
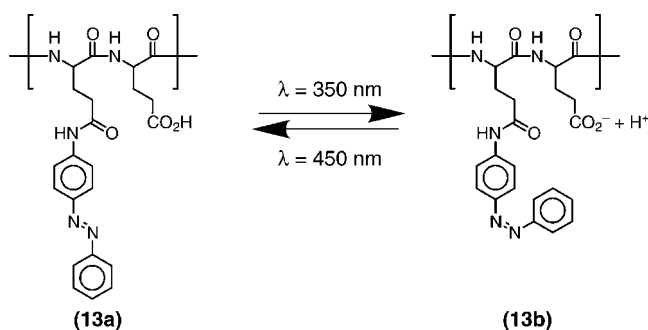


Fig. 5: (A) CD spectra of: (a) **12a** polymer; (b) **12b** polymer.
(B) Schematic presentation of the α -helix/random-coil transition of the photoisomerizable polymer **12**.

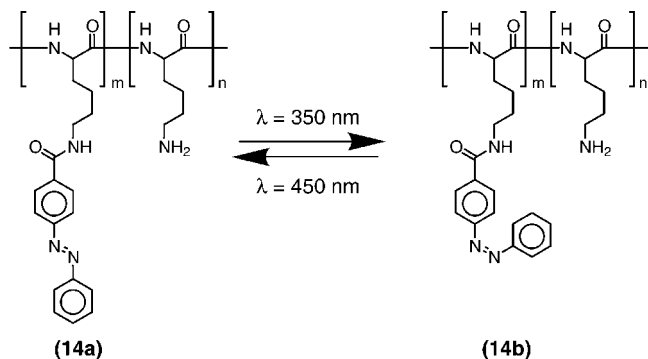
layers,^[22,23] or polymers^[20,21] have been found to be controllable by light. The wettability,^[25] effective volume viscosity,^[27] permeability, or transport properties^[28] of photoisomerizable polymers and film interfaces have also been reported to be controllable by light. The light-switchable properties of photoisomerizable macromolecules, and polymers in particular, have been extensively reviewed.^[15,16] Accordingly, only representative examples of light-induced structural control over several photoisomerizable assemblies will be addressed here, in order to highlight the feasibility of regulating the microscopic structures and properties of these systems by photochemical means.

Poly-(L-glutamic acid) was modified with nitrospiropyran units to yield the photoisomerizable polymer **12a** (Figure 5). The polymer, solubilized in hexafluoropropanol (HFP) containing some trifluoroacetic acid, was stabilized in the open, protonated nitromerocyanine state (**12b**). Visible light irradiation of the solution resulted in the formation of the nitrospiropyran polymer state (**12a**), which relaxed thermally to **12b**. The nitrospiropyran polymer exhibited an α -helix structure, reflected in the typical CD curves, with two negative bands at $\lambda = 208$ nm and 222 nm.^[39,40] Thermal isomerization of the polymer to the protonated nitromerocyanine state resulted in depletion of the CD bands, implying that the peptide had been transformed into an extended coil configuration lacking a defined structural pattern (Figure 5). The cause of the light-stimulated structural assembly of **12a** into the α -helix structure was attributed to its hydrophobic polar properties, which enabled the polymer to form intramolecular H-bonds and to adopt the α -helix structure. Thermal isomerization of the polymer into state **12b** resulted in electrostatic repulsions between the tagged isomer units. These electrostatic repulsions perturbed the α -helix structure and so produced the extended coil configuration. The structural transformations of the polymer between the α -helix and random coil structures were reversible. Closely related photoregulation of polypeptide structures has been accomplished with azobenzene-modified poly(L-glutamic acid) (**13**)^[41] and azobenzene-modified poly(L-lysine) (**14**),^[42] using surfactant solutions as the reaction media for the structural isomerization of the photoisomerizable polymers. *Trans*-azobenzene poly(L-glutamic acid) (**13a**) underwent reversible light-induced isomerization, with irradiation ($\lambda = 350$ nm) of **13a** yielding the *cis*-azobenzene polymer **13b**, whereas illumination of the latter isomer with visible light ($\lambda = 450$ nm) regenerated the *trans*-azobenzene polymer **13a**. The pKa values of the free carboxylic acid functions of the polymer backbone (35 % loading with azobenzene units) depended on the isomeric state of the azobenzene sites (pKa = 6.8 for **13a** and 6.3 for **13b**). This difference in the pKa values was attributed to the polarity of the *cis*-azobenzene units, which enhances the local dielectric constant of neighboring carboxylic acid residues. This light-stimulated alteration of the protonation/deprotonation features of the polymer was used to control the structural properties of the polymer. In a dodecylammonium chloride micellar solution at pH = 6.5, the *trans*-azobenzene poly(L-glutamic acid) **13a** (20 mol% loading) exists in the random coil configuration. Photoisomerization of **13a** to **13b** induces the transition of the polymer structure from a coil form to an α -helix form, evident from the CD bands at $\lambda = 210$ and 228 nm. The existence of the *trans*-isomer **13a** in the disordered structure was attributed to the hydrophobic character

of the polymer. The polymer exists in a protonated, uncharged state, which results in the incorporation of the polymer in the hydrophobic core of the micelles. Incorporation of the polymer units in the micelles inhibits possibilities for self-assembly and organization, and the polymer adopts the coil structure. Photoisomerization to the *cis*-azobenzene poly(L-glutamic acid) yields a hydrophilic, negatively charged polymer structure. The polymer units are expelled from the micellar microenvironment into the bulk aqueous phase, in which the intramolecular H-bonded α -helix structure is favored.



Similar photomodulated control was observed in the case of the structural features of azobenzene-poly(L-lysine) (**14**) in a hexafluoropropanol/water/dodecylsulfate solution. In the *trans*-azobenzene configuration (**14a**), the polymer (43 mol% loading of azobenzene units) exists in a β -sheet configuration. Irradiation ($\lambda = 350 \text{ nm}$) of the polymer yielded the *cis*-azobenzene poly(L-lysine) state (**14b**), in which the β -sheet structure was disrupted and the α -helix configuration promoted (50 % α -helix content). These examples of light-stimulated, reversible, structural control over polypeptides tagged with photoisomerizable units, are intended to highlight the feasibility of controlling structural patterns of polypeptides through tethering with synthetic photoisomerizable units. An excellent recent review^[15b] addressed different photoisomerizable polypeptide systems and discussed the different effects that control the structural features of the polypeptides.



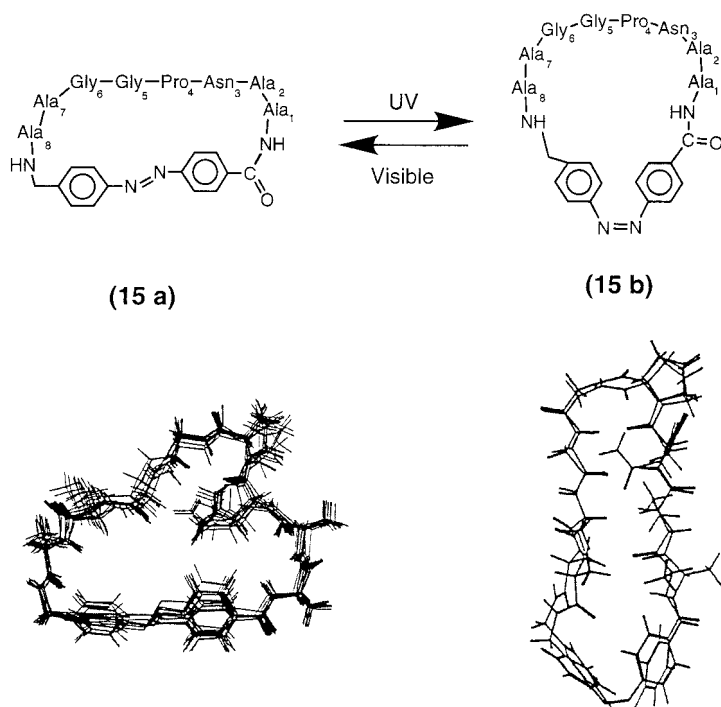


Fig. 6: Energy-minimized structures of a photoisomerizable cyclic azobenzene polypeptide.

The structure of the cyclic photoisomerizable azobenzene-functionalized peptide **15** (Figure 6) was found to be controllable by light.^[43] Detailed NMR studies, that included double quantum filtered COSY and NOESY experiments, made it possible to elucidate the structural features of the *trans*-azobenzene cyclic peptide **15a** and the *cis*-azobenzene peptide **15b**. The NMR data for the **15a** isomer indicate a β -strand extending from residue Ala₂ to Gly₆, interrupted by a bend at Pro₄, with bends at residues Ala₁, Ala₇, and Ala₈, adjacent to the azobenzene unit. In the *trans* configuration (**15a**), only one H-bond exists – between the side chain NH of Asn₃ and the carbonyl unit of Gly₅. In turn, in the *cis* configuration (**15b**), the NMR data support the existence of a type II β -turn from residues Gly₆ to Asn₃, with a hydrogen bond between the carbonyl of Gly₆ and the backbone NH site of Asn₃, and an anti-parallel β -sheet extending from the residues adjacent to the azobenzene group up to the β -turn, with H-bonds between the NH of Gly₆ and the backbone carbonyl moiety of Asn₃, and the NH of Ala₈ and the carbonyl of Ala₁. The NMR data were used as constraints in molecular dynamic simulations of the energy-minimized configurations of the structures **15a** and **15b** (Figure 6).

Monolayers representing two-dimensional arrays of membrane-mimetic assemblies, consisting of azobenzene (poly-L-lysine) with 43 % loading of the photoisomerizable units, were prepared.^[44] The compressed *trans*-azobenzene polymer monolayer exhibited a surface pressure of $7 \text{ mN} \cdot \text{m}^{-1}$, whereas photoisomerization of the monolayer to the *cis*-azobenzene state by UV light decreased the surface pressure to

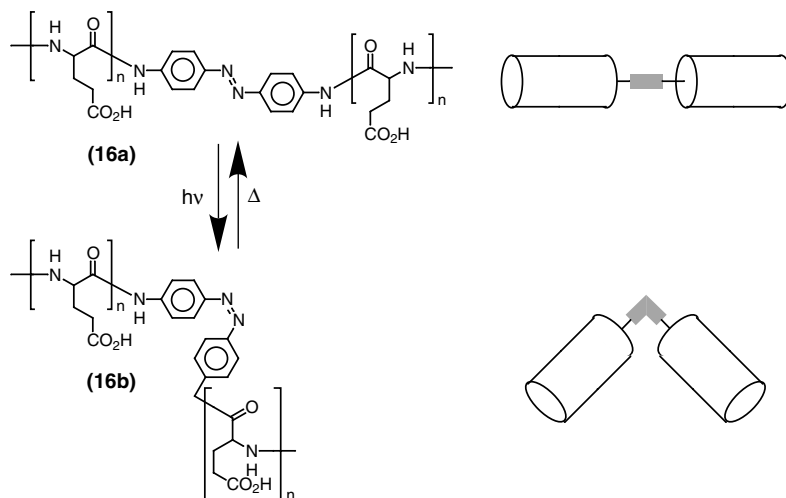
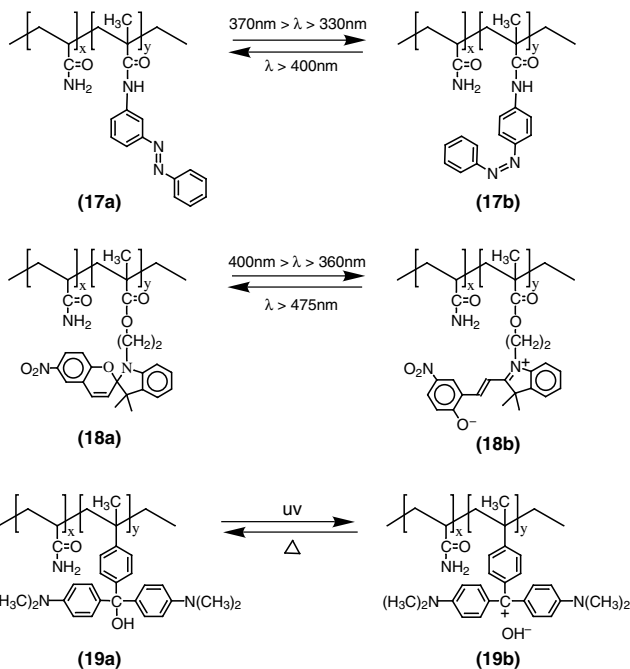
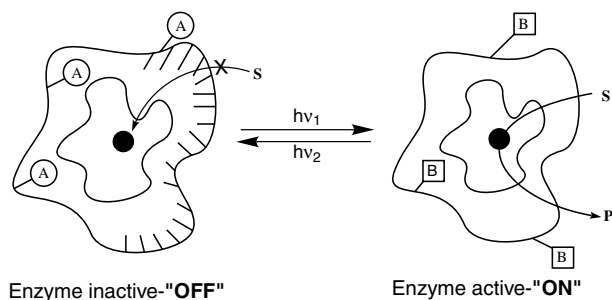


Fig. 7: Schematic structural transformation of the photoisomerizable polyglutamic acid **16**.

(1.8 ± 0.2) $\text{mN} \cdot \text{m}^{-1}$. Cyclic photoisomerization of the polymer monolayer between the *trans*- and *cis*-azobenzene states results in reversible alteration of the monolayer surface pressure between high and low values, respectively, implying that photoisomerization induces structural changes in the compressed polymer.^[44] An interesting photoresponsive polypeptide consisting of two α -helical poly(L-glutamate) units ($M_w = 11,000$) linked by an azobenzene moiety (**16**) was reported^[45] to alter its helical configuration as a result of the action of light (Figure 7). Monolayers of the *trans*-azobenzene bis- α -helical polymer (**16a**) were generated at a water-air interface. Photoisomerization of the monolayer to the *cis*-azobenzene state (**16b**) resulted in a decrease in the area of the monolayer. From the extent of the decrease in area per molecule, it was concluded that in the *cis*-azobenzene configuration the two α -helices exist in a bent structure, with a bending angle of ca. 140° .

Light-stimulated permeability and substrate transport through photoisomerizable polymers makes it possible to use polymer membranes as matrices for photoregulation of the functions of biomaterials^[46–48] (Scheme 6). The enzyme is embedded in the polymer matrix. In one photoisomer state of the polymer, the membrane is permeable to the substrate, and the immobilized enzyme catalyzes its biological process. In the second isomer state of the polymer, a nonpermeable membrane is generated, and the biocatalytic functions of the enzyme are blocked. The activity of α -chymotrypsin was photoregulated by this method,^[47,48] by immobilizing the biocatalyst in one of the following photosensitive, crosslinked, isomerizable polymers: the azobenzene-acrylamide copolymer **17**, the nitrospiropyran-acrylamide copolymer **18**, and the bis-dimethylamino triphenyl carbinol-acrylamide copolymer **19**. Figure 8(A) illustrates the hydrolysis of N-(3-carboxypropionyl)-L-phenylalanine-*p*-nitroanilide (**20**) by α -chymotrypsin immobilized in the azobenzene-acrylamide copolymer **17**. With a polymer loading of 0.5 mol% of photoisomerizable azobenzene units, the hydrolytic activity of the immobilized enzyme is totally blocked in the *trans*-azoben-



Scheme 6: Photoswitching of α -chymotrypsin through its immobilization in photoisomerizable polymers.

zene polymer configuration **17a**. Photoisomerization of the polymer to the *cis*-azobenzene state **17b** ($330 \text{ nm} < \lambda < 370 \text{ nm}$) switches on the biocatalyst's activity, and **20** is hydrolyzed to **21** ($V = 2 \mu\text{M} \cdot \text{min}^{-1}$). Photoisomerization of **17b** back to the *trans*-state **17a** ($\lambda > 400 \text{ nm}$), switches the enzyme activity off. The biocatalytic hydrolysis of **20** can hence be cycled between "ON" and "OFF" states by the reversible photoisomerization of the polymer between the structures **17b** and **17a**.^[47,48]

Similar results are observed with the nitrospiropyran-acrylamide copolymer **18** (Figure 8(B)). The enzyme activity is almost entirely blocked in the presence of the copolymer **18a** incorporating 0.12 mol% of nitrospiropyran units.^[47b] Photoisomeri-

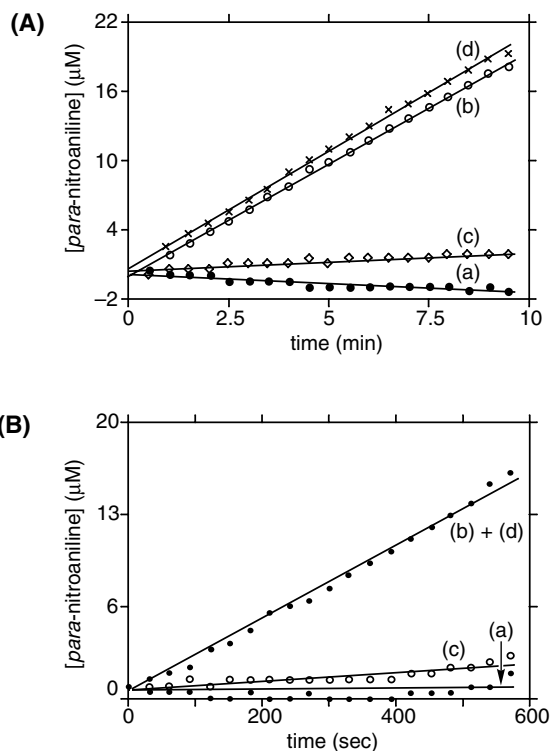
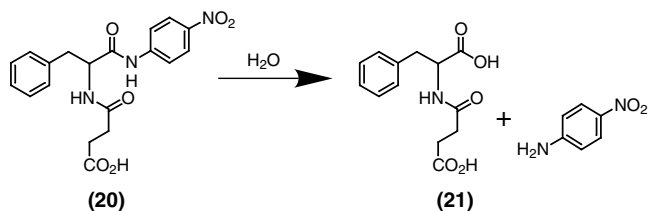


Fig. 8: Photoswitchable hydrolysis of **(20)** by α -chymotrypsin immobilized in photoisomerizable acrylamide copolymers. (A) α -Chymotrypsin immobilized in copolymer **17**; (a) and (c): hydrolysis of **(20)** in the presence of **17a** copolymer, (b) and (d): hydrolysis of **(20)** in the presence

of α -chymotrypsin in **17b**. (B) Hydrolysis of **(20)** in the presence of α -chymotrypsin immobilized in copolymer **18**; (a) and (c): hydrolysis in the presence of copolymer **18a**, (b) and (d): hydrolysis in the presence of **18b**.

zation of the polymer to the nitromerocyanine state **18b** activates α -chymotrypsin towards the hydrolysis of **(20)** ($V = 1.5 \mu M \cdot \text{min}^{-1}$). The photostimulated hydrolysis of **(20)** can be switched reversibly between “ON” and “OFF” states by means of light-induced isomerization of the polymer membrane between the configurations **18b** and **18a**. Copolymer **19** does not display reversible photoisomerizable properties, but can be cycled between the structures **19b** and **19a** by a photochemical/thermal cycle.

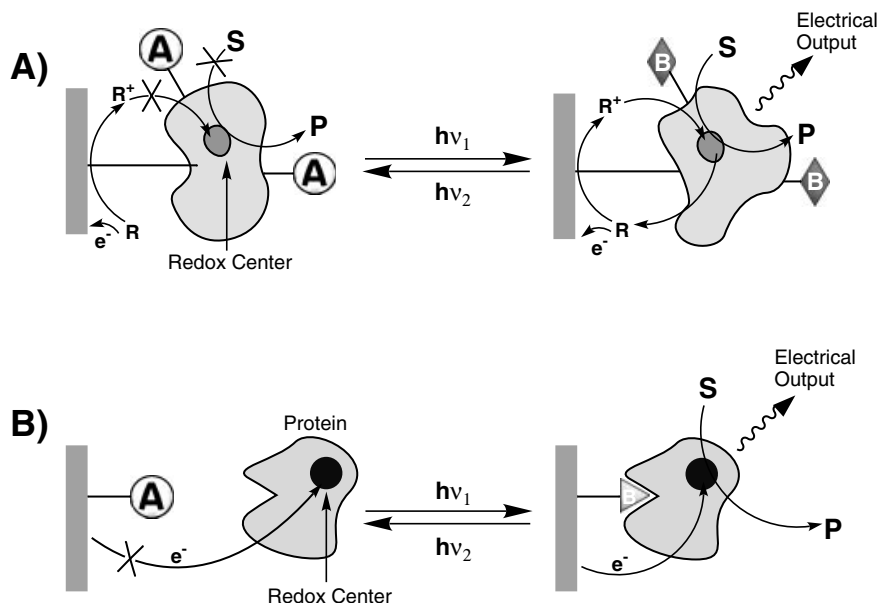
The biocatalyst α -chymotrypsin's ability to hydrolyze **20** is inhibited in the presence of copolymer **19a** loaded with 0.2 mol% of the triphenyl carbinol units.^[47b] Photoirradiation of **19a** results in heterolytic bond cleavage and the formation of the cationic copolymer **19b**. In this polymer structure, the biocatalyzed hydrolysis of **20** is activated ($V = 1.0 \mu\text{M} \cdot \text{min}^{-1}$). The polymer-induced photostimulated activation and deactivation of α -chymotrypsin in the different membrane environments correlates with the permeability and transport properties of the substrate **20** through the different structures of the polymer membranes.^[47] Flow dialysis experiments showed that the polymer states **17a**, **18a**, and **19a** are nonpermeable to **20**, and hence the biocatalytic functions of the immobilized enzyme are blocked. The polymer structures **17b**, **18b**, and **19b** are permeable to **20**, and the effective transport of the substrate through these polymer membranes activates the biocatalytic process. It was suggested that the polarity or charge on the polymer membranes facilitate the transport of **20** through the polymer matrices. The dipole moment of *cis*-azobenzene units is approximately 3.0 D, compared to $\mu = 0$ for *trans*-azobenzene units. The polar structure of polymer **17b**, and the electrical charges associated with **18b** and **19b**, result in porous environments as a product of electrical repulsion within the polymers, a structural feature that facilitates the transport of **20**.

6.2

Electronic Transduction of Photoswitchable Redox Functions of Biomaterials

Photochemical activation (or deactivation) of biomaterials represents the fundamental event of triggering on (or switching off) of a chemical process by the registering of a photonic signal. The activation of an enzymatic process by a photonic signal leads to amplification of the optical stimulus through the cyclic, biocatalyzed formation of the product. Accordingly, photochemical switching of the biocatalytic functions of redox proteins could lead to activation (or deactivation) of biocatalytic electron transfer cascades that might translate the photonic triggering signal into an output of electrochemical current. Such systems represent "smart" biological interfaces, in which photonic signals are recorded and stored by the photosensitive biomaterial, and the encoded information can be transduced and amplified by the biocatalytic electron transfer cascade of the redox protein.^[1,2,49] The electronic transduction of recorded photonic signals requires the integration and coupling of the photoswitchable redox biomaterial with an electronic transducer element, and provides the basis for future optobioelectronic and sensory devices (cf. Section 6.3).

Two general methodologies for photoregulation of electron transfer reactions at electrode interfaces may be envisaged (Scheme 7). One method (Scheme 7(A)), involves photoisomerizable units tethered to a redox enzyme. In configuration A, the active site environment of the enzyme is distorted and the bioelectrocatalytic properties of the enzyme are blocked, in a switched "OFF" state. Photoisomerization of the photoactive groups to state B restores the active site structure, and the enzyme is activated for its bioelectrocatalytic process, and hence in a switched ON state. The resulting electrical contact between the biocatalyst and the electrode, together with



Scheme 7: Electronic transduction of photo-switchable bioelectrocatalytic functions of proteins, (A) by the tethering of photoisomerizable units to the protein (R is a diffusional electron mediator that electrically contacts the redox

site of the protein with the electrode support), (B) by application of a photoisomerizable command interface that controls the electrical contact between the redox protein and the electrode.

the activation of the bioelectrocatalytic process, result in the transduction of a current to the macroscopic environment. Cyclic photoisomerization of the photoactive groups between the states B and A makes it possible to switch amperometric transduction between ON and OFF states.

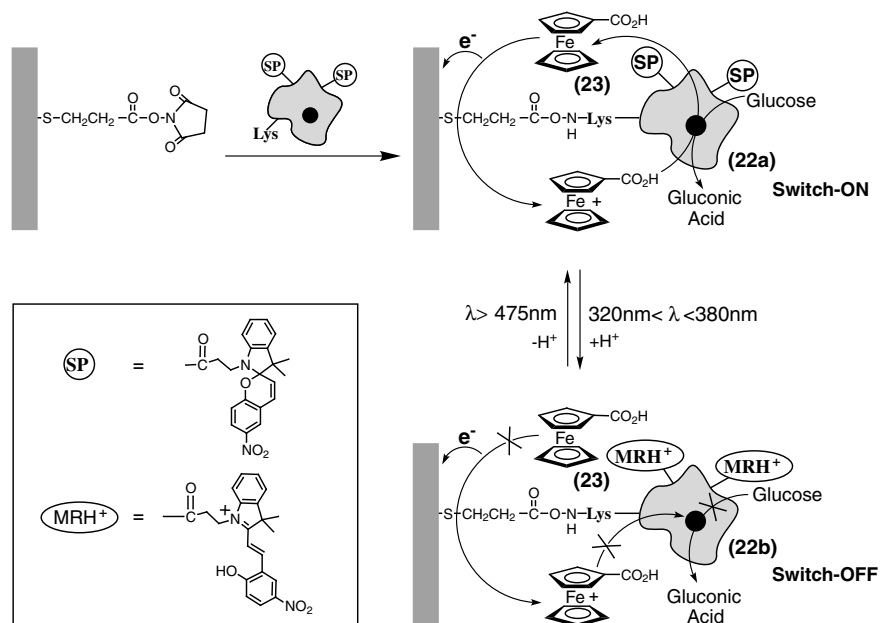
A different approach to photostimulation of redox biomaterials and electronic transduction of photonic stimuli is shown in Scheme 7(B), and involves control of the electronic coupling between the biomaterial and the transducer by means of a photosensitive interface associated with the electronic support. In this method, the transducer element is functionalized with a photoisomerizable interface. In the interface photoisomer state A, no affinity interactions exist between the redox protein (or the redox enzyme) and the photosensitive interface associated with the solid support. As a result, no electronic coupling occurs between the redox biomaterial and the transducer (electrode), and the system is in a mute, switched off state. Photoisomerization of the interface to state B results in binding of the redox biomaterial to the surface through the agency of affinity interactions or intermolecular recognition properties. This results in the electronic coupling of the biomaterial and the electronic transducer, producing electronic or amperometric transduction of the photonic information, recorded by the photoactive interface. That is, the photoisomerizable interface acts as a “photo-command” interface for controlling the electrical communication between the redox biomaterial and the electronic transducer.

In the next section, we will address different systems tailored along these lines, leading to the electronic transduction of photoswitchable redox biomaterial functions.

6.2.1

Amperometric Transduction of Optical Signals Recorded by Photoisomerizable Enzyme Electrodes

Glucose oxidase, GOx, has been employed as a redox enzyme to engineer a photoisomerizable enzyme electrode for the photoswitchable bioelectrocatalyzed oxidation of glucose, and for the amperometric transduction of the photonic information recorded by the enzyme interface.^[50] Photoisomerizable nitrospiropyran units were tethered to GOx lysine residues, and the photoisomerizable protein was assembled on an Au electrode as shown in Scheme 8. A primary *N*-hydroxysuccinimide monolayer was assembled on the conductive support, and the photoisomerizable enzyme was covalently coupled to the monolayer to yield the integrated photoactive enzyme electrode. The enzyme monolayer was found to undergo reversible photoisomerization, and photoirradiation of the nitrospiropyran-tethered GOx **22a** with UV light ($320 \text{ nm} < \lambda < 380 \text{ nm}$) generated the protonated nitromerocyanine-tethered GOx **22b**. Further irradiation of the **22b** monolayer with visible light ($\lambda > 475 \text{ nm}$) restored the nitrospiropyran-tethered protein **22a**. The photoisomerizable enzyme monolayer electrode displayed a photoswitchable bioelectrocatalytic function (Figure 9).



Scheme 8: Assembly of a photoisomerizable glucose oxidase monolayer electrode and the reversible photoswitchable activation/deactivation of the bioelectrocatalytic functions of the enzyme electrode.

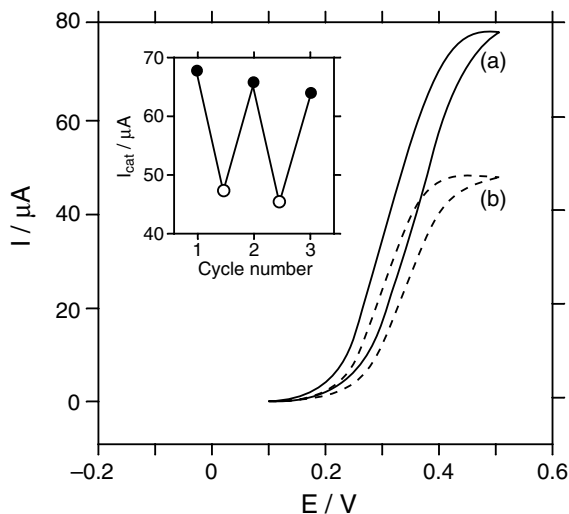
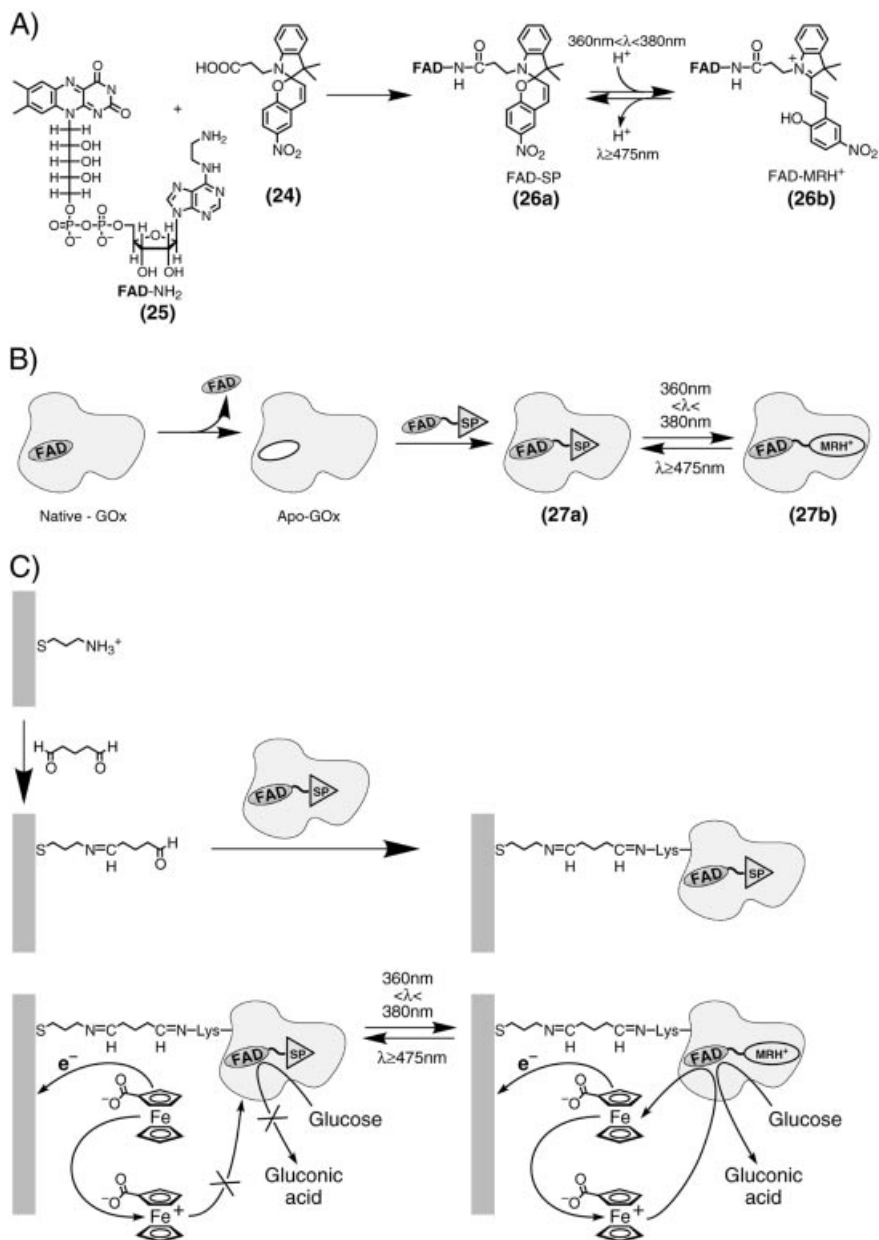


Fig. 9: Photostimulated bioelectrocatalyzed oxidation of glucose (2.5×10^{-2} M) in the presence of ferrocenecarboxylic acid (**23**) (5×10^{-3} M), as a diffusional electron mediator in the presence of: (a) nitrospiropyran-tethered GOx (**22a**). (b) protonated nitromerocyanine-tethered GOx, (**22b**). Inset: Reversible photo-switchable amperometric transduction of the bioelectrocatalyzed oxidation of glucose by **22a** – (●) and **22b** – (○).

In the presence of ferrocene carboxylic acid (**23**) as an electron transfer mediator, the nitrospiropyran-tethered GOx **22a** displayed a high bioelectrocatalytic activity, reflected in a high electrocatalytic anodic current. The protonated nitromerocyanine GOx **22b** exhibited half the activity, reflected in the decreased bioelectrocatalytic current. By exploiting reversible photoisomerization of the enzyme electrode between the **22a** and **22b** monolayer electrodes, it was possible to cycle the current responses between high and low values (Figure 9 (inset)). Although the tethering of photoisomerizable units to the protein had resulted in photoswitchable bioelectrocatalytic properties, the “OFF” state of the photoisomerizable GOx exhibited residual bioelectrocatalytic properties. This was due to the fact that the photoisomerizable units were tethered randomly to the protein, and the structural distortion of the active site environment upon photoisomerization of the protein to the **22b** state was not optimized (cf. Section 6.1.1 for a related discussion).

To optimize the photoswitchable bioelectrocatalytic features of the protein, site-specific functionalization or mutation of the active site microenvironment is essential. This was accomplished by a semisynthetic approach involving the reconstitution of the flavoenzyme-glucose oxidase with a semisynthetic photoisomerizable FAD cofactor (Scheme 9).^[51] The photoisomerizable nitrospiropyran carboxylic acid (**24**) was covalently coupled to N^6 -(2-aminoethyl)-FAD (**25**), to yield the synthetic photoisomerizable nitrospiropyran-FAD cofactor **26a** (Scheme 9(A)). The native FAD cofactor was removed from glucose oxidase, and the synthetic photoisomerizable-FAD cofactor **26a** was reconstituted into the apo-glucose oxidase (apo-GOx), to yield the photoisomerizable enzyme **27a** (Scheme 9(B)). This reconstituted protein



Scheme 9: (A) Synthesis of a semisynthetic photoisomerizable FAD cofactor. (B) Reconstitution of apo-glucose oxidase with semisynthetic nitrospiropyran-FAD photoisomerizable cofactor to yield a photoisomerizable glucose

oxidase. (C) Assembly of nitrospiropyran-FAD-reconstituted GOx as a monolayer on the electrode and the reversible photoswitchable bioelectrocatalytic activation/deactivation of the enzyme electrode.

features a photoisomerizable unit directly attached to the redox center of the protein, and hence the redox enzyme was expected to display optimized photoswitchable bioelectrocatalytic properties. The resulting enzyme was incorporated onto an Au electrode, as shown in Scheme 9(C), to yield an integrated electronic assembly consisting of the photoisomerizable enzyme-layered electrode. Photoinduced bioelectrocatalytic oxidation of glucose was stimulated in the presence of ferrocenecarboxylic acid (**23**) as a diffusional electron transfer mediator. The nitrospiropyran state of the reconstituted enzyme (**27a**) was inactive towards the bioelectrocatalytic transformation, but photoisomerization of the enzyme electrode to the protonated nitromerocyanine state (**27b**) activated the enzyme towards bioelectrocatalyzed oxidation of glucose (Figure 10). Cyclic photoisomerization of the enzyme monolayer interface between the nitrospiropyran and the protonated nitromerocyanine states resulted in biocatalyzed oxidation of glucose cycling between the completely “OFF” state and a switched “ON” state (Figure 10 (inset)). It was also found that the direction of the photobiocatalytic switch of the nitrospiropyran-FAD-reconstituted enzyme was controlled by the electrical properties of the electron transfer mediator.^[52] With ferrocenedicarboxylic acid (**28**) as the diffusional electron transfer mediator, the enzyme in the nitrospiropyran-FAD state (**27a**) was found to correspond (for glucose oxidation) to the switched off biocatalyst, while the protonated nitromerocyanine state of the enzyme (**27b**) exhibited switched “ON” bioelectrocatalytic properties. In the presence of the protonated 1-[1-(dimethylamino)ethyl]ferrocene **29**, the direction of the photobiocatalytic switch was reversed. The nitrospiropyran enzyme state

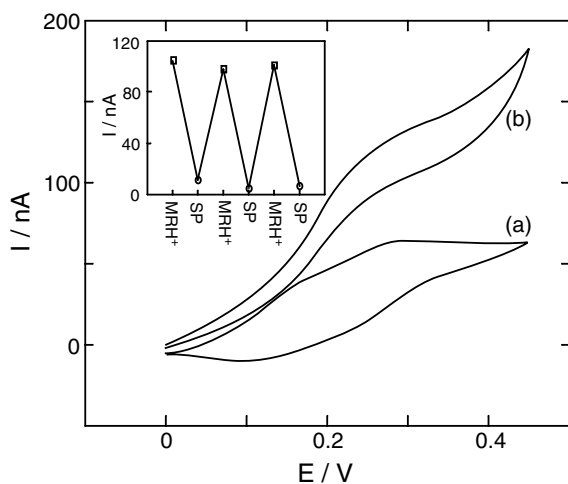
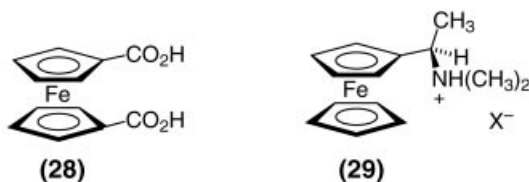


Fig. 10: Photoswitchable bioelectrocatalyzed oxidation of glucose (5×10^{-2} M) by a photoisomerizable FAD-reconstituted GOx assembled as a monolayer on an Au electrode and using ferrocenecarboxylic acid (**23**) (5×10^{-5} M) as a diffusional electron mediator. (a) By the nitrospiropyran-FAD-reconstituted GOx (**27a**) monolayer. (b) By the protonated

nitromerocyanine-FAD-reconstituted GOx (**27b**) monolayer. Inset: Cyclic amperometric transduction of the bioelectrocatalyzed oxidation of glucose by the photoisomerizable reconstituted GOx monolayer electrode. (□) – Monolayer in the (**27b**)-state. (○) – Monolayer in the (**27a**)-state.

(27a) was activated towards electrocatalyzed oxidation of glucose, while the protonated nitromerocyanine enzyme state was switched “OFF”, and so was inactive for electrochemical oxidation of glucose. This control of the photoisomerizable reconstituted enzyme’s photoswitching direction was attributed to electrostatic interactions between the diffusional electron mediator and the photoisomerizable unit linked to the FAD, acting as a “gate” for electrical contact between the redox cofactor and the electrode support. The protonated nitromerocyanine photoisomer state attracted the oxidized negatively charged electron mediator **28**, but repelled the oxidized positively charged relay **29**. As a result, the photoisomer state of the enzyme **27b** was switched “ON” in the presence of **28**, but existed in the switched “OFF” state when the positively charged electron transfer mediator **29** was used.

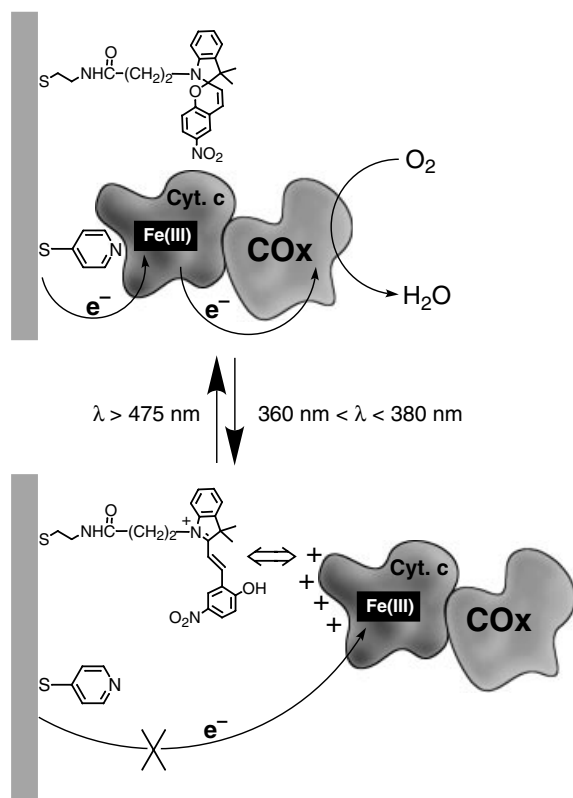


6.2.2

Light-Switchable Activation of Redox Proteins by Means of Photoisomerizable “Command Interfaces” Associated with Electrodes

Photoswitchable electrical transduction of recorded photonic signals using functionalized “command interfaces” on electrodes to control electrical contact between redox proteins and their conductive support according to Scheme 7(B), has been accomplished with various systems.^[53,54] Redox proteins do not usually enter into direct electrical contact with electrodes, since the redox site is embedded in the protein. Electrical communication between the redox site and the electrode is hence blocked, due to the spatial separation between the protein redox site and the electrode support. For redox proteins of low molecular weight, such as the hemoprotein cytochrome c (Cyt. c), chemical functionalization of the electrode surfaces with molecular promoter units was found to facilitate electron transfer communication between the protein redox centers and the conductive supports.^[55,56] Binding of the redox proteins to the promoter sites aligns the redox centers with respect to the electrode surface. This results in the shortening of electron transfer distances, and leads to electrical contact with the redox sites. For example, pyridine units^[56] or negatively charged promoter sites,^[57] assembled on electrode surfaces, have been reported to align Cyt. c on electrodes through affinity or electrostatic interactions, and to facilitate electrical communication between the heme site and the electrode. At neutral pH, cytochrome c is a positively charged hemoprotein. This suggests that the nanoengineering of an electrode with a composite layer consisting of Cyt. c binding sites and photoisomerizable units that could be transformed from neutral to positively charged states would make it possible to achieve electrostatic photoswitchable

binding of Cyt. c to the electrode, and dissociation from it.^[53] To photoregulate electrical communication between Cyt. c and the electrode, a mixed monolayer consisting of pyridine sites and photoisomerizable nitrospiropyran units was assembled on an Au electrode (Scheme 10). This monolayer binds Cyt. c to the surface, aligns the heme center of the protein, and so electrical contact with the electrode is stimulated (Figure 11(A), curve (a)). Photoisomerization of the monolayer to the positively charged, protonated nitromerocyanine state results in electrostatic repulsion of Cyt. c from the monolayer. As a result, electrical communication between the hemoprotein and the electrode is blocked (Figure 11(A), curve (b)). Cyclic photoisomerization of the monolayer between the nitrospiropyran and the protonated nitromerocyanine states makes reversible light-induced binding and dissociation of Cyt. c to and from the monolayer possible, and so electrical contact between the hemoprotein and the electrode is switched between “ON” and “OFF” states. Cytochrome c acts as an electron transfer mediator (cofactor) that activates many secondary biocatalyzed transfor-



Scheme 10: Reversible photoswitchable activation/deactivation of the electrical contact between cytochrome c and the electrode and the secondary activation/deactivation of the COx-biocatalyzed reduction of oxygen using a thiolated nitrospiropyran and thiolated pyridine mixed monolayer as a command interface.

mations through the formation of interprotein Cyt. c-enzyme complexes. Specifically, Cyt. c transfers the electrons to cytochrome oxidase, COx, which mediates the four-electron reduction of oxygen to water. This photoswitchable electrical activation

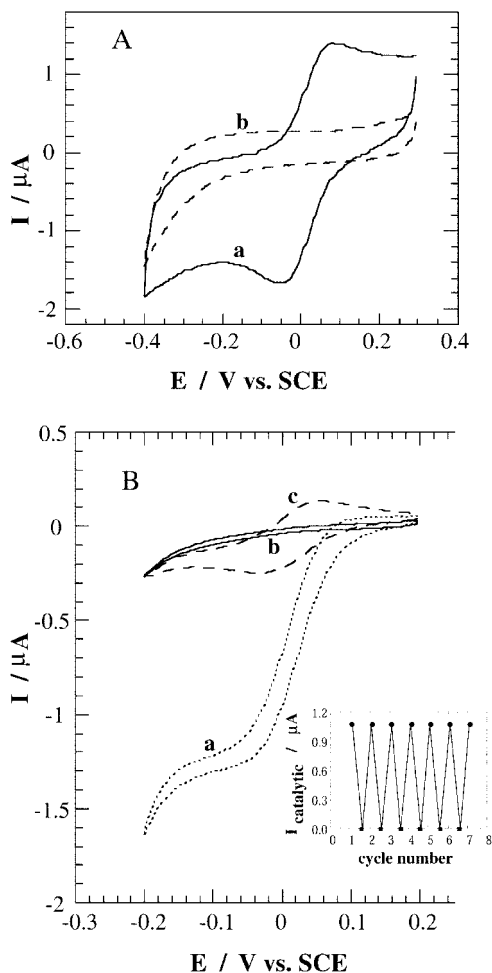
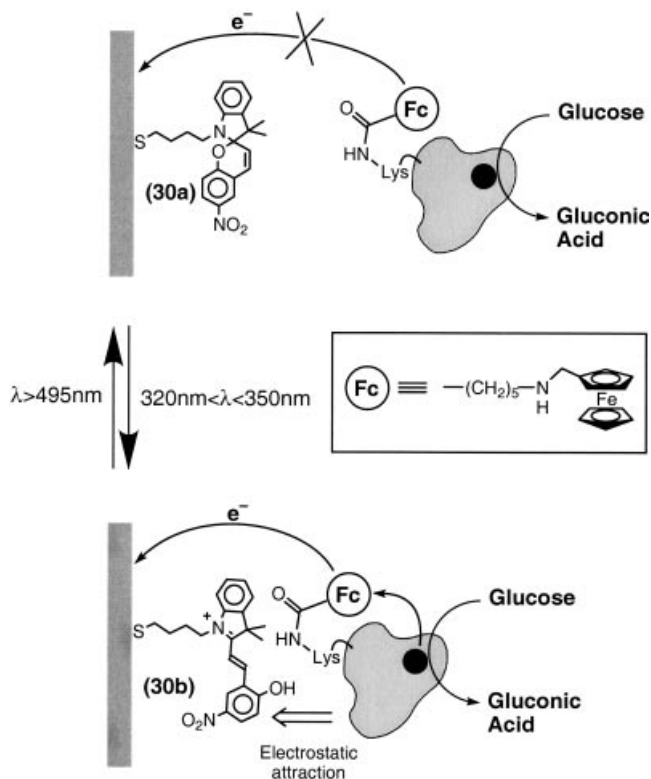


Fig. 11: (A) Cyclic voltammograms of cytochrome c (Cyt. c) (1×10^{-4} M), in the presence of: (a) the pyridine-nitrospiropyran mixed monolayer electrode, (b) the pyridine-protonated-nitromerocyanine mixed monolayer electrode. Data recorded at a scan rate of $50 \text{ mV} \cdot \text{sec}^{-1}$. (B) Cyclic voltammograms of the Cyt.c/COx system corresponding to the photo-stimulated bioelectrocatalyzed reduction of O_2 in the presence of the photoisomerizable monolayer electrode. (a) Bioelectrocatalyzed reduction of O_2 by Cyt. c/COx in the presence of pyridine-nitrospiropyran mixed monolayer

electrode. (b) Cyclic voltammogram of the Cyt. c/COx system under O_2 in the presence of the pyridine-protonated-merocyanine mixed monolayer electrode. (c) Cyclic voltammogram of Cyt. c alone (under O_2) in the presence of the pyridine-nitrospiropyran mixed monolayer electrode. Data recorded at scan rate $2 \text{ mV} \cdot \text{sec}^{-1}$. Inset: Photoswitchable amplified amperometric transduction of photonic signals recorded by the photoisomerizable monolayer electrode through the Cyt. c/COx bioelectrocatalyzed reduction of O_2 .

of Cyt. c thus makes photostimulated triggering of the COx-biocatalyzed reduction of O₂ possible (Scheme 10). In the presence of the pyridine-nitrospiropyran monolayer electrode, electron transfer to Cyt. c activates the electron transfer cascade to COx, and the bioelectrocatalyzed reduction of O₂ to water is accomplished, reflected in the transduced electrocatalytic cathodic current (Figure 11(B), curve (a)). Photoisomerization of the monolayer into the protonated nitromerocyanine configuration results in the repulsion of Cyt. c from the electrode interface. This, in turn, blocks interfacial electron transfer to Cyt. c and the secondary bioelectrocatalytic activation of the COx-mediated reduction of O₂ (Figure 11(B), curve (b)). Note that the electrocatalytic cathodic current transduced by the Cyt. c-COx protein assembly is enhanced approximately 10-fold compared to the amperometric current resulting from Cyt. c alone (Figure 11(B), curve (c) versus curve (a)). This is due to the fact that COx induces a bioelectrocatalytic process and the photonic activation of the Cyt. c-COx system drives the reduction of O₂ with a high turnover. Thus, the amperometric response of the Cyt. c-COx layered electrode represents the amplified amperometric transduction of the photonic information recorded by the monolayer. Cyclic photoisomerization of the monolayer between the nitrospiropyran and protonated nitromerocyanine states results in reversible cycling of the system's amperometric responses between "ON" and "OFF" states (Figure 11(B), inset). The system mimics certain functions of the natural vision process, in that the photoisomerizable monolayer assembled on the electrode mimics the functions of the rhodopsin-embedded protein membrane. Photoisomerization of the monolayer to the nitrospiropyran and binding of Cyt. c is analogous to the association of Protein G to the protein membrane. The Cyt. c electron transfer activation of COx towards O₂ reduction, and the resulting amplified transduced current from the system mimics the Protein G activation of the enzyme cascade leading to the generation of c-GMP, which activates the neural response of the vision process.

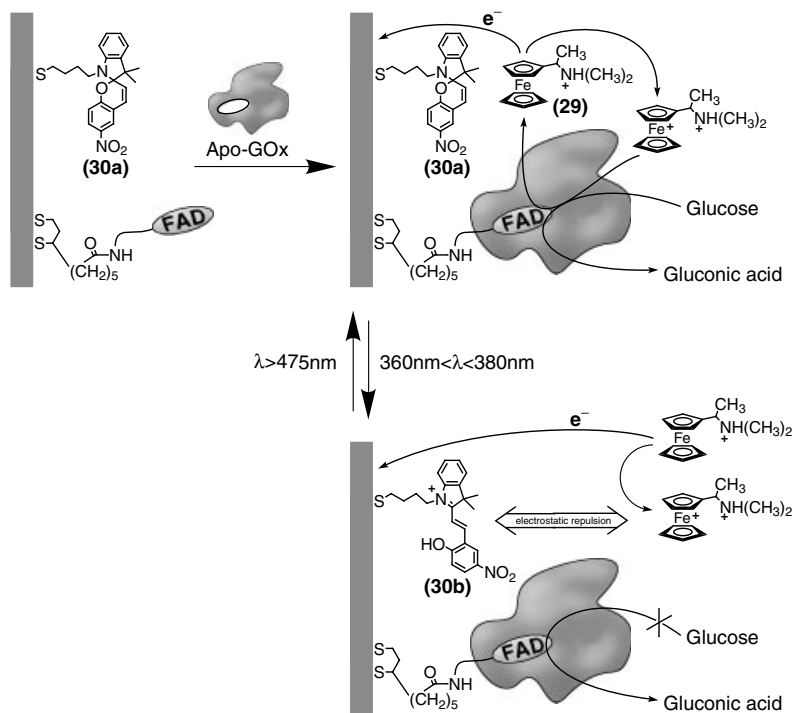
Electrostatic control over electrical contact between redox proteins and electrodes by means of "photo-command interfaces" has further been demonstrated by the photochemical switching of the bioelectrocatalytic properties of glucose oxidase (Scheme 11).^[54] Ferrocene units were tethered to the protein backbone of glucose oxidase, to yield an "electrically-wired" enzyme activated for the bioelectrocatalyzed oxidation of glucose. The enzyme is negatively charged at neutral pH values (pI = 4.0), and hence could be electrostatically attracted by positively charged surfaces. Accordingly, a thiolated nitrospiropyran (**30a**) monolayer was assembled on an Au electrode. In this photoisomer state of the functionalized electrode monolayer, inefficient electrical interactions exist between the protein and the modified electrode, and moderate bioelectrocatalyzed oxidation of glucose occurred. Photoisomerization of the monolayer to the protonated nitromerocyanine state (**30b**) resulted in the electrostatic attraction of the biocatalyst to the electrode support. The resulting concentration of the enzyme at the electrode surface produced effective electrical communication between the biocatalyst and the electrode. This yielded enhanced bioelectrocatalyzed oxidation of glucose and the photochemical activation of the redox protein. The current transduced by the bioelectrocatalyzed oxidation of glucose represents an amplified signal resulting from the photonic activation of the monolayer. Cyclic photoisomerization of the monolayer between the nitro-



Scheme 11: Photochemical control of electrical contact between a ferrocene-tethered glucose oxidase and the electrode using a thiolated nitrospiropyran as a command interface.

merocyanine state and the nitrospiropyran state engendered switching of the enzyme between surface-associated and surface-dissociated configurations, respectively, leading to reversible “ON”-“OFF” photochemical activation of the bioelectrocatalytic functions of the enzyme.

A further approach to controlling electrical communication between redox proteins and their electrode support through a photo-command interface includes photostimulated electrostatic control over the electrical contact between the redox enzyme and the electrode in the presence of a diffusional electron mediator (Scheme 12).^[58] A mixed monolayer, consisting of the photoisomerizable thiolated nitrospiropyran units **30** and the semi-synthetic FAD cofactor **25**, was assembled on an Au electrode. Apo-glucose oxidase was reconstituted onto the surface FAD sites to yield an aligned enzyme-layered electrode. The surface-reconstituted enzyme ($2 \times 10^{-12} \text{ mole} \cdot \text{cm}^{-2}$) by itself lacked electrical communication with the electrode. In the presence of the positively charged, protonated diffusional electron mediator 1-[1-(dimethylamino)ethyl]ferrocene **29**, however, the bioelectrocatalytic functions of the enzyme-layered electrode could be activated and controlled by the photoisomerizable component co-immobilized in the monolayer assembly (Figure 12). In the



Scheme 12: Surface reconstitution of apo-glucose oxidase on a mixed monolayer associated with an electrode consisting of an FAD cofactor and photoisomerizable nitrospiropyran units, and reversible photoswitching of the bioelectrocatalytic functions of the enzyme electrode.

monolayer's neutral nitrospiropyran state, the positively charged electron mediator was oxidized at the electrode, and it mediated electrical communication between the surface-bound redox enzyme and the electrode in diffusional manner. The electrical contact between the surface-associated glucose oxidase (GOx) and the conductive support activated the bioelectrocatalyzed oxidation of glucose, a process reflected in an electrocatalytic anodic current (Figure 12, curve (a)). Photoisomerization of the monolayer to the protonated nitromerocyanine state resulted in the electrostatic repulsion of the positively charged electron mediator from the electrode surface, both before and after its oxidation. This blocked the mediated electrical communication between the redox enzyme and the electrode, and the bioelectrocatalytic functions of the GOx layer were switched off (Figure 12, curve (b)). Cyclic photoisomerization of the monolayer, between its nitrospiropyran and protonated nitromerocyanine states, produced reversible switching on and switching off of amperometric transduction of the photonic signals, recorded at the monolayer, in the modified bioelectrocatalytic interface (Figure 12 (inset)).

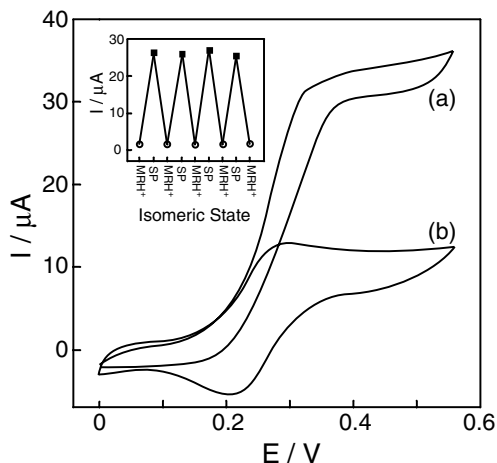


Fig. 12: Photoswitchable bioelectrocatalyzed oxidation of glucose (8×10^{-2} M) by a composite monolayer consisting of GOx reconstituted onto FAD units and nitrospiropyran photoisomerizable units in the presence of **29** as a diffusional electron mediator. (a) In the presence

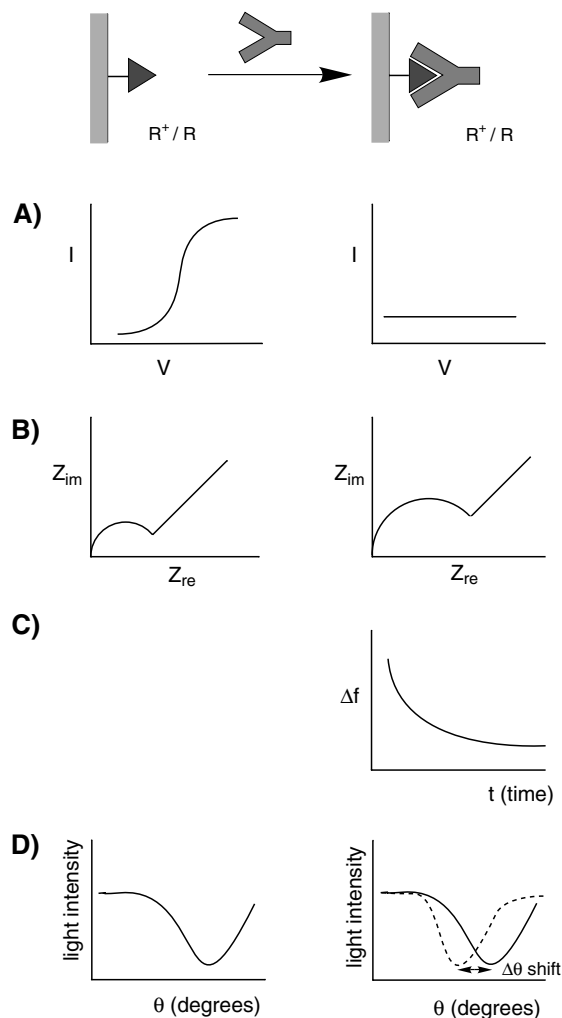
of the nitrospiropyran state (**30a**). (b) In the presence of the protonated nitromerocyanine state (**30b**). Inset: Cyclic amperometric transduction of photonic signals recorded by the photoisomerizable monolayer electrode by the bioelectrocatalyzed oxidation of glucose.

6.3

Electronic Transduction of Photoswitchable Antigen–Antibody Interactions at Solid Supports

The electronic transduction of the formation of antigen–antibody complexes at electronic transducers is the basis of bioelectronic immunosensor devices.^[59,60] Several means of transduction, including electrochemical transduction (potentiometric,^[61,62] amperometric,^[63,64] and impedometric^[65] signals), microgravimetric quartz crystal microbalance (QCM) analysis,^[66,67] and surface plasmon resonance (SPR) spectroscopy,^[68,69] have been used to follow the formation of antigen–antibody complexes on surfaces. Scheme 13 shows schematic representations of amperometric, impedometric, microgravimetric, and SPR transduction of antigen–antibody layer formation on solid supports. The formation of an antigen–antibody complex on an electrode insulates the conductive support, and introduces a barrier to electron transfer at electrode surfaces. The formation of the antigen–antibody complex on the electrode results, as a consequence of the electrical insulation of the surface, in the blocking of the amperometric response of a redox label solubilized in the electrolyte solution (Scheme 13(A)). Impedance spectroscopy – and, specifically, Faradaic impedance spectroscopy – is a useful method for probing electron transfer resistance and capacitance at the electrode surface. Upon application of an alternating voltage at the electrode, the complex impedance (the real impedance ($Z_{re}(\omega)$) plus the imaginary impedance ($Z_{im}(\omega)$) components) is determined as a function of the applied frequency. The interfacial electron transfer resistance at the electrode

support – R_{et} – is derived from the respective Nyquist plot, (Z_{im} versus Z_{re}), where the semicircle diameter of the impedance spectrum corresponds to the electron transfer resistance at the electrode surface. Accordingly, the formation of the antigen–antibody complex on the electrode surface is reflected in an increase in the interfacial electron transfer resistance and an enlarged semicircle diameter in the respective impedance spectrum (Scheme 13(B)). Formation of the antigen–antibody complex on the transducer alters its mass. The resonance frequency of a piezoelec-



Scheme 13: Electronic and optical transduction of the formation of antigen–antibody affinity complexes on transducers: (A) amperometric transduction at an electrode (R^+/R is a redox label in the electrolyte solution), (B)

transduction by Faradaic impedance spectroscopy, (C) microgravimetric Quartz Crystal Microbalance (QCM) transduction in the presence of a piezoelectric quartz crystal. (D) Surface plasmon resonance transduction.

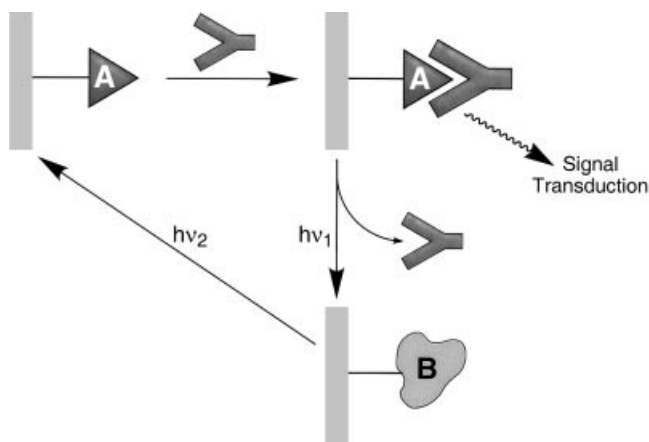
tric crystal – such as a quartz crystal – is dependent on the mass associated with the crystal. An increase in the quartz crystal mass, as a consequence of the formation of the antigen–antibody complex, is accompanied by a decrease in the resonance frequency of the crystal (Eq. 6.3.1; Scheme 13(C)).

$$\Delta f = -C_f \Delta m \quad (\text{where } C_f = 1.83 \times 10^8 \text{ (Hz} \times \text{cm}^2 \times \text{g}^{-1})) \quad (6.3.1)$$

Indeed, different immunosensor devices based on the frequency changes of the crystal have been reported.^[66,67]

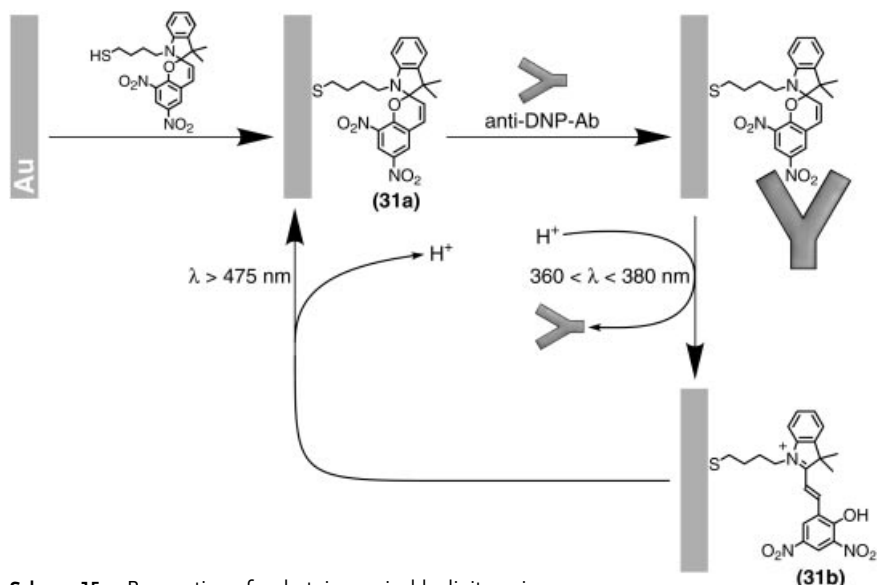
Surface plasmon resonance spectroscopy is a further means by which the formation of antigen–antibody complexes may be followed. Thin metal layers – Au or Ag, for example – give rise to a surface plasmon. The interaction of the metal layer with p-polarized light gives rise to resonance excitation of the plasmon, resulting in the absorption of the light energy at an appropriate angle of incident light. The angle of minimum reflectivity, as a product of the plasmon resonance excitation, is controlled by the dielectric constant and the thickness of the dielectric layer associated with the metal support. The formation of the antigen–antibody complex at the metal surface alters the dielectric constant of the interface and increases the thickness of the dielectric layer, resulting in a shift in the minimum reflectivity angle of the plasmon resonance absorbance (Scheme 13(D)). The surface plasmon resonance (SPR) phenomenon is frequently exploited to characterize the formation of antigen–antibody complexes at metal layers.^[68,69]

Antigen–antibody affinity interactions usually exhibit high binding constants ($K_a \approx 10^7\text{--}10^{10} \text{ M}^{-1}$), resulting in the formation of tightly bound complexes on the respective transducers. This causes most of the immunosensor devices to act as single-cycle bioelectronic systems, in which regeneration of the sensor is precluded. The concept of photoswitchable binding between a photoisomerizable substrate and a receptor (cf. Section 6.1.1) has been extended to tailoring of photostimulated formation and dissociation of antigen–antibody complexes on electronic transducers as



Scheme 14: Assembly of a reversible immunosensor using a photoisomerizable antigen-functionalized transducer.

a generic methodology for producing cyclic, reusable immunosensors (Scheme 14).^[70] A photoisomerizable antigen is assembled on the sensing interface as a monolayer. In one photoisomer configuration, state A, the monolayer exhibits affinity for the antibody. The formation of the antigen–antibody complex on the surface is transduced to the environment, thus enabling sensing of the antibody. After completion of the sensing cycle, the monolayer is photoisomerized to the complementary structure, state B. The latter monolayer configuration lacks antigen affinity properties for the antibody. This enables the antibody to be washed off from the monolayer interface. In a secondary illumination process, the resulting monolayer is once more isomerized from state B to state A, a process that transforms the monolayer into the original antigen interface. Thus, by means of a two-step photochemical isomerization of the monolayer, with intermediate elimination of the analyzed antibody by a rinsing process, the sensing interface is recycled and the functionalized transducer acts as a reversible, reusable immunosensor.^[70] The reversible cyclic sensing of anti-dinitrophenyl-antibody (anti-DNP-Ab) was accomplished by this method, through the application of a photoisomerizable dinitrospiropyran monolayer on an Au support. A thiolated dinitrospiropyran photoisomerizable monolayer (**31a**) was assembled on Au electrodes or Au quartz crystals (Scheme 15). The dinitrospiropyran monolayer acted as an antigen for the DNP-Ab, while the protonated dinitromerocyanine monolayer state lacked antigen affinity for the DNP-Ab. This allowed for cyclic sensing of the DNP-Ab by the monolayer-modified transducers (Scheme 15). The association of the DNP-Ab to the dinitrospiropyran antigen monolayer was transduced electrochemically, using amperometric^[71] or Faradaic impedance spectroscopy,^[72] microgravimetrically in the presence of the piezoelectric Au quartz crystal as a transducer,^[71] or optically, using surface plasmon resonance (SPR).^[73] Association of the DNP-Ab with the antigen monolayer-functionalized electrode resulted in electrical insulation of the electrode support and the introduction of an electron barrier at the electrode surface. Thus, in the presence of an “electrically wired” enzyme, ferrocene-tethered glucose oxidase, the bioelectrocatalytic oxidation of glucose, and the resulting electrocatalytic current, were inhibited on the formation of the DNP-Ab/dinitrospiropyran complex on the electrode support (Figure 13(A), curve (b)).^[71] Similarly, the association of DNP-Ab to the antigen monolayer increased the interfacial electron transfer resistance.^[72] In the presence of $\text{Fe}(\text{CN})_6^{3-}/\text{Fe}(\text{CN})_6^{4-}$ as a redox label, the electron transfer resistance increased from $R_{\text{et}} = 60 \pm 2 \text{ k}\Omega$ to $R_{\text{et}} = 80 \pm 2 \text{ k}\Omega$ upon formation of the DNP-Ab/antigen complex (Figure 13(B), curves (b) and (c), respectively). Photoisomerization of the DNP-Ab/dinitrospiropyran monolayer interface ($360 \text{ nm} < \lambda < 380 \text{ nm}$) to the protonated dinitromerocyanine state, followed by rinsing off of the DNP-Ab, resulted in the original amperometric response of the monolayer-functionalized electrode (Figure 13(A), curve (c)), and a low electron transfer resistance ($R_{\text{et}} = 47 \pm 2 \text{ k}\Omega$) in the Faradaic impedance spectrum (Figure 13(B), curve (a)), indicating that the antibody had been removed from the electrode support upon isomerization of the monolayer to the protonated dinitromerocyanine state. Note that the electron transfer resistance at the protonated dinitromerocyanine-functionalized electrode was lower than at the dinitrospiropyran-modified electrode, using $\text{Fe}(\text{CN})_5^{3-}/\text{Fe}(\text{CN})_6^{4-}$ as the redox



Scheme 15: Preparation of a photoisomerizable dinitrospiropyran monolayer on a transducer and the reversible sensing of anti-DNP-Ab.

probe (Figure 13(B), curves (a) and (b), respectively). This arises from the fact that the positively charged protonated dinitromerocyanine monolayer interface attracted the redox label electrostatically, thereby facilitating the interfacial electron transfer. Further photochemical isomerization of the protonated dinitromerocyanine monolayer to the dinitrospiropyran interface ($\lambda > 475$ nm) regenerated the sensing interface. Cyclic amperometric and Faradaic impedance transduction of DNP-Ab sensing by the reusable photoisomerizable monolayer electrode are demonstrated in Figure 13(A) and (B) (insets), respectively.

Microgravimetric quartz crystal microbalance (QCM) transduction provides a further means to probe the binding interactions of the DNP-Ab with the photoisomerizable monolayer interface (Figure 14(A)).^[71] The DNP-Ab binds effectively to the dinitrospiropyran layer associated with the Au quartz crystal, as reflected in the decrease in the crystal frequency ($\Delta f = -120$ Hz; Figure 14(A), curve (a)). From the extent of the frequency decrease, the surface coverage of the DNP-Ab on the dinitrospiropyran antigen layer was calculated to be approximately 3.8×10^{-12} mole \times cm⁻². The frequency of the protonated dinitromerocyanine monolayer-functionalized Au quartz crystal was only slightly affected upon interaction with the DNP-Ab ($\Delta f = -40$ Hz; Figure 14(A), curve (b)). (This low decrease in the crystal frequency was attributed to non-specific adsorption of the antibody to the surface.) The photoisomerization of the dinitrospiropyran/DNP-Ab layered Au quartz crystal to the protonated dinitromerocyanine enabled the DNP-Ab to be washed off, a process reflected in the frequency increase of the Au quartz crystal (Figure 14(B)). Further photochemical isomerization of the protonated dinitromerocyanine mono-

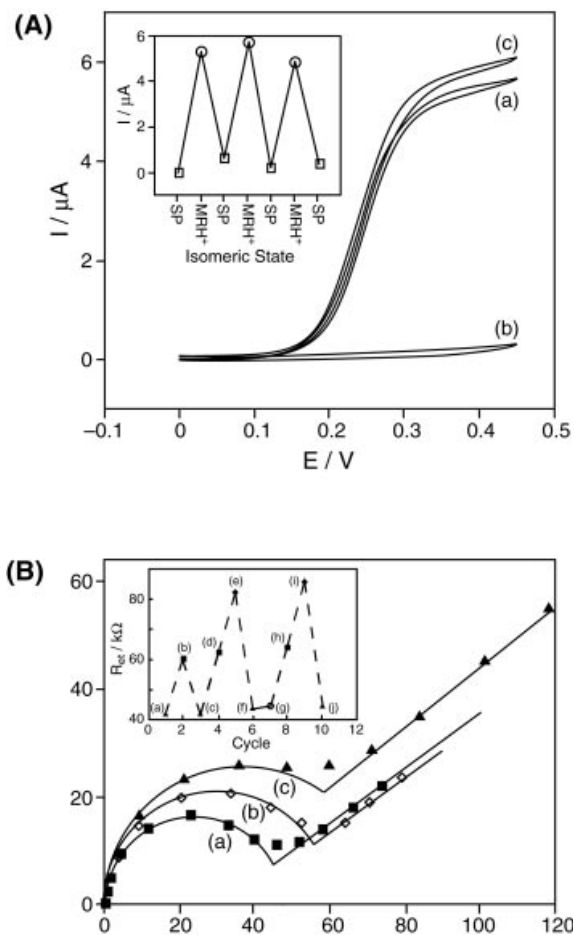


Fig. 13: (A) Cyclic voltammograms of: (a) the dinitrospiropyran (**31a**) monolayer electrode. (b) After addition of anti-DNP-Ab to the dinitrospiropyran (**31a**) monolayer electrode. (c) After photoisomerization of the dinitrospiropyran/anti-DNP-Ab to the protonated dinitromerocyanine monolayer and the washing off of the antibody. All data were recorded in the presence of ferrocene-tethered GOx as a redox biocatalyst and glucose (5×10^{-2} M, scan rate $5 \text{ mV} \cdot \text{sec}^{-1}$). Inset: Cyclic amperometric sensing of the DNP-Ab by the dinitrospiropyran photoisomerizable monolayer electrode. (B) Faradaic impedance spectra (Nyquist plots) of: (a) the protonated dinitromerocyanine monolayer electrode, (b) the dinitrospiropyran monolayer electrode, (c) the dinitrospiropyran monolayer electrode upon

addition of the anti-DNP-Ab. Impedance spectra were recorded in the presence of $\text{Fe}(\text{CN})_6^{3-}/\text{Fe}(\text{CN})_6^{4-}$ (1×10^{-2} M) as a redox label. Inset: Interfacial electron transfer resistances at the functionalized electrodes upon cyclic photoisomerization of the monolayer and the reversible sensing of the anti-DNP-Ab. (a) and (c) – Monolayer in the protonated dinitromerocyanine state. (b), (d), and (h) – Monolayer in the dinitrospiropyran state. (e) and (i) – After binding of DNP-Ab to the dinitrospiropyran monolayer electrode. (f) and (j) – After photoisomerization of the dinitrospiropyran (**31a**)/DNP-Ab monolayer electrode to the protonated dinitromerocyanine and washing off of the DNP-Ab. (g) – Addition of the DNP-Ab to the protonated dinitromerocyanine monolayer electrode (**31b**).

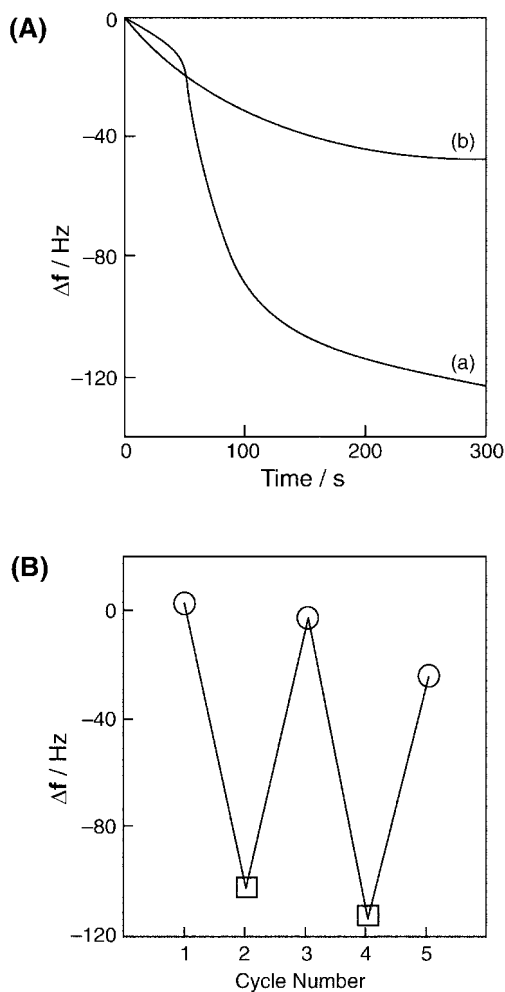


Fig. 14: (A) Time-dependent frequency changes of: (a) The dinitrospiropyran (**31a**) monolayer associated with an Au quartz crystal upon addition of anti-DNP-Ab. (b) The protonated dinitromerocyanine monolayer on an Au quartz crystal upon addition of the anti-DNP-Ab. (B) Cyclic microgravimetric sensing of the anti-DNP-Ab by the photoisomerizable dinitrospiropyran monolayer Au quartz crystal.

(□) Frequency of the crystal after addition of the DNP-Ab to the dinitrospiropyran (**31a**)-functionalized crystal. (O) Frequency of the crystal after photoisomerization of the (**31a**)/DNP-Ab monolayer to the protonated dinitromerocyanine (**31b**), washing off of the DNP-Ab, and back isomerization to (**31a**) monolayer state.

layer to the dinitrospiropyran monolayer state restored the active antigen monolayer interface for second-cycle sensing of the DNP-Ab. Cyclic photoisomerization of the monolayer between the protonated dinitromerocyanine and dinitrospiropyran states enables the DNP-Ab to be washed off from the transducer, and the sensing interface is regenerated, hence yielding a reversible immunosensor device (Figure 14(B)).

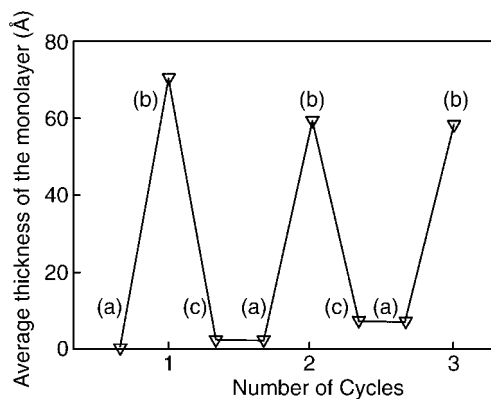


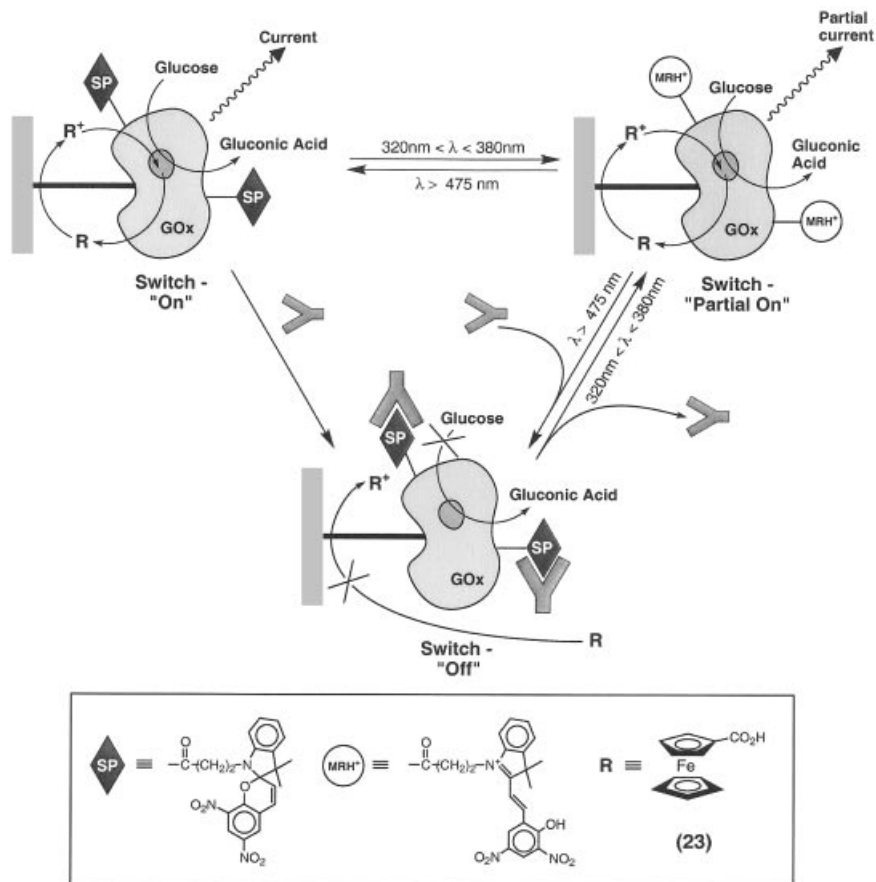
Fig. 15: Average thickness of the monolayer (determined from the respective surface plasmon resonance spectra). (a) The dinitrospiropyran (**31a**) monolayer. (b) The (**31a**) monolayer after binding of the anti-DNP-Ab. (c) After photoisomerization of the (**31a**)/DNP-Ab monolayer to the (**31b**) state, and washing off of the DNP-Ab.

Surface plasmon resonance spectroscopy (SPR) provides an optical transduction-based means to follow the reversible binding and dissociation of the DNP-Ab to and from the photoisomerizable monolayer. The thiolated dinitrospiropyran **31a** was assembled on an Au thin film coating a glass support.^[73] Upon binding of the DNP-Ab to the antigen layer, the minimum reflectivity angle was shifted by $\Delta\theta = 0.54^\circ$. Further photoisomerization of the modifying interface to the protonated dinitromerocyanine state **31b**, followed by washing off of the DNP-Ab, restored the characteristic minimum reflectivity angle of the monolayer without antibody. Theoretical fitting, according to the Fresnel equation, of the SPR spectrum observed upon the association of the DNP-Ab to the dinitrospiropyran (**31a**) antigen monolayer, indicated that the refractive index and thickness of the antigen-antibody complex layer corresponded to 1.41 and 70 Å, respectively. From the layer thickness, it was implied that approximately 60 % of a random, densely-packed monolayer is formed upon association of the DNP-Ab with the dinitrospiropyran (**31a**) antigen monolayer. Figure 15 shows the light-induced reversible binding of the DNP-Ab to the dinitrospiropyran (**31a**) antigen monolayer, and its dissociation from the protonated dinitromerocyanine (**31b**), as reflected by the thickness of the sensing interface as elucidated by SPR.^[73]

6.4

Complex Photochemical Biomolecular Switches

The ability to use light to electrochemically transduce photoswitchable electrocatalytic functions of photoisomerizable redox proteins associated with electrodes, and to regulate the binding between a substrate and its receptor – the binding of a photoisomerizable antigen with the respective antibody, for example – offers the potential to design complex photochemical bioswitches by integrating several light-controlled biomaterials. A biphasic photochemical bioswitch exhibiting “ON”, “partial-ON”, and “OFF” states has been designed through the assembly of dinitrospiropyran-functionalized glucose oxidase (GOx) on an Au electrode and the integration of the



Scheme 16: Biphasic optobioelectronic switch by means of coupling anti-DNP-Ab with a dinitrospiropyran-functionalized GOx monolayer electrode.

enzyme electrode with the anti-dinitrophenyl antibody DNP-Ab (Scheme 16).^[74] The dinitrospiropyran-modified GOx monolayer electrode exhibited bioelectrocatalytic properties, and in the presence of ferrocenecarboxylic acid (**23**) as a diffusional electron mediator, the biocatalytic interface electrocatalyzed the oxidation of glucose. This process was reflected in a high electrocatalytic anodic current response (Figure 16(A), curve (a)). Reversible photoisomerization of the enzyme monolayer between the dinitrospiropyran state and the protonated dinitromerocyanine state allowed the system to be cycled between a switched on bioelectrocatalytic state and a partially switched on configuration, respectively (Figure 16(A), curve (b)).

Since the photoisomerizable dinitrospiropyran units tethered to the redox enzyme act as photoisomerizable antigen sites for the anti-dinitrophenyl antibody DNP-Ab, the light-controlled association and dissociation of the antibody to and from the antigen-functionalized redox enzyme layer may control the bioelectrocatalytic functions

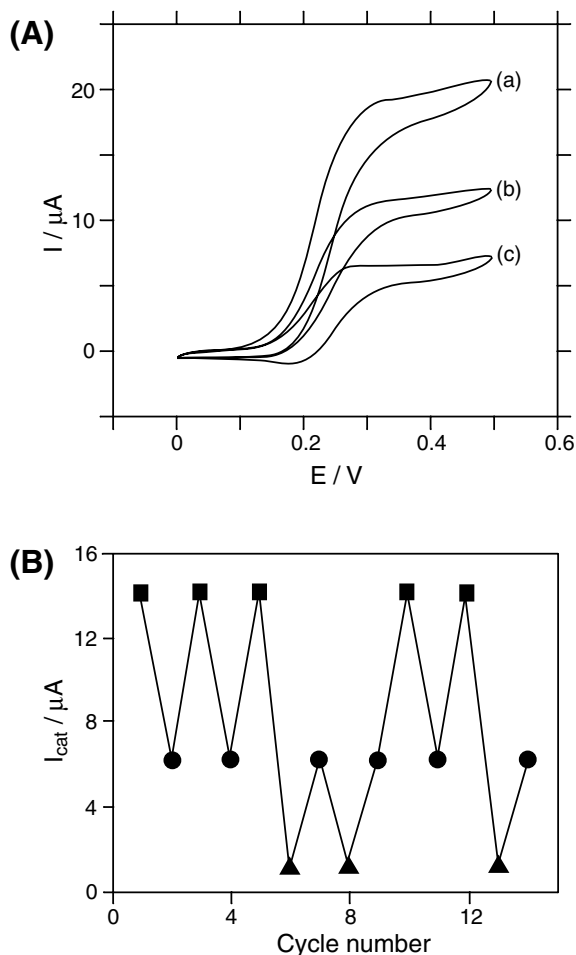
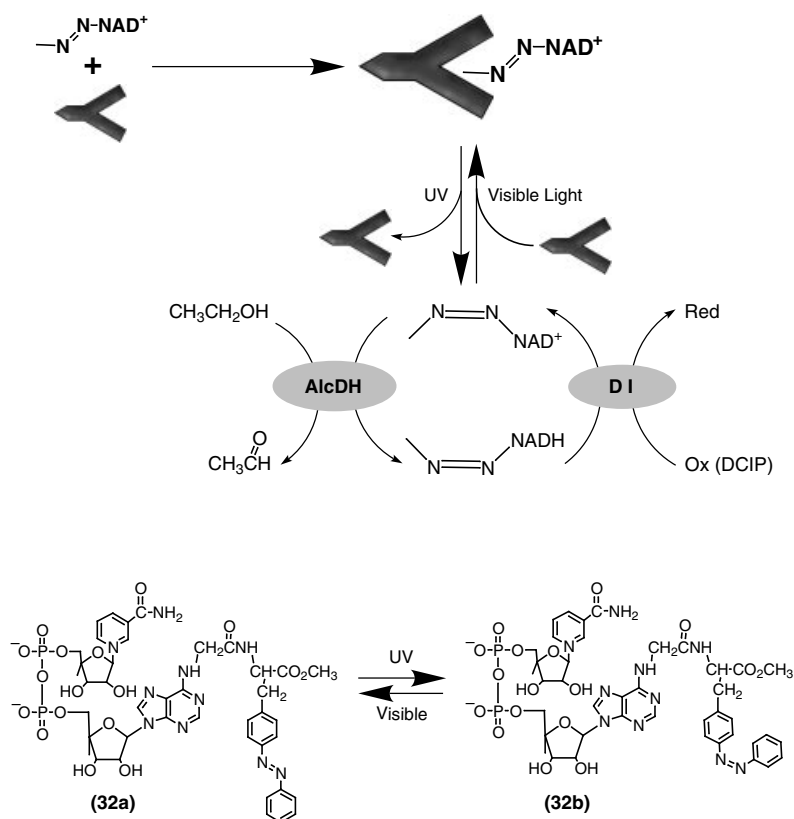


Fig. 16: (A) Cyclic voltammograms of: (a) the dinitrospiropyran-tethered GOx monolayer electrode, (b) the protonated dinitromerocyanine-tethered GOx monolayer electrode, (c) the dinitrospiropyran-tethered GOx monolayer electrode in the presence of the anti-DNP-Ab. Data were recorded in the presence of ferrocenecarboxylic acid (4×10^{-4} M) as a diffusional electron mediator and glucose

(5×10^{-2} M), scan rate $2 \text{ mV} \cdot \text{s}^{-1}$. (B) Biphasic switchable amperometric transduction of photonic signals recorded by the photoisomerizable GOx/DNP-Ab system. (■) The electrode in the dinitrospiropyran-GOx state. (●) The electrode in the protonated-dinitromerocyanine-state. (▲) The electrode in the presence of the dinitrospiropyran-GOx monolayer with associated DNP-Ab.

of the enzyme-layered electrode. Interaction of the switched on dinitrospiropyran-functionalized GOx monolayer electrode with the DNP-Ab resulted in the association of the antibody with the antigen sites. Binding of the antibody to the interface blocked electrical contact between the redox enzyme and the conductive support through the diffusional electron mediator. This prohibited the bioelectrocatalyzed oxidation of glucose by the enzyme-layered electrode, and the amperometric

response of the system was fully switched off (Figure 16(A), curve (c)). Photoisomerization of the composite monolayer electrode (consisting of the dinitrospiropyran-GOx/DNP-Ab complex array) to its protonated dinitromerocyanine state yielded a photoisomer state that lacked antigen features for the DNP-Ab. This resulted in the dissociation of the antibody from the interface. The resulting protonated dinitromerocyanine-functionalized GOx monolayer electrode exhibited partially switched on bioelectrocatalytic functions. Alternatively, the DNP-Ab could be washed off from the system, and the protonated dinitromerocyanine GOx electrode photoisomerized ($\lambda > 475$ nm) to the dinitrospiropyran state. This regenerated the switched on bioelectrocatalytic functions of the light-active enzyme electrode. Thus, photochemical isomerization of the GOx-layered electrode between the dinitrospiropyran and the protonated dinitromerocyanine states, and the coupling of the interface with the DNP-Ab allowed the bioelectrocatalytic functions of the electrode to be cycled between three states: “ON”, “partial ON”, and “OFF”, respectively (Figure 16(B)).



Scheme 17: Reversible photostimulation of alcohol dehydrogenase (AlcDH) by the application of the photoisomerizable azobenzene-modified NAD⁺ (32a) in the presence of the Z1HO1 monoclonal antibody. Disphorase (DI) is used to regenerate the oxidized cofactor.

Photochemical control over the biocatalytic functions of an enzyme has been accomplished by conjugation of a photoisomerizable antigen-modified cofactor and its respective antibody as a gate assembly for enzyme activation/deactivation.^[75] The monoclonal antibody to *trans*-azobenzene (cf. Section 6.1.1) was used to control the bioelectrocatalytic functions of the NAD⁺-dependent enzyme alcohol dehydrogenase, AlcDH (Scheme 17). The *trans*-azobenzene-modified NAD⁺-cofactor (**32a**) exhibits reversible photoisomerizable properties, and underwent photoisomerization ($\lambda = 320$ nm) to the *cis*-azobenzene-NAD⁺-cofactor (**32b**). The latter *cis* isomer was isomerized back to **32a** by visible light irradiation ($\lambda > 400$ nm). In the presence of the *trans*-azobenzene-NAD⁺-cofactor (**32a**) and the respective monoclonal antibody, formation of the antigen–antibody complex resulted in the expulsion of the diffusional cofactor, and the biocatalytic functions of the AlcDH enzyme were switched off. Photochemical isomerization of the *trans*-azobenzene-NAD⁺-cofactor (**32a**) to the *cis*-azobenzene-NAD⁺-cofactor (**32b**) released the cofactor from the antibody. The free cofactor was reduced by ethanol in the presence of AlcDH, and the resulting NADH was oxidized by 2,6-dichlorophenol-indophenol (DCIP) in the presence of diaphorase (DI). This process regenerated the cofactor, and as long as the cofactor existed in the *cis*-azobenzene configuration, biocatalyzed oxidation of ethanol took place. Photoisomerization of the cofactor to the **32a** state resulted in the formation of the *trans*-azobenzene-NAD⁺/antibody complex and the inhibition of the cofactor-driven transformation. This indirect approach to gating and photomodulating enzyme activities through the coupling of a photoisomerizable cofactor and antibody seems to be a general method for designing photoswitchable biomaterials. That is, tailoring of photoisomerizable antigen-functionalized inhibitors, coenzymes, or activating proteins, and coupling them with their respective antibodies in biocatalytic systems, provides a general route to bind or release the enzyme-triggering components.

6.5

Applications of Photoswitchable Biomaterials

The development of photoswitchable biomaterials is at the level of basic research, and the possible practical applications of photobiological switches are a matter of vision and imagination. As the fundamental concept of light-controlled activation and deactivation of biological functions is established, the broad applicability of such systems in various disciplines is possible. In fact, the native bacteriorhodopsin system, and its bioengineered mutants, represent optical “write and erase” systems.^[76] Indeed, various optical applications,^[77] such as holographic pattern recording,^[78] dynamic optical filtering,^[79] and associative optical memory,^[80] have been developed using the bacteriorhodopsin photosensor system. The utilization of the native system as a biocomputer and information storage device has been extensively discussed in the literature.^[81] This chapter addresses, however, photosensory biomaterial assemblies exhibiting greater complexity and, hence, increased potential applicabilities:

- 1) Photoswitchable activation of enzymes provides a means to trigger a biocatalytic transformation “ON” and “OFF”. This feature shows two important functions:
 - The biocatalytic transformation generates a product, and hence the light-triggered formation or inhibition of the respective product may be tailored.
 - The biocatalytic transformation and the enzyme turnover provides a means to amplify the light-triggered process.
- 2) The concept of photoswitchable biomaterial can be extended to different biological functions, such as cofactors, inhibitors, enzymes, receptors, hormones, antigens/antibodies, DNA, etc. This opens a broad spectrum of applications in different biomaterial science disciplines.
- 3) The integration of photoswitchable biomaterials with solid supports, and specifically with electronic transducers, is of particular interest. It enables electronic transduction of photoswitchable biological functions through integrated biomaterial-transducer assemblies. Moreover, photoswitchable activation of redox enzymes on electrode supports permits amplified amperometric transduction of photonic signals that trigger the biological functions.

Table 2 summarizes different possible applications of photoswitchable biomaterials, while detailing the nature of the biomaterial, the area of application, and, when possible, specific examples. Reversible light-induced activation and deactivation of redox proteins (enzymes) corresponds to “write”-“read”-“erase” functions. The photonic activation of the biomaterial corresponds to the “write” function, whereas the amperometric transduction of the recorded optical information represents the “read” function of the systems. Switching off of the redox functions of the proteins erases the stored photonic information and regenerates the photosensory biomaterial. These integrated, photoswitchable redox enzyme electrode assemblies mimic logic functions of computers, and may be considered as first step into the era of biocomputers.

Photonic activation of redox enzymes results in the light-induced bioelectrocatalytic activation of an enzyme cascade. This permits application of photoswitchable enzymes as amplifiers of weak photonic signals. Alternatively, sensitive actinometers, measuring low irradiation doses, might be envisaged.

Redox enzymes are the active component in many electrochemical enzyme electrode biosensor devices.^[82] The integration of two different redox enzymes with an electrode support, in which one of the biocatalysts is photoswitchable between “ON” and “OFF” states, can establish a composite multisensor array. The biomaterial interface that includes the photoswitchable enzyme in the “OFF” state electrochemically transduces the sensing event of the substrate corresponding to the nonphotoswitchable enzyme. Photochemical activation of the light-active enzyme leads to the full electrochemical response, corresponding to the analysis of the substrates of the two enzymes. As a result, the processing of the signals transduced by the composite biomaterial interface in the presence of the two substrates permits the assay of the

Tab. 2: Areas for the Application of Biomaterial Photoswitches

Photoswitchable Biomaterial	Area of Application	System Configuration
Photoswitchable redox-enzymes	<ol style="list-style-type: none"> 1. Amperometric transduction of optical information – biocomputers 2. Amplification of weak optical signals – photonic amplifiers 3. Multisensor arrays – biosensor and bioelectronics 4. Photoelectrochemical systems 	Enzyme immobilized on electronic transducer
Photoswitchable enzymes – light-triggered biotransformations	<ol style="list-style-type: none"> 1. Localized activation of therapeutic enzymes or proteins (e.g. blood clotting) 2. Light-controlled biotechnological processes (light-mediated sensoric/processing and feedback biotransformation) 	Enzyme solubilized in solution or immobilized on inert polymers or conductive supports
Photoswitchable antigen/antibody (substrate/receptor) complexes	<ol style="list-style-type: none"> 1. Reversible immunosensors 2. Patterning of surfaces with biomaterials using antigen/antibody-biomaterial conjugates (Design of biosensor arrays, biochips) 	1. Immobilization of systems on electronic transducers (electrodes, piezoelectric crystals, FET) or the assembly of biomaterials on inert supports by non-covalent interactions (e.g. glass, polymers)
Photoswitchable substrate–protein/cofactor– enzyme/antigen–antibody interactions	Light-stimulated affinity chromatography	Immobilization of photoactive separation component on solid matrices

individual analytes. Furthermore the organization of several photoswitchable biomaterials in which the photoactive units undergo isomerization at different wavelengths might lead, through sequential wavelength-controlled activation of the different enzymes, to multisensor arrays for different substrates.

Photoswitchable enzymes might find important applications in the preparation of targeted therapeutic materials. Enzymes and proteins have wide therapeutic uses, but often their nonlocalized activities are harmful and prevent their medical use. For example, thrombin is an important factor in inducing blood clotting in individuals affected by hemophilia. Nontargeted blood clotting could lead, however, to thrombosis, with fatal consequences. Light-regulated blood clotting in injured locations might be an elegant approach for using photoswitchable enzymes in medicinal chemistry.

Photoswitchable enzymes could have an important role in controlling biochemical transformations in bioreactors. Various biotechnological processes generate an inhibitor, or alter the environmental conditions (pH, for example) of the reaction medium. Photochemical activation of enzymes that adjust environmental conditions or deplete the inhibitor to a low concentration may maintain the bioreactor at optimal performance. More specifically, integration of the photoswitchable biocatalytic matrix with a sensory electrode might yield a feedback mechanism in which the sensor element triggers the light-induced activation/deactivation of the photosensitive biocatalyst.

The use of photoisomerizable antigens as active components for tailoring reversible immunosensors has been extensively discussed (cf. Section 6.3). Photoswitchable binding interactions between photoisomerizable antigens and antibodies can be used for patterning of surfaces with biomaterials.^[83] The patterning of surfaces with addressable biomaterial domains is important for developing biochips and biosensor arrays.^[84,85] The patterning of antibodies on surfaces is demonstrated in Scheme 18. A dinitrospiropyran antigen layer is assembled on a glass support and irradiated with UV light ($320 \text{ nm} < \lambda < 360 \text{ nm}$) through a mask. Areas exposed to the light are isomerized into the protonated dinitromerocyanine state, lacking affi-

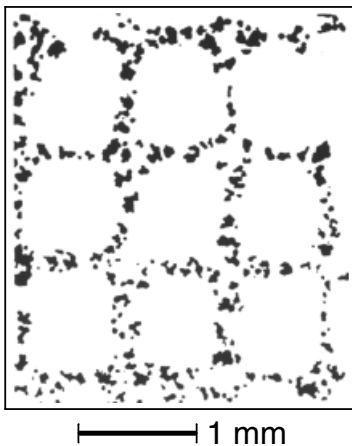
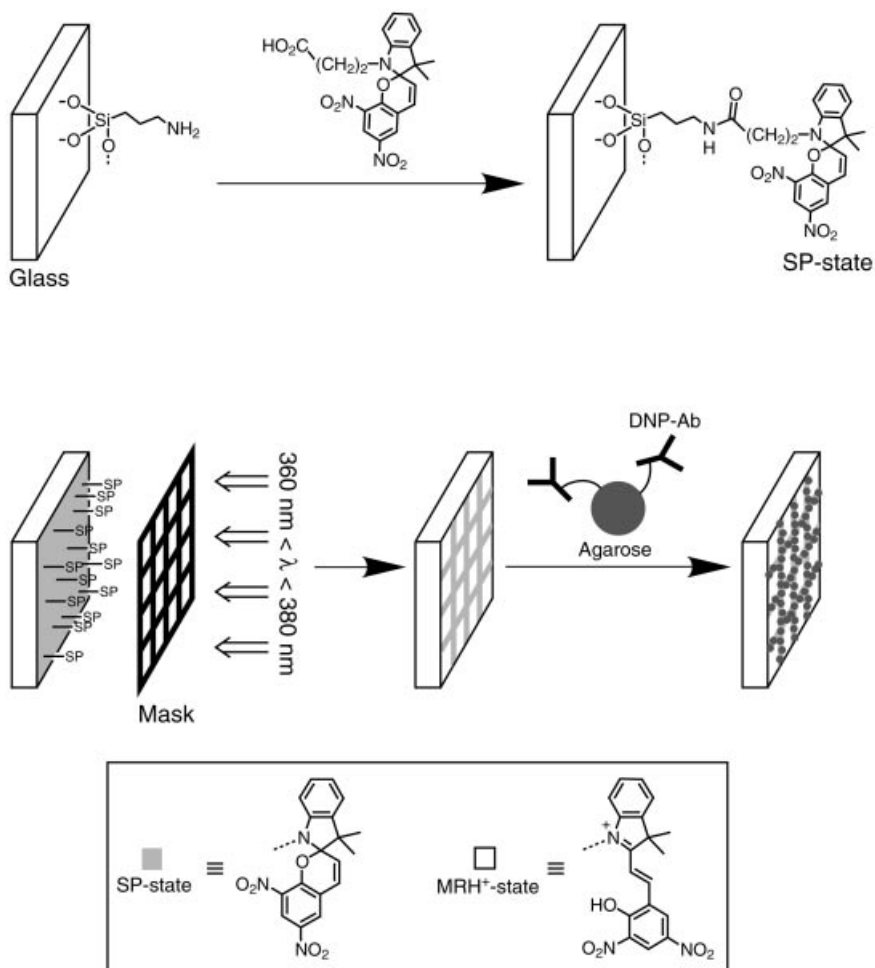


Fig. 17: Pattern of DNP-Ab-functionalized agarose beads on a glass support functionalized with a dinitrospiropyran photoisomerizable layer.



Scheme 18: Photochemical patterning of a photoisomerizable dinitrospiropyran monolayer associated with a glass support with agarose beads functionalized with DNP-Ab.

nity for the dinitrophenyl antibody DNP-Ab. Interaction of the photopatterned interface with DNP-Ab results in the selective association of the antibody with the dinitrospiropyran antigen domains. Figure 17 shows the pattern of DNP-Ab on a glass support. The dinitrospiropyran layer was irradiated through a grid acting as a mask. The resulting photopatterned surface was treated with agarose beads (50 μm) functionalized with the DNP-Ab. Figure 17 shows the self-organization of the DNP-Ab-functionalized beads on the photopatterned surface. This patterning process can be extended to yield any biomaterial structure on the surface. By application of DNP-biomaterial conjugates, one might use the DNP-Ab as a directing arrow leading the different biomaterials to light-activated addressable antigen domains. Alternatively,

using the anti-antibody/biomaterial conjugate, the biomaterial might be targeted to a pre-organized DNP-pattern.

Finally, photoswitchable binding interactions between photoisomerizable substrates and their receptors – photoisomerizable antigens and their antibodies or photoisomerizable inhibitors and the respective proteins, for example – could provide a general means to design novel chromatographic separation methods. Affinity chromatography provides a general route for the separation of biomaterials through biorecognition interactions. Complementary affinity interactions between enzyme-substrate, antigen-antibody, hormone-receptor, and other recognition pairs on solid supports permits the separation of the biomaterial from other biological ingredients. The dissociation of the ligated biomaterial from the separation matrix is often accompanied by difficulties arising from the high affinity binding interaction between the ligand and the complementary biomaterial. The application of photoisomerizable ligand-functionalized supports allows tailoring of separation matrices in which binding and dissociation events can be controlled by external light stimuli. That is, photoisomerization of the ligand to a state of low affinity for the substrate could permit its elution from the separation matrix, while subsequent photoisomerization of the ligand to the complementary state would regenerate the separation matrix by generation of the ligand with high affinity for the biomaterial.

6.6

Conclusions and Future Perspectives

This chapter addresses recent scientific accomplishments in the rapidly developing area of photoswitchable biomaterials and optobioelectronics. We have addressed different methodologies for tailoring photoswitchable functions such as recognition, catalysis or transport functions. We have also reviewed the different scientific approaches to integrating photoswitchable biomaterials with electronic transducers, and have discussed means for the electronic transduction of photoswitchable biological events on the respective transducers. Specifically, the application of these systems as information storage assemblies, photonic signal amplifiers, and sensory devices has been addressed. The recording of photonic signals through photoswitchable biomaterial (photosensor), and the amplified electronic transduction of the recorded optical information, duplicates certain functions of the vision process. One might envisage broad applications of such “synthetic biomaterial-based eyes” in robotics, micromachinery, or prosthetic uses.

Science is entering into the nanoscale world, and the organization of microscale or nanoscale biomaterial structures on surfaces has been demonstrated and is a subject of extensive research effort.^[84,85] Single biomaterial molecules have been imaged on surfaces,^[86,87] and the individual affinity interactions of biomaterials probed at the molecular level.^[88,89] While the different scanning microscopy techniques provide useful means to image and manipulate biomaterials on surfaces, the use of the near-field scanning optical microscope (NSOM)^[90] in the activation of photoswitchable biomaterials on surfaces should be emphasized specifically. One

could use this nanoscale light source as a tool for the photonic activation of biomaterials on surfaces. Clearly, this could lead to dense storage of photonic information, or, alternatively, could provide a means to engineer addressable nanoscale sensing domains (nanobiochips). Photoswitchable biomaterials are certainly expected to offer exciting new perspectives at the frontiers of chemistry, biology, physics, medicine, and material science.

Acknowledgments

Special gratitude is expressed to the students and research associates who participated in this research project. Their names appear in the reference list. Their skill and enthusiasm turned fundamental thoughts into a mature research field. Parts of the research were supported by The Israel Science Foundation.

References

- 1 (a) I. Willner, S. Rubín, *Angew. Chem. Int. Ed. Engl.* **1996**, *35*, 367–385. (b) I. Willner, B. Willner in *Biological Applications of Photochemical Switches, Bioorganic Photochemistry*, Vol. 2 (Ed.: H. Morrison), Wiley, New York, **1993** pp. 1–110.
- 2 I. Willner, *Acc. Chem. Res.* **1997**, *30*, 347–356.
- 3 (a) A.M. Gurney, H.A. Lester, *Physiol. Rev.* **1987**, *67*, 583–617. (b) A.P. Somlyo, A.V. Somlyo, *Ann. Rev. Physiol.* **1990**, *52*, 857–874. (c) I. Parker, in *Neuromethods*, Vol. 20, Intracellular Messengers, (Eds.: A. Boulton, G. Baker, C. Taylor) Humana Press, Totowa, N.J. **1992**, pp. 369–396.
- 4 (a) H.A. Lester, J.M. Nerbonne, *Ann. Rev. Biophys. Bioeng.* **1982**, *11*, 151–175. (b) S.R. Adams, R.Y. Tsien, *Annu. Rev. Physiol.* **1993**, *55*, 755–783. (c) J.A. McCray, D.R. Trentham, *Annu. Rev. Biophys. Biophys. Chem.* **1989**, *18*, 239–270.
- 5 (a) A.D. Turner, S.V. Pizzo, G.W. Rozakis, N.A. Porter, *J. Am. Chem. Soc.* **1988**, *110*, 244–250. (b) N.A. Porter, J.D. Bruhnke, *Photochem. Photobiol.* **1990**, *51*, 37–43.
- 6 (a) P.M. Koenigs, B.C. Faust, N.A. Porter, *J. Am. Chem. Soc.* **1993**, *115*, 9371–9379. (b) N.A. Porter, J.D. Bruhnke, P. Koenigs, in *Biological Applications of Photochemical Switches, Bioorganic Photochemistry Series*, Vol. 2, (Ed.: H. Morrison) Wiley, New York, **1993**, pp. 197–241.
- 7 (a) S.R. Adams, J.P.Y. Kao, R.Y. Tsien, *J. Am. Chem. Soc.* **1989**, *111*, 7957–7968. (b) G.C.R. Ellis-Davies, J.H. Kaplan, *J. Org. Chem.* **1988**, *53*, 1966–1969.
- 8 R. Warmuth, E. Grell, J.-M. Lehn, J.W. Bats, G. Quinkert, *Helv. Chim. Acta* **1991**, *74*, 671–681.
- 9 J. Nargeot, J.M. Nerbonne, J. Engels, H.A. Lester, *Proc. Natl. Acad. Sci. USA* **1983**, *80*, 2395–2399.
- 10 J.M. Nerbonne, S. Richard, J. Nargeot, H.A. Lester, *Nature* **1984**, *310*, 74–76.
- 11 (a) J.H. Kaplan, R.J. Hollis, *Nature* **1980**, *288*, 587–589. (b) J.W. Walker, G.P. Reid, J.A. McCray, D.R. Trentham, *J. Am. Chem. Soc.* **1988**, *110*, 7170–7177.
- 12 J.W. Walker, A.V. Somlyo, Y.E. Goldman, A.P. Somlyo, D.R. Trentham, *Nature* **1987**, *327*, 249–252.
- 13 (a) L. Fabbrizzi, A. Poggi, *Chem. Soc. Rev.* **1995**, *24*, 197–202. (b) R.A. Bissel, A.P. DeSilva, H.Q.N. Gunarante, P.L.M. Lynch, G.E.M. Maguire, C.P. McCoy, K.R.A.S. Sandanayake, *Top. Curr. Chem.* **1993**, *168*, 223–264.
- 14 (a) I. Willner, B. Willner, *J. Mater. Chem.* **1998**, *8*, 2543–2556. (b) I. Willner, B. Willner, *Adv. Mater.* **1997**, *9*, 351–355.
- 15 (a) O. Pieroni, F. Ciardelli, *Trends Polym. Sci.* **1995**, *3*, 282–287. (b) O. Pieroni, A. Fissi, G. Popova, *Prog. Polym. Sci.*, Vol. 23 **1998**, 81–123.
- 16 (a) M. Irie, *Adv. Polym. Sci.* **1990**, *94*, 27–67. (b) M. Irie in *Applied Photochromic Polymer Systems* (Ed.: C.B. McArdle) Chapman & Hall, New York, **1992**, p. 174–206.
- 17 (a) H. Rau, *Angew. Chem., Int. Ed. Engl.* **1973**, *12*, 224–235. (b) H. Rau in *Photochromism: Molecules and Systems* (Eds.: H. Dürr, H. Bouas-Laurent) Elsevier, Amsterdam, **1990**, pp. 165–191.
- 18 R. Guglielmetti in *Photochromism: Molecules and Systems* (Eds.: H. Dürr, H. Bouas-Laurent) Elsevier, Amsterdam, **1990**, p. 314–466.
- 19 J. Whittall in *Photochromism: Molecules and Systems* (Eds.: H. Dürr, H. Bouas-Laurent) Elsevier, Amsterdam, **1990**, p. 467–492.
- 20 J. Anzai, K. Sakamura, T. Osa, *J. Chem. Soc., Chem. Commun.* **1992**, 888–889.
- 21 G.S. Kumar, D.C. Neckers, *Chem. Rev.* **1989**, *89*, 1915–1925.
- 22 (a) T. Seki, K. Tanaka, K. Ichimura, *Macromolecules* **1997**, *30*, 6401–6403. (b) T. Seki, K. Fukuda, K. Ichimura, *Langmuir* **1999**, *15*, 5098–5101. (c) H. Menzel, B. Weichart, A. Schmidt, S. Paul, W. Knoll, J. Stumpe, T. Fischer, *Langmuir* **1994**, *10*, 1926–1933.
- 23 (a) I. Willner, A. Doron, E. Katz, *J. Phys. Org. Chem.* **1998**, *11*, 546–560. (b) H. Menzel, *Macromol. Chem. Phys.* **1994**, *195*, 3747–3757. (c) H. Menzel, M.L. Hallensleben, A. Schmidt, W. Knoll, T. Fischer, J. Stumpe, *Macromolecules* **1993**, *26*, 3644–3649.
- 24 T. Sato, M. Kijima, M. Shiga, Y. Yonezawa, *Langmuir* **1991**, *7*, 2330–2335.
- 25 K. Ishihara, A. Okazaki, N. Negishi, I. Shinohara, T. Okano, K. Kataoka, Y. Sakurai, *J. Appl. Polym. Sci.* **1982**, *27*, 239–245.
- 26 A. Mamada, T. Tanaka, D. Kungwachakun, M. Irie, *Macromolecules* **1990**, *23*, 1517–1519.

- 27 M. Irie, K. Hayashi, *J. Macromol. Sci. Chem.* **1979**, *413*, 511.
- 28 I. Willner, S. Sussan, S. Rubin, *J. Chem. Soc., Chem. Commun.* **1992**, 100–101.
- 29 I. Willner, S. Rubin, J. Wonner, E. Effenberger, P. Bäuerle, *J. Am. Chem. Soc.* **1992**, *114*, 3150–3151.
- 30 E. Zahavy, S. Rubin, I. Willner, *Mol. Cryst. Liq. Cryst.* **1994**, *246*, 195–199.
- 31 I. Willner, S. Rubin, Y. Cohen, *J. Am. Chem. Soc.* **1993**, *115*, 4937–4938.
- 32 E. Zahavy, S. Rubin, I. Willner, *J. Chem. Soc., Chem. Commun.* **1993**, 1753–1755.
- 33 M. Harada, M. Sisido, J. Hirose, M. Nakanishi, *FEBS Lett.* **1991**, *285*, 6–8.
- 34 (a) M. Aizawa, K. Namba, S. Suzuki, *Arch. Biochem. Biophys.* **1977**, *182*, 305–310. (b) S. Monti, G. Montagnoli, L. Nannicini, *J. Am. Chem. Soc.* **1977**, *99*, 3808–3811.
- 35 (a) I. Willner, S. Rubin, A. Riklin, *J. Am. Chem. Soc.* **1991**, *113*, 3321–3325. (b) I. Willner, M. Lion-Dagan, S. Rubin, J. Wonner, F. Effenberger, P. Bäuerle, *Photochem. Photobiol.* **1994**, *59*, 491–496.
- 36 T. Ueda, K. Murayama, T. Yamamoto, S. Kimura, Y. Imanishi, *J. Chem. Soc., Perkin Trans. 1* **1994**, 225–230.
- 37 (a) T. Seki, M. Sakuragi, Y. Kawanishi, Y. Suzuki, T. Tamaki, R. Fukuda, K. Ichimura, *Langmuir* **1993**, *9*, 211–218. (b) K. Aoki, T. Seki, Y. Suzuki, T. Tamaki, A. Hosoki, K. Ichimura, *Langmuir* **1992**, *8*, 1007–1013.
- 38 (a) A. Suzuki, T. Tanaka, *Nature* **1990**, *346*, 345–347. (b) T. Amiya, T. Tanaka, *Macromolecules* **1987**, *20*, 1162–1164.
- 39 F. Ciardelli, D. Fabbri, O. Pieroni, A. Fissi, *J. Am. Chem. Soc.* **1989**, *111*, 3470–3472.
- 40 O. Pieroni, A. Fissi, A. Viegi, D. Fabbri, F. Ciardelli, *J. Am. Chem. Soc.* **1992**, *114*, 2734–2736.
- 41 O. Pieroni, J.L. Houben, A. Fissi, P. Costantino, F. Ciardelli, *J. Am. Chem. Soc.* **1980**, *102*, 5913–5915.
- 42 J.L. Houben, A. Fissi, D. Baccida, N. Rosato, O. Pieroni, F. Ciardelli, *Int. J. Biol. Macromol.* **1983**, *5*, 94–100.
- 43 L. Ulysse, J. Cubillos, J. Chmielewski, *J. Am. Chem. Soc.* **1995**, *117*, 8466–8467.
- 44 B.R. Malcolm, O. Pieroni, *Biopolymers* **1990**, *29*, 1121–1123.
- 45 M. Higuchi, N. Minoura, T. Kinoshita, *Colloid Polym. Sci.* **1995**, *273*, 1022–1027.
- 46 (a) I. Karube, Y. Nakamoto, K. Namba, S. Suzuki, *Biochim. Biophys. Acta* **1976**, *429*, 975–981. (b) Y. Hasebe, J.-I. Anzai, A. Ueno, T. Osa, *J. Phys. Org. Chem.* **1988**, *1*, 309–315.
- 47 (a) I. Willner, S. Rubin, T. Zor, *J. Am. Chem. Soc.* **1991**, *113*, 4013–4014. (b) I. Willner, S. Rubin, R. Shatzmiller, T. Zor, *J. Am. Chem. Soc.* **1993**, *115*, 8690–8694.
- 48 I. Willner, S. Rubin, *React. Polym.* **1993**, *21*, 177–186.
- 49 I. Willner, E. Katz, B. Willner, R. Blonder, V. Heleg-Shabtai, A.F. Bückmann, *Biosens. Bioelectron.* **1997**, *12*, 337–356.
- 50 (a) M. Lion-Dagan, E. Katz, I. Willner, *J. Am. Chem. Soc.* **1994**, *116*, 7913–7914. (b) I. Willner, M. Lion-Dagan, S. Marx-Tibbon, E. Katz, *J. Am. Chem. Soc.* **1995**, *117*, 6581–6592.
- 51 I. Willner, R. Blonder, E. Katz, A. Stocker, A.F. Bückmann, *J. Am. Chem. Soc.* **1996**, *118*, 5310–5311.
- 52 R. Blonder, E. Katz, I. Willner, V. Wray, A.F. Bückmann, *J. Am. Chem. Soc.* **1997**, *119*, 11747–11757.
- 53 M. Lion-Dagan, E. Katz, I. Willner, *J. Chem. Soc., Chem. Commun.* **1994**, 2741–2742.
- 54 I. Willner, A. Doron, E. Katz, S. Levi, A.J. Frank, *Langmuir* **1996**, *12*, 946–954.
- 55 (a) F.A. Armstrong, H.A.O. Hill, N.J. Walton, *Q. Rev. Biophys.* **1985**, *18*, 261–322. (b) P.M. Allen, H.A.O. Hill, N.J. Walton, *J. Electroanal. Chem.* **1984**, *178*, 69–86.
- 56 F.A. Armstrong, H.A.O. Hill, N.J. Walton, *Acc. Chem. Res.* **1988**, *21*, 407–413.
- 57 M.J. Tarlov, E.F. Bowden, *J. Am. Chem. Soc.* **1991**, *113*, 1847–1849.
- 58 R. Blonder, I. Willner, A.F. Bückmann, *J. Am. Chem. Soc.* **1998**, *120*, 9335–9341.
- 59 P. Skladal, *Electroanalysis* **1997**, *9*, 737–745.
- 60 A.L. Ghindilis, P. Atanasov, M. Wilkins, E. Wilkins, *Biosens. Bioelectron.* **1998**, *13*, 113–131.
- 61 (a) A.L. Ghindilis, O.V. Skorobogat'ko, V.P. Gavrilova, A.I. Yaropolov, *Biosens. Bioelectron.* **1992**, *7*, 301–304. (b) U. Pfeifer, W. Baumann, *Fresenius J. Anal. Chem.* **1993**, *345*, 504–511.
- 62 (a) L. Engel, W. Baumann, *Fresenius J. Anal. Chem.* **1993**, *346*, 745–751. (b) L. Engel, W. Baumann, *Fresenius J. Anal. Chem.* **1993**, *349*, 447–450.
- 63 (a) W.O. Ho, D. Athey, C.J. McNeil, *Biosens. Bioelectron.* **1995**, *10*, 683–691. (b) L.X. Tiefenauer, S. Kossek, C. Padeste, P. Thiébaud, *Biosens. Bioelectron.* **1997**, *12*, 213–223.

- (c) D. Ivnitski, J. Rishpon, *Biosens. Bioelectron.* **1996**, *11*, 409–417. (d) G. Wittstock, H. Emons, W.R. Heineman, *Electroanalysis* **1996**, *8*, 143–146. (e) S. Zhang, K. Jiao, H. Chen, *Electroanalysis* **1999**, *11*, 511–516.
- 64** (a) R. Blonder, E. Katz, Y. Cohen, N. Itzhak, A. Riklin, I. Willner, *Anal. Chem.* **1996**, *68*, 3151–3157. (b) E. Katz, I. Willner, *J. Electroanal. Chem.* **1996**, *418*, 67–72. (c) H.T. Tang, C.E. Lunte, H.B. Halsall, W.R. Heineman, *Anal. Chim. Acta* **1988**, *214*, 187–195. (d) O. Niwa, Y. Xu, H.B. Halsall, W.R. Heineman, *Anal. Chem.* **1993**, *65*, 1559–1563. (e) N. Kaneki, Y. Xu, A. Kumari, H.B. Halsall, W.R. Heineman, P.T. Kissinger, *Anal. Chim. Acta* **1994**, *287*, 253–258.
- 65** (a) M.S. DeSilva, Y. Zhang, P.J. Hesketh, G.J. Maclay, S.M. Gendel, J.R. Stetter, *Biosens. Bioelectron.* **1995**, *10*, 675–682. (b) H. Maupas, A.P. Soldatkin, C. Martelet, N. Jaffrezic-Renault, B. Mandrand, *J. Electroanal. Chem.* **1997**, *421*, 165–171.
- 66** (a) I. Ben-Dov, I. Willner, E. Zisman, *Anal. Chem.* **1997**, *69*, 3506–3512. (b) A.A. Suleiman, G.G. Guilbault, *Anal. Lett.* **1991**, *24*, 1283–1292. (c) A.A. Suleiman, G.G. Guilbault, *Analyst* **1994**, *119*, 2279–2282.
- 67** (a) B. König, M. Grätzel, *Anal. Chim. Acta* **1993**, *276*, 323–333. (b) B. König, M. Grätzel, *Anal. Chim. Acta* **1993**, *280*, 37–41. (c) B. König, M. Grätzel, *Anal. Chim. Acta* **1993**, *281*, 13–18. (d) B. König, M. Grätzel, *Anal. Chim. Acta* **1995**, *309*, 19–25.
- 68** (a) B. Liedberg, C. Nylander, I. Lundström, *Biosens. Bioelectron.* **1995**, *10*, R1-R9. (b) S. Sasaki, R. Nagata, B. Hock, I. Karube, *Anal. Chim. Acta* **1998**, *368*, 71–76.
- 69** (a) L.C. Gruen, J.L. McKimm-Breschkin, J.B. Coldwell, E.C. Nice, *J. Immunol. Methods* **1994**, *168*, 91–100. (b) G. Zeder-Lutz, D. Altschuh, H.M. Geysen, E. Trifilieff, G. Sommermeyer, M.H.V. Van Regenmortel, *Molec. Immunol.* **1993**, *30*, 145–155.
- 70** (a) I. Willner, R. Blonder, A. Dagan, *J. Am. Chem. Soc.* **1994**, *116*, 9365–9366. (b) I. Willner, B. Willner, *Biotechnology Progress* **1999**, *15*, 991–1002.
- 71** R. Blonder, S. Levi, G. Tao, I. Ben-Dov, I. Willner, *J. Am. Chem. Soc.* **1997**, *119*, 10467–10478.
- 72** F. Patolsky, B. Filanovsky, E. Katz, I. Willner, *J. Phys. Chem. B* **1998**, *102*, 10359–10367.
- 73** E. Kaganer, R. Pogreb, D. Davidov, I. Willner, *Langmuir* **1999**, *15*, 3920–3923.
- 74** I. Willner, M. Lion-Dagan, E. Katz, *Chem. Commun.* **1996**, 623–624.
- 75** T. Hohsaka, K. Kawashima, M. Sisido, *J. Am. Chem. Soc.* **1994**, *116*, 413–414.
- 76** N. Hampp, C. Bräuchle, D. Oesterhelt, *Biophys. J.* **1990**, *58*, 83–93.
- 77** *Optical Processing and Computing* (Eds.: H.H. Arsenault, T. Szoplik, B. Macukow) Academic Press, New York, **1989**.
- 78** N. Hampp and C. Bräuchle in *Photochromism: Molecules and Systems* (Eds.: H. Dürr, H. Bouas-Laurent) Elsevier, Amsterdam, **1990**, p. 954–975.
- 79** R. Thoma, N. Hampp, C. Bräuchle, D. Oesterhelt, *Opt. Lett.* **1991**, *16*, 651–653.
- 80** A. Yariv, S.K. Kwong, *Opt. Lett.* **1986**, *11*, 186–188.
- 81** (a) R.R. Birge, *Annu. Rev. Phys. Chem.* **1990**, *41*, 683–733. (b) R.R. Birge, *Am. Sci.* **1994**, *82*, 348–355.
- 82** (a) I. Willner, E. Katz, B. Willner, *Electroanalysis* **1997**, *9*, 965–977. (b) I. Willner, E. Katz, *Angew. Chem. Int. Ed.* **2000**, *39*, 1180–1218.
- 83** I. Willner, R. Blonder, *Thin Solid Films* **1995**, *266*, 254–257.
- 84** (a) L.F. Rozsnyai, D.R. Benson, S.P.A. Fodor, P.G. Schultz, *Angew. Chem., Int. Ed. Engl.* **1992**, *31*, 759–761. (b) A.S. Blawas, T.F. Oliver, M.C. Pirrung, W.M. Reichert, *Langmuir* **1998**, *14*, 4243–4250. (c) B.D. Martin, B.P. Gaber, C.H. Patterson, D.C. Turner, *Langmuir*, **1998**, *14*, 3971–3875.
- 85** (a) A. Schwarz, J.S. Rossier, E. Roulet, N. Mermod, M.A. Roberts, H.H. Girault, *Langmuir* **1998**, *14*, 5526–5531. (b) N. Dontha, W.B. Nowall, W.G. Kuhr, *Anal. Chem.* **1997**, *69*, 2619–2625. (c) A. Bernard, E. Delamarche, H. Schmid, B. Michel, H.R. Bosshard, H. Biebuyck, *Langmuir* **1998**, *14*, 2225–2229. (d) M. Mrksich, G.M. Whitesides, *ACS Sym. Ser.* **1997**, *680*, 361–373.
- 86** (a) M. Rief, M. Gautel, F. Oesterhelt, J.M. Fernandez, H.E. Gaub, *Science* **1997**, *276*, 1109–1112. (b) A.L. Weisenhorn, M. Egger, F. Ohuesorge, S.A.C. Gould, S.P. Heyn, H.G. Hansma, R.L. Sinsheimer, H.E. Gaub, P.K. Hansma, *Langmuir* **1991**, *7*, 8–12. (c) M. Rief, F. Oesterhelt, B. Heymann, H.E. Gaub, *Science* **1997**, *275*, 1295–1297.

- 87 (a) L.I. Pietrasanta, D. Thrower, W. Hsieh, S. Rao, O. Stemmann, J. Lechner, J. Carbon, H. Hansma, *Proc. Natl. Acad. Sci. U.S.A.* **1999**, *96*, 3757–3762. (b) M.B. Viani, T.E. Schaffer, G.T. Paloczi, L.I. Pietrasanta, B.L. Smith, J.B. Thompson, M. Richter, M. Rief, H.E. Gaub, K.W. Plaxco, A.N. Cleland, H.G. Hansma, P.K. Hansma, *Rev. Sci. Instrum.* **1999**, *70*, 4300–4303.
- 88 M. Ludwig, W. Dettmann, H.E. Gaub, *Biophysical J.* **1997**, *72*, 445–448.
- 89 H. Clausen-Schaumann, H.E. Gaub, *Langmuir* **1999**, *15*, 8246–8251.
- 90 (a) P.F. Barbara, D.M. Adams, D.B. O'Connor, *Annu. Rev. Mater. Sci.* **1999**, *29*, 433–450. (b) A. Shchemelinin, M. Rudman, K. Liebermann, A. Lewis, *Rev. Sci. Instr.* **1993**, *64*, 3538–3541. (c) R.C. Dunn, *Chem. Rev.* **1999**, *99*, 2891–2928.

7

Switchable Catenanes and Molecular Shuttles

Françisco M. Raymo and J. Fraser Stoddart

7.1

Introduction

Catenanes and rotaxanes are molecules composed of two or more mechanically interlocked components.^[1,2] In an $[n + 1]$ catenane (Figure 1a), $n + 1$ macrocycles interlock to form a molecular sized chain. In an $[n + 1]$ rotaxane (Figure 1b), n macrocycles encircle a single linear component terminated by bulky stoppers. In both instances, the components are held together by mechanical bonds which can be reinforced by intercomponent noncovalent bonding interactions. Because of the structural features associated with catenanes and rotaxanes, their syntheses posed quite a challenge for most of the twentieth century. Indeed, even though their preparation was discussed^[3] before 1912, the first catenanes^[4,5] and the first rotaxanes^[6,7] were only synthesized in the 1960s. These early procedures relied on either low yielding statistical approaches^[4,6] or on multistep directed covalent syntheses.^[5,7] With the advent of supramolecular chemistry,^[8] efficient template-directed syntheses^[9] of catenanes and rotaxanes have been developed,^[1,2] exploiting the ability of transition metals to coordinate with organic ligands and/or assistance from cooperative noncovalent bonding interactions. Indeed, catenanes and rotaxanes and their polymeric counterparts^[10] can nowadays be made in remarkably high yields, starting from relatively inexpensive materials.

The relative movements of the interlocked components of a $[2]$ catenane and of a $[2]$ rotaxane can be exploited^[11,12] to perform switching operations at the molecular level. Indeed, there are two states associated with a $[2]$ catenane (Figure 2a) incorporating two different units (0 and 1) in one of its two macrocyclic components. In *State 0*, the unit 0 is located inside the cavity of the other macrocyclic component and the unit 1 is positioned alongside. In *State 1*, the unit 1 is located 'inside' and

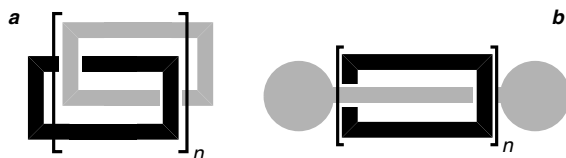


Fig. 1: Schematic representations of (a) an $[n + 1]$ catenane and (b) an $[n + 1]$ rotaxane.

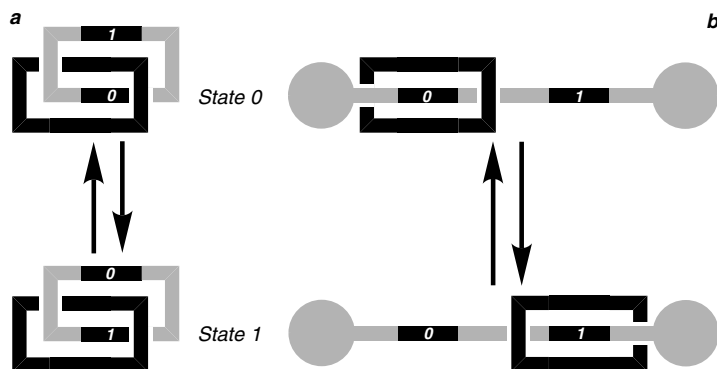


Fig. 2: Schematic representations of (a) a switchable [2]catenane and (b) a switchable [2]rotaxane.

the unit 0 'alongside'. Switching between *State 0* and *State 1* requires the circumrotation of the macrocyclic component incorporating the units 0 and 1 through the cavity of the other. Similarly, there are two states associated with a [2]rotaxane (Figure 2b) incorporating two units (0 and 1) in the dumbbell-shaped component. In *State 0*, the unit 0 is located inside the cavity of the macrocyclic component and the unit 1 is positioned alongside. In *State 1*, the unit 1 is located 'inside' and the unit 0 'alongside'. Switching between *State 0* and *State 1* requires the shuttling of the macrocyclic component along the linear portion of the dumbbell-shaped component. By employing chemically, electrochemically, and/or photochemically active groups as the units 0 and/or 1, the relative movements of the interlocked components of such [2]catenanes and [2]rotaxanes can be controlled from outside by means of chemical, electrochemical, and/or photochemical stimuli, respectively.

7.2

Catenanes and Rotaxanes Containing Transition Metals

The ability of transition metals to coordinate organic ligands has been exploited by Sauvage et al.^[13] for the synthesis of catenanes and rotaxanes for more than 15 years now. The template-directed synthesis of their 'first' [2]catenane^[14] is summarized in Figure 3. Upon mixing equimolar amounts of $\text{Cu}(\text{MeCN})_4\text{BF}_4$ and the phenanthroline-containing compounds 1 and 2 in solution, the complex $[\text{1:2}\cdot\text{Cu}]\cdot\text{BF}_4$ self-assembles^[14a,c] spontaneously. In this complex, the macrocycle 1 is threaded onto the linear component 2 and the Cu^+ ion coordinates the two phenanthroline ligands in a tetrahedral manner. Treatment of $[\text{1:2}\cdot\text{Cu}]\cdot\text{BF}_4$ with $\text{I}[(\text{CH}_2)_2\text{O}]_4(\text{CH}_2)_2\text{I}$ in the presence of Cs_2CO_3 gave the [2]catenane $[\text{3}\cdot\text{Cu}]\cdot\text{BF}_4$ in 42 % yield.^[14a,c] Treatment of this [2]catenane with KCN afforded^[14,15] the [2]catenand 3 quantitatively. Interestingly, the demetallation of $[\text{3}\cdot\text{Cu}]\cdot\text{BF}_4$ was accompanied (Figure 3) by a co-conformational^[16] change, as suggested^[14,15] by ^1H NMR spectroscopy and confirmed^[17] by X-ray crystallographic analyses of $[\text{3}\cdot\text{Cu}]\cdot\text{BF}_4$ and 3. Indeed, after demetallation, one macrocyclic component had circumrotated through the cavity of the other and

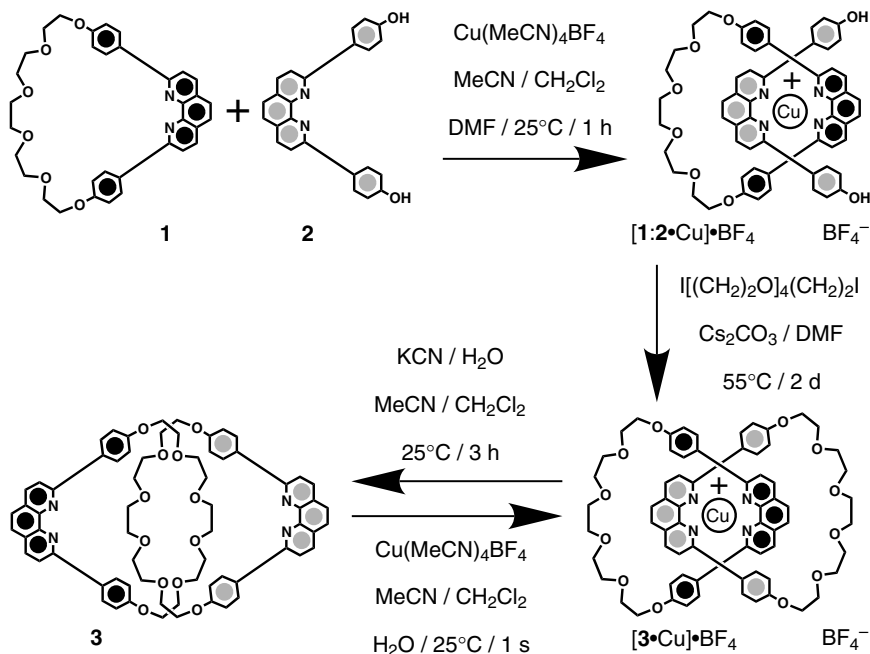


Fig. 3: The template-directed synthesis of the [2]catenane $[\mathbf{3}\cdot\text{Cu}]\cdot\text{BF}_4$ and its reversible demetallation.

vice versa, and in the [2]catenand **3** the two phenanthroline units were situated well away from each other. Complete rearrangement of the [2]catenand **3** occurred^[18] (Figure 3) upon addition of $\text{Cu}(\text{MeCN})_4\text{BF}_4$; the macrocyclic components circumrotated through each other's cavities to yield the [2]catenane $[\mathbf{3}\cdot\text{Cu}]\cdot\text{BF}_4$ once again. A similar result was observed^[19,20] upon metallation of the [2]catenand **3** with a variety of metal ions and upon protonation with HClO_4 .

The template-directed strategy developed to prepare the [2]catenane $[\mathbf{3}\cdot\text{Cu}]\cdot\text{BF}_4$ was subsequently employed^[21] (Figure 4) to generate a [2]catenane incorporating two different macrocyclic components. Upon mixing equimolar amounts of $\text{Cu}(\text{MeCN})_4\text{BF}_4$ and the phenanthroline-containing compounds **2** and **4** in solution, the complex $[\mathbf{2}:\mathbf{4}\cdot\text{Cu}]\cdot\text{BF}_4$ self-assembled spontaneously. Treatment of $[\mathbf{2}:\mathbf{4}\cdot\text{Cu}]\cdot\text{BF}_4$ with $\text{I}[(\text{CH}_2)_2\text{O}]_5(\text{CH}_2)_2\text{I}$ in the presence of Cs_2CO_3 gave the [2]catenane $[\mathbf{5}\cdot\text{Cu}]\cdot\text{BF}_4$ in 10 % yield. Treatment of $[\mathbf{5}\cdot\text{Cu}]\cdot\text{BF}_4$ with KCN afforded the [2]catenand **5** quantitatively.

In the [2]catenane, the circumrotation of the terpyridine-containing macrocyclic component can be reversibly controlled^[21,22] (Figure 5), by altering the redox state of the metal. The absorption spectrum of a red-brown solution of $[\mathbf{5}\cdot\text{Cu}]\cdot\text{BF}_4$ in MeCN shows a band, centered on 437 nm, characteristic of a Cu^+ ion tetraordinated to two phenanthroline ligands. Upon oxidative electrolysis, or upon addition of Br_2 , Cu^+ is oxidized (step 1 in Figure 5) to Cu^{2+} and the solution turns deep green. The absorption spectrum shows a band, centered on 670 nm, typical of a Cu^{2+} ion tetraordinated to two phenanthroline ligands. However, this absorption band shifts to

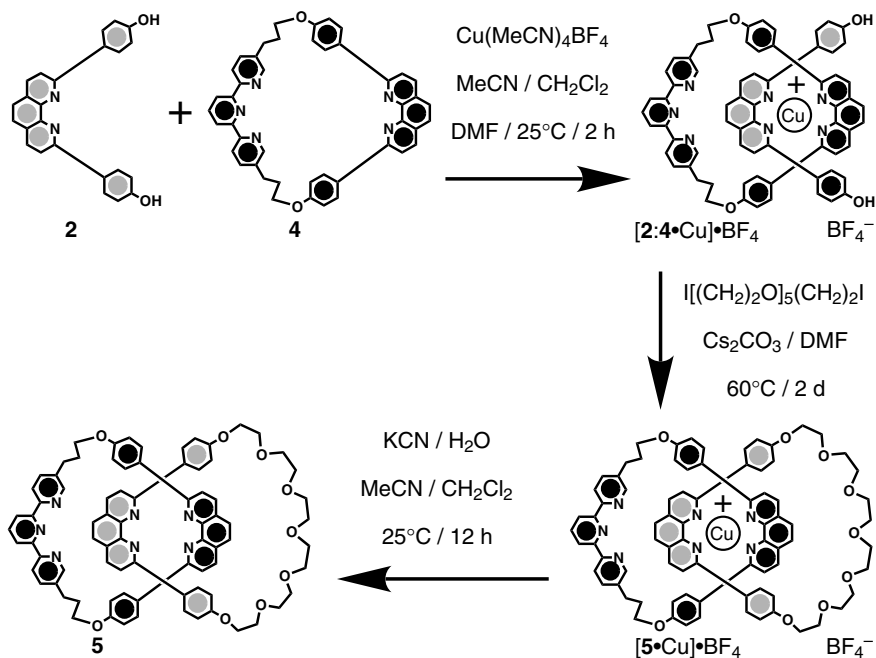


Fig. 4: The template-directed synthesis of the [2]catenate $[5 \cdot \text{Cu}] \cdot \text{BF}_4^-$ and its demetallation.

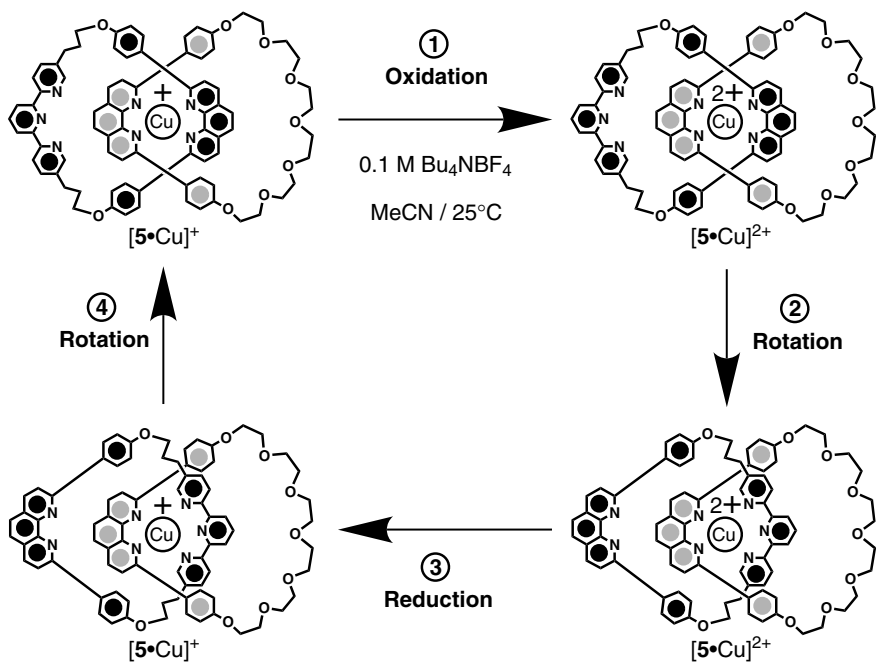


Fig. 5: The redox-controllable switching of the [2]catenane $[5 \cdot \text{Cu}]^+$.

640 nm after some hours, as the terpyridine-containing macrocycle circumrotates (step 2 in Figure 5) through the cavity of the other macrocyclic component and the Cu^{2+} ion becomes pentacoordinated by a phenanthroline and a terpyridine ligand. Upon reductive electrolysis, or upon addition of ascorbic acid, Cu^{2+} is reduced (step 3 in Figure 5) to Cu^+ , the terpyridine-containing macrocycle circumrotates (step 4 in Figure 5) through the cavity of the other macrocyclic component, and the solution becomes reddish-brown in color.

The template-directed synthesis of a [2]catenate incorporating two terpyridine-containing macrocyclic components has been accomplished^[23] as illustrated in Figure 6. Upon mixing $\text{Cu}(\text{MeCN})_4\text{BF}_4$ with two equivalents of the phenanthroline-containing compound **2**, the complex $[\text{2}_2 \cdot \text{Cu}] \cdot \text{BF}_4$ self-assembled spontaneously. Treatment of $[\text{2}_2 \cdot \text{Cu}] \cdot \text{BF}_4$ with two equivalents of the terpyridine-containing compound **6** in the presence of Cs_2CO_3 and ascorbic acid gave the [2]catenate $[\text{7} \cdot \text{Cu}] \cdot \text{PF}_6$ in a yield of 21 % after counterion exchange.

In this [2]catenate, the circumrotation of the macrocyclic components through each others' cavities can be reversibly controlled (Figure 6) by oxidation/reduction of the metal ion. The absorption spectrum of the dark red $[\text{7} \cdot \text{Cu}] \cdot \text{PF}_6$ in MeCN shows a band, centered on 439 nm, characteristic of a Cu^+ ion tetraordinated to two phenanthroline ligands. Upon addition of NOBF_4 , Cu^+ is oxidized (step 1 in Figure 7) to Cu^{2+} and the solution turns green. The absorption spectrum shows a band, centered on 670 nm, typical of a Cu^{2+} ion tetraordinated to two phenanthroline ligands. However, the intensity of this absorption band decreases with time as each one of the macrocyclic components circumrotates (steps 2 and 3 in Figure 7) through the other's cavity and the Cu^{2+} ion becomes hexacoordinated to two terpyridine ligands. Upon reductive electrolysis, Cu^{2+} is reduced (step 4 in Figure 7) to Cu^+ and the

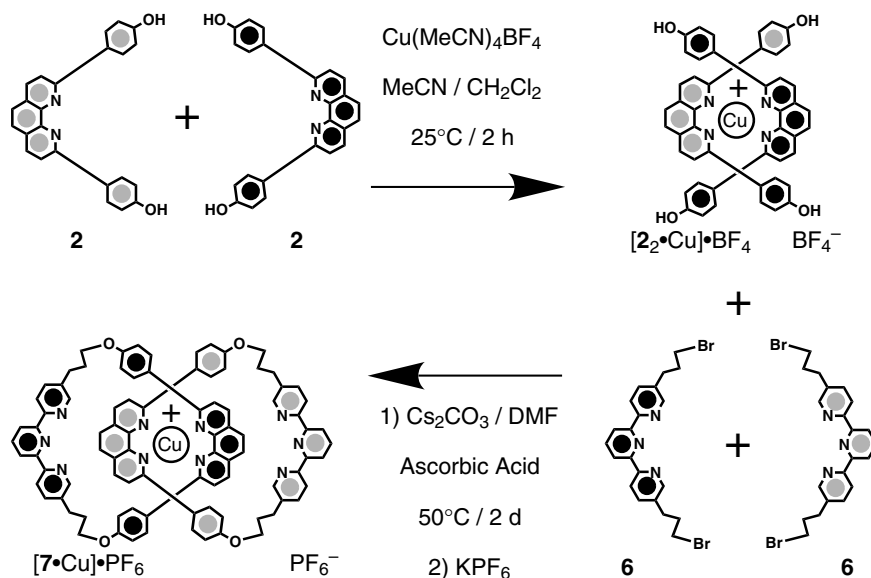


Fig. 6: The template-directed synthesis of the [2]catenate $[\text{7} \cdot \text{Cu}] \cdot \text{BF}_4$.

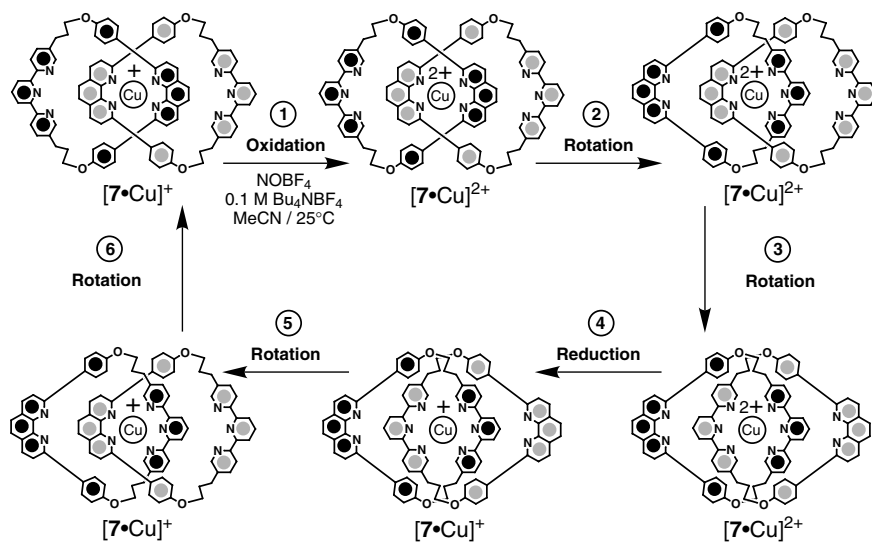


Fig. 7: The redox-controllable switching of the [2]catenate $[7\cdot\text{Cu}]^+$.

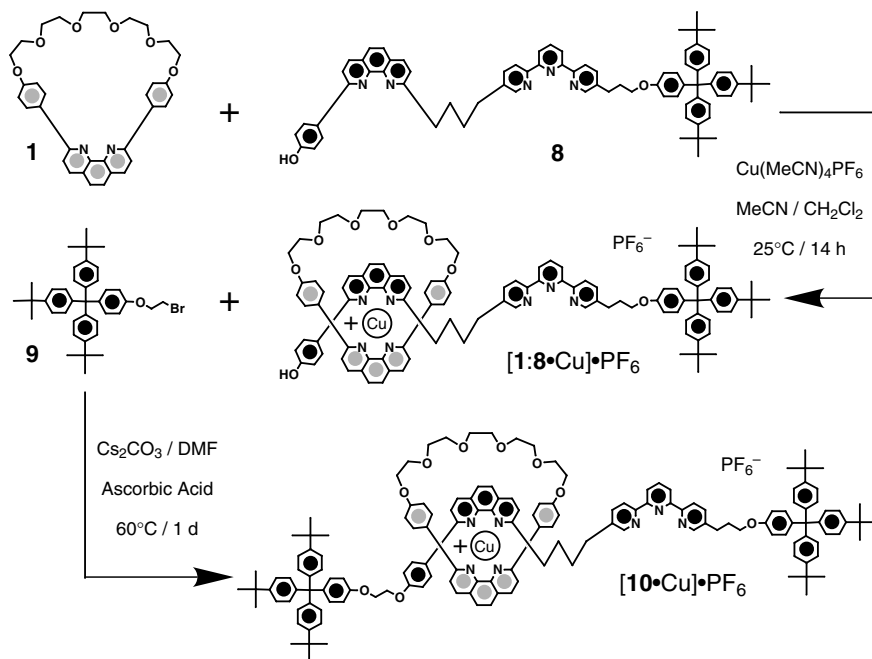


Fig. 8: The template-directed synthesis of the [2]rotaxane $[10\cdot\text{Cu}]\cdot\text{PF}_6$.

macrocyclic components again circumrotate (steps 5 and 6 in Figure 7) through each others' cavities and the Cu^+ ion becomes tetracoordinated to two phenanthroline ligands.

The template-directed synthesis of a [2]rotaxane incorporating a phenanthroline and a terpyridine recognition site in the dumbbell-shaped component and a phenanthroline ligand in the macrocyclic component has been accomplished,^[24] as shown in Figure 8. Upon mixing equimolar amounts of $\text{Cu}(\text{MeCN})_4\text{PF}_6$ and the phenanthroline-containing compounds **1** and **8**, the complex $[\mathbf{1}:\mathbf{8}\cdot\text{Cu}]\cdot\text{PF}_6$ self-assembled spontaneously. Treatment of $[\mathbf{1}:\mathbf{8}\cdot\text{Cu}]\cdot\text{PF}_6$ with the tetraarylmethane-based compound **9** in the presence of Cs_2CO_3 and ascorbic acid gave the [2]rotaxane $[\mathbf{10}\cdot\text{Cu}]\cdot\text{PF}_6$ in 40 % yield.

In this [2]rotaxane, the shuttling of the macrocycle component along the linear portion of the dumbbell-shaped component can be reversibly controlled^[24b,25] (Figure 9) by oxidation/reduction of the metal ion. The cyclic voltammogram of a dark red solution of $[\mathbf{10}\cdot\text{Cu}]\cdot\text{PF}_6$ in MeCN shows a reversible redox wave at +0.68 V, corresponding to the oxidation/reduction of a $\text{Cu}^+/\text{Cu}^{2+}$ ion tetracoordinated to two phenanthroline ligands. After oxidative electrolysis, the Cu^+ ion is oxidized (step 1 in Figure 9) to Cu^{2+} and the dark red solution turns light green. However, cyclic voltammetry reveals the gradual disappearance of the redox wave at +0.68 V and the concomitant growth of a redox wave at -0.3 V. This redox wave corresponds to the oxidation/reduction of a pentacoordinated $\text{Cu}^+/\text{Cu}^{2+}$ ion obtained after the shuttling (step 2 in Figure 9) of the macrocyclic component along the linear portion of the

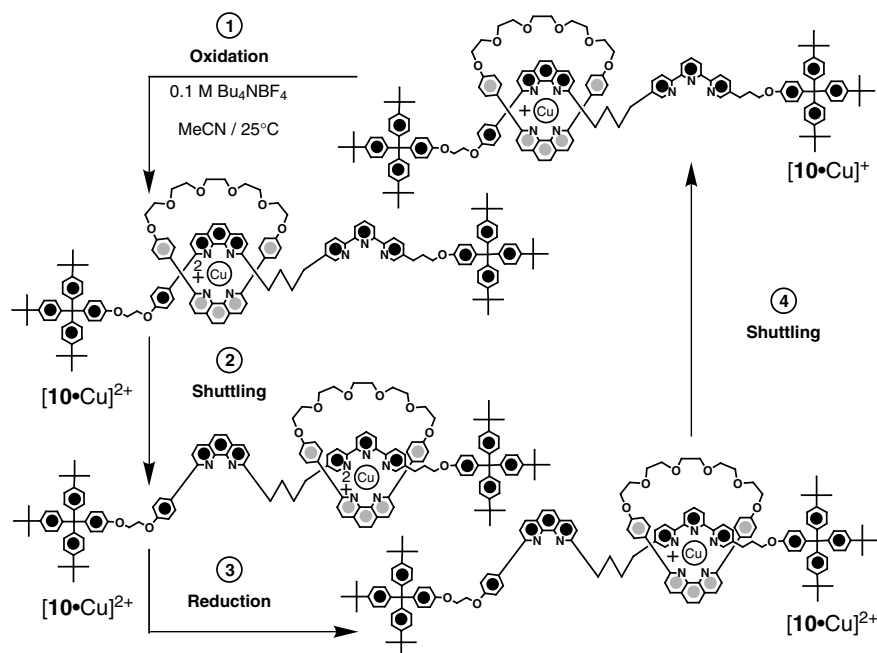


Fig. 9: The redox-controllable switching of the [2]rotaxane $[\mathbf{10}\cdot\text{Cu}]^+$.

dumbbell-shaped component. Upon reductive electrolysis, Cu^{2+} is reduced (step 3 in Figure 9) to Cu^+ and the macrocyclic component shuttles^[26] (step 4 in Figure 9) back to afford a Cu^+ ion tetracoordinated to two phenanthroline ligands.

7.3

Catenanes and Rotaxanes Containing π -Electron-deficient and π -Electron-rich Recognition Sites

Over the last decade, noncovalent bonding interactions between appropriate π -electron-deficient and π -electron-rich recognition sites have been exploited in our laboratories for the synthesis of catenanes and rotaxanes.^[27] In the example illustrated in Figure 10, the bis(hexafluorophosphate) salt $\mathbf{11} \cdot 2\text{PF}_6$ was treated^[28] with *trans*-bis(pyridine)ethylene ($\mathbf{12}$) in the presence of the previously formed macrocyclic polyether bis-*p*-phenylene-34-crown-10 ($\mathbf{13}$). The resulting [2]catenane $\mathbf{14} \cdot 4\text{PF}_6$ was isolated in 43 % yield after counterion exchange.

This [2]catenane is composed of a π -electron-deficient tetracationic cyclophane interlocked with a π -electron-rich macrocyclic polyether. In addition to a mechanical bond, $[\pi \cdots \pi]$ stacking interactions between the complementary aromatic units, [C–H \cdots O] hydrogen bonds between the α -bipyridinium hydrogen atoms and the polyether oxygen atoms, and [C–H \cdots π] interactions between the 1,4-dioxybenzene hydrogen atoms and the *p*-phenylene spacers in the tetracationic cyclophane hold the two macrocyclic components together and control their relative movements in solution. As a result of the asymmetry of the tetracationic cyclophane, two transla-

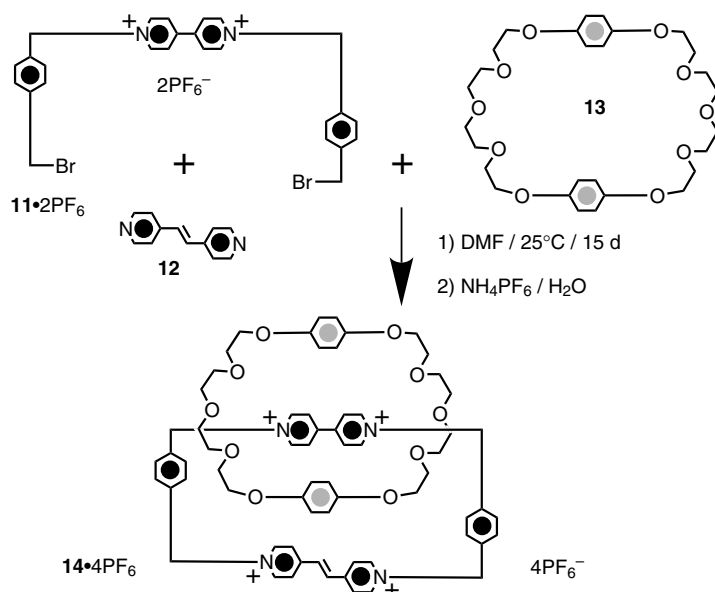


Fig. 10: The template-directed synthesis of the [2]catenane $\mathbf{14} \cdot 4\text{PF}_6$.

tional isomers are observed for $14 \cdot 4PF_6$. One of the two translational isomers has the bipyridinium unit incorporated inside the cavity of the macrocyclic polyether, while the other has the *trans*-bis(pyridinium)ethylene unit inside. 1H NMR spectroscopic investigation [$(CD_3)_2CO$, -60 °C] of $14 \cdot 4PF_6$ found^[28,29] an isomer ratio of 92:8 in favor of the isomer with the bipyridinium unit 'inside' and the *trans*-bis(pyridinium)ethylene unit 'alongside'. In the major translational isomer, the circumrotation of the tetracation cyclophane through the cavity of the macrocyclic polyether can be controlled (Figure 11) electrochemically by reducing and then oxidizing the bipyridinium unit. Indeed, monoelectronic reduction (step 1 in Figure 11) of the 'inside' bipyridinium unit is followed by circumrotation (step 2 in Figure 11) of the tetracation cyclophane through the cavity of the macrocyclic polyether. Oxidation (step 3 in Figure 11) of the now 'alongside' bipyridinium unit is followed by circumrotation (step 4 in Figure 11) of the tetracation cyclophane back through the cavity of the macrocyclic polyether to afford the original translational isomer of $14 \cdot 4PF_6$ once again.

A similar template-directed synthetic strategy was employed^[30] (Figure 12) to generate [2]catenanes incorporating a tetrathiafulvalene unit in their π -electron-rich macrocyclic component. The bis(hexafluorophosphate) salt $15 \cdot 2PF_6$ was treated with the dibromide **16** in the presence of a previously formed macrocyclic polyether **17** or **18**. The resulting [2]catenanes $19 \cdot 4PF_6$ and $20 \cdot 4PF_6$ were isolated in yields of 43 and 23 %, respectively, after counterion exchange. X-ray crystallographic analysis of $20 \cdot 4PF_6$ revealed that the tetrathiafulvalene unit preferentially resides 'inside' the

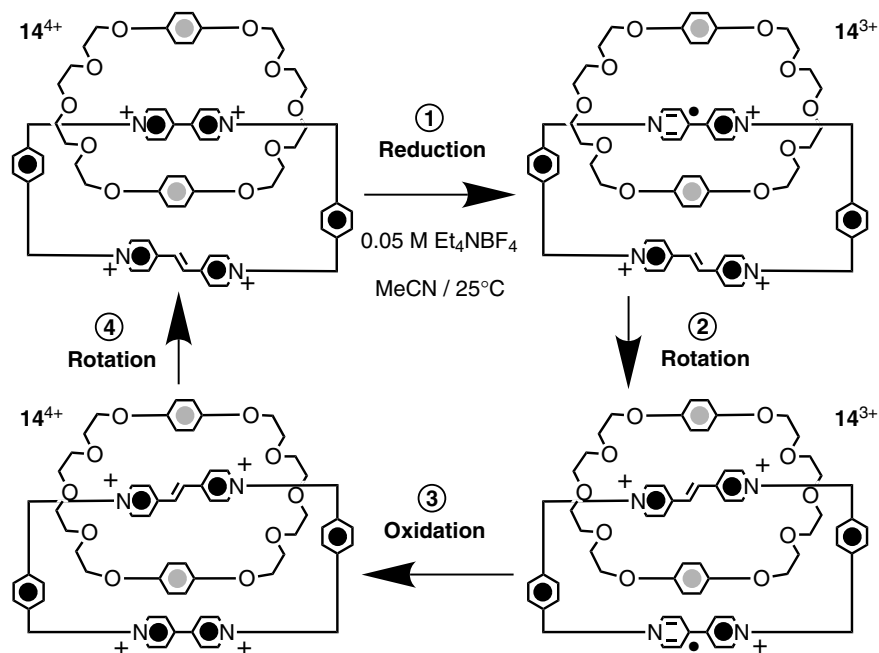


Fig. 11: The redox-controllable switching of the [2]catenane 14^{4+} .

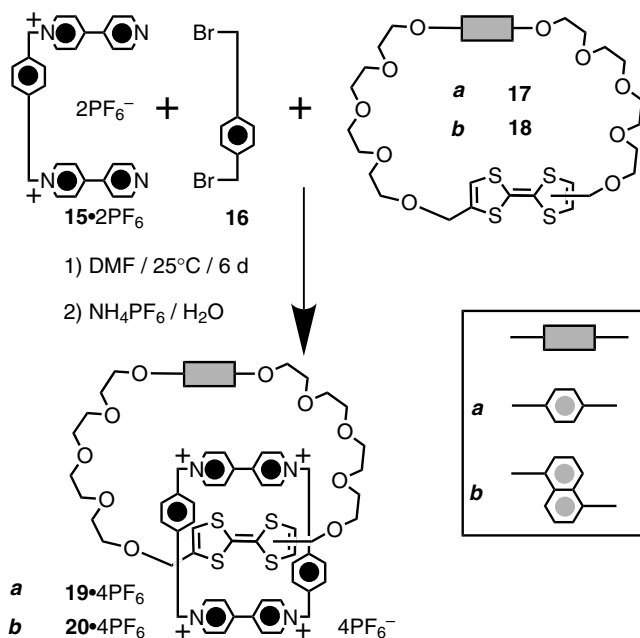


Fig. 12: The template-directed syntheses of the [2]catenanes $19 \cdot 4PF_6^-$ and $20 \cdot 4PF_6^-$.

cavity of the tetracationic cyclophane in the solid state. Consistent with this, the absorption spectra of $19 \cdot 4PF_6^-$ and $20 \cdot 4PF_6^-$ in MeCN show a band at 850 nm, corresponding to charge transfer interactions between the tetrathiafulvalene unit and the sandwiching bipyridinium units.

In both [2]catenanes, the circumrotation of the macrocyclic polyether component through the cavity of the tetracationic cyclophane can be reversibly controlled by oxidizing and then reducing the tetrathiafulvalene unit. Upon addition of one equivalent of $Fe(ClO_4)_3$, the tetrathiafulvalene unit is oxidized (step 1 in Figure 13) to its radical monocation. As a result of electrostatic repulsion between this monocationic unit and the sandwiching bipyridinium units, circumrotation (step 2 in Figure 13) of the macrocyclic polyether through the cavity of the tetracationic cyclophane occurs, and the charge transfer band centered on 850 nm in the absorption spectra disappears. Upon addition of one equivalent of $Na_2S_2O_5$ and H_2O , the tetrathiafulvalene unit is reduced (step 3 in Figure 13) back to its neutral state and the macrocyclic polyether once again circumrotates (step 4 in Figure 13) through the cavity of the tetracationic cyclophane, restoring the original state.

In both [2]catenanes, the circumrotation of the macrocyclic polyether component through the cavity of the tetracationic cyclophane can also be reversibly controlled by adding and then removing a 'sequestering' agent. In CD_3CN , the equilibrium between the two possible translational isomers of 19^{4+} and of 20^{4+} lies (step 1 in Figure 14) in favor of the isomer possessing the tetrathiafulvalene unit 'inside' the cavity of the tetracationic cyclophane. Indeed, the concentration of the minor isomer – in which the tetrathiafulvalene unit is positioned 'alongside' the tetracationic

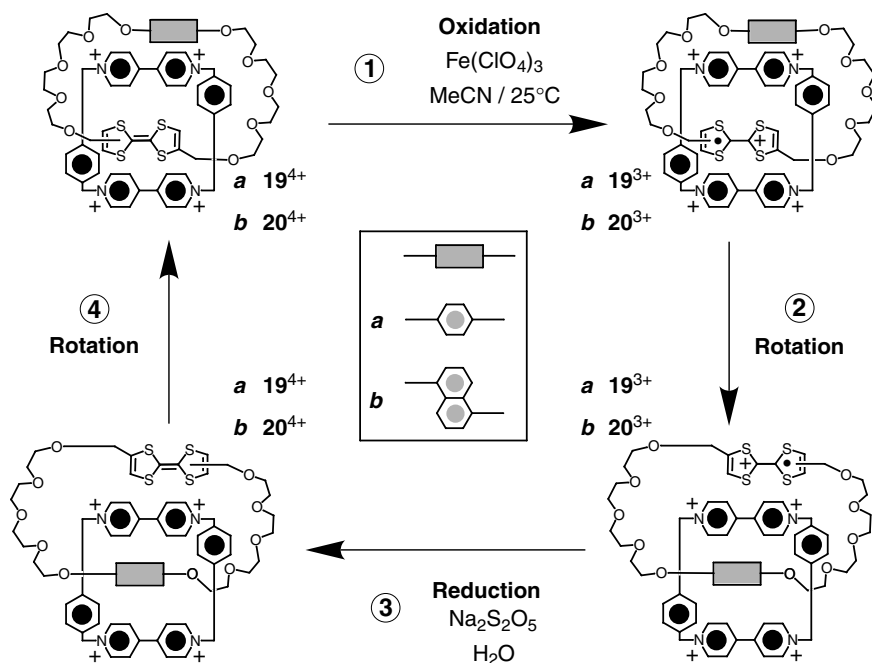


Fig. 13: The redox-controllable switching of the [2]catenanes 19^{4+} and 20^{4+} .

cyclophane – is so low that this species cannot even be detected using ^1H NMR spectroscopy. However, upon addition of two equivalents of *o*-chloroanil (**21**), the major translational isomer is converted completely into the minor isomer which, in turn, is complexed (step 2 of Figure 14) by **21** to form the 1:1 adducts $[19:\mathbf{21}]^{4+}$ and $[20:\mathbf{21}]^{4+}$. In these adducts, the tetrathiafulvalene unit is held ‘alongside’ the cavity of the tetracationic cyclophane as a result of charge transfer interactions between the tetrathiafulvalene unit and *o*-chloroanil. The overall process can be monitored using ^1H NMR spectroscopy, by following the chemical shift change associated with the dioxylene protons. For example, in the case of 19^{4+} , the protons of the ‘alongside’ 1,4-dioxybenzene ring resonate at about δ 6.5 in the ^1H NMR spectrum recorded in CD_3CN at 25°C . After the addition of **21**, the circumrotation of the macrocyclic polyether through the cavity of the tetracationic cyclophane moves the 1,4-dioxybenzene ‘inside’. As a result, the set of signals at about δ 6.5 for the protons of the ‘alongside’ 1,4-dioxybenzene ring disappear and are replaced by a set of signals at about δ 3.5, associated with the protons of the ‘inside’ 1,4-dioxybenzene ring. This remarkable chemical shift change is a result of shielding effects experienced by the protons of the ‘inside’ 1,4-dioxybenzene ring and exerted by the sandwiching bipyridinium units.

Porphyrin-containing [2]catenanes have been synthesized by Gunter et al.,^[31] following the template-directed synthetic strategy outlined in Figure 15. The bis(hexafluorophosphate) salt $15 \cdot 2\text{PF}_6$ was treated with the dibromide **16** in the presence of the previously formed macrocyclic polyether **22** or **23**. After counterion exchange,

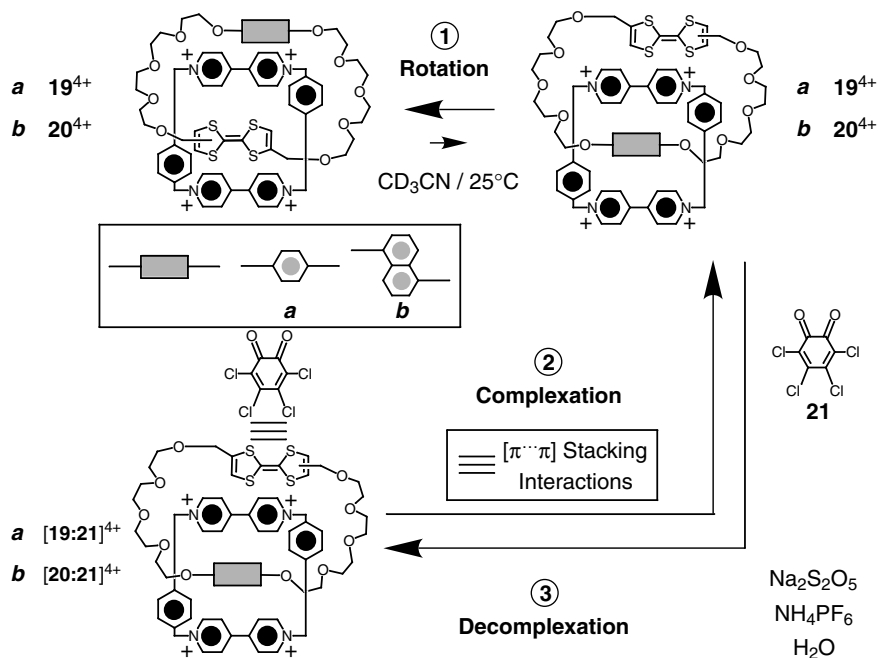


Fig. 14: The supramolecularly controllable switching of the [2]catenanes 19^{4+} and 20^{4+} .

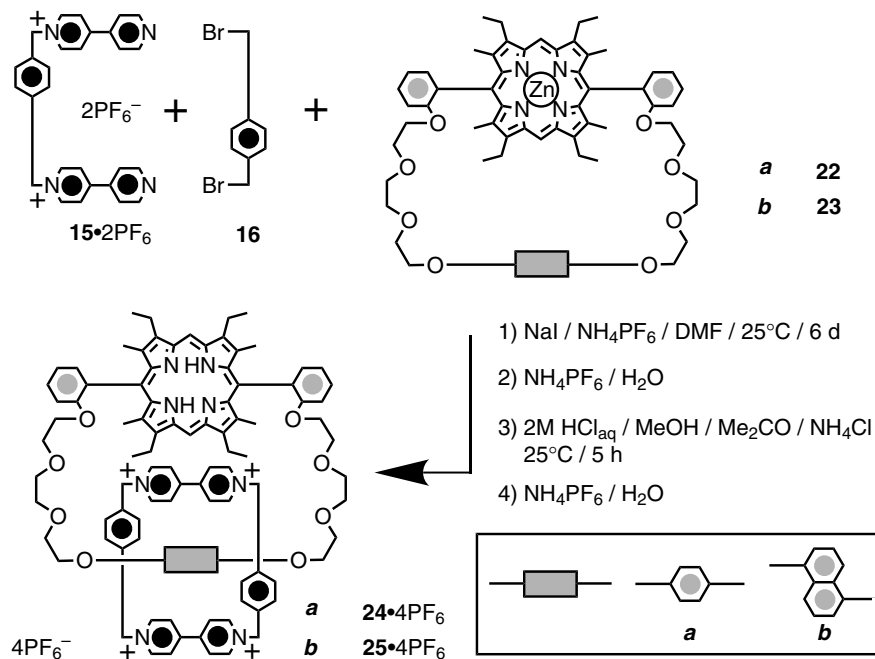


Fig. 15: The template-directed syntheses of the [2]catenanes $24 \cdot 4\text{PF}_6^-$ and $25 \cdot 4\text{PF}_6^-$.

demetallation, and further counterion exchange, the resulting porphyrin-containing [2]catenanes **24**·4PF₆ and **25**·4PF₆ were isolated in yields of 28 and 45 %, respectively.

The ¹H NMR spectra of **24**·4PF₆ and **25**·4PF₆, recorded in (CD₃)₂CO, show that the dioxyarene protons experience pronounced shielding effects and give rise to signals that are shifted upfield relative to those observed in the case of the 'free' macrocyclic polyethers. These observations indicate that, in both instances, the dioxyarene units reside inside the cavity of the tetracationic cyclophane. Similarly, one of the two bipyridinium units is positioned inside the cavity of the macrocyclic polyether and is engaged in $[\pi \cdots \pi]$ stacking interactions with the sandwiching dioxyarene and porphyrin units. Upon addition of CF₃CO₂H to a (CD₃)₂CO solution of **24**⁴⁺ or **25**⁴⁺, the porphyrin ring system is protonated^[32] (step 1 in Figure 16). As a result of electrostatic repulsion between the dicationic porphyrin ring system and the 'inside' bipyridinium unit, circumrotation of the tetracationic cyclophane through the cavity of the macrocyclic polyether occurs (step 2 in Figure 16) and the positively charged 'inside' bipyridinium is replaced by a neutral *p*-phenylene ring. Consistent with this,

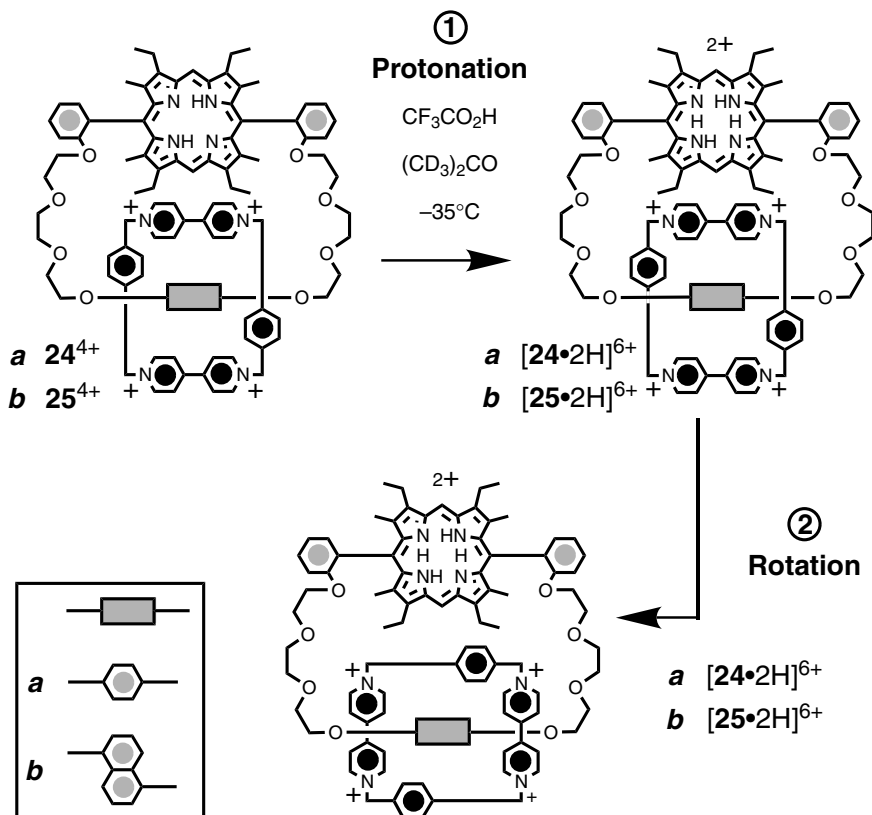


Fig. 16: The co-conformational change accompanying the protonation of the [2]catenanes **24**⁴⁺ and **25**⁴⁺.

the ^1H NMR spectrum recorded after protonation, at $-35\text{ }^\circ\text{C}$, shows two different environments for the ‘inside’ and ‘alongside’ *p*-phenylene rings and the adjacent methylene groups. The chemical shift differences between the ‘inside’ and ‘alongside’ *p*-phenylene protons, for $[\mathbf{24}\cdot\text{H}]^{6+}$ and $[\mathbf{25}\cdot\text{H}]^{6+}$, respectively, are $\Delta\delta -0.39$ and -0.50 ppm, and those for the ‘inside’ and ‘alongside’ methylene protons are $\Delta\delta -1.63$ and -1.03 ppm.

Chemically and electrochemically controllable [2]rotaxanes that rely upon $[\pi\cdots\pi]$ stacking interactions and $[\text{N}\cdots\text{H}\cdots\text{O}]$ and/or $[\text{C}\cdots\text{H}\cdots\text{O}]$ hydrogen bonds between complementary recognition sites have been synthesized.^[33] In the example illustrated in Figure 17, the bis(hexafluorophosphate) salt $\mathbf{15}\cdot 2\text{PF}_6$ was treated^[34] with the dibromide $\mathbf{16}$ in the presence of the π -electron-rich, dumbbell-shaped compound $\mathbf{26}$ to afford the [2]rotaxane $\mathbf{27}\cdot 4\text{PF}_6$ in 19 % yield after counterion exchange.

The dumbbell-shaped component of this [2]rotaxane incorporates recognition sites for benzidine and biphenol moieties. As a result, two translational isomers are associated with the [2]rotaxane $\mathbf{27}\cdot 4\text{PF}_6$ in solution. At $-44\text{ }^\circ\text{C}$, the ^1H NMR spectrum of a CD_3CN solution of $\mathbf{27}\cdot 4\text{PF}_6$ shows distinct signals for the two translational isomers, in a ratio of 84:16 in favor of the isomer incorporating the benzidine unit inside the cavity of the tetracationic cyclophane. The presence, in solution, of two translational isomers was also found by absorption spectroscopy. Indeed, the absorption spectrum of a solution of $\mathbf{27}\cdot 4\text{PF}_6$ in MeCN shows two bands centered on 490 and 690 nm. These arise from charge transfer interactions between the bipyridinium units of the tetracationic cyclophane and the biphenol and benzidine units,

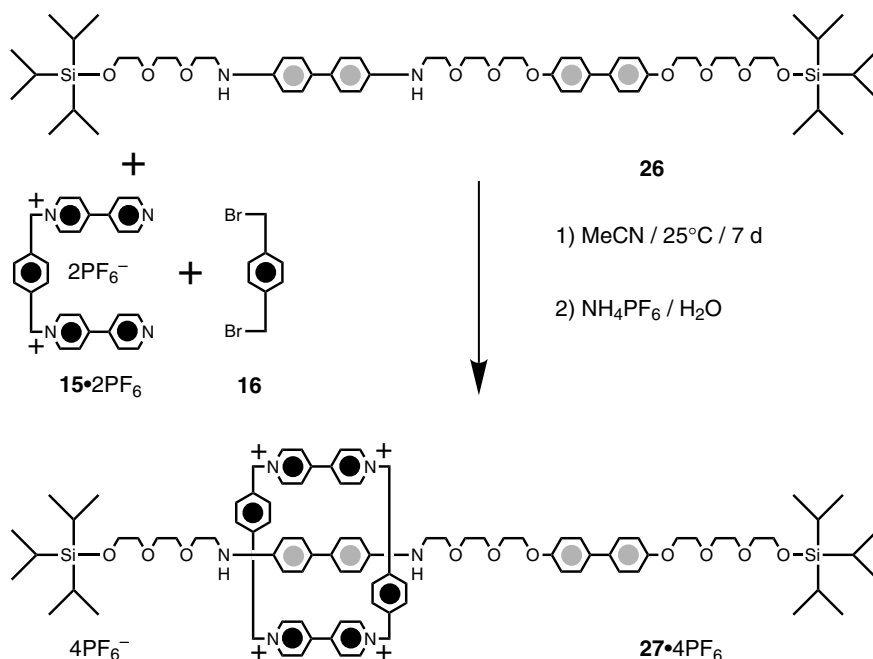


Fig. 17: The template-directed syntheses of the [2]rotaxane $\mathbf{27}\cdot 4\text{PF}_6$.

respectively, of the dumbbell-shaped component. Upon addition of an excess of $\text{CF}_3\text{CO}_2\text{H}$, the benzidine unit is protonated (step 1 in Figure 18). As a result of electrostatic repulsion, the tetracationic cyclophane shuttles (step 2 in Figure 18) away from this newly formed dicationic unit, and the band centered on 690 nm disappears. Upon addition of $\text{C}_5\text{H}_5\text{N}$, deprotonation occurs (step 3 in Figure 18) and the tetracationic cyclophane shuttles back (step 4 in Figure 18) to encircle the neutral benzidine unit.

The shuttling of the tetracationic cyclophane along the linear portion of the dumbbell-shaped component can also be reversibly controlled by electrochemical oxidation and then reduction of the benzidine unit. The electrochemical oxidation of the benzidine unit to a radical monocation (step 1 in Figure 19) is followed by the shuttling (step 2 in Figure 19) of the tetracationic cyclophane, which moves from the newly formed monocationic unit to the neutral biphenol ring system. The electrochemical reduction of the radical monocation to its neutral state (step 3 in Figure 19) is accompanied by the shuttling (step 4 in Figure 19) of the tetracationic cyclophane back to encircle the benzidine unit.

A [2]rotaxane containing a 2,6-dioxyanthracene moiety has also been prepared^[35] (Figure 20) by employing the usual template-directed approach. Treatment of the bis(hexafluorophosphate) salt $15 \cdot 2\text{PF}_6$ with the dibromide **16** in the presence of the

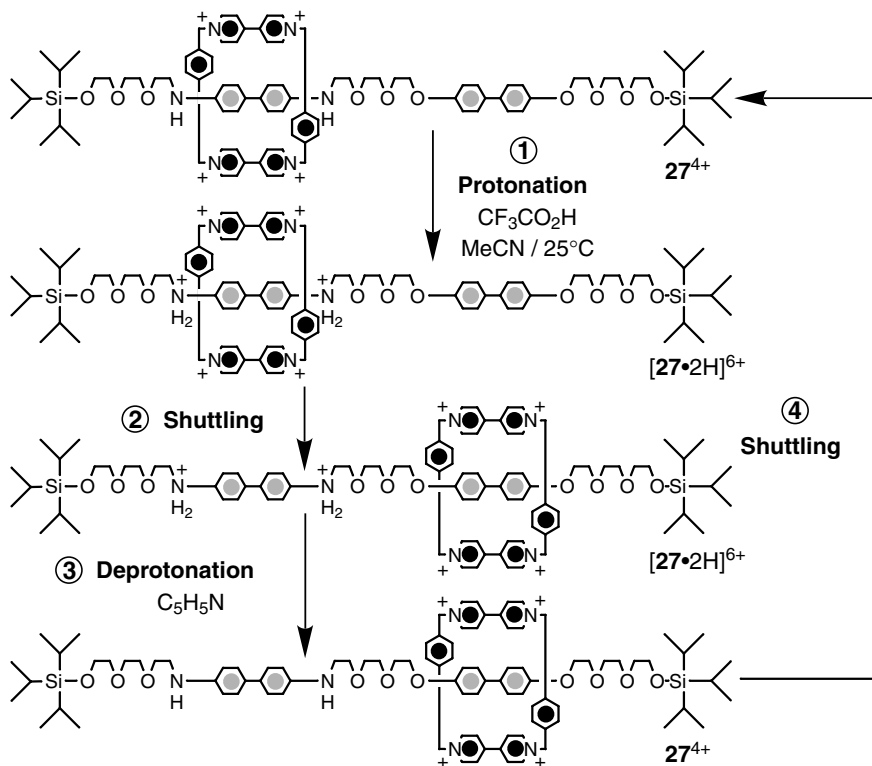


Fig. 18: The acid/base-controllable switching of the [2]rotaxane 27^{4+} .

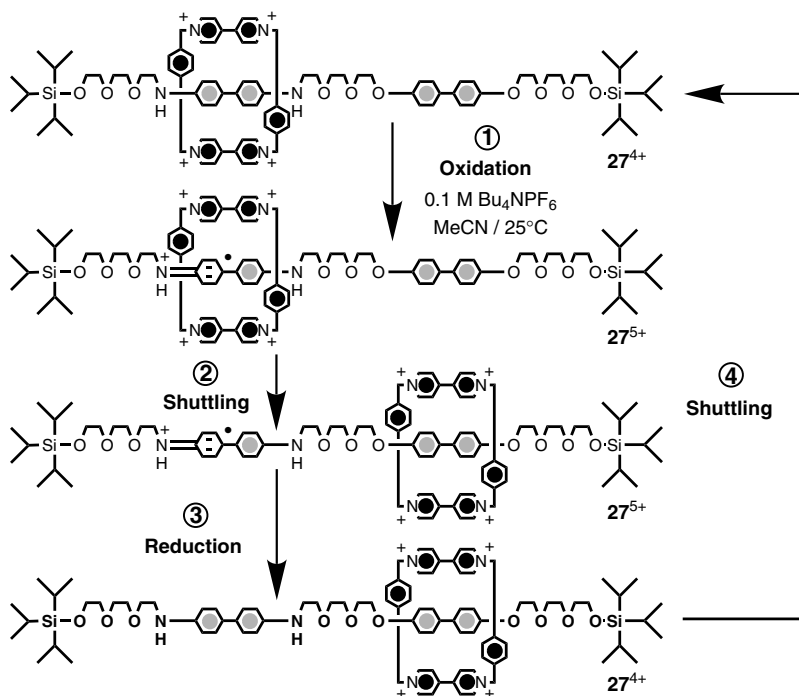


Fig. 19: The redox-controllable switching of the [2]rotaxane 27^{4+} .

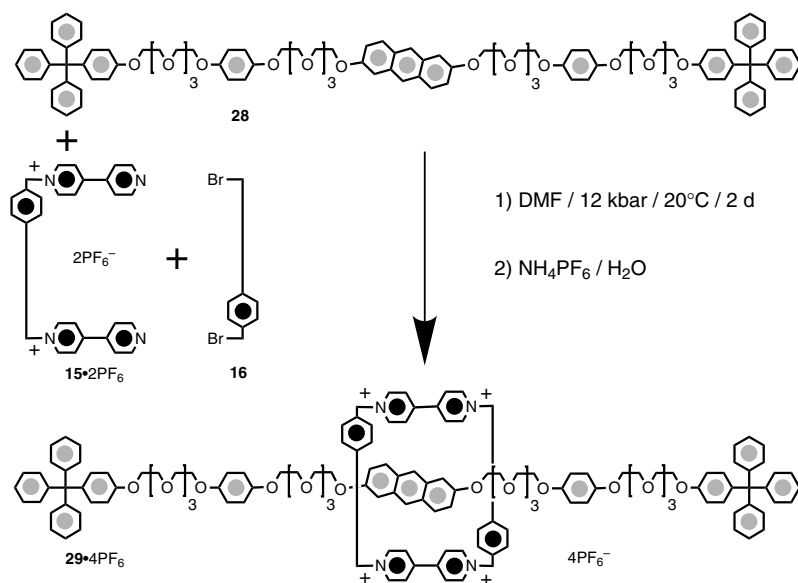


Fig. 20: The template-directed syntheses of the [2]rotaxane $29 \cdot 4PF_6$.

2,6-dioxyanthracene-containing, dumbbell-shaped compound **28** afforded the [2]rotaxane **29**·4PF₆, in a yield of 17 %, after counterion exchange.

The ¹H NMR spectrum of the [2]rotaxane **29**·4PF₆ in (CD₃)₂CO showed that the tetracationic cyclophane component resides exclusively around the 2,6-dioxyanthracene ring system. Indeed, the singlet associated with the 9,10-protons of the 2,6-dioxyanthracene ring system is shifted by $\Delta\delta$ -3.86 ppm upon rotaxane formation. This remarkable chemical shift change is a result of shielding effects exerted by the sandwiching bipyridinium units. In contrast, the protons on the two equivalent 1,4-dioxybenzene rings are unaffected by the presence of the tetracationic cyclophane. Upon electrochemical oxidation of the 2,6-dioxyanthracene ring system, a positive charge is generated (step 1 in Figure 21) on this unit. As a result of electrostatic repulsion, the tetracationic cyclophane shuttles (step 2 in Figure 21) to encircle one of the two 1,4-dioxybenzene rings.

[2]Rotaxanes incorporating dialkylammonium recognition sites have been synthesized,^[36] as illustrated in Figure 22. Treatment of the bis(hexafluorophosphate) salts [30·H]·2PF₆ and [31·H]·2PF₆ with the benzylic bromide **32** in the presence of

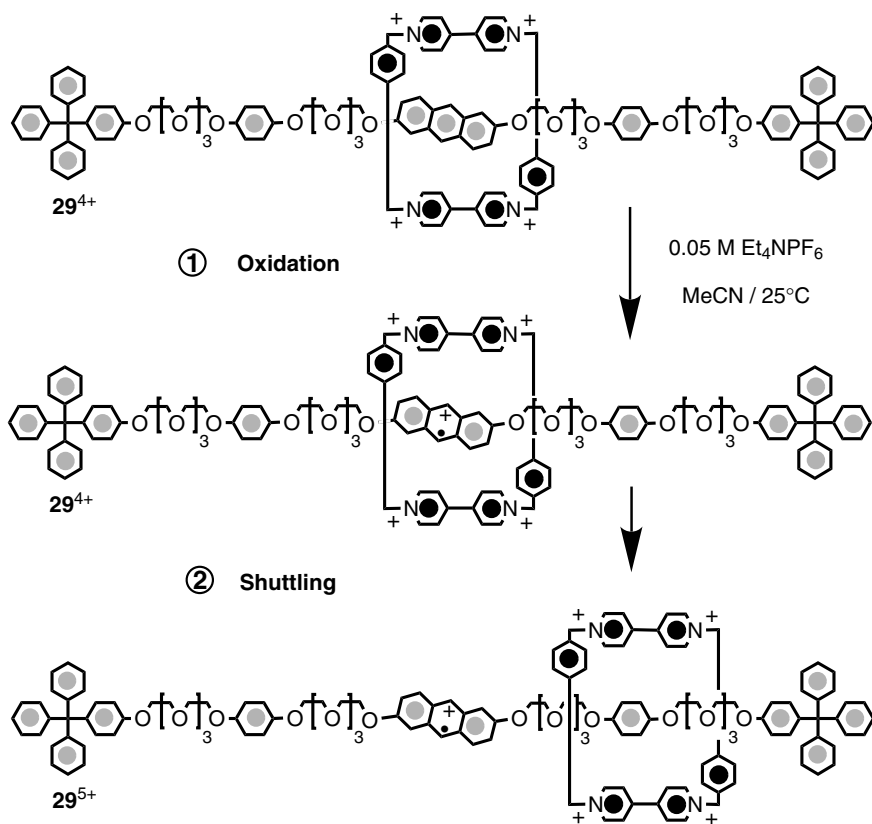


Fig. 21: The co-conformational change accompanying the oxidation of the [2]rotaxane **29**⁴⁺.

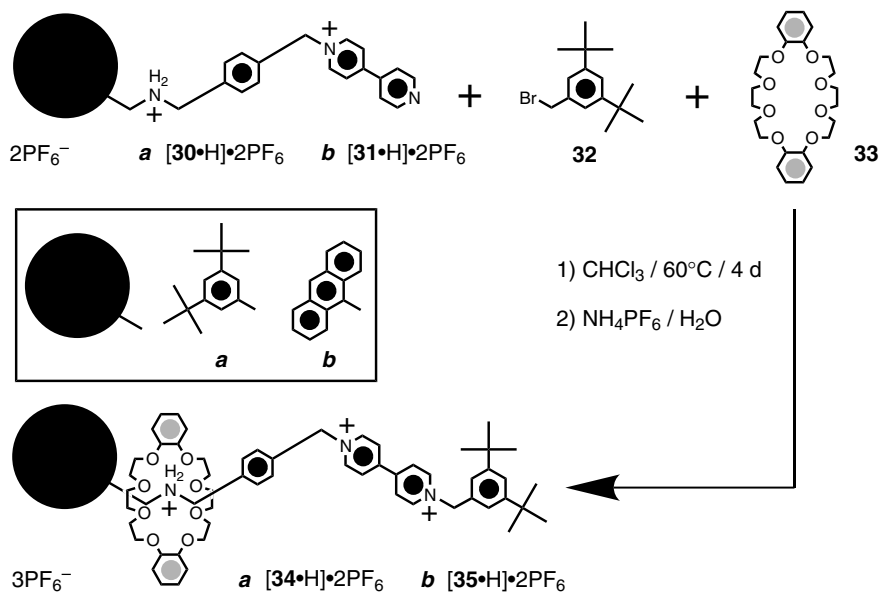


Fig. 22: The template-directed syntheses of the [2]rotaxanes $[\mathbf{34}\cdot\text{H}]\cdot 3\text{PF}_6$ and $[\mathbf{35}\cdot\text{H}]\cdot 3\text{PF}_6$.

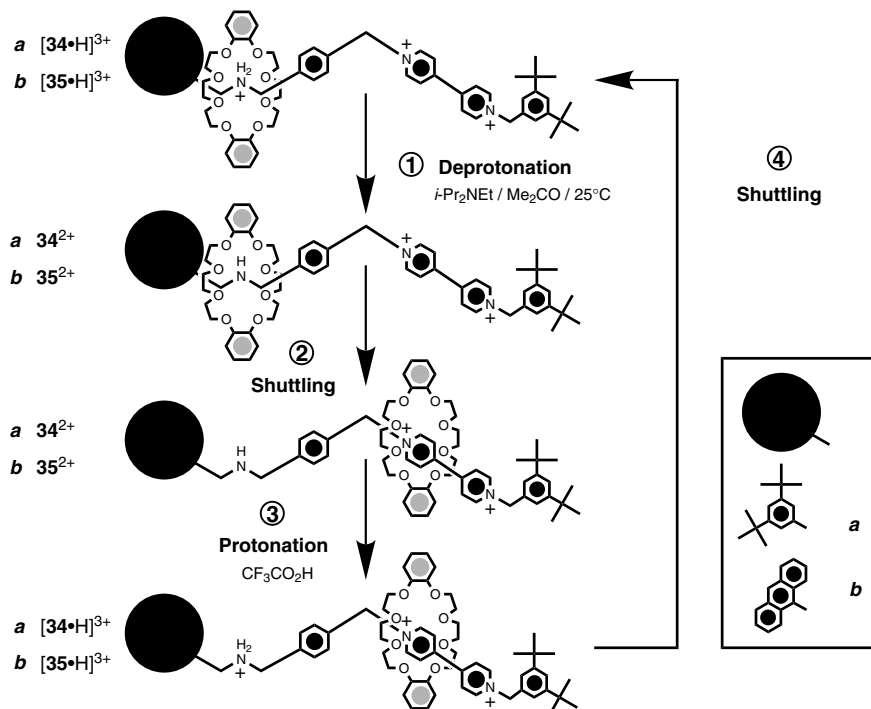


Fig. 23: The acid/base-controllable switching of the [2]rotaxanes $[\mathbf{34}\cdot\text{H}]^{3+}$ and $[\mathbf{35}\cdot\text{H}]^{3+}$.

dibenzo[24]crown-8 (**33**) gave the [2]rotaxanes $[34 \cdot H] \cdot 3PF_6$ and $[35 \cdot H] \cdot 3PF_6$, respectively, in yields of 38 and 30 % after counterion exchange.

In both [2]rotaxanes, the macrocyclic polyether is positioned around the dialkylammonium recognition site as a result of a combination of $[^+N-H \cdots O]$ and $[C-H \cdots O]$ hydrogen bonds between the polyether oxygen atoms and the $[^+NH_2]$ and $[CH_2]$ dialkylammonium hydrogen atoms, respectively. However, upon addition of 2.4 equivalents of $i-Pr_2NEt$ to an Me_2CO solution of either $[34 \cdot H]^{3+}$ or $[35 \cdot H]^{3+}$, deprotonation of the dialkylammonium recognition site occurs (step 1 in Figure 23) and the intercomponent hydrogen bonds are destroyed. As a result, the macrocyclic polyether shuttles (step 2 in Figure 23) to encircle the bipyridinium recognition site. Upon addition of 3.2 equivalents of CF_3CO_2H , protonation restores the dialkylammonium recognition site (step 3 in Figure 23) and the macrocyclic polyether shuttles (step 34 in Figure 23) back from the bipyridinium to the dialkylammonium recognition site.

7.4

Rotaxanes Containing Cyclodextrins

The ability of cyclodextrins to bind organic guests with rotaxane-like geometries in aqueous solution has been exploited^[37] for the self-assembly of rotaxanes. In the example illustrated in Figure 24, the synthesis^[38] of a cyclodextrin-containing [2]rotaxane incorporating a photoactive azobenzene unit is illustrated. The bis(perchlorate) salt $36 \cdot 2ClO_4$ was treated with **37** in the presence of α -cyclodextrin (**38**) to afford the [2]rotaxane $39 \cdot 4ClO_4$, in 30 % yield after counterion exchange.

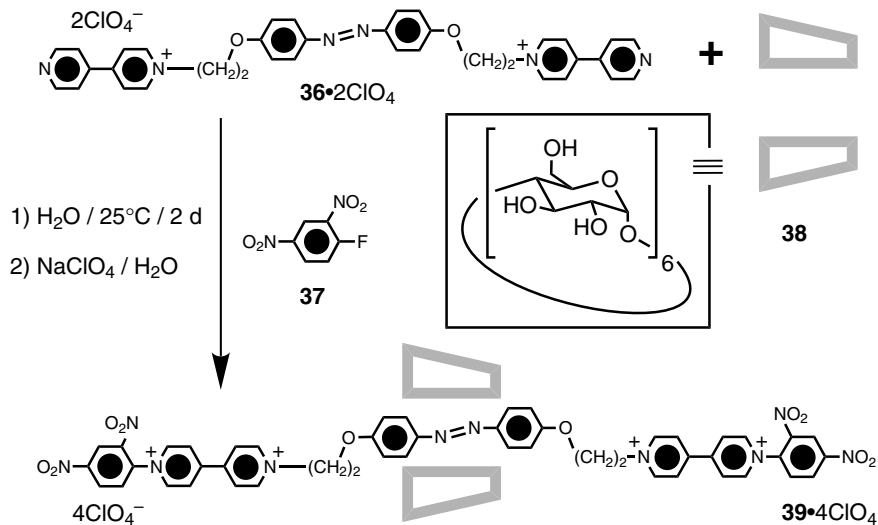


Fig. 24: The template-directed syntheses of the [2]rotaxane $39 \cdot 4ClO_4$.

In this [2]rotaxane, the cyclodextrin component preferentially encircles the *trans*-azobiphenoxy unit. However, upon irradiation ($\lambda = 360$ nm) of an aqueous solution of 39^{4+} , isomerization of the azobiphenoxy unit from the *trans* to the *cis* form occurs (step 1 in Figure 25). As a result, the cyclodextrin component shuttles (step 2 in Figure 25) to encircle the bismethylene spacer bridging the *cis*-azobiphenoxy unit and one of the two bipyridinium units. Upon further irradiation ($\lambda = 430$ nm), the isomerization of the azobiphenoxy unit back from the *cis* to the *trans* form takes place (step 3 in Figure 25) and is followed (step 4 in Figure 25) by the shuttling of the cyclodextrin component back to the *trans*-azobiphenoxy unit. The light-controlled switching of this [2]rotaxane can be followed by circular dichroism measurements. Before irradiation, a positive circular dichroism induced band ($\lambda = 360$ nm), corresponding to the π - π^* transition associated with the azobiphenoxy unit, is observed. After irradiation ($\lambda = 360$ nm), the intensity of this band decreases, but it is restored after irradiation at a longer wavelength ($\lambda = 430$ nm). Since the sign of a π - π^* transition associated with a guest encircled by an α -cyclodextrin is positive, the observed results indicate that the azobiphenoxy unit is initially inserted inside the cyclodextrin cavity and that it is expelled after irradiation at a wavelength of 360 nm.

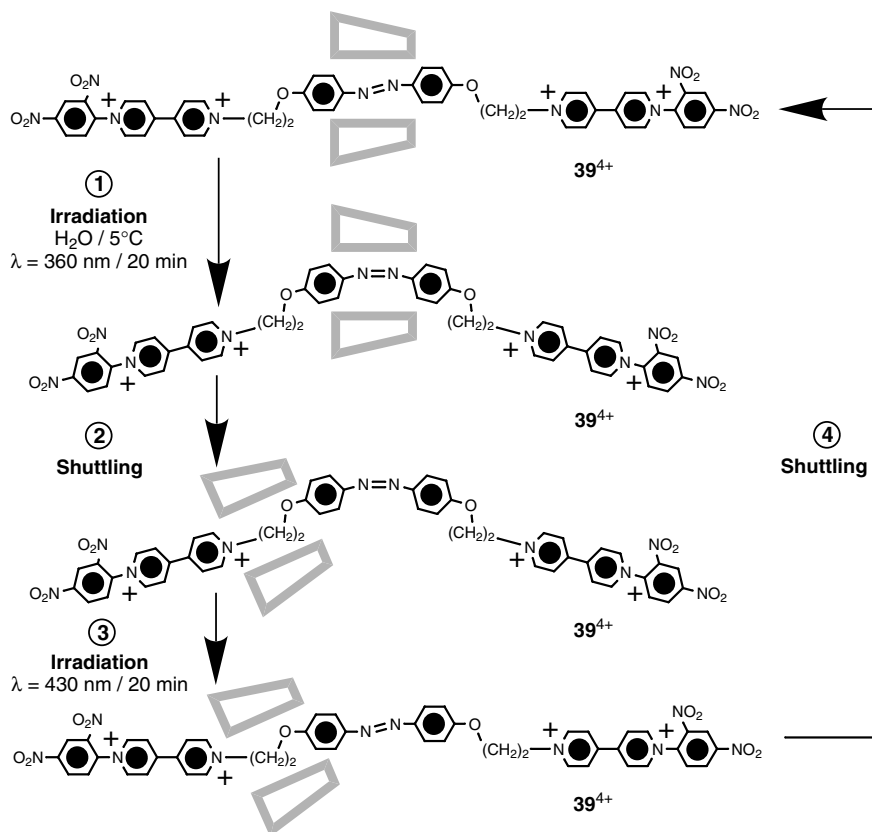


Fig. 25: The light-controllable switching of the [2]rotaxane 39^{4+} .

7.5 Molecule-based Logic Gates

It is possible to perform logic operations^[11,39] at the supramolecular level by employing appropriate molecular components in [2]pseudorotaxanes. In particular, macrocyclic hosts capable of reversibly binding to linear guests under the influence of chemical, electrochemical, and/or photochemical stimuli can be used to generate molecule-based logic gates with one or more input signals and one output signal. Figure 26 shows an exclusive OR (XOR) gate based^[40] on a [2]pseudorotaxane and the corresponding truth table.

This logic gate can be controlled by consecutive additions of $\text{CF}_3\text{SO}_3\text{H}$ and $n\text{-Bu}_3\text{N}$ – the two input signals – and its state can be read by monitoring the fluorescence associated with the 2,3-dioxynaphthalene ring systems – the output signal. In its free form, the macrocyclic polyether **40** shows a fluorescence band at 343 nm. This is quenched upon complexation (step 1 in Figure 26) with the diazapyrenium-based compound $\mathbf{41}^{2+}$ to form the nonemitting [2]pseudorotaxane $[\mathbf{40}\cdot\mathbf{41}]^{2+}$. Upon addition of $\text{CF}_3\text{SO}_3\text{H}$ (step 2A in Figure 26), the [2]pseudorotaxane $[\mathbf{40}\cdot\mathbf{41}]^{2+}$ dissociates as a result of the formation of the fluorescent complex $[\mathbf{40}\cdot\text{H}]^+$. Upon addition of $n\text{-Bu}_3\text{N}$ (step 3A in Figure 26), the complex $[\mathbf{40}\cdot\text{H}]^+$ dissociates and the nonemitting [2]pseudorotaxane $[\mathbf{40}\cdot\mathbf{41}]^{2+}$ is reformed. Similarly, the addition of $n\text{-Bu}_3\text{N}$ (step 2B in Figure 26) to a solution of the [2]pseudorotaxane $[\mathbf{40}\cdot\mathbf{41}]^{2+}$ induces its dissociation as the charge-transfer complex $[\mathbf{40}\cdot 2n\text{-Bu}_3\text{N}]^{2+}$ is formed. This process is accompanied by the release of the fluorescent macrocyclic polyether **40**. However, upon addition of $\text{CF}_3\text{SO}_3\text{H}$ (step 3B in Figure 26), the charge-transfer complex

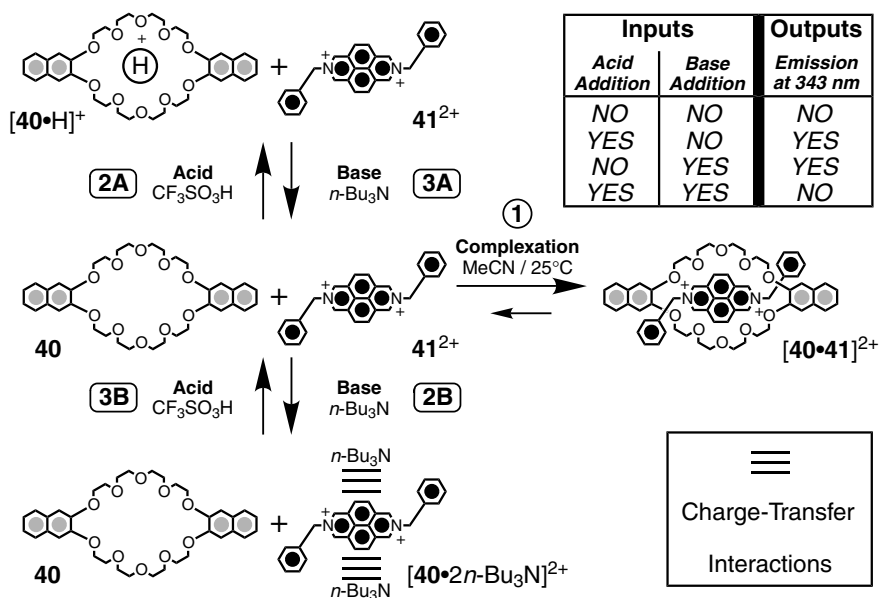


Fig. 26: The acid/base-controllable XOR gate based on the [2]pseudorotaxane $[\mathbf{40}\cdot\mathbf{41}]^{2+}$.

$[40 \cdot 2n\text{-Bu}_3\text{N}]^{2+}$ is destroyed and the nonemitting $[2]$ pseudorotaxane $[40 \cdot 41]^{2+}$ is reformed.

An electrochemically-controllable exclusive NOR (XNOR) logic gate has been demonstrated,^[41] using a $[2]$ pseudorotaxane composed of a tetrathiafulvalene-based guest and a bipyridinium-based host. This logic gate can be controlled by oxidizing and then reducing the tetrathiafulvalene unit or the bipyridinium recognition sites – the two input signals – and its state can be read by monitoring the charge-transfer band associated with the $[2]$ pseudorotaxane – the output signal. Upon mixing equimolar amounts of the guest **42** and the host **43**⁴⁺, the $[2]$ pseudorotaxane $[42 \cdot 43]^{4+}$ self-assembles (step 1 in Figure 27) spontaneously and a charge-transfer band associated with the $[\pi \cdots \pi]$ stacking interactions between the tetrathiafulvalene and the bipyridinium units appears in the visible region. The electrochemical oxidation (step 2A in Figure 27) of the tetrathiafulvalene unit generates a positive charge on the guest, which is expelled (step 3A in Figure 27) from the cavity of the tetracationic host. The decomplexation is accompanied by the disappearance of the charge-transfer band. It is restored, however, after the electrochemical reduction (step 4A in Figure 27) of the guest back to its neutral state **42** and the reformation of the $[2]$ pseudorotaxane $[42 \cdot 43]^{4+}$. Similarly, the charge-transfer band associated with $[42 \cdot 43]^{4+}$ disappears after the electrochemical reduction (step 2B in Figure 27) of the bipyridinium units of the host, which causes decomplexation (step 3B in Figure 27).

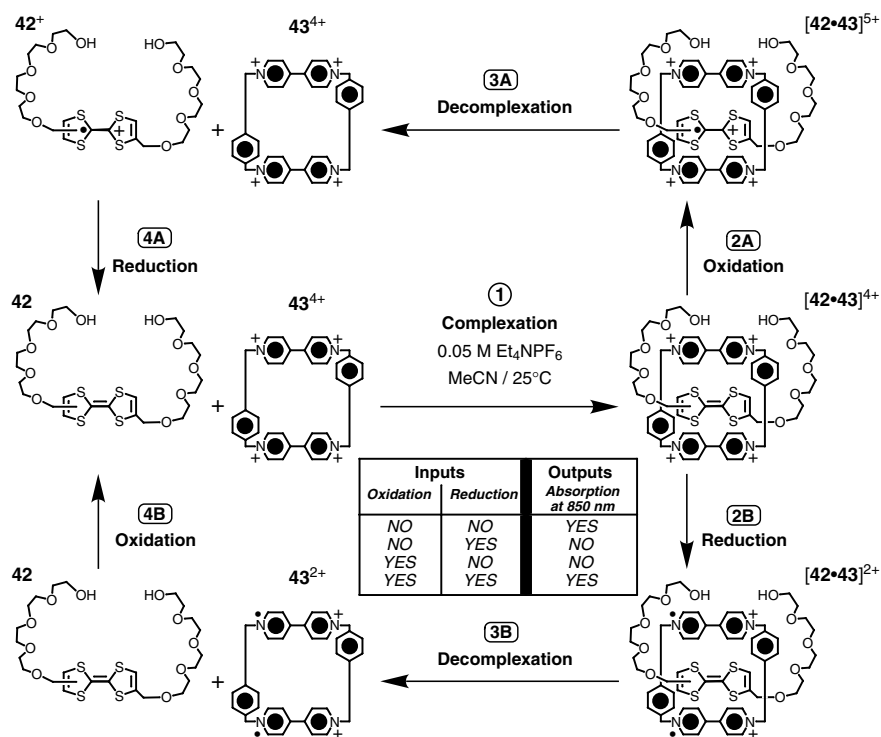


Fig. 27: The redox-controllable XNOR gate based on the $[2]$ pseudorotaxane $[42 \cdot 43]^{4+}$.

Upon electrochemical oxidation (step 4B in Figure 27) of the host, the dicationic bipyridinium units are restored and the green-colored [2]pseudorotaxane [42·43]⁴⁺ is reformed.

Bipyridinium-containing catenanes and rotaxanes form^[42] stable monolayers at air/water interfaces. In particular, amphiphilic rotaxanes, composed of 1,4-dioxymethylene-based macrocyclic polyethers encircling triply branched bipyridinium-based compounds, self-organize^[42b] into monolayers which can be transferred onto solid supports. These observations suggested^[43] the possibility of fabricating devices composed of a monolayer of amphiphilic rotaxanes sandwiched between two electrodes. Appropriate rotaxanes were self-assembled (Figure 28) by slippage on heating a THF solution of the dumbbell-shaped compound **44**·4PF₆ with 19 equivalents of bis-*p*-phenylene-34-crown-10 (**13**) at 55 °C for 10 d. The resulting [2]rotaxane **45**·4PF₆ and [3]rotaxane **46**·4PF₆ were isolated in yields of 14 and 52 %, respectively.

The dumbbell-shaped compound and the two rotaxanes were dissolved separately in THF and the solutions were deposited individually at the air/water interface of a Langmuir trough. After evaporation of the solvent, the molecules were compressed into a close-packed monolayer. The corresponding surface pressure/area per molecule isotherms indicated that, in all three monolayers, the molecules adopt a V-shaped conformation, with the hydroxymethyl group pointing towards, and the tetraarylmethane-based stoppers away from, the water. By employing the Langmuir–Blodgett technique, monolayers of the dumbbell-shaped compound and of

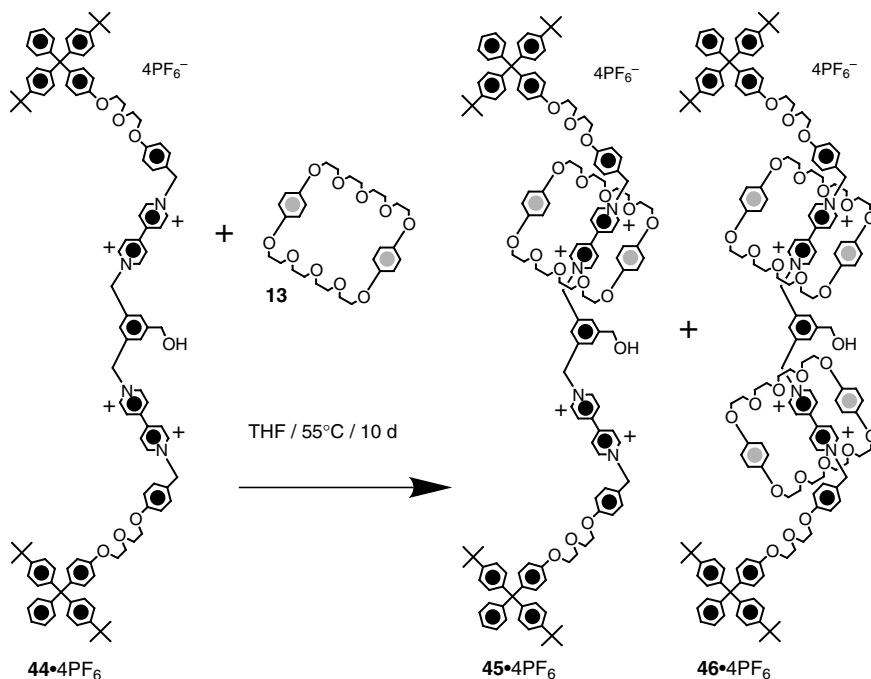


Fig. 28: The template-directed syntheses of the [2]rotaxane **45**·4PF₆ and of the [3]rotaxane **46**·4PF₆.

the two rotaxanes were transferred onto a pattern of parallel aligned Al/Al₂O₃ wires supported by an SiO₂/Si substrate. These wires had been deposited previously on the SiO₂/Si substrate using lithographic techniques, and each of them had a width of 6000 nm. A second set of wires perpendicular to this first one was evaporated onto the monolayer through a contact shadow mask, using an electron beam deposition technique. These wires were composed of a layer of Ti (5 nm) and one of Al (100 nm) and had a width of 11,000 nm. A portion of the resulting device is illustrated in Figure 29. Here, an Al/Ti wire overlays six Al/Al₂O₃ wires, forming a linear array of six junctions. A section of one of these junctions is also illustrated in Figure 29 and shows a monolayer of V-shaped [2]rotaxane molecules sandwiched between the two perpendicular wires. When the voltage, applied to the Al/Al₂O₃ wire of one of the junctions, was gradually reduced to -2 V, electrons passed from this wire to the overlying Al/Ti wire through the monolayer of [2]rotaxane molecules. Concomitantly, the current intensity, measured on the Al/Ti wire, increased sharply up to about 0.7 nA. When the voltage applied to the Al/Al₂O₃ wire was increased to +0.7 V, irreversible oxidation of the [2]rotaxane molecules occurred and, when the voltage was reduced again to -2 V, the current intensity was approximately 20 % of its original value. Thus, each of these junctions behaves as a switch that can be closed irreversibly by applying a positive voltage to one of its two terminals. It should be stressed that essentially the same switching phenomenon was observed in devices constructed using the dumbbell-shaped compound 44·4PF₆ and the [3]rotaxane 46·4PF₆, as described above for the [2]rotaxane 45·4PF₆. By interconnecting some of these irreversible switches appropriately, logic gates can be generated. Indeed, both AND and OR logic gates have been constructed using a linear array of junctions similar to the one shown in Figure 29.

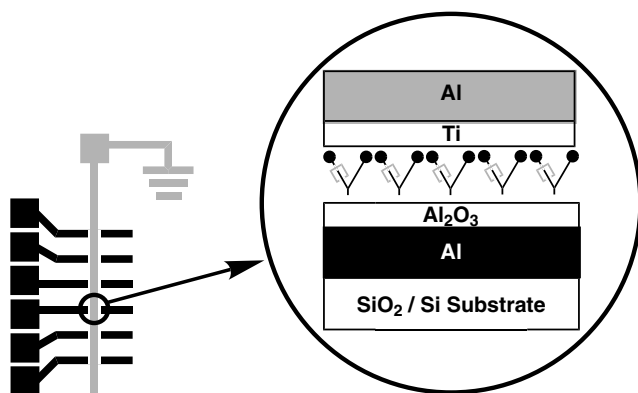


Fig. 29: Top view of a linear array of six devices and a section of a single junction containing a monolayer of [2]rotaxanes.

7.6

Electronically Reconfigurable Molecular Devices

The dimiristoylphosphatidyl salts of the switchable [2]catenanes **19**⁴⁺ and **20**⁴⁺ form stable monolayers at the air/water interface.^[44a] The monolayers can be transferred on Au(111) and can be studied by scanning tunneling spectroscopy.^[44a] The current-voltage behavior of the resulting materials is dictated by the redox state of the tetrathiafulvalene unit and by the co-conformation of the [2]catenane. Virtually no current is detected between -0.5 and 0.0 V when the tetrathiafulvalene unit is initially in its neutral state and located inside the cavity of the tetracationic cyclophane. Relatively high tunneling currents are obtained instead when the tetrathiafulvalene unit is initially in its oxidized state and located alongside the cavity of the tetracationic cyclophane.

These findings suggested the design of electronically reconfigurable molecular devices.^[44b] By employing the Langmuir-Blodgett technique, monolayers of the dimiristoylphosphatidyl salt of the [2]catenane **20**⁴⁺ were transferred onto a pattern of parallel aligned SiO₂/Si wires supported by a SiO₂/Si substrate. These wires had been deposited previously on the substrate by direct chemical vapor deposition and each of them had a width of 7 μm . A second set of wires perpendicular to the first was evaporated on the monolayer through a contact shadow mask, using an electron beam deposition technique. These wires were composed of a layer of Ti (5 nm) and one of Al (100 nm) and had a width of 10 μm . A portion of the resulting device is illustrated in Figure 30. Here, an Al/Ti wire overlays six SiO₂/Si wires, forming a linear array of six junctions. A section of one of these junctions is also illustrated in Figure 30 and shows the two perpendicular wires sandwiching a film of dimiristoylphosphatidyl anions laying on a monolayer of switchable [2]catenanes. The reversible switching between the two states of the [2]catenanes is achieved by alternating

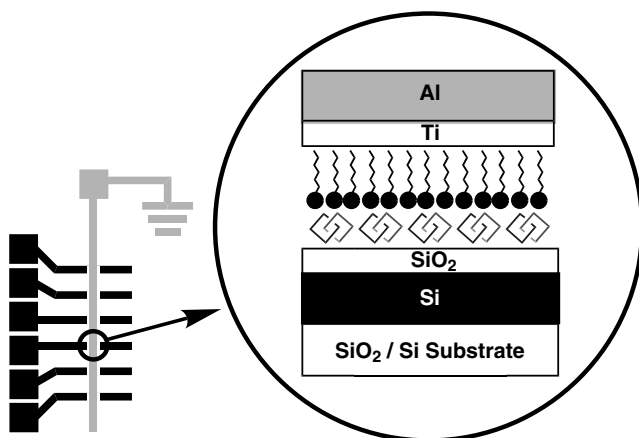


Fig. 30: Top view of a linear array of six devices and a section of a single junction containing a monolayer of catenanes anchored with amphiphilic counterions.

voltage pulses of +2 and -2 V. In between the switching pulses, the resistance of the device is measured maintaining the voltage at +0.1 V. An average change of $5 \times 10^8 \Omega$ was observed over ten consecutive switching cycles. This electronically reconfigurable device is a unique example of bistable molecule-based switch that can be operated under ambient conditions and might be useful for the generation of random access memories.

7.7

Conclusions

Catenanes and rotaxanes can be prepared efficiently, relying upon template-directed synthetic approaches. The ability of transition metals such as Cu^+ to coordinate phenanthroline ligands with tetrahedral geometry has been employed successfully to synthesize interlocked molecules in remarkably high yields. Similarly, a combination of noncovalent bonds – such as $[\pi \cdots \pi]$, $[\text{C}-\text{H} \cdots \text{O}]$, and $[\text{C}-\text{H} \cdots \pi]$ interactions – has been exploited to self-assemble catenanes and rotaxanes incorporating π -electron-rich and π -electron-deficient components. The complexation of organic guests by cyclodextrin hosts has also been employed to template the formation of cyclodextrin-containing rotaxanes. These template-directed synthetic procedures have permitted the introduction of chemically, electrochemically, and/or photochemically active units into these interlocked molecules. By employing chemical, electrochemical, and/or photochemical stimuli, the relative movements of the interlocked components of these catenanes and rotaxanes can be controlled externally and reversibly. As a result, these molecular systems can be switched reversibly between two states (*State 0* and *State 1*) in a manner reminiscent of conventional transistors. Importantly, the dimensions of these switchable catenanes and rotaxanes are approximately two orders of magnitude smaller than those of commercially available transistors. Thus, their incorporation into appropriate devices could pave the way for the fabrication of a new generation of nanometer scale electronic circuits.

References

- 1 For books on catenanes and rotaxanes, see: (a) Schill, G. *Catenanes, Rotaxanes and Knots*, Academic Press, New York, **1971**. (b) *Molecular Catenanes, Rotaxanes and Knots* (Eds. Sauvage, J.-P.; Dietrich-Buchecker, C.O.), VCH-Wiley, Weinheim, **1999**.
- 2 For reviews on catenanes and rotaxanes, see: (a) Walba, D.M. *Tetrahedron* **1985**, *41*, 3161–3212. (b) Dietrich-Buchecker, C.O.; Sauvage, J.-P. *Chem. Rev.* **1987**, *87*, 795–810. (c) Dietrich-Buchecker, C.O.; Sauvage, J.-P. *Bioorg. Chem. Front.* **1991**, *2*, 195–248. (d) Chambbron, J.-C.; Dietrich-Buchecker, C.O.; Sauvage, J.-P. *Top. Curr. Chem.* **1993**, *165*, 131–162. (e) Amabilino, D.B.; Stoddart, J.F. *Chem. Rev.* **1995**, *95*, 2725–2828. (f) Belohradsky, M.; Raymo, F.M.; Stoddart, J.F. *Collect. Czech. Chem. Commun.* **1996**, *61*, 1–43. (g) Fujita, M.; Ogura, K. *Coord. Chem. Rev.* **1996**, *148*, 249–264. (h) Belohradsky, M.; Raymo, F.M.; Stoddart, J.F. *Collect. Czech. Chem. Commun.* **1997**, *62*, 527–557. (i) Jäger, R.; Vögtle, F. *Angew. Chem., Int. Ed. Engl.* **1997**, *36*, 930–944. (j) Nepogodiev, S.A.; Stoddart, J.F. *Chem. Rev.* **1998**, *98*, 1959–1976. (k) Fujita, M. *Acc. Chem. Res.* **1999**, *32*, 53–61. (l) Breault, G.A.; Hunter, C.A.; Mayers, P.C. *Tetrahedron* **1999**, *55*, 5265–5293.
- 3 Wasserman E. *Molecular Catenanes, Rotaxanes and Knots* (Eds. Sauvage, J.-P.; Dietrich-Buchecker, C.O.), VCH-Wiley, Weinheim, **1999**, 1–6.
- 4 Wasserman E. *J. Am. Chem. Soc.*, **1960**, *82*, 4433–4434.
- 5 Schill, G.; Luttringhaus, A. *Angew. Chem., Int. Ed. Engl.* **1964**, *3*, 546–547.
- 6 Harrison, I.T.; Harrison, S. *J. Am. Chem. Soc.*, **1967**, *89*, 5723–5724.
- 7 Schill, G.; Zollenkopf, H. *Liebigs Ann. Chem.*, **1969**, *721*, 53–74.
- 8 (a) Vögtle, F. *Supramolecular Chemistry*, Wiley, New York, **1991**. (b) Lehn, J.-M. *Supramolecular Chemistry*, VCH, Weinheim, **1995**. (c) *Comprehensive Supramolecular Chemistry* (Eds. Lehn, J.-M.; Atwood, J.L.; Davies, J.E.D.; MacNicol, D.D.; Vögtle, F.), Pergamon, Oxford, **1996**.
- 9 For accounts and reviews on template-directed syntheses, see: (a) Busch, D.H.; Stephenson, N.A. *Coord. Chem. Rev.* **1990**, *100*, 119–154. (b) Lindsey, J.S. *New J. Chem.* **1991**, *15*, 153–180. (c) Whitesides, G.M.; Mathias, J.P.; Seto, C.T. *Science* **1991**, *254*, 1312–1319. (d) Philp, D.; Stoddart, J.F. *Synlett* **1991**, 445–458. (e) Busch, D.H. *J. Inclusion Phenom.* **1992**, *12*, 389–395. (f) Anderson, S.; Anderson, H.L.; Sanders, J.K.M. *Acc. Chem. Res.* **1993**, *26*, 469–475. (g) Cacciapaglia, R.; Mandolini, L. *Chem. Soc. Rev.* **1993**, *22*, 221–231. (h) Hoss, R.; Vögtle, F. *Angew. Chem., Int. Ed. Engl.* **1994**, *33*, 375–384. (i) Schneider, J.P.; Kelly, J.W. *Chem. Rev.* **1995**, *95*, 2169–2187. (j) Philp, D.; Stoddart, J.F. *Angew. Chem., Int. Ed. Engl.* **1996**, *35*, 1155–1196. (k) Raymo, F.M.; Stoddart, J.F. *Pure Appl. Chem.* **1996**, *68*, 313–322. (l) Fyfe, M.C.T.; Stoddart, J.F. *Acc. Chem. Res.* **1997**, *30*, 393–401. (m) Hubin, T.J.; Kolchinski, A.G.; Vance, A.L.; Busch, D.L. *Adv. Supramol. Chem.* **1999**, *5*, 237–357. (n) Hubin, T.J.; Busch, D.H. *Coord. Chem. Rev.* **2000**, *200*, 5–52. (o) Li, Z.T. *Chinese J. Org. Chem.* **2000**, *20*, 655–662.
- 10 For reviews on polycatenanes and polyrotaxanes, see: (a) Gibson, H.W.; Marand, H. *Adv. Mater.* **1993**, *5*, 11–21. (b) Gibson, H.W.; Bheda, M.C.; Engen, P.T. *Prog. Polym. Sci.* **1994**, *19*, 843–945. (c) Amabilino, D.B.; Parsons, I.W.; Stoddart, J.F. *Trends Polym. Sci.* **1994**, *2*, 146–152. (d) Gibson, H.W. *Large Ring Molecules*, Ed. Semlyen, J.A., Wiley, New York, **1996**, 191–202. (e) Raymo, F.M.; Stoddart, J.F. *Trends Polym. Sci.* **1996**, *4*, 208–211. (f) Raymo, F.M.; Stoddart, J.F. *Chem. Rev.* **1999**, *99*, 1643–1664.
- 11 For accounts, books, and reviews on switchable molecular and supramolecular systems, see: (a) Balzani, V.; Scandola, F. *Supramolecular Photochemistry*, Horwood, Chichester, **1991**. (b) Balzani, V. *Tetrahedron* **1992**, *48*, 10443–10514. (c) Bissell, R.A.; de Silva, A.P.; Gunaratne, H.Q.N.; Lynch, P.L.M.; Maguire, G.E.M.; McCoy, C.P.; Sandanayake, K.R.A.S. *Top. Curr. Chem.* **1993**, *168*, 223–264. (d) De Silva, A.P.; McCoy, C.P. *Chem. Ind.* **1994**, 992–996. (e) Fabbrizzi, L.; Poggi, A. *Chem. Soc. Rev.* **1995**, *24*, 197–202. (f) Shinkai, S. *Compr. Supramol. Chem.*, **1996**, *1*, 671–700. (g) de Silva, A.P.; Gunaratne, H.Q.N.; Gunnlaugsson, T.; Huxley, A.J.M.; McCoy, C.P.; Rademacher, J.T.; Rice, T.E. *Chem. Rev.* **1997**, *97*, 1515–1566. (h) Ward, M.D. *Chem. Ind.* **1997**, 640–645. (i) Beer, P.D. *Acc. Chem. Res.*

- 1998, 31, 71–80. (j) Boulas, P.L.; Gómez-Kaifer, M.; Echegoyen, L. *Angew. Chem. Int. Ed.* **1998**, 37, 216–247. (k) Bryce, M.R. *Adv. Mater.* **1999**, 11, 11–23. (l) Niemz, A.; Rotello, V.M. *Acc. Chem. Res.* **1999**, 32, 42–52. (m) Asanuma, H.; Hishiyama, T.; Komiyama, M. *Adv. Mater.* **2000**, 12, 1019–1030.
- 12 For accounts and reviews on switchable catenanes, rotaxanes, and pseudorotaxanes, see: (a) Stoddart, J.F. *Chem. Aus.* **1992**, 59, 576–577. (b) Preece, J.A.; Stoddart, J.F. *Nanobiology* **1994**, 3, 149–166. (c) Benniston, A.C. *Chem. Soc. Rev.* **1996**, 25, 427–435. (d) Gómez-López, M.; Preece, J.A.; Stoddart, J.F. *Nanotechnology* **1996**, 7, 183–192. (e) Balzani, V.; Gómez-López, M.; Stoddart, J.F. *Acc. Chem. Res.* **1998**, 31, 405–414. (f) Sauvage, J.-P. *Acc. Chem. Res.* **1998**, 31, 611–619. (g) Sauvage, J.-P. *Bull. Pol. Acad. Sci. Chem.* **1998**, 46, 289–307. (h) Chambron, J.-C.; Sauvage, J.-P. *Chem. Eur. J.* **1998**, 4, 1362–1366. (i) Kaifer, A.E. *Acc. Chem. Res.* **1999**, 32, 62–71. (j) Leigh, D.A.; Murphy, A. *Chem. Ind.* **1999**, 178–183. (k) Balzani, V.; Credi, A.; Raymo, F.M.; Stoddart, J.F. *Angew. Chem. Int. Ed.* **2000**, 39, 3349–3391. (l) Joachim, C.; Gimzewski, J.K.; Aviram, A. *Nature* **2000**, 408, 541–548.
- 13 (a) Sauvage, J.-P. *Acc. Chem. Res.* **1990**, 23, 319–327. (b) Chambron, J.-C.; Dietrich-Buchecker, C.O.; Hemmert, C.; Khemiss, A.K.; Mitchell, D.; Sauvage, J.-P.; Weiss, J. *Pure Appl. Chem.* **1990**, 62, 1027–1034. (c) Chambron, J.-C.; Chardon-Noblat, S.; Harri-man, A.; Heitz, V.; Sauvage, J.-P. *Pure Appl. Chem.* **1993**, 65, 2343–2349. (d) Chambron, J.-C.; Dietrich-Buchecker, C.O.; Nierengarten, J.-F.; Sauvage, J.-P. *Pure Appl. Chem.* **1994**, 66, 1543–1550. (e) Chambron, J.-C.; Dietrich-Buchecker, C.O.; Heitz, V.; Nierengarten, J.-F.; Sauvage, J.-P.; Pascard, C.; Guilhem, J. *Pure Appl. Chem.* **1995**, 67, 233–240.
- 14 (a) Dietrich-Buchecker, C.O.; Sauvage, J.-P.; Kintzinger, J.-P. *Tetrahedron Lett.* **1983**, 46, 5095–5098. (b) Dietrich-Buchecker, C.O.; Sauvage, J.-P.; Kern, J.-M. *J. Am. Chem. Soc.* **1984**, 106, 3043–3045. (c) Dietrich-Buchecker, C.O.; Sauvage, J.-P. *Tetrahedron* **1990**, 46, 503–512.
- 15 Albrecht-Gary, A.-M.; Saad, Z.; Dietrich-Buchecker, C.O.; Sauvage, J.-P. *J. Am. Chem. Soc.* **1985**, 107, 3205–3209.
- 16 For a definition of the term ‘co-conformation’, see: Fyfe, M.C.T.; Glink, P.T.; Menzer, S.; Stoddart, J.F.; White, A.J.P.; Williams, D.J. *Angew. Chem., Int. Ed. Engl.* **1997**, 36, 2068–2070.
- 17 Cesario, M.; Dietrich-Buchecker, C.O.; Guilhem, J.; Pascard, C.; Sauvage, J.-P. *J. Chem. Soc., Chem. Commun.* **1985**, 244–247.
- 18 Albrecht-Gary, A.-M.; Dietrich-Buchecker, C.O.; Saad, Z.; Sauvage, J.-P. *J. Am. Chem. Soc.* **1988**, 110, 1467–1472.
- 19 (a) Cesario, M.; Dietrich-Buchecker, C.O.; Edel, A.; Guilhem, J.; Kintzinger, J.-P.; Pascard, C.; Sauvage, J.-P. *J. Am. Chem. Soc.* **1986**, 108, 6250–6254. (b) Albrecht-Gary, A.-M.; Dietrich-Buchecker, C.O.; Saad, Z.; Sauvage, J.-P. *J. Chem. Soc., Chem. Commun.* **1992**, 280–282. (c) Armaroli, N.; De Cola, L.; Balzani, V.; Sauvage, J.-P.; Dietrich-Buchecker, C.O.; Kern, J.-M.; Bailal, A. *J. Chem. Soc., Dalton Trans.* **1993**, 3241–3246.
- 20 Similar co-conformational changes have been observed upon demetallation/metallation and upon demetallation/protonation of analogous phenanthroline-containing [3]catenanes, as well as upon demetallation/metallation of a phenanthroline-containing [2]catenane incorporating π -electron-rich and π -electron-deficient recognition sites. (a) Sauvage, J.-P.; Weiss, J. *J. Am. Chem. Soc.* **1985**, 107, 6108–6110. (b) Dietrich-Buchecker, C.O.; Khemiss, A.; Sauvage, J.-P. *J. Chem. Soc., Chem. Commun.* **1986**, 1376–1378. (c) Armaroli, N.; Balzani, V.; De Cola, L.; Hemmert, C.; Sauvage, J.-P. *New J. Chem.* **1994**, 18, 775–782. (d) Amabilino, D.B.; Dietrich-Buchecker, C.O.; Livoreil, A.; Pérez-García, L.; Sauvage, J.-P.; Stoddart, J.F. *J. Am. Chem. Soc.* **1996**, 118, 3905–3913.
- 21 (a) Livoreil, A.; Dietrich-Buchecker, C.O.; Sauvage, J.-P. *J. Am. Chem. Soc.* **1994**, 116, 9399–9400. (b) Livoreil, A.; Sauvage, J.-P.; Armaroli, N.; Balzani, V.; Flamigni, L.; Ventura, B. *J. Am. Chem. Soc.* **1997**, 119, 12114–12124.
- 22 Baumann, F.; Livoreil, A.; Kaim, W.; Sauvage, J.-P. *Chem. Commun.* **1997**, 35–36.
- 23 Cárdenas, D.; Livoreil, A.; Sauvage, J.-P. *J. Am. Chem. Soc.* **1996**, 118, 11980–11981.
- 24 (a) Gaviña, P.; Sauvage, J.-P. *Tetrahedron Lett.* **1997**, 38, 3521–3524. (b) Armaroli, N.; Balzani, V.; Collin, J.-P.; Gaviña, P.; Sauvage, J.-P.; Ventura, B. *J. Am. Chem. Soc.* **1999**, 121, 4397–4408.
- 25 Collin, J.-P.; Gaviña, P.; Sauvage, J.-P. *New J. Chem.* **1999**, 21, 525–528.

- 26 For a definition of the term 'molecular shuttle', see: Anelli, P.-L.; Spencer, N.; Stoddart, J.F. *J. Am. Chem. Soc.* **1991**, *113*, 5131–5133.
- 27 (a) Amabilino, D.B.; Stoddart, J.F. *Pure Appl. Chem.* **1993**, *65*, 2351–2359. (b) Pasini, D.; Raymo, F.M.; Stoddart, J.F. *Gazz. Chim. Ital.* **1995**, *125*, 431–435. (c) Langford, S.J.; Stoddart, J.F. *Pure Appl. Chem.* **1996**, *68*, 1255–1260. (d) Amabilino, D.B.; Raymo, F.M.; Stoddart, J.F. *Compr. Supramol. Chem.*, **1996**, *9*, 85–130. (e) Raymo, F.M.; Stoddart, J.F. *Pure Appl. Chem.* **1997**, *69*, 1987–1997. (f) Gillard, R.E.; Raymo, F.M.; Stoddart, J.F. *Chem. Eur. J.* **1997**, *3*, 1933–1940. (g) Raymo, F.M.; Stoddart, J.F. *Chemtracts* **1998**, *11*, 491–511.
- 28 (a) Ashton, P.R.; Ballardini, R.; Balzani, V.; Gandolfi, M.T.; Marquis, D.J.F.; Pérez-García, L.; Prodi, L.; Stoddart, J.F.; Venturi, M. *J. Chem. Soc., Chem. Commun.* **1994**, 177–180. (b) Ashton, P.R.; Ballardini, R.; Balzani, V.; Credi, A.; Gandolfi, M.T.; Menzer, S.; Pérez-García, L.; Prodi, L.; Stoddart, J.F.; Venturi, M.; White, A.J.P.; Williams, D.J. *J. Am. Chem. Soc.* **1995**, *117*, 11171–11197.
- 29 For the solvent-dependence of the translational isomerism associated with some catenanes and rotaxanes, see: (a) Ashton, P.R.; Blower, M.; Philp, D.; Spencer, N.; Stoddart, J.F.; Tolley, M.S. *New J. Chem.* **1993**, *17*, 689–695. (b) Ballardini, R.; Balzani, V.; Gandolfi, M.T.; Gillard, R.E.; Stoddart, J.F.; Tabellini, E. *Chem. Eur. J.* **1998**, *4*, 449–459. (c) Asakawa, M.; Ashton, P.R.; Dehaen, W.; L'abbé, G.; Menzer, S.; Nouwen, J.; Raymo, F.M.; Stoddart, J.F.; Tolley, M.S.; Toppet, S.; White, A.J.P.; Williams, D.J. *Chem. Eur. J.* **1997**, *3*, 772–787. (d) Leigh, D.A.; Moody, K.; Smart, J.P.; Watson, K.J.; Slawin, A.M.Z. *Angew. Chem., Int. Ed. Engl.* **1996**, *35*, 306–310. (e) Lane, A.X.; Leigh, D.A.; Murphy, A. *J. Am. Chem. Soc.* **1997**, *119*, 11092–11093. (f) Clegg, W.; Gimenez-Saiz, C.; Leigh, D.A.; Murphy, A.; Slawin, A.M.Z.; Teat, S.J. *J. Am. Chem. Soc.* **1999**, *121*, 4124–4129. (g) Gong, C.; Gibson, H.W. *Angew. Chem., Int. Ed. Engl.* **1997**, *36*, 2331–2333.
- 30 (a) Asakawa, M.; Ashton, P.R.; Balzani, V.; Credi, A.; Hamers, C.; Mattersteig, G.; Montalti, M.; Shipway, A.N.; Spencer, N.; Stoddart, J.F.; Tolley, M.S.; Venturi, M.; White, A.J.P.; Williams, D.J. *Angew. Chem., Int. Ed.* **1998**, *37*, 333–337. (b) Balzani, V.; Credi, A.; Mattersteig, G.; Matthews, O.A.; Raymo, F.M.; Stoddart, J.F.; Venturi, M.; White, A.J.P.; Williams, D.J. *J. Org. Chem.* **2000**, *65*, 1924–1936.
- 31 (a) Gunter, M.J.; Johnston, M.R. *J. Chem. Soc., Chem. Commun.* **1992**, 1163–1165. (b) Gunter, M.J.; Hockless, D.C.R.; Johnston, M.R.; Skelton, B.W.; White, A.H. *J. Am. Chem. Soc.* **1994**, *116*, 4810–4823.
- 32 Gunter, M.J.; Johnston, M.R. *J. Chem. Soc., Chem. Commun.* **1994**, 829–830.
- 33 For related photoactive [2]rotaxanes, see: (a) Benniston, A.C.; Harriman, A. *Angew. Chem., Int. Ed. Engl.* **1993**, *32*, 1459–1461. (b) Benniston, A.C.; Harriman, A.; Lynch, V.M. *Tetrahedron Lett.* **1994**, *35*, 1473–1476. (c) Benniston, A.C.; Harriman, A.; Lynch, V.M. *J. Am. Chem. Soc.* **1995**, *117*, 5275–5291.
- 34 Bissell, R.A.; Córdova, E.; Kaifer, A.E.; Stoddart, J.F. *Nature* **1994**, *369*, 133–137.
- 35 Ballardini, R.; Balzani, V.; Dehaen, W.; Dell'Erba, A.E.; Raymo, F.M.; Stoddart, J.F.; Venturi, M. *Eur. J. Org. Chem.* **2000**, 591–602.
- 36 (a) Martínez-Díaz, M.-V.; Spencer, N.; Stoddart, J.F. *Angew. Chem., Int. Ed. Engl.* **1997**, *36*, 1904–1907. (b) Ashton, P.R.; Ballardini, R.; Balzani, V.; Baxter, I.; Credi, A.; Fyfe, M.C.T.; Gandolfi, M.T.; Gómez-López, M.; Martínez-Díaz, M.-V.; Piersanti, A.; Spencer, N.; Stoddart, J.F.; Venturi, M.; White, A.J.P.; Williams, D.J. *J. Am. Chem. Soc.* **1998**, *120*, 11932–11942.
- 37 For examples of cyclodextrin-containing rotaxanes, see: (a) Stoddart, J.F. *Angew. Chem., Int. Ed. Engl.* **1992**, *31*, 846–848. (b) Wylie, R.S.; Macartney, D.H. *J. Am. Chem. Soc.* **1992**, *114*, 3136–3138. (c) Ogino, H. *New J. Chem.* **1993**, *17*, 683–688. (d) Wenz, G.; Wolf, F.; Wagner, M.; Kubik, S.; *New J. Chem.* **1993**, *17*, 729–738. (e) Isnin, R.; Kaifer, A.E. *Pure Appl. Chem.* **1993**, *65*, 495–498. (f) Harada, A. *Polym. News* **1993**, *18*, 358–363. (g) Harada, A.; Li, J.; Kamachi, M. *Proc. Jpn. Acad.* **1993**, *69*, 39–44. (h) Wylie, R.S.; Macartney, D.H. *Supramol. Chem.* **1993**, *3*, 29–35. (i) Wenz, G. *Angew. Chem., Int. Ed. Engl.* **1994**, *33*, 802–822. (j) Anderson, S.; Anderson, H.L. *Angew. Chem., Int. Ed. Engl.* **1996**, *35*, 1956–1959. (k) Harada, A. *Coord. Chem. Rev.* **1996**, *148*, 115–133. (l) Macartney, D.H. *J. Chem. Soc., Perkin Trans. 2* **1996**, 2775–2778. (m) Harada, A. *Large Ring Molecules*, Ed. J. A. Semlyen, Wiley, New York, **1996**, 406–432. (n) Harada, A. *Supramol. Sci.*, **1996**, *3*, 19–23. (o) Harada, A. *Adv. Polym.* **1997**,

- 133, 142–191. (p) Anderson, S.; Claridge, T.D.W.; Anderson, H.L. *Angew. Chem., Int. Ed. Engl.* **1997**, *36*, 1310–1313. (q) Harada, A. *Carbohydr. Polym.* **1997**, *34*, 183–188. (r) Lyon, A.P.; Macartney, D.H. *Inorg. Chem.* **1997**, *36*, 729–736. (s) Harada, A. *Acta Polym.* **1998**, *49*, 3–17. (t) Anderson, S.; Clegg, W.; Anderson, H.L. *Chem. Commun.* **1998**, 2379–2380. (u) Anderson, A.; Aplin, R.T.; Claridge, T.D.W.; Goodson III, T.; Maciel, A.C.; Rumbles, G.; Ryan, J.F.; Anderson, H.L. *J. Chem. Soc., Perkin Trans. 1* **1998**, 2383–2397.
- 38** Murakami, H.; Kawabuchi, A.; Kotoo, K.; Kunitake, M.; Nakashima, N. *J. Am. Chem. Soc.* **1997**, *119*, 7605–7606.
- 39** de Silva, A.P.; Gunaratne, H.Q.N.; McCoy, C.P. *Nature* **1993**, *364*, 42–44
- 40** Credi, A.; Balzani, V.; Langford, S.J.; Stoddart, J.F. *J. Am. Chem. Soc.* **1997**, *119*, 2679–2681.
- 41** Asakawa, M.; Ashton, P.R.; Balzani, V.; Credi, A.; Mattersteig, G.; Matthews, O.A.; Montalti, M.; Spencer, N.; Stoddart, J.F.; Venturi, M. *Chem. Eur. J.* **1997**, *3*, 1992–1996.
- 42** (a) Ahuja, R.C.; Caruso, P.L.; Mobius, D.; Philp, D.; Preece, J.A.; Ringsdorf, H.; Stoddart, J.F.; Wildburg, G. *Thin Solid Films* **1996**, *285*, 671–677. (b) Arnabilino, D.B.; Asakawa, M.; Ashton, P.R.; Ballardini, R.; Balzani, V.; Belohradsky, M.; Credi, A.; Higuchi, M.; Raymo, F.M.; Shimizu, T.; Stoddart, J.F.; Venturi, M.; Yase, K. *New J. Chem.*, **1998**, 959–972.
- 43** (a) Collier, C.P.; Wong, E.W.; Belohradsky, M.; Raymo, F.M.; Stoddart, J.F.; Kuekes, P.J.; Williams, R.S.; Heath, J.R. *Science*, **1999**, *285*, 391–394. (b) Wong, E.W.; Collier, C.P.; Belohradsky, M.; Raymo, F.M.; Stoddart, J.F.; Heath, J.R. *J. Am. Chem. Soc.* **2000**, *122*, 5831–5840.
- 44** (a) Asakawa, M.; Higuchi, M.; Mattersteig, G.; Nakamura, T.; Pease, A.R.; Raymo, F.M.; Shimizu, T.; Stoddart, J.F. *Adv. Mater.* **2000**, *12*, 1099–1102. (b) Collier, C.P.; Mattersteig, G.; Wong, E.W.; Lou, Y.; Beverly, K.; Sampaio, J.; Raymo, F.M.; Stoddart, J.F.; Heath, J.R. *Science* **2000**, *289*, 1172–1175.

8

Metallo-Rotaxanes and Catenanes as Redox Switches: Towards Molecular Machines and Motors

Jean-Paul Collin, Jean-Marc Kern, Laurence Raehm, and Jean-Pierre Sauvage

8.1

Introduction

8.1.1

Generalities Regarding Machines and Motors

Although controlled molecular motions have been known for many years, existing in a very large variety of compounds ranging from purely organic structures to inorganic complexes, the field of „molecular machines and motors“ is just emerging. Today, molecular chemists are consciously designing and constructing molecular ensembles that will undergo some particular form of motion under the influence of an external physical or chemical signal.

Molecules possessing shapes that can be modified from the outside by sending some form of signal to the system are, of course, numerous. However, „molecular machines“ tends to refer to *large-amplitude* motions resulting in real translocation of some parts of the compound, reversibility being an essential feature of the system.

In order for an object to be regarded as a motor, several basic requirements have to be fulfilled. Even without trying to apply a strict thermodynamic definition, the system will have to convert a certain type of energy into another form of energy, while undergoing some kind of continuous motion.

8.1.2

Proteins Undergoing Folding–Defolding Processes

Both natural and synthetic proteins have been shown to undergo large conformational changes under the action of a variety of signals; a recent issue of *Accounts of Chemical Research* has been devoted to „Protein Folding“.^[1] Cytochrome c (cyt c) has been used in many studies,^[2–6] because of its simplicity and due to the fact that its three-dimensional structure is known.^[7] Another important advantage of cyt c lies in the reversible nature of the folding-defolding processes.

Particularly relevant to this chapter is work done on protein folding triggered by electron transfer. This electron transfer step can be either electrochemical^[8] or photochemical using such means as $\text{Ru}(\text{bipy})_3^{2+}$ in its ³MLCL excited state as an elec-

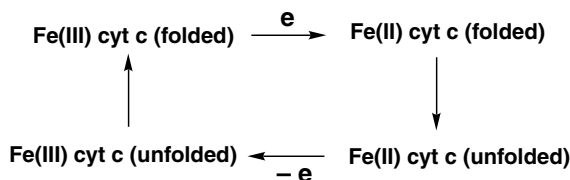


Fig. 1: Simplified view of the redox-triggered folding-defolding process in cyt c.

tron donor (bipy = 2,2'-bipyridine ; MLCT = metal-to-ligand charge transfer). The main advantage of the photochemical method is that it allows fast reduction of the heme iron(III) state of cyt c.^[8]

The following square scheme (Figure 1) gives a simplified view of the redox-triggered folding-defolding process:^[8]

Addition of increasing concentrations of guanidinium chloride favors the unfolded form of ferri cyt c (Fe(III)), due to binding to the iron center by chloride.

The conformational changes seen in cyt c are based on principles very similar to those operating in the metallo-rotaxanes and catenanes discussed in this paper. To a large extent, the geometry of the enzyme is determined by the coordination of various ligands to the iron center of the heme, and modification of the redox state of the metal (Fe(III)/Fe(II)) will induce rearrangement through ligation changes.

Reversible chemical oxidation reactions have also been used to control and modulate the conformation of polypeptide chains.^[9,10] By converting methionine to its sulfoxide, Gellman and co-workers were able to control the secondary structure of an 18-residue peptide. The side chain of a methionine residue (containing a CH₂CH₂SCH₃ fragment) is hydrophobic and favors α -helical folding. Oxidation to the methionine sulfoxide state results in a preference for a β -strand situation.

8.1.3

Biological Molecular Motors

Molecular motors of various kinds are very common in biology.^[11] Roughly, biological motors can be classified into two families: linear and rotary motors. The most classical examples of linear motors are the myosin-actin complex^[12-15] present in muscles and the kinesin-containing system.^[16-17] Rotary motors have recently attracted much attention since the extremely common enzyme ATP synthase^[18-22] has been shown to behave in a fashion reminiscent of a rotary motor. A „shaft“ (γ protein) rotates inside a hollow stator ($\alpha_3\beta_3$ aggregate of six proteins, Figure 2), this spinning motion inducing formation of ATP from ADP and inorganic phosphate (3 moles per round).

Another example of a rotary motor is that of bacterial flagella,^[23] which are responsible for bacterial motility.

Very generally, the creation of molecules that, under the action of an external signal, can change their shape or position in space, or in which certain components can be set into motion at will is a challenging target, both in relation to natural systems mimics, but also as components of long-term potential information storage or processing devices.

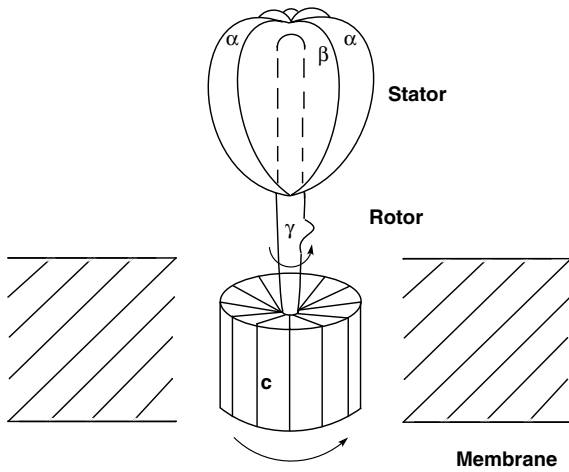


Fig. 2: A schematic representation of ATP synthase, a biological rotary motor, γ (and c) are mobile whereas the aggregate $\alpha\beta$ is fixed to the membrane and constitutes the stator of the motor.

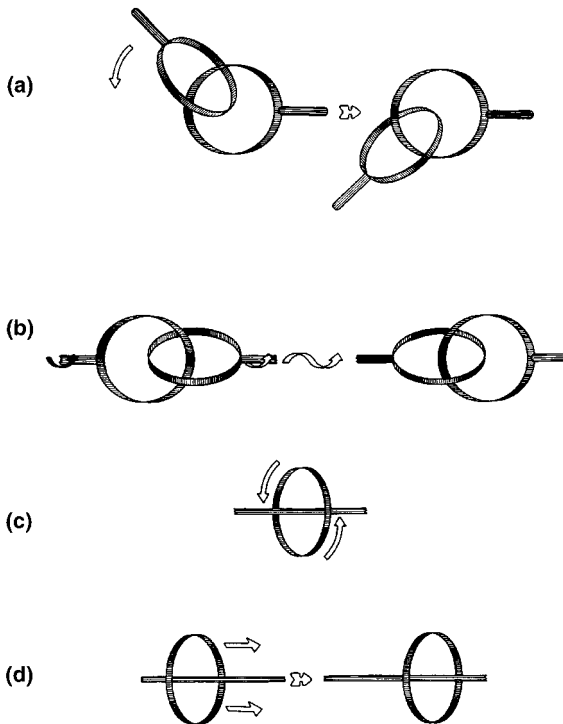


Fig. 3: Interlocking rings and threaded systems can be considered as elemental working components of future molecular machines. (a) A prototype molecular „ball and socket“ joint. (b) A crude „universal joint“: the action

of twisting the axle on the left clockwise is followed by the effect of rotating the right hand axle, due to the mechanical action of one ring on the other. (c) A wheel and axle in action. (d) Lateral movement of a ring on an axle.

Compounds containing interlocking rings (catenanes) or rings threaded on an acyclic fragment are ideal precursors to molecular machines^[24–26] and motors. The interlocking and threaded topologies provide the working components of the machines and motors to be elaborated, as represented schematically in Figure 3.

8.1.4

Previously Described Synthetic Systems based on Purely Organic Components

Photochemistry offers many examples of large-scale movement at the molecular level. The *cis*–*trans* isomerization^[27–33] of an azo group is a very attractive process for modification of the geometry and the properties of compounds, although several other photochemical reactions can be utilized,^[34–37] including the photoisomerization of stilbene-like compounds.

A chemical signal can also be used, as in the recently described „molecular brake“.^[38] In this case, rather than its shape, it is more the motion dynamic properties of the compound (rotation of a group about a C–C bond) that are modified, by addition of a transition metal.

Stoddart's group has recently created a new and vast family of interlocking and threaded compounds constructed on acceptor-donor aromatic complexes.^[39] This remarkable synthetic work has been sustained by very elegant photochemical and electrochemical studies carried out, respectively, by the groups of Balzani^[40–43] and Kaifer.^[44] These have demonstrated that molecular movements can be induced in such systems, either by irradiating the compounds with visible light in the presence of other additional reagents, or by using electrochemical reactions. A few recent examples of molecules undergoing large-amplitude photochemically or electrochemically driven conformational changes are indicated in Figure 4.

8.1.5

Motion in Transition Metal-based Molecules

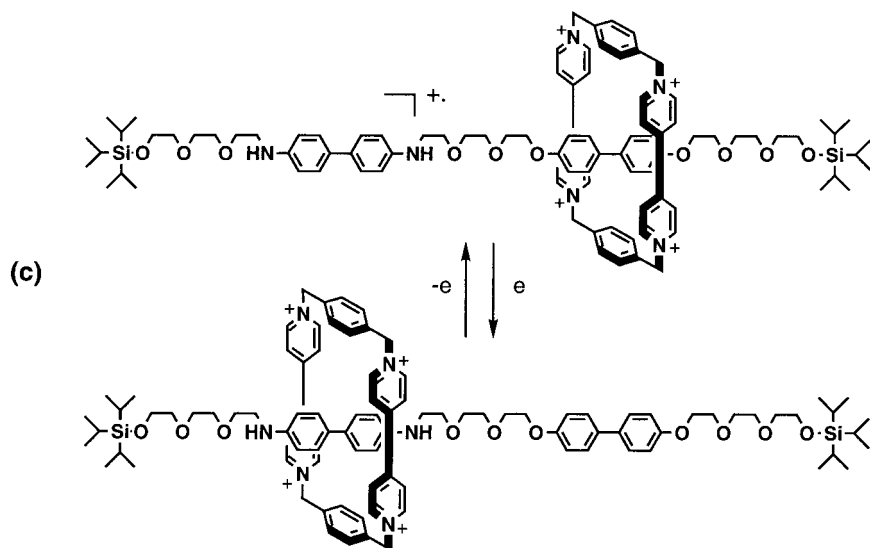
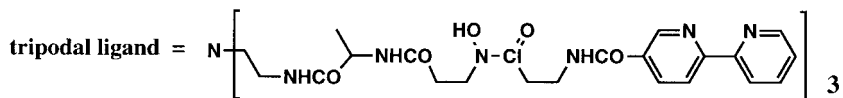
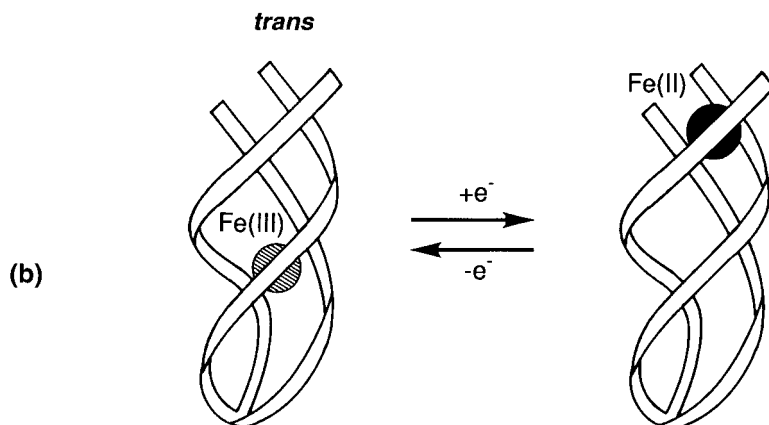
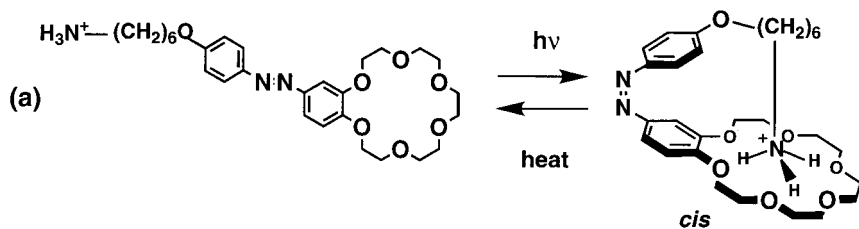
Inorganic systems featuring linkage isomerism induced by changing the oxidation state of a metal are also known.^[45–56] For instance, a sulfoxide is O-bonded to ruthenium(III) in its stable form (Ru-OSR₂). On reduction of the metal to the divalent state, the initially obtained O-bonded species rearranges to afford the stable S-

Fig. 4: A few examples of machine-like compounds, able to undergo drastic geometrical changes under the action of an external signal. In some cases, this shape modification induces new properties and is followed by a subsequent reaction.

(a) Photoresponsive crown ether^[31] whose ammonium group can complex the coordination site („tail-biting“) in the *cis* form, thus partly masking the ability of the crown to bind and extract alkali cations. As expected, the *trans* isomer has much better complexation power.

(b) Hopping of an iron center between two ligands of the 2,2'-bipyridine type. After oxidation to Fe(III), the metal center moves to the anionic site (left).^[57]

(c) A switchable rotaxane based on acceptor-donor complexes.^[44] Before oxidation (bottom), the electron acceptor (ring) interacts preferentially with the benzidine nucleus (donor). After electrochemical oxidation of the latter, the ring is shifted towards the biphenol group. The process is reversible.



bonded complex $[\text{Ru-S}(\text{O})\text{R}_2]$. In an elegant study, Taube and Sano have shown that this principle can result in molecular hysteresis.^[52–56] Another pertinent example of redox-induced movement is based on a multifunctional system incorporating sets of ligands forming two distinct coordination sites, adapted to either $\text{Fe}(\text{II})$ or $\text{Fe}(\text{III})$.^[57,58] On changing the iron oxidation state, translocation of the metal is observed (Figure 4b). Another interesting example is that of anion translocation, as recently reported by Fabbrizzi et al.^[59] In a heterometallic trinuclear compound consisting of two nickel(II) cyclam-like fragments covalently attached to a central copper(II) bipy complex (bipy = 2,2'-bipyridine), the anion (N_3^- , SCN^- , or OCN^-) is preferably bound to the copper center. Electrochemical oxidation of nickel(II) to nickel(III) triggers motion of the anion, which jumps from the central copper onto one of the peripheral nickel(III) centers.

8.2

Rotaxanes Containing Transition Metals: From Electronic to Molecular Motion

8.2.1

Photoinduced Intramolecular Electron Transfer Within Porphyrinic Rotaxanes

Rotaxanes can be defined as molecular systems consisting of a “string” threaded through one or more rings, the two ends of the string bearing bulky groups acting as stoppers and preventing the molecular string from unthreading.^[60]

In making rotaxanes usable as parts of molecular devices and with the purpose of studying long range electron transfer processes within large molecular systems of well controlled geometries, the introduction of photoactive and electroactive compounds has been a valuable development. Photoinduced electron transfer between porphyrin species has a particular relevance to the primary events occurring in bacterial photosynthetic reaction center complexes, and so is a well studied phenomenon.

Molecular systems in which two porphyrins are held apart by a covalently linked spacer function give rise to bis-porphyrins with flexible or constrained geometries. Rotaxane architectures incorporating similar or dissimilar porphyrins as stoppers have been widely developed in our group, with the goal of building such systems capable of allowing modulation of electron transfer.

With the aim of mimicking structurally^[61] and functionally the association of cofactors SP / BPh (SP is a bacteriochlorophyll dimer called ‘Special Pair’ and BPh is a bacteriopheophytin) in the reaction center^[62–67] of the bacterium *Rhodospseudomonas viridis*, bis-porphyrin **1** was synthesized^[68,69] (Figure 5). Compound **1** is composed of zinc (II) and gold (III) mesotetraaryl porphyrins, separated by the rigid 2,9-diphenyl-1,10-phenanthroline (dpp) spacer. Zn (II) porphyrin is a powerful reductant in its singlet excited state ($E^0(\text{Zn}(\text{II})\text{P}^{\bullet+} / * \text{Zn}(\text{II})\text{P}) = -1.44 \text{ V}$), while the ground state of the Au (III) porphyrin is easily reduced ($E^0(\text{Au}(\text{III})\text{P}^+ / \text{Au}(\text{III})\text{P}^\bullet) = -0.59 \text{ V}$).

Specifically, light excitation of SP leads to very fast electron transfer to BPh, within 3 ps. In bis-porphyrin **1**, the electron donor (the zinc porphyrin) is in its sing-

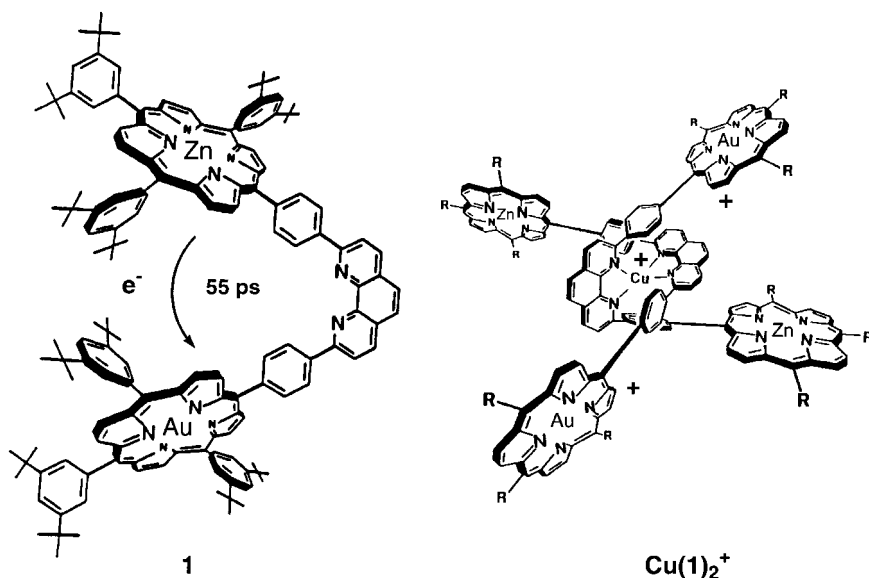


Fig. 5: a) A synthetic model **1** of the natural system. SP and BPh are mimicked by a zinc(II) and a gold(III) porphyrin, respectively, bridged by a dpp spacer. b) Complex $\text{Cu}(1)_2^+$

let excited state, and the electron acceptor (the gold porphyrin) in its ground state. The latter is also a very poor energy acceptor. Accordingly, photoinduced intramolecular electron transfer was shown to occur,^[70] and to take place in 55 ps.

The dpp core is a good ligand for Cu(I), and it was possible to prepare the corresponding $\text{Cu}(1)_2^+$ complex.^[70] In this complex, the two porphyrin-bearing ligands are entwined around the metal center. For this type of complex, NMR and crystallographic studies clearly showed that the dpp core of one coordinating subunit was inside the cleft formed by the other bis-porphyrin dpp ligand. Here, again, electron transfer occurs between the zinc and the gold porphyrin, but its rate increases dramatically (17 times faster). Moreover, the rate found (3 ps) is close to that observed in the natural system!

In order to explain this increase in electron transfer rate and to elucidate which pathway was followed (intra- or interligand), a rotaxane structure was elaborated^[71,72] (Figure 6). Here, the principle of construction of the architecture was again based on the 3-dimensional template effect of copper (I).

The homoleptic $\text{Cu}(1)_2^+$ complex and the bis-porphyrinic rotaxane 2^+ both incorporate the same coordinating core: $\text{Cu}(\text{dpp})_2^+$. In the rotaxane, one of the coordinating moieties (dpp) is incorporated in a macrocycle, which plays the role of a wheel. The second coordinating core is incorporated in the molecular thread – the axle of the rotaxane – the two ends of which bear the gold and the zinc porphyrin, respectively.

Figure 7 illustrates the principle of the construction of this [2]-rotaxane, which bears two different porphyrin stoppers.

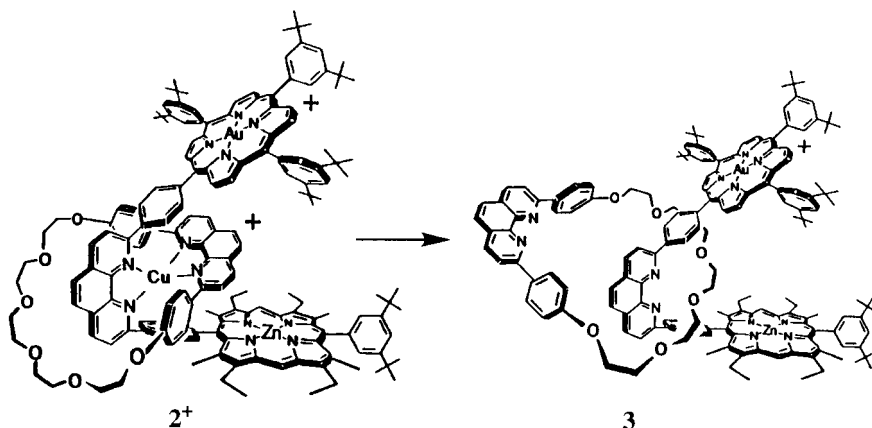


Fig. 6: Cu(I)-complexed [2]-rotaxane **2** and demetallated [2]-rotaxane **3**, bearing metalloporphyrins as stoppers.

This copper rotaxane could be demetallated, producing the free rotaxane **3** (Figure 6). As observed in some other cases, the demetallation reaction was accompanied by a pirouetting of the macrocycle, moving its dpp chelate outside the cleft formed by the porphyrin stoppers.^[73,74] In fact, free rotaxane **3** and bis-porphyrin thread **1** differ mainly in the fact that, in **3**, ligand **1** is mechanically incarcerated in macrocycle **4**.

The rates of photoinduced electron transfer between the zinc porphyrin and the gold(III) porphyrin are 1.7 ps for the Cu(I)-complexed [2]-rotaxane, and 36 ps for

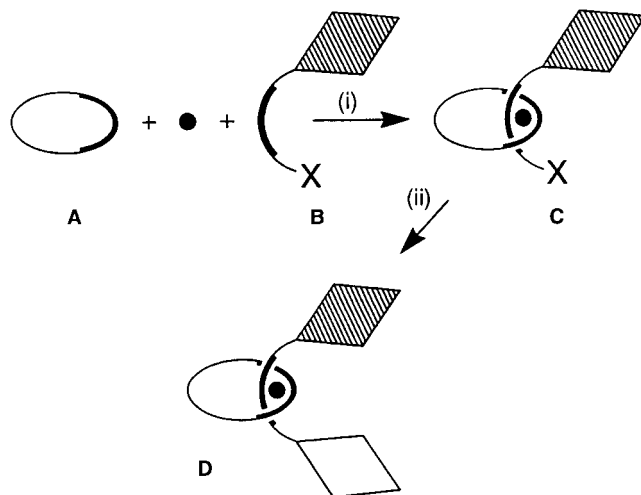


Fig. 7: Principle of transition metal-templated construction of a [2]-rotaxane with two different porphyrin stoppers. The white diamond is a zinc porphyrin, and the hatched diamond is a gold porphyrin. The black disk is Cu(I).
(i) Macrocycle **A** is threaded onto chelate **B**,

end-blocked by a porphyrin at one extremity and functionalized with a reactive group **X**, which is a precursor to the second porphyrin stopper, affording prerotaxane **C**; (ii) construction of the second porphyrin, resulting in metal-complexed [2]-rotaxane **D**.

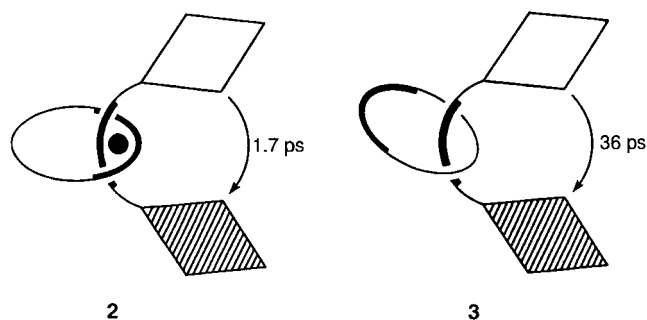


Fig. 8: Schematic representation of the electron transfer events occurring in copper(I)-complexed and template-free [2]-rotaxanes **2** and **3** (same conventions as in Figure 7).

the free [2]-rotaxane^[75–77] (Figure 8). Therefore, what had initially been observed in the case of the homoleptic complex $\text{Cu}(\text{I})_2^+$ was corroborated by the Cu(I)-complexed [2]-rotaxane, suggesting that, in the former molecule, electron transfer can take place between porphyrins of the same ligand. The rate obtained for the free [2]-rotaxane was consistent with that found for the bis-porphyrin conjugate **1** (the difference arising from a slightly more exergonic process in the case of the [2]-rotaxane).

The increase in the rate of electron transfer arising from coordination of Cu(I) to the dpp bridging chelate was interpreted in terms of the superexchange effect.^[78–80] If it is assumed that the electron transfer is a through-bond process, then coordination of Cu(I) to the dpp spacer reduces the energy of the LUMO of this bridge and therefore increases the electronic coupling between the excited state of the zinc porphyrin and the ground state of the gold porphyrin electron acceptor.^[77]

This work was carried out in the context of a study of models of photosynthesis. Rotaxanes revealed themselves to be particularly interesting systems, in which it is possible to modulate the magnitude of electronic coupling between the photoactive porphyrin stoppers.

8.2.2

Lateral Translation of a Ring on the Molecular String on which it is Threaded: Electrochemically-driven Motion

The synthetic strategy developed in our group for making rotaxanes relies on the ability of copper(I) to attract two constituent organic fragments (a ring incorporating a bidentate chelate and an open chain component) together, and to force the string to thread through the ring. This threading step is generally quantitative, provided that the stoichiometry of the reaction is carefully respected, thanks to the selective formation of very stable, tetrahedral copper(I) complexes (Figure 9(a)). It can be extended to strings containing two identical coordination sites, thus permitting the threading of two identical rings (Figure 9 (b)).^[81,82] It can also be generalized to molecular strings containing two *different* sites, such as bidentate and terdentate

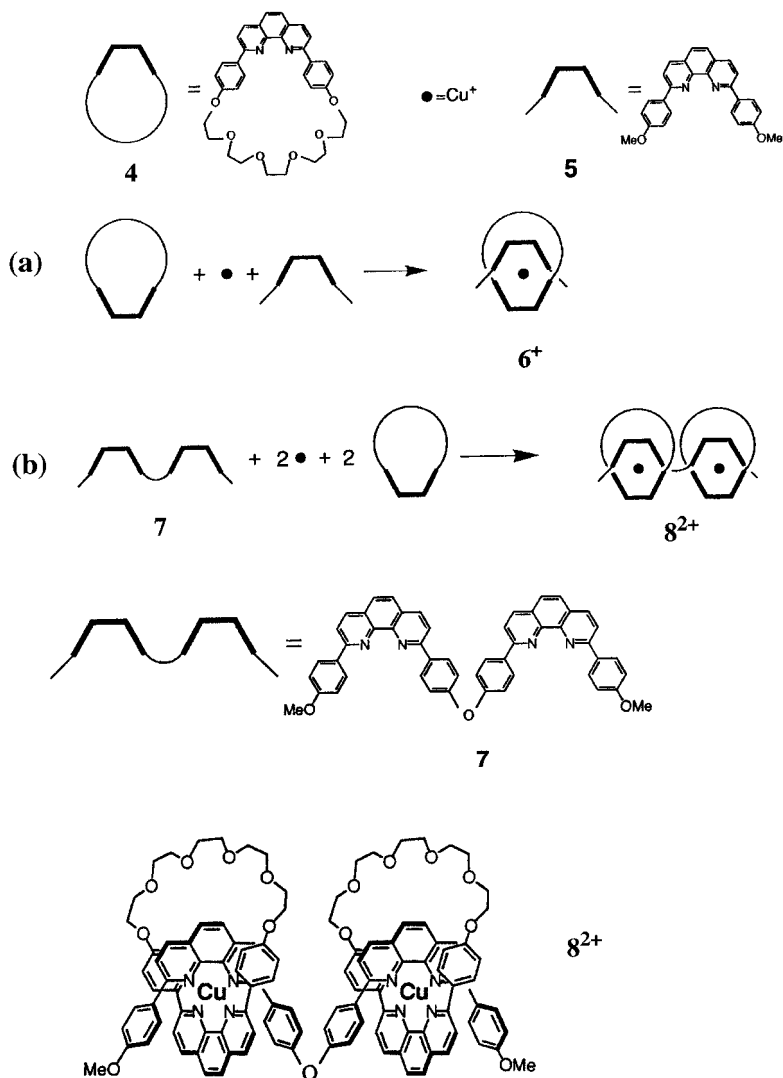


Fig. 9 (a) and (b): Copper(I)-induced threading of one or two rings onto a molecular string. Compound 4 is a 30-membered ring, containing a bidentate ligand.

(a) The acyclic fragment 5 is a simple phenanthroline derivative. This threading process has been used in our group since the early 1980s to make catenanes.^[88]

(b) The string 7 now incorporates two identical bidentate units; as in (a), the process is quantitative.^[82]

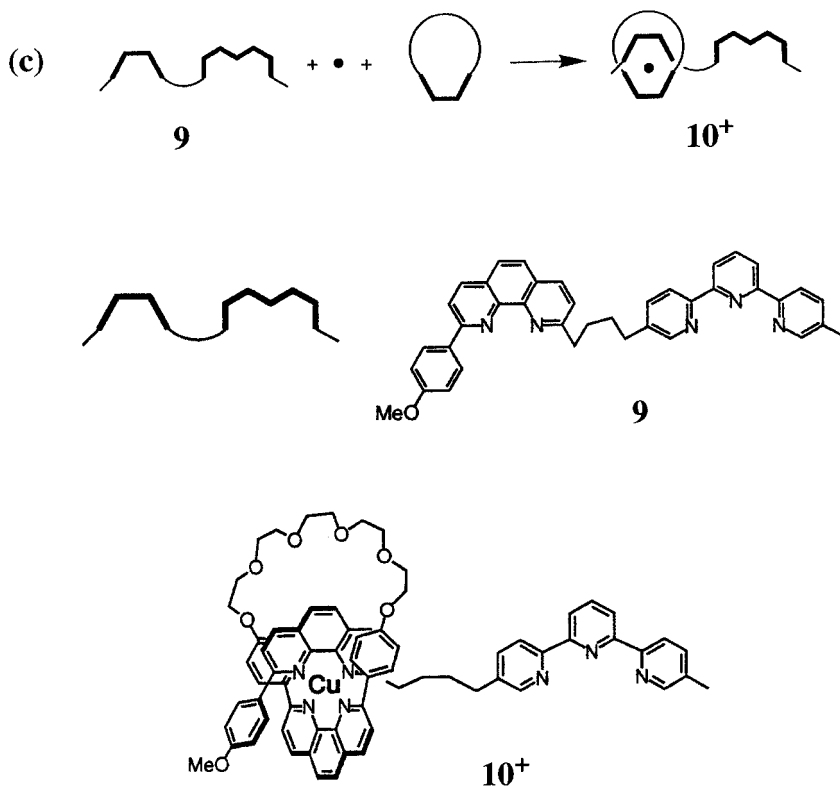


Fig. 9 (c): A slightly more complex case: the acyclic component contains both a bidentate ligand and a terdentate coordinating unit

(2,2',6',2''-terpyridine). With copper(II) as gathering metal, exclusive formation of the 4-coordinate complex **10⁺** is observed.

coordinating units (Figure 9 (c)). In this case, again because of the very strong preference of copper(I) for tetracoordinate complexes (tetrahedral or distorted tetrahedral), the threading process will be very selective and result in a situation in which the ring is exclusively associated with the bidentate chelate fragment of the string, through its coordination to copper(I), as indicated in Figure 9(c).^[83]

It is, of course, this last compound that will be prompted to undergo motion on changing the redox state. This particular system, and all the other „molecular machines“ elaborated and studied in our group, function on the same principle. Of the first row transition metal ions, copper displays unusual features regarding the geometrical properties of its complexes. The stereoelectronic requirements of copper(I) and copper(II) are markedly different, and this characteristic provides the driving force for setting our systems into motion. Whereas a coordination number (CN) of 4, usually with a roughly tetrahedral arrangement of ligands, suits stable, monovalent systems, copper(II) requires higher coordination numbers. The most commonly encountered copper(II) complexes have CNs of 5 (square pyramidal or trigonal bipyramidal geometries) or 6 (octahedral arrangement, with Jahn-

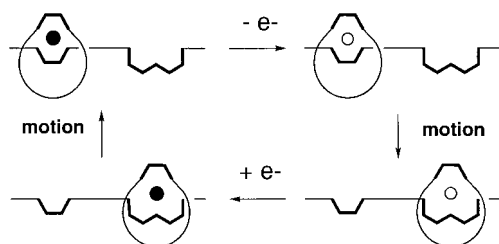


Fig. 10: Principle behind electrochemically induced molecular motion in a copper(I) complex pseudorotaxane. The stable, four-coordinate, monovalent complex is oxidized to an intermediate tetrahedral, divalent species. This compound undergoes a rearrangement to afford the stable, five-coordinate

copper(II) complex. Upon reduction, the five-coordinate, monovalent state is formed as a transient species. Finally, this undergoes the reorganization process that regenerates the starting complex (the black circle represents Cu^{I} and the white circle represents Cu^{II}).

Teller distortion). Thus, by switching alternatively from copper(I) to copper(II), it should be possible to induce changes in the molecule so as to afford a coordination environment favorable to the corresponding oxidation state. The principle is illustrated in Figure 10,^[83] using the threaded system of Figure 9, (c).

Of course, if the acyclic molecular fragment that threads the ring does not bear blocking groups at its ends, unthreading may occur. This is indeed observed in polar solvents (CH_3CN), mostly at the 2+ stage, affording a bis-terpy-like (terpy=2,2',6',2''-terpyridine) complex obtained when two strings are taken up by the same copper(II) center. The obvious improvement is to attach one or, better, two bulky groups at the extremities of the string in order to prevent unthreading.^[84] These new systems are represented in Figure 11.

The semi-rotaxane was obtained simply by mixing stoichiometric amounts of **11** (which is an improved version of **9** (Figure 9b)), $\text{Cu}(\text{CH}_3\text{CN})_4^+$, and **4** (Figure 9a). If, in **11**, the OCH_3 group attached to the phen unit of the string (phen = 1,10-phenanthroline) is replaced by a phenol function (**12**), threading will lead to a 13^+ -type compound, with a reactive end. Activation of the $-\text{OH}$ function and covalent attachment of the blocking group affords the real rotaxane **14**⁺. (It is real in the sense that demetallation furnishes a copper-free system (**15**) with an acyclic component that will not unthread from the 30-membered ring.)

The electrochemical behavior of **14**⁺ is particularly clean and interesting, since only the 4- and the 5-coordinate geometries can be obtained on translating the metal-complexed ring from the phen site to the terpy site.^[84] The electrochemically induced molecular motions (square scheme^[85]), similar to those represented in Figure 10 but now involving “stopped” compounds, can be monitored by cyclic voltammetry (CV) and controlled potential electrolysis experiments.^[85]

From CV measurements at different scan rates (from 0.005 to 2 Vs^{-1}) on both the copper(I) and the copper(II) species, it could be inferred that the chemical steps (movements of the ring from the phenanthroline to the terpyridine and vice-versa) are slow on the timescale of the experiments. As the two redox couples involved in these systems are separated by 0.7 V, the concentration of the species

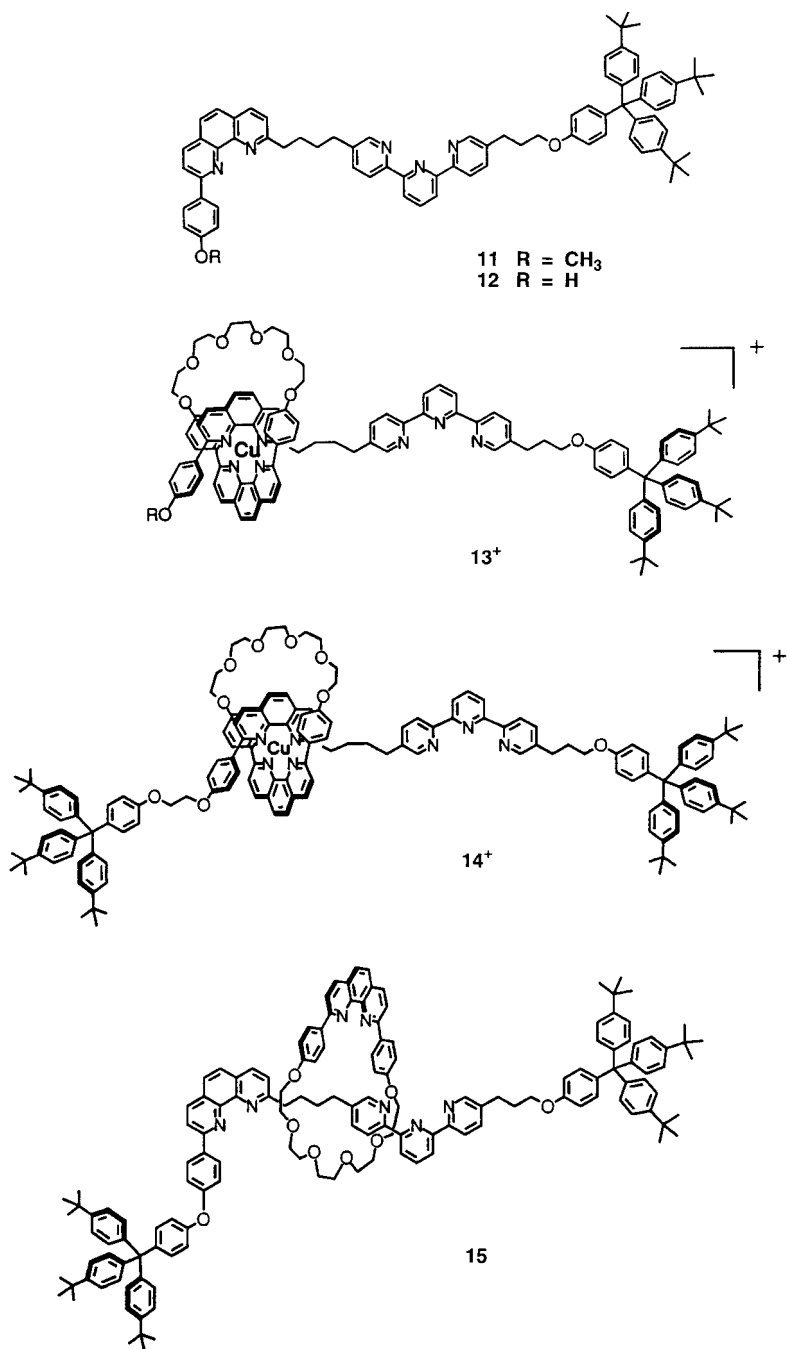


Fig. 11: The semi-rotaxane 13^+ , the real copper-containing rotaxane 14^+ and the demetallated rotaxane **15**.

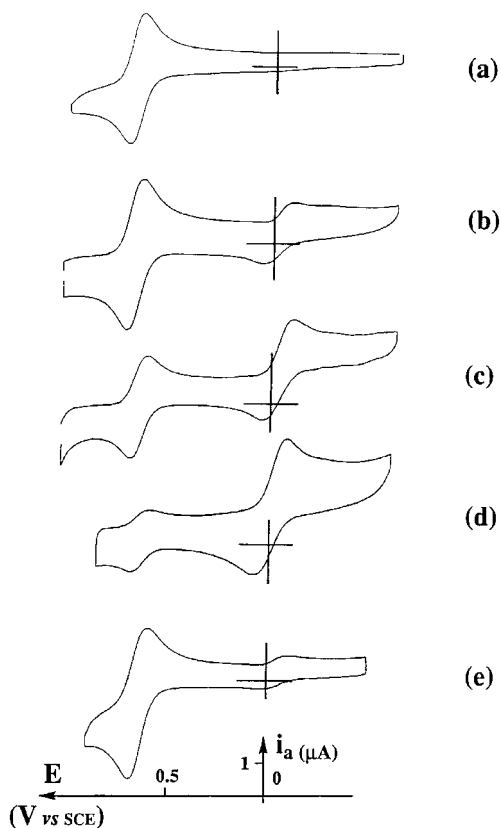


Fig. 12: a) Cyclic voltammogram of 14^+ ; b) after electrolysis for 1 h at +1.0 V; c) and d) evolution of a 14^{2+} solution with time [after 2 h (c) and after 4 h (d)]; (e) cyclic voltammogram immediately after electrolysis of 14^{2+} solution at -0.3 V. Conditions: MeCN (0.1M, $n\text{-Bu}_4\text{NBF}_4$), Pt electrode, $v = 100 \text{ mVs}^{-1}$, 25°C .

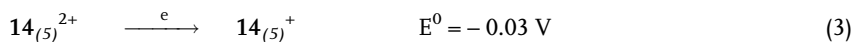
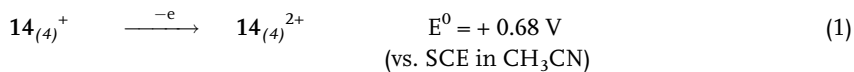
in each environment (tetracoordination or pentacoordination) can be directly deduced from the peak intensities of the redox signals. Figure 12 displays some voltammograms (curves a–e) obtained on different oxidation states of the rotaxane 14^+ at different times.

Curve (a) displays the voltammogram of a (red) solution of 14^+ in degassed acetonitrile. A reversible redox wave at 0.68 V (versus SCE) attests to the tetrahedral environment around the copper(I) atom.^[86,87] During the potential scan, for rates between 0.005 and 2 Vs^{-1} , no redox signal corresponding to pentacoordination could be observed. This fact is evidence of the high kinetic stability of the tetra-coordinate copper(II) rotaxane generated at the electrode. At this stage, a controlled potential electrolysis (applied potential = $+1.0 \text{ V}$) was performed until one Faraday per mole of complex had been exchanged. During the electrolysis, the red color of the solution changed to light green. Immediately after the coulometry, the voltammogram of the

copper(II) species (curve b) showed the same redox couple at +0.68 V and an additional small reversible couple at -0.03 V. These signals are characteristic of the $\text{Cu}^{\text{II}}_{(4)}/\text{Cu}^{\text{I}}_{(4)}$ and $\text{Cu}^{\text{II}}_{(5)}/\text{Cu}^{\text{I}}_{(5)}$ couples, respectively (the subscripts 4 and 5 indicate the coordination number of the copper center).^[86,87] After several hours at room temperature, without any visible color change, the progressive disappearance of the redox couple at +0.68 V (tetracoordinate state) and the concomitant growth of the couple at -0.03 V (pentacoordinate state) evidences the coordination change around the copper(II) ion (curves c and d). Analysis of the concentration of the two different copper(II) species with time produces a first-order rate constant of $1.5 \times 10^{-4} \text{ s}^{-1}$ for the chemical reaction: $\text{Cu}^{\text{II}}_{(4)} \rightarrow \text{Cu}^{\text{II}}_{(5)}$. From the invariance in the shape of the signals with the scan rate of the copper(II) solution, it can be inferred that the rate constant for the reaction $\text{Cu}^{\text{I}}_{(5)}$ to $\text{Cu}^{\text{I}}_{(4)}$ is smaller than 10^{-2} s^{-1} . Subsequent second electrolysis at -0.3 V restores the initial red solution. The voltammogram (curve e) performed immediately after the reductive electrolysis displays the redox couple of 14^+ and is invariant with time. As all the $\text{Cu}^{\text{I}}_{(5)}$ species formed electrochemically are quantitatively transformed into $\text{Cu}^{\text{I}}_{(4)}$ species during the electrolysis, a lower limit of 10^{-4} s^{-1} is reasonable for the rate constant of the chemical reaction. The residual signal at -0.03 V simply reflects incomplete electrolysis.

The behavior of the systems comprised of the semirotaxane 13^{+} ^[83,84] is related to that of the fully blocked rotaxane 14^+ , i.e., the same redox couple can be observed. Some variations of peak intensities with the scan rate also indicate an acceleration of the chemical processes as compared to 14^+ . However, additional signals corresponding to the species $\text{Cu}^{\text{I}}(\text{MeCN})_4^+$ ($E_{1/2} = +1.02 \text{ V}$) and $\text{Cu}^{\text{II}}_{(6)}$ (hexacoordinate state, $E_{1/2} = -0.41 \text{ V}$)^[87] show that the unthreading process becomes significant and occurs primarily with the copper(II) species. The hexacoordinate complex evidenced by CV originates from the unthreading of two linear fragments and their coordination to a copper center through their terpy units.

It is noteworthy that oxidation of 14^+ to the divalent copper(II) state exclusively affords the pentacoordinate species after rearrangement of the system. The bis-terpy complex, which would be formed by decomplexation of the copper(II) center and recoordination to the terpy fragments of two different molecules of **15**, is not detected. This observation is important in relation to the general mechanism of the changeover step in converting a tetracoordinate Cu(II) species ($\text{Cu}(\text{II})_{(4)}$) into the corresponding, stable 5-coordinate complex ($\text{Cu}(\text{II})_{(5)}$) (the subscripts 4 and 5 indicate the coordination number of the copper center). It tends to indicate that the conversion does not involve full demetallation of $\text{Cu}(\text{II})_{(4)}$ followed by recomplexation, but is rather an intramolecular reaction, probably consisting of several elementary dissociation-association steps involving the phen and terpy fragments of the string as well as solvent molecules and, possibly, counterions. The square scheme involving the fully blocked rotaxanes 14^{n+} ($n = 1$ or 2) corresponds to the following sequence of reactions:



8.2.3

Towards Rotary Motors: Pirouetting of a Two-coordinate Ring on its Thread

Previous sections have discussed the gliding motion of one ring around another (Figure 3a, 3b) in the case of a catenane,^[86] or translational motion along a molecular thread (Figure 3d) in the case of a rotaxane.^[84] We will now consider a rotaxane in which a new type of motion, pirouetting of the wheel around its axle (Figure 13), can be triggered electrochemically.

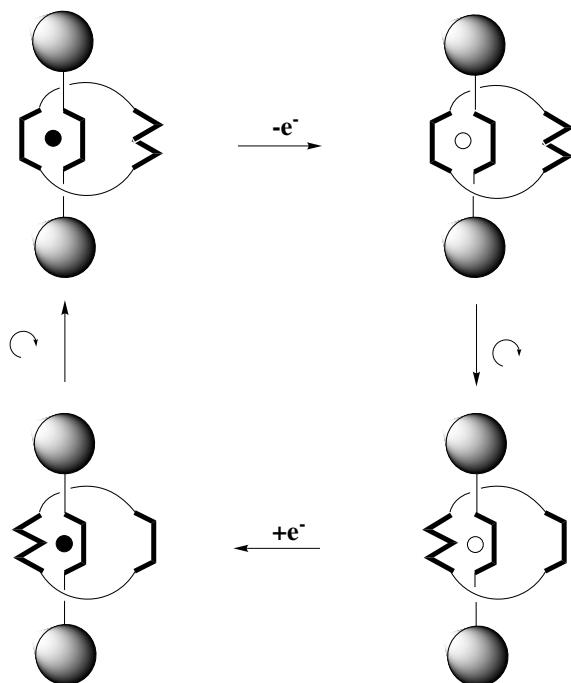


Fig. 13: Principle of the electrochemically induced molecular motion in a rotaxane copper complex. The stable, four-coordinate monovalent complex is oxidized to an intermediate tetrahedral divalent species. This compound undergoes a rearrangement to afford the stable, five-coordinate copper(II) complex.

Upon reduction, the five-coordinate monovalent state is formed as transient. Finally, this undergoes the reorganization process that regenerates the starting complex (the black circle represents Cu^I and the white circle represents Cu^{II}).

The driving force of this motion here is again based on the different geometrical preferences of Cu(I) and Cu(II). In this case, however, the wheel of the rotaxane is a bis-coordinating macrocycle and the axle incorporates only one bidentate moiety.

The three-dimensional template effect of Cu(I), first reported over fifteen years ago, made catenanes, rotaxanes, and related systems reasonably easily accessible from a preparative point of view.^[88–90] The strategy leading to the preparation of catenanes is based on a precursor consisting of two phenanthroline-type ligands entwined around a Cu(I) center. In the case in which one of these ligands is macrocyclic, the structure of the precursor is singular: the acyclic ligand is threaded through the macrocycle. Treatment of the terminal functions of the acyclic ligand of this complex with an appropriate difunctionalized molecular fragment results in the formation of a catenane, while treating them with two monofunctionalized and bulky fragments produces a rotaxane.

The principle of the synthesis is as described earlier, slightly modified by application of an alternative strategy consisting of the use of a monostoppered species to form the prerotaxane intermediate and the subsequent addition of the second stopper (Figure 14). The advantage of this method is that it limits unthreading of the macrocycle during the stopping reaction.

The rotaxane $16_{(4)}^+$ (the rotaxane nomenclature used here is $16_{(N)}^{n+}$, where N refers to the coordination number of the metal (4 or 5) and n to its charge) synthesized here is composed of two subunits: a macrocycle and a molecular thread (Figure 15). The macrocycle^[86] **17** (Figure 15 (a) and (b)) possesses two different coordi-

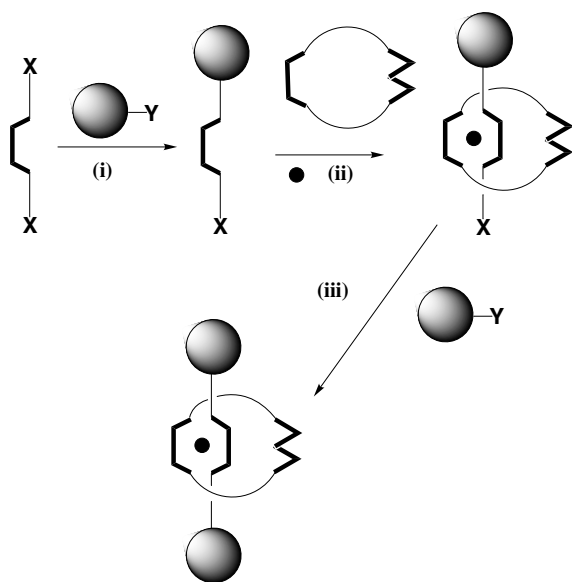


Fig. 14: Principle of the synthesis of rotaxane $16_{(4)}^+$ (see Figure 15). (i) Formation of a monostoppered axle. (ii) Threading of the axle through the wheel. (iii) Unthreading of the macrocycle is prevented by adding a second blocking group.

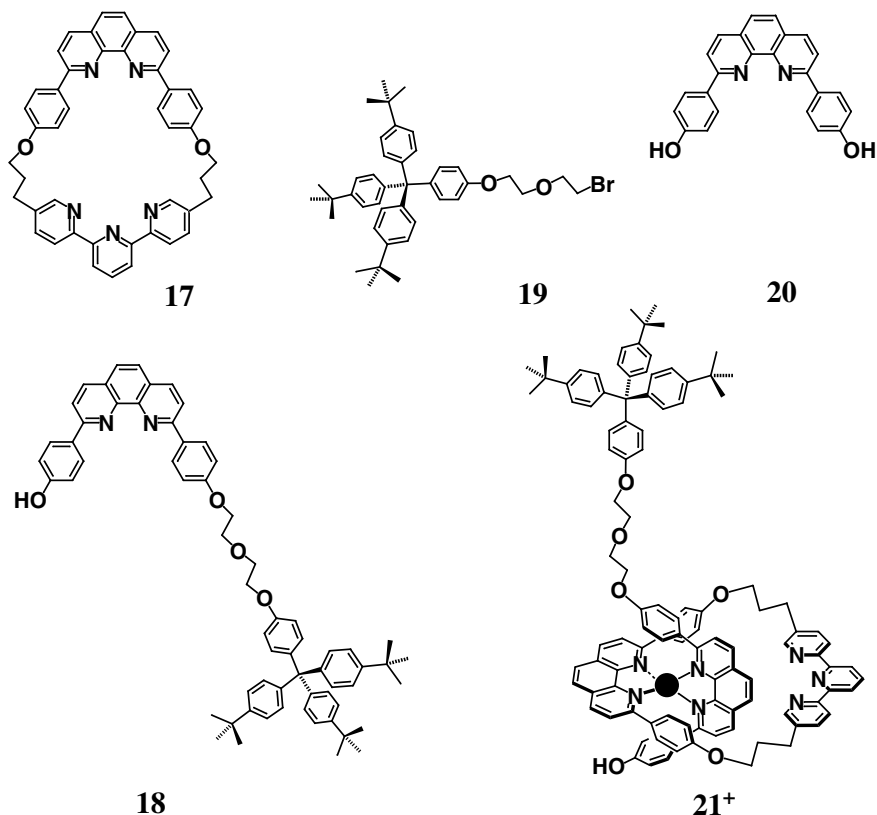


Fig. 15 (a): Molecular representation of the precursors of the metallated rotaxane **16**₍₄₎⁺.

nating sites: a terpyridine and a 1,10-phenanthroline moiety. A phenanthroline moiety in which the α -positions of the coordinating atoms were substituted with phenyl groups (2,9-diphenyl-1,10-phenanthroline, „dpp“) was used. It has been shown that low oxidation states are strongly stabilized in dpp-based transition metal complexes; this is particularly true for copper complexes.^[91] The two units are joined by two C₃ chains, which are linked to the 5- and 5'-positions of the terpyridine on one side and on the other side through oxygen atoms to the 4- and 4'-positions of the phenyl groups attached to phenanthroline. The resulting macrocycle is 33-membered.

The monostoppered thread **18** was obtained by treating the electrophile **19** with a large excess of 2, 9-di(*p*-hydroxyphenyl)-1,10-phenanthroline^[92] **20** in basic medium. These last species were selected as blocking groups since they are large enough to prevent unthreading of the 33-membered ring **17**. In order to lessen solubility problems, lipophilic groups (*t*-butyl fragments) were introduced at the *para* positions of three of the aryl groups. The stoppers and the coordinating site are linked through bisethoxy-ether spacers.

The monostoppered thread **18** was obtained by treating the electrophile **19** with a large excess of 2, 9-di(*p*-hydroxyphenyl)-1,10-phenanthroline^[92] **20** in basic medium.

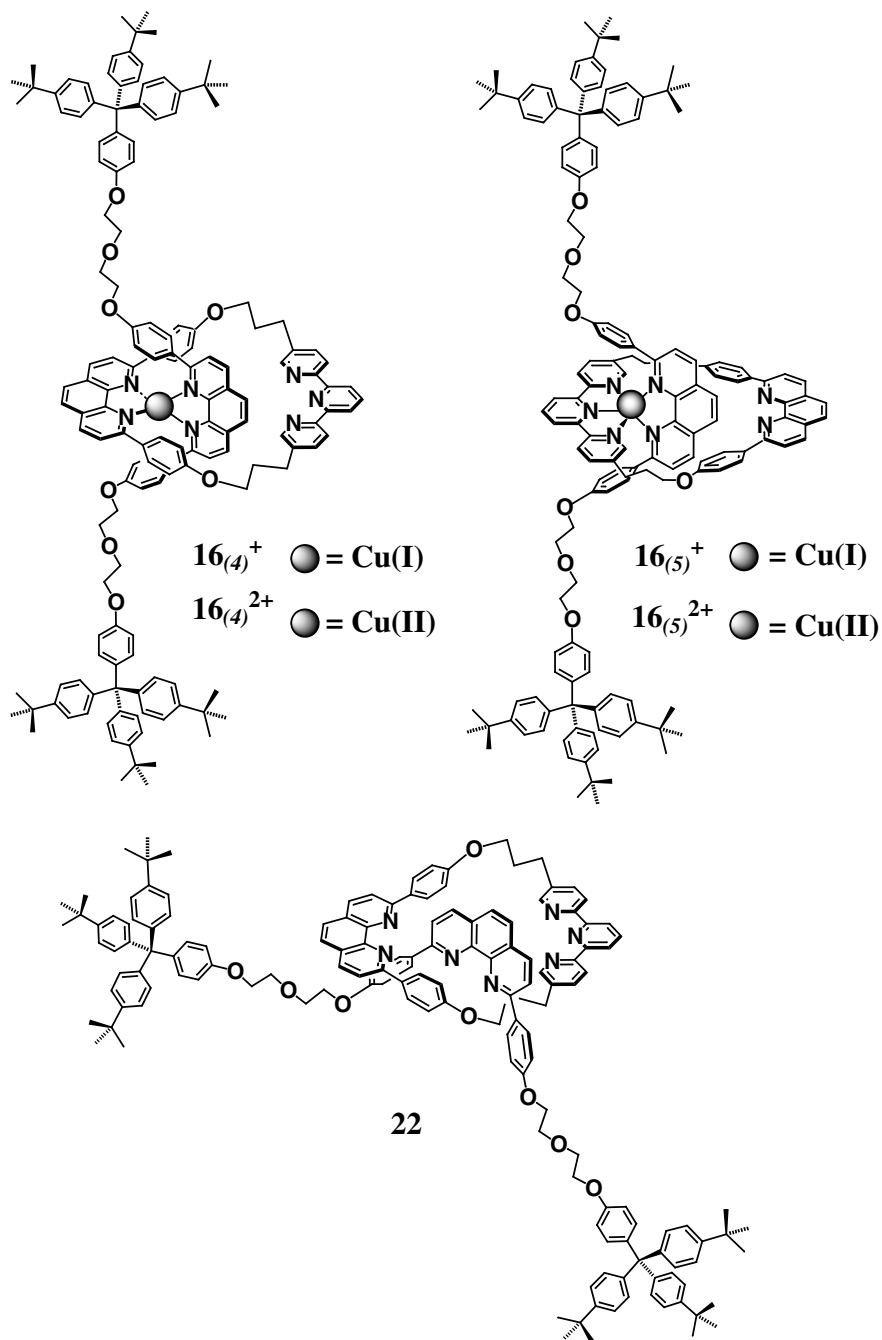


Fig. 15 (b): Molecular representation of the metallated rotaxanes $16_{(4)}^+$, $16_{(5)}^+$, $16_{(4)}^{2+}$, $16_{(5)}^{2+}$ and of the metal-free rotaxane **22**.

The powerful template effect of Cu(I) was exploited to force the threading of **18** through the hetero bis-chelating macrocycle **17**, producing prerotaxane **21**⁺.

The completion of the synthesis of the fully blocked rotaxane **16**₍₄₎⁺ was performed by treating **21**⁺ with **19**. Cu(I) complex rotaxane could easily be demetalated.^[92] by reaction with cyanide, producing rotaxane **22**, with free coordination sites. Transformation of the free rotaxane **22** into the Cu(I) complex **16**₍₅₎²⁺ was accomplished by metallation of **22** with Cu(BF₄)₂.

The electrochemical behavior of tetracoordinated Cu(I) complexes (i.e., Cu(dpp)₂-based cores) is well established.^[93,94] The reversible redox potential for the Cu(II)/Cu(I) transition is around 0.6–0.7 V versus SCE. This relatively high potential underlines the stability of the 4-coordinate Cu(I) complexes relative to their Cu(II) counterparts. The redox potential of pentacoordinated copper complexes^[84,86] is observed in a much more cathodic range. For example, for the 5-coordinate complex Cu(1, dap)^{2+/+} (dap = 2,9-di-*p*-anisyl-1,10-phenanthroline), in which the terpy fragment of the ring is bound to the metal, the redox potential is –0.035 V. This potential shift when going from tetracoordinated to pentacoordinated copper systems is due to the better stabilization of the Cu(II) state, thanks to the presence in the coordination sphere of five donor atoms.

8.2.3.1 Electrochemical Behavior of Chemically Isolated **16**₍₄₎⁺ and **16**₍₅₎²⁺

The electrochemical behavior of **16**₍₄₎⁺ in a CH₂Cl₂–CH₃CN solution has been studied by cyclic voltammetry (CV) and is represented in Figure 16 a). A reversible signal appears at 0.545 V.

In the rotaxane **16**₍₄₎⁺, in which the metal is tetracoordinated, the signal occurring at 0.54 V corresponds to the tetracoordinated Cu(II)/Cu(I) couple. The ratio of the intensi-

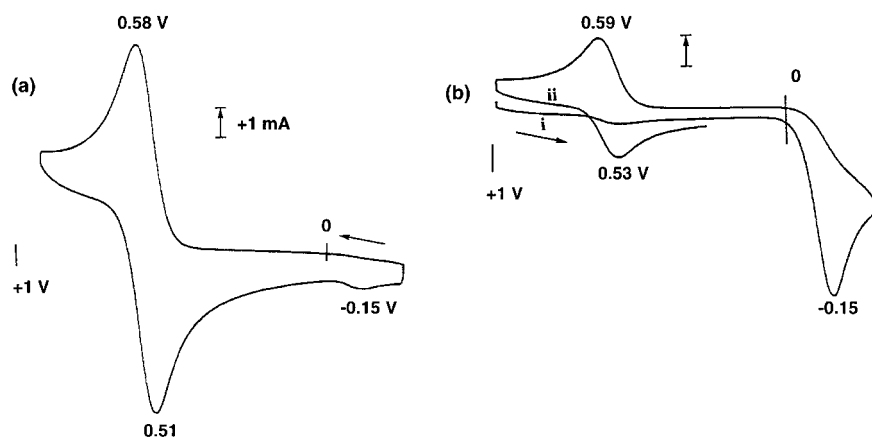


Fig. 16: Cyclic voltammograms recorded using a Pt working electrode at a 100 mV s⁻¹ sweep rate (CH₃CN–CH₂Cl₂ 4:1, supporting electrolyte: tetrabutylammonium tetrafluoro-

borate, 0.1 mol L⁻¹, Ag wire pseudo-reference). (a) Compound **16**₍₄₎⁺ (b) Chemically prepared **16**₍₅₎²⁺. Curve (ii) refers to a second potential sweep immediately following the first one (i).

ties of the anodic and cathodic peaks i_{pc}/i_{pa} is 0.95 (i_{pc} and i_{pa} respectively being the intensities of the cathodic and anodic peaks), showing that no transformation or reorganization of the coordination sphere of the tetracoordinated Cu(II) complex occurs in the timescale of the measurements (sweep rate of potential : $100 \text{ mV}\cdot\text{s}^{-1}$). The weak signal at -0.15 V is due to the presence of small amounts of $\mathbf{16}_{(5)}^{2+}$.

The cyclic voltammetric behavior of the Cu(II) rotaxane $\mathbf{16}_{(5)}^{2+}$ (Figure 16 b) is very different from that of $\mathbf{16}_{(4)}^+$. The potential sweep for the measurement was started at $+0.9 \text{ V}$, a potential at which no electron transfer should occur, whatever the surroundings of the central Cu(II) might be (pentacoordinated or tetracoordinated). Curve (i) (first scan, recorded at 100 mV s^{-1}) shows two cathodic peaks: one very small one, located at $+0.53 \text{ V}$, followed by an intense one at -0.15 V . Only one anodic peak, at 0.59 V , appears during the reverse sweep. If a second scan (ii) immediately follows the first one (i), the intensity of the cathodic peak at 0.53 V increases noticeably.

The weak peak at 0.53 V (i) is due to the presence of small quantities of $\mathbf{16}_{(4)}^+$. The main cathodic peak at -0.15 V is characteristic of pentacoordinated Cu(II). Thus, in $\mathbf{16}_{(5)}^{2+}$ prepared from the free rotaxane by metallation with Cu(II) ions, the central metal is coordinated to the terdentate terpyridine of the wheel and to the bidentate dpp of the axle. On the other hand, the irreversibility of this peak means that the pentacoordinated Cu(II) species formed in the diffusion layer when sweeping cathodically is transformed very rapidly and in any case before the electrode potential again becomes more anodic than the potential of the pentacoordinated $\text{Cu}^{2+}/\text{Cu}^+$ redox system. The irreversible character of the wave at -0.15 V and the appearance of an anodic peak at the value of $+0.53 \text{ V}$ indicates that the transient species, formed by reduction of $\mathbf{16}_{(5)}^{2+}$, has undergone a complete reorganization, producing a tetracoordinated copper rotaxane. The second scan (ii) which immediately follows the first one (i) confirms this assertion. Indeed, a cathodic peak ($+0.53 \text{ V}$) has appeared, corresponding to the reduction of this tetracoordinated species.

These two complementary cyclic voltammetry experiments confirm that, in this rotaxane, as in related systems studied previously, the tetracoordinated Cu(I) state is more stable than the pentacoordinated one and the pentacoordinated Cu(II) state is more stable than the tetracoordinated one. Moreover, it was observed that the rearrangement rates from the less stable to the most stable geometries are drastically different for the two oxidation states of the metal.

The irreversibility of the reduction peak of $\mathbf{16}_{(5)}^{2+}$, combined with the appearance of a reversible peak corresponding to tetracoordinated copper, suggests that the reorganization of the rotaxane in its pentacoordinated form $\mathbf{16}_{(5)}^+$ (i.e., with the copper coordinated to terpy and to dpp units) to its tetracoordinated form ($\mathbf{16}_{(4)}^+$, in which the copper is surrounded by two dpp units) occurs within the timescale of the cyclic voltammetry. Indeed, the cyclic voltammetry response located at -0.15 V becomes progressively reversible when increasing the potential sweep rate, as expected for an electrochemical process in which an electron transfer is followed by an irreversible chemical reaction (EC). Following the method of Nicholson and Shain,^[95] the rate constant value, k , of the chemical reaction, i.e., the transformation of pentacoordinated Cu(II) into tetracoordinated Cu(I), was determined. A value of 17 s^{-1} was

found for k , corresponding to a half-life $t_{1/2}$ of 56 ms for the pentacoordinated Cu(I) complex.

On the other hand, Figure 16 a) testifies to the inertness of the reorganization of the tetracoordinated Cu(II) rotaxane. Thus, a total conversion of tetracoordinated $16_{(4)}^+$ into tetracoordinated $16_{(4)}^{2+}$ was performed by preparative electrolysis and the subsequent rearrangement of tetracoordinated $16_{(4)}^{2+}$ into pentacoordinated $16_{(5)}^{2+}$ was followed by monitoring the current (versus time) flowing through a rotating disk electrode polarized at +0.3 V. Indeed, at that potential, the cathodic current observed is representative of the presence and concentration of $16_{(4)}^{2+}$, the tetracoordinated Cu(II) complex only. This remains true even if the electrolytic solution contains tetracoordinated $16_{(4)}^+$, which will be electrochemically silent in the potential range used.

Current versus time was recorded and an exponential decrease in the intensity of the current was observed. When the current was close to 0, a new cyclic voltammetry curve of the solution was recorded, resulting in a voltammogram similar to the one represented in Figure 16 b). This confirmed that the electrogenerated tetracoordinated Cu(II) rotaxane had undergone a rearrangement to form the pentacoordinated Cu(II) rotaxane $16_{(5)}^{2+}$.

The kinetic constant, k' , of this rearrangement can be derived from the variation of the cathodic current versus time; its average value is $0.007 \pm 0.003 \text{ s}^{-1}$. In other words, the half-life of tetracoordinated Cu(II) rotaxane is $120 \pm 50 \text{ s}$.

These experiments underline the noticeable difference between the kinetic rate constants k and k' for the reorganization processes leading respectively from $16_{(5)}^+$ to $16_{(4)}^+$ and from $16_{(4)}^{2+}$ to $16_{(5)}^{2+}$. Indeed, the ratio k/k' is about 3000. In analogous systems studied previously,^[84,86] an important difference between the related rate constants had also been observed. Nevertheless, for the systems based on a copper [2]-catenate (see below), in which one of the macrocycles is monochelating and the other hetero-bischelating, the two processes are much slower. For the rotaxane^[84] (see above) in which the axle is a hetero-bischelating molecular thread and the wheel a monochelating macrocycle, the reorganization processes implying a translation of the ring along the string, the values determined for k and k' are respectively 10^{-2} and $1.5 \times 10^{-4} \text{ s}^{-1}$. Thus, on comparison with the rate constant values determined for the rotaxane studied in this work ($k = 17$ and $k' = 0.007 \text{ s}^{-1}$), it appears that the pirouetting, induced by changing the redox state of the central metal, of a macrocycle around its axle is also faster than the translation of a macrocycle along a molecular thread, using the same triggering process.

These different types of molecular motion – gliding, translation, and pirouetting – are possible thanks to the kinetic lability of copper complexes. As mentioned above, the k/k' ratio is high in all the cases studied so far, which means that the reorganization process around Cu(I) is much faster than that around Cu(II). Both rearrangements require a decoordination step in one of the chelates, followed by recomplexation by the other chelate. The activation barrier to this decoordination step might be higher for the process from tetracoordinated Cu(II) to pentacoordinated Cu(II) than for that from pentacoordinated Cu(I) to tetracoordinated Cu(I), due to the greater electronic requirements of Cu(II). Thus, the difference

in molecular motion rates induced by changing the redox state of the metal might be partially attributed to ligand field effects.

8.3

Electrochemically Driven Ring Gliding Motion in Catenanes

8.3.1

A Two-geometry Catenane

The first molecular motor elaborated and studied in our group was a catenane containing two different interlocking rings. Its principle is explained in Figure 17.^[86]

The actual system and the full square-scheme are indicated in Figure 18. The starting copper(I) complex $23_{(4)}^+$ is a 4-coordinate species, the high redox potential of which (+ 0.63 V versus SCE in CH_3CN) clearly indicates that the geometry of the system (tetrahedral or distorted tetrahedral) is well adapted to copper(I). This redox state being very stable in the environment provided by $23_{(4)}^+$, a relatively high redox potential will have to be applied for the monovalent copper center to be oxidized to the divalent state. Interestingly, the 4-coordinate Cu(II) complex $23_{(4)}^{2+}$ is an intense green species, with a d-d absorption band at 670 nm ($\epsilon = 800$) in CH_3CN . This compound can be generated either by chemical (Br_2 or NOBF_4) or electrochemical oxidation.

The changeover reaction converting $23_{(4)}^{2+}$ to the stable 5-coordinate species $23_{(5)}^{2+}$ is quantitative. It is easily monitored by visible absorption spectroscopy, since the product of the rearrangement reaction is only slightly colored (pale olive green ; $\lambda_{\text{max}} = 640$ nm ; $\epsilon = 125$). The geometry of the copper(II) catenane obtained through decomplexation and remetalation has been confirmed by comparison of its physi-

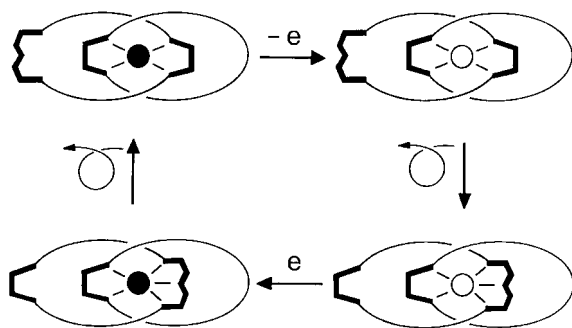


Fig. 17: Electrochemically triggered rearrangement of a [2]-catenane containing two different rings. The stable, 4-coordinate monovalent complex [top left, the black circle represents Cu(I)] is oxidized to an intermediate, tetrahedral, divalent species [top right, the white circle represents Cu(II)]. This compound

undergoes a complete reorganization process to afford the stable, 5-coordinate Cu(II) complex [bottom right]. Upon reduction, the 5-coordinate, monovalent state is formed as a transient [bottom left]. Finally, this undergoes the conformational change that regenerates the starting complex.

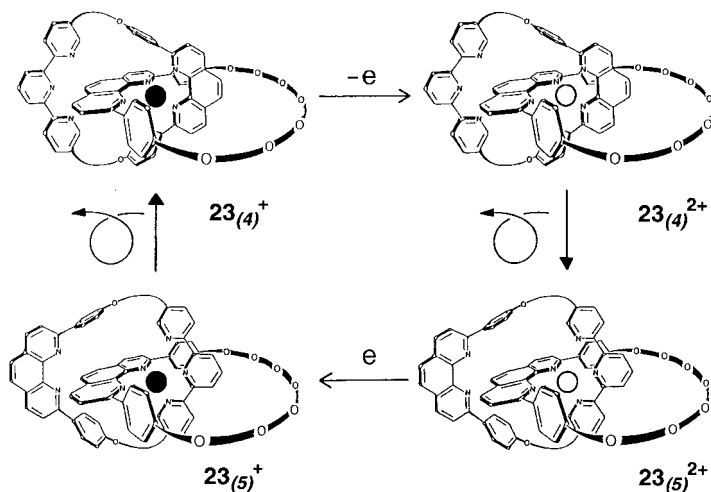


Fig. 18: Electrochemically induced molecular rearrangements undergone by the copper catenate $23^{2+/+}$. In the text, the subscript 4 or 5 indicates the number of nitrogen atoms coordinated to the metal. This number is indicated on the figure.

cal and chemical properties with those of literature compounds with structures that have already been established. Its redox potential is -0.07V versus SCE in acetonitrile, indicating good stabilization of the copper(II) state. UV-visible absorption spectroscopy in acetonitrile reveals a band centered at 636nm ($\epsilon = 125$), corresponding to a d–d transition, resulting in a pale olive-green solution. This value can be compared with that obtained for the 5-coordinated complex $\text{Cu}^{\text{II}}(\text{terpy})(\text{bipy})(\text{ClO}_4)_2$: 640 nm ($\epsilon = 120$),^[96] as well as for the same complex present in a recently synthesized copper(II) helicate.^[97] In collaboration with Kaim and Baumann, we also performed EPR spectroscopic measurements on the catenate;^[98] these showed an anisotropic signal characteristic of axial symmetry coordination around $\text{Cu}(\text{II})$ ($g_{\parallel} = 2.233$; $g_{\perp} = 2.045$; $A_{\parallel} = 16.6\text{ mT}$ in acetonitrile at 110K). We compared these data with those measured for a 5-coordinate complex $[\text{Cu}(\eta^3\text{-L})(\eta^2\text{-L})](\text{ClO}_4)_2$, containing the potential terdentate 2,6-bis(benzimidazol-2'-yl)pyridine ligand L and showing square-pyramidal configuration at the metal ion ($g_{\parallel} = 2.23$, $g_{\perp} = 2.03$; $A_{\parallel} = 16.7\text{ mT}$).^[99] The similarity of all these data tends to confirm the 5-coordination of the metal cation in our catenate, through intertwining of one dpp and the terpy, as summarized in the notation $\text{Cu}^{\text{II}}\text{N}_5$.

Both copper(II) complexes $23_{(4)}^{2+}$ and $23_{(5)}^{2+}$ have electronic spectra typical of 4-coordinate and 5-coordinate species, respectively, in accordance with previously reported complexes possessing analogous ligand sets.^[99,100] The same interconversion process can also be monitored by EPR,^[98,101] and it was demonstrated in an unambiguous fashion that $23_{(4)}^{2+}$ is a distorted tetrahedral complex and that the product of the changeover, $23_{(5)}^{2+}$, is a square pyramidal compound.

An interesting question deals with the rate of the ring gliding motion that transforms $23_{(4)}^{2+}$ into $23_{(5)}^{2+}$ or, after reduction of the latter, $23_{(5)}^+$ into $23_{(4)}^+$. It was

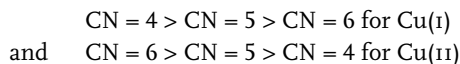
observed that this last process, involving Cu(I), is fast (a few seconds at room temperature, regardless of the solvent) whereas the copper(II) complex rearrangement $23_{(4)}^{2+} \rightarrow 23_{(5)}^{2+}$ is slow and depends enormously on experimental conditions. This linkage isomerization reaction was shown to take place in a few minutes in anhydrous acetonitrile but it required hours or even days to go to completion in noncoordinating solvents or in the absence of coordinating counterions. The strong accelerating influence of CH_3CN (over CH_2Cl_2) or Cl^- (over PF_6^-) may give some indications regarding the rearrangement mechanism. In the course of the changeover process, removal of a dpp unit (dpp = 2,9-diphenyl 1,10-phenanthroline) from the copper(II) coordination sphere has to proceed before any interaction between the metal center and the entering terpy ligand is possible. This implies that the copper(II) atom should be “half-naked” at some stage. If coordinating ions or solvent molecules are present in the medium, they could interact in a transitory fashion with the metal in this coordinatively unsaturated complex, and thus lower the activation barrier of the rearrangement by stabilizing intermediate states.

8.3.2

A Three-configuration Copper Catenane

The last system that we shall discuss is based on a [2]-catenane that can adopt three distinct geometries^[87] and contains two identical, interlocking rings. Multistage systems seem to be uncommon, although they are particularly challenging and promising with regard to photochemical and electrochemical devices aimed at important electronic functions and information storage. In particular, if molecules or molecular assemblies are one day to be utilized as information storage devices, it is obvious that the use of three-state systems will produce a great increase in information density compared to that attainable with bistable systems. For instance, an assembly of ten distinct molecules, each individual molecular component of which can occupy two states (say, + or -) will afford 2^{10} different states (i.e., 1024 states) whereas, if the same collection of 10 distinct molecules is such that each compound can now occupy three states (+, 0 and -), the overall number of states is now 3^{10} (i.e., 59 049).

The principle of the three-state, electromediated catenane is represented in Figure 19. Again, it relies on the drastic differences in stereochemical requirements for coordination of Cu(I) and Cu(II), the sequence of preferred coordination numbers (CN) being :



The compound was synthesized in modest yield, but following a very straightforward approach. The entwined complex 24^+ , used in many syntheses in our group,^[102] was treated with the difunctionalized terpy **25**, in the presence of Cs_2CO_3 under high dilution conditions. This one-pot, two-ring-forming reaction (Figure 20) afforded $26_{(4)}^+$ in 21 % yield, as a deep red, 4-coordinate complex ($\lambda_{\text{max}} = 439 \text{ nm}$; $\epsilon = 2570 \text{ mol}^{-1} \text{ L cm}^{-1}$ in CH_3CN).^[87]

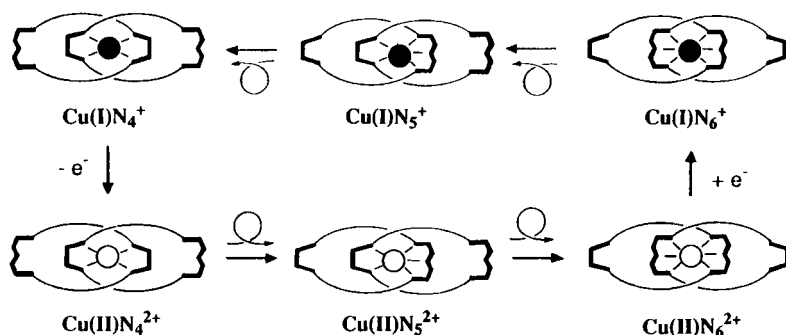


Fig. 19: A three-configuration Cu(I) catenate, the general molecular shape of which can be dramatically modified by oxidizing the central metal [Cu(I) to Cu(II)] or by reducing it back to the monovalent state. Each ring of the [2]-catenate now incorporates two different coordinating units: a bidentate unit and a terdentate fragment. Starting from the tetracoordinated monovalent Cu complex (Cu(I)N_4^+ ; top left) and oxidizing it to the divalent state (Cu(II)N_4^{2+}), a thermodynamically unstable species is obtained, which should first

rearrange to the 5-coordinate complex Cu(II)N_5^{2+} through the gliding of one ring (left) within the other and, finally, to the hexacoordinate stage Cu(II)N_6^{2+} by rotation of the second cycle (right) within the first one. Cu(II)N_6^{2+} is expected to be the thermodynamically stable divalent complex. The double ring-gliding motion following oxidation of Cu(I)N_4^+ can be inverted by reducing Cu(II)N_6^{2+} to the monovalent state (Cu(I)N_6^+ ; top right), as represented in the top line.

The free catenand **27** was easily obtained from $\mathbf{26}_{(4)}^+$ by removing the metal with KCN. Interestingly, remetalation of **27** by the divalent copper salt $\text{Cu}(\text{BF}_4)_2$ afforded the hexacoordinate species $\mathbf{26}_{(6)}^{2+}$ (see Figure 21) as a very pale green complex ($\lambda_{\text{max}} = 687 \text{ nm}$; $\epsilon = 100 \text{ mol}^{-1} \text{ L cm}^{-1}$).

Detailed electrochemical studies have been carried out on $\mathbf{26}_{(4)}^+$. Although we will not discuss them in this chapter, they afford very conclusive data and, in particular, they demonstrate unambiguously that the compound undergoes the rearrangement reactions schematically represented in Figure 19.

The sequence of electron transfer steps and ring-gliding motions corresponding to the cyclic process of Figure 19 can also be induced by using chemical reagents. For instance, when a dark red solution of $\mathbf{26}_{(4)}^+$ is oxidized by NO^+BF_4^- in CH_3CN , an intense green solution of $\mathbf{26}_{(4)}^{2+}$ is first obtained. As expected, the cyclic voltammogram (CV) of this species is the same as for the starting complex, which is in

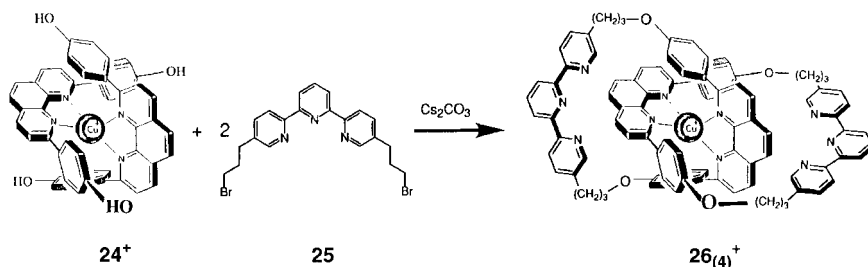


Fig. 20: Synthesis of the symmetrical catenate $\mathbf{26}_{(4)}^+$. ($\mathbf{26}^+ = [\text{Cu}(\mathbf{27})]^+$).

accordance with the 4-coordinate situation for both oxidized and reduced forms. The visible absorption spectrum shows a band at $\lambda_{\text{max}} = 670 \text{ nm}$ with a high extinction coefficient ($\epsilon = 810 \text{ mol}^{-1} \text{ L cm}^{-1}$ in CH_3CN), typical of tetrahedral complexes with nitrogen ligands. The ring-gliding step subsequently produces a hexacoordinate complex, the 5-coordinate compound being characterized as a transient species by electrochemistry only. As for the changeover reaction of the disymmetrical catenane ($23_{(4)}^{2+} \rightarrow 23_{(5)}^{2+}$), the rearrangement $26_{(4)}^{2+} \rightarrow [26_{(5)}^{2+}] \rightarrow 26_{(6)}^{2+}$ depends critically on the experimental conditions used and can be performed in minutes or hours.

Reversing the process, reduction of the stable species $26_{(6)}^{2+}$ affords $26_{(6)}^+$, which rapidly rearranges to the stable monovalent complex $26_{(4)}^+$. The intermediate $26_{(5)}^+$ has not been isolated nor spectroscopically characterized, but its formation was clearly evidenced by cyclic voltammetry, due to its analogy with $23_{(5)}^+$.

The three forms of the catenane are represented in Figure 21.

The redox potentials for the three situations (CN = 4, 5, or 6) are in perfect agreement with those of similar systems with identical CNs. The pentacoordinate com-

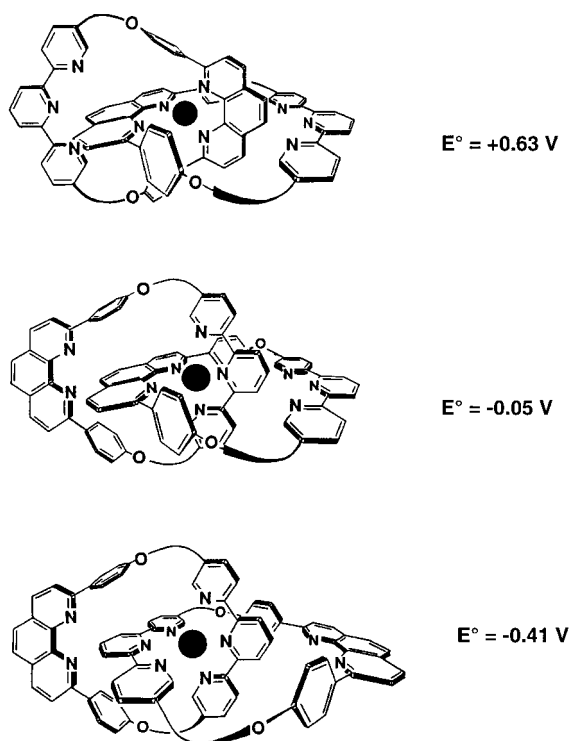


Fig. 21: The 4-, 5-, and 6-coordinate copper complexes involved. The corresponding $\text{Cu}(\text{II})/\text{Cu}(\text{I})$ redox potentials are also indicated. They clearly show the sequence of preferred stabilities for copper(II) versus copper(I), the hexacoordinate complex producing the most stable divalent complex.

plexes were characterized as transient species, but in principle, the present system does not permit stopping motion at this stage.

8.4

Conclusion and Prospects

The first template-directed synthesis of a catenane,^[88–90] making these molecules accessible from a preparative viewpoint, was published almost 15 years ago, although highly elegant but less practical work, based purely on organic chemistry, had been reported previously.^[103] Since those early days, more and more functionality has been introduced into these molecules, either in relation to electron and energy transfer processes or with regard to controlled molecular motion. The use of transition metals as templates, and of their complexes as electroactive and mobile components, has turned out to be particularly useful in the construction of *electromechanical molecular machines* based on coordination compounds. It would of course be unwise to predict that nanoscopic motors and related machines will have any practical application in the future as molecular information storage devices, or as nanoscale components in electronics, but the search for such molecules or molecular assemblies is important in itself.

Molecular machines constitute an emerging field of research, at an interface with many areas of molecular sciences. For instance, the concepts discussed in the present paper can certainly be generalized to organized assemblies of molecules (liquid crystals) or to molecular components attached to an electrode surface. The overall properties of the system (now a „device“), such as liquid crystal character, ability to carry electrons or transport molecules, etc..., could be switched just by applying a given signal. The variety of impulses that might be used is immense: redox (as in the present examples), photonic, heat or pressure change, magnetic field variation, pH-change, chemical signal (recognition of a molecule), electric field, and so on... The effect obtained is also multifarious and might lead to dramatic modifications of the bulk properties of the system. Since a simple signal can change the shape and the volume of a compound and of its assemblies, fascinating features related to mechanics (contraction or stretching) may be imagined, reminiscent of biological systems such as muscles or other biological molecular machines.

Finally, the making of real motors at the molecular level remains a challenge. Not only will the motion have to be continuous, in the sense that cyclic processes, with a turnover, are required, but directionality will be essential. This is especially true for molecular ensembles aimed at mimicking the dynamic properties of ATP synthase. Although still relatively remote from continuous directional rotary motion, one interesting chemical system with behavior reminiscent of rotary motors has recently been proposed.^[104] For a photochemical driven unidirectional rotor,^[105] see Chapter 5. Other systems, based on related or different principles, will no doubt be reported in the future.

Acknowledgments

This work was supported by the CNRS (France) and EC HCM network ERB CHR XCT 940492 „Transitions Metals in Supramolecular Catalysis“. Special thanks are also due to all the researchers who contributed to the work described here with so much enthusiasm.

References

- 1 *Acc. Chem. Res.* **1998**, *31*, number 11.
- 2 J. R. Telford, P. Wittung-Stafshede, H. B. Gray, J. R. Winkler, *Acc. Chem. Res.* **1998**, *31*, 755–763, and references therein.
- 3 S.-R. Yeh, S. Han, D. L. Rousseau, *Acc. Chem. Res.* **1998**, *31*, 727–736, and references therein.
- 4 T. Pascher, J. P. Chesick, J. R. Winkler, H. B. Gray, *Science* **1996**, *271*, 1858–1860, and references therein.
- 5 M. C. R. Shastry, J. M. Sauder, H. Roder, *Acc. Chem. Res.* **1998**, *31*, 717–725, and references therein.
- 6 S. W. Englander, T. R. Sosnick, L. C. Mayne, M. Shtilerman, P. X. Qi, Y. Bai, *Acc. Chem. Res.* **1998**, *31*, 737–744, and references therein.
- 7 G. W. Bushnell, G. V. Louie, G. D. Brayer, *J. Mol. Biol.* **1990**, *214*, 585–595.
- 8 J. Bixler, G. Bakker, G. McLendon, *J. Am. Chem. Soc.* **1992**, *114*, 6938–6939.
- 9 H. L. Schenck, G. P. Dado, S. H. Gellman, *J. Am. Chem. Soc.* **1996**, *118*, 12487–12494.
- 10 G. P. Dado, S. H. Gellman, *J. Am. Chem. Soc.* **1993**, *115*, 12609–12610.
- 11 J. Howard, *Nature* **1997**, *389*, 561–567.
- 12 K. Kitamura, M. Tokunaga, A. H. Iwane, T. Yanagida, *Nature* **1999**, *397*, 129–134.
- 13 I. Rayment, W. R. Rypniewski, K. Schmidt-Bäse, R. Smith, D. R. Tomchick, M. M. Benning, D. A. Winkelmann, G. Wesenberg, H. M. Holden, *Science* **1993**, *261*, 50–58.
- 14 I. Rayment, H. M. Holden, M. Whittaker, C. B. Yohn, M. Lorenz, K. C. Holmes, R. A. Milligan, *Science* **1993**, *261*, 58–64.
- 15 I. Dobbie, M. Linari, G. Piazzesi, M. Reconditi, N. Koubassova, M. A. Ferenczi, V. Lombardi, M. Irving, *Nature* **1998**, *396*, 383–387.
- 16 E. P. Sablin, F. J. Kull, R. Cooke, R. D. Vale, R. J. Fletterick, *Nature* **1996**, *380*, 555–559.
- 17 F. J. Kull, E. P. Sablin, R. Lau, R. J. Fletterick, R. D. Vale, *Nature* **1996**, *380*, 550–555.
- 18 J. P. Abrahams, A. G. W. Leslie, R. Lutter, J. E. Walker, *Nature* **1994**, *370*, 621–628.
- 19 H. Noji, R. Yasuda, M. Yoshida, K. Kinosita, *Nature* **1997**, *386*, 299–302.
- 20 J. E. Walker, *Angew. Chem. Int. Ed.* **1998**, *37*, 2308–2319.
- 21 W. S. Allison, *Acc. Chem. Res.* **1998**, *31*, 819–826.
- 22 P. D. Boyer, *Angew. Chem. Int. Ed.* **1998**, *37*, 2296–2307.
- 23 L. Stryer, *Biochemistry*, 2nd ed., W. H. Freeman and Company, San Francisco, 1981; pp 906–907.
- 24 K. E. Drexler, *Nanosystems, molecular machinery, manufacturing and computation*; Wiley, New-York, 1992.
- 25 A. Ikeda, T. Tsudera, S. Shinkai, *J. Org. Chem.* **1997**, *62*, 3568–3574.
- 26 D. W. Urry, *Angew. Chem., Int. Ed. Engl.* **1993**, *32*, 819–841.
- 27 S. Shinkai, T. Nakaji, Y. Nishida, T. Ogawa, O. Manabe, *J. Am. Chem. Soc.* **1980**, *102*, 5860–5862.
- 28 S. Shinkai, T. Ogawa, Y. Kusano, O. Manabe, K. Kikikawa, T. Goto, T. Matsuda, *J. Am. Chem. Soc.* **1982**, *104*, 1960–1967.
- 29 S. Shinkai, T. Minama, O. Manabe, Y. Kusano, *Tetrahedron Lett.* **1982**, *23*, 2581–2584.
- 30 S. Shinkai, T. Minami, Y. Kusano, O. Manabe, *J. Am. Chem. Soc.* **1983**, *105*, 1851–1856.
- 31 S. Shinkai, M. Ishihara, K. Ueda, O. Manabe, *Chem. Commun.* **1984**, 727–729.
- 32 F. Vögtle, W. M. Müller, U. Müller, M. Bauer, K. Rissanen, *Angew. Chem., Int. Ed. Engl.* **1993**, *32*, 1295–1297.
- 33 M. Bauer, W. M. Müller, U. Müller, K. Rissanen, F. Vögtle, *Liebigs Ann.* **1995**, 649–656.
- 34 H. Bouas-Laurent, A. Castellan, M. Daney, J.-P. Desvergnès, G. Guinand, P. Marseau, M.-H. Riffaud, *J. Am. Chem. Soc.* **1986**, *108*, 315–317.
- 35 M. T. Staufer, D. B. Knowles, C. Brennan, L. Funderburk, F.-T. Lin, S. G. Weber, *Chem. Commun.* **1997**, 287–288.
- 36 S. M. Fatah-ur Rahman, K. Fukunishi, *Chem. Commun.* **1994**, 917–918.
- 37 S. Wu, A. Mori, H. Takeshita, *Chem. Commun.* **1994**, 919–920.
- 38 T. R. Kelly, M. C. Bowyer, K. V. Bhaskar, D. Bebbington, A. Garcia, F. Lang, M. H. Kim, M. P. Jette, *J. Am. Chem. Soc.* **1994**, *116*, 3657–3658.
- 39 D. Philp, *Angew. Chem., Int. Ed. Engl.* **1996**, *35*, 1154–1196.
- 40 A. Credi, V. Balzani, S. J. Langford, J. F. Stoddart, *J. Am. Chem. Soc.* **1997**, *119*, 2679–2681.
- 41 P. R. Ashton, R. Ballardini, V. Balzani, S. Boyd, A. Credi, M. T. Gandolfi, M. Gómez-

- López, D. Philp, J. A. Preece, L. Prodi, H. G. Ricketts, J. F. Stoddart, M. S. Tolley, M. Venturi, A. J. P. White, D. J. Williams, *Chem. Eur. J.* **1997**, *3*, 152–170.
- 42 P. R. Ashton, R. Ballardini, V. Balzani, A. Credi, M. T. Gandolfi, S. Menzer, L. Pérez-García, L. Prodi, J. F. Stoddart, M. Venturi, A. J. P. White, D. J. Williams, *J. Am. Chem. Soc.* **1995**, *117*, 11171–11197.
- 43 R. Ballardini, V. Balzani, M. T. Gandolfi, L. Prodi, M. Venturi, D. Philp, H. G. Ricketts, J. F. Stoddart, *Angew. Chem. Int. Ed. Engl.* **1993**, *32*, 1301–1303.
- 44 R. A. Bissel, E. Córdova, A. E. Kaifer, J. F. Stoddart, *Nature* **1994**, *369*, 133–137.
- 45 W. E. Geiger Jr, *J. Am. Chem. Soc.* **1979**, *3407*–3408.
- 46 M. M. Bernardo, P. V. Robandt, R. R. Schroeder, D. B. Rorabacher, *J. Am. Chem. Soc.* **1989**, *111*, 1224–1231.
- 47 N. E. Katz, F. Fagalde, *Inorg. Chem.* **1993**, *32*, 5391–5393.
- 48 J. Moraczewski, C. A. Sassano, C. A. Mirkin, *J. Am. Chem. Soc.* **1995**, *117*, 11379–11380.
- 49 E. T. Singewald, C. A. Mirkin, C. L. Stern, *Angew. Chem., Int. Ed. Engl.* **1995**, *34*, 1624–1627.
- 50 J. A. Wytko, C. Boudon, J. Weiss, M. Gross, *Inorg. Chem.* **1996**, *35*, 4469–4470.
- 51 T. T. Chin, W. E. Geiger, A. L. Rheingold, *J. Am. Chem. Soc.* **1996**, *118*, 5002–5010.
- 52 M. Sano, H. Taube, *J. Am. Chem. Soc.* **1991**, *113*, 2327–2328.
- 53 M. Sano, H. Taube, *Inorg. Chem.* **1994**, *33*, 705–709.
- 54 M. Sano, H. Sago, A. Tomita, *Bull. Chem. Soc. Jpn.* **1996**, *69*, 977–981.
- 55 A. Tomita, M. Sano, *Inorg. Chem.* **1994**, *33*, 5825–5830.
- 56 A. Tomita, M. Sano, *Chem. Lett.* **1996**, 981–982.
- 57 L. Zelikovich, J. Libman, A. Shanzer, *Nature* **1995**, *790*–792.
- 58 C. Canevet, J. Libman, A. Shanzer, *Angew. Chem., Int. Ed. Engl.* **1996**, *35*, 2657–2660.
- 59 G. De Santis, L. Fabbri, D. Iacopino, P. Pallavicini, A. Perotti, A. Poggi, *Inorg. Chem.* **1997**, *36*, 827–832.
- 60 G. Schill *Catananes, Rotaxanes and Knots*; Academic Press: New York and London, 1971.
- 61 C. Pascard, J. Guilhem, S. Chardon-Noblat, J.-P. Sauvage, *New J. Chem.* **1993**, *17*, 331–335.
- 62 J. Deisenhofer, O. Epp, K. Miki, R. Huber, H. Michel, *J. Mol. Biol.* **1984**, *180*, 385–398.
- 63 R. Huber, *Angew. Chem. Int. Ed. Engl.* **1989**, *28*, 848–849.
- 64 J. Deisenhofer, H. Michel, *Angew. Chem. Int. Ed. Engl.* **1989**, *28*, 829–847.
- 65 N. W. Woodbury, M. Becker, D. Middendorf, W. W. Parson, *Biochemistry* **1985**, *24*, 7516–7521.
- 66 J. Breton, J.-L. Martin, A. Migus, A. Antonetti, A. Orszag, *Proc. Natl. Acad. Sci. U.S.A.* **1986**, *83*, 5121–5125.
- 67 J.-L. Martin, J. Breton, A. J. Hoff, A. Migus, A. Antonetti, *Proc. Natl. Acad. Sci. U.S.A.* **1986**, *83*, 957–961.
- 68 S. Chardon-Noblat, J.-P. Sauvage, *Tetrahedron* **1991**, *47*, 5123–5132.
- 69 V. Heitz, S. Chardon-Noblat, J.-P. Sauvage, *Tetrahedron Lett.* **1991**, *32*, 197–198.
- 70 A. M. Brun, S. Atherton, A. Harriman, V. Heitz, J.-P. Sauvage, *J. Am. Chem. Soc.* **1992**, *114*, 4632–4639.
- 71 J.-C. Chambron, V. Heitz, J.-P. Sauvage, *J. Am. Chem. Soc.* **1993**, *115*, 12378–12384.
- 72 J.-C. Chambron, V. Heitz, J.-P. Sauvage, *J. Chem. Soc., Chem. Commun.* **1992**, 1131–1133.
- 73 C. Wu, P. R. Lecavalier, Y. X. Shen, H. W. Gibson, *Chem. Mater.* **1991**, *3*, 569–572.
- 74 D. J. Cárdenas, P. Gaviña, J.-P. Sauvage, *J. Am. Chem. Soc.* **1997**, *119*, 2656–2664.
- 75 J.-C. Chambron, A. Harriman, V. Heitz, J.-P. Sauvage, *J. Am. Chem. Soc.* **1993**, *115*, 6109–6114.
- 76 J.-C. Chambron, A. Harriman, V. Heitz, J.-P. Sauvage, *J. Am. Chem. Soc.* **1993**, *115*, 7419–7425.
- 77 A. Harriman, V. Heitz, J.-C. Chambron, J.-P. Sauvage, *Coord. Chem. Rev.* **1994**, *132*, 229–234.
- 78 R. A. Marcus, N. Sutin, *Biochim. Biophys. Acta* **1985**, *811*, 265–322.
- 79 N. S. Hush, *Coord. Chem. Rev.* **1985**, *64*, 135–157.
- 80 M. D. Todd, A. Nitzan, M. A. Ratner, *J. Phys. Chem.* **1993**, *97*, 29–33.
- 81 J.-C. Chambron, C. O. Dietrich-Buchecker, J.-F. Nierengarten, ; J.-P. Sauvage, *New J. Chem.*, **1993**, *17*, 331–335; J.-C. Chambron, C. O. Dietrich-Buchecker, J.-F. Nierengarten, J.-P. Sauvage, N. Solladié, A.-M. Albrecht-Gary, M. Meyer, *New J. Chem.*, **1995**, *19*, 409–426.

- 82 D. B. Amabilino, C. O. Dietrich-Buchecker, J.-P. Sauvage, *J. Am. Chem. Soc.*, **1996**, *118*, 3285–3286.
- 83 P. Gaviña, J.-P. Sauvage, *Tetrahedron Letters* **1997**, *38*, 3521–3524; J.-P. Collin, P. Gaviña, J.-P. Sauvage, *J. Chem. Soc., Chem. Commun.* **1996**, 2005–2006.
- 84 J.-P. Collin, P. Gaviña, J.-P. Sauvage, *New J. Chem.* **1997**, *21*, 525–528.
- 85 D. H. Evans, *Chem. Rev.* **1990**, *90*, 739.
- 86 A. Livoreil, C. O. Dietrich-Buchecker, J.-P. Sauvage, *J. Am. Chem. Soc.* **1994**, *116*, 9399–9400. A. Livoreil, J.-P. Sauvage, N. Armaroli, V. Balzani, L. Flamigni, B. Ventura *J. Am. Chem. Soc.* **1997**, *119*, 12114–12124.
- 87 D.J. Cárdenas, A. Livoreil, J.-P. Sauvage, *J. Am. Chem. Soc.* **1996**, *118*, 11980–11981.
- 88 C. Dietrich-Buchecker, J.-P. Sauvage, *Tetrahedron Lett.* **1983**, *24*, 5091–5094.
- 89 C. Dietrich-Buchecker, J.-P. Sauvage, J.-P. Kintzinger, *Tetrahedron Lett.* **1983**, *24*, 5095–5098.
- 90 C. Dietrich-Buchecker, J.-P. Sauvage, J.-M. Kern, *J. Am. Chem. Soc.* **1984**, *106*, 3043–3045.
- 91 F. Arnaud-Neu, E. Marques, M.-J. Schwing-Weill, C. O. Dietrich-Buchecker, J.-P. Sauvage, J. Weiss, *New J. Chem.* **1988**, *12*, 15–20.
- 92 C. Dietrich-Buchecker, J.-P. Sauvage, *Tetrahedron* **1990**, *46*, 503–512.
- 93 C. Dietrich-Buchecker, J.-M. Kern, J.-P. Sauvage, *J. Am. Chem. Soc.* **1989**, *111*, 7791–7800.
- 94 P. Federlin, J.-M. Kern, A. Rastegar, C. Dietrich-Buchecker, P. A. Marnot, J.-P. Sauvage, *New J. Chem.* **1990**, *14*, 9–12.
- 95 R.S. Nicholson, I. Shain, *Anal. Chem.* **1964**, *36*, 706–723.
- 96 C.M. Harris, T.N. Lockyer, *Aust. J. Chem.* **1970**, *23*, 673–682; G. Arena, R.P. Bonomo, S. Musumeci, R. Purello, E. Rizzarelli, S. Sammartano, *J. Chem. Soc. Dalton Trans.* **1983**, 1279–1283.
- 97 B. Hasenknopf, J.-M. Lehn, G. Baum, D. Fenske, *Proc. Natl. Acad. Sci. USA* **1996**, *93*, 1397–1400.
- 98 Baumann, F.; Livoreil, A.; Kaim; W.; Sauvage, J.P. *J. Chem. Soc. Chem. Commun.* **1997**, 35–36.
- 99 Sanni, S.B.; Behm, H.J.; Beurskens, P.T.; Van Albada, G.A.; Reedijk, J.; Lenstra, A.T.H.; Addison, A.W.; Palaniandavar, M. *J. Chem. Soc. Dalton Trans.* **1988**, 1429–1435.
- 100 For previous studies on 5-coordinate Cu(I) and Cu(II) complexes with imine-type ligands, see; J. A. Goodwin, D. M. Stanbury, L. J. Wilson, C. W. Eigenbrot, W.R. Scheidt, *J. Am. Chem. Soc.*, **1987**, *109*, 2979–2991; J. A. Goodwin, G. A. Bodager, L. J. Wilson, D. M. Stanbury, W. R. Scheidt, *Inorg. Chem.*, **1989**, *28*, 35–42; Goodwin, J. A. ; Wilson, L. J. Stanbury, D. M.; Scott, R. A. *Inorg. Chem.*, **1989**, *28*, 42–50;
- 101 For the EPR properties of copper(II) complexes with coordination spheres similar to those in $23_{(4)}^{2+}$ or $23_{(5)}^{2+}$ see : B. A. Goodman, J. B. Raynor, *Adv. Inorg. Chem. Radiochem.*, **1970**, *13*, 135; M. Geoffroy, M. Wermeille, C. O. Dietrich-Buchecker, J.-P. Sauvage, G. Bernadinelli, *Inorg. Chem. Acta*, **1990**, 1429; W. Kaim, *Coord. Chem. Rev.*, **1987**, *76*, 187.
- 102 C.O. Dietrich-Buchecker, J.-P. Sauvage, *Bioorganic Chemistry Frontiers*; Springer-Verlag Berlin, **1991**, Vol. 2, pp. 197–248
- 103 E. Wasserman, *J. Am. Chem. Soc.* **1960**, *82*, 4433 ; G. Schill, *Catenanes, Rotaxanes and Knots*, **1971**, Academic Press, New-York, London ; I.T. Harrison, S. Harrison, *J. Am. Chem. Soc.*, **1967**, *89*, 5723–5724.
- 104 T.R. Kelly, H. De Silva, R.A. Silva, *Nature*, **1999**, *401*, 150.
- 105 N. Koumura, R.W.J. Zylstra, R.A. van Delden, N. Harada, B.L. Feringa, *Nature*, **1999**, *401*, 152.

9

Switchable Molecular Receptors and Recognition Processes: From Photoresponsive Crown Ethers to Allosteric Sugar Sensing Systems

Seiji Shinkai

We entered this research field in 1979, with a new concept involving “photoresponsive crown ethers”. This enabled us, for the first time, to change the size and the shape of crown ethers by means of a nano-scale photomanipulator and to control the metal affinity and metal selectivity by means of an external stimulus. This concept has been extended from the unimolecular to supramolecular systems. In addition, it has provided a strong background for our recent research interest; namely the molecular design of allosteric sugar sensing systems.

9.1

Introduction: Why is the Switch Function Indispensable in Molecular Receptors?

The concept of an “enthalpy-entropy compensation relationship” was proposed by Leffler in the 1960s.^[1] This concept was very valuable for gaining insights into a number of thermodynamic data for association and kinetic processes. However, it also implies that high selectivity and high activity cannot appear in one reaction series, as this would represent deviation from the linear relationship. In this light, the starting point of our chemistry was to become *how can we create an exceptional system, with high selectivity and high activity, and which deviates from the enthalpy-entropy compensation relationship?* This question becomes especially important for mimicking the high selectivity and high activity of enzymes in a biomimetic chemistry field. Eventually, we arrived at one potential breakthrough. In essence, it is that as long as one association process or one kinetic process is treated independently, it is still restricted by the relationship, but if two or more systems are coupled together reversibly, it may be possible to find an exceptional process to which the relationship does not apply, thanks to “switching” to and from other conjugated systems. This original concept has enabled us to create a number of new ion and molecule recognition systems, which can be combined with switch-functionalized systems and molecular-assembly systems (Figure 1). We believe that this breakthrough is applicable to the basic concept of the so-called “molecular machine”.

Nature is filled with molecules and ions, and we are frequently required to measure the concentrations of selected ions and small organic molecules both in in vivo and in in vitro processes. One possible strategy in this research field is the direct

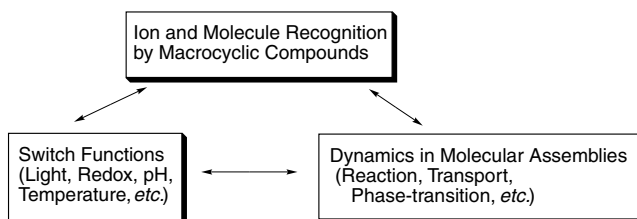


Fig. 1: A concept for molecular design of switch-functionalized recognition systems.

application, after appropriate modifications, of biomaterials such as proteins, biomembranes, etc. created in nature. This approach has had some impact: for example, “biosensors” may be cited as representative and successful systems. However, this system in which naturally evolved “tools” are “borrowed” is frequently hampered by their inherent boundary conditions, such as poor solubility in organic media, instability at high temperature, degradation and denaturation, lack of broad specificity, and so on, since they have not arisen for our practical convenience, but fulfil nature’s own purposes. Thus, artificial molecular design of man-made receptors, displaying high affinity and high selectivity comparable with natural systems, has long been a dream for scientists and has recently become a very active area of endeavor. However, it should be noted that this concept is only one component in the design of a total sensing system; even if an artificial receptor can recognize a selected ion or molecule precisely, it is still useless unless the guest-binding event can be read out as some convenient physical signal. To provide a total sensing system, therefore, the binding event must be transduced into some sort of change in a molecular system and eventually converted into some form of physical signal. Hence, the total sensing system consists of three different components: (1) an ion or molecule recognition site, (2) a signal conversion site, and (3) a signal read-out site. This system may be called a unimolecular “molecular machine” and the function performed by component (2) frequently plays a key role (Figure 2). To integrate such multicomponent functions into one small molecular system appears to be quite difficult. However, there are a considerable number of successful examples in which slight structural changes induced by ion or molecule binding are efficiently transduced into changes in the subsequent physical signaling processes. These examples teach us that, to achieve precise molecular design, a small molecular system is frequently more advantageous than a polymeric system or a molecular

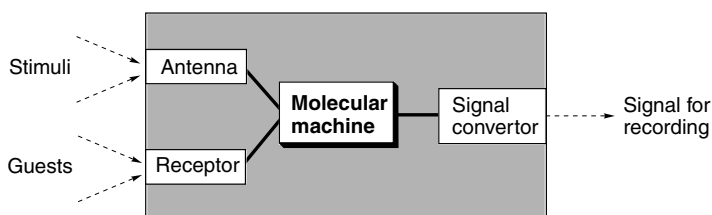


Fig. 2: Conceptual scheme for the design of a total sensing system.

assembly system. Furthermore, it is now possible to predict the guest-induced structural change precisely, utilizing recently developed computational methods.

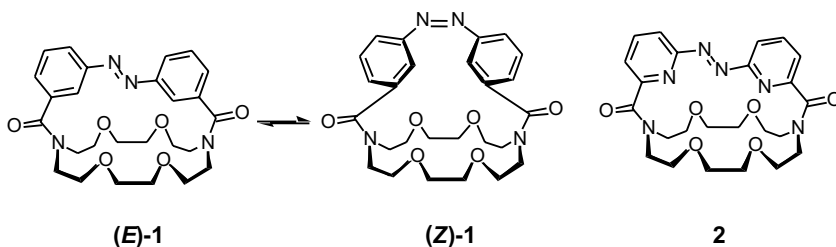
In this chapter, we introduce the concept of the molecular design of several sensing or switching systems for selected ions and molecules, focusing particularly on our own recent research achievements.

9.2

The Origination of Photoresponsive Crown Ethers

Photoresponsive systems are seen ubiquitously in nature, and light is intimately associated with the subsequent life processes. In these systems, a photoantenna to capture a photon is neatly combined with a functional group to mediate some subsequent events. Important is the fact that these events are frequently linked with photoinduced structural changes in the photoantennae. This suggests that chemical substances that exhibit photoinduced structural changes may serve as potential candidates for the photoantennae. To date, such photochemical reactions as *E/Z* isomerism of azobenzenes, dimerization of anthracenes, spiropyran-merocyanine interconversion, and others have been exploited in practical photoantennae. It may be expected that if one of these photoantennae were adroitly combined with a crown ether, it would then be possible to control many crown ether family physical and chemical functions by means of an “ON/OFF” photoswitch. This is the basic concept underlying the designing of photoresponsive crown ethers. We believe that this is one of the earliest examples of “molecular machines”.

Compound **1** is an early example of a photoresponsive crown ether.^[2,3] It has a photofunctional azobenzene cap on an N_2O_4 crown ring, so it may be expected that the conformational change in the crown ring occurs in response to the photoinduced configurational change in the azobenzene cap. Isomer (*E*)-**1**, with the (*E*)-azobenzene cap, selectively binds Na^+ . However, isomer (*Z*)-**1**, produced by photoisomerization upon irradiation with UV light, binds more strongly to K^+ . This finding suggests that the N_2O_4 ring is apparently stretched by the photoinduced *E/Z* isomerization. X-ray crystallographic studies of the closely related (*E*)-**2** confirmed that the N_2O_4 crown in **2** has two anti C-C bonds, resulting in an oval-shaped crown ring. In contrast, all the C-C bonds in 18-crown-6 complexed with K^+ are gauche.^[4] Conceivably, this is the reason why (*E*)-**1** favors small Na^+ rather than K^+ .

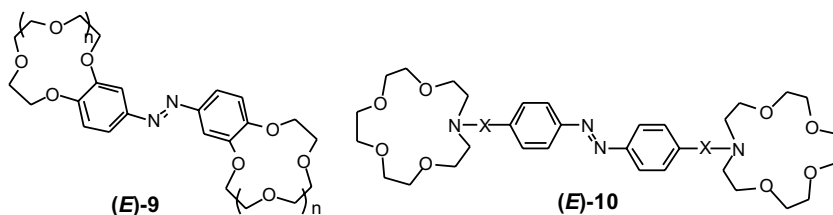


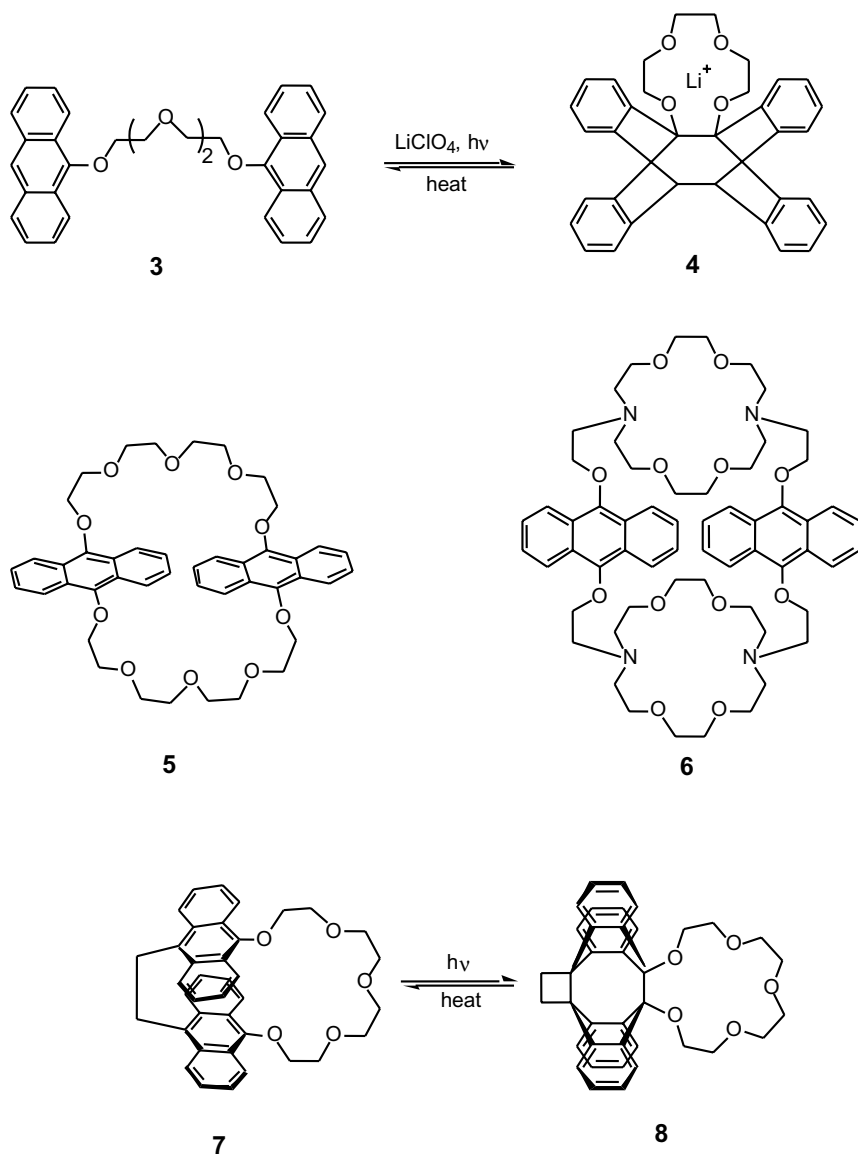
Photodimerization of anthracene is also usable as a photochemical switch to create photoresponsive crown ethers. Photoirradiation of **3** in the presence of Li^+ gives the photocycloisomer **4**.^[5,6] Compound **4** is fairly stable in the presence of Li^+ , but readily reverts to the open form **3** when Li^+ is removed from the ring.

In this system, however, intermolecular dimerization may take place competitively with intramolecular dimerization. To rule out this possibility, compound **5**, in which two anthracenes are linked by two polyether chains, was synthesized.^[7] It was found that intramolecular photodimerization proceeds rapidly in the presence of Na^+ as the template metal cation. Compound **6** was also synthesized.^[8] Although this compound has not been applied in a photoswitch system, it displays a remarkable fluorescence change upon binding with RbClO_4 or $\text{H}_3\text{N}^+(\text{CH}_2)_7\text{NH}_3$.^[8] Yamashita et al.^[9] also synthesized **7**, in which intermolecular photodimerization of anthracene is completely suppressed. The photochemically produced cyclic form **8** displayed excellent Na^+ selectivity.

It has been established that those alkali metal cations that exactly fit the size of the crown ether ring form 1:1 complexes, whereas those that have larger cation radii form 1:2 sandwich complexes. This view has been clearly substantiated by the use of bis(crown ethers). Kimura et al.,^[10] for instance, reported that the maleate diester of monobenzo-15-crown-5 (*Z* form) extracts K^+ from an aqueous phase 14 times more efficiently than its fumarate counterpart (*E* form). The difference stems from the formation of the intramolecular 1:2 complex with the *Z* form. If the $\text{C}=\text{C}$ double bond were replaced by an azo linkage, the resultant bis(crown ethers) would exhibit interesting photoresponsive behavior. This is the essential idea in this section: that a photoinduced change in the spatial separation between two crown rings should be reflected in a change in ion binding ability.

Shinkai et al.^[11–15] synthesized a series of azobis(benzocrown ethers) called “butterfly crown ethers”, of which compounds **9** and **10** are examples. Their photoresponsive molecular motion resembles that of a flying butterfly. It was found that the proportion of their *Z* forms at the photostationary state increases remarkably with increasing concentration of Rb^+ and Cs^+ , which interact with two crown rings in a 1:2 sandwich fashion. This is clearly due to the bridge effect of the metal cations with the two crowns, results that support the view that the *Z* forms make an intramolecular 1:2 complex with these metal cations. As expected, the *Z* forms extracted alkali metal cations with large ion radii more efficiently than did the corresponding *E* forms. In particular, the photoirradiation effect on **9** is quite remarkable: for example, (*E*)-**9** ($n = 2$) extracts Na^+ 5.6 times more efficiently than (*Z*)-**9** ($n = 2$), whereas (*Z*)-**9** ($n = 2$) extracts K^+ 42.5 times more efficiently than (*E*)-**9** ($n = 2$).^[13]





The solution properties of complexes formed from **9** ($n = 3$) and polymethylene-diammonium cations, $\text{H}_3\text{N}^+(\text{CH}_2)_m\text{NH}_3^+$ have been studied in detail.^[16] It was found that when the distance between the two ammonium cations is shorter than that between the crown rings in (*E*)-**9** ($n = 3$), (e.g., $m = 6$), they form a polymeric complex (Figure 3). When the two distances are comparable (for example, $m = 12$), they form a 1:1 pseudo-cyclic complex. Photoisomerized (*Z*)-**9** ($n = 3$) displayed a different mode of aggregation, because of the change in the distance between the

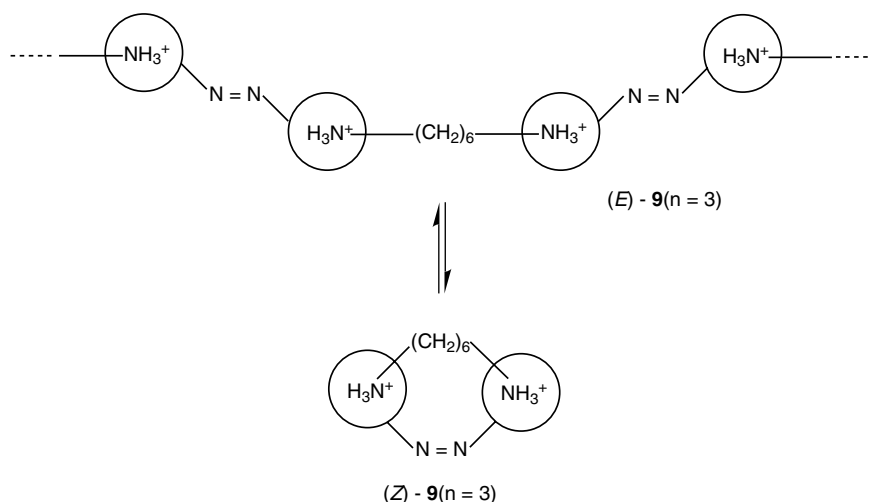


Fig. 3: Photoregulation of polymer/pseudo-macrocycle interconversion in a **9** (n = 3) + $\text{H}_3\text{N}^+(\text{CH}_2)_6\text{NH}_3^+$ system. The circle indicates benzo-18-crown-6.

two crown rings, producing the 1:1 complex for (Z)-**9** (n = 3) and the (m = 6) diammonium salt and the 2:2 complex for (Z)-**9** (n = 3) and the (m = 12) diammonium salt. This is a novel example of reversible interconversion between polymers and low molecular weight pseudomacrocycles. Since the interconversion process is sensitively reflected by electrical conductance, this may be viewed as the conversion of light energy into an electrical signal.^[16]

Cations are known to be transported through membranes by synthetic macrocyclic polyethers, as well as by antibiotics. When the rate-determining step is ion extraction from the IN aqueous phase to the membrane phase, the transport rate increases with increasing stability constant. On the other hand, when the rate-determining step is ion release from the membrane phase to the OUT aqueous phase, the carrier must reduce its stability constant if efficient decomplexation is to be attained. Some polyether antibiotics feature the interconversion between their cyclic and noncyclic forms in the membrane, a characteristic by means of which the transport system is able to escape from the limitation of the rate-determining step. In this system, energy arising from the pH gradient is consumed to balance cyclic–noncyclic interconversion. This gives rise to an interesting possibility: provided that the ion binding ability of the carrier at the rate-determining step can be changed by light, then the rate of ion transport can also be changed. This idea should be of particular importance when the ion release is rate-determining. For the case of K^+ transport across a liquid membrane with **9** (n = 2), Shinkai et al.^[13] found that the rate was accelerated by UV irradiation, which mediated E/Z isomerization. The rate enhancement was attributed to the increased speed of extraction from the IN aqueous phase to the membrane phase. The rate was further enhanced by alternating irradiation with UV

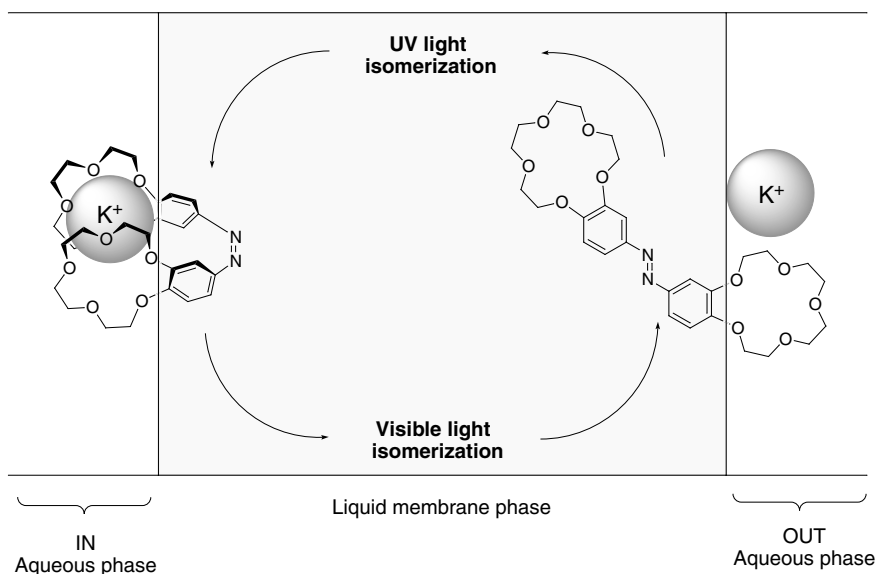


Fig. 4: Schematic representation of K^+ transport with **9** ($n = 2$) accelerated by alternate irradiation with UV and visible light.

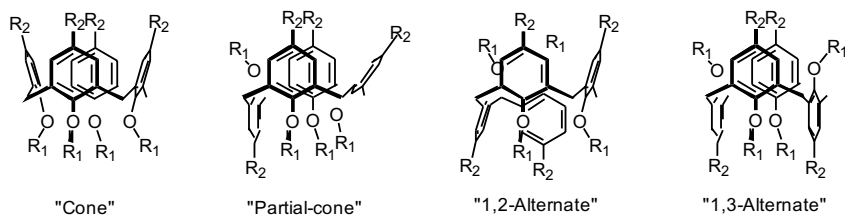
and visible (which mediates *Z/E* isomerization) light (Figure 4).^[17] This effect was attributed to the increased speed of release from the membrane phase to the OUT aqueous phase. In other words, the pH gradient utilized in ion transport by some polyether antibiotics can be replaced by light energy in these light-driven systems.

9.3

Dynamic Actions of Calixarenes in Ion and Molecule Recognition

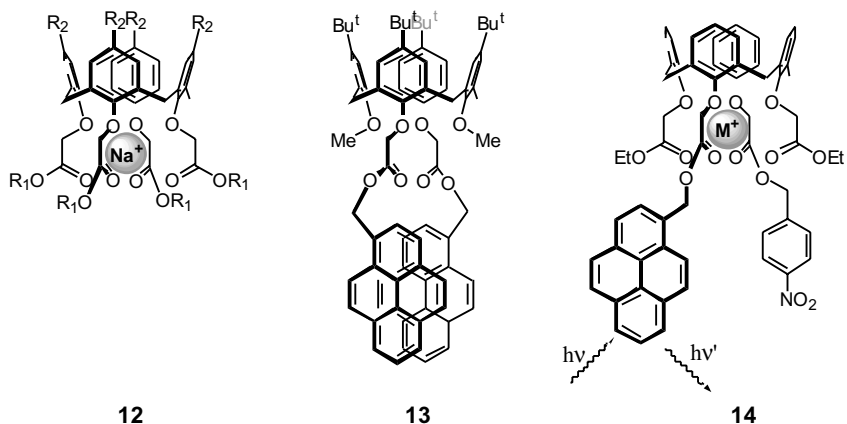
Calixarenes are $[1_n]$ metacyclophanes, made up of phenol units linked through alkylidene groups.^[18] They preferably adopt a cone conformation, because of the stabilization effect from intramolecular hydrogen-bonding interaction. Unless bulky substituents are introduced onto the OH groups, rotation of the phenyl units is allowed.^[18,19] Hence, the cavity shape, which governs the guest-binding properties, can be controlled by changing the phenol moieties' rotation. Compound **11** is conformationally mobile and four conformers (cone, partial-cone, 1,2-alternate, and 1,3-alternate) can interconvert by rotation in which the oxygen passes through the annulus.^[19,20] Although the most stable conformer is partial-cone,^[19–22] it changes in response to added guests.^[23] This conformational freedom, characteristic of the calixarene family, is very attractive for designing molecular switches. For example, ^1H NMR studies established that, when LiClO_4 or NaClO_4 was added, new peaks appeared and were attributable to the cone-**11** ($R_2 = \text{Bu}^t$)· M^+ complex.^[23] On the other hand, the spectrum was scarcely affected by the addition of KClO_4 .^[23] The findings suggested that, to bind alkali metal cations, four oxygens must be arranged

on the same side of the cone-shaped calix[4]arene and that the size of the oxygen cavity thus formed is comparable with the size of Li^+ or Na^+ . In contrast, Ag^+ is efficiently bound by 1,3-alternate-**11** ($\text{R}_2 = \text{H}$).^[23–25] 1,3-Alternate-**11** ($\text{R}_2 = \text{H}$) has two ionophoric cavities, one either side, each of which is composed of two ethereal oxygens and two benzene rings. It is now considered that the binding of Ag^+ is due to the “ π -donor participation” characteristic of these cavities.^[24,25] These results indicate that, if the equilibrium between cone and 1,3-alternate forms can be regulated by some switch function, this will produce a change in the metal binding ability of calix[4]arenes.

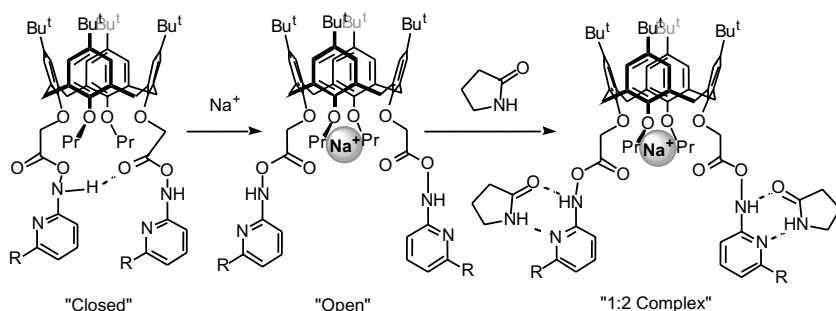


11

It has been shown that calix[4]aryl esters **12** exhibit remarkably high selectivity towards Na^+ .^[26–30] This is attributable to the internal size of the ionophoric cavity made up by the four $\text{OCH}_2\text{C}=\text{O}$ groups, which is comparable with the ion size of Na^+ .^[18] In the absence of guest metals, the carbonyls are oriented in the *exo*-annulus direction to reduce electrostatic repulsion, whereas in the presence of guest metals they rotate to the *endo*-annulus direction to coordinate to the bound metal cation. The metal-induced molecular motion of the ester groups enables the design of a new fluorogenic calix[4]arene **13**. In this compound, strong excimer emission (480 nm) was observed in the absence of metal cations, because of the mutual proximity of the two pyrene moieties. With increasing metal (Li^+ , Na^+ , or K^+) concentration, however, monomer emission increased because of the separation of the two pyrene moieties.^[31] Thus, it was possible to achieve fluorimetric metal sensing over a wide pH range. A similar idea was also reported by Jin et al.^[32] and Diamond et al.^[33] In **14**, a pyrene fluorophore is combined intramolecularly with a *p*-nitrophenyl quencher.^[34] As expected, fluorescence was efficiently quenched in the absence of metal cations, while the quenching efficiency became low in the presence of Na^+ , because of the separation of the fluorophore and the quencher.^[34]

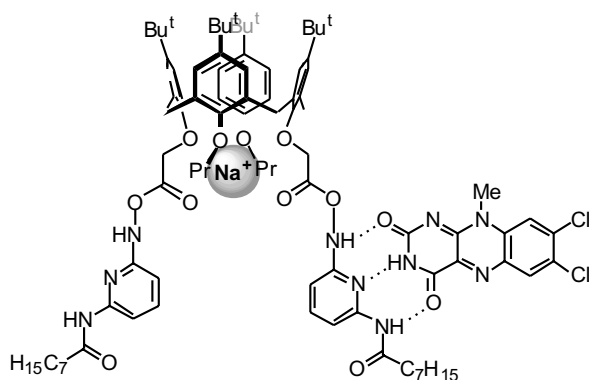


Molecular design of artificial receptors largely relies upon hydrogen-bonding interactions. However, an artificial receptor bearing both hydrogen bond donors and hydrogen bond acceptors within one molecule inevitably tends to associate intramolecularly. To avoid such undesired intramolecular association, a rigid segment may be inserted between the donor and the acceptor, so that the two sites cannot form intramolecular hydrogen bonds. This limitation frequently hampers the design of artificial receptors with a structure complementary to the guest molecule. We were thus motivated to design new artificial receptors, in which an “open” form, active to the guest, is generated from an intramolecularly hydrogen-bonded “closed” form only when it perceives a “stimulus”. We already know that in calix[4]aryls esters and amides the four carbonyl groups are turned outward to reduce electrostatic repulsion between carbonyl oxygens, while bound Na⁺ induces the *exo*-annulus carbonyls to rotate to the *endo*-annulus orientation, trapping the Na⁺ ion.^[31–34] We thus considered that such a metal-induced structural change might be useful for generating an “open” form from a “closed” form. In chloroform:acetonitrile = 9:1 (v/v), compound 15 exists as a “closed” form because of the formation of intramolecular hydrogen bonds, and cannot bind its complementary guests (such as lactams).^[35] However, when Na⁺ binds to the ionophoric cavity, this cleaves the intramolecular hydrogen bonds and the exposed receptor sites can bind the guests by means of intermolecular hydrogen bonds.



15

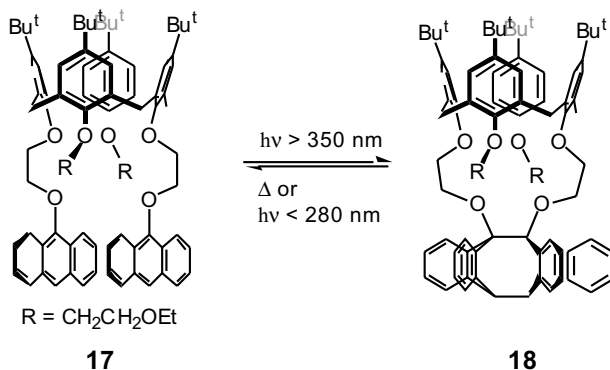
In compound **16**, the 2,6-diaminopyridine receptor sites are capable of binding guest molecules with a pteridine moiety. In the absence of metal cations, **16** is “closed”, because of the intramolecular hydrogen bonds. On the other hand, binding of Na^+ disrupts the intramolecular hydrogen bonds, and the receptor sites may associate with the pteridine moiety of a flavin.^[36a] Since the flavin is strongly fluorescent, the association process can be conveniently “read out” from a change in the fluorescence intensity.^[36a] Barbituric acid derivatives have two $\text{C}(=\text{O})\text{-NH-C}(=\text{O})$ binding sites complementary with the 2,6-diamidopyridine group. A 1:1 mixture of “closed” **16** and barbituric acid does not give any new peak in the ^1H NMR spectrum, but when an equimolar amount of NaClO_4 is added, a spectral change is induced and the formation of polymeric aggregates is confirmed.^[36b] The results indicate that one barbituric acid cross-links with two “open”-form 2,6-diamidopyridine moieties in **16** to form the polymers. This demonstrates that monomer-polymer interconversion can be achieved not only photochemically,^[16] but also by addition of metal cations.



16

To produce a calixarene-based photoregulated ion binding system, we introduced two anthracenes near the metal binding site of calix[4]arene.^[37–40] Compound **17** itself showed poor ion affinity, whereas the photochemically produced isomer **18**, with a dimeric anthracene cap, showed much improved ion affinity and sharp Na^+ selectivity.^[38,39] Although the ionophoric cavity in **18** is not so closed as to form a kinetically stable Na^+ complex, the ^1H and ^{23}Na NMR spectra established that the association-dissociation rate was much slower than that for **17**.^[38,39] Interestingly, when immobilized in a PVC membrane plasticized with di(2-ethylhexyl)sebacate, **17** underwent ring-closure to **18** when photoirradiated at 381 nm.^[40] The thermal ring-opening reaction **18**→**17** took place slowly.^[40] Although the reverse reaction could be accelerated by photoirradiation at 279 nm, this resulted in serious photodecomposition. We found that in the presence of NaClO_4 the thermal reverse reaction was completely inhibited and that it could be induced only when the membrane was photoirradiated at 279 nm.^[40] The addition of NaClO_4 efficiently suppressed the

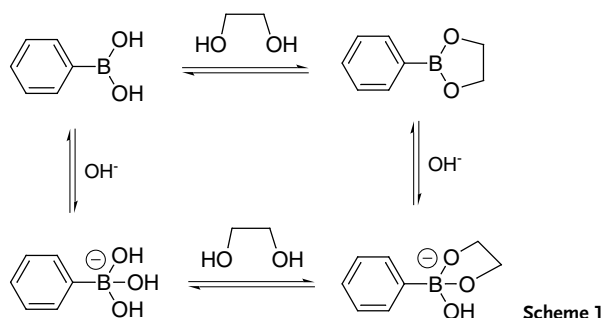
photodecomposition and the reversibility became excellent. The results indicate that this system satisfies both the thermal stability and the light stability requirements for photodevices: that is, in the presence of NaClO_4 , photochemically written memories can be safely stored, while being erasable with the aid of 279 nm irradiation.



9.4

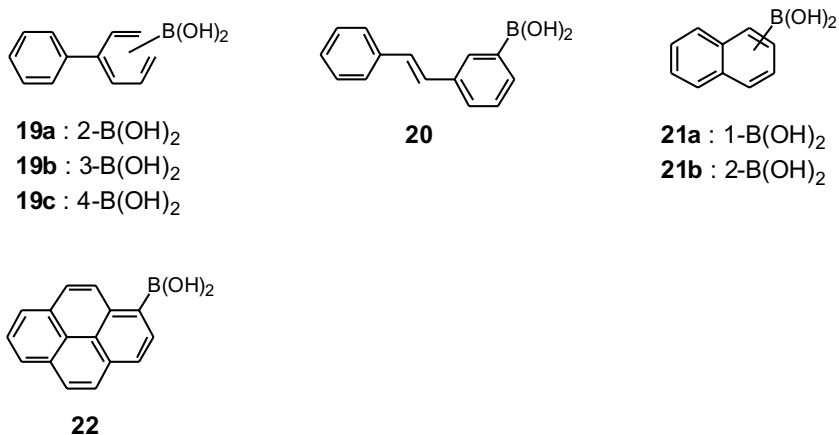
Artificial Sugar-sensing Systems utilizing Photoinduced Electron Transfer (PET)

A survey of previously published literature teaches us that hydrogen bonding interactions can be used in a versatile manner for recognition of guest molecules.^[41] We, however, are currently interested in sugar recognition and in read-out of the recognition process,^[42–45] and although hydrogen bonding interactions have also proved useful for sugar recognition in several systems,^[46–48] the effect is exerted only in aprotic organic solvents. Hence, hydrogen bonding interactions are useless for sugar recognition in water, while sugars display significant solubility only in this medium. So, *how can we “touch” sugars and “recognize” them in water?* In an attempt to solve this dilemma, we proposed the use of a boronic acid, which self-associatively forms covalent complexes with a variety of sugar molecules in water (Scheme 1).^[42–45,49–51] Since this covalent bond formation process is reversible, and the rate is much faster than the human timescale, this system may be treated like the noncovalent



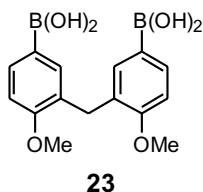
lent interactions frequently used for molecular recognition. Although this mode of operation is quite different from that found in nature (which uses hydrogen bonding interactions),^[41,46–48] it is undoubtedly a practical (and probably the sole) way to “touch” sugars in water.

It is known that the acidity of monoboric acids is intensified when they form covalent complexes with diols.^[50] Hence, at a constant pH, saccharide addition can induce a change of neutral sp^2 -hybridized boronic acids into anionic sp^3 -hybridized boronate esters. In fluorescent monoboric acids, this change is reflected in a decrease in the fluorescence intensity (I) of the neighboring fluorophore.^[47,50,52] Typical examples are compounds **19–22**.^[50,52] Among these, **19b** and **21b** can satisfy three prerequisites that may be necessary for saccharide sensing: strong fluorescence intensity, a large, pH-dependent change in I , and a shift of the pH- I profile to a lower pH region in the presence of saccharides.^[52] However, the affinity order of monoboric acids for saccharides is always the same: namely, D-fructose > D-arabinose > D-mannose > D-glucose for monosaccharides. We thus decided to direct our research effort towards selective recognition of particular saccharides.

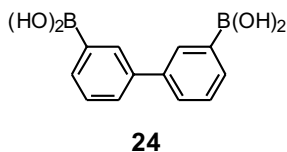


Regular monosaccharides have five OH groups. Since a boronic acid can react with a 1,2-diol (HO-C-C-OH) or a 1,3-diol (HO-C-C-C-OH) group, diboronic acids can immobilize four of these five OH groups. We thus expected that diboronic acids would show selectivity toward certain selected saccharides, and that the selectivity would depend on the relative spatial positions of the two boronic acids. Compound **23** is the first diboronic acid synthesized for this purpose. It is relatively flexible, but when it adopts a folded *syn* conformation the distance between the two boronic acids is comparable with that between the 1,2-diol and 4,6-diol in monosaccharides (about 6 Å). It was shown that, at 25 °C and pH 11.3, **23** can complex several monosaccharides, such as glucose, mannose, galactose, and talose, to form cyclic 2:1 boron/saccharide complexes.^[42] The highest affinity ($K_{\text{ass}} = 19000 \text{ M}^{-1}$) was observed for glucose.^[42] Thus, this is the first case in which boronic acid derivatives show the highest affinity for some saccharide other than fructose. D-Glucose gave a

CD spectrum with positive exciton coupling, whereas D-glucose gave a CD spectrum with negative exciton coupling.^[42] The results indicate that two dipoles present in *p*-anisylboronic acid units are oriented in an asymmetric fashion (e.g., in the clockwise direction in the **23**- D-glucose complex). D-Galactose gave a CD spectrum with negative exciton coupling, while all other D-monosaccharides and D-disaccharides tested gave CD spectra with positive exciton coupling.^[42] The results thus indicate that the absolute configuration of saccharides can be conveniently predicted from the sign and the strength of CD spectra of **23**. This means that the CD spectroscopic method using **23** as a receptor probe can serve as a new sensory system for sugar molecules.

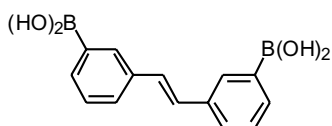


For disaccharides, compound **24** was designed, since the spacing between its two boronic acid units is similar to the spacing between the 1,2-diol and the 4'-OH and 5'-OH of disaccharides (about 7 Å).^[44] In the presence of D-maltose , a distinct CD band appeared. A split CD band crossing the $[\eta] = 0$ line at 210 nm ($\lambda_{\text{max}} = 207$ nm in the absorption spectrum) is ascribed to exciton coupling. The negative sign for the first Cotton effect (223 nm) and the positive sign for the second Cotton effect (201 nm) indicate that the two dipoles along the phenylboronic acid molecular axis are oriented in a chiral, anti-clockwise direction when they interact in the excited state. These findings reveal that when **24** forms a complex with D-maltose , the two dipoles preferentially adopt *S* chirality. Very interestingly, D-cellobiose induced a positive first Cotton effect, whereas D-lactose induced a negative one. The results imply that the complexes with D-cellobiose and D-lactose display *R* and *S* chirality, respectively. On the other hand, D-saccharose was totally CD-silent. These results consistently support the view that saccharide selectivity is achieved as a function of the separation and the relative spatial position of two intramolecular boronic acid groups.



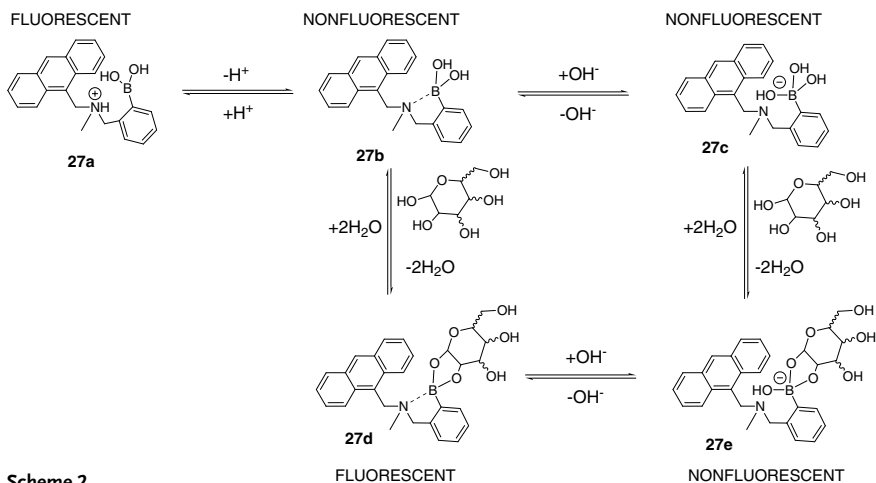
The diboronic acids **23** and **24** form rigid cyclic complexes with chiral monosaccharides and disaccharides; this is the origin of the CD observations. The induced chirality upon formation of rigid, chiral complexes was monitored by CD spectroscopy, and this rigidification process can be utilized in the design of spectroscopic

sensors. The main pathway for nonradiative deactivation of the lowest excited singlet state of stilbene is known to be through rotation of the ethylenic double bond. For stilbenes in solid matrices, viscous solvents, and cyclodextrin inclusion complexes, inhibited bond rotation followed by enhanced fluorescence emission is known to take place. The fluorescence of stilbene-3,3'-diboronic acid **25** increases upon binding to disaccharides in basic aqueous media.^[53] Large fluorescence increases have specifically been observed for the disaccharide D-(+)-melibiose in basic aqueous media, compared to small increases observed for monosaccharides (D-(+)-glucose, D-(+)-mannose, and D-(-)-arabinose). This fluorescence increase was attributed to the formation of a cyclic complex of diboronic acid with disaccharide and subsequent freezing of ethylenic bond rotation in the excited state. It seems that out of these three disaccharides, which all possess a 1,6'-ether linkage between sugar monomers, D-(+)-melibiose has the best fit with the diboronic acid receptor.

**25**

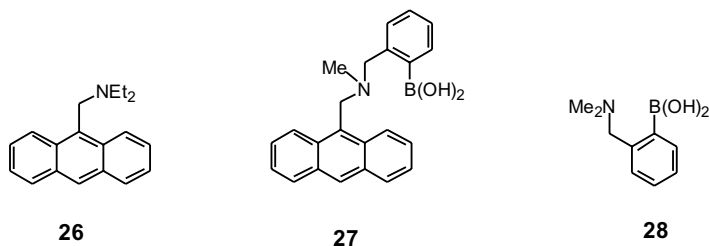
Photoinduced electron transfer (PET) has been wielded as a tool of choice in fluorescent sensor design for protons and metal ions.^[54] The design of fluorescent sensors for neutral organic species presents a harsher challenge, due to the lack of electronic changes upon inclusion. Designing a fluorescent sensor based on the boronic acid-saccharide interaction has been difficult, owing to the lack of sufficient electronic changes found in either the boronic acid moiety or in the saccharide moiety. Furthermore, facile boronic acid-saccharide complexation occurs only under the high pH conditions required to create a boronate anion.

In order to overcome these disadvantages of boronic acid-saccharide interactions, we modified the boronic acid binding site to create an improved electron center around the boronic acid moiety.^[55] It is known that saccharide complexation changes the pK_a of the boronic acid moiety,^[50,52,55–58] and we reasoned that this pK_a shift could be useful for designing new PET sensors that might drastically change fluorescence intensity and bind saccharides even in neutral pH regions. In compound **27**, the basic skeleton of a known PET sensor **26**, which exhibits an $N \rightleftharpoons NH^+$ pH dependence, is preserved (Scheme 2),^[54] while an improved binding site with an intramolecular tertiary amine, as in **28**, is also incorporated. In addition, the amine can interact intramolecularly with the boronic acid, creating a five membered ring and an sp^3 -hybridized boron atomic center. Thus, this boronic acid can bind saccharides without the aid of OH^- . The fluorescence-pH profile of **27** in unbuffered aqueous media gave one large step at low pH ($pK_a = 2.9$) and a possible small step at high pH. The pK_a of **26** is known to be 9.3 (fluorescence measurements in ethanolic aqueous media).^[54] The large shift of the pK_a to an acidic pH region is due to the interaction found between the boronic acid moiety and the amine group. However,



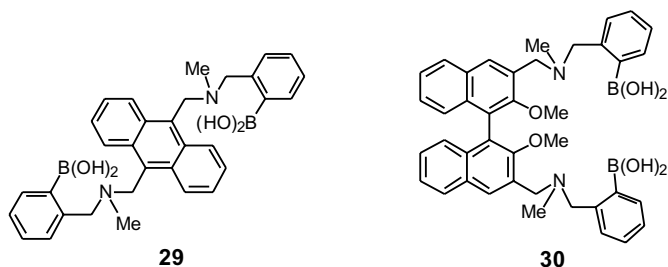
Scheme 2

the boronic acid-amine interaction does not inhibit the photoinduced electron transfer quenching process in the complex.^[55] Complete separation of the amine and the boronic acid moiety at very high pH further quenched the anthracene fluorescence. However, the fluorescence decrease was insufficient for calculation of the pK_a . The introduction of saccharides (*D*-glucose and *D*-fructose) remarkably changed the fluorescence of 27 over a large pH range. The intensified interaction between boronic acid and amine, induced upon saccharide binding,^[50,52] inhibited the electron transfer process, giving more intense fluorescence. This increased interaction is to be expected, since the binding of the saccharide to boronic acid increases its acidity, creating a more electron-deficient boron atomic center. From pH-fluorescence intensity plots, it is now obvious that 27, with the aid of the intramolecular amine, can bind saccharides even in neutral pH regions, just as simple monoboronic acids do in alkaline pH region with the aid of OH^- . The pK_a of the saccharide complex, as calculated from fluorescence measurements at high pH ($pK_a = 11.1$), is comparable with the second pK_a of 28, the parent binding moiety of 27, in the absence of saccharide ($pK_a = 11.8$).



Many monosaccharides possess at least two binding sites, by which they may be distinguished from each other. Thus, by careful manipulation of the spatial disposition of two 2-aminomethylphenylboronic acid groups, it should be possible to con-

struct saccharide-selective PET sensors. Our molecular design strategy is illustrated in compound **29**.^[56,57] The “switch-on” factor (ratio of maximum to minimum fluorescence intensity) for **29** is also greater than that for **27**. Upon 1:1 binding of glucose to **29**, the formation of a large, macrocyclic structure causes glucose to be held close to the anthracene aromatic face. Such cooperative binding of saccharides, in this case specifically glucose, occurs at very low saccharide concentrations. Because of the PET design, non-cyclic 1:1 bound species could not be detected by fluorescence spectroscopy; only the 1:1 cyclic and 1:2 complexes gave fluorescent signals. In human blood, three main monosaccharides are present: D-glucose (0.3–1.0 mM), D-fructose (≤ 0.1 mM) and D-galactose (≤ 0.1 mM). Competitive binding studies show that **29** is suitable for the detection of glucose at physiological levels.^[57]



In the case of compound **30**, chiral recognition of saccharides exploits both steric and electronic factors.^[58] The asymmetric fixing of the amine groups on the chiral binaphthyl moiety upon 1:1 complexation of saccharide D or L isomers produces a difference in PET. This difference is manifested in the maximum fluorescence intensity of the complex. Steric factors arising from the chiral binaphthyl building block are chiefly reflected in the stability constant of the complex. However, interdependency of electronic and steric factors is not ruled out. This new “molecular cleft”, with a longer spacer unit than in the anthracene-based diboronic acid **29**, gave the best recognition for fructose. D-Fructose was best bound by (R)-**30**, with a large increase in fluorescence. In this system, steric factors and electronic factors discriminate the chirality of the saccharide in bimodal fashion. Competitive studies with D- and L-monosaccharides demonstrated the possibility of selective detection of saccharide isomers. The availability of both R and S isomers of this particular molecular sensor is an important advantage, since concomitant detection by two probes is possible. Compound **30** is the first molecular sensor that can discriminate between saccharide enantiomers.^[59]

In conclusion, the recognition of saccharides by molecular receptors based on boronic acid has shown tremendous growth during the last few years: from inherent saccharide selectivity with monoboronic acids and controlled selectivity with simple diboronic acids through to the chiral recognition of saccharides. The biggest breakthrough in this study was a combination of the PET sensor concept with the boronic acid binding of sugars, which enabled us to solve two difficult problems at once: sugar-binding in neutral pH regions and read-out of the sugar-binding process. It is

undeniable that such adroit molecular design has become possible thanks to broad accumulation of knowledge on “molecular machines”.

9.5

Dynamic and Efficient Guest-binding Achieved through Allosteric Effects

Positive or negative allostery is frequently seen in nature when biological events must be efficiently regulated in response to chemical or physical signals from the outside world. Typical examples are to be observed in cooperative dioxygen binding to hemoglobin,^[60] hexamerization of arginine repressor,^[61] a cooperative effect in the concentration of arachidonate-containing phospholipids in cytosolic phospholipase A₂,^[62] and elsewhere.^[63] The biomimetic design of such allosteric systems is of great significance for regulation of complexation ability or catalytic activity of artificial receptors in allosteric fashion.^[64–72] Furthermore, the methodology is very useful for amplification and conversion of weak chemical or physical signals into other signals that may be conveniently read out and recorded. It is undeniable, therefore, that “molecular machines” can play important roles in these processes. Essentially, the allosteric systems may be classified into four different categories:

- 1) negative heterotropic,
- 2) positive heterotropic,
- 3) negative homotropic, and
- 4) positive homotropic.

There are several demonstration cases that successfully reproduce heterotropic allosteric systems.^[64–70] Design of homotropic allosteric systems, on the other hand, is more difficult, but more important for the efficient regulation of equilibria and catalysis.^[71,72] Here we introduce several examples of four different allosteric systems, designed mainly with regard to sugar recognition.

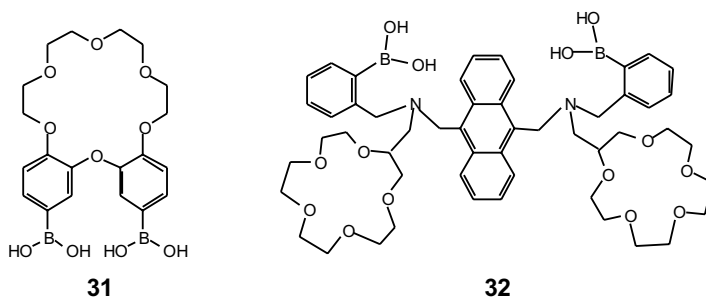
9.5.1

Negative Heterotropic Systems

The first negative heterotropic receptor in which covalent interactions (the formation of saccharide boronate esters) are coupled with metal ion complexation is compound **31**.^[73] In the design of an allosteric system, binding at the first or main site should thereby deactivate binding at the second site. To facilitate deactivation, the binding at the first site should induce a major conformational change in the molecule. From our previous work with diphenylmethane-3,3'-diboronic acid (**23**),^[42] we know that the binding of a saccharide immobilizes the two phenyls, imparting a chiral twist. This asymmetric immobilization can readily be “read-out” as a change in the circular dichroism (CD) of the benzene chromophore.^[42] If the second binding site requires a different disposition of the two aromatic rings, then negative cooperativeness, or negative allostericity, will be observed. Conversely, if both sites align with the same disposition, positive cooperativeness, or positive allostericity,

will result. One possible secondary site is a metal binding site; crown ethers are the obvious first choice in this case. If a crown ether is employed in the molecular design, then the ideal starting structure **31** should include the replacement of the methylene bridge of **23** with an oxygen. In this molecule, metal binding should induce the classic “crown” of oxygens, and this will force the phenyls into the same plane. Therefore, negative cooperativeness, or negative allostereism, is predicted.

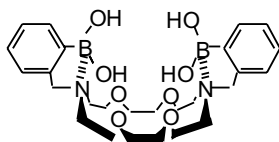
With this work we present the first example in which a saccharide (covalent) binding site and a metal (electrostatic) binding site are allosterically coupled.^[73] Conformational reorganization of the host (**31**) concomitant with metal ion complexation causes a reduction in the population of 1:1 saccharide-diboronic acid complex, which is easily monitored by the decrease in the CD intensity. Presumably, the reorganization produces a disposition of boronic acids that is unsuitable for 1:1 binding with saccharides. The adroit combination of saccharide and metal ion recognition opens the way for a chiral allosteric device in which the binding of chiral ammonium ion to the crown moiety regulates the binding of chiral saccharides.



The second example of a negative heterotropic system utilizes the crown ether metal-binding characteristic of tending to form 1:1 complexes when the metal size fits the crown cavity size and 1:2 sandwich complexes when the metal size is larger than the crown cavity size.^[74] Our earlier allosteric diboronic acid^[73] showed that boronate esters are just as useful in the construction of allosteric devices as metal ion coordination or lipophilic interactions. With diboronic acids **29** and **30**, by modifying the shape of the cleft we were able to vary the inherent selectivity of the diboronic acid. With compound **29**, glucose selectivity^[56,57] was achieved, with compound **30** chiral selectivity.^[58] In both these systems, the 1:1 intramolecular complex produced was shown to be the important CD-active and fluorescent species. From this work, we took a step towards controlling the saccharide selectivity of our fluorescent saccharide cleft **29** by means of external stimuli. On examination of CPK models for compound **32**, it can be seen that when the two 15-crown-5 rings form a metal ion sandwich, the distance between the two boronic acid moieties is increased, making the formation of the 1:1 fluorescent saccharide complex impossible. Indeed, we found that both the CD intensity and the fluorescence intensity are reduced after metal addition.^[74] With 0.1 M metal ion, the decrease in CD intensity at 258 nm is proportional to the change in fluorescence intensity. Decreases in CD intensity were observed for sodium (35 %), potassium (69 %), strontium (65 %), and barium (96 %)

and decreases in fluorescence intensity were also measured for sodium (29 %), potassium (65 %), strontium (60 %), and barium (100 %). Clearly, decomposition of the 1:1 complex with D-glucose was the cause of this decrease in fluorescence intensity. In conclusion, this is a novel negative heterotropic system, which mimics the action of the Na⁺/D-glucose cotransport protein in nature.

The third example features the more direct coupling between a diazacrown ether and a diboronic acid function, in the form of a novel diaza-18-crown-6-based sugar receptor (**33**), bearing two boronic acid groups.^[75] The purpose of this study was to design a new saccharide receptor in which a saccharide-binding site and a metal-binding site “communicated” with each other. This system can be regarded as a metal-controllable sugar receptor, or as a saccharide-controllable metal receptor. It is to be expected for **33** that boronic acids in the side arms and a metal cation bound to the crown cavity would competitively interact as “Lewis acids” with the two basic nitrogens in diaza-18-crown-6. Compound **33** forms a 1:1 complex with D-fructose or D-glucose, assisted by the intramolecular B···N interaction. Added Ca²⁺ competes with the boronic acids for the nitrogens, and hence the B···N interaction is weakened by the Ca²⁺···N interaction. In neutral pH regions, without the assistance of the B···N interaction, the diboronic acid cleft loses its saccharide-binding capability and releases the saccharide.^[75] Therefore, this study represented a novel example for the design of artificial sugar receptors in which sugar and Ca²⁺ interact competitively with the binding-sites.



33

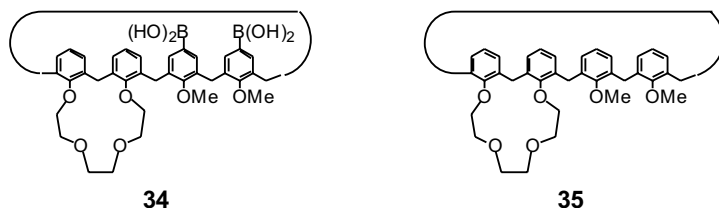
9.5.2

Positive Heterotropic Systems

It is frequently said that multipoint interaction is the origin of precise molecular recognition with high guest selectivity. These systems are more or less static, but can behave as positive heterotropic systems when they are combined with proper dynamic factors. That is, in negative heterotropic systems, two different guests produce opposing influences, whereas in positive heterotropic systems they give rise to cooperative influence. Generally speaking, it is more difficult to design for positive allosterism than for negative allosterism.

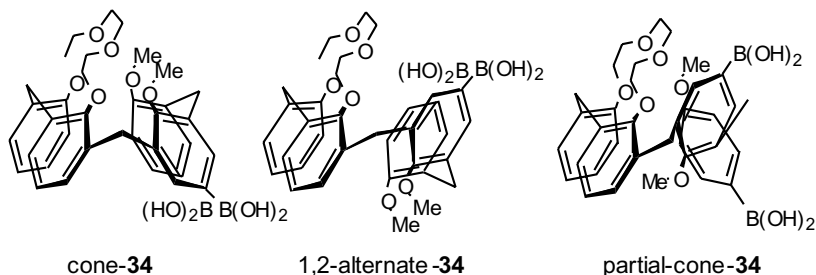
Calix[4]arenes are composed of repeating 3,3'-diphenylmethane units, useful for designing a boronic acid-based glucose receptor.^[42] Accordingly, if two boronic acids are introduced into the *para* positions of the proximal phenyl units, the compound will include the basic structure of **23** within the calix[4]arene skeleton. It is known that calix[4]arenes may change their conformation in response to metal binding.^[76,77] This

suggests that two boronic acids situated in the upper rim, acting as a saccharide binding site, may “communicate” with the metal binding site located on the lower rim. In other words, the metal binding event can change the conformation, resulting in a change in the relative spatial positions of the two boronic acids. With these objects in mind, we designed compound **34**; a crown “strap” was used to hold two proximal phenol units in a *syn* conformation (and to make the resultant ^1H NMR analysis easier).^[78]



Firstly, we investigated the metal-induced conformational change, using a model compound **35** because the conformational analysis of **34** by ^1H and ^{13}C NMR was extremely complicated. It was found that in the presence of “hard” metal cations, such as Na^+ , Mg^{2+} , and Ca^{2+} , the cone conformer was favored by the metal binding to the lower rim oxygenic site.^[78] Although cone **34** can form a CD-active 1:1 complex with *D*-glucose, the cone **34**·metal complexes cannot bind *D*-glucose, because of the significant degree of “flattening” of the phenyl groups (in other words, the distance between the two boronic acid groups is increased).^[78] On the other hand, addition of “soft” metal cations, such as K^+ , Rb^+ , and Cs^+ , increased the proportion of 1,2-alternate conformer. The appearance of the 1,2-alternate conformer is attributable to the cation- π interaction between crown-bound K^+ and two inverted benzene rings. The two boronic acids in 1,2-alternate-**34** are suitable for binding *D*-glucose, to yield a CD-active 1:1 complex.^[78]

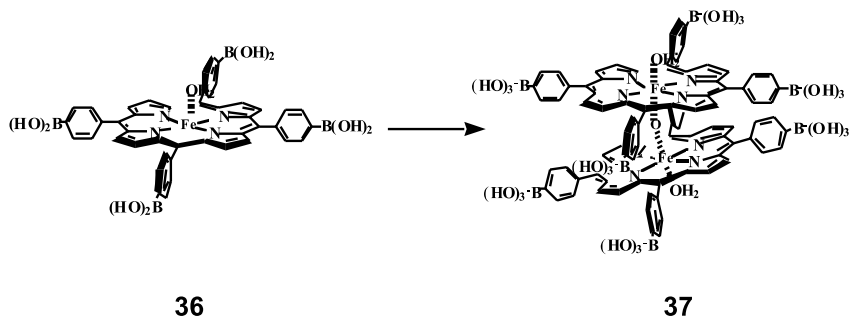
We tested whether the saccharide binding site on the upper rim could “communicate” with the metal binding site on the lower rim through the calix[4]arene cavity. The CD band weakened with increasing concentrations of Na^+ , Mg^{2+} , or Ca^{2+} .^[78] On the other hand, when K^+ , Rb^+ , or Cs^+ was added, the CD intensities increased and the spectral shape was changed.^[78] For a number of reasons, we consider the new band to be attributable to the 1,2-alternate-**34**·*D*-glucose·metal complexes. Therefore, this system is a unique example that exhibits both negative and positive allosteric interactions between metal ions and saccharides in a calix[4]arene host.



9.5.3

Negative Homotropic Systems

We previously showed that porphyrins with appended boronic acid moieties act as very useful spectroscopic sensors for detecting saccharides in water by fluorescence and for predicting their absolute configurations by circular dichroism (CD).^[79–81] Through these studies it has become clear that two boronic acids must be manipulated in appropriate spatial positions to achieve successful two-point interrogation of a specific saccharide guest.^[79–81] In these systems, it is known that only when two boronic acids are intramolecularly bridged by a saccharide do the resultant saccharide-containing macrocycles become CD-active. Here, it occurred to us that, in order to arrange two porphyrins with appended boronic acid moieties into an appropriate spatial position, a μ -oxo dimer (37) of porphinatoiron(III) 36 would have great potential: the μ -oxo dimer is formed stably in basic aqueous solution, as is the boronic acid-saccharide complex. Furthermore, the distance between two porphyrin planes (3.8 Å)^[82] is comparable with the molecular size of monosaccharides. Examination of the absorption spectra of 37 at pH 10.5 in the absence and in the presence of saccharides showed that they are scarcely affected by saccharide addition.^[83] In CD spectra, of the many monosaccharides tested, only glucose and galactose could produce the strong CD bands at Soret band wavelengths.^[83] The CD signal could be detected even for $\sim 10^{-5}$ M glucose and galactose. Thus, it may be concluded that 37 acts as a highly selective and sensitive “sugar tweezer” for glucose and galactose.



To obtain quantitative insights into the mode of binding, we estimated the stoichiometry of the complexes by a continuous variation plot of CD intensity. A sharp maximum appeared at 0.5. D-Galactose also gave the maximum at 0.5. The results indicate that even though 37 has eight boronic acid residues, only two are used in forming the 1:1 37/saccharide complexes. Examination of CPK molecular models revealed that when two boronic acid moieties react with four OH groups in these saccharides, they must approach each other closely, and the Fe-O-Fe bond angle is tilted to 150° from its regular 180° . As a result, the distance between two boronic acids in the remaining three pairs becomes too long to complex saccharides intramolecularly. Hence, this binding mode is classified as homotropic negative allostery. From plots of CD intensity (θ_{obs} at 380 nm) versus [saccharide], we estimated

the association constants (K_{ass}) to be $1.51 \times 10^5 \text{ M}^{-1}$ for glucose and $2.43 \times 10^4 \text{ M}^{-1}$ for galactose. These values are the largest for artificial saccharide receptors and one to two orders of magnitude greater than those achieved previously. The results clearly indicate that μ -oxo dimers provide an excellent platform for designing saccharide receptors based on boronic acids.

9.5.4

Positive Homotropic Systems

As mentioned above, the μ -oxo dimer **37** was formed from **36** in alkaline pH regions and showed extraordinarily high affinity and selectivity for glucose and galactose.^[83] However, only one pair of boronic acid groups was used to form 1:1 complexes with saccharides, and the remaining three pairs of boronic acids did not bind saccharides.^[83] The strong negative homotropic allosterism was attributed to an inclination of the two porphyrin planes, induced by the binding of the first saccharide guest.^[83] Hence, if the first guest could suppress the rotation of the two porphyrin planes and maintain their parallel arrangement, the second guest should be bound more efficiently and the system should exhibit positive homotropic allosterism.

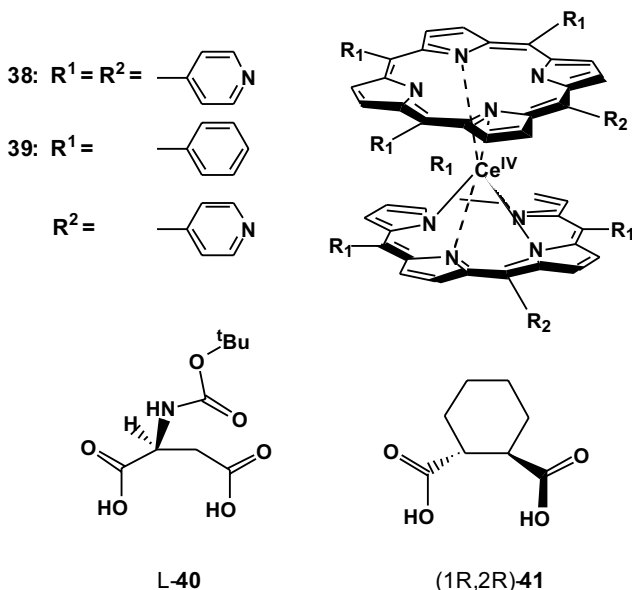
To construct such a porphyrin-based positive allosteric system, we chose a cerium(IV) bis(porphyrinate) double decker compound:^[84–86] namely the tetrakis(4-pyridyl)porphyrin derivative **38**.^[87] This molecule satisfies the aforementioned requirements: firstly, slow rotation of the two porphyrin planes with respect to one another should be possible at room temperature,^[88] in analogy to similar cerium(IV) bis(diarylporphyrin) and bis(tetraarylporphyrin) complexes studied by Aida et al.^[86] Secondly, tilting of two porphyrin planes is more difficult than in **37**, and thirdly, four pairs of 4-pyridyl groups are available as hydrogen bond acceptor sites for diols, hydroxycarboxylic acids, and dicarboxylic acids. Compound **39**, which has only one pair of pyridyl groups, was used as a reference.

Firstly, circular dichroism (CD) spectra of **38** and **39** were recorded in the presence of each of the eight guest molecules. Exciton-coupling CD bands were clearly observed for **38** in the presence of BOC-L-aspartic acid (**L-40**; BOC = *tert*-butoxycarbonyl) or (1*R*,2*R*)-1,2-cyclohexanedicarboxylic acid ((1*R*,2*R*)-**41**). Compound **39** was CD-inactive in the presence of these guest molecules. Therefore, the strong CD bands can be observed for only a proportion of the host-guest combinations. The $[\theta]_{\text{max}}$ at 310 nm was plotted against the guest concentration. The sigmoidal curvature observed for this binding system indicates that the binding of the guest to **38** is “self-accelerating”. This cooperative guest binding process can be analyzed with the Hill equation^[89]

$$\log(\gamma/(1-\gamma)) = n \log[G] + \log K, \quad (1)$$

where $[G]$ is the concentration of the guest, K the association constant, and n the Hill coefficient, and $\gamma = K/([G]^{-n} + K)$. From the slope and the intercept of the linear plots, we obtained $K = 2.63 \times 10^{11} \text{ M}^{-4}$ and $n = 3.9$ for **L-40** (correlation coefficient 0.988) and $K = 2.75 \times 10^9 \text{ M}^{-4}$ and $n = 4.0$ for (1*R*,2*R*)-**41** (correlation coefficient

0.995). The 1:4 composition of the CD-active complexes was further corroborated by Job diagram^[90]: a plot of $[\theta]_{\max}$ at 310 nm against $[38]/([38]+[L-40])$ has a maximum at 0.2. This supports the view that the complex consists of one **38** host and four **L-40** guests. These findings consistently indicate that four pairs of pyridyl groups in **38** cooperatively bind these chiral guest molecules through hydrogen bonding interactions, and that the two porphyrin planes are immobilized in a chiral conformation to give the CD-active complexes. Hence, this is a rare example of an artificial system with a strong positive allosteric effect and $n = 4$.^[91]



Here, two important questions come to mind. Firstly, why can **38** bind dicarboxylic acids, whereas **39** cannot? Secondly, why do only **40** and **41** form CD-active complexes with **38**? ¹H NMR studies established that some proton signals had shifted to lower magnetic field in the **38**·**L-40** complex, while a mixture of **39** and **L-40** did not display any such chemical shift change at all.^[87] This difference revealed the mechanism responsible for the positive allosteric effect in this system. Although host **39** has a pair of pyridyl groups, and could therefore potentially bind **40** or **(1R,2R)-41** by hydrogen bonding, the unchanged chemical shifts in the ¹H NMR spectrum suggest that this site exhibits at most only a very weak interaction with dicarboxylic acids. In other words, the first association constant K_1 for binding the first guest is very small for **39**. Conceivably, the gain in Gibbs free energy from the pyridine/carboxylic acid interaction is overcompensated by the loss of Gibbs free energy associated with suppression of the rotation of the porphyrin rings. This is also the case in **38**, for the binding of the first guest. In **38**, however, once the rotation of the porphyrin rings has been suppressed by the first guest, successive binding of the second, third, and fourth guests can occur without

such a loss of Gibbs free energy. Thus, as the number of the bound guests increases, rotation of the porphyrin rings becomes more strongly suppressed, and guest binding becomes increasingly favorable. This type of guest binding is possible only in the 1:4 complex. This is the origin of the unique positive allosterism observed for **38**.

In conclusion, it has been demonstrated that the cerium(IV) bis[tetrakis(4-pyridyl)porphyrinate] double-decker compound displays a highly homotropic positive allosteric effect, with a Hill coefficient of 4. Such strong allosteric effects are very rare in an artificial system.^[72] The origin of the cooperative guest binding is attributable to the successive suppression of the rotation of the porphyrin rings, without deformation of the basic structure of the cerium double-decker. Thus, this system should be readily applicable to the regulation of association processes and catalytic activity. For example, **38** is useful for the efficient release or capture of **L-40** and (1*R*,2*R*)-**41** in solution, and the catalytic activity of porphyrins can be regulated by means of these chiral guests.

9.6

Concluding Remarks

It seems to us that the progress of ion sensing and molecule sensing consists of three stages: (1) direct utilization of biomaterials, (2) artificial modification or semi-synthesis of biomaterials, and (3) design of totally manmade sensors. Each stage certainly has a historical reason, role, and significance. From the viewpoints of versatility and future developments, however, stage 3 seems to be most promising and active. This chapter surveys the basic molecular design concepts leading towards such manmade, artificial chemosensors. Through the work described in this survey, we have learned that dynamic events frequently play indispensable and crucial roles in designing sensing systems leading to “molecular machines”. On the other hand, if ion or molecular recognition is understood only on the basis of static events, they would appear to remain in an inadequate, closed field. Only when adroitly combined with dynamic events can they exhibit vivid, viable enhancement, sometimes mimicking important life processes. We believe that such efficient combination will find many applications for both the monitoring and the mapping of important recognition targets. This relatively new field is going to attract many scientists’ attention in the years to come.

References

- 1 J. E. Leffler, E. Grunwald, *Rates and Equilibria of Organic Reactions*, Wiley, New York, N. Y., 1963.
- 2 S. Shinkai, T. Ogawa, T. Nakajima, Y. Kusano, O. Manabe, *Tetrahedron Lett.* **1979**, 20, 4569.
- 3 S. Shinkai, T. Nakaji, Y. Nishida, T. Ogawa, O. Manabe, *J. Am. Chem. Soc.* **1980**, 102, 5860.
- 4 H. L. Ammon, S. K. Bhattacharjee, S. Shinkai, Y. Honda, *J. Am. Chem. Soc.* **1984**, 106, 262.
- 5 J.-P. Desvergne, H. Bouas-Laurent, *J. Chem. Soc., Chem. Commun.* **1978**, 403.
- 6 H. Bouas-Laurent, A. Castellan, J.-P. Desvergne, *Pure Appl Chem.* **1980**, 52, 2633.
- 7 H. Bouas-Laurent, A. Castellan, M. Daney, J.-P. Desvergne, G. Guinand, P. Marsau, M.-H. Riffaud, *J. Am. Chem. Soc.* **1986**, 108, 315.
- 8 F. Fages, J.-P. Desvergne, H. Bouas-Laurent, J.-M. Lehn, J. P. Konopelski, P. Marsau, Y. Barrans, *J. Chem. Soc., Chem. Commun.* **1990**, 655.
- 9 I. Yamashita, M. Fujii, T. Kaneda, S. Misumi, T. Otsubo, *Tetrahedron Lett.* **1980**, 21, 541.
- 10 K. Kimura, H. Tamura, T. Tsuchida, T. Shono, *Chem. Lett.* **1979**, 611.
- 11 For a comprehensive review for photoresponsive crown ethers see S. Shinkai, O. Manabe, *Top. Curr. Chem.* **1984**, 121, 67.
- 12 S. Shinkai, T. Ogawa, Y. Kusano, O. Manabe, *Chem. Lett.* **1980**, 283.
- 13 S. Shinkai, T. Nakaji, T. Ogawa, K. Shigematsu, O. Manabe, *J. Am. Chem. Soc.* **1981**, 103, 111.
- 14 S. Shinkai, K. Shigematsu, Y. Kusano, O. Manabe, *J. Chem. Soc., Perkin Trans. 1* **1981**, 3279.
- 15 S. Shinkai, T. Ogawa, Y. Kusano, O. Manabe, K. Kikukawa, T. Goto, T. Matsuda, *J. Am. Chem. Soc.* **1982**, 104, 1960.
- 16 S. Shinkai, T. Yoshida, O. Manabe, F. Fuchita, *J. Chem. Soc., Perkin Trans. 1* **1988**, 1431.
- 17 Shinkai S, Shigematsu K, Sato M, Manabe O, *J. Chem. Soc., Perkin Trans. 1* **1982**, 2735.
- 18 Comprehensive reviews for calixarene chemistry see C. D. Gutsche, *Calixarenes*, Royal Society of Chemistry, Cambridge, **1989**.
- 19 K. Iwamoto, K. Araki, S. Shinkai, *J. Org. Chem.* **1991**, 56, 4955.
- 20 S. Shinkai, K. Iwamoto, K. Araki, T. Matsuda, *Chem. Lett.* **1990**, 1263.
- 21 P. D. J. Grootenhuis, P. A. Kollman, L. C. Groenen, D. N. Reinhoudt, G. J. van Hummel, F. Ugozzoli, G. D. Andreetti, *J. Am. Chem. Soc.* **1990**, 122, 4165.
- 22 T. Harada, J. M. Rudzinski, S. Shinkai, *J. Chem. Soc., Perkin Trans. 2* **1990**, 2109.
- 23 K. Iwamoto, A. Ikeda, K. Araki, T. Harada, S. Shinkai, *Tetrahedron* **1993**, 49, 9937.
- 24 A. Ikeda, S. Shinkai, *Tetrahedron Lett.* **1992**, 33, 7385.
- 25 A. Ikeda, S. Shinkai, *J. Am. Chem. Soc.* **1994**, 116, 3102.
- 26 A. Arduini, A. Pochini, S. Reverberi, R. Ungaro, *Tetrahedron* **1986**, 42, 2089.
- 27 S.-K. Chang, I. Cho, *J. Chem. Soc., Perkin Trans. 1* **1986**, 211.
- 28 F. Arnard-Neu, E. M. Collins, M. Deasy, G. Ferguson, S. J. Harris, B. Kaitner, A. J. Lough, M. A. McKervey, E. Marques, B. L. Ruhl, M. J. Schwing-Weill, E. M. Seward, *J. Am. Chem. Soc.* **1989**, 111, 8681.
- 29 T. Arimura, M. Kubota, T. Matsuda, O. Manabe, S. Shinkai, *Bull. Chem. Soc. Jpn.* **1989**, 62, 1674.
- 30 K. Iwamoto, S. Shinkai, *J. Org. Chem.* **1992**, 57, 7066.
- 31 I. Aoki, Y. Kawahara, K. Nakashima, S. Shinkai, *J. Chem. Soc., Chem. Commun.* **1991**, 1771.
- 32 T. Jin, K. Ichikawa, T. Koyama, *J. Chem. Soc., Chem. Commun.* **1992**, 499.
- 33 C. Perez-Jimenez, S. J. Harris, D. Diamond, *J. Chem. Soc., Chem. Commun.* **1993**, 480.
- 34 I. Aoki, T. Sakaki, S. Shinkai, *J. Chem. Soc., Chem. Commun.* **1992**, 730.
- 35 H. Murakami, S. Shinkai, *Tetrahedron Lett.* **1993**, 34, 4237.
- 36 a) H. Murakami, S. Shinkai, *J. Chem. Soc., Chem. Commun.* **1993**, 1533; b) P. Lhotak, S. Shinkai, *Tetrahedron Lett.* **1995**, 36, 4829.
- 37 G. Deng, T. Sakaki, Y. Kawahara, S. Shinkai, *Tetrahedron Lett.* **1992**, 33, 2163.
- 38 G. Deng, T. Sakaki, K. Nakashima, S. Shinkai, *Chem. Lett.* **1992**, 1287.
- 39 G. Deng, T. Sakaki, Y. Kawahara, S. Shinkai, *Supramol. Chem.* **1993**, 2, 71.
- 40 G. Deng, T. Sakaki, S. Shinkai, *J. Polym. Sci., Polym. Chem.* **1993**, 31, 1915.
- 41 For comprehensive reviews see a) J. Rebek Jr., *Angew. Chem. Int. Ed. Engl.* **1990**, 29, 245; b) A. D. Hamilton, *Bioorg. Chem. Front.* **1991**, 2, 115.
- 42 a) K. Tsukagoshi, S. Shinkai, *J. Org. Chem.* **1991**, 56: 4089; b) Y. Shiomi, M. Saisho, K. Tsukagoshi, S. Shinkai, *J. Chem. Soc., Perkin Trans. 1* **1993**, 2111.

- 43 S. Shinkai, K. Tsukagoshi, Y. Ishikawa, T. Kunitake, *J. Chem. Soc., Chem. Commun.* **1991**, 1039.
- 44 K. Kondo, Y. Shiomi, M. Saisho, T. Harada, S. Shinkai, *Tetrahedron* **1992**, *48*, 8239.
- 45 T. D. James, T. Harada, S. Shinkai, *J. Chem. Soc., Chem. Commun.* **1993**, 857.
- 46 K. Kano, K. Yoshiyasu, S. Hashimoto, *J. Chem. Soc., Chem. Commun.* **1988**, 801.
- 47 Y. Aoyama, Y. Tanaka, H. Toi, H. Ogoshi, *J. Am. Chem. Soc.* **1988**, *110*, 634.
- 48 Y. Kikuchi, K. Kobayashi, Y. Aoyama, *J. Am. Chem. Soc.* **1992**, *114*, 1351.
- 49 J. P. Lorand, J. O. Edwards, *J. Org. Chem.* **1959**, *24*, 769.
- 50 J. Yoon, A. W. Czarnik, *J. Am. Chem. Soc.* **1992**, *114*, 5874.
- 51 L. K. Mohler, A. W. Czarnik, *J. Am. Chem. Soc.* **1993**, *115*, 2998.
- 52 a) K. Nakashima, S. Shinkai, *Chem. Lett.* **1994**, 1267; b) H. Suenaga, M. Mikami, K. R. A. S. Sandanayake, S. Shinkai, *Tetrahedron Lett.* **1995**, *36*, 4825.
- 53 K. R. A. S. Sandanayake, K. Nakashima, S. Shinkai, *J. Chem. Soc., Chem. Commun.* **1994**, 1621.
- 54 a) A. J. Bryan, A. P. de Silva, R. A. D. Rupasingha, K. R. A. S. Sandanayake, *Biosensors* **1989**, *4*, 169; b) A. P. de Silva, R. A. D. Rupasingha, *J. Chem. Soc., Chem. Commun.* **1985**, 1669.
- 55 T. D. James, K. R. A. S. Sandanayake, S. Shinkai, *J. Chem. Soc., Chem. Commun.* **1994**, 477.
- 56 T. D. James, K. R. A. S. Sandanayake, S. Shinkai, *Angew. Chem. Int. Ed. Engl.* **1994**, *33*, 2207.
- 57 T. D. James, K. R. A. S. Sandanayake, R. Iguchi, S. Shinkai, *J. Am. Chem. Soc.* **1995**, *117*, 8982.
- 58 T. D. James, K. R. A. S. Sandanayake, R. Iguchi, S. Shinkai, *Nature* **1995**, *374*, 345.
- 59 For an extension of this study see M. Takeuchi, S. Yoda, S. Shinkai, *Tetrahedron* **1997**, *53*, 8335.
- 60 a) M. F. Perutz, *Ann. Rev. Biochem.* **1979**, *48*, 327; b) J. Monod, J.-P. Changeux, F. Jacob, *J. Mol. Biol.* **1963**, *6*, 306; c) M. F. Perutz, G. Fermi, B. Luisi, B. Shaanan, R. C. Liddington, *Acc. Chem. Res.* **1987**, *20*, 309.
- 61 R. Gramdori, T. A. Lavoie, M. Pflumm, G. Tian, H. Niersbach, W. K. Maas, R. Fairman, J. Carey, *J. Mol. Biol.* **1995**, *254*, 150.
- 62 J. R. Burke, M. R. Witmer, J. Tredup, R. Micanovic, K. R. Gregor, J. Lahiri, K. M. Trampusch, J. J. Villafranca, *Biochemistry* **1995**, *34*, 15165.
- 63 a) A. M. Filenko, V. M. Danilova, A. Sobieszek, *Biophys. J.* **1997**, *73*, 1593; b) S. Modi, D. E. Gilham, M. J. Sutcliffe, L.-Y. Lian, W. V. Primrose, C. R. Wolf, G. C. K. Roberts, *Biochemistry* **1997**, *36*, 4461; c) F. J. Bruzzese, P. R. Connelly, *ibid.* **1997**, *36*, 10428; d) J. A. Schetz, D. R. Sibley, *J. Neurochem.* **1997**, *68*, 1990.
- 64 T. G. Traylor, M. Mitchell, J. P. Ciconene, S. Nelson, *J. Am. Chem. Soc.* **1982**, *104*, 4986.
- 65 a) J. Rebek, Jr., *Acc. Chem. Res.* **1984**, *17*, 258; b) J. Rebek, Jr., T. Costello, L. Marshall, R. Wattle, R. C. Gadwood, K. Onan, *J. Am. Chem. Soc.* **1985**, *107*, 7481.
- 66 a) I. Tabushi, S. Kugimiya, M. G. Kinnaird, T. Sasaki, *J. Am. Chem. Soc.* **1985**, *107*, 4129; b) I. Tabushi, S. Kugimiya, *ibid.* **1986**, *108*, 6926.
- 67 P. D. Beer, A. S. Rothin, *J. Chem. Soc., Chem. Commun.* **1988**, 52.
- 68 R. C. Petter, J. S. Salek, C. T. Sikorski, G. Kumaravel, F.-T. Lin, *J. Am. Chem. Soc.* **1990**, *112*, 3860.
- 69 H.-J. Schneider, D. Ref, *Angew. Chem. Int. Ed. Engl.* **1990**, *29*, 1159.
- 70 R. P. Sijbesma, J. R. Nolte, *J. Am. Chem. Soc.* **1991**, *113*, 6695.
- 71 Y. Kobuke, Y. Satoh, *J. Am. Chem. Soc.* **1992**, *114*, 789.
- 72 K. Kobayashi, Y. Asakawa, Y. Kato, Y. Aoyama, *J. Am. Chem. Soc.* **1992**, *114*, 10307.
- 73 G. Deng, T. D. James, S. Shinkai, *J. Am. Chem. Soc.* **1994**, *116*, 4567.
- 74 T. D. James, S. Shinkai, *J. Chem. Soc., Chem. Commun.* **1995**, 1483.
- 75 K. Nakashima, S. Shinkai, *Chem. Lett.* **1994**, 1267.
- 76 S. Shinkai, K. Iwamoto, K. Araki, T. Matsuda, *Chem. Lett.* **1990**, 1263.
- 77 K. Iwamoto, A. Ikeda, K. Araki, T. Harada, S. Shinkai, *Tetrahedron* **1993**, *49*, 9937.
- 78 F. Ohseto, H. Yamamoto, H. Matsumoto, S. Shinkai, *Tetrahedron Lett.* **1995**, *36*, 6911.
- 79 T. Imada, H. Murakami, S. Shinkai, *J. Chem. Soc., Chem. Commun.* **1994**, 1557.
- 80 T. Imada, H. Kijima, M. Takeuchi, S. Shinkai, *Tetrahedron* **1996**, *52*, 2817.

- 81 M. Takeuchi, H. Kijima, I. Hamachi, S. Shinkai, *Bull. Chem. Soc. Jpn.* **1997**, *70*, 699.
- 82 B. Cheng, J. D. Hobbs, P. G. Debrunner, J. Erlebacher, J. A. Shelnut, W. R. Scheidt, *Inorg. Chem.* **1995**, *34*, 102.
- 83 a) M. Takeuchi, T. Imada, S. Shinkai, *J. Am. Chem. Soc.* **1996**, *118*, 10658; b) Idem, *Bull. Chem. Soc. Jpn.* **1998**, *71*, 1117.
- 84 J. W. Buchler, M. Nawra, *Inorg. Chem.* **1994**, *33*, 2830 and references cited therein.
- 85 J. Jiang, K. Machida, G. Adachi, *J. Alloys Compd.* **1993**, *32*, 950 and references cited therein.
- 86 K. Tashiro, K. Konishi, T. Aida, *Angew. Chem. Int. Ed. Engl.* **1997**, *36*, 856.
- 87 M. Takeuchi, T. Imada, S. Shinkai, *Angew. Chem. Int. Ed. Engl.* **1998**, *37*, 2096.
- 88 M. Takeuchi, T. Imada, M. Ikeda, S. Shinkai, *Tetrahedron Lett.* **1998**, *39*, 7897.
- 89 K. A. Connors, *Binding Constants*, Wiley, New York, **1987**.
- 90 A. Job, *Ann. Chem. (Paris)* **1928**, *9*, 113.
- 91 To the best of our knowledge, there exists only one precedent that achieves positive homotropic allosterism with $n=4$: see Ref. 72.

10

Multistate/Multifunctional Molecular-level Systems – Photochromic Flavylum Compounds

Mauro Maesri, Fernando Pina, and Vincenzo Balzani

10.1

Introduction

Great interest is currently being devoted to molecular or supramolecular species existing in two forms, interconversion of which can be modulated by means of an external stimulus.^[1–6] The design of such molecular-level switching devices is directly related to the chemistry of signal generation, transfer, conversion, storage, and detection (semiochemistry).^[3]

Typical bistable species are the so-called photochromic compounds: molecules that can be reversibly interconverted, with at least one of the reactions being induced by light excitation, between two forms displaying different absorption spectra.^[7,8]

Photochromism was first described in the scientific literature in 1876.^[7] In his famous paper entitled “The Photochemistry of the Future” (1912), G. Ciamician^[9] discussed the importance of photochromic substances and mentioned the possibility of using such compounds for fashion purposes. Photochromism is also a natural phenomenon; most biologic photoreceptors exhibit photochromic behavior.^[10] Until the middle of this century research on photochromic compounds was mainly carried out in academic centers, but around 1960 it was recognized that this subject is also of considerable commercial interest and since then most of the research has been done in industrial laboratories. The applications of photochromic materials can be classified as follows:^[7]

- (i) applications depending upon sensitivity to radiation of some kind (for example, self-developing photography, protective materials, camouflage, decoration);
- (ii) applications depending upon reversibility (such as protection against sunlight, smart windows, protection against intense flashes of light, data storage and retrieval);
- (iii) applications depending upon thermal, chemical, or physical properties (such as temperature indicators, photoresist technology, photocontractile polymers, Q-switches, security printing). Currently, much interest is being devoted to the possibility of using photochromic compounds for information processing at the molecular level.

The first scientist to carry out systematic investigations on photochromic compounds as computer memory elements was Hirshberg.^[11,12] In the years following, there has been strong development of research into photochromic molecular memories, with a great number of patents granted, particularly in Japan.^[7] By reducing switching elements to molecular size, it would be possible to increase the memory density of computers by several orders of magnitude and to reduce their power requirements very significantly.^[13] The potential of information storage in chemical system is demonstrated by DNA, which has an estimated capacity of 10^{21} bits/cm³. A CD-ROM (compact disk, read only memory) holds approximately 10^8 bits/cm². Photochromic materials can offer (although not necessarily simultaneously) increased capacity (to $>10^{12}$ bits/cm²), a simple readout mechanism, the possibility of optical replication, and selective erase and rewrite facilities.

Apart from future applications for information processing at the molecular level,^[14] the study of compounds capable of existing in different forms that can be interconverted by means of external stimuli is a topic of great fundamental interest.^[1–6] Recently it has been shown that suitably designed photochromic compounds may

- (i) be used to obtain switchable quadratic non linear optic properties,^[15]
- (ii) behave as logic gates,^[16–19]
- (iii) exhibit very complex chemical reaction patterns,^[17–19] and
- (iv) be used as components of rudimentary neuron-like networks.^[20]

In this chapter, we discuss the multistate/multifunctional character of the chemistry of synthetic photochromic flavylum compounds and show that the examination of complex chemical systems from novel viewpoints may reveal very interesting features and may be useful to introduce new concepts in the field of chemical research.

10.2

Multistate/Multifunctional Compounds

The simplest photochromic compounds are bistable species that can be interconverted between two forms (X and Y) exhibiting different colors.^[7,8,21] Most photochromic compounds change their color as a result of photoexcitation and revert more or less slowly to their initial state when kept in the dark (Figure 1a). Compounds exhibiting this behavior are useless for information storage (or switching purposes), since the written information (switching state) is spontaneously erased (back-converted) after a relatively short time.

Other photochromic compounds do not revert to their initial state thermally, but can undergo reversible photoisomerization (Figure 1b).^[22] Such compounds can be used in optoelectronic devices. However they present a severe problem. The light used for reading the written data (detecting the switching state) causes the back-conversion of the sampled molecules, and thus the gradual loss of information (state definition). Several attempts have been made to overcome this difficulty, including

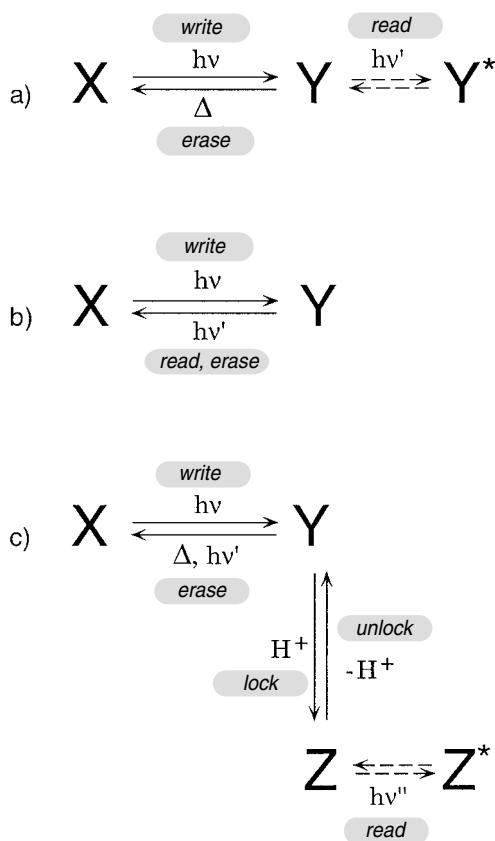


Fig. 1: Schematic representation of the behavior of three types of photochromic systems. (a) The photochemical reaction of the form **X** reverts by thermal means in the dark, (b) The photochemical reaction of the form **X** reverts only through light excitation of the form **Y**; (c) The form **Y**, which reverts to **X** through light excitation, can be transformed by means of a second stimulus (such as an acid/base reaction) into another form **Z**, which is stable toward light excitation and, when necessary, can be reconverted to **Y**. For more details, see text.

the use of photochemically inactive infrared light to read the status of the system.^[23,24]

A general approach to avoiding destructive reading is to combine two reversible processes that can be addressed by means of two different stimuli (dual-mode systems).^[25–30] The additional stimulus can be another photon,^[26] heat,^[27] an electron,^[25,28] a proton,^[29] or something even more subtle, such as formation of a hydrogen bond.^[30] In such systems (Figure 1c), light is used to convert **X** to **Y** (write), then a second stimulus (such as a proton, as in Figure 1c) is employed to transform **Y** (which would be reconverted back to **X** by a direct photon reading process) into **Z**, a different, stable state of the system (lock), which can be optically detected without being destroyed (read). This process safeguards the change initially induced by the writing photon. When the written information is to be erased, **Z** is reconverted back to **Y** (unlock; for example, by addition of a base, as in the example of Figure 1c) and **Y** is then reconverted back to **X** (erase). Such a write-lock-read-unlock-erase cycle could constitute the basis for an optical memory system with multiple storage and nondestructive readout capacity.

The concept of dual-mode stimulation can be expanded further. It is possible to devise systems capable of existing in several forms (multistate) that can be interconverted by different external stimuli (multifunctional). Such systems can give rise to intricate networks of reactions that, when examined from the viewpoint of “molecular-level devices”^[31] reveal very interesting properties.^[32]

Like anthocyanins,^[33] which are one of the most important sources of color in flowers and fruits, synthetic flavylum salts in aqueous solutions undergo various structural transformations^[34–37] that can be driven by pH changes and light excitation. Such transformations are often accompanied by quite dramatic color changes or color disappearance. In the last few years, the thermal and photochemical reactions of several synthetic flavylum salts have been investigated in great detail,^[17–19,34–43] and it has been shown that some of these compounds can perform write-lock-read-unlock-erase cycles and can also exhibit multistate/multifunctional behavior.

10.3

Natures of the Species Involved in the Chemistry of Flavylum Compounds

The basic scheme relevant to discussion of the structural transformations of flavylum-type compounds is that shown in Figure 2.^[33–37] As we will see below, other forms may also be involved, depending on the nature of the substituents in the 4-, 7-, and 4'-positions. The flavylum cation AH^+ , the stable form in strongly acidic solution, can easily be prepared by acidic condensation of salicylaldehyde and acetophenone derivatives, as well as by other routes.^[44] In moderately acidic or neutral solution, the thermodynamically stable form is generally the neutral *trans*-2-hydroxychalcone species **Ct**, which is formed from AH^+ through the two intermediate compounds **B2** and **Cc**. **B2** is a hemiacetal species, obtained by hydration at the 2-position of the flavylum cation, and **Cc** is a *cis*-2-hydroxychalcone, formed from the hemiacetal **B2** through a tautomerism process. The interesting feature of these systems is that the AH^+ and **B2** forms can be reversibly interconverted by changing the pH,^[34–37] whereas **Cc** and **Ct** can be interconverted by photoexcitation.^[17–19,38–43,45–48] Since the **B2** and **Cc** forms are in tautomeric equilibrium, it follows that pH and photostimulation can be used to induce interconversion of the four fundamental forms (Figure 2). Furthermore, the AH^+ form exhibits acid properties not only at the 2-position, but also at the 4-position, to give the **B4** basic species. In their turn, **Cc** and **Ct** can undergo deprotonation to give the respective Cc^- and Ct^- monoanions which, being *cis/trans* isomers, can in principle be interconverted by light excitation. As we will see later, depending on the nature of the substituents, other acid/base equilibria and *cis/trans* couples may be present. It is therefore clear that in these systems, pH changes coupled with light excitation may produce very intricate series of chemical reactions, with dramatic changes in absorption spectra (i.e., in the color of the system). A further interesting aspect is that some of the species exhibit fluorescence, which is not only another analytical “handle” to control the behavior of the system, but also a very interesting signal for the purpose of information processing.

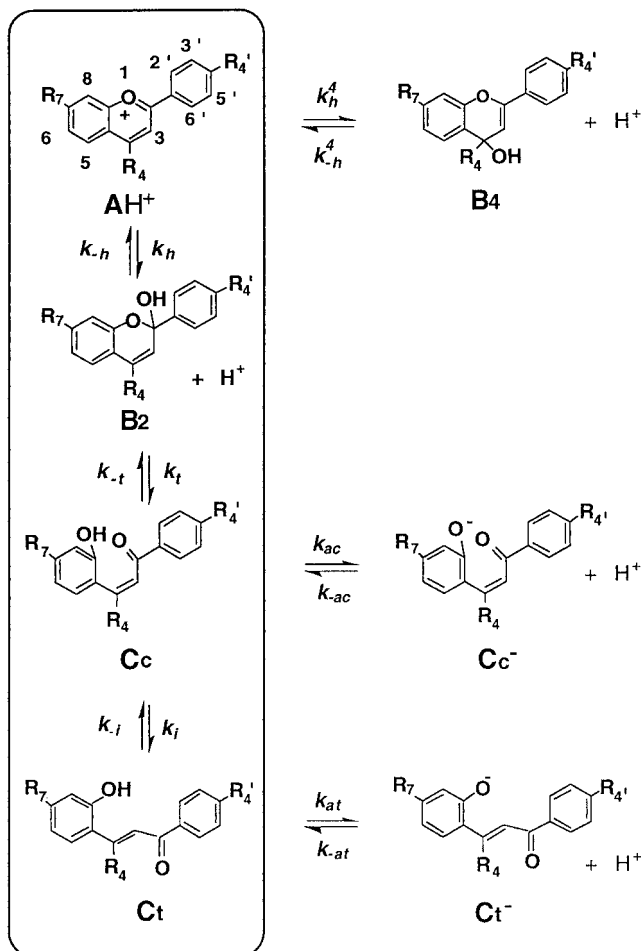


Fig. 2: Structural transformations of flavylum-type compounds. Only the most important forms are shown.

Several investigations concerning the thermodynamic and kinetic aspects of the thermal reactions of flavylum-type compounds have long been in the literature,^[33–37] while photochemical and photophysical aspects have been systematically examined more recently.^[17–19,38–43] As we shall see below, pH jump, temperature jump, and flash photolysis experiments permit measurement of the rate constants of some of the reactions involved, and steady state titration experiments (using UV/Vis and NMR techniques) allow the measurement of equilibrium constants. In order to illustrate the complex reaction network in which these systems operate, we will now focus on the behavior of the 4'-methoxyflavylum ion (Figure 2; $R_4 = R_7 = \text{H}$, $R_4' = \text{OCH}_3$).^[39]

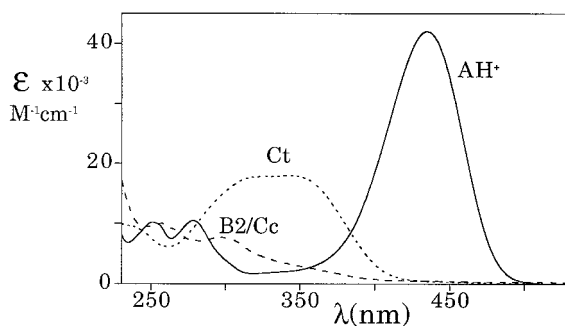


Fig. 3: Absorption spectra in aqueous solution at 25 °C of the 4'-methoxyflavylium compound: **AH⁺** at pH = 1.0, **Ct** at pH = 4.0 and **B2/Cc** mixture at pH = 7.0.^[39]

10.4

Thermal Reactions of the 4'-Methoxyflavylium Ion

A very careful spectroscopic and kinetic investigation of the transformations undergone by the 4'-methoxyflavylium ion was originally performed by McClelland and Gedge.^[36] Using the pH-jump technique, they found that seven different species were involved as transient or equilibrium compounds, depending on the experimental conditions (Figure 2). The absorption spectra of the strongly colored 4'-methoxyflavylium cation **AH⁺** ($\lambda_{\text{max}} = 435 \text{ nm}$, $\epsilon = 42,000 \text{ M}^{-1} \text{ cm}^{-1}$), the colorless *trans*-4'-methoxychalcone **Ct** ($\lambda_{\text{max}} = 350 \text{ nm}$, $\epsilon = 18,000 \text{ M}^{-1} \text{ cm}^{-1}$), and the **B2** and **Cc** mixture are shown in Figure 3.

The molar fraction distribution^[36,47a] of the various species as a function of pH, in aqueous solution at 25 °C, was obtained from the equilibrium constants (vide infra) and is shown in Figure 4. The thermodynamically stable form in the pH range 2–8 is the *trans*-4'-methoxychalcone, **Ct**, which, at higher pH, is transformed into its anion, **Ct⁻** (Figure 4, solid lines). In strongly acidic solutions, **AH⁺** becomes thermodynamically stable; however, **Ct** cannot convert into **AH⁺** because of the very large activation barrier, which reflects the isomerization of **Ct** to the intermediate compound **Cc** (Figure 2). Furthermore, a solution of **AH⁺** is almost indefinitely stable at room temperature below pH 3, since under such conditions a very large kinetic barrier prevents conversion of **AH⁺** to the thermodynamically stable **Ct** form via the hydrated (pseudobase) species **B2** and the **Cc** isomer (Figure 2). At higher pH, however, **AH⁺** is very reactive.^[36] For example, when starting from an aqueous solution of **AH⁺** at 25 °C and pH = 1, a pH jump to pH = 4.29 leads within a few seconds to a pseudoequilibrium consisting of 50 % **AH⁺**, 33.2 % **B2**, 0.3 % **B4**, and 16.5 % **Cc** (Figure 4, dashed lines). A much slower reaction follows (half-life 19.7 h), resulting in complete conversion to the thermodynamically stable form **Ct**.

At pH 8, **AH⁺** reacts mainly with solvent water (half-life 0.44 s) to produce 64 % **B4**, 24 % **B2**, and 12 % **Cc**, the last two existing in equilibrium with each other (equilibration half-life, $7 \times 10^{-5} \text{ s}$).^[36] This is followed by another fast reaction (half-life 66 s) in which **B4**, a product of kinetic control of the initial neutralization of **AH⁺**, is converted via **AH⁺** to **B2** and **Cc**, yielding a pseudoequilibrated mixture of

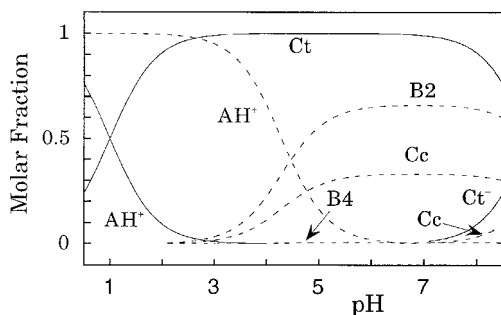


Fig. 4: Molar fraction distribution as a function of pH, in aqueous solution at 25 °C, for the 4'-methoxyflavylium compound. Solid lines refer to the species obtained at the thermodynamic equilibrium. Dashed lines refer to species obtained by bringing

AH^+ solutions from pH = 1 to higher pH values by the pH-jump technique or by exciting **Ct** solutions by a light flash. Such species reach a pseudoequilibrium on a time scale of seconds and then undergo a very slow, thermal transformation to **Ct**.^[39]

66.3 % **B2**, 33.1 % **Cc**, and 0.6 % **B4** (Figure 4, dashed lines). A much slower reaction (half-life 9.9 h) then occurs, resulting in complete conversion to **Ct**.

10.5

Photochemical Behavior of the 4'-Methoxyflavylium Ion

As described above, in the pH range 2–8 the colorless *trans*-4'-methoxychalcone **Ct** is the thermodynamically stable species and therefore it is the final product of the transformations of the strongly colored 4'-methoxyflavylium ion AH^+ . Even at pH = 1, at which AH^+ is the thermally stable species, **Ct** can be kinetically stable because of the high energy barrier of its transformation into **Cc**. **Ct**, however, can be converted into AH^+ photochemically.^[39] As might be expected from the thermal behavior of the system, the photoreaction may result either in a transient or in an almost permanent effect, depending on the temperature and the pH of the irradiated solution.

10.5.1

Continuous Irradiation

Continuous irradiation of 2.3×10^{-5} M aqueous solutions of **Ct** at pH = 1.0 with 365 nm light causes strong spectral changes, with five isosbestic points and formation of a very intense band in the visible region, with its maximum at 435 nm (Figure 5a).^[39] Analysis of the spectral changes shows that the photoreaction converts **Ct** into AH^+ , without formation of sizeable amounts of other products. The quantum yield of the photoreaction is 0.04, independent of the presence of dioxygen in solution. At pH = 1.0, no back-reaction takes place and irradiation with 434 nm light, corresponding to the maximum of the absorption band of AH^+ (Figure 3), does not have any effect.

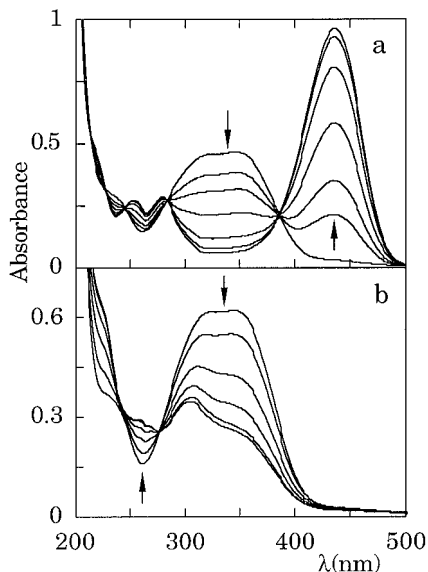


Fig. 5: Spectral changes caused by continuous irradiation of aqueous solutions of the **Ct** form of 4'-methoxyflavylium ion with 365 nm light: (a) pH = 1.0, $[\text{Ct}] = 2.5 \times 10^{-5}$ M; the curves correspond to the following irradiation

times : 0; 0.5; 1; 2; 4; 7; 12 minutes. (b) pH 7.0, $[\text{Ct}] = 3.2 \times 10^{-5}$ M; the curves correspond to the following irradiation times: 0; 0.25; 1.5; 3; 6; 10 minutes.^[39]

When irradiation of **Ct** is carried out at pH = 4.0, the quantum yield of the photo-reaction leading from **Ct** to **AH⁺** does not change, but the expected thermal back-reaction of **AH⁺** to **Ct** is observed. The rate of the back-reaction increases with temperature (activation energy 93 kJ mol⁻¹ at pH = 4.0). Irradiation at pH = 7.0 causes the spectral changes shown in Figure 4b. At this pH, the disappearance of **Ct** does not cause any increase of absorbance in the visible spectral region, thus showing that **AH⁺** is not formed. Furthermore, the back-reaction is very fast, so complete disappearance of **Ct** cannot be observed. This is in full agreement with expectations

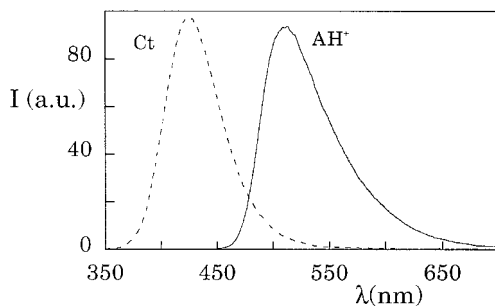


Fig. 6: Fluorescence spectra in aqueous solution at 25 °C of the **AH⁺** (pH = 1.0) and **Ct** (pH = 4.0) forms of the 4'-methoxyflavylium ion.^[39]

based on the data shown in Figure 4, which indicate that at pH = 7.0 the pseudo-equilibrated mixture of products is composed essentially of the open **Cc** and the closed **B2 cis** forms. As is always the case for aromatic derivatives of ethylene,^[49] the absorption spectrum of this mixture of *cis* species is less intense than the spectrum of the *trans* form (Figure 3), and slightly blue-shifted. Under such conditions, irradiation of the mixture with 313 nm light causes the reverse *cis*→*trans* photoisomerization reaction with an apparent quantum yield of approximately 0.5 (based on the total light absorbed by **Cc** and **B2**).

Interestingly, **Ct** and **AH⁺** exhibit intense fluorescence bands with λ_{max} at 430 and 530 nm, respectively (Figure 6).^[39] The fluorescence lifetime is shorter than 1 nanosecond in both cases. It is worth noting that the occurrence of the thermal and photochemical reactions described above can also be followed by fluorescence measurements.

10.5.2

Pulsed Irradiation

Flash photolysis is a powerful technique for investigating the kinetics of conversion of the various forms of flavylium ions.^[47c] Even with a simple flash-photolysis apparatus, with a time resolution of approximately 0.2 s, it is possible to obtain kinetic data that can complement and/or replace those obtainable by the pH-jump technique.

Flash excitation^[39] of 6.0×10^{-5} M aqueous solutions of **Ct** at 25 °C and pH = 3.0 or 7.0 causes a bleaching in the 300–400 nm region, which can be assigned to the disappearance of **Ct**. At pH 3, a strong increase in absorbance in the 400–500 nm region is observed, as expected for the formation of **AH⁺**. Absorbance versus time traces show that **Ct** disappears within the timescale of the flash, but that its disappearance does not lead directly to **AH⁺**. One or more intermediate products are formed (**Cc** and **B2** according to the scheme of Figure 2), and these then convert completely to **AH⁺** in a few seconds. At pH = 7.0, the decrease in absorbance in the 300–400 nm region, corresponding to the disappearance of **Ct**, is not accompanied by an increase in absorbance in the visible region, because **AH⁺** is not stable in neutral solution and the main products of the photoreaction are **B2** and **Cc** (Figure 4). None of the thermal and photochemical processes observed are affected by the presence of dioxygen in the solution.

In order to check the degree of reversibility of the observed reactions, a 1.0×10^{-5} M aqueous solution of **Ct** at pH = 3.0 and 60 °C was irradiated at 365 nm. After 20 minutes of irradiation, resulting in the formation of the colored form **AH⁺**, the solution was kept in the dark, at 60 °C, until practically complete bleaching of the **AH⁺** visible absorption had occurred. Then, photoexcitation was again performed. Figure 7 shows the changes in absorbance (at 435 nm) obtained on repeating these light/dark cycles five times. As can be seen, the degree of reversibility of the system is satisfactory.^[39]

In conclusion, the photochemical behavior is in agreement with that observed in pH-jump experiments. Although **Cc** is obviously the primary product of flash excitation, the observed species and their survival time (*from seconds to years*) before reversion to the thermodynamically stable form **Ct** depend on temperature and pH.

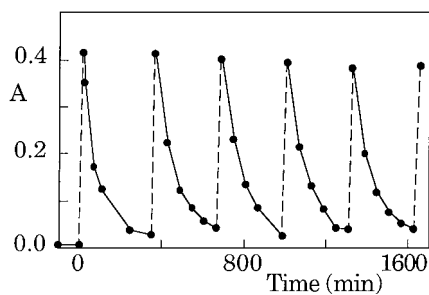


Fig. 7: Behavior of a 1.0×10^{-5} M aqueous solution of the Ct form of the 4'-methoxyflavylium ion at pH = 3.0 and 60 °C on 365 nm photoexcitation (dashed lines) followed by dark periods (full lines).^[39]

10.6 Flavylium Ions with OH Substituents

In flavylium compounds that bear OH substituents in their 4'- and/or 7-positions, deprotonation of the OH group can result in other forms being obtained, not seen in the case of the 4'-methoxyflavylium compound discussed above. Figure 8 illustrates this for the 4'-hydroxyflavylium ion.^[17] The new species are the quinoidal base A, obtained by simple deprotonation of the AH⁺ flavylium cation, and the dianionic Cc²⁻ and Ct²⁻ forms, obtained by second deprotonations of Cc and Ct. The roles played by these forms depend on the specific compound and the pH conditions. For

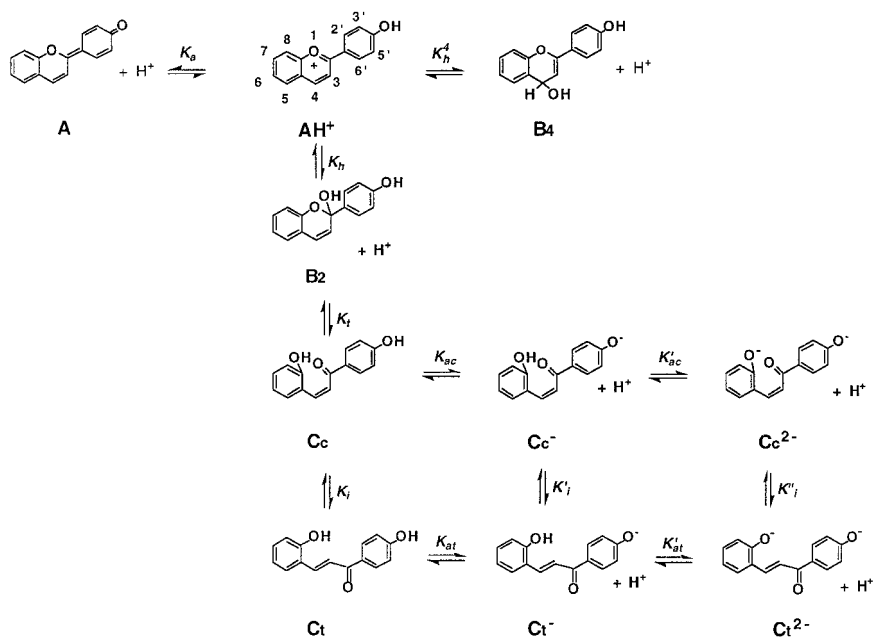


Fig. 8: Species obtained upon deprotonation of the OH groups contained in the 4'-hydroxyflavylium ion.^[17]

example, in the case of 4'-hydroxyflavylium ion, the Ct^{2-} species exhibits fluorescence and its Cc^{2-} counterpart undergoes photoisomerization to Ct^{2-} (for more details, vide infra). Interestingly, for the 4-methyl-7-hydroxy- and the 4',7-dihydroxyflavylium compounds, both the AH^+ cation and the **A** quinoidal base exhibit fluorescence. Moreover, in the former compound, in which only two forms (AH^+ and **A**) are observed, the pK_a of the ground state (4.4) is higher than the apparent pK_a of the excited state (0.7) and a very efficient adiabatic excited state proton transfer reaction (yield = 0.95) transforms $*AH^+$ into $*A$. These results show that the 4-methyl-7-hydroxy-flavylium compound behaves as a four-level system and suggests that it could be used, in principle, to obtain laser effects.^[40]

10.7

Energy Level Diagrams

As discussed above for the 4'-methoxyflavylium compound, pH jump, temperature jump, and flash photolysis experiments permit the measurement of the rate constants of some of the reactions involved, while steady state titration experiments (using UV-Vis and NMR techniques) enable equilibrium constants to be determined. The values obtained for the most important processes in five flavylium compounds are gathered in Table 1.

Tab. 1: Thermodynamic and kinetic constants for some structural transformations of synthetic flavylium compounds.^a

	<i>substituent</i> 7-OH ^b	4'-7-diOH ^c	None ^d	4'-OH ^e	4'-OMe ^f
K'_a	2.0×10^{-3}	8.9×10^{-4}	2.3×10^{-2}	1.26×10^{-2} ^g	8.0×10^{-2}
K_a	2.8×10^{-4}	1.0×10^{-4}		3.16×10^{-6}	
K_h	8.0×10^{-6}	1.4×10^{-6}	9.8×10^{-4}	3.6×10^{-6}	3.4×10^{-5}
K_t	–	–	0.06	1	0.50
K_i	500	1.4×10^3	400	3500	ca 100
k_h	0.48 s^{-1} ^a	$1.8 \times 10^{-2} \text{ s}^{-1}$	4.6 s^{-1}	$8.9 \times 10^{-2} \text{ s}^{-1}$	0.47 s^{-1}
k_{-h}	$3 \times 10^4 \text{ s}^{-1} \text{M}^{-1}$ ^h	$1.3 \times 10^4 \text{ s}^{-1} \text{M}^{-1}$ ^h	$4.7 \times 10^3 \text{ s}^{-1} \text{M}^{-1}$	$2.5 \times 10^4 \text{ s}^{-1} \text{M}^{-1}$ ^h	$1.38 \times 10^4 \text{ s}^{-1} \text{M}^{-1}$
k_i	0.57 s^{-1} ^h	0.26 s^{-1} ^h	$4.1 \times 10^{-4} \text{ s}^{-1}$	$3.7 \times 10^{-5} \text{ s}^{-1}$	$5.8 \times 10^{-5} \text{ s}^{-1}$
k_{-i}	$8.3 \times 10^{-4} \text{ s}^{-1}$	$1.8 \times 10^{-4} \text{ s}^{-1}$	$1.1 \times 10^{-6} \text{ s}^{-1}$	$< 10^{-7} \text{ s}^{-1}$	$< 10^{-6} \text{ s}^{-1}$

[a] Measured by means of pH jump techniques at 25 °C, unless otherwise noted.

[b] Ref. 41.

[c] Ref. 38.

[d] Refs.43.

[e] Refs. 17 and 37.

[f] Refs. 36 and 39.

[g] At 60° C.

[h] Measured by flash photolysis.

From an operational viewpoint, the complex equilibria involving those species present at moderately acidic pH (Figure 8) can be described in terms of a single acid-base equilibrium between the acid species AH^+ and a conjugated base "CB" with its concentration equal to the sum of the concentrations of the species A, B4, B2, Cc, and Ct:



where $K'_a = K_a + K_h + K_h^4 + K_h K_t + K_h K_i K_i$. The equilibrium constant of such an overall process is also given in Table 1. By using the data shown in the table, an energy level diagram can be constructed for each compound. Simplified versions of such diagrams (Figures 9–13) can then be used to illustrate the behavior of the various compounds^[17–19,38–43] and for discussion of the effect of the substituents.

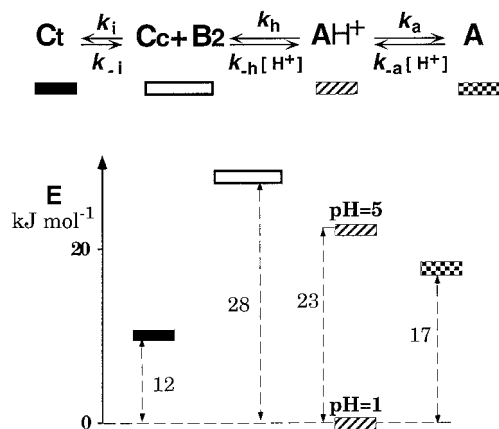


Fig. 9: Energy level diagram for the species involved in the equilibria of the 4',7-dihydroxyflavylium compound.^[41]

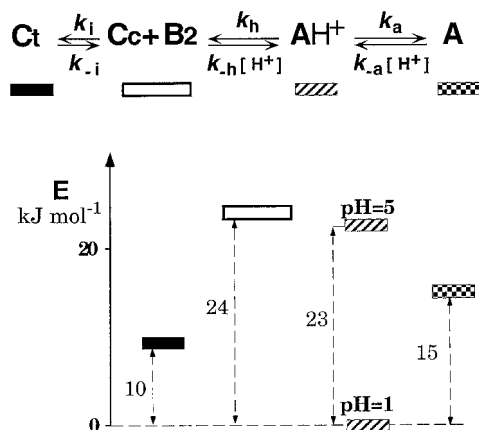


Fig. 10: Energy level diagram for the species involved in the equilibria of the 7-hydroxyflavylium compound.^[41]

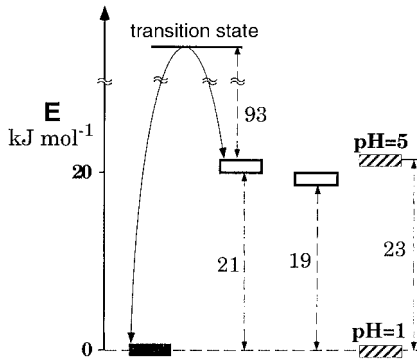
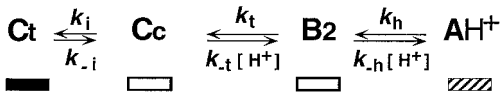


Fig. 11: Energy level diagram for the species involved in the equilibria of the 4'-methoxyflavylium compound.^[39]

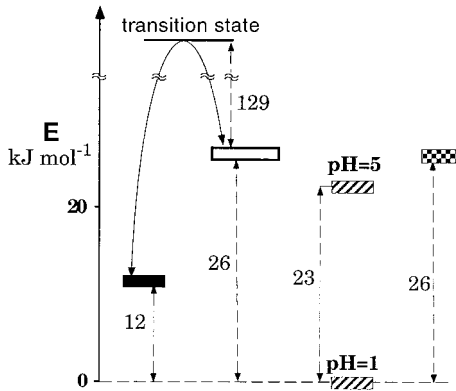
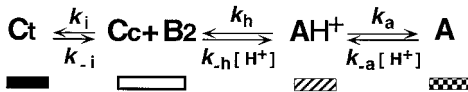


Fig. 12: Energy level diagram for the species involved in the equilibria of the 4'-hydroxyflavylium compound.^[17]

An intuitive way to describe the interconversion processes in flavylium-type compounds is their description by a hydraulics analogy.^[41] By such an analogy, the behavior of aqueous solution of flavylium ions upon a pH-jump from 1.0 to 4.2 can be schematically represented as in Figure 14. In the case of 4'-hydroxyflavylium, Cc

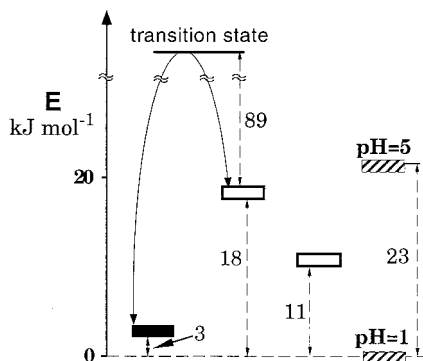
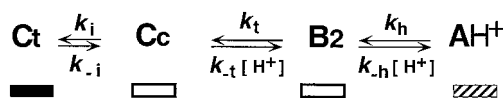


Fig. 13: Energy level diagram for the species involved in the equilibria of the unsubstituted flavilyium compound.^[43]

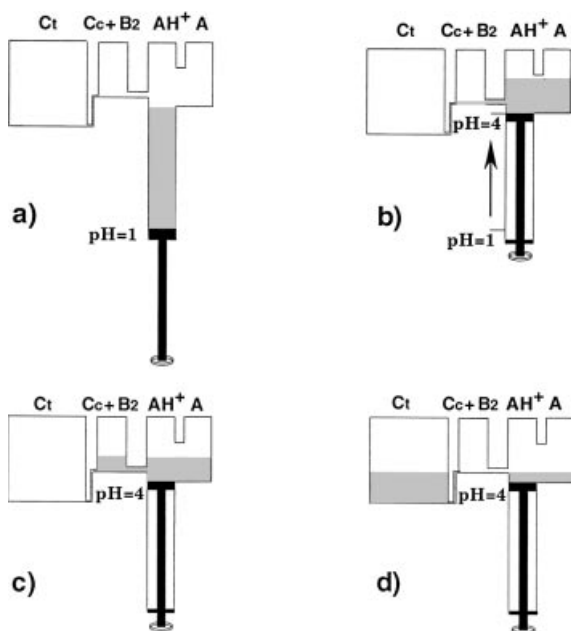
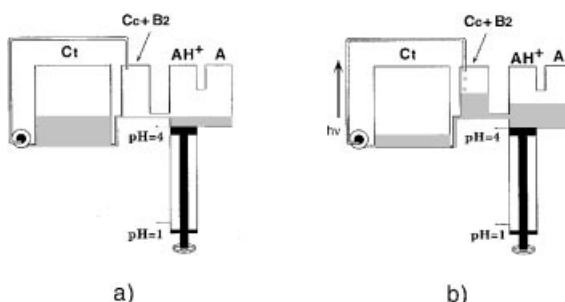


Fig. 14: Hydraulic analogy for the description of the behavior of flavilyium compounds upon a pH-jump from pH = 1.0 to pH = 4.0.^[41] (a) the system is equilibrated at pH = 1.0; (b) the pH is changed to 4.0; the pH-jump has an effect comparable to driving in the piston, and the figure represents the situation

immediately after the proton transfer process; (c) when the *cis-trans* isomerization is very slow, it is possible to obtain an intermediate (pseudoequilibrium) state involving the species AH^+ , A , B , and C ; (d) thermodynamic equilibrium at pH = 4.0.^[41]

Fig. 15: Hydraulic analogy for the photochemical reaction of the **Ct** form of the flavylum compounds. Light behaves like a pump that increases (in a transient mode as represented, or in a steady state) the quantity of liquid in the reservoir.

a) before irradiation;
b) immediately after the light flash.^[41]



converts very slowly to **Ct** and thus **B2** and **Cc** accumulate, whereas for 4',7-dihydroxyflavylium and 7-hydroxyflavylium, **Cc** converts very rapidly to **Ct** so that **Cc** and **B2** disappear as soon as they are formed.

The hydraulic analogy can also be used to illustrate the photochemical behavior of these compounds, the light playing the role of a pump. The scheme shown in Figure 15 is appropriate for 4'-hydroxyflavylium.

10.8

Chemical Process Networks

As mentioned in the introduction, molecular or supramolecular systems capable of existing in different forms (multistate) that can be interconverted by different external stimuli (multifunctional) are interesting both for fundamental reasons and for their applications. As we have seen above (Figures 2 and 8), the flavylum compounds can be interconverted into a number of different transient and stable forms by using two different inputs: namely light and changes in pH. Several interesting aspects emerge when the resulting networks of chemical processes are analyzed in terms of “molecular level devices” and “molecular level logic functions”, as illustrated below. To illustrate these aspects, we will mainly discuss the cases of the 4'-methoxy-, 4'-hydroxy-, and unsubstituted flavylum compounds in which the high activation energy of the **Cc**→**Ct** reaction imparts an appreciable kinetic stability to **Cc** and related structures. For the sake of simplicity, the **A**, **B4**, and **B2** transient species are neglected in the following discussion, since in the compounds under examination they are always in rapid equilibrium with either **AH**⁺ or **Cc**.

10.8.1

Write-lock-read-unlock-erase Cycles

As discussed at the beginning of this chapter, photochromic systems represent potential molecular level memory devices. A number of problems, however, must be solved for practical applications. A challenge problem is to find systems with multiple storage and nondestructive readout capacity; those in which the record can be

erased when necessary, but is not destroyed merely by the act of reading out. The 4'-hydroxyflavylium^[17] and 4'-methoxyflavylium^[39] ions can operate through the write-lock-read-unlock-erase cycle illustrated in Figure 1c, and therefore they can be taken as a basis for optical memory systems with multiple storage and nondestructive readout capability.

The behavior of the 4'-methoxyflavylium ion can be described with reference to Figure 16 (which refers to a solution at pH = 3.0), in which Ct, Cc, and AH⁺ play the roles of the generic species X, Y, and Z of Figure 1c (B2 is not shown because it is always in equilibrium with Cc):

- (i) a stable form (Ct≡X) can be photochemically converted by irradiation with 365 nm light (write) into a form (Cc≡Y) that can be reconverted back either thermally or on optical reading;
- (ii) by means of a second stimulus (addition of acid, which can also be present from the beginning without perturbing the behavior of the system), Cc≡Y can be converted into a kinetically inert form AH⁺≡Z (lock);
- (iii) the AH⁺≡Z form exhibits a spectrum (Figure 3) clearly distinct from that of Ct≡X and is photochemically inactive, so it can be optically detected (read) without being erased;
- (iv) by addition of base, AH⁺≡Z can be reconverted into Cc≡Y (unlock);
- (v) Cc≡Y can be thermally or photochemically reconverted into the initial Ct≡X form (erase).

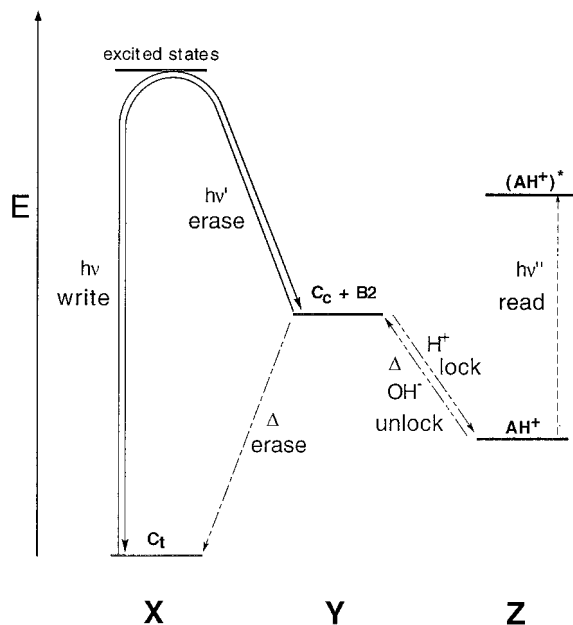


Fig. 16: Schematic energy level diagram for the species involved in the write-lock-read-unlock-erase cycle in the case of the 4'-methoxyflavylium ion.^[39]

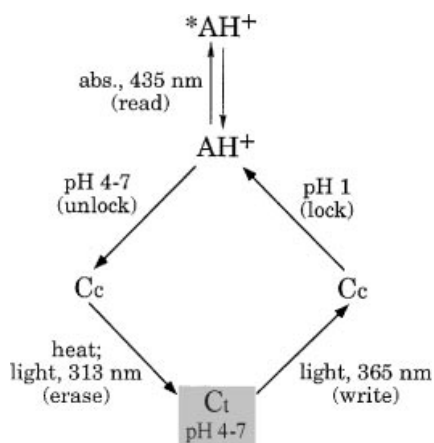


Fig. 17: Write-lock-read-unlock-erase cycle starting from the C_t form of the 4'-hydroxyflavylium compound.^[17]

It should be noted that the locking time of the written information bit is not indefinite (at 25 °C and pH = 3.0, the half-life of the back-reaction from AH^+ to C_t is about 8 days).

In the case of the 4'-hydroxyflavylium ion,^[17] similar behavior is observed. It can be described on the basis of the energy level diagram of Figure 12 or the simpler scheme shown in Figure 17:

- (i) at pH = 4–7, the stable or kinetically inert (depending on pH), colorless C_t species can be photochemically converted (365 nm light) into the thermodynamically unstable, but relatively inert, C_c form (write);
- (ii) by means of a second stimulus (addition of acid), C_c can be converted into the kinetically inert or thermodynamically stable (depending on pH) AH^+ form (lock). If the initial pH is 1, the C_c species autolocks as AH^+ ;
- (iii) the AH^+ species is photochemically inactive and shows an absorption spectrum clearly distinct from that of C_t , so it can be optically detected (read);
- (iv) by addition of base, AH^+ can be reconverted into C_c (unlock);
- (v) C_c can be reconverted to the initial C_t form by a thermal or a photochemical reaction (erase).

10.8.2

Reading without Writing in a Write-lock-read-unlock-erase Cycle

An often overlooked difficulty with photochromic systems is that the starting form (C_t in the above discussion) is the photoreactive one, so it cannot be read by absorption spectroscopy without overwriting it. With the 4'-hydroxyflavylium ion, this difficulty can be overcome by starting from AH^+ , which at pH = 1 is the thermodynamically stable form, and performing a write-lock-read-unlock-erase cycle as illustrated in Figures 18 and 19.^[17] Since AH^+ is not photosensitive, it can be read by light excitation (i.e., by recording its absorption spectrum) without overwriting. It can then be unlocked by a pH-jump to 12, yielding the metastable C_c^{2-} form. At this

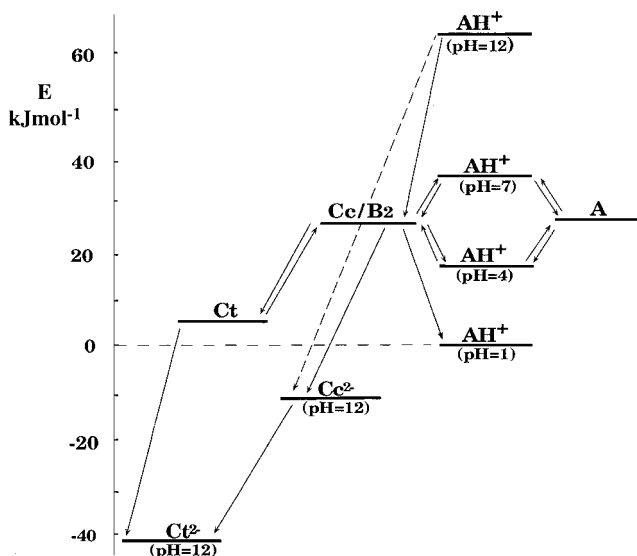


Fig. 18: Energy level diagram for the species involved in experiments carried out on the 4'-hydroxyflavylum compound in the pH range 1–12.^[17]

stage, it is possible to write the optical information, obtaining the stable (locked) Ct^{2-} form, which can then be read. When necessary, the information stored in Ct^{2-} can be unlocked by a pH-jump, yielding Ct and can then be erased by light excitation. The same performance can be obtained starting from Ct^{2-} .

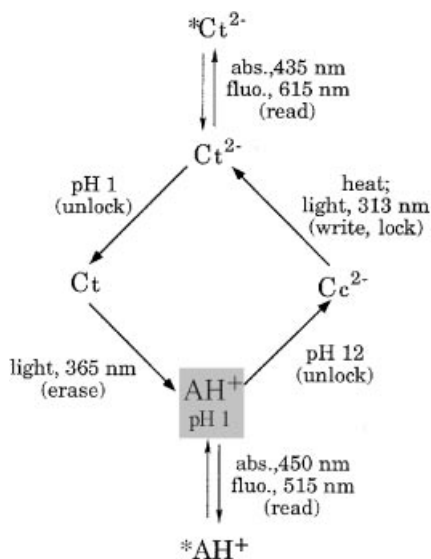


Fig. 19: Read-write-lock-read-unlock-erase cycle starting from the AH^+ form of the 4'-hydroxyflavylum compound.^[17]

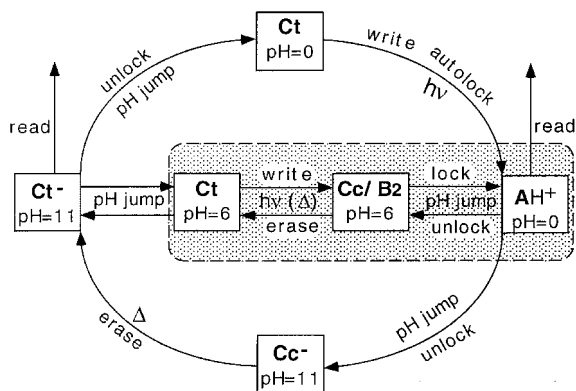


Fig. 20: Write-lock-read-unlock-erase cycles for the unsubstituted flavylum ion.^[43] For more detail, see text.

In the case of the unsubstituted flavylum cation,^[43] as well as a cycle like that schematized in Figure 17, it is also possible to perform a cycle based on the anionic species present in basic media (Figure 20). This second cycle starts at pH = 11, with the **Ct⁻** form. This, not being photosensitive, can be read without overwriting. Two different paths can then be followed. The first one begins with a pH-jump to pH = 6, leading to **Ct** and continuing as described above (shaded area in Figure 20). The second path starts with a pH-jump from 11 to 0. This produces **Ct**, which can be photochemically written (and locked, thanks to the low pH), giving **AH⁺**. In this form, the information can be stored permanently and read without erasing, since **AH⁺** is thermally and photochemically stable. When necessary, **AH⁺** can be unlocked by a pH-jump to 11 and thermally erased to give back **Ct⁻**. An advantage of this cycle lies in the possibility of reading the system in both the initial (nonwritten) and final (written) states without overwriting or erasing. Moreover, **Ct⁻** is more stable than **Ct**, so that durability of the system could be increased. A disadvantage lies in the fact that, in this cycle, autolocking (and auto-unlocking) cannot occur, so that two pH changes per cycle are needed.^[43]

10.8.3

Micelle Effect on the Write-lock-read-unlock-erase Cycle

For the 4'-hydroxyflavylium ion, the **AH⁺** form is stabilized by negatively charged sodium dodecyl sulfate (SDS) micelles, whereas positively charged cetyltrimethylammonium bromide (CTAB) and neutral polyoxyethylene(10)-isooctylphenylether (Triton X-100) micelles stabilize the uncharged (basic) forms.^[18] Besides affecting the molar fraction distribution of the various species, the presence of micelles also influences their interconversion rates. Addition of micelles can therefore be considered as a third external stimulus (together with light excitation and pH-jump) capable of changing the state of this multistate/multifunctional molecular level system. Particularly interesting is the possibility of changing the autolock pH of a photochromic reaction by addition of micelles. For example, starting from a **Ct** solution at pH = 5.5, as well as the previously described write-lock-read-unlock-erase cycle, it is possible to design an alternative cycle

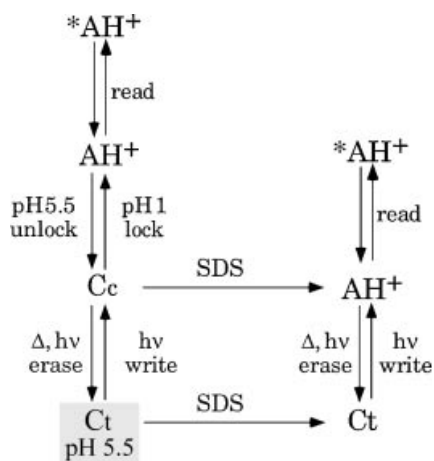


Fig. 21: Write-lock-read-unlock-erase cycles for the 4'-hydroxyflavylium ion, starting from the Ct form at pH = 5.5. Left-hand side: light and pH-jump inputs in the absence of micelles. This part is equivalent to the cycle shown in Figure 16. Right-hand side: light input at the autolocking pH in the presence of SDS micelles.^[18]

based on addition of SDS micelles and exploitation of the autolocking and thermal erasing processes of this system (Figure 21).^[18]

10.8.4

Permanent and Temporary Memories

The human brain displays shallow and deep memory processes.^[50] The network of processes interconverting the various species of the 4'-hydroxyflavylium ion permits the operation of different levels of memory.^[17] Once the permanent (deep) AH⁺ form of memory has been obtained (write and lock, Figure 22), a jump to pH 12 results in the formation of a temporary (shallow) memory state Cc²⁻, spontaneous

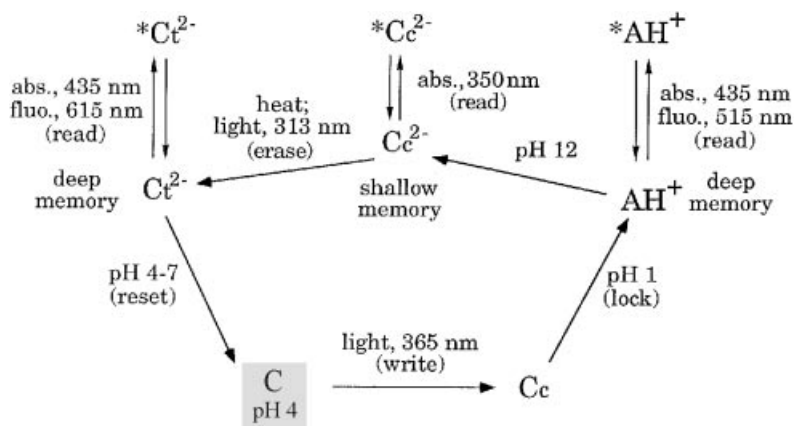


Fig. 22: A write-lock-read-unlock-erase cycle with two memory levels, based on the 4'-hydroxyflavylium compound.^[17]

slow erasure of which to give the deep Ct^{2-} memory can be accelerated by light. Reset can then be accomplished by means of a back pH-jump to pH 4.

10.8.5

Oscillating Absorbance Patterns

Another feature of the 4'-hydroxyflavylium ion should be pointed out.^[17] Starting from AH^+ , alternation of pH-jump and light excitation causes oscillation patterns of absorbance at different wavelengths, as shown in Figure 23. Such patterns may be interesting for signal generation and information processing.^[51]

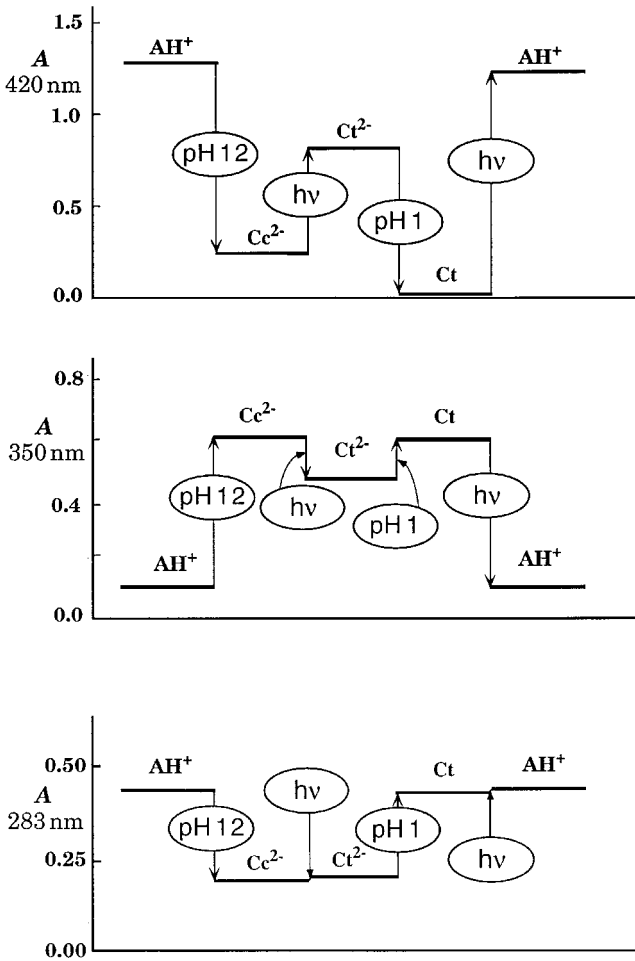


Fig. 23: Absorbance oscillations resulting from alternating pH-jump and light excitation in a 3.3×10^{-5} M aqueous solution starting from the AH^+ form of the 4'-hydroxyflavylium compound at pH = 1.^[17]

10.8.6

Color-tap Effect

Because of the competition between the pH-dependent rate of the reaction leading from the uncolored Cc form to the colored AH⁺ and A species and the pH-independent *cis*→*trans* back-isomerization, the amount of colored species formed upon light excitation of the Ct solution depends on pH. In other words, the pH plays the role of a tap for the color intensity generated by light excitation.^[41] This also means that this system can be viewed as a light-switchable pH indicator. The color-tap effect is larger in the case of 4',7-dihydroxyflavylium than in that of 7-hydroxyflavylium.

10.8.7

Logic Operations

From the point of view of logic operations,^[5,52,53] simple (bistable) photochromic systems perform YES/NO functions. Multistate/multifunctional molecular level systems can be taken as bases for more complex logic operations. Chemical systems capable of performing AND,^[52] OR,^[52] XOR,^[54] and XNOR^[55] logic operations, as well as integration of logic functions and sequential operation of gates on the molecular scale have recently been reported.^[56] (A complete survey of chemical systems able to perform as logic gates is given in Chapter 11 in this volume, by A.P. de Silva). With the 4'-hydroxyflavylium compound, light excitation and pH-jumps can be viewed as inputs, and absorbance or fluorescence as outputs. Starting from the non-emitting Ct species, and taking the emission of AH⁺ at 515 nm as the output signal, neither a jump to pH = 1 alone, nor light excitation alone are sufficient to generate the output. When these two inputs are applied in series, however, the output is obtained (AND logic function, Table 2).^[17]

For the 4'-hydroxyflavylium compound in the presence of micelles,^[18] starting from Ct at pH 5.0 and taking the formation of the AH⁺ absorption at 436 or 450 nm as an output, the truth table for the effect of the three inputs (pH-jump to 1.0, addition of SDS, light excitation) shows a peculiar pattern (Table 3) corresponding to an OR function, which is activated only in the presence of the third input (enabled OR).

Tab. 2: Truth table for the AND logic behavior of the 4'-hydroxyflavylium compound, starting from Ct at pH = 5.5.

<i>Input 1</i> ^a	<i>Input 2</i> ^b	<i>Output</i> ^c
0	0	0
1	0	0
0	1	0
1	1	1

[a] pH jump to pH 1.

[b] Light excitation at 365 nm.

[c] Absorbance at 435 nm or emission at 515 nm of the AH⁺ form.

Tab. 3: Truth table for the enabled OR logic behavior of the 4'-hydroxyflavylium compound, starting from Ct at pH = 5.5.

Input 1 ^a	Input 2 ^b	Input 3 ^c	Output ^d
1	0	0	0
0	1	0	0
1	1	0	0
0	0	0	0
1	0	1	1
0	1	1	1
1	1	1	1
0	0	1	0

[a] pH jump to pH 1.

[b] SDS micelle.

[c] Light excitation at 365 nm.

[d] Absorbance at 435 nm or emission at 515 nm of the AH⁺ form.

An interesting system, based on the 4'-methoxyflavylium ion and capable of behaving according to an XOR (eXclusive OR) logic has recently been reported.^[20] The system consists of an aqueous solution containing the Ct form of the 4'-methoxyflavylium ion (AH⁺), and the Co(CN)₆³⁻ complex ion (as a potassium salt). The absorption spectra of Ct and Co(CN)₆³⁻ are shown in Figure 24. For the current discussion, the most relevant aspects of the thermal and photochemical reactions of these two compounds, which have been studied in great detail in our laboratories,^[39,57] are as follows. Excitation of Ct, the thermodynamically stable form of the flavylium species in the pH range 3–7, by 365 nm light causes the *trans*→*cis* photoisomerization reaction discussed previously (quantum yield: 0.04).^[39]

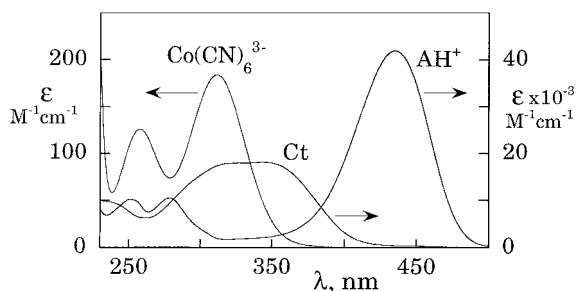
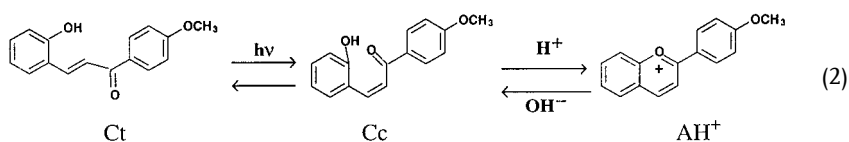
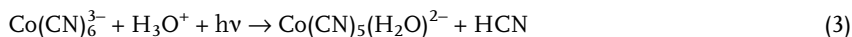


Fig. 24: Absorption spectra of Co(CN)₆³⁻ and of the Ct and AH⁺ forms of the 4'-methoxyflavylium compound in aqueous solution.

As we have seen above, if the solution is sufficiently acidic ($\text{pH} < 4$), the **Cc** isomer is rapidly protonated, with conversion to the 4'-methoxyflavilyium ion AH^+ , which is kinetically stable under such pH conditions and exhibits an intense absorption band with a maximum at 434 nm (Figure 24) and an emission band with maximum at 530 nm (Figure 6). At higher pH values, however, protonation does not occur and the **Cc** photoproduct is back-converted into **Ct**. As far as $\text{Co}(\text{CN})_6^{3-}$ is concerned, excitation by 254 or 365 nm light in acidic or neutral aqueous solution causes the dissociation of a CN^- ligand from the metal coordination sphere (quantum yield = 0.31), with a consequent increase in pH.^[57]



When an acidic solution ($\text{pH} = 3.6$) containing $2.5 \times 10^{-5} \text{ M Ct}$ and $2.0 \times 10^{-2} \text{ M Co}(\text{CN})_6^{3-}$ is irradiated at 365 nm, most of the incident light is absorbed by **Ct** (Figure 23), which undergoes photoisomerization to **Cc**. Since the pH of the solution is sufficiently acidic, **Cc** is rapidly protonated (Equation 2), with the consequent appearance of the absorption band with its maximum at 434 nm (Figure 24) and of the emission band characteristic of the AH^+ species, with its maximum at 530 nm (Figure 6).

On continuing the irradiation, it can be observed that the absorption (Figure 25) and emission bands increase in intensity, reach a maximum value, and then decrease, finally disappearing completely. These results show that AH^+ first forms and then disappears with increasing irradiation time. The reason for the off-on-off behavior of AH^+ under continuous light excitation relates to the effect of reaction 2 on reaction 1. As **Ct** is consumed by reaction 1, with formation of AH^+ , an increasing fraction of the incident light is absorbed by $\text{Co}(\text{CN})_6^{3-}$, which undergoes reaction 2. Such a photoreaction causes an increase in the pH of the solution. This not only prevents further formation of AH^+ , which would imply protonation of the **Cc** molecules that continue to be formed by light excitation of **Ct**, but also causes the back-reaction to **Cc** (and, then, to **Ct**) of the previously formed AH^+ molecules. Clearly, the examined solution performs like a threshold device as far as the input (light)/output (spectroscopic properties of AH^+) relationship is concerned. Instead of a con-

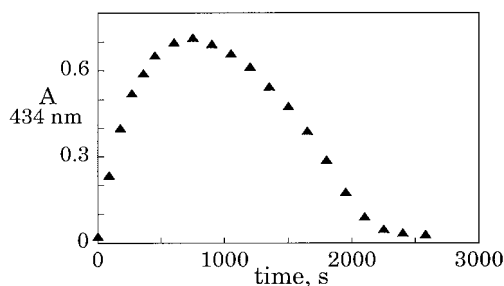


Fig. 25: Changes in absorbance at 434 nm with increasing irradiation time upon continuous irradiation with 365 nm light of solutions containing $\text{Co}(\text{CN})_6^{3-}$ and the **Ct** form of the 4'-methoxyflavilyium compound.^[20]

tinuous light source, pulsed (flash) irradiation can be used. After input of only one flash, a strong change in absorbance at 434 nm is observed, due to the formation of AH^+ . After 2 flashes, however, the change in absorbance practically disappears. In other words, an output (434 nm absorption) can be obtained only when *either* input 1 (flash I) or input 2 (flash II) are used, whereas there is no output under the action of *none* or *both* inputs. This shows (Table IV) that the system described behaves according to an XOR (eXclusive OR) logic, under control of an intrinsic threshold mechanism. It is noteworthy that the input and output signals are of the same nature (light).^[20]

Tab. 4: Truth table for the XOR (eXclusive OR) logic behavior of the 4'-methoxyflavylium/ $Co(CN)_6^{3-}$ system, starting from pH = 3.6.

<i>Input 1</i> ^a	<i>Input 2</i> ^a	<i>Output</i> ^b
0	0	0
1	0	1
0	1	1
1	1	0

[a] The two inputs are identical and consist of the amount of photons necessary to achieve the absorbance value corresponding to the top of the curve of Figure 25.

[b] Absorbance at 435 nm or emission at 515 nm of the AH^+ form.

10.8.8

Multiple Reaction Patterns

In the case of the unsubstituted flavylium cation, we have seen that it is possible to follow different paths to obtain the same result (Figure 20). For the 4'-hydroxyflavylium compound, the network of processes is even more intricate, and several species are interconnected by multiple reaction patterns.^[17] For example, in order to go from AH^+ to Ct, three different routes can be chosen, as represented pictorially in Figure 26:

- (i) jump to pH 12, with formation of Cc^{2-} , followed by excitation with 313 nm light to obtain Ct^{2-} , and by a jump to pH = 6;
- (ii) jump to pH = 6 to form Cc; at this stage, one can choose between two sub-routes: (iia) light excitation with 313 nm light, or (iib) jump to pH 12 to merge into the preceding path that leads to Ct via Cc^{2-} and Ct^{2-} .

Once Ct has been obtained, one can return to AH^+ by two different routes:

- (iii) light excitation at 365 nm to obtain Cc and subsequent jump to pH = 1;
- (iv) jump to pH = 1 and subsequent light excitation at 365 nm.

Interestingly, in some cases, such as when starting from Ct at pH 6, the same result (AH^+) is obtained regardless of the order in which light excitation (365 nm) and pH-jump (pH = 1) take place. In other cases, however, this is not true. For exam-

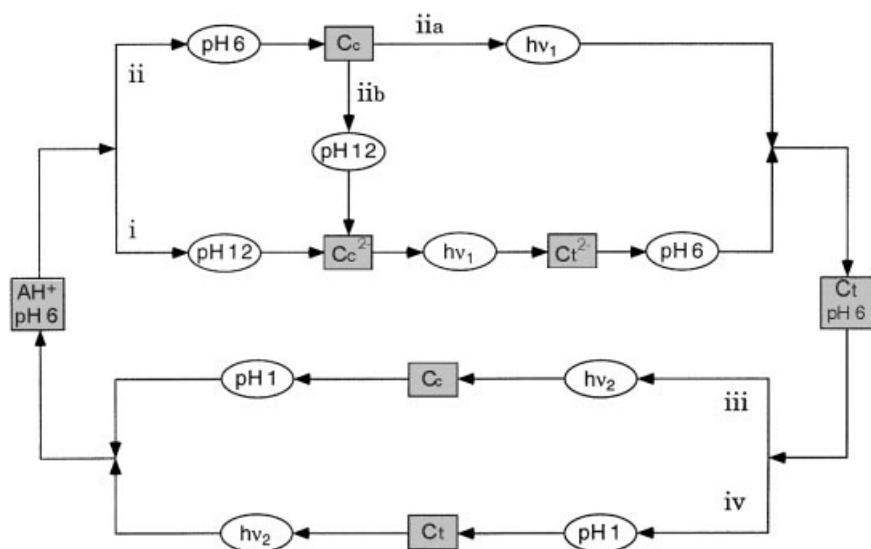


Fig. 26: The network of processes resulting from pH jumps and light excitations interconnecting the AH^+ and Ct forms of the 4'-hydroxyflavylium compound.^[17]

ple (not shown in Figure 26), when starting from AH^+ at $pH = 1$, light excitation followed by pH-jump to 12 leads to Cc^{2-} , whereas when the two inputs are applied in the reverse order, Ct^{2-} results. Since Cc^{2-} and Ct^{2-} exhibit very different spectroscopic properties (for example, Ct^{2-} exhibits fluorescence whereas Cc^{2-} does not), from the state of the system after the two inputs it is possible to establish the sequence in which the two inputs were applied.

A network of processes governed by external inputs can be used as a model system^[51,58,59] for understanding the chemical basis of complex biological systems.^[60,61]

10.9

Conclusions

Synthetic flavylium compounds can exist in several forms (multistate), which can be interconverted by more than one type of external stimulus (multifunctional). The intricate network made up by their reactions, when examined from the viewpoints of “molecular level devices” and “molecular level logic functions”, reveals that these systems exhibit very interesting properties.

In our brain, neurons store, exchange, and retrieve information by means of extremely complicated chemical processes.^[60,61] Synthetic multistate/multifunctional systems may play the role of models in initial attempts to understand the chemical basis of complex biological processes.^[20] It is not at all clear whether “wet”

artificial systems can find real applications, for example in molecular scale computers.^[62,63] However, the study of molecular or supramolecular species capable of existing in different forms that can be interconverted by external stimuli is a topic of great interest, since it introduces new concepts in the field of chemistry and stimulates the ingenuity of research workers engaged in the “bottom up” approach to nanotechnology.

Acknowledgments

This work was supported in Portugal by Fundação para a Ciência e Tecnologia (project PRAXIS /P/QUI/10074/1998) and Fundação Gulbenkian, and in Italy by MURST (Toward Artificial Photosynthesis) and the University of Bologna (Funds for Selected Research Topics) and CNR (Sensori Fluorescenti Supramolecolari). F.P. and M.M. thank a grant from FCT (Portugal)/CNR Bologna (Italy).

References

- 1 V. Balzani, F. Scandola, *Supramolecular Photochemistry*, Ellis Horwood, Chichester, **1991**.
- 2 L.B. Feringa, W.F. Jager, B. de Lange, *Tetrahedron*, **1993**, 49, 8267.
- 3 J.-M. Lehn, *Supramolecular Chemistry. Concepts and Perspectives*, VCH, Weinheim, **1995**.
- 4 V. Balzani, F. Scandola, in *Comprehensive Supramolecular Chemistry* (Ed.: D.N. Reinhoudt), Pergamon Press, Oxford, **1996**; Vol. 10, 687.
- 5 A.P. de Silva, H.Q.N. Gunaratne, T. Gunnlaugsson, A.J.M. Huxley, C.P. McCoy, J.T. Rademacher, T.E. Rice, *Chem. Rev.*, **1997**, 97, 1515.
- 6 (a) V. Balzani, M. Gómez-López, J.F. Stoddart, *Acc. Chem. Res.*, **1998**, 31, 405. (b) J.-P. Sauvage, *Acc. Chem. Res.*, **1998**, 31, 611. (c) V. Balzani, A. Credi, F. Raymo, J.F. Stoddart, *Angew. Chem. Int. Ed.*, **2000**, 39, 3348.
- 7 *Photochromics* (Ed.: G.H. Brown), Wiley-Interscience, New York, **1971**.
- 8 *Photochromism – Molecules and Systems* (Eds.: H. Dürr, H. Bouas-Laurent), Elsevier, Amsterdam, **1990**.
- 9 G. Ciamician, *Science*, **1912**, 36, 385.
- 10 S. Braslawsky, in *Photochromism - Molecules and Systems* (Eds.: H. Dürr, H. Bouas-Laurent), Elsevier, Amsterdam, **1990**, p. 738.
- 11 Y. Hirshberg, *J. Am. Chem. Soc.*, **1956**, 78, 2303.
- 12 Y. Hirshberg, *New Scientist*, **1960**, 7, 1243.
- 13 a) *Molecular Electronic Devices* (Eds.: F.L. Carter, R.E. Siatkowsky, H. Woltjien), Elsevier, Amsterdam, **1988**; b) K.E. Drexler, *Nanosystems: Molecular Machinery, Manufacturing, and Computation*, Wiley, New York, **1992**; c) T. Thompson, *Byte*, **1996**, 45.
- 14 D. Rouvray, *Chem. Brit.*, **1998**, 34(2), 26.
- 15 B.J. Coe, *Chem. Eur. J.*, **1999**, 5, 2464.
- 16 M.P. O'Neil, M.P. Niemczyk, W.A. Svec, D. Gosztola, G.L. Gaines III, M.R. Wasielewski, *Science*, **1992**, 257, 63. See also the chapter by M.R. Wasielewski in this volume.
- 17 F. Pina, A. Roque, M. J. Melo, M. Maestri, L. Belladelli, V. Balzani, *Chem. Eur. J.*, **1998**, 4, 1184.
- 18 A. Roque, F. Pina, S. Alves, R. Ballardini, M. Maestri, V. Balzani, *J. Mater. Chem.*, **1999**, 9, 2265.
- 19 F. Pina, M. Maestri, V. Balzani, *Chem. Commun.*, **1999**, 107.
- 20 F. Pina, M. J. Melo, M. Maestri, P. Passaniti, V. Balzani, *J. Am. Chem. Soc.*, **2000**, 122, 4496.
- 21 For seminal examples concerning photochromic systems, see: a) J. Daub, J. Salbeck, T. Knöchel, C. Fischer, H. Kunkely, K.M. Rapp, *Angew. Chem. Int. Ed. Eng.*, **1989**, 28, 1494; b) T. Iyoda, T. Saika, K. Honda, T. Shimidzu, *Tetrahedron Letters*, **1989**, 30, 5429; c) J. Daub, C. Fischer, J. Salbeck, K. Ulrich, *Adv. Mater.*, **1990**, 8, 366; d) Y. Yokoyama, T. Yamane, Y. Kurita, *J. Chem. Soc. Chem. Commun.*, **1991**, 1722; g) S. Kobatake, M. Yamada, T. Yamada, M. Irie, *J. Am. Chem. Soc.*, **1999**, 121, 8450; f) M. Irie, *Mol. Cryst. Liquid Cryst.* **1993**, 227, 263; g) M. Irie, O. Miyatake, K. Uchida, T. Eriguchi, *J. Am. Chem. Soc.*, **1994**, 116, 9894; h) M.J. Preigh, F.-T. Lin, K.Z. Ismail, S.G. Weber, *J. Chem. Soc. Chem. Commun.* **1995**, 2091; k) S.H. Kawai, S.L. Gilat, R. Posinet, J.-M. Lehn, *Chem. Eur. J.* **1995**, 1, 285; j) G.M. Tsivgoulis, J.-M. Lehn, *Chem. Eur. J.* **1996**, 2, 1399; i) M. Inouye, K. Akamatsu, H. Nakazumi, *J. Am. Chem. Soc.*, **1997**, 119, 916
- 22 For relevant examples, see: (a) M. Irie, M. Mohri, *J. Org. Chem.*, **1988**, 53, 803; (b) M. Hana-zawa, R. Sumiya, Y. Horikawa, M. Irie, *J. Chem. Soc., Chem. Commun.*, **1992**, 206; (c) F. Buchholtz, K. Zelichenok, V. Krongauz, *Macromolecules*, **1993**, 26, 906; (d) J. Wals, K. Ulrich, H. Port, H.C. Wolf, J. Wonner, F. Effenberger, *Chem. Phys. Letters*, **1993**, 213, 321; (e) T. Saika, M. Irie, T. Shimidzu, *J. Chem. Soc., Chem. Commun.*, **1994**, 2123; (f) M. Coursan, J.-P. Desvergne, A. Deffieux, *Macromol. Chem. Phys.*, **1996**, 197, 1599.
- 23 A.S. Dvornikov, P.M. Rentzepis, *Mol. Cryst. Liq. Cryst.*, **1994**, 246, 379.
- 24 M. Seibold, H. Port, *Chem. Phys. Letters*, **1996**, 252, 135.
- 25 S.H. Kawai, S.L. Gilat, R. Posinet, J.-M. Lehn, *Chem. Eur. J.*, **1995**, 1, 285.
- 26 K. Uchida, M. Irie, *J. Am. Chem. Soc.*, **1993**, 115, 6442.
- 27 M. Irie, *Mol. Cryst. Liquid Cryst.*, **1993**, 227, 263.
- 28 (a) J. Daub, J. Salbeck, T. Knöchel, C. Fischer, H. Kunkely, K.M. Rapp, *Angew. Chem. Int. Ed. Eng.* **1989**, 28, 1494; (b) T. Iyoda, T. Saika, K. Honda, T. Shimidzu, *Tetrahedron Letters* **1989**, 30, 5429; (c) J. Daub, J. Fischer, J. Salbeck, K. Ulrich, *Adv. Mater.*, **1990**, 8, 366.

- 29 Y. Yokoyama, T. Ymamane, Y. Kurita, *J. Chem. Soc., Chem. Commun.*, **1991**, 1722.
- 30 M. Irie, O. Miyatake, K. Uchida, T. Eriguchi, *J. Am. Chem. Soc.*, **1994**, *116*, 9894.
- 31 V. Balzani, A. Credi, M. Venturi, in *Supramolecular Science: Where It Is and Where It Is Going* (Eds.: R. Ungaro, E. Dalcanele), Kluwer, Dordrecht, **1999**, p. 1.
- 32 For multiplexing optical systems based on mixtures of photochromic compounds, see: G.M. Tsigoulis, J.-M. Lehn, *Adv. Mater.* **1997**, *9*, 627.
- 33 a) R. Brouillard, In *The Flavonoids, Advances in Research*, (Ed.: J.B. Harborne), Chapman and Hall, London, **1988**; p. 525; b) R. Brouillard, in *Anthocyanins as food colors* (Ed.: P. Markakis, Academic Press, New York, **1982**, Chapter 1.
- 34 R. Brouillard, J.E. Dubois, *J. Am. Chem. Soc.*, **1997**, *99*, 1359.
- 35 R. Brouillard, J. Delaporte, *J. Am. Chem. Soc.*, **1997**, *99*, 8461.
- 36 R.A. McClelland, S. Gedge, *J. Am. Chem. Soc.*, **1980**, *102*, 5838.
- 37 R.A. McClelland, G.H. McGall, *J. Org. Chem.*, **1982**, *47*, 3730.
- 38 F. Pina, M. J. Melo, L. Flamigni, R. Ballardini, M. Maestri, *New J. Chem.*, **1997**, *21*, 969
- 39 F. Pina, M. J. Melo, M. Maestri, R. Ballardini, V. Balzani, *J. Am. Chem. Soc.*, **1997**, *119*, 5556.
- 40 F. Pina, M. J. Melo, M. H. Santos, J. C. Lima, I. Abreu, R. Ballardini, M. Maestri *New J. Chem.*, **1998**, 1093.
- 41 F. Pina, M. J. Melo, A. J. Parola, M. Maestri, V. Balzani, *Chem. Eur. J.*, **1998**, *4*, 2001.
- 42 F. Pina, *J. Chem. Soc. Faraday Trans.*, **1998**, *94*, 2109.
- 43 F. Pina, M. J. Melo, P. Passaniti, N. Camaioni, M. Maestri, V. Balzani, *Eur. J. Org. Chem.*, **1999**, *11*, 3199.
- 44 a) C. Michaelis, R. Wizinger, *Helv. Chim. Acta*, **1951**, *34*, 1761. b) A. W. Johnson, R. R. Melhuish, *J. Chem. Soc.* **1947**, 346.
- 45 W. von Sperling, F.C. Werner, and H. Kuhn, *Ber. Bunsenges. Phys. Chem.*, **1966**, *70*, 530.
- 46 G. Haucke, P. Czerney, C. Igney, H. Hartmann, *Ber. Bunsenges. Phys. Chem.*, **1989**, *93*, 805; b) G. Haucke, P. Czerney, D. Steen, W. Rettig, H. Hartmann *Ber. Bunsenges. Phys. Chem.*, **1993**, *97*, 561.
- 47 P. Figueiredo, J.C. Lima, H. Santos, M.-C. Wigand, R. Brouillard, F. Pina, *J. Am. Chem. Soc.*, **1994**, *116*, 1249; b) F. Pina, L. Bedito, M.J. Melo, A.J. Parola, M.A. Bernardo, *J. Chem. Soc. Faraday Trans.*, **1996**, *92*, 1693; c) M. Maestri, R. Ballardini, F. Pina, M.J. Melo, *J. Chem. Educ.*, **1997**, *74*, 1314.
- 48 R. Matsushima, H. Mizuno, H. Itoh, *J. Photochem. Photobiology A*, **1995**, *89*, 251; b) R. Matsushima, H. Mizuno, A. Kajiura, *Bull. Chem. Soc. Jpn.*, **1994**, *67*, 1762; c) R. Matsushima, M. Suzuki, *Bull. Chem. Soc. Jpn.*, **1992**, *65*, 39.
- 49 J. Saltiel, Y.-P. Sun, in *Photochromic systems-Molecules and Systems* (Ed.: H. Dürr, H. Bouas-Laurent), Elsevier, Amsterdam, **1990**, Chapter 3.
- 50 H. Eichenbaum, *Science* **1997**, *277*, 330. For an example of an artificial system showing deep and shallow memory forms, see ref. 21b.
- 51 (a) H.M. Cartwright, *Application of artificial intelligence in chemistry*, Oxford University Press Inc., New York, **1993**. (b) N.J. Nilson, *Artificial intelligence: a new synthesis*, M. Kaufmann Publishers, San Francisco, **1998**.
- 52 A.P. de Silva, H.Q.N. Gunaratne, C.P. McCoy, *Nature*, **1993**, *364*, 42.
- 53 V. Balzani, A. Credi, F. Scandola, *Chim. Ind. (Milan)*, **1997**, *79*, 751.
- 54 A. Credi, V. Balzani, S. J. Langford, J. F. Stoddart, *J. Am. Chem. Soc.*, **1997**, *119*, 2679.
- 55 M. Asakawa, P. R. Ashton, V. Balzani, A. Credi, G. Matternsteig, O.A. Matthews, M. Montalti, N. Spencer, J. F. Stoddart, M. Venturi, *Chem. Eur. J.*, **1997**, *3*, 1992.
- 56 A.P. de Silva, I.M. Dixon, H.Q.N. Gunaratne, T. Gunnlaugsson, P.R.S. Maxwell, T.E. Rice, *J. Am. Chem. Soc.*, **1999**, *121*, 1393.
- 57 L. Moggi, F. Bolletta, V., Balzani, F. Scandola, *J. Inorg. Nuclear Chem.*, **1966**, *28*, 2589.
- 58 C. Amatore, L. Thouin, J.-S. Warkocz, *Chem. Eur. J.*, **1999**, *5*, 456.
- 59 S. Faulkner, D. Parker, J.A.G. Williams, in *Supramolecular Science: Where It Is and Where It Is Going* (Eds.: R. Ungaro, E. Dalcanele), Kluwer, Dordrecht, **1999**, p. 53.
- 60 R. Beale, T. Jackson, *Neural computing: an introduction*, Adam Hilger, Bristol, **1990**.
- 61 D.H. Hubel, *Eye, brain and vision*, Scientific American Library, New York, **1995**.
- 62 P. Ball, L. Garvin, *Nature*, **1992**, *355*, 761.
- 63 D. Bradley, *Science*, **1993**, *259*, 890.

11

Molecular Logic Systems

A. Prasanna de Silva, Nathan D. McClenaghan, and Colin P. McCoy

11.1

Introduction

Luminescence is one of the few techniques commonly available to the molecular scientist that retains its potency as smaller and smaller populations are addressed, right down to the single molecule limit.^[1,2] The ease with which luminescence can be quenched^[3–7] is a useful starting point for designing molecule-based optical switches. When the quenching mechanism is known, it is possible to arrange for the removal of quenching. The simplest switches are operated by a single, usually chemical, stimulus. Systems which respond to a given combination of multiple stimuli open the way to more complex switches – logic gates^[8,9] – at the molecular scale. In this short chapter, we focus on one guiding principle for the design of molecular scale logic systems, based mainly on chemical (usually ionic) inputs and optical (usually luminescent) output. For a wider perspective, the interested reader is referred to companion reviews.^[10,11]

Green plant photosynthesis, which feeds the world, runs on photoinduced electron transfer (PET).^[12] This principle was developed in chemical contexts by Albert Weller over three decades ago,^[13] and became adapted for use in fluorescent switching contexts in the late 1970s and early 1980s.^[14–21] A general design principle emerged soon afterwards.^[22]

11.2

YES Logic

The finite (usually nanoseconds or longer) lifetime of an electronically excited state is long enough to permit three-dimensional diffusional encounters between it and other species. The resulting quenching becomes even more efficient when the quencher unit is covalently held in the proximity of the fluorophore. Such modular ‘lumophore-spacer-receptor’ systems allow for easy development in a variety of formats,^[23] as later sections will illustrate. PET can easily be arranged in such situations if proper attention is paid to thermodynamic requirements. In other words, the fluorescence output is switched ‘off’ if the guest input is absent (Figure 1).

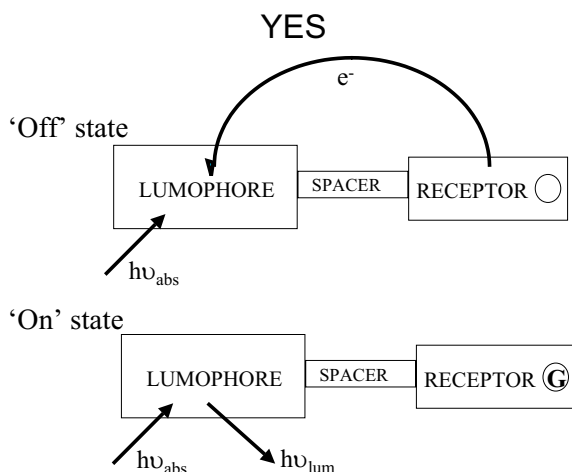
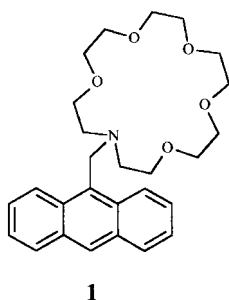


Fig. 1: Design principle of YES logic gates with luminescence output and chemical input according to photoinduced electron transfer (PET) concepts.

The arrival of the input guest species can be arranged to block this PET channel by making the thermodynamics unfavorable. At the simplest level, this switching of the thermodynamic conditions can be electrostatic in origin. A more complex situation can exploit a strategically placed hydrogen bond to bind a crucial lone electron pair. Another can exploit a guest-induced conformational switch to attenuate electroactivity. Now, the luminescence output is switched 'on' when the guest input is present (Figure 1). Thus, quenched/recoverable luminescent systems allows us a simple access into YES logic (Figure 2). The conventional symbols used in electronics for this and other logic gates will also be shown alongside the truth tables in each instance.

We note in passing that a large number of YES logic gates are already available in the literature relating to PET-based sensors.^[24] One example would be the anthracene-appended azacrown ether **1**,^[21] which responds to a K^+ input by increasing its fluorescence quantum yield 47-fold. An even larger number of YES logic systems can be discerned within the literature of general fluorescent sensors and reagents concerned with a variety of mechanisms and designs.^[25–28]



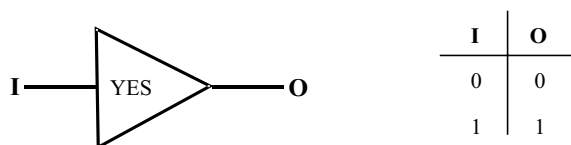


Fig. 2: A YES logic gate and its corresponding truth table.

11.3 NOT Logic

The directness of the thermodynamic analysis for PET allows us simply to reverse the above argument when required. This takes the first step in generalizing the PET switching principle. It can be arranged for the PET channel to be unfavorable when the guest input is absent, but for PET to become permitted if the guest input is present (Figure 3). Bright luminescence is observed only when the guest is absent from the receptor site. This leads easily to NOT logic (Figure 4). The Δ^2 -pyrazoline derivative 2, with an attached pyridyl unit,^[31] illustrates this situation. PET is encouraged only when the pyridine unit is protonated, to give the electron-deficient pyridinium group. The proton input is considered low (digital 0) at a concentration of 10^{-7} M or less, and high (digital 1) at 10^{-3} M or more.

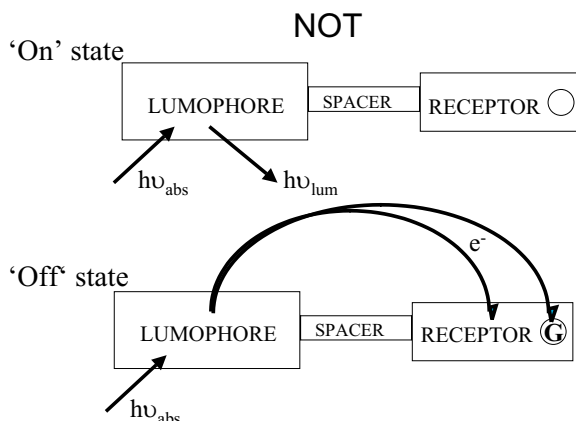


Fig. 3: Design principle of NOT logic gates with luminescence output and chemical input according to photoinduced electron transfer (PET) concepts.

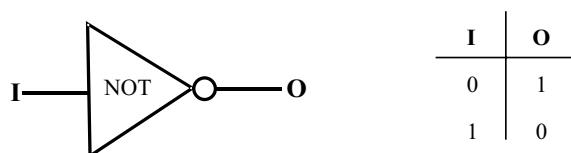
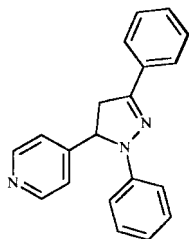
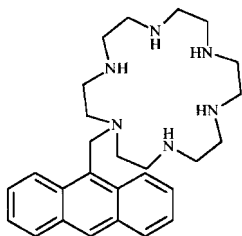


Fig. 4: A NOT logic gate and its corresponding truth table.

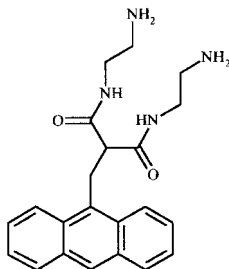


2

Another way of designing NOT logic gates is to arrange PET involving the input guest species (Figure 3). Examples from the supramolecular era can be illustrated from publications by Czarnik and Fabbrizzi, with **3**^[32,33] and **4**,^[34,35] respectively.

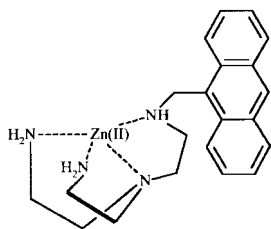


3



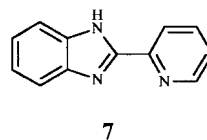
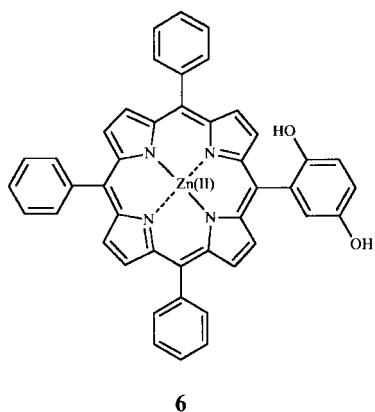
4

Fabbrizzi's **5**^[36] is unusual in using a nonmetallic, redox-active guest with a metal center serving as the receptor. An anionic nitrobenzoate guest is held by coordination of the carboxylate to the free apical position in Zn^{2+} . The electron-deficient nitrobenzoate engages in PET with the anthracene fluorophore to switch the fluorescence 'OFF'.



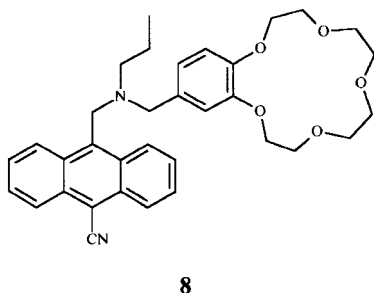
5

D'Souza's **6**^[37] achieves a similar end-result of NOT logic with no metal-centred interactions at all. In this case, the hydrogen bonding and π - π stacking interactions are sufficient to cause association of **6** and benzoquinone. Classical examples of NOT logic can be found in the analytical chemistry literature^[28] if we broaden our search to look for the phenomenon rather than a particular mechanism. For instance the fluorescence of **7**^[38] is extinguished upon arrival of Hg^{2+} .



11.4 AND Logic

The modular 'lumophore-spacer-receptor' systems illustrated in the previous sections are clearly designed to handle one input (though see later under OR gates). Addition of extra receptors via suitable spacers to maintain modularity would be a rational approach to logic systems which handle two or more inputs. In fact, the development of molecular scale logic as a subject would require this step, since the single-input systems are already seeing service as straightforward sensors which monitor the presence/absence of a chosen chemical species by means of a luminescence signal.^[39,25–27]



The first case of a molecular scale logic gate designed for that very purpose was the AND gate **8**, which can be viewed as a 'lumophore-spacer₁-receptor₁-spacer₂-receptor₂' system.^[40] It displayed the property that two possible PET channels from the two receptors needed to be suppressed if a strong fluorescence output was to be obtained. This was arranged by providing the two guest species that these two receptors were selectively looking for. The amine unit required H⁺ (input₁) whereas the benzocrown ether moiety required Na⁺ (input₂). This satisfied AND logic (Figure 5).

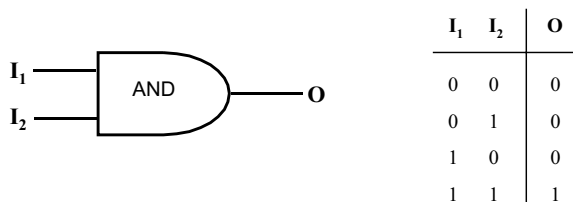
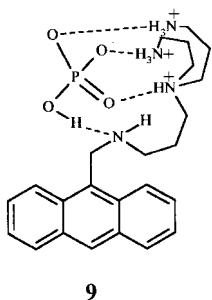
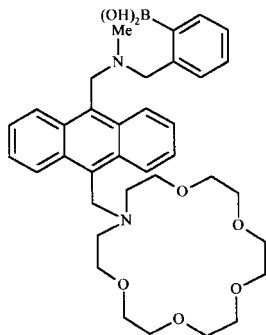


Fig. 5: An AND logic gate and its corresponding truth table.

Czarnik^[41] adapted a partially protonated polyamine receptor to serve as a receptor with a PET channel that was blocked upon arrival of an HPO_4^- anion, as seen in complex **9**. Although not discussed in a logical context, with protons and HPO_4^- serving as inputs, a large fluorescence switching 'ON' can be seen in the presence of both inputs, thus conferring an AND logic function upon the complex. While this is fine operationally, it can be seen to be noncommutative at the molecular scale, as binding of an HPO_4^- anion can take place only upon binding protons. The overall strategy for anion recognition can be seen to build upon an earlier example of cooperative binding put forward by Lehn,^[42] discussed in Section 11.5.



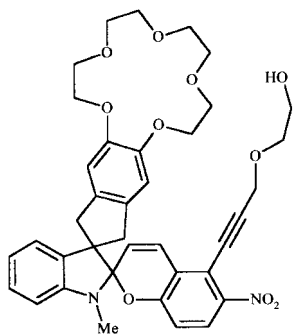
The case of **10**^[43] can be seen to exhibit AND logic behavior under appropriately controlled pH conditions. Two receptor moieties can be identified in this molecule: a boronic acid to bind saccharides and an azacrown ether for recognition of an ammonium ion. Thus, a molecule of *D*-glucosamine possesses the necessary components to enable switching 'on' of fluorescence (output 1) when the amine group is protonated. Using a coding such that the unprotonated amine is one input and protons the other, in a concentration such that the *D*-glucosamine is able to be protonated and hence bound, an AND action can be imposed on the molecule. The proton concentration must not be high enough to protonate the nitrogen center in the azacrown ether, of course. Thus, this example varies from the others in that no binding is seen in the presence of only one input, but rather when both are present.

**10**

Compound **10** can also be employed as a fluorescent AND logic gate if we supply a saccharide –glucose, say – and ammonium ions as the two inputs. This case again illustrates the point that fluorescent molecular logic gates serve immediately as sensors for important biological parameters, a D-glucosamine concentration in this case.

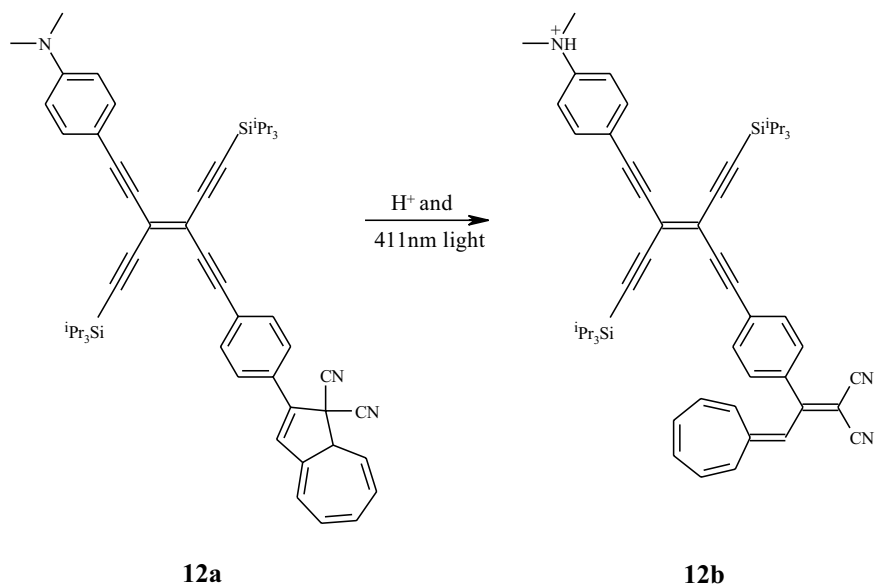
The simple molecule 1-bromonaphthalene can also provide the basis for a sharp AND logic action. The strong phosphorescence of naphthalenes derivatized with heavy atoms and embedded in low temperature glasses has a history of fifty years.^[44] However, this phosphorescence usually does not survive aerated fluid solutions at room temperature. β -Cyclodextrin encapsulation goes a long way towards overcoming this problem,^[45] but oxygen-insensitive phosphorescence remains a rarity. Nocera's solution was to encapsulate 1-bromonaphthalene inside the extended cylinder of glucosyl β -cyclodextrin and to cap the complex with *t*-butanol.^[46] The fact that these last two chemicals are both needed to create conditions for phosphorescence emission is quintessential AND logic action. The prospect of a simple test for alcohol in breath makes this system particularly attractive.

In the discussion so far, the inputs employed have been all chemical. It is also possible to combine light and chemical inputs. If light absorption is taken as the output, such systems translate as chemically responsive photochromics.^[47] Inouye has extended his photochromic spiropyrans in this direction. Unlike many spiropyrans, **11**^[48] produces little coloration upon ultraviolet irradiation. Strong coloration is seen, however, if Li^+ is present during irradiation, thus representing AND logic with Li^+ and ultraviolet light inputs, together with visible absorption as output. Other dual mode transducers with electrochemical stimulation and light irradiation as inputs are also known.^[49–53] Related systems in which the metal ion can be held by the phenolate oxygen develop the colored ring-opened form in response either to metal ion or to ultraviolet irradiation. In other words, they function as OR gates and can be compared with the examples in Section 11.6.



11

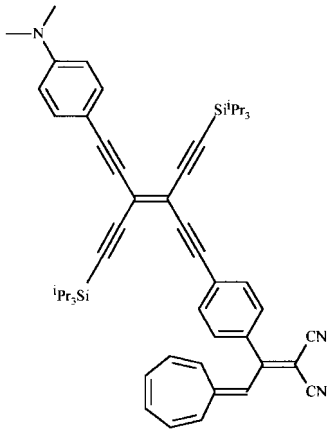
Pina, Maestri, and Balzani have exploited the photochromism of flavylum salts in this way. These flavylum salts have the added advantage of fluorescence output.^[54] This case is discussed in more detail in Chapter 10 and in a companion review.^[10] Diederich^[55] reports similar logic properties with **12**, as depicted in Figure 6, similarly employing a mix of ionic and photonic inputs, but utilizing absorption (500nm) as the output. This case has been interpreted as an AND logic gate, since protonation (using CF_3COOH) followed by 411nm irradiation clearly leads to **12b**. Overall this system is reversible as, following deprotonation of **12b** with NEt_3 , the system is thermally restored to **12a**. An ideal AND operation should show commutation: i.e., in the case at hand, irradiation followed by protonation should give the same end result. However, this is apparently not the case as a rapid thermal electrocyclic ring-closure of the nonprotonated, ring-opened form **13** gives **12a**.



12a

12b

Fig. 6: An AND logic with **12** based on absorption output using proton and light inputs.



13

11.5 NAND Logic

The NAND logic gate (Figure 7) enjoys a special place in the contemporary semiconductor electronics industry, since most other logic gates can be constructed from appropriate wiring of multiple units of this device. Of course, the present generation of molecular scale logic systems cannot be physically integrated in a direct way, because of their qualitatively different input and output types. Nevertheless, the very fact that molecular scale NAND gates are already available demonstrates how the ‘wiring problem’ can be circumvented in favorable situations. This issue will be discussed in more detail in Section 11.7, which deals with NOR gates designed from scratch while paying attention to integration issues. In the meantime, we illustrate molecular systems producing end results that are certainly NAND logic action.

Tanaka and Iwata^[56] have described an interesting system (14) that displayed all the hallmarks of a NAND logic gate at the molecular scale. The fluorescence of the heteroaromatic unit is quenched only when Ba^{2+} and SCN^- ions are simultaneously present at suitably high concentrations. The fluorescence-quenching PET process comes into action only when the electron-rich SCN^- is held near the fluorophore by coordination to an available site on the crown-complexed Ba^{2+} ion.

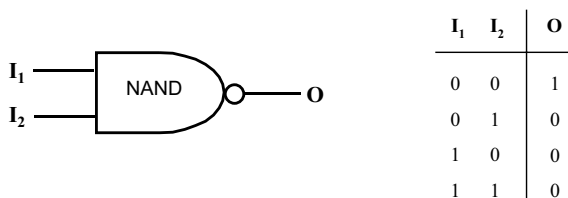
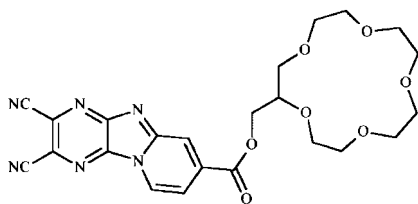


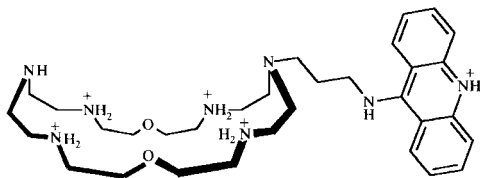
Fig. 7: A NAND logic gate and its corresponding truth table.



14

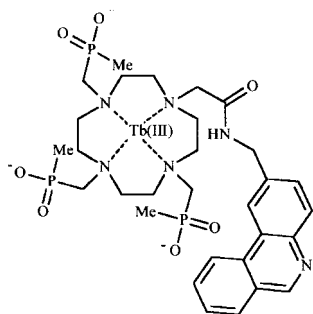
As far back as 1984, Wolfbeis described the quenching of fluorescence of dibenzo-18-crown-6 ether in the presence of K^+ and I^- ions;^[57] this can now be viewed as NAND logic behavior. It is likely that the oxidizable I^- is ion-paired to the crown-bound K^+ in much the same way as in the system involving **14**, Ba^{2+} , and SCN^- .

Lehn^[42] has reported a system in which a similar strategy is employed. Observed fluorescence changes are small, so this action cannot be described as digital, but it is significant. It is another early case in which a light emission response was obtained thanks to a sequence of ionic inputs: H^+ and adenosine triphosphate (ATP), in that order. In the current context, the decreasing fluorescence emission on binding protons and ATP makes **15** interpretable as a NAND logic gate. The fluorescence decrease can be assigned to the π - π interaction between the aminoacridinium moiety of **15** and the adenine component in ATP.



15

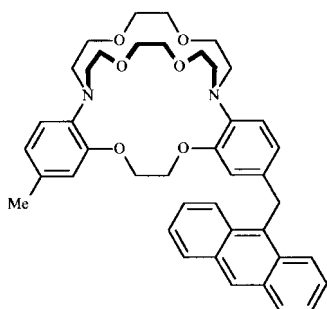
Parker and Williams recently reported NAND logic action in the terbium complex **16**.^[58] The delayed emission of the lanthanide ion is switched 'off' when H^+ and O_2 are present simultaneously. Protonation of the phenanthridine side chain causes its triplet excited state to approach the $Tb(III)$ 5D_4 excited state energetically. This leads to equilibration of these two excited states and sharing of their properties. Thus, the metal-centered state displays the O_2 sensitivity usually only found in organic triplets.



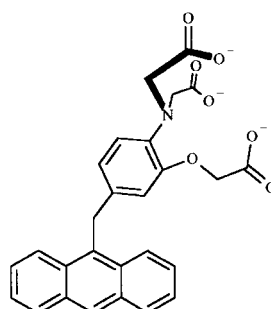
16

11.6 OR Logic

Molecular OR gates, as currently implemented, should be relatively easily produced, as all that is required is a set of nonselective receptors giving a positive optical response upon binding. The less selective the receptor, the operationally better the resulting OR action. It is important to note that in this instance this is going against the flow of most chemistry, in which the impetus is toward receptors of ever increasing selectivity. An inelegance in the strategy as currently implemented is perhaps that a receptor is not being provided for each of the ionic inputs, but rather the different inputs compete for a single receptor site. From another point of view, however, this demonstrates atom economy within an operational molecular scale device.



17



18

One of the earlier nonselective sensors of this type,^[59] subsequently interpreted as a photoionic OR gate (Figure 8), was 17. Sufficient quantities of K^+ or Rb^+ elicited the correct fluorescence output, with K^+ and Rb^+ giving almost equal fluorescence enhancements. Only with neither input species present was the fluorescence seen to be switched 'off'. However, the first intentionally designed OR logic gates^[60] were 18 and 19, in which Ca^{2+} and Mg^{2+} produce essentially identical fluorescence enhancements. The receptor employed in this instance is one put forward by London:^[61] compound 20.

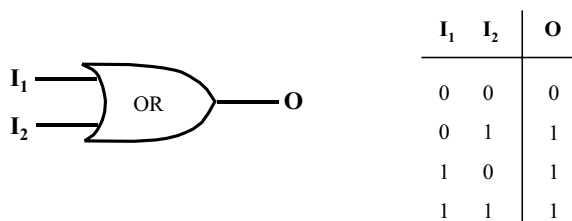
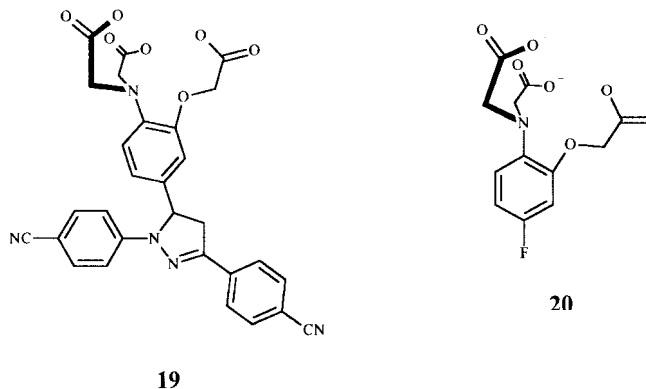
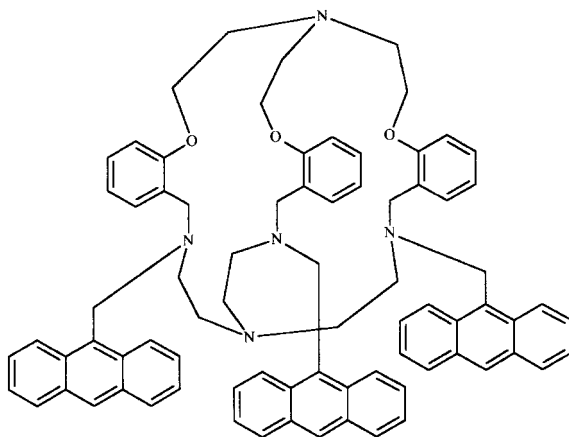


Fig. 8: An OR logic gate and its corresponding truth table.



This receptor shows a remarkable selectivity for Mg^{2+} over Ca^{2+} under physiological conditions and has found applications in ^{19}F NMR probes and ratiometric fluorescent sensors based on wavelength shifts.^[62] In high concentrations, however, both Ca^{2+} and Mg^{2+} can be bound. The similarity of fluorescence enhancements with both ions is the result of essentially identical conformational changes produced upon complexation. Each ion-bound state effectively decouples the amine substituent from the oxybenzene unit, so that PET is similarly suppressed. This means that the charge density difference between the two cations is of secondary importance in these conformationally switchable systems.

Molecule **21** also serves an example of an interesting OR gate, because various transition metal ions serve to switch fluorescence 'ON' by more or less similar amounts.^[63,64] The surprise in this system is that transition metal ions are acting here contrarily to their normal behavior. Transition metal ions have a history of quenching fluorescence very efficiently by several mechanisms: heavy atom effects, PET, electronic energy transfers, and paramagnetic effects. The authors of **21** appear to have eliminated the possibility of artifacts arising from protonation originating from the hydration shell of the highly charged transition metal ion.



21

11.7 NOR Logic

As Figure 9 shows, NOR logic involves a particular combination of NOT and OR operations. If we follow the electronic symbology to its logical conclusion, this would require the physical connection of the output from the OR gate into the input of the NOT gate. Though not impossible in principle, such ‘wiring’ would be quite difficult to achieve in systems with qualitatively different inputs and outputs. However, such issues can be sidestepped if we opt for functional rather than physical integration. After all, the end result will be the same. Functional integration of NOT and OR operations can be achieved by noting the requirement for a nonselective receptor for the OR operation and for ion-induced fluorescence quenching for the NOT operation. Therefore, the NOT logic function simply becomes the achievement of fluorescence quenching through the occupation of a nonselective receptor by one or other of two guest ions.

Two examples of molecular NOR logic gates can be seen in molecules 22 and 23.^[65] For 22, zinc ions and protons are coded as the inputs, and fluorescence is the

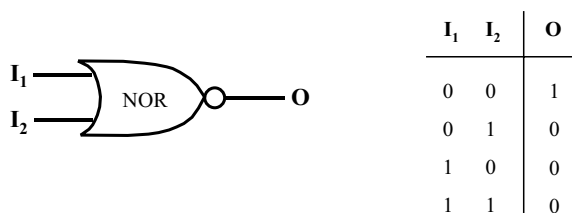
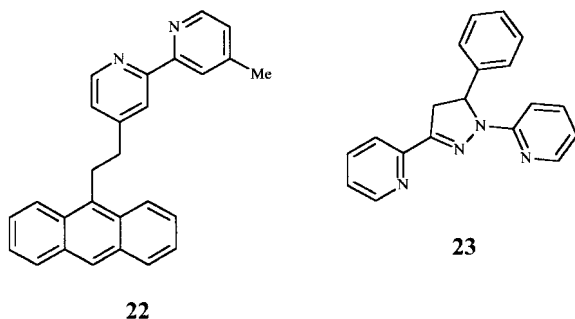


Fig. 9: A NOR logic gate and its corresponding truth table.

output. The mode of action is evident, as binding of either ion results in a positive charge and induced planarization in the bipyridyl receptor. Planarization of a bipyridyl makes it more reducible, as does a positive charge, and so good electron transfer is ensured on ion binding.^[66,67] This electron transfer proceeds from the excited state of the anthryl fluorophore and serves to disable the fluorescence emission. This fluorescence quenching in the presence of one or both of the inputs, in sufficient quantities, along with observed fluorescence emission in the absence of either, can be seen to correspond to the NOR truth table in Figure 9.



NOR gates can also be approached by utilization of switching mechanisms other than PET, as highlighted by 23. In this instance, protons cause quenching by introducing a vibrational loss mechanism^[68] through binding to the imine nitrogen of the central heterocycle. This nonradiative loss mechanism is seen to be more efficient than the radiative one. Additionally, Hg^{2+} binds to the 2,2':6',2''-terpyridyl-like ligation site and creates a ligand to metal charge transfer (LMCT) excited state which is non-emissive. The efficiency of these quenching processes is clearly illustrated in Figure 10. The LMCT state can be anticipated because of the facile one-electron reducibility of Hg^{2+} . Non-emissive LMCT states have some similarities with

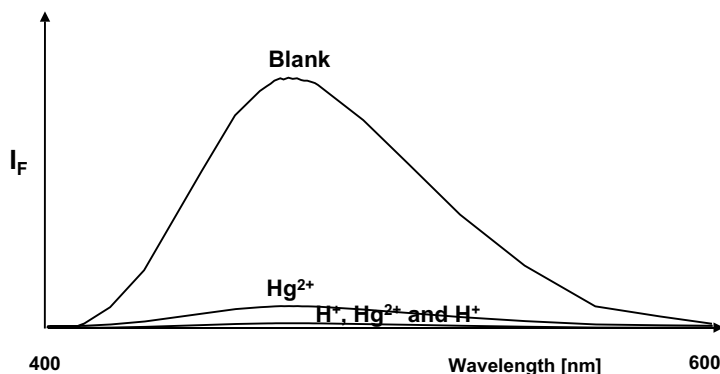
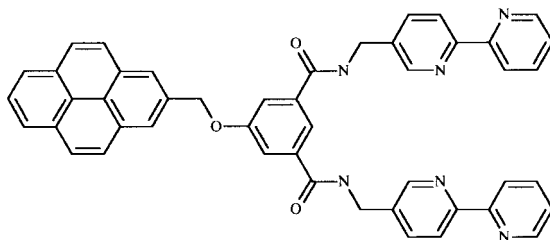


Fig. 10: NOR logic gate action of system 23. A family of fluorescence spectra under various conditions is shown. I_F is the fluorescence intensity. 'Blank' refers to the absence of high levels of H^+ and Hg^{2+} .

PET. The key difference is that PET requires clear separation between donor and acceptor units, which is not the case in **23**.

The pyrene-based fluorescence of **24**^[69] was recently demonstrated by Fages et al. to be switched 'OFF' by Zn^{2+} . Similar action of H^+ on this receptor can also be envisaged, thereby making the mode of action similar to **22**.

**24**

11.8 XOR Logic

XOR is a particularly interesting type of double-input logic, for two reasons. Firstly, it achieves a high output only if the two inputs are digitally different: i.e., 1 and 0, or 0 and 1 (Figure 11). Secondly, it is a vital half of the half-adder, from which arithmetic is performed in current computers and calculators. The other vital half is the AND operation, which has a longer history of emulation at the molecular scale (Section 11.4). So the achievement of molecular XOR logic is likely to cause a domino effect in the movement towards molecular scale arithmetic.

The only reported example of this type of behavior comes from the work of Balzani and Stoddart and their teams. It is based upon the threading/unthreading processes of a pseudorotaxane (see Chapters 7 and 8),^[70] with concomitant fluorescence output changes. The constituent components of the pseudorotaxane are a naphthocrown ether, **25**, and a diazapyrenium dication, **26**. On accommodation of the diazapyrenium thread, a nonfluorescent complex is formed, abolishing the fluorescent properties of the individual components. This corresponds to the first row of the truth table as no inputs are present and no fluorescence output is observed. The introduction of protons (in the form of CF_3SO_3H) causes an unthreading of the

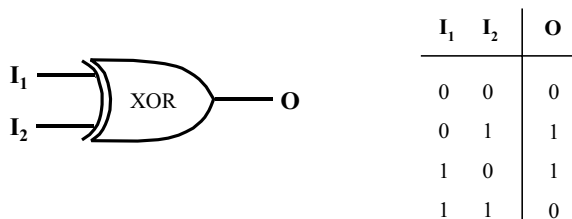
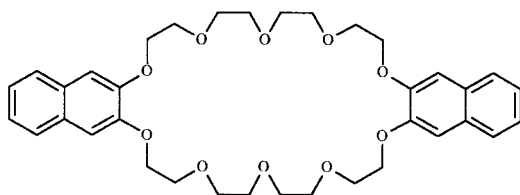
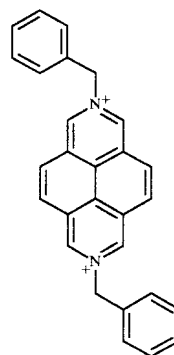


Fig. 11: An XOR logic gate and its corresponding truth table.

complex formed. This is due to the poorly solvating CH_3CN medium enabling a protonation of the crown ether oxygens and facilitating the unthreading procedure, displacing the diazapyrenium dication. Fluorescence is thus restored, corresponding to the second row of the truth table. Fortunately, the protonated crown ether fluoresces in the same region as the unprotonated crown ether on its own. The second input is Bu_3N , which, when supplied on its own, binds rather strongly to the diazapyrenium unit, displacing the naphthocrown ether. Hence, fluorescence from the free naphthocrown ether can again be seen as the output. The fourth row of the truth table is reached by providing equimolar amounts of $\text{CF}_3\text{SO}_3\text{H}$ and Bu_3N so that neutralization takes place. This is equivalent to an ion-free situation, and so no fluorescence output is observed.



25



26

11.9 XNOR Logic

The XNOR logic gate combines the NOT and XOR operations (Figure 12), both of which have molecular scale counterparts. Nevertheless, only one example of this type of behavior is known, and it comes from the same stable as the case in Section 11.8. Again it involves pseudorotaxane chemistry (see Chapters 7 and 8), produced this time from components 27 and 28.^[71]

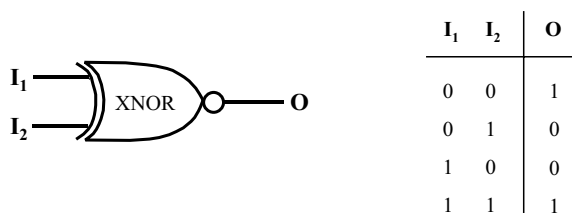
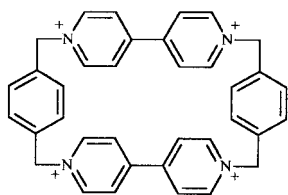
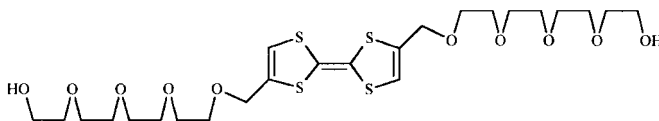


Fig. 12: An XNOR logic gate and its corresponding truth table.



27



28

This complex displays a charge transfer (CT) absorption band, equivalent to an output 1. The first input is considered to be a reduction potential large enough to reduce the component 27 within the 27.28 complex. Upon reduction, the CT interaction between the two components is sufficiently weakened such that unthreading occurs, with concomitant loss of the absorption signature. This is taken as output 0. Similarly, the second input can be considered to be the application of an oxidation potential sufficient to oxidize component 28 within the 27.28 complex. Again an unthreading process occurs, with the loss of the CT absorption. This is read as output 0. The fourth row of the truth table must be imagined as the simultaneous application of equal oxidation and reduction potentials, resulting in mutual annihilation: i.e., a potential of 0. With no applied potential, no perturbation of the complex 27.28 occurs. Thus the CT absorption is seen to persist, and hence output 1, in a similar fashion to that of the first row of the truth table. Viewed more generally, this is a nice example of electrochromic effects within a supramolecular system being exploited for a logic-centered end result.

11.10 INHIBIT Logic

The previous logic functions relied upon a minimum of one or two inputs. The INHIBIT gate, in its usual manifestation, is the first of the gates under consideration which relies upon a minimum of three inputs, and hence can be considered a more complex gate. This is reflected in the difficulty of its implementation in a molecular regime. Additionally, as the electronic symbol denotes, this operation requires the appropriate connection of NOT and AND gates (Figure 13). This type of integration is a major challenge to the further growth of molecular scale logic devices.

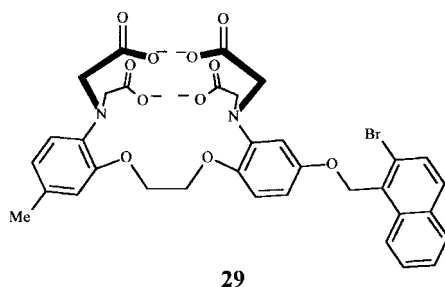


Fig. 13: An INHIBIT gate with its corresponding truth table.

This type of integration of molecular logic functions has obviously been accomplished one way or another in the NOR, NAND, and XNOR cases discussed previously. However, predictive integration of modular logic devices is in its infancy. In the case of NOR gates, integration was achieved functionally rather than physically, avoiding the “wiring together” of NOT and OR devices, which would have proved particularly challenging.

The development of the INHIBIT logic gate can be discussed in terms of a similar process of functional and physical integration. As the electronic symbol shows, the INHIBIT gate is a 3-input AND gate, with the output of a NOT gate serving as the third input to the AND gate. Viewed from a different perspective, the third input serves as a disable signal to the entire AND gate. Disabling is easily implementable at the molecular scale after we note that luminescence quenching is such a process. Therefore, a molecular scale AND gate is required, the luminescence of which can be quenched overall upon provision of the third input while being preserved when this third input is absent.^[65]

The third input selected was molecular oxygen; its paramagnetism allows it to be a powerful quencher of room temperature phosphorescence in fluid solution.^[45] AND logic behavior was arranged in a phosphorescent system, by using β -cyclodextrin as one input and Ca^{2+} as the second input. Room temperature phosphorescent systems such as **29** suffer triplet-triplet annihilations, hence quenching their phosphorescence unless the phosphors are sterically prevented from encountering one another.



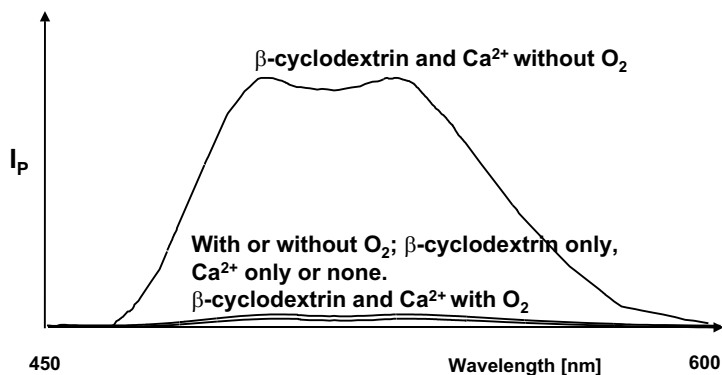


Fig. 14: INHIBIT logic gate action of system **29**. A family of phosphorescence spectra under various conditions are shown. I_P is the phosphorescence intensity.

β -Cyclodextrins achieve this steric protector role by acting as an optically transparent “sleeve”, which envelops the 1-bromonaphthalene phosphor.^[72,73] Ca^{2+} serves as the second input for the inhibit gate, as the PET process (from the tetracarboxylate receptor to the 1-bromonaphthalene phosphor) engineered into **29** can be arrested on binding Ca^{2+} . Therefore it is only when Ca^{2+} and β -cyclodextrin are present in sufficiently high concentrations and when molecular oxygen is absent that bright phosphorescence can be observed, demonstrating the INHIBIT operation (Figure 14).

The use of phosphorescent systems in molecular scale logic devices opens up the possibility of operating gates in a controlled sequence. A fluorescent gate and a phosphorescent gate coexisting in solution can be interrogated at will by two different strategies. The first is time-resolved observation following pulse excitation, such that the fluorescence gate responds within nanoseconds and is lost during the ‘blind’ period of observation. The millisecond duration of the phosphorescence allows it to be observed without any contamination by the fluorescence signal. Secondly, the phosphorescent gate can be disabled by addition of oxygen so that its output remains silent, whereas the fluorescent gate loses very little efficiency (if any), especially if short lived (picosecond) fluorophores are selected.

11.11

Enabled OR Logic

The enabled OR – another type of gate that requires a minimum of three inputs – has just become available. Figure 15 shows the equivalent electronic representation, with the appropriate connection of AND and OR gates. In this context we note that the INHIBIT gate discussed in Section 11.10 also involves an enabling/disabling input. One strand of Pina, Maestri, and Balzani’s novel exploitation of flavylum derivative photochemistry was briefly mentioned in Section 11.4. This AND logic system used protons and ultraviolet photons as the two inputs, to create a visible

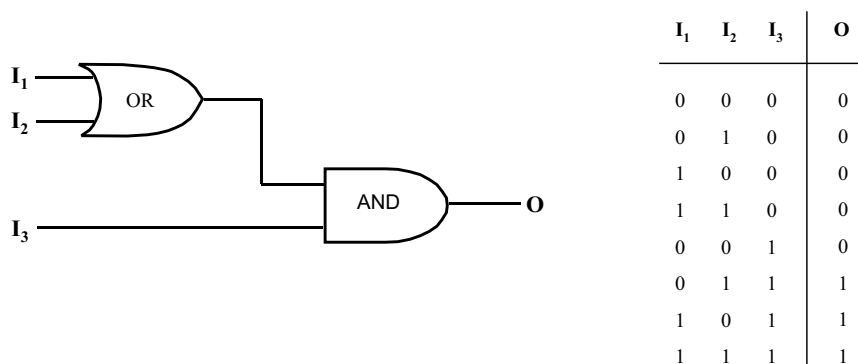
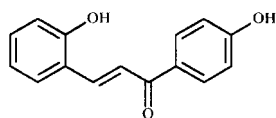


Fig. 15: An Enabled OR logic gate and corresponding truth table.

absorption output. Such a system (30) has been extended to produce a hitherto undescribed three-input logic gate – the enabled OR.



30

The extension is simple but effective. Fluorescent sensors that migrate to interfacial regions of detergent micelles can experience highly enhanced proton densities in their vicinities as a result of electrostatic concentration.^[75,76] Addition of negatively charged sodium dodecyl sulfate (SDS) micelles raises formerly low proton densities (bulk pH = 5.5) to the high levels necessary (local pH ~1) to switch the molecular scale gate if ultraviolet photons are simultaneously present. Hence, the AND truth table can now be expanded to give the enabled OR case. The ultraviolet photons are naturally the enabling input I_3 , because the gate would not switch without them. Protons serve as input I_1 , with the high level being bulk pH = 1 and the low level being bulk pH = 5.5. SDS micelles serve as input I_2 . We close this section by noting that this paper includes far more than the point relevant to our discussion.

11.12

Conclusion

The preceding pages demonstrate that the input-output behavior of many molecular systems can already be described in terms of fundamental logic operations. It has also been suggested above that what is explicitly described is the tip of an iceberg when one takes into account the rich literature on analytical reagents in various domains. The identification and taxonomy of individual cases must be a natural

early step in the development of any field of this type. In addition to this exploratory step, an equally natural step of generalization and expansion of individual classes must also occur early on. This is a design step. When these two steps are being taken with growing confidence, we should be in a position to exploit what has been learned to solve the problems of other disciplines. This is the step of application. The fact that this sequence of steps has already been successfully taken on several occasions in the sister field of luminescent sensors^[39,25] augurs well for the subject of this chapter.

Acknowledgments

Our recent endeavors in this area depend on the support of the Department of Education in Northern Ireland, the Engineering and Physical Sciences Research Council (UK) and the European Social Fund.

References

- 1 M. Sauer, J. Wolfrum in *Applied Fluorescence in Chemistry, Biology and Medicine*, Eds. W. Rettig, B. Strehmel, S. Schrader, H. Seifert, Springer Verlag, Berlin, 1999, 39.
- 2 S. Weiss, *Science* 1999, **283**, 1676.
- 3 J.B. Birks, *Photophysics of Aromatic Molecules*, Wiley, London, 1970.
- 4 J.R. Lakowicz, *Principles of Fluorescence Spectroscopy*, Plenum, New York, 1983.
- 5 G.G. Guilbault, *Practical Fluorescence*; 2nd Edition, Dekker, New York, 1990.
- 6 N.J. Turro, *Modern Molecular Photochemistry*, University Science Books, Mill Valley, CA, 1991.
- 7 V. Balzani, F. Scandola, *Supramolecular Photochemistry*, Ellis-Horwood, Chichester, 1991.
- 8 A.P. Malvino, J.A. Brown, *Digital Computer Electronics* 3rd Ed., Glencoe, Lake Forest, 1993.
- 9 J. Millman, A. Grabel, *Microelectronics*, McGraw-Hill, London, 1988.
- 10 A.P. de Silva, N.D. McClenaghan, C.P. McCoy in *Handbook of Electron Transfer in Chemistry*, Ed. V. Balzani, Wiley-VCH, Weinheim, 2000.
- 11 A.P. de Silva, D.B. Fox, T.S. Moody in *Stimulating Concepts in Chemistry*, Eds. M. Shibasaki, J.F. Stoddart and F. Vogtle, Wiley-VCH, Weinheim, 2000, in press.
- 12 G.J. Kavarnos, *Fundamentals of Photoinduced Electron Transfer*, VCH, Weinheim, New York, 1993.
- 13 A. Weller, *Pure Appl. Chem.* **1968**, *16*, 115.
- 14 Y.C. Wang, H. Morawetz, *J. Am. Chem. Soc.* **1976**, *98*, 3611.
- 15 H. Morawetz, *J. Lumin.* **1989**, *43*, 59.
- 16 H. Shizuka, M. Nakamura, T. Morita, *J. Phys. Chem.* **1979**, *83*, 2019.
- 17 B.K. Selinger, *Aust. J. Chem.* **1977**, *30*, 2087.
- 18 A.P. de Silva, R.A.D.D. Rupasinghe, S.L.A. Peiris, *Proc. Sri Lanka Assoc. Advmt. Sci.*, **1982**, *38*, 68.
- 19 J.P. Konopelski, F. Kotzyba-Hibert, J.-M. Lehn, J.-P. Desvergne, F. Fages, A. Castellan, H. Bouas-Laurent, *J. Chem. Soc., Chem. Commun.* **1985**, 433.
- 20 A.P. de Silva, R.A.D.D. Rupasinghe, *J. Chem. Soc. Chem. Commun.* **1985**, 1669.
- 21 A.P. de Silva, S.A. de Silva, *J. Chem. Soc. Chem. Commun.* **1986**, 1709.
- 22 A.J. Bryan, A.P. de Silva, S.A. de Silva, R.A.D.D. Rupasinghe, K.R.A.S. Sandanayake, *Biosensors* **1989**, *4*, 169.
- 23 R.A. Bissell, A.P. de Silva, H.Q.N. Gunaratne, P.L.M. Lynch, G.E.M. Maguire, K.R.A.S. Sandanayake, *Chem. Soc. Rev.* **1992**, *21*, 187.
- 24 R.A. Bissell, A.P. de Silva, H.Q.N. Gunaratne, P.L.M. Lynch, G.E.M. Maguire, C.P. McCoy, K.R.A.S. Sandanayake, *Top. Curr. Chem.* **1993**, *168*, 223.
- 25 A.P. de Silva, H.Q.N. Gunaratne, T. Gunnlaugsson, A.J.M. Huxley, C.P. McCoy, J.T. Rademacher, T.E. Rice, *Chem. Rev.* **1997**, *97*, 1515.
- 26 *Fluorescent Chemosensors for Ion and Molecule Recognition*, Ed., A.W. Czarnik, ACS Books, Washington DC, 1993.
- 27 *Chemosensors for Ion and Molecule Recognition*, Eds., A.W. Czarnik, J.-P. Desvergne, Kluwer, Dordrecht, 1997.
- 28 A. Fernandez-Gutierrez, A. Munoz de la Pena, in *Molecular Luminescence Spectroscopy. Methods and Applications. Part 1*, Ed. S.G. Schulman, Wiley, New York, 1985, 371.
- 29 L. Fabbrizzi, A. Poggi, *Chem. Soc. Rev.* **1995**, *24*, 197.
- 30 B. Valeur, in *Topics in Fluorescence Spectroscopy. Vol. 4. Probe Design and Chemical Sensing*, Ed., J.R. Lakowicz, Plenum, New York, 1994, 21.
- 31 A.P. de Silva, H.Q.N. Gunaratne, P.L.M. Lynch, *J. Chem. Soc. Perkin Trans. 2* **1995**, 685.
- 32 E.U. Akkaya, M.E. Huston, A.W. Czarnik, *J. Am. Chem. Soc.* **1990**, *112*, 3590.
- 33 A.W. Czarnik, *Acc. Chem. Res.* **1994**, *27*, 302.
- 34 L. Fabbrizzi, M. Licchelli, P. Pallavicini, D. Sacchi, *Angew. Chem., Int. Ed. Engl.* **1994**, *33*, 1975.
- 35 L. Fabbrizzi, M. Licchelli, P. Pallavicini, *Acc. Chem. Res.* **1999**, *32*, 846.
- 36 G. De Santis, L. Fabbrizzi, M. Licchelli, A. Poggi, A. Taglietti, *Angew. Chem., Int. Ed. Engl.* **1996**, *35*, 202.
- 37 F. D'Souza, *J. Am. Chem. Soc.* **1996**, *118*, 923.
- 38 L.S. Bark, A. Rixon, *Analyst* **1970**, *95*, 786.
- 39 A.P. de Silva, J. Eilers, G. Zlokarnik, *Proc. Natl. Acad. Sci. USA* **1999**, *96*, 8336.
- 40 A.P. de Silva, H.Q.N. Gunaratne, C.P. McCoy, *Nature* **1993**, *364*, 42.

- 41 M.E. Huston, E.V. Akkaya, A.W. Czarnik, *J. Am. Chem. Soc.* **1989**, *111*, 8735.
- 42 M.W. Hosseini, A.J. Blacker, J.-M. Lehn, *J. Am. Chem. Soc.* **1990**, *112*, 3896.
- 43 C.R. Cooper, T.D. James, *Chem. Commun.*, **1997**, 1419.
- 44 D.S. McClure, *J. Chem. Phys.* **1949**, *17*, 905.
- 45 J.D. Bolt, N.J. Turro, *Photochem. Photobiol.* **1982**, *35*, 305.
- 46 A. Ponce, P.A. Wong, J.J. Way, D.G. Nocera, *J. Phys. Chem.* **1993**, *93*, 11137.
- 47 *Photochromism. Molecules and Systems*, Eds. H. Dürr, H. Bouas-Laurent, Elsevier, Amsterdam, 1990.
- 48 M. Inouye, K. Akamatsu, H. Nakazumi, *J. Am. Chem. Soc.* **1997**, *119*, 9160.
- 49 J. Daub, J. Salbeck, T. Knochel, C. Fischer, H. Kunkely, K.M. Rapp, *Angew. Chem., Int. Ed. Engl.* **1989**, *28*, 1494.
- 50 J. Achatz, C. Fischer, J. Salbeck, J. Daub, *J. Chem. Soc., Chem. Commun.* **1991**, 504.
- 51 A.K. Newell, J.H.P. Utley, *J. Chem. Soc., Chem. Commun.* **1992**, 800.
- 52 T. Saika, T. Iyoda, K. Honda, T. Shimidzu, *J. Chem. Soc., Perkin Trans. 2* **1993**, 1181.
- 53 S.H. Kawai, S.L. Gilat, J.-M. Lehn, *J. Chem. Soc., Chem. Commun.* **1994**, 1011.
- 54 F. Pina, M. Maestri, V. Balzani, *Chem. Commun.* **1999**, 107.
- 55 L. Gobbi, P. Seiler, F. Diederich, *Angew. Chem., Int. Ed. Engl.* **1999**, *38*, 674.
- 56 S. Iwata, K. Tanaka, *J. Chem. Soc., Chem. Commun.* **1995**, 1491.
- 57 O.S. Wolfbeis, H. Offenbacher, *Monatsh. Chem.* **1984**, *115*, 647.
- 58 D. Parker, J.A.G. Williams, *Chem. Commun.* **1998**, 245.
- 59 A.P. de Silva, H.Q.N. Gunaratne, K.R.A.S. Sandanayake, *Tetrahedron Lett.* **1990**, *31*, 5193.
- 60 A.P. de Silva, H.Q.N. Gunaratne, G.E.M. Maguire, *J. Chem. Soc., Chem. Commun.* **1994**, 1213.
- 61 L.A. Levy, E. Murphy, B.Raju, R.E. London, *Biochemistry* **1988**, *27*, 4041.
- 62 B. Raju, E. Murphy, L.A. Levy, R.D. Hall, R.E. London, *Am. J. Physiol.* **1989**, *256*, C540.
- 63 P. Ghosh, P.K. Bharadwaj, S. Mandal, S. Ghosh, *J. Am. Chem. Soc.* **1996**, *118*, 1553.
- 64 D.K. Chand, P. Ghosh, R. Shukla, S. Sengupta, G. Das, P. Bandyopadhyay, P.K. Bharadwaj, *Proc. Indian Acad. Sci., Chem. Sci.* **1996**, *108*, 229.
- 65 A.P. de Silva, I.M. Dixon, H.Q.N. Gunaratne, T. Gunnlaugsson, P.R.S. Maxwell, T.E. Rice, *J. Am. Chem. Soc.* **1999**, *121*, 1393.
- 66 M. Cesario, C.O. Dietrich, A. Edell, J. Guilhem, J.P. Kintzinger, C. Pascard, J.-P. Sauvage, *J. Am. Chem. Soc.* **1986**, *108*, 6250.
- 67 M. Yagi, T. Kaneshima, Y. Wada, K. Takemura, Y. Yokoyama, *J. Photochem. Photobiol. A: Chem.* **1994**, *84*, 27.
- 68 M.D.P. De Costa, A.P. de Silva, S.T. Pathirana, *Can. J. Chem.* **1987**, *65*, 1416.
- 69 J.-E. Sohma, P. Jaumier, F. Fages, *J. Chem. Res.* **1999**, 134.
- 70 A. Credi, V. Balzani, S.J. Langford, J.F. Stoddart, *J. Am. Chem. Soc.* **1997**, *119*, 2679.
- 71 M. Asakawa, P.R. Ashton, V. Balzani, A. Credi, G. Matternsteig, O.A. Matthews, M. Montalti, N. Spencer, J.F. Stoddart, M. Venturi, *Chem. Eur. J.* **1997**, *3*, 1992.
- 72 M. Bender, M. Komiyama, *Cyclodextrin Chemistry*: Springer-Verlag: New York, 1971.
- 73 R.A. Bissell, A.P. de Silva, *J. Chem. Soc. Chem. Commun.* **1991**, 1148.
- 74 A. Roque, F. Pina, S. Alves, R. Ballardini, M. Maestri, V. Balzani, *J. Mater. Chem.* **1999**, *9*, 2265.
- 75 M. Fernandez, P. Fromherz, *J. Phys. Chem.* **1977**, *31*, 1755.
- 76 R.A. Bissell, A.J. Bryan, A.P. de Silva, C.P. McCoy, *J. Chem. Soc. Chem. Commun.* **1994**, 405.

12

Liquid Crystal Photonics: Opto-photochemical Effects in Photoresponsive Liquid Crystals

Tomiki Ikeda and Akihiko Kanazawa

12.1

Introduction

It is expected that we will soon have an information society, in which a huge amount of information will be exchanged simultaneously all over the world. This is evidenced by trends in communication; its annual volume grows each year and is expected to increase abruptly in the early part of the 21st century, due to construction of optical fiber networks not only in North America, Europe, and Asia, but also in other areas of the world. Through optical fiber networks, it will be possible to receive several hundreds of gibabits to several terabits of optical data per second, and this tremendously large amount of optical data will have to be processed in a short time. However, it is very difficult to achieve this with electron processes alone, as has so far been done, because of limitations to the capability of electron processes in information processing. It is necessary to develop a new system incorporating photon processes (photonics), which display superior properties to electron processes in three aspects, certainly advantageous for information processing. Time-wise, fast processing of signals is possible both with photon processes and with electron processes. However, photons feature two additional domains crucial in photon processes: the wavelength domain and the spatial domain. In the wavelength domain, multiplex processing is achievable; in the spatial domain, two-dimensional processing of information is possible. Furthermore, the photon process shows an additional merit that also makes photon processes much more efficient: high signal to noise (S/N) ratios. With these advantageous properties, multimedia based on photon processes are expected to be the most promising technology in information processing in the next generation.

Liquid crystals (LCs) exhibit some unique and invaluable properties:

- 1) self-organizing nature in a certain temperature range with fluidity and long-range order;
- 2) cooperative effect: if a small portion of LCs change alignment, the remainder will also change their alignment;
- 3) anisotropy in refractive index, which means birefringence;
- 4) alignment change produced by external fields at surfaces and interfaces.

A large change in refractive index can be obtained by changing the alignment of LCs. This property of LCs is very useful for optical data processing, because changing the refractive index of materials or devices by means of an external field is the most effective way to control optical signals. The LC materials can be used not only in LC displays (LCDs) but also in various photonic applications, such as optical storage, optical switching, optical display, and optical computing.

12.2

LC Alignment Change by Means of Photochemical Processes

12.2.1

Photochemical Phase Transitions in Guest/Host Systems

Thanks to cooperative effects, changes in alignment of whole LC systems can be effected by only a small amount of trigger molecules capable of changing their molecular shape on photoirradiation. Many photochromic compounds have been used as photoswitchable guest molecules, among them azobenzenes, stilbenes, spiropyrans, and fulgides. Advantages of these photochromic compounds as trigger molecules are:

- 1) they undergo changes in molecular shape, which in most cases results in changes in other properties of the molecules, such as polarity;
- 2) photochromic reactions are reversible and two isomers can usually be inter-switched effectively with the aid of light of different wavelengths. Thus, the alignment of LCs can be altered reversibly by these means;
- 3) photochromic reactions are in most cases very fast, occurring in a timescale of picoseconds, which can give rise to very fast alignment changes in LCs.

The first example of induction of LC alignment changes arising from photochromic reactions was reported by Sackmann in 1971. He discovered that the pitch of cholesteric LCs could be changed on *trans-cis* photoisomerization of azobenzene moieties dispersed in host cholesteric LCs, as evidenced by a change in the wavelength of reflected light.^[1] Since this first report, many studies on photoinduced LC alignment change have been performed (see also Chapter 5). Attention has mainly been directed towards:

- photochemically induced phase transitions of LCs: smectic (Sm) cholesteric (Ch) phase transitions^[2] and nematic (N) isotropic (I) phase transitions^[3,4] induced by photoisomerization of azobenzenes dispersed in LCs; N–I phase transitions induced by photochemical reaction of spiropyrans;^[5]
- change in pitch of Ch LCs caused by photoisomerization of fulgides;^[6]
- helix inversion in Ch LCs induced by photoisomerization of thiopyranilidene-thioxanthenes.^[7]

Photochemically induced phase transition (*photochemical phase transition*) of LCs in guest/host systems is interpreted as follows.^[8] If a small population of photochromic compounds such as azobenzene are dispersed in nematic LCs (NLCs), the phase structure of the NLCs is susceptible to change induced by photochemical reac-

tion of the photochromic guest molecules. The *trans* form of azobenzene is a rod-like shape, which stabilizes the phase structure of NLCs. Its *cis* form isomer, however, is bent and tends to destabilize NLC phase structure. Accordingly, the N→I phase transition temperature, T_{NI} , of the *cis*-azobenzene/NLC mixture is much lower than that of the *trans*-azobenzene/NLC mixture. This phenomenon is similar to the depression of freezing point observed in the presence of a small amount of an impurity. In this case, an impurity (*cis* form) is produced on photoirradiation. Depression of freezing point is a colligative property of materials; the temperature change does not depend on the structure of the impurity, only on its concentration. The photochemically induced decrease in T_{NI} , however, depends strongly on the structure of the impurity. For instance, 4-pentyl-4'-cyanobiphenyl (5CB) was used as a host NLC, two types of azobenzenes were used as guest molecules, and the T_{NI} s of the mixtures were examined before and after photoirradiation-induced *trans-cis* photoisomerization. It was found that a 4-butyl-4'-methoxyazobenzene (BMAB)/5CB mixture showed a much larger value of ΔT ($= T_{NI}(\textit{trans}) - T_{NI}(\textit{cis})$) than an unsubstituted azobenzene/5CB mixture did. If an NLC sample that contains an azobenzene guest is kept at a temperature between $T_{NI}(\textit{cis})$ and $T_{NI}(\textit{trans})$ and then irradiated to induce *trans-cis* isomerization of the azobenzene guest molecules, the N→I phase transition of the sample is induced isothermally. Suppose that, in its initial state, the guest molecule is in the *trans* form. Before photoirradiation, the temperature of the sample is below $T_{NI}(\textit{trans})$ and the sample is in an N phase. On photoirradiation to induce *trans-cis* photoisomerization, the concentration of the *cis* form in the sample increases, and the T_{NI} of the mixture decreases concomitantly. When the T_{NI} is lowered below the experimental temperature, an N→I phase transition takes place. Put another way, when the *cis* form concentration exceeds a threshold value in the phase diagram of the *cis*-azobenzene/NLC system, the mixture will be in an I phase at the temperature of irradiation. Since the *trans-cis* photoisomerization is reversible, this process is also reversible; with *cis* to *trans* back-isomerization (either photochemical or thermal), the initial N phase is restored. This is the mechanism proposed for the photochemical phase transition of NLCs in the guest/host systems. The photochemical phase transition of NLCs in the guest/host systems has been explored extensively, particular in terms of effects such as temperature of the sample, structure of guest molecules, concentration of the guest molecules, and the structure of host LCs on photochemical phase transition behavior.^[9-14]

12.2.2

Photochemical Phase Transitions in Guest/Polymer LC Systems

Polymer liquid crystals (PLCs) are high-performance materials that exhibit properties of both polymers and LCs. PLCs are currently regarded as a promising materials for information processing, due to their film-forming nature and the high birefringence observed in ultrathin films of PLCs.

The first example of PLC photoresponse was reported by Wendorff et al., as holographic recording in PLCs. They successfully produced holograms in LC copolymers

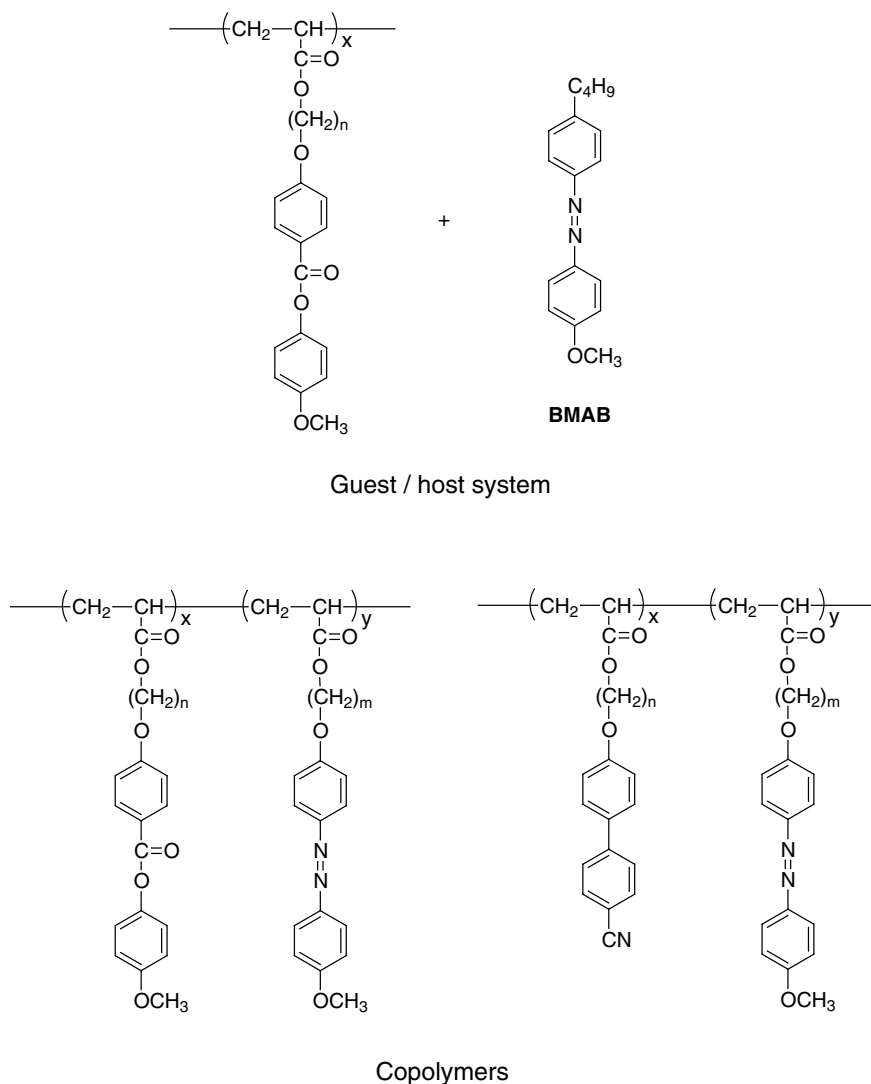


Fig. 1: Structure of polymer liquid crystals involved in photochemically induced phase transition.

containing azobenzene moieties, by means of irradiation with two coherent beams from an Ar^+ laser.^[15,16] The first report of photochemically induced phase transition in guest/PLC host systems was from the authors' group.^[17-19] In studies of the BMAB/PLC mixture shown in Figure 1, it was found that on photoirradiation to induce *trans-cis* isomerization of the guest BMAB molecule the system underwent $\text{N} \rightarrow \text{I}$ phase transition, as in photochromic guest/low-molecular-weight (LMW) LC systems. The dye-doped PLC systems were then extended to copolymer systems, on which detailed studies were performed (Figure 1).^[19-22]

Photochemical phase transition response time has been investigated in detail. The response time is one of the crucial factors in the manipulation of light waves by means of refractive index modulation by light-induced change in alignment of LCs. For use in information processing, fast response is essential. Response times were measured for N–I phase transitions in azobenzene/LMWLC systems.^[23,24] A thermostated sample composed of an azobenzene guest and an NLC host was placed between a pair of crossed polarizers and irradiated with a YAG laser third harmonic at 355 nm (10 ns fwhm) to bring about the *trans-cis* photoisomerization of the azobenzene guest molecules. Transmittance of a probe light at 633 nm from a He-Ne laser was measured as a function of time. In the azobenzene/LMWLC systems, the N–I phase transition, as verified by loss of birefringence of the LC sample, occurred in 100 ms.^[23] The response time for azobenzene/PLC systems was also examined and it was observed that the N–I phase transition took place in 50–200 ms in azobenzene-doped PLCs^[25] and copolymer LCs containing side chain azobenzene moieties.^[21]

12.3

Novel Approach to Alignment Change in LCs through Photochemical Processes

It is very difficult to obtain fast responses in guest/NLC host systems. As mentioned above, most photochromic reactions are very fast, occurring on a timescale of picoseconds. Therefore, if ultrafast lasers with a pulse width of picoseconds or nanoseconds are used as an excitation light source for the photochemical phase transition of guest/host systems, photochemical reactions of the guest molecules can be completed in picoseconds or nanoseconds, and the T_{NI} of the system can also be lowered below the irradiation temperature in these timescales. This means that, immediately after pulse irradiation, a nonequilibrium state appears which is thermodynamically isotropic in its equilibrium state in the phase diagram but shows birefringence due to nonrelaxation of mesogens. From this state, relaxation of mesogens takes place to their equilibrium state: an I state. Change in refractive index of samples depends on this relaxation process; the relaxation of mesogens is a rate-determining step in the modulation refractive index. LCs possess a high viscosity, so that relaxation of alignment of LCs takes a relatively long time.

To obtain fast LC photoresponse, a new guest/host system was developed, in which ferroelectric LCs (FLCs) were used as a host LC. FLCs exhibit spontaneous polarization (P_s) and show microsecond responses to change in applied electric field (flip of polarization) in a surface-stabilized state.^[26] If a flip of polarization of FLC molecules in the surface-stabilized state can be induced by light in the presence of an applied electric field, photoresponse in the microsecond time region might be achievable.

A mixture of an azobenzene derivative and an FLC (Figure 2), in which the concentration of the azobenzene guest was 3 mol%, was prepared in the surface-stabilized state in a very thin LC cell. Then the mixture was irradiated with light at 366 nm to cause *trans-cis* photoisomerization of the azobenzene guest molecule. It

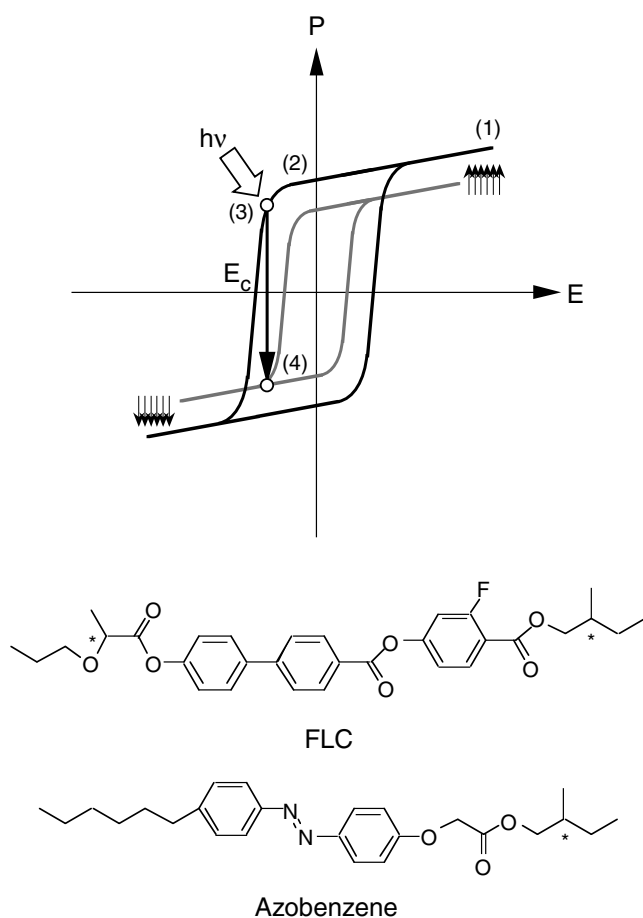


Fig. 2: Photochemical flip of polarization in ferroelectric liquid crystals.

was found that a threshold electric field for the polarization flip (coercive force) of FLC was changed on photoirradiation.^[27] FLC in the surface-stabilized state displayed hysteresis between applied electric field and polarization.^[26] It was observed that the hysteresis of the mixture with the azobenzene guest molecule in *trans* form was different from that of the mixture with the azobenzene in *cis* form. It has already been mentioned in Section 12.2.1 that, in the azobenzene guest/NLC mixtures, T_{NI} (*trans*) is different from T_{NI} (*cis*), and that this difference arises mainly from the molecular shape of the guest molecule. In azobenzene guest/FLC host systems, a change in the threshold value for the polarization flip between the *trans* azobenzene mixture and that with a *cis* azobenzene is also similarly interpreted in terms of change in the molecular shape of the guest molecule. When the azobenzene guest is in its *trans* form, the rod-shaped azobenzene molecules do not disorganize the phase structure of the chiral smectic C (SmC^*) phase of FLCs to any great extent, and the mixture shows an electric field threshold value for the polarization flip similar to that in the absence of guest molecule. However, when the azobenzene

is in its *cis* form, the phase structure of the SmC* phase is significantly disorganized on account of the bent shape of the guest molecules, and the threshold value for the flip of polarization is much reduced. On the basis of these experimental observations, a new mode of FLC photoresponse (*photochemical flip of polarization of FLC*) was proposed (Figure 2).^[27,28]

- (1) polarization of the FLC cell, containing a small population of azobenzene guest molecules, is aligned in one direction by an electric field;
- (2) an opposite electric field, sufficiently small as not to affect the initial direction of polarization, is applied across the FLC cell;
- (3) with this opposite electric field as a bias, the FLC cell is irradiated to cause *trans-cis* photoisomerization of the azobenzene guest molecule, changing the hysteresis of the cell;
- (4) the threshold value for the flip of polarization of the FLC cell is reduced on photoirradiation and becomes smaller than the bias voltage, which positively induces the flip of polarization of the FLC molecules.

In other words, the bias voltage remains unchanged before and after photoirradiation; however, the threshold value for the flip of polarization of FLC cell is reduced through the *trans-cis* photoisomerization of the guest molecules. As a result, a polarization flip is induced at irradiated sites, which leads to change in alignment of the FLC molecules (*photochemical flip of polarization of FLC*). FLC molecules in a surface-stabilized state show bistability of polarization in upward and downward directions with respect to the normal to the cell surface and hence two alignments of FLC molecules are stabilized. Furthermore, these two states remain unchanged even after the electric field is removed. Thanks to these properties of FLCs in the surface-stabilized state, once the polarization flip is induced on photoirradiation, the directions of polarization in the irradiated site and in the nonirradiated site are opposite, and the alignment of FLC molecules differs between the two sites. These changes in polarization and alignment of FLCs result in optical contrast between the irradiated and unirradiated sites, and they remain unchanged (memory effect). Time-resolved measurements of change in mesogen alignment due to polarization flip in the azobenzene guest/FLC host mixtures were performed on pulse irradiation. It was observed that the mixture composed of the azobenzene and FLC shown in Figure 2 displayed the polarization flip in 500 μ s on pulse irradiation with the YAG laser third harmonic (fwhm, 10 ns).^[27] This is the first example in which FLC polarization flip was induced by photochemical reactions.^[27] Since this first report, detailed studies have been performed on polarization flip in photochromic guest/FLC host systems: notably the effects of structure of FLC hosts,^[29,30] structures of photochromic guests,^[31] temperature,^[32] bias voltage,^[28] and change in P_s .^[32]

Photochemical polarization flip was immediately extended to antiferroelectric LCs (AFLCs), and it was found that in azobenzene guest/AFLC host systems, polarization flip could be induced photochemically and effectively, as shown in Figure 3.^[33] Novel photochromic molecules to induce polarization flip effectively have been explored, and molecular design on the basis of large P_s resulting from chiral cyclic carbonates has been found to be quite effective. An azobenzene dopant containing a

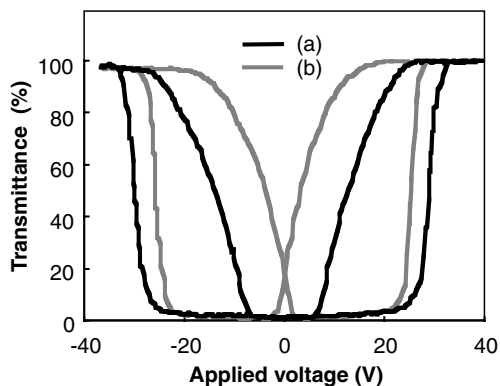
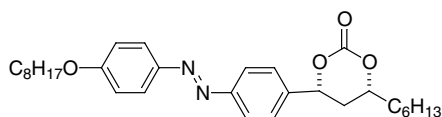
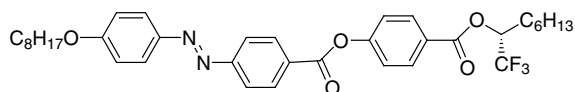
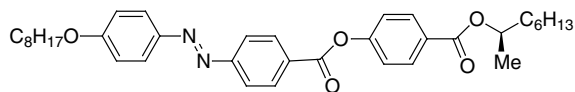


Fig. 3: Change in transmittance of an antiferroelectric liquid crystal containing an azobenzene: (a) in the dark; (b) under photoirradiation.

chiral cyclic carbonate was synthesized and used as a chiral dopant to induce the SmC* phase (Figure 4). In this system, the photosensitive azobenzene acts as a chiral dopant, which is essential if the dopant/host LC mixtures is to exhibit the SmC* phase, and therefore the change in molecular shape of the dopant is expected to affect the phase structure of the mixture significantly. It was observed that in this system the flip of polarization was induced in 90 μ s on pulse irradiation.^[34] Furthermore, a very interesting photoresponsive molecule has been developed, possessing both a photochromic nature and antiferroelectric properties (Figure 4). The photoresponsive property of this AFLC molecule has been extensively investigated.^[35] Polarization flip in AFLCs is very effective and reliable, and so devices based on this mechanism have been keenly explored.^[36]



Azobenzene dopant



Azobenzene antiferroelectric liquid crystal

Fig. 4: Structure of azobenzene dopant and azobenzene antiferroelectric liquid crystal.

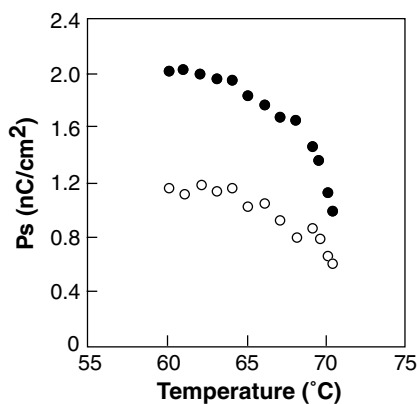
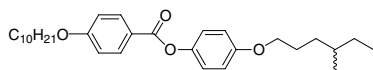
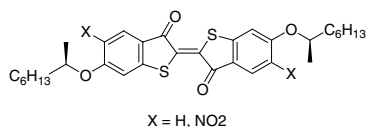


Fig. 5: Spontaneous polarization as a function of temperature: (●), *cis* isomer of thioindigo; (○), *trans* isomer of thioindigo

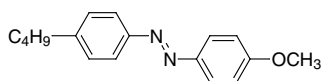


Thioindigo has two isomers, with parallel (*cis* form) and antiparallel (*trans* form) arrangements of the carbonyl groups attached to the α -carbons of the double bond; the two isomers exhibit distinct dipole moments. The *cis* form has a high dipole moment, due to the parallel arrangement of the carbonyl moiety, while in the *trans* isomer antiparallel dipole moments associated with the carbonyl moieties are canceled out, producing a very small overall dipole moment. Another feature of thioindigo as a photoresponsive molecule is its small change in molecular shape on isomerization. Thus, thioindigo derivatives are distinguished as a novel class of guest molecules in guest/FLC host systems, because they possess a “tunable dipole moment” characteristic independent of significant change in the molecular shape.^[37,38] Optical modulation of P_s of FLCs has so far been achieved by employing this unique feature of thioindigo. Photoirradiation (>505 nm) to cause *trans-cis* photoisomerization resulted in 1.5-fold enhancement of the P_s , due to the increase in dipole moment of the guest thioindigo molecules (Figure 5).

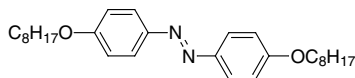
12.4

New Concept for Fast LC Response through the Agency of Photochemical Processes

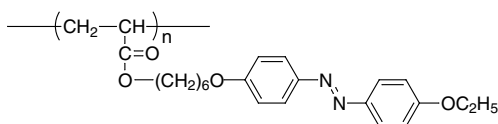
As described above, the temperature range in which to induce photochemical phase transition of NLCs in guest/host systems is limited. In the temperature ranges above the T_{NI} of *trans*-azobenzene/NLC mixtures and below the T_{NI} of *cis*-azoben-



BMAB
K 35 N 48 I



8AB8
K 99 N 113 I



PA6AB2
G 45 N 155 I
 $M_n = 9,100; M_w/M_n = 1.3$

Fig. 6: Structures of azobenzene liquid crystals.

zene/NLC mixtures, phase transitions cannot be induced even if *trans-cis* photoisomerization of guest molecules is effected. To make this temperature range for photochemical phase transition wider, a new system has been developed in which every mesogen is equipped with a photosensitive moiety. Through extensive studies on photochemical alignment change of LCs in guest/host systems, in which a large number of azobenzene derivatives have been used as guest molecules, it has been found that some azobenzene derivatives exhibit LC phase character. Put another way, the azobenzene moiety plays the roles both of a mesogen and of a photosensitive molecule (Figure 6). For instance, BMAB exhibits an N phase between 35 °C and 48 °C, and 4, 4'-dioctylazobenzene (8AB8) displays one around 100 °C. Furthermore, polyacrylate with side chain azobenzene moieties (PA6AB2 in Figure 6) shows a very stable N phase between 45 °C, the glass transition temperature (T_g) of this polymer, and 155 °C.

These azobenzene LCs display the liquid crystalline phase only when the azobenzene moiety is in the *trans* form, and no liquid crystalline phase at any temperature when the azobenzene moiety is in the *cis* form. In these azobenzene LC system, it was predicted that phase transition should be induced on essentially the same time-scale as the photochemical reaction of the photoresponsive moiety in each mesogen, if the photochemical reactions of a large number of mesogens were induced simultaneously by the use of a short laser pulse (Figure 7).^[39] On the basis of such a new concept, the photoresponse of azobenzene LCs with the laser pulse was examined, and it was found that the N to I phase transition was induced in 200 μ s.^[39,40] This fast response, on the microsecond timescale, had been demonstrated for the first time in NLCs. From the viewpoint of application of LCs to photonic devices, such a fast response is quite encouraging.

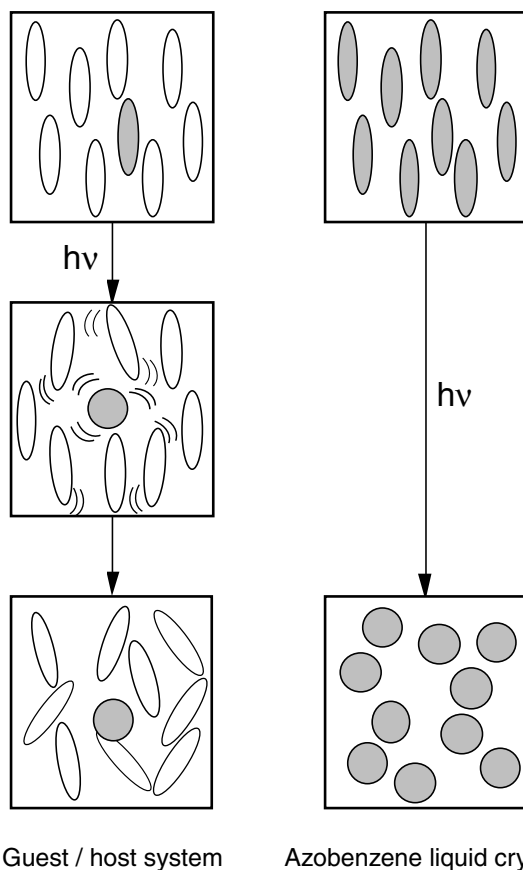


Fig. 7: Fast optical switching by means of azobenzene liquid crystals.

In general, the response time of PLCs is longer than that of LMWLCs, since in the PLCs, mobility of mesogens is highly restricted by the main chain of the polymer. In the photochemical phase transition behavior of azobenzene LCs, however, there is no response difference between polymer and LMW samples. It is worth mentioning that the polymer azobenzene LCs show a similar 200 μs response even below T_g .^[39,40] Figure 8 shows a typical result observed for PA6AB2. In the polymer azobenzene LCs, the photochemical phase transition can be induced in an extremely wide temperature range of over 150 $^{\circ}\text{C}$. This advantageous photonic material feature is specific to the azobenzene LCs, because in the guest/host systems the temperature range in which to induce photochemical phase transition is about 20 $^{\circ}\text{C}$. A relationship between the structure of polymer azobenzene LCs and their photochemical phase transition behavior has been explored extensively, to develop high-performance photonic materials. It was found that the structure of the polymer backbone, as well as the spacer of the side chain component, is a crucial factor for the photo-response of PLCs.^[41–44]

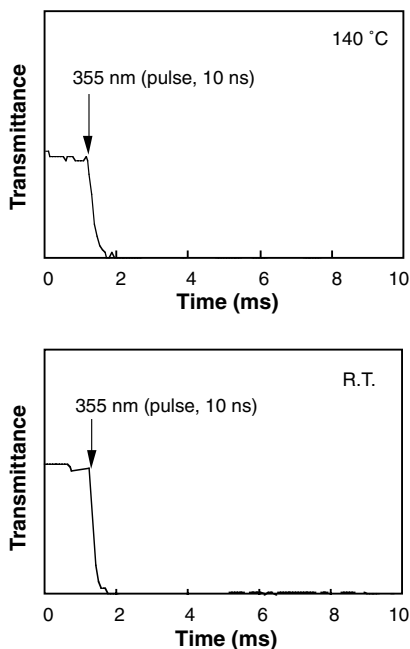


Fig. 8: Time-resolved measurements of the photochemical phase transition of the polymer azobenzene liquid crystal.

Since the photochemical phase transition is accompanied by a large change in refractive index, the polymer azobenzene LCs may be potential candidates for all-optical switching materials and dynamic holographic materials. In these applications, it is necessary to rapidly induce not only the N–I phase transition, but also the I–N phase transition (the recovery of the N phase). After photoirradiation of the polymer azobenzene LC film (N–I phase transition), once irradiation has ceased, the initial N phase can be restored thanks to thermal *cis-trans* back-isomerization, due to the thermal instability of *cis*-azobenzenes. With the goal of accelerating the thermal recovery of the LC phase, the mechanism of the I–N phase transition has been investigated in detail. The recovery is composed of two processes: thermal *cis-trans* back-isomerization of the azobenzene moieties and reorientation of the mesogenic *trans*-azobenzenes, and it was found that *cis-trans* back-isomerization is a rate-determining process.^[40] On the basis of the results of the kinetic studies on the I–N phase transition, polymer azobenzene LCs with both donor and acceptor moieties in a molecule, characterized by very fast *cis-trans* thermal back-isomerization, have been designed. With such donor-acceptor azobenzenes, a very fast recovery of the N phase (800 ms) was achieved (Figure 9).^[41] This response is faster than that of conventional azobenzene LCs by one order of magnitude.

As another approach to fast I–N phase transition, the optical switching behavior of LMW and polymer azobenzene LCs has been explored by means of reflection-mode analysis (Figure 10).^[45] On laser-pulse irradiation, it is possible to switch the

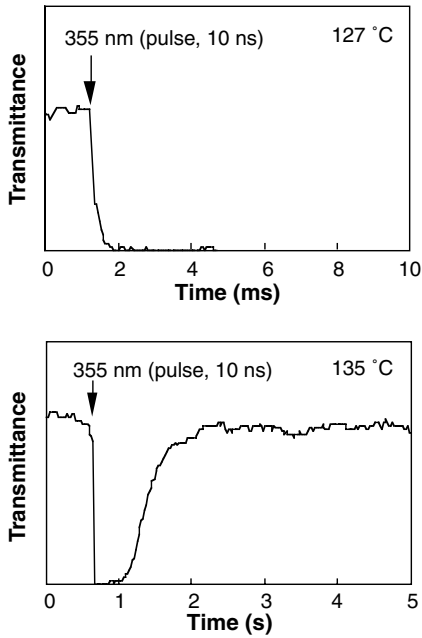


Fig. 9: Time-resolved measurements of the photochemical phase transition of the “push-pull” polymer azobenzene liquid crystal.

incident probe light reflected from the interface between the LC and the substrate, as a result of modulation of reflectivity arising from photoinduced change in the refractive index of the LC materials. In BMAB, the reflection-mode system gave a response time of 100 μ s, very similar to that observed in the usual transmission-mode analysis, and a decay time of 1 ms, which was significantly shorter than that obtained in the transmission-mode analysis (Figure 11).

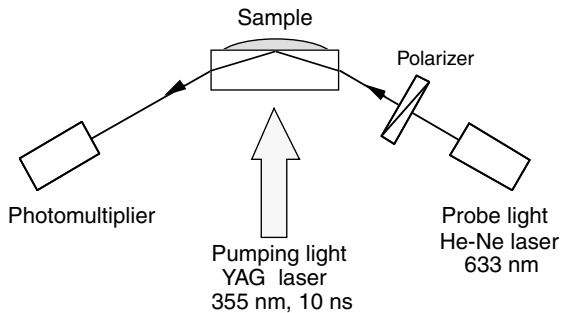


Fig. 10: Reflection-mode optical switching of azobenzene liquid crystals.

The molar extinction coefficients of the azobenzene moieties are very large (approximately 10^4) at 355 nm, and hence pumping light is absorbed entirely at the surface of the sample. Thus, *trans-cis* photoisomerization is also only induced near the surface, and so the N–I phase transition occurs solely in the surface region, leaving the bulk area intact as an N phase. In reflection-mode analysis, the probe light can only penetrate the surface area, so if molecules in the *cis* form produced at the surface by photoirradiation diffuse into the bulk phase, while simultaneously being replaced by molecules in the *trans* form from the bulk phase, recovery of the initial N phase can be achieved without involving the slow *cis-trans* back-isomerization process. Since the diffusion and the reorientation processes are much faster than the *cis-trans* back-isomerization process, optical switching in reflection-mode experiments has thus become much faster (Figure 11).^[46] Such reflection-mode analysis has another superior characteristic for optical switching. For the practical use of optical switching devices containing organic dyes as a key component, there is a very important prerequisite, which is stability. Optical switching in the ordinary transmission mode generally exhibits low fatigue resistance. With the aim of achieving highly fatigue-resistant optical switching, detailed optical switching behavior of azobenzene LCs was explored with the aid of reflection-mode analysis. The reflection-mode optical switching was found to be repeatable over 15,000 cycles, representing stability 10 times greater than that obtained with the transmission mode switching.^[47] This fact suggests that the optimization of this optical system for photoresponsive LCs may be an effective approach to producing more stable optical switching devices.

A unique feature of polymer azobenzene LCs as optical image storage materials has been demonstrated. In nematic glasses (solid state azobenzene LC films retaining an N

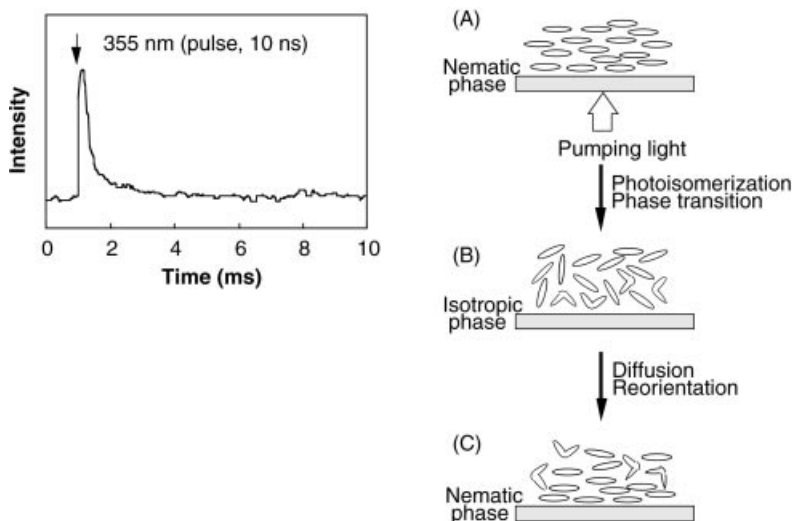


Fig. 11: Time-resolved measurements of reflection-mode optical switching and the possible mechanism.

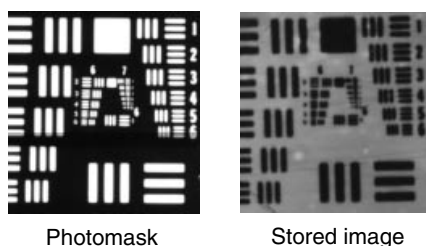


Fig. 12: Optical image storage in the polymer azobenzene liquid crystal.

phase structure below T_g), only the N–I phase transition can be induced and the I–N phase transition never occurs. Figure 12 shows photographs of a photomask and a binary test pattern recorded in azobenzene LC films by pulse irradiation at 355 nm.^[39,40] Pulse irradiation was performed at room temperature below T_g , and it was found that the irradiated site became isotropic as observed under exclusion of light by polarizing microscope. The stored optical image has been kept stable over two years. In the polymer films, it was observed that the thermal *cis-trans* back-isomerization took place in 24 h at room temperature. Although the *trans* form was recovered nearly completely, the isotropic glass induced at the irradiated site below T_g still remained unchanged at room temperature even after two years.^[40] These results imply that, below T_g , the orientation of the mesogenic *trans*-azobenzenes had become disordered through the process of thermal *cis-trans* back-isomerization. Even though the *trans* form was recovered thermally, orientation of the mesogens could scarcely be attained in the absence of segmental motion of the main chain of the polymer below T_g . Consequently, the polymer azobenzene LCs can be used as optical switching materials above T_g and as optical image storage materials below T_g .

In addition, more recently, an interesting approach to fast response of photoresponsive LCs has been reported. Crosslinked PLC networks containing azobenzene molecules were prepared by polymerization of ternary mixtures of monofunctional and difunctional LC monomers together with a LMW azobenzene LC, as shown in Figure

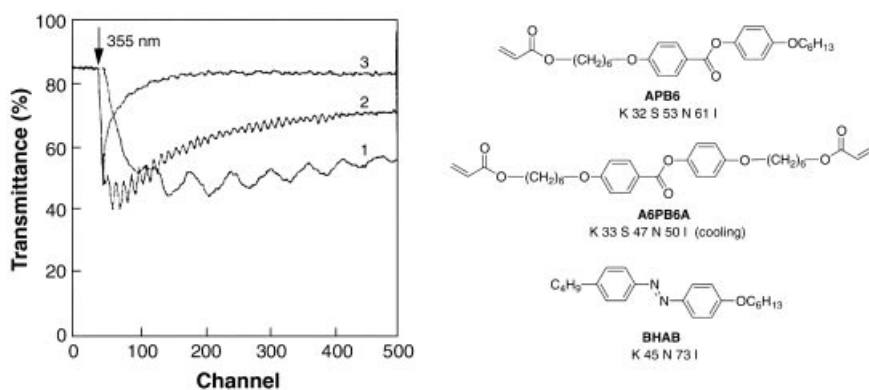


Fig. 13: Time-resolved measurements of changes in the transmittance of the crosslinked polymer network. 1: 10 ns/ch; 2: 50 ns/ch; 3: 1 μ s/ch.

13, and their photoresponsive behavior was evaluated by monitoring changes in the intensity of the probe light transmitted through a pair of crossed polarizers, with the sample film showing birefringence between them, on pulse irradiation at 355 nm.^[48] As can be seen in Figure 13, the response time and the decay time were 1 μ s and 100 μ s, respectively. This very fast response seems to be attributable to the suppression of motion of the mesogenic groups by crosslinking. Indeed, non-crosslinked PLC analogs showed no such fast response. From intensive studies, it has been concluded that the stabilization of an initial ordered state by crosslinking results in a fast order-disorder transition, induced by slight changes in the orientational order of mesogens, and a fast disorder-order transition, due to relaxation of the strain generated on irradiation by the photoisomerization of the azobenzene molecules.

12.5

Photochemical Control of LC Alignment by Linearly Polarized Light

The nature of light may be simply represented as electromagnetic waves with oscillating electric dipoles. The key idea in understanding the interaction of light with molecules is that electrons may be set into motion by the oscillating electric field of the light. The major force operating on the electrons of a molecule as a consequence of a passing light wave is that due to the undulating electric field. Light absorption to give excited molecules is subject to exclusive preconditions, including the coincidence of the electric field vector of light with the direction of a transition moment of the corresponding ground state chromophores.

In the case of the *trans*-azobenzene moiety, light is absorbed when the electric field vector of radiation is not perpendicular to the transition moment of the azobenzene moiety. The *trans* form possesses π - π^* transition moments approximately parallel to the molecular long axis. Light is considered to be "linearly polarized" when it contains waves that only fluctuate in one specific plane. Thus, it can be concluded that the *trans*-azobenzene moieties exhibit angular-dependent absorption (photoselection) of linearly polarized light. *Trans*-azobenzene molecules with their transition moment parallel to the polarization direction of light are activated to undergo *trans-cis* isomerization, while molecules with their transition moment perpendicular to the polarization direction are inactive towards isomerization. After each isomerization cycle, the azobenzene moieties may have different orientations, because the *trans* and *cis* isomers have different molecular shapes and the isomerization causes a perturbation on the molecular environment. Once, after repetition of the *trans-cis-trans* isomerization cycles, the azobenzene moieties have fallen perpendicular to the polarization direction of the irradiation light, they become inactive. At the end of the multicycles, there will be a net population of azobenzene groups aligned in the direction perpendicular to the light polarization. Taking advantage of this photoselection of azobenzene moieties, the possibility of using a polymer system containing azobenzene molecules as an optical recording medium was first advanced in 1983, with azo dyes (methyl red and methyl orange) dispersed in a polymer matrix (poly(vinyl alcohol)).^[49] When the polymer system was irradiated with a linearly polarized

laser beam at 488 nm (close to the absorption maximum of the moiety), the optical transmittance for light polarized along the polarization direction of the writing light increased and that for light perpendicular to the direction of the writing light decreased. Optical dichroism, therefore, had been induced because of the anisotropic rearrangement of *trans*-azobenzenes. However, this report has shown that the induced anisotropy can only be maintained for a short time, even in the dark. This shortcoming was overcome by Natansohn and co-workers, who developed amorphous azobenzene polymers, and also by other groups.^[50–54] By attaching the azobenzene moieties to polymer backbones through covalent bonds, stable birefringence was achieved in the amorphous polymers at ambient temperatures below T_g . The induced alignment can be erased thermally and photochemically and reinduced by irradiation with linearly polarized light.

Since these reports concerning non-LC systems, photoinduction of molecular alignment has been extended to copolymer LC systems possessing both mesogens and azobenzene moieties in the side chains. Several studies on photoinduced reorientation behavior showed that non-photoactive mesogens were able to undergo reorientation concomitantly with azobenzene moieties above T_g . This was explained in terms of cooperative motion of adjacent groups, due to the similar shapes of the rigid structures. On the other hand, different arguments were presented concerning reorientation behavior below T_g . Anderle et al. reported that only reorientation of azobenzene moieties was induced below T_g and the orientational direction of the mesogens was unchanged.^[55] Wiesner et al.,^[56] in contrast, observed cooperative motion of mesogens resulting from the reorientation of azobenzene moieties even below T_g . Recent works on the photoinduced alignment behavior of side chain PLCs have revealed that dipole-dipole interaction affecting cooperative motion is a more important effect in the reorientation process.^[54]

Through evaluation of the photoinduced alignment properties of a variety of PLCs with azobenzene moieties in their side chains, the important factors for the reorientation process were found to be: azobenzene content,^[57] enthalpy change during the phase transition,^[58] morphology of the sample before irradiation,^[59,60] intensity of linearly polarized light as an incident light,^[61] spacer length of the side chain,^[62] and so on. On the other hand, structural effects of azobenzene moieties on photoinduced alignment behavior were investigated systematically for a series of side chain PLCs containing different azobenzene moieties, and interesting results were obtained (Figure 14).^[63–65] With increasing strength of donor and acceptor at the 4- and 4'-positions of the azobenzene groups, the possibility of alignment change in PLCs possessing the same methacrylate backbone decreased, due to the slightly increased enthalpic stability of the mesophase and the significantly reduced concentration of *cis*-azobenzene (*i.e.*, an increased *cis-trans* isomerization rate). However, high alignment efficiency was observed in ACB-ABA6, a polyacrylate with strong donor-acceptor pairs in the azobenzene moiety and exhibiting low mesophase stability, since both the rate of *cis-trans* isomerization and the mobility of mesogens are favorable for alignment change. These results demonstrate that the photoalignment behavior can be regulated by appropriate choice of azobenzene unit or polymer backbone.

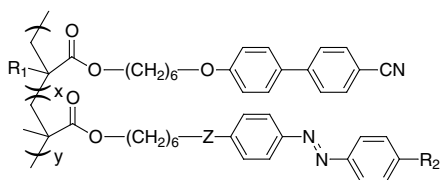


Fig. 14: Polymer liquid crystals containing various azobenzene moieties.

polymer	R ₁	Z	R ₂	x : y
MACB-AB6	CH ₃	O	C ₂ H ₅	94 : 6
MACB-CNAB6	CH ₃	O	CN	93 : 7
MACB-NAB6	CH ₃	O	NO ₂	93 : 7
MACB-ABA6	CH ₃	N-CH ₃	NO ₂	95 : 5
ACB-ABA6	H	N-CH ₃	NO ₂	95 : 5

The azobenzene-containing polymer systems described above are capable of controlling alignment direction in a two-dimensional fashion, by changing the direction of polarization of the irradiation light. During the in-plane alignment process, photoinduced biaxiality of azobenzene moieties was observed in liquid-crystalline and amorphous polymer films, and also in Langmuir–Blodgett films.^[50,66–68] This phenomenon was interpreted in terms of the realignment of the azobenzene moi-

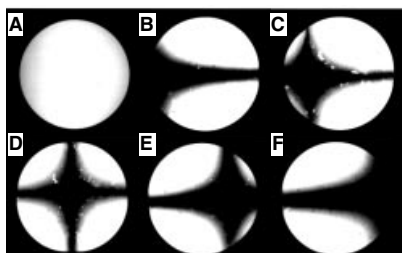
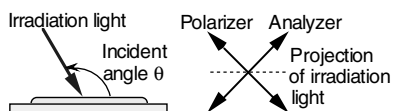
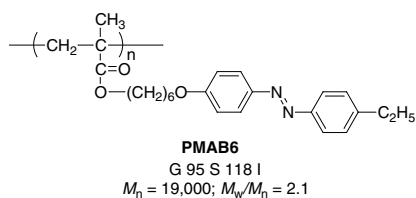


Fig. 15: Conoscopic observation of the alignment of azobenzene mesogens as a function of change in incident angle. From A to F: before irradiation, after irradiation at incident angles of 30°, 60°, 90°, 120°, and 150°, respectively.

eties along the propagation direction of the irradiating light; in other words, the existence of out-of-plane alignment was demonstrated.^[50] When the azobenzene moieties are aligned with the molecular long axis along the propagation direction of the irradiating light, photoisomerization hardly takes place, since the propagation direction of light is always perpendicular to its electric field vector. In the case of unpolarized light, only the propagation direction is, in principle, perpendicular to the electric field vector of the unpolarized light. Thus, when unpolarized light is used, it is expected that the azobenzene moieties become aligned only in the propagation direction of the irradiating light. In fact, several studies have been reported on out-of-plane alignment behavior on using unpolarized light.^[69–72] Recently, an attractive result was found in a polymer azobenzene LC, in which, by changing the incident direction of the irradiation light, it was possible to bring about effective three-dimensional manipulation of PLCs at room temperature, about 70 degrees below the T_g of the polymer (Figure 15).^[73,74] This result is expected to open a new dimension for high-density data storage, since information can be stored as a change in the three-dimensional alignment direction of the azobenzene moieties. The stored information may be read nondestructively with light outside the absorption band of the azobenzene moieties, as the difference in transmittance.

12.6

Manipulation of LC Alignment through Photoactive Surface Layers

Control over the alignment of LCs is important for their optical and optoelectrical applications, such as in LCDs and LC spatial light modulators (LC-SLM), and homogeneous LC alignment is conventionally achieved by mechanical rubbing of a polymer alignment layer coated on the substrates. Should it be possible to change chemical and/or physical properties of the surface layer of a substrate through an external field, LC alignment might be controllable through changes in the surface property of substrates. Recently, control of LC alignment by light has been a hot

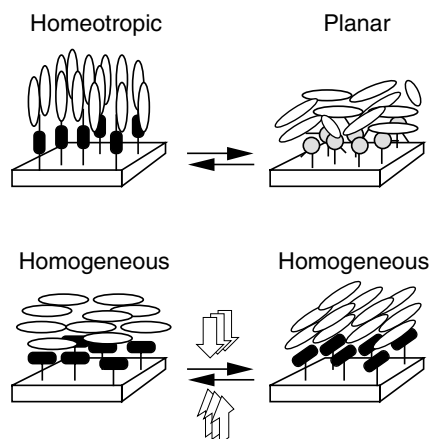


Fig. 16: Photoalignment by "Command Surface".

topic. Ichimura and co-workers employed azobenzene monolayers, formed on glass substrates by silane coupling agents, and demonstrated the possibility of photoalignment LCs by exploitation of photoactive surface layers. This basic concept of the photoalignment technique is illustrated in Figure 16. In the cell filled with an NLC constructed out of the surface-treated substrates, the NLC molecules display a homeotropic alignment when the azobenzene immobilized on the substrates is the *trans* form. Photoirradiation to induce *trans-cis* isomerization of the azobenzene moieties enables repeatable changes of alignment from homeotropic to planar forms to be performed. Such photoactive surface layers are called “command surfaces”.^[75] A similar photoalignment of LCs has also been reported for polymer films containing azobenzene moieties, and the effects of structure and density of azobenzene molecules on the photoalignment behavior have been explored systematically.^[76,77]

A closely related phenomenon induced by linearly polarized light was found independently by Gibbons et al., who employed a polyimide (PI) film doped with azobenzene molecules as a dichroic dye and showed that the direction of homogeneous

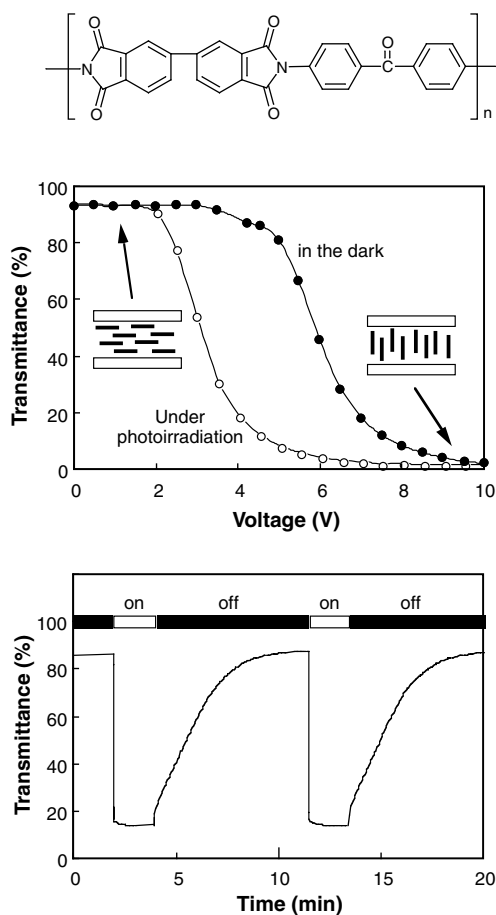


Fig. 17: T-V profile for 5CB with the photosensitive PI as an alignment layer, and optical switching behavior.

alignment of LC molecules can be established and altered using polarized light.^[78] An NLC cell fabricated from a substrate coated with a dye/PI mixture and a substrate coated only with PI, with the rubbing directions of both substrates mutually parallel, was exposed to linearly polarized light of polarization parallel to the rubbing direction. It was found that LC molecules at the irradiated dye-doped surface became aligned perpendicular to the polarization of the light, whereas those at the undoped PI surface remained parallel to the rubbing direction, resulting in a twisted nematic structure in the irradiated region. The photoinduced alignment could subsequently be erased or rewritten by altering the polarization of the light. Furthermore, unidirectional alignment of LCs has been also achieved with a variety of materials with photoactive surfaces, such as poly(vinyl alcohol) thin films containing a hydrophilic azo dye,^[79] glass substrate modified by azobenzene monolayers (Figure 16),^[80] polymer azobenzene films,^[72,81] and polyvinyl cinnamate with photodimerization properties.^[82] Such photoalignment techniques using linearly polarized light are more favorable from the viewpoint of improvement of the performance of existing LC devices and development of novel LC devices with new functions, because the photoalignment process is free from dust particles and static surface charges generated in the conventional rubbing process.

A unique LC alignment technique based on a novel principle is represented by dynamic and static control of LCs by means of photoresponsive PIs as an alignment layer. The most significant characteristic of this system is the non-utilization of photochemical reactions as a trigger to control alignment of LCs. Optical switching of NLCs with a photosensitive PI containing benzophenone moieties as an alignment layer has been reported (Figure 17).^[83] LC cells with a gap of 5 μm , in which substrates were coated with PI films and then rubbed, were fabricated to evaluate the optical response of 5CB. Figure 17 shows the change in the transmittance as a function of applied voltage for the sample cell.

It is clear that the threshold voltages, at which change in the LC alignment takes place, are quite different in the irradiated and unirradiated states. When a bias voltage of 4.5 V was applied across the cell, it was found that photoirradiation at 366 nm resulted in an immediate change in transmittance (Figure 17). Since the transmittance recovered when photoirradiation ceased, it was assumed that the optical switching observed is based on an alignment change between a homogeneous state and a homeotropic one. Although the switching mechanism is not well understood at this stage, formation of intra- or intermolecular charge transfer complexes in the surface area of PI films as a result of photoirradiation (*i.e.*, a change in the polarity) seems to participate in the optical switching. Furthermore, these photoresponsive PI films have been also applied to photoalignment (nonrubbing alignment) techniques for LC devices. As early as 1995, Hasegawa and co-workers achieved homogeneous alignment of NLCs by anisotropic photodegradation of PIs exposed to linearly polarized UV light of short wavelength (254, 257, or 313 nm).^[84] However, this method was accompanied by chemical reaction, resulting in deterioration of the thermal stability of PIs due to serious degradation of backbone structure. Recently, aromatic PIs exposed to linearly polarized UV light of long wavelength (366 nm) were reported to show high photoalignment efficiency without significant change in

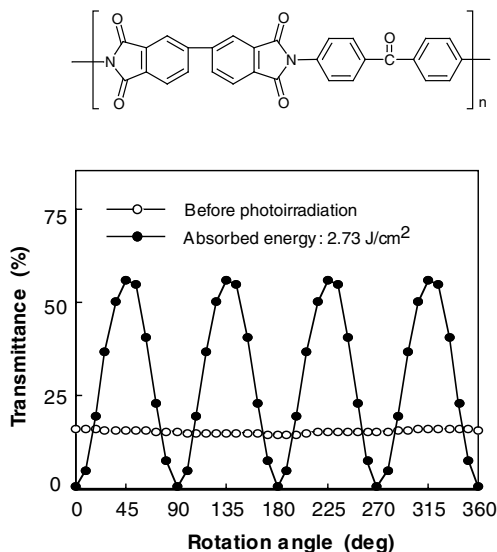


Fig. 18: Alignment behavior of 5CB by means of PI film exposed to linearly polarized UV light.

the chemical structure of the PIs.^[85–87] To evaluate alignment ability, a PI film formed on the glass substrate was irradiated with linearly polarized light at 366 nm, an LC cell with a gap of 5 μm was assembled with two pieces of the exposed PI-coated substrates, and then the cell was filled with 5CB. As can be seen in Figure 18, the transmittance of probe light through crossed polarizers, with the unexposed cell between them, displays no distinct angular dependence. With the exposed cell, in contrast, transmittance maxima and minima appear regularly at every 90° interval. It is obvious that unidirectional homogeneous alignment of 5CB is successfully induced with the photoresponsive PI film. The degree of uniformity of LC alignment is strongly affected by the structure of PIs and it has been demonstrated that an aromatic PI with a diphenyl ether diamine unit is a more favorable photoalignment film in terms of photosensitivity and chemical stability.

12.7

Modulation of Light Waves in Polymer/LC Composite Films

The photoresponsive LC systems presented in the previous section enjoy a dominant position in control of light by light; however, loss of optical efficiency in the LC devices is unavoidable due to the use of a pair of crossed polarizers. This problem can be overcome by modifying the morphology of materials. Polymer/LC composite films, consisting of a polymer matrix and an LC component, can be converted from a light-scattering state to a transparent state by application of an external electric field. They remove the need for polarizers with LC devices and possess high processability and flexibility because of the absence of substrates coated with an alignment

layer, so that these polymer/LC composite films are now at a stage of practical utility.^[88,89]

Although such polymer/LC composite films are usually prepared by emulsification and phase separation techniques, the resulting composites have a variety of morphological characteristics arising from differences in conditions and compositions during sample preparation. The polymer/LC composite films are mainly classified into four types:

- nematic curvilinear aligned phase (NCAP) material, with an encapsulated LC structure,^[90,91]
- polymer-dispersed liquid crystal (PDLC) material, with LC droplets dispersed in a polymer matrix by means of polymerization-induced or solvent-induced phase separation,^[92,93]
- polymer network liquid crystal (PNLC) material, with micrometer scale LC domains,^[94] and
- polymer-stabilized liquid crystal (PSLC) material, with a small amount of polymer network.^[95]

Currently, to develop more highly functionalized LC devices, intensive studies are being carried out on electrically controllable polymer/LC composite films with such advantageous features as high electric field response, high contrast, and wide viewing angle, as well as reverse-mode and haze-free characteristics.^[96–100]

With respect to photonic application of the polymer/LC composite films, a projection light valve has been reported by Takizawa et al.^[101] This is an SLM, the function of which is to display large images on a screen by projecting an image created on a small valve. It is illustrated schematically in Figure 19. The PDLC-SLM consists mainly of two components: one is a PDLC layer, which modulates the probe light, and the other is a photoconductive layer ($\text{Bi}_{12}\text{SiO}_{20}$), which detects the stimulus light. In the initial state, some voltage as bias is applied to the two layers. Upon irradiation by the stimulus light, the resistance of the photoconductive layer decreases. The voltage, therefore, becomes centered mainly on the PDLC layer. The increase in the voltage across the PDLC layer brings about unidirectional alignment of LC droplets. Consequently, the probe light reflected by the dielectric mirror can be modulated according to the transformation between light-scattering state and

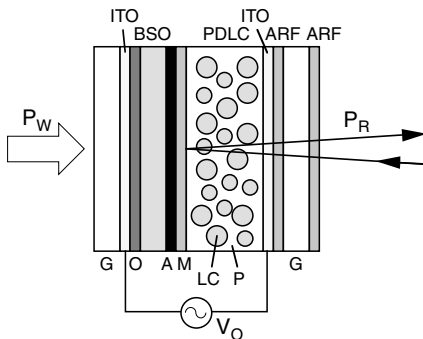


Fig. 19: PDLC-SLM. LC: liquid crystal droplet; M: dielectric mirror; A: light absorption layer; BSO: photoconductive layer; O: optical cement; PW: writing beam; PR: reading beam.

transparent state in the PDLC layer. A high contrast ratio of 178 : 1, a response time of 14 ms, and a decay time of 15 ms have been achieved.

Light addressing and optical image recording by means of polymer/LC composite films displaying electric field frequency-dependent optical properties have been reported by Kajiyama et al.^[102] A composite film consisting of a side chain PLC with a polysiloxane backbone and LMWLCs, shown in Figure 20, displays remarkable light scattering characteristics on application of a low frequency electric field, while becoming highly transparent on application of a high frequency electric field. This composite system is inactive towards light as a stimulus, because the LC component used has no photoresponsive character in itself. An azobenzene derivative was added to the composite film as a photoresponsive molecule. The threshold frequency, defined as the critical frequency at which the composite films change from a transparent state to a turbid one, was demonstrated to be alterable using light irradiation as an external stimulus. The threshold frequency in the composites containing the *trans*-azobenzene, f_c , was smaller than that in the composites with *cis*-azobenzene, f_{cs} (Figure 20). The transmittance of the composites can be therefore switched by stimulation in the presence of an electric field with frequency of f_d , situated between f_c and f_{cs} as shown in Figure 20. Since both the transparent and the turbid states of the composite films are memorized stably even after removal of electric fields, they can be applied to rewritable optical image recording media. In addition, a similar phenomenon can be induced by laser irradiation, resulting in the formation of both positive and negative images from a thermal process.^[103]

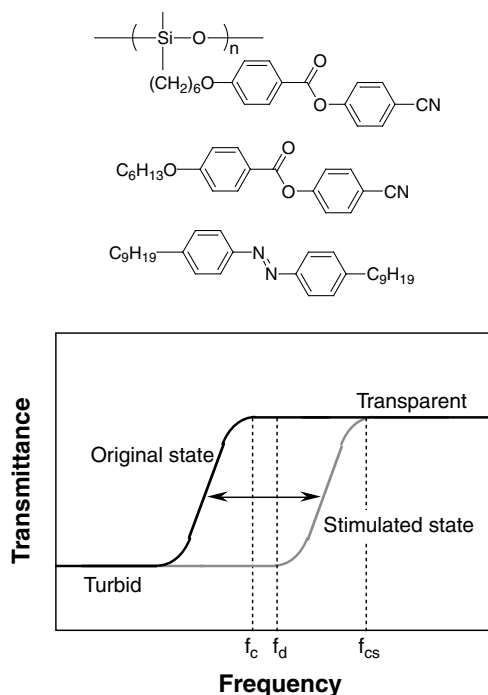


Fig. 20: Frequency dependence of transmittance of the composite film.

All-optically controllable polymer/LC composite films, driven by photon mode processes in the absence of electric fields, have been achieved by means of photochemical phase transitions. Kawanishi et al. prepared polymer/LC composite films with a thickness of 2–3 μm from a mixture of NLC and azobenzene derivatives dispersed in an aqueous solution of poly(vinyl alcohol), using the solvent-induced phase separation technique.^[104] Although the composite films showed very low transmittance because of the opacity of the composite film, they became transparent on irradiation at 366 nm, as a result of the N–I phase transition in the LC droplets in the polymer matrix, caused by *trans-cis* photoisomerization of the azobenzene molecules. The recovery of the initial opaque state could be achieved by irradiation using visible light, causing *cis-trans* back-isomerization of the azobenzenes. In this system, the degree of change in transmittance was as low as 10–50 %. With the aim of constructing novel photoresponsive polymer/LC composite systems possessing superior optical properties, a ternary mixture of bifunctional acrylate monomers, NLCs, and azobenzene compounds was polymerized in a 10 μm gap cell under a variety of conditions, and optical properties of the resulting polymer networks were appraised systematically.^[105,106] It was found that the transmittance of these composites can be modulated throughout the range from approximately 0 % to 100 % on photoirradiation to induce photochemical phase transition (Figure 21). Furthermore, by choosing network-forming materials and by tuning polymerization conditions, optical image storage and reverse-mode switching could be also achieved.^[107,108]

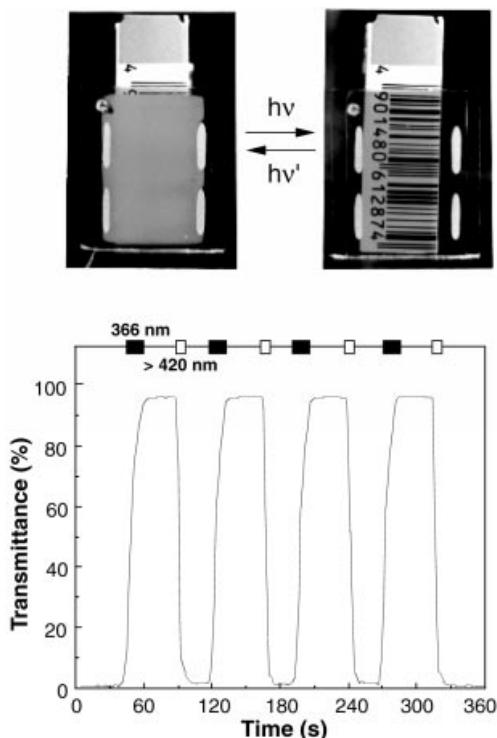


Fig. 21: Reversible change in transmittance of the composite film.

A second harmonic generation (SHG) property also exists as a nonlinear optical effect as a unique feature of polymer/LC composite films. For this SHG, the key requirement is the presence of a noncentrosymmetric (polar) environment. In these molecule-based systems, materials can possess the SHG activity only when the noncentrosymmetric molecules are incorporated into a noncentrosymmetric macroscopic structure. Achievement of such a macroscopic ordering (*i.e.*, dipolar alignment), however, is a formidable task, since the permanent electric dipoles of noncentrosymmetric molecules tend to pair in opposite directions to give rise to a centrosymmetric macroscopic structure. Although an NLC molecule itself usually possesses dipole moments parallel to the molecular long axis, due to its noncentrosymmetric molecular shape, no SHG can be observed in the N phases because of cancellation of the dipolar vectors. The surfaces and interfaces of substances invariably show a noncentrosymmetric nature, however. This implies that the SHG is generated from the surfaces or interfacial regions of substances. In polymer/LC composite films, numerous interfaces are present, since micrometer-sized LC droplets are dispersed in a polymer matrix. Through this structural characteristic, LCs lend themselves to wavelength-controllable materials. Several studies have to date been carried out on the SHG behavior of these composite films.^[109,110]

12.8

Holography as a Future Technology in Photonics

12.8.1

Distinct Image-recording and Image-displaying Techniques

Holography is an image-recording process essentially different from other processes: both the phase and the amplitude of the light wave that intercepts the recording medium are recorded. Holography's most attractive feature is that it can record and display a complete three-dimensional image of an object. In holography, the phase and amplitude of light waves are modulated through periodic alternation of various physical properties of the medium. Therefore, holography can be regarded as a photonic application. Amplitude can be recorded by any of numerous photosensitive materials; many of these materials, however, are insensitive to phase differences between various parts of the wave front. In 1948, to overcome this, Gabor introduced the use of a background wave, generally referred to as the reference beam.^[111] Interference between the reference beam and the object beam (the wave front reflected by the object, the image of which is to be recorded) converts phase differences into amplitude differences, which can be recorded by photosensitive materials. Gabor coined the name "holography", meaning the "whole record", for this technique because it contains all the information necessary to reconstruct the object beam. The hologram can be "played back" by illumination with a beam of coherent light identical to the reference beam (*i.e.*, readout beam). On passing through the hologram, this beam acquires the phase and amplitude modulations of the object beam, reconstructing the wave front that originally came from the object,

the image of which was recorded. For holography, a coherent light source is the prerequisite optical component. Laser, which was developed as early as around 1960, is now readily available as a coherent light source. Thanks to progress in laser technology, the greatest attention is being focused on the holographic process, since the information packing density can be considerably increased by exploiting its unique storage techniques in the form of interference patterns. Therefore, holography is viewed as the most promising candidate for storage of high-density information, as well as for recording three-dimensional objects. Moreover, holographic storage permits information to be written and read simultaneously as parallel processes, resulting in an extremely high transmission rate.

Holograms are mainly classified into two types, according to the manner of recording of the interference pattern.^[112,113] The first is an amplitude-type hologram. The interference pattern is recorded as a density variation in the recording medium, and thus the amplitude of the illuminating wave is modulated. The other is a phase-type hologram. The fringe pattern is recorded as a change in thickness or refractive index, and accordingly the phase of the illuminating wave is modulated. In terms of diffraction efficiency, it is well known that the theoretically calculated diffraction efficiency of phase-type holograms is always higher than that of amplitude-type holograms. Therefore, most studies on holography involve phase-type holograms.

In early stages of research into holography, silver halide emulsions and dichromated gelatin were widely used as a holographic materials. These materials, however, have certain drawbacks, such as the need for wet-process post-treatment, low exposure sensitivity, and high-grain noise in the holograms. Organic materials, especially polymer materials, for holographic recording have been under investigation for many years, thanks to their ease of molecular design and good mechanical properties in comparison with inorganic materials.^[113] Recent trends in holographic recording materials include photorefractive materials,^[114–118] thermoplastics,^[119–121] photochromic compounds,^[122–134] and ordinary photopolymers.^[135–140] All of these materials can be used in phase-type holography, and all possess some advantages, but also some limitations. For instance, photorefractive materials are erasable and have unique nonlinear optical properties, but have only moderate diffraction efficiency and relatively low stability of stored information. Thermoplastics have relatively high exposure sensitivity and are erasable, but have only moderate diffraction efficiency and high scattering noise. Photochromic compounds, meanwhile, have high resolution and high exposure sensitivity and are erasable, but have relatively low diffraction efficiency, while, finally, photopolymers have excellent diffraction efficiency and noise properties, but are not erasable and require post-treatment. For holographic recording, therefore, it is preferable that materials should simultaneously possess a number of specific characteristics, such as high diffraction efficiency, high spatial resolution, and high S/N ratio. To construct phase-type holograms with high diffraction efficiency, large modulation either of refractive index or of thickness of recording materials is required. In application of the holographic technique to active recording devices, holograms should be erasable and rewritable. Furthermore, for dynamic holography, with which it would be possible to recon-

struct 3-D moving objects, rapid response in the processes both of formation and of wiping of the holograms would be needed in the materials.

12.8.2

LC Materials in Holography

As described above, LC materials possess large optical anisotropies, resulting from self-assembly characteristics, and offer additional features such as an ability to respond to applied external fields. These features are quite favorable from the perspective of producing rewritable phase-type holograms, as well as that of achieving dynamic holography. In the past decade, with the goal of 2-D or 3-D image-recording, many extensive studies have been performed on holographic gratings based on modulation of refractive index, using LC materials that are variously LMWLCs,^[78,141–158] PDLCs,^[159–167] and PLCs.^[15,16,168–180] The holographic gratings are essentially formed by means of photorefractive effects or photochromism. In gratings based on photorefractive effects, Khoo et al. have obtained high diffraction efficiencies of 30 % at low writing beam intensities of 40 $\mu\text{W}/\text{cm}^2$ in LMWLC systems.^[152] Ono and Kawatsuki have also shown that the periodic modulation of LC alignment induced by the spatial charge distribution can result in relatively large changes in refractive index ($\Delta n = 3.6 \times 10^{-3}$) in LMWLC cells coated with photoconductive layers.^[153] Furthermore, photorefractive rise times as short as 40 ms were obtained in LMWLCs containing donor and acceptor molecules in which photoinduced electron transfer reactions occur effectively,^[146] and photorefractive grating memory effects were observed in PDLCs.^[160]

On the other hand, photochromism-based grating formation has been achieved in LC materials containing azobenzene derivatives as a photochromic elements. It is expected that such systems should enable dynamic and/or effective control of grating formation, as the photoisomerization of azobenzene molecules produces very fast changes in alignment of LCs, resulting in large changes in refractive index, as mentioned above. In fact, dynamic holography has been achieved using dye-doped NLCs.^[141,142] Although the grating formation is largely due to the realignment of LCs in the bright region in interference patterns, changes in refractive index arising from N–I phase transitions also seem to participate in the grating formation.^[141] In LMWLCs, however, it is often difficult to obtain a holographic grating displaying narrow fringe spacing (*i.e.*, high resolution) and high stability, because of the high mobility of LC molecules. It is easy to imagine that side chain PLCs may be one of the most promising materials in holography, because they possess not only high viscosity, due to their polymeric structure, but also superior LC properties, in which flexible side chain spacers play a crucial role in decoupling the motion of the polymer backbone from that of the aligned mesogens. Wendorff et al. have shown for the first time that a holographic recording can be built into PLCs containing azobenzene moieties in the side chain as discussed above.^[15,16,168–170] This holographic image storage appears to originate from periodically photoinduced LC alignment by linearly polarized writing beams.

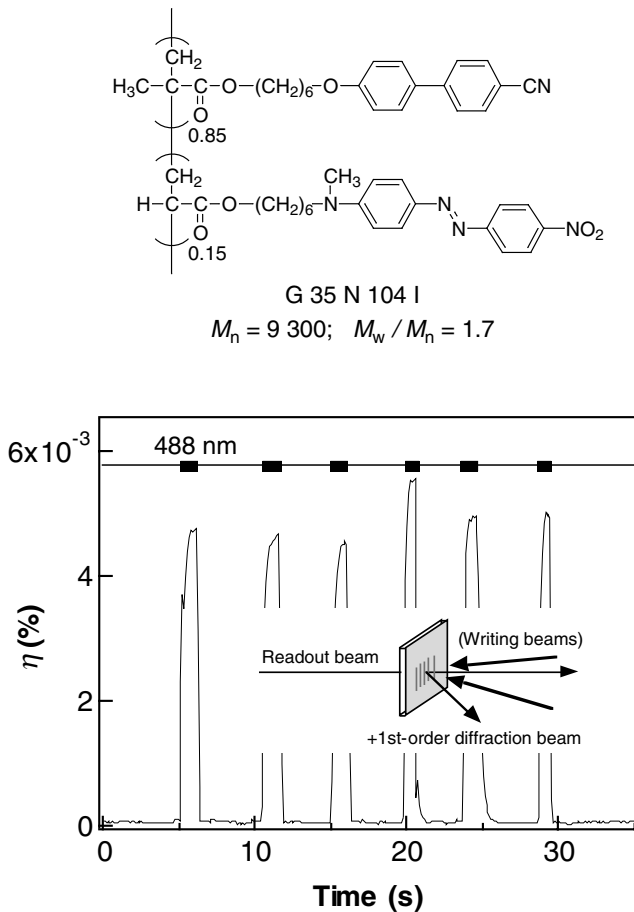


Fig. 22: Switching behavior of the diffraction beam on turning on and off the writing beams.

Recently, formation of phase-type holograms by means of photochemical phase transition has been attempted in side chain PLCs containing azobenzene moieties at various temperatures at which sample films display LC phases or solid states retaining an LC structure.^[181–185] A typical result with dynamic gratings is shown in Figure 22.^[181,182] The holographic diffraction in the N phase was observed repeatedly by turning on and off the writing beams. In this system, the formation and disappearance of the grating, exhibiting a narrow fringe spacing of $1.4\ \mu\text{m}$, were achieved within about 150 ms and 190 ms, respectively. It is worth mentioning that the magnitude of refractive index modulation reached the order of 10^{-2} . Phase-type gratings based on photochemical phase transitions have been also obtained in glassy ordered films.^[184,185] A sinusoidal variation of the thickness of the films (surface-relief structure) was confirmed to be generated through irradiation by two interfering beams: results similar to those obtained in azobenzene-containing amorphous polymers and reported by Natansohn et al.^[126–128] The gratings recorded in the

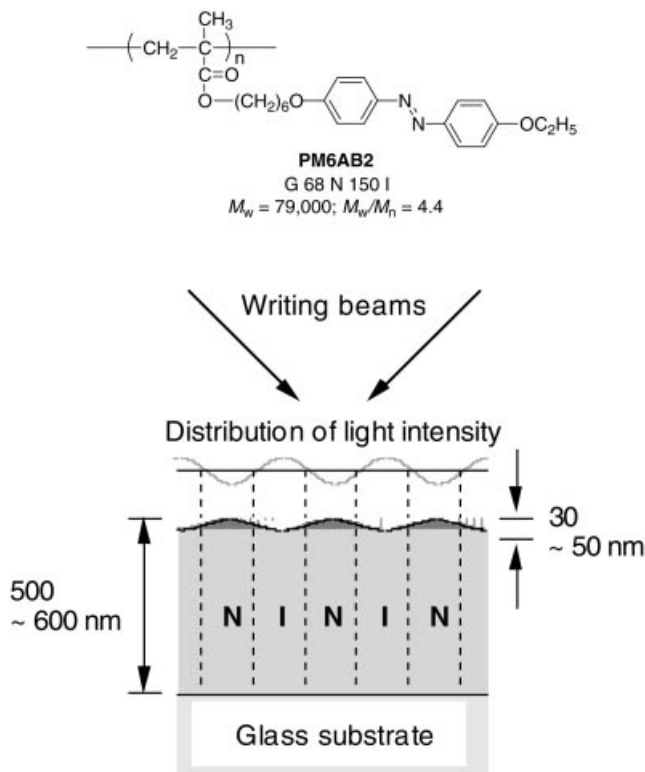


Fig. 23: Plausible structure of the holographic diffraction grating, with an alternating arrangement of N and I phases present under the relief structure.

ordered sample, with a thickness of about 500 nm, showed a high diffraction efficiency of approximately 28 %; however, the surface modulation was slight (33–53 nm). Through theoretical calculation of the degree of surface modulation, it was found that the gratings cannot only be characterized as conventional surface relief gratings. These results demonstrated that the large enhancement of diffraction efficiency is mainly governed by spatial modulation of molecular alignment resulting from alternate arrangement of N and I phases (Figure 23).^[184,185] The grating formation, therefore, is associated with photochemical phase transitions in azobenzene-containing PLCs. This system has also proved capable of holographic recording of 2-D or 3-D objects with high resolution.^[185]

References

- 1 E. Sackmann, *J. Am. Chem. Soc.*, **93**, 7088 (1971).
- 2 K. Ogura, H. Hirabayashi, A. Uejima, and K. Nakamura, *Jpn. J. Appl. Phys.*, **21**, 969 (1982).
- 3 S. Tazuke, S. Kurihara, and T. Ikeda, *Chem. Lett.*, 911 (1987).
- 4 C.h. Legge and G.R. Mitchell, *J. Phys. D: Appl. Phys.*, **25**, 492 (1992).
- 5 S. Kurihara, T. Ikeda, S. Tazuke, and J. Seto, *J. Chem. Soc. Faraday Trans.*, **87**, 3251 (1991).
- 6 Y. Yokoyama and T. Sagisaka, *Chem. Lett.*, 687 (1997).
- 7 B.L. Feringa, N.P.M. Huck, and J.A. van Doren, *J. Am. Chem. Soc.*, **117**, 9929 (1995).
- 8 T. Ikeda, *EKISHO*, **2**, 257 (1998).
- 9 S. Kurihara, T. Ikeda, and S. Tazuke, *Mol. Cryst. Liq. Cryst.*, **178**, 117 (1990).
- 10 T. Ikeda, T. Miyamoto, S. Kurihara, M. Tsukada, and S. Tazuke, *Mol. Cryst. Liq. Cryst.*, **182B**, 357 (1990).
- 11 T. Ikeda, T. Miyamoto, S. Kurihara, M. Tsukada, and S. Tazuke, *Mol. Cryst. Liq. Cryst.*, **182B**, 373 (1990).
- 12 T. Ikeda, T. Miyamoto, S. Kurihara, and S. Tazuke, *Mol. Cryst. Liq. Cryst.*, **188**, 207 (1990).
- 13 T. Ikeda, T. Miyamoto, S. Kurihara, and S. Tazuke, *Mol. Cryst. Liq. Cryst.*, **188**, 223 (1990).
- 14 T. Ikeda, T. Miyamoto, S. Kurihara, and S. Tazuke, *Mol. Cryst. Liq. Cryst.*, **188**, 235 (1990).
- 15 M. Eich, J.H. Wendorff, B. Reck, and H. Ringsdorf, *Makromol. Chem. Rapid Commun.*, **8**, 59 (1987).
- 16 M. Eich and J.H. Wendorff, *Makromol. Chem. Rapid Commun.*, **8**, 467 (1987).
- 17 T. Ikeda, S. Horiuchi, D.B. Karanjit, S. Kurihara, and S. Tazuke, *Chem. Lett.*, 1679 (1988).
- 18 T. Ikeda, S. Horiuchi, D.B. Karanjit, S. Kurihara, and S. Tazuke, *Macromolecules*, **23**, 36 (1990).
- 19 T. Ikeda, S. Horiuchi, D.B. Karanjit, S. Kurihara, and S. Tazuke, *Macromolecules*, **23**, 42 (1990).
- 20 T. Ikeda, S. Kurihara, D.B. Karanjit, and S. Tazuke, *Macromolecules*, **23**, 3938 (1990).
- 21 T. Sasaki, T. Ikeda, and K. Ichimura, *Macromolecules*, **25**, 3807 (1992).
- 22 O. Tsutsumi, Y. Demachi, A. Kanazawa, T. Shiono, T. Ikeda, and Y. Nagase, *J. Phys. Chem.*, **102**, 2869 (1998).
- 23 S. Kurihara, T. Ikeda, T. Sasaki, H.-B. Kim, and S. Tazuke, *J. Chem. Soc., Chem. Commun.*, 1751 (1990).
- 24 S. Kurihara, T. Ikeda, T. Sasaki, H.-B. Kim, and S. Tazuke, *Mol. Cryst. Liq. Cryst.*, **195**, 251 (1991).
- 25 T. Ikeda, T. Sasaki, and H.-B. Kim, *J. Phys. Chem.*, **95**, 509 (1991).
- 26 A. Fukuda and H. Takezoe, *Structures and Properties of Ferroelectric Liquid Crystals*, Corona, Tokyo (1990).
- 27 T. Ikeda, T. Sasaki, and K. Ichimura, *Nature*, **361**, 428 (1993).
- 28 T. Sasaki, T. Ikeda, and K. Ichimura, *J. Am. Chem. Soc.*, **116**, 625 (1994).
- 29 T. Sasaki and T. Ikeda, *Ferroelectrics*, **149**, 343 (1993).
- 30 T. Sasaki and T. Ikeda, *J. Phys. Chem.*, **99**, 13002 (1995).
- 31 T. Sasaki and T. Ikeda, *J. Phys. Chem.*, **99**, 13008 (1995).
- 32 T. Sasaki and T. Ikeda, *J. Phys. Chem.*, **99**, 13013 (1995).
- 33 T. Moriyama, J. Kajita, Y. Takanashi, K. Ishikawa, H. Takezoe, and A. Fukuda, *Jpn. J. Appl. Phys.*, **32**, L589 (1993).
- 34 M. Negishi, O. Tsutsumi, T. Ikeda, T. Hiyama, J. Kawamura, M. Aizawa, and S. Takehara, *Chem. Lett.*, 319 (1996).
- 35 M. Negishi, K. Kanie, T. Ikeda, and T. Hiyama, *Chem. Lett.*, 583 (1996).
- 36 K. Shirota and I. Yamaguchi, *Jpn. J. Appl. Phys.*, **36**, L1035 (1997).
- 37 L. Dinescu and R.P. Lemieux, *Liq. Cryst.*, **20**, 741 (1996).
- 38 L. Dinescu and R.P. Lemieux, *J. Am. Chem. Soc.*, **119**, 8111 (1997).
- 39 T. Ikeda and O. Tsutsumi, *Science*, **268**, 1873 (1995).
- 40 O. Tsutsumi, T. Shiono, T. Ikeda, and G. Galli, *J. Phys. Chem. B*, **101**, 1332 (1997).
- 41 O. Tsutsumi, T. Kitsunai, A. Kanazawa, T. Shiono, and T. Ikeda, *Macromolecules*, **31**, 355 (1998).
- 42 O. Tsutsumi, Y. Miyashita, S. Hirano, A. Shishido, A. Kanazawa, T. Shiono, and T. Ikeda, *Mol. Cryst. Liq. Cryst.*, **312**, 33 (1998).
- 43 A. Kanazawa, A. Shishido, M. Hasegawa, O. Tsutsumi, T. Shiono, T. Ikeda, Y. Nagase, E. Akiyama, and Y. Takamura, *Mol. Cryst. Liq. Cryst.*, **300**, 201 (1997).

- 44 A. Kanazawa, S. Hirano, A. Shishido, M. Hasegawa, O. Tsutsumi, T. Shiono, T. Ikeda, Y. Nagase, E. Akiyama, and Y. Takamura, *Liq. Cryst.*, **23**, 293 (1997).
- 45 A. Shishido, O. Tsutsumi, A. Kanazawa, T. Shiono, T. Ikeda, and N. Tamai, *J. Phys. Chem. B*, **101**, 2806 (1997).
- 46 A. Shishido, O. Tsutsumi, A. Kanazawa, T. Shiono, T. Ikeda, and N. Tamai, *J. Am. Chem. Soc.*, **119**, 7791 (1997).
- 47 A. Shishido, A. Kanazawa, T. Shiono, T. Ikeda, and N. Tamai, *J. Mater. Chem.*, **9**, 2211 (1999).
- 48 S. Kurihara, A. Sakamoto, and T. Nonaka, *Macromolecules*, **31**, 4648 (1998).
- 49 T. Todorov, N. Tomova, and L. Nikolova, *L. Opt. Commun.*, **47**, 123 (1983).
- 50 P. Rochon, J. Gosselin, A. Natansohn, and S. Xie, *Appl. Phys. Lett.*, **60**, 4 (1992).
- 51 M. S. Ho, A. Natansohn, and P. Rochon, *Macromolecules*, **28**, 6124 (1995).
- 52 O. K. Song, C. H. Wang, and M. A. Pauley, *Macromolecules*, **30**, 6913 (1997).
- 53 T. Buffeteau, A. Natansohn, P. Rochon, and M. Pézolet, *Macromolecules*, **29**, 8783 (1996).
- 54 A. Natansohn, P. Rochon, X. Meng, C. Barrett, T. Buffeteau, S. Bonenfant, and M. Pézolet, *Macromolecules*, **31**, 1155 (1998).
- 55 K. Anderle, R. Birenheide, M. J. A. Werner, and J. H. Wendorff, *Liq. Cryst.*, **9**, 691 (1991).
- 56 U. Wiesner, N. Reynolds, C. Roeffel, and H. W. Spiess, *Makromol. Chem. Rapid Commun.*, **12**, 457 (1991).
- 57 J. Stumpe, L. Läscher, Th. Fischer, M. Rutloh, S. Kostromin, and R. Ruhmann, *Thin Solid Film*, **284**, 252 (1996).
- 58 Th. Fischer, L. Läscher, J. Stumpe, and S. Kostromin, *J. Photochem. Photobiol. A: Chem.*, **80**, 453 (1994).
- 59 L. Läscher, J. Stumpe, Th. Fischer, M. Rutloh, S. Kostromin, and R. Ruhmann, *Mol. Cryst. Liq. Cryst.*, **261**, 371 (1995).
- 60 L. Läscher, Th. Fischer, J. Stumpe, S. Kostromin, S. Ivanov, V. P. Shibaev, and R. Ruhmann, *Mol. Cryst. Liq. Cryst.*, **253**, 1 (1994).
- 61 Y. Wu, Y. Demachi, O. Tsutsumi, A. Kanazawa, T. Shiono, and T. Ikeda, *Macromolecules*, **31**, 349 (1998).
- 62 Y. Wu, Y. Demachi, O. Tsutsumi, A. Kanazawa, T. Shiono, and T. Ikeda, *Macromolecules*, **31**, 1104 (1998).
- 63 Y. Wu, Y. Demachi, O. Tsutsumi, A. Kanazawa, T. Shiono, and T. Ikeda, *Macromolecules*, **31**, 4457 (1998).
- 64 Y. Wu, Q. Zhang, A. Kanazawa, T. Shiono, and T. Ikeda, *Polymer*, **40**, 4787 (1999).
- 65 Y. Wu, Q. Zhang, A. Kanazawa, T. Shiono, T. Ikeda, and Y. Nagase, *Macromolecules*, **32**, 3951 (1999).
- 66 U. Wiesner, N. Reynolds, Ch. Boeffel, and H. W. Spiess, *Liq. Cryst.*, **11**, 251 (1992).
- 67 Th. Fischer, L. Läscher, S. Czaplá, J. Rübner, and J. Stumpe, *Mol. Cryst. Liq. Cryst.*, **298**, 213 (1997).
- 68 M. Schönhoff, M. Mertesdorf, and M. Lösche, *J. Phys. Chem.*, **100**, 7558 (1996).
- 69 H. J. Haitjema, G. L. von Morgen, Y. Y. Tan, and G. Challa, *Macromolecules*, **27**, 6201 (1994).
- 70 F. H. Kreuzer, Ch. Bräuchle, A. Miller, and A. Petri, *Polymers as Electrooptical and Photo-optical Active Media*, V. P. Shibaev, Ed., Springer (1996), Chapter 3.
- 71 M. Pfaadt, C. Boeffel, and H. W. Spiess, *Acta Polymer*, **47**, 35 (1996).
- 72 K. Ichimura, S. Morino, and H. Akiyama, *Appl. Phys. Lett.*, **73**, 921 (1998).
- 73 Y. Wu, T. Ikeda, and Q. Zhang, *Adv. Mater.*, **11**, 300 (1999).
- 74 Y. Wu, J. Mamiya, A. Kanazawa, T. Shiono, T. Ikeda, and Q. Zhang, *Macromolecules*, **32**, 8829 (1999).
- 75 K. Ichimura, Y. Suzuki, T. Seki, A. Hosoki, and K. Aoki, *Langmuir*, **4**, 1214 (1988).
- 76 K. Ichimura, Y. Suzuki, T. Seki, A. Kawanishi, and K. Aoki, *Makromol. Chem. Rapid Commun.*, **10**, 5 (1989).
- 77 T. Seki, M. Sakuragi, A. Kawanishi, T. Tamaki, R. Fukuda, and K. Ichimura, *Langmuir*, **9**, 211 (1993).
- 78 W. M. Gibbons, P. J. Shannon, S. T. Sun, and B. J. Swetlin, *Nature*, **351**, 49 (1991).
- 79 Y. Iimura, J. Kusano, S. Kobayashi, T. Aoyagi, and T. Sugano, *Jpn. J. Appl. Phys. Part 2*, **32**, L93 (1993).
- 80 K. Ichimura, Y. Hayashi, H. Akiyama, and N. Ishizuki, *Langmuir*, **9**, 3298 (1993).
- 81 K. Ichimura, H. Akiyama, N. Ishizuki, and A. Kawanishi, *Makromol. Chem. Rapid Commun.*, **14**, 813 (1993).
- 82 M. Schadt, H. Seiberle, and A. Schuster, *Nature*, **381**, 212 (1996).

- 83 G.-H. Kim, S. Enomoto, A. Kanazawa, T. Shiono, T. Ikeda, and L.-S. Park, *Appl. Phys. Lett.*, **75**, 3458 (1999).
- 84 M. Hasegawa and Y. Taira, *J. Photopolym. Sci. Technol.*, **8**, 241 (1995).
- 85 Y. Wang, A. Kanazawa, T. Shiono, T. Ikeda, Y. Matsuki, and Y. Takeuchi, *Appl. Phys. Lett.*, **72**, 545 (1998).
- 86 Y. Wang, C. Xu, A. Kanazawa, T. Shiono, T. Ikeda, Y. Matsuki, and Y. Takeuchi, *J. Appl. Phys.*, **84**, 181 (1998).
- 87 Y. Wang, C. Xu, A. Kanazawa, T. Shiono, T. Ikeda, Y. Matsuki, and Y. Takeuchi, *J. Appl. Phys.*, **84**, 4573 (1998).
- 88 G. P. Montgomery, Jr., G. W. Smith, and N. A. Vaz, *Liquid Crystalline and Mesomorphic Polymers*, Springer (1994).
- 89 H. Kitzerow, *Liq. Cryst.*, **16**, 1 (1994).
- 90 J. L. Ferguson, *SID Int. Symp. Digest of Tech. Papers*, **16**, 68 (1985).
- 91 P. S. Drzaic, *J. Appl. Phys.*, **60**, 2142 (1986).
- 92 J. L. West, *Mol. Cryst. Liq. Cryst.*, **157**, 427 (1988).
- 93 J. W. Doane, N. A. Vaz, B.-G. Wu, and S. Zumer, *Appl. Phys. Lett.*, **48**, 269 (1986).
- 94 H. Takatsu, *Kinouzairyou (Functional Materials)*, **15**, 22 (1995).
- 95 C. V. Rajaram and S. D. Hudson, *Chem. Mater.*, **8**, 2451 (1996).
- 96 D.-K. Yang, L.-C. Chien, and J. W. Doane, *Appl. Phys. Lett.*, **60**, 3102 (1992).
- 97 P. P. Crooker and D. K. Yang, *Appl. Phys. Lett.*, **57**, 2529 (1990).
- 98 R. A. M. Hikmet, H. M. Boots, and M. Michielsen, *J. Appl. Phys.*, **79**, 8098 (1996).
- 99 Y.-D. Ma, B.-G. Wu, and G. Xu, *Proc. SPIE*, **1257**, 46 (1990).
- 100 A.Y.-G. Fuh, C.-Y. Huang, C.-R. Sheu, G.-L. Lin, and M.-S. Tsai, *Jpn. J. Appl. Phys.*, **33**, L870 (1994).
- 101 K. Takizawa, H. Kikuchi, H. Fujikake, Y. Namikawa, and K. Tada, *Jpn. J. Appl. Phys.*, **33**, 1346 (1994).
- 102 T. Kajiyama, H. Kikuchi, and K. Nakamura, *Proc. SPIE*, **1911**, 111 (1993).
- 103 R. Yamaguchi, H. Ookawara, and S. Sato, *Jpn. J. Appl. Phys.*, **31**, L1093 (1992).
- 104 Y. Kawanishi, T. Tamaki, and K. Ichimura, *J. Phys. D: Appl. Phys.*, **24**, 782 (1991).
- 105 H.-K. Lee, A. Kanazawa, T. Shiono, T. Ikeda, T. Fujisawa, M. Aizawa, and B. Lee, *Chem. Mater.*, **10**, 1402 (1998).
- 106 H.-K. Lee, A. Kanazawa, T. Shiono, T. Ikeda, T. Fujisawa, M. Aizawa, and B. Lee, *J. Appl. Phys.*, **86**, 5927 (1999).
- 107 S. Kurihara, K. Masumoto, and T. Nonaka, *Appl. Phys. Lett.*, **73**, 160 (1998).
- 108 H.-K. Lee, K. Doi, A. Kanazawa, T. Shiono, T. Ikeda, T. Fujisawa, M. Aizawa, and B. Lee, *Polymer*, **41**, 1757–1763 (2000).
- 109 L. Li, H. J. Yuan, and P. Palffy-Muhoray, *Mol. Cryst. Liq. Cryst.*, **198**, 239 (1991).
- 110 T. Vogeler, M. Kreuzer, T. Tschudi, and F. Simoni, *Mol. Cryst. Liq. Cryst.*, **282**, 419 (1996).
- 111 D. Gabor, *Nature*, **161**, 777 (1948).
- 112 R. J. Collier, C. B. Burckhardt, and L. H. Lin, *Optical Holography*, Academic Press: New York (1971).
- 113 H. M. Smith, *Holographic Recording Materials*, Springer-Verlag: Berlin (1977).
- 114 W. E. Moerner and S. M. Silence, *Chem. Rev.*, **94**, 127 (1994).
- 115 J. F. Heanue, M. C. Bashaw, and L. Hesselink, *Science*, **265**, 749 (1994).
- 116 N. Cheng, B. Swedek, and P. N. Prasad, *Appl. Phys. Lett.*, **71**, 1828 (1997).
- 117 B. P. Ketchel, G. L. Wood, R. J. Anderson, and G. J. Salamo, *Appl. Phys. Lett.*, **71**, 7 (1997).
- 118 S. Stepanov, N. Komeev, A. Gerwens, and K. Buse, *Appl. Phys. Lett.*, **72**, 879 (1998).
- 119 K. Kinoshita, *Jpn. J. Appl. Phys.*, **31**, 1677 (1992).
- 120 F. Carreno and E. Bernabeu, *Appl. Phys. Lett.*, **66**, 798 (1995).
- 121 I. Banyasz, *Appl. Opt.*, **37**, 2081 (1998).
- 122 V. Weiss, A. A. Friesem, and V. A. Krongauz, *Opt. Lett.*, **18**, 1089 (1993).
- 123 A. Akella, S. L. Sochava, and L. Hesselink, *Opt. Lett.*, **22**, 919 (1997).
- 124 T. Kardinahl and H. Franke, *Appl. Phys. A*, **61**, 23 (1995).
- 125 R. Wortmann, P. M. Lundquist, R. J. Twieg, C. Geletnek, C. R. Moylan, Y. Jia, R. G. Devoe, D. M. Burland, M. P. Bernal, H. Coufal, R. K. Grygier, J. A. Hoffnagle, C. M. Jefferson, R. M. Macfarlane, R. M. Shelby, and G. T. Sincerbox, *Appl. Phys. Lett.*, **69**, 1657 (1996).
- 126 A. Natansohn, P. Rochon, M. S. Ho, and C. Barrett, *Macromolecules*, **28**, 4179 (1995).
- 127 C. J. Barrett, A. Natansohn, and P. L. Rochon, *J. Phys. Chem.*, **100**, 8836 (1996).
- 128 F. L. Labarthe, P. Rochon, and A. Natansohn, *Appl. Phys. Lett.*, **75**, 1377 (1999).

- 129 D.Y. Kim, L. Li, X.L. Jiang, V. Shivshankar, J. Kumar, and S.K. Tripathy, *Macromolecules*, **28**, 8835 (1995).
- 130 S. Bian, L. Li, J. Kumar, D.Y. Kim, J. Williams, and S.K. Tripathy, *Appl. Phys. Lett.*, **73**, 1817 (1998).
- 131 T. Todorov, L. Nikolova, and N. Tomova, *Appl. Opt.*, **23**, 4588 (1984).
- 132 T. Todorov, L. Nikolova, and N. Tomova, *Appl. Opt.*, **24**, 785 (1985).
- 133 R.H. Berg, S. Hvilsted, and P.S. Ramanujam, *Nature*, **383**, 505 (1996).
- 134 P.H. Rasmussen, P.S. Ramanujam, S. Hvilsted, and R.H. Berg, *J. Am. Chem. Soc.*, **121**, 4738 (1999).
- 135 B.M. Monroe, W.K. Smothers, D.E. Keys, R.R. Krebs, D.J. Mickish, A.F. Harrington, S.R. Schicker, M.K. Armstrong, D.M. Chan, and C.I. Weathers, *J. Imag. Sci.*, **35**, 19 (1991).
- 136 T. Hotta and T. Yamaoka, *Polym. Adv. Tech.*, **5**, 90 (1994).
- 137 A. Blendez, A. Fimia, L. Carretero, and F. Mateos, *Appl. Phys. Lett.*, **67**, 3856 (1995).
- 138 C. Zhang, H. Tao, and W. Mei, *Appl. Opt.*, **36**, 4862 (1997).
- 139 K.T. Weitzel, U.P. Wild, and V.N. Mikhailov, *Opt. Lett.*, **22**, 1899 (1997).
- 140 L. Carretero, S. Blaya, R. Mallavia, R.F. Mandrigal, and A. Fimia, *J. Mod. Opt.*, **45**, 2345 (1998).
- 141 A. Chen and D.J. Brady, *Opt. Lett.*, **17**, 441 (1992).
- 142 A. Chen and D.J. Brady, *Appl. Phys. Lett.*, **62**, 2920 (1993).
- 143 S. Bartkiewicz, A. Januszko, A. Miniewix, and J. Parka, *Pure Appl. Opt.*, **5**, 799 (1996).
- 144 F. Simoni, O. Francescangeli, Y. Reznikov, S. Slussarenko, *Opt. Lett.*, **22**, 549 (1997).
- 145 S. Slussarenko, O. Francescangeli, F. Simoni, and Y. Reznikov, *Appl. Phys. Lett.*, **71**, 3613 (1997).
- 146 G.P. Wiederrecht, B.A. Yoon, and M.R. Wasielewski, *Science*, **270**, 1794 (1995).
- 147 G.P. Wiederrecht, B.A. Yoon, W.A. Svec, and M.R. Wasielewski, *J. Am. Chem. Soc.*, **119**, 3358 (1997).
- 148 I.C. Khoo and Y.R. Shen, *Opt. Eng.*, **24**, 579 (1985).
- 149 I.C. Khoo, R.G. Lindquist, R.R. Michael, R.J. Mansfield, and P. Lopresti, *J. Appl. Phys.*, **69**, 3853 (1991).
- 150 I.C. Khoo, H. Li, and Y. Liang, *Opt. Lett.*, **19**, 1723 (1994).
- 151 I.C. Khoo, *Opt. Lett.*, **20**, 2137 (1995).
- 152 I.C. Khoo, S. Slussarenko, B.D. Guenther, M.Y. Shih, P. Chen, and W.V. Wood, *Opt. Lett.*, **23**, 253 (1998).
- 153 H. Ono and N. Kawatsuki, *Appl. Phys. Lett.*, **71**, 1162 (1997).
- 154 R. Ortler, C. Brauchle, A. Miller, and G. Riepl, *Makromol. Chem. Rapid Commun.*, **10**, 189 (1989).
- 155 H.J. Eichler, G. Heppke, R. Macdonald, and H. Schmid, *Mol. Cryst. Liq. Cryst.*, **223**, 159 (1992).
- 156 H.J. Eichler, R. Elschner, and R. Macdonald, *Mol. Cryst. Liq. Cryst.*, **250**, 293 (1994).
- 157 J. Contzen, G. Heppke, D. Kitzerow, and H. Schmid, *Appl. Phys. B*, **63**, 605 (1996).
- 158 R. Elschner and R. Macdonald, *Mol. Cryst. Liq. Cryst.*, **282**, 107 (1996).
- 159 F. Simoni, F. Bloisi, and L. Vicari, *Mol. Cryst. Liq. Cryst.*, **223**, 169 (1992).
- 160 H. Ono and N. Kawatsuki, *Jpn. J. Appl. Phys.*, **36**, 6444 (1997).
- 161 G.P. Wiederrecht and M.R. Wasielewski, *J. Am. Chem. Soc.*, **120**, 3231 (1998).
- 162 G. Cipparrone, A. Mazzulla, and F. Simoni, *Opt. Lett.*, **23**, 1505 (1998).
- 163 A. Golemme, B. Kippelen, and N. Peyghambarian, *Appl. Phys. Lett.*, **73**, 2408 (1998).
- 164 V.P. Tondiglia, L.V. Natarajan, R.L. Sutherland, T.J. Bunning, and W.W. Adams, *Opt. Lett.*, **20**, 1325 (1995).
- 165 A.Y.G. Fuh, C.Y. Huang, M.S. Tsai, J.M. Chen, and L.C. Chien, *Jpn. J. Appl. Phys.*, **35**, 630 (1996).
- 166 A.Y.G. Fuh, M.S. Tsai, T.C. Liu, and L.C. Chien, *Jpn. J. Appl. Phys.*, **36**, 6839 (1997).
- 167 A.Y.G. Fuh, T.C. Ko, M.S. Tsai, C.Y. Huang, and L.C. Chien, *J. Appl. Phys.*, **83**, 679 (1998).
- 168 M. Eich, B. Reck, H. Ringsdorf, and J.H. Wendorff, *Proc. SPIE*, **682**, 93 (1986).
- 169 M. Eich and J.H. Wendorff, *J. Opt. Soc. Am. B*, **7**, 1428 (1990).
- 170 M. Eich and J.H. Wendorff, *Mol. Cryst. Liq. Cryst.*, **243**, 51 (1994).
- 171 S. Hvilsted, F. Andruzzi, and P.S. Ramanujam, *Opt. Lett.*, **17**, 1234 (1992).
- 172 P.S. Ramanujam, S. Hvilsted, and F. Andruzzi, *Appl. Phys. Lett.*, **62**, 1041 (1993).
- 173 S. Hvilsted, F. Andruzzi, C. Kulinna, H. W. Siesler, and P.S. Ramanujam, *Macromolecules*, **28**, 2172 (1995).

- 174 N.C.R. Holme, P.S. Ramanujam, and S. Hvilsted, *Appl. Opt.*, **35**, 4622 (1996).
- 175 L. Nikolova, T. Todorov, M. Ivanov, F. Andruzzi, S. Hvilsted, and P.S. Ramanujam, *Appl. Opt.*, **35**, 3835 (1996).
- 176 P.S. Ramanujam, N.C.R. Holme, and S. Hvilsted, *Appl. Phys. Lett.*, **68**, 1329 (1996).
- 177 N.C.R. Holme, L. Nikolova, P.S. Ramanujam, and S. Hvilsted, *Appl. Phys. Lett.*, **70**, 1518 (1997).
- 178 I. Naydenova, L. Nikolova, T. Todorov, N.C.R. Holme, P.S. Ramanujam, and S. Hvilsted, *J. Opt. Soc. Am. B*, **15**, 1257 (1998).
- 179 L. Andruzzi, A. Altomare, F. Ciardelli, R. Solaro, S. Hvilsted, and P.S. Ramanujam, *Macromolecules*, **32**, 448 (1999).
- 180 X. Wei, X.Z. Yan, D.R. Zhu, D. Mo, Z.X. Liang, and W.Z. Lin, *Appl. Phys. Lett.*, **68**, 1913 (1996).
- 181 M. Hasegawa, T. Yamamoto, A. Kanazawa, T. Shiono, and T. Ikeda, *Adv. Mater.*, **11**, 675 (1999).
- 182 M. Hasegawa, T. Yamamoto, A. Kanazawa, T. Shiono, and T. Ikeda, *Chem. Mater.*, **11**, 2764 (1999).
- 183 M. Hasegawa, T. Yamamoto, A. Kanazawa, T. Shiono, T. Ikeda, Y. Nagase, E. Akiyama, and Y. Takamura, *J. Mater. Chem.*, **9**, 2765 (1999).
- 184 T. Yamamoto, M. Hasegawa, A. Kanazawa, T. Shiono, and T. Ikeda, *J. Phys. Chem. B*, **103**, 9873 (1999).
- 185 T. Yamamoto, M. Hasegawa, S. Yoneyama, A. Kanazawa, T. Shiono, and T. Ikeda, *Mat. Res. Soc. Symp. Proc.*, **559**, 153 (1999).

13

Photoswitchable Polypeptides

Francesco Ciardelli and Osvaldo Pieroni

13.1

Introduction

13.1.1

Photoresponsive Polymers

Photoresponsive polymers are quite special polymers, able to respond to light and dark conditions and thus giving rise to reversible variations in their structure and conformation. These photoinduced structural changes may in turn be accompanied by reversible changes in the physical and chemical properties of the polymeric materials.

Photoresponsive polymers can be obtained by introducing photochromic units, such as azobenzene or spiropyran groups, into the macromolecules of polymeric compounds. As described in Chapter 1 of this book, photochromic compounds can exist in two different states, such as two isomeric structures that can be interconverted by means of a light stimulus, and the relative concentrations of which depend on the wavelength of the incident light. For instance, in azobenzene compounds, photochromism is due to *trans-cis* photoisomerization around the N=N double bond, while in spiropyran compounds photochromism involves interconversion between the neutral spiro form and the zwitterionic merocyanine form (Figure 1).

The occurrence of two different structures that can be interconverted through the agency of an external light stimulus can be the basis of a molecular switch. Moreover, when photochromic molecules are incorporated into polymeric compounds, their photoisomerization can affect the structure and the physical properties of the attached macromolecules. Therefore, photochromic polymers may be highly promising materials for application in optical technologies, as well as in the design of photoswitchable devices.

Some fine review articles dealing with various aspects of photochromic polymers are reported in the literature,^[1–9] and several photoresponse effects have been described. These include light-induced conformational changes, photostimulated variations of viscosity and solubility, photocontrol of membrane functions, and photomechanical effects. Here we provide an overview of the photoresponse effects

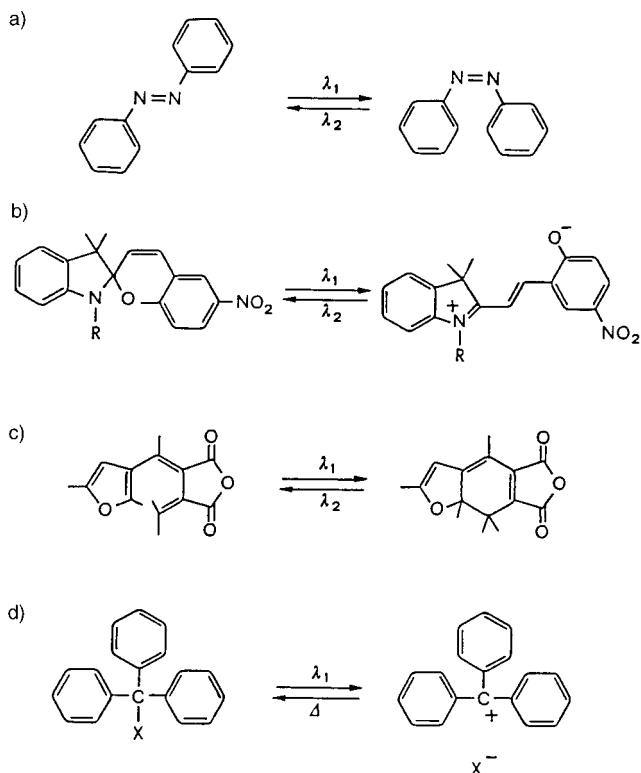


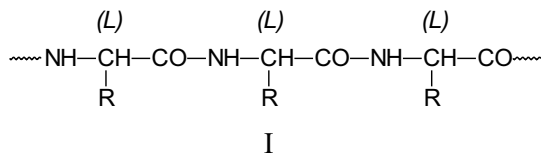
Fig. 1: Photochemical reactions responsible for photochromic behaviour in a) azobenzene derivatives, b) spirocyclic compounds, c) fulgides, and d) triphenylmethane derivatives.

observed in the field of photochromic polypeptides. Other photoresponsive systems, including several involving polymers, such as photosensitive liquid crystals and biological photosensors, are examined in separate chapters of this book.

13.1.2

Structure and Conformation of Polypeptides

Polypeptides and poly(α -amino acid)s are polymers of α -amino acids, with the chemical structure I:



Scheme 1 Chemical structure of polypeptides (I).

They can be synthesized easily, up to a molecular weight of 10^6 , by polymerization of *N*-carboxy anhydride derivatives of amino acids. When the configuration of the chiral carbon atoms is L for all the amino acid monomer units along the macromolecular chains, they can be considered simple synthetic analogues of proteins.

Polypeptides and poly(α -amino acid)s have a quite unique position amongst synthetic polymers. The reason for this is that most common synthetic polymers have very little long range order in solution and their properties are the products of statistical random coil conformations. Polypeptides, in contrast, can adopt well defined, ordered structures typical of those existing in proteins, such as α -helix and β -structures. Moreover, the ordered structures can undergo conformational changes to the random coil state as cooperative transitions, analogous to the denaturation of proteins.

The most widely known ordered structure in polypeptides is the α -helix. When the repeating units are amino acid residues of L configuration, the α -helix is right-handed: i.e., the chain backbone follows the pattern of the thread of a right-hand screw. Each turn of the helix is made up of 3.6 residues, so the helix is nonintegral. An exact repeat of the backbone structure occurs every 18 monomeric units. This repeat corresponds to five turns of the helix, with a linear translation along the axis of 27 Å and a pitch of 5.4 Å. The helix diameter, neglecting side chains, is about 6 Å.

An important feature of the α -helix is the pattern of the hydrogen bonds. When the α -helix is viewed with the *N*-terminus at the bottom and the *C*-terminus at the top, all the carbonyl groups point upwards and all the N-H groups point downwards. The spatial positions of the atoms are such that every C=O group forms a hydrogen bond with the N-H group four residues away, almost parallel to the axis of the helix. A well defined, ordered structure can thus be formed and stabilized within a single polypeptide chain without any intermolecular interactions being involved.

All side chains of L-amino acid residues point away from the axis; thus the structure can accommodate almost any kind of flexible side chain, and it is not necessary that the macromolecules have chemically identical repeating units. Since the chain backbone is the same for all the amino acids, units with different side groups can be accommodated within the same structure.

Another common ordered structure occurring in polypeptides is the β -structure. The conformational angles of the β -structure are relatively close to the fully extended conformation: the macromolecules therefore have an almost planar, zig-zag geometry. Their C=O and N-H groups participate in hydrogen bonding, but these bonds are all *interstrand* rather than *intrastrand*, and link two polypeptide chains, thus generating sheets. These sheets are puckered, with side chains above and below the plane of the sheet; the side chains in adjacent macromolecules are parallel and sufficiently close to stabilize the structure through hydrophobic interactions. Alternate chains can be arranged either parallel or antiparallel to one another. In the parallel β -structure, all the chains are aligned in the same direction; in the antiparallel β -structure, alternate chains have opposite directions. The antiparallel case is more common in synthetic polypeptides.

13.1.3

Chiroptical Properties of Polypeptide Structures

The detection of ordered structures such as α -helix or β -structures, and quantitative measurements of their populations, are essential aspects of structural investigation in polypeptides. The most sensitive technique for such investigation is certainly circular dichroism (CD) spectroscopy, because the various structures are characterized by typical and standard CD spectra.

13.1.3.1 CD Spectrum of the α -Helix

The right-handed α -helix formed by polypeptides of amino acids of L-configuration is surely the best characterized structure. It exhibits a highly distinctive CD spectrum (Figure 2).^[10,11] The general spectral features are two negative bands at 222 nm ($[\Theta] = -35,000$) and 208 nm ($[\Theta] = -33,000$), and a positive band at 190 nm ($[\Theta] +70,000$). The negative 222 nm band is due to the peptide $n\text{-}\pi^*$ transition, while the negative 208 nm and positive 190 nm bands result from exciton splitting of the peptide $\pi\text{-}\pi^*$ transition. The CD spectra of a variety of different α -helical polypeptides have been reported and a number of different solvents have been used.^[11] Although there may be small differences in the exact amplitudes of extrema, the spectrum shown in Figure 2 is highly characteristic of simple α -helical polypeptides. A theoretical CD curve calculated by Woody^[12] for α -helical poly(L-alanine) was found to fit

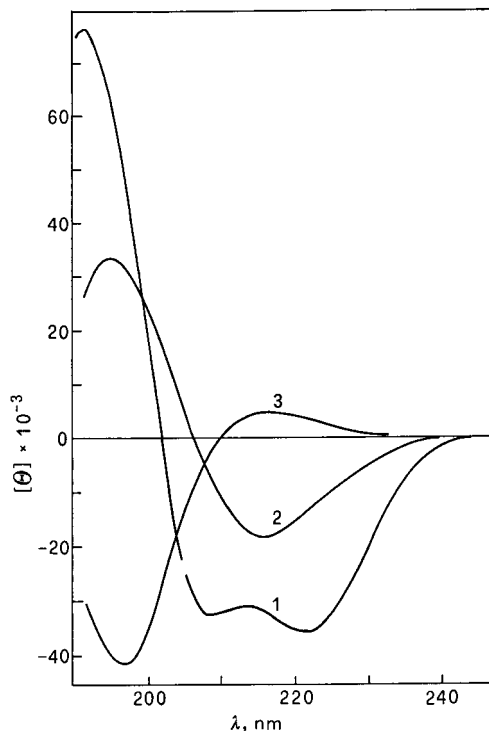


Fig. 2: Standard circular dichroism (CD) spectra of the most common polypeptide structures: 1) α -helix; 2) β -structure; 3) random coil.

very well with the experimental spectrum. However, although differences in solvent and amino acid residues do not generally affect qualitative features of the α -helix CD spectrum, they may affect more subtle aspects, including the relative amplitudes of the 222 and 208 nm bands. Significant variations have been observed for polypeptides in hexafluoro-2-propanol.^[11,13]

13.1.3.2 CD spectrum of the β -Structure

Polypeptides adopting a β -structure exhibit CD spectra, the characteristic features of which are a negative band at about 216 nm ($[\Theta] \approx -18,000$) and a positive band of comparable magnitude near 195 nm (Figure 2). However, the CD spectra of β -structures show much more pronounced variations with solvent and amino acid residues than those of the α -helix, both in amplitude and in the position of the bands. In the presence of sodium dodecyl sulfate, the β -form of poly(L-lysine), though still a β -structure by infrared criteria, gives a 218 nm CD band only about half as large as that in the absence of the surfactant.^[11]

This variability may result from the limited CD characterization of the β -structure, which has proven to be more difficult than for the case of the α -helix. The solubility of polypeptides in the β -conformation is usually limited. In addition, the β -structure is less well defined than the α -helix. Indeed, β -sheets can be found with adjacent strands either parallel or antiparallel. Theoretical calculations have indicated though that, on the basis of CD alone, it is difficult to distinguish between parallel and antiparallel β -structures.^[14]

13.1.3.3 CD Spectra of Random Coil Structures

The CD spectrum associated with a random coil structure is usually characterized by an intense, negative band near 200 nm and a weak, positive band at about 220 nm (Figure 2). The described CD spectrum, however, may show large variations both from one polypeptide to another and as function of temperature and solvent composition.^[15] The spectra of proteins which have been denatured by urea or guanidine hydrochloride do not show the positive band at 220 nm.^[16] In contrast, a negative shoulder of approximately the same intensity is seen at the same wavelength for polypeptides containing ionic side chains, such as poly(L-glutamate) and poly(L-lysine) in concentrated solutions of salts. The variability of the CD spectra of disordered polypeptides is not surprising if one considers that polypeptide chains can adopt many different conformations: as conditions are varied or the sequence is changed, the distribution of conformations is altered, and this leads to changes in the magnitude of the 200 nm band and profound effects, even sign changes, in the more sensitive band at 220 nm.^[17]

13.1.3.4 CD Spectra of Polypeptides with Chromophoric Side Chains

If the side chains have strongly chromophoric groups near the backbone, such as in polymers of aromatic amino acids like poly(L-phenylalanine), poly(L-tyrosine), and poly(L-tryptophan), the CD spectrum is strongly dependent on the side chains and is totally different from the standard spectra of polypeptides lacking chromophoric groups in the side chains. This is due to the interactions between amide and aro-

matic transitions and to the presence of the CD contributions of the chromophoric side chains in the peptide region, which strongly perturb the CD spectra.

This aspect must be carefully taken into account when strongly absorbing chromophores, such as photochromic dyes, are attached to the side chains. In the case of azobenzene-containing polypeptides, for instance, a correct assignment of the conformation on the basis of CD spectra can be complicated by the presence of overlapping contributions of peptide and azo chromophores. In addition, the azobenzene chromophore is characterized by different electric and magnetic transition moments for the *trans* and the *cis* isomers. Thus, isomerization of the azo side chains could in principle produce marked changes of CD spectra, independently of the actual conformation of the macromolecular backbone. Usually, aromatic substituents at carbon atoms beyond the γ -carbon atom lead to negligible perturbations. For instance, poly(γ -benzyl-L-glutamate) and poly(N^{ϵ} -carbobenzoxy-L-lysine) have normal α -helix CD spectra, indicating that the aromatic groups in these polypeptides are sufficiently remote from the backbone as to perturb the spectra to a negligible extent.^[11]

13.2

Photomodulation of Polypeptide Macromolecular Structure

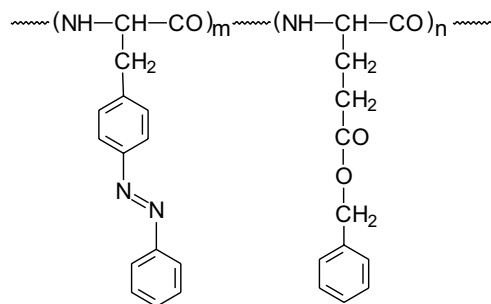
13.2.1

UV Light-induced Conformational Transitions in Azobenzene-containing Polypeptides

13.2.1.1 *p*-Phenylazo-L-phenylalanine Polypeptides

In pioneering articles published in 1966 and 1967, Goodman et al. described a series of polypeptides derived from *p*-phenylazo-L-phenylalanine and γ -benzyl-L-glutamate by polymerization of the corresponding *N*-carboxy anhydrides (Scheme 2).^[18,19]

These polypeptides exhibited photochromic behavior associated with the photoisomerization of their azobenzene moieties, as discussed in Section 13.1 (Figure 1). At room temperature, in the dark, azo groups exist in the more stable *trans* config-



II

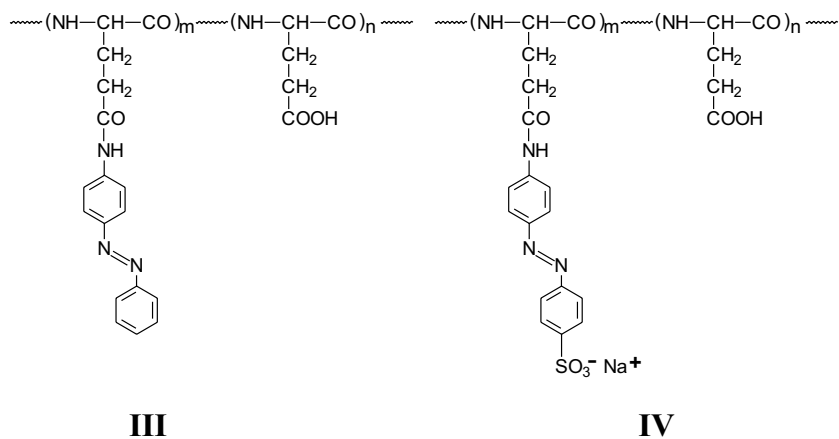
Scheme 2 Chemical structure of polypeptides containing *p*-phenylazo-L-phenylalanine and γ -benzyl-L-glutamate residues (II).

uration; irradiation results in isomerization to the *cis* isomer. The azo-polypeptides were directly irradiated at 320 nm in a Cary 60 spectropolarimeter and the *trans-cis* isomerization reaction was followed by recording changes in optical rotation. Under these irradiation conditions, the extent of azo residue photoconversion from the *trans* to the *cis* isomer was about 40–50%.

Studies were carried out in the helicogenic solvent dioxane and in the denaturing solvent trifluoroacetic acid. In both solvents, irradiation caused changes in the optical rotatory dispersion (ORD) curves in the region of the absorption of the azo chromophore (300–500 nm). Prior to irradiation, in dioxane, ORD spectra exhibited a Cotton effect trough at 233 nm, consistent with a helical main chain structure for the polypeptides. After irradiation at 320 nm, the Cotton effect at 233 nm remained essentially unchanged. In trifluoroacetic acid, in contrast, ORD curves revealed no Cotton effects, indicating that the backbone conformation was nonhelical for both the *trans*- and the *cis*-azo-polypeptides. For these polypeptides, therefore, the change in chiroptical properties at 300–500 nm had to have been the result of the *trans-cis* isomerization of the azobenzene units – and not the consequence of photoinduced variation of the macromolecular conformation.

13.2.1.2 Azobenzene-containing Poly(L-glutamic acid)

A detailed investigation of photochromism, conformation, and CD properties has been carried out on poly(L-glutamic acid) containing azobenzene units in the side chains (Scheme 3, Structure III). The polymers were obtained by treating high molecular weight poly(L-glutamic acid) with *p*-aminoazobenzene in the presence of dicyclohexylcarbodiimide (DCCI) and *N*-hydroxy-benzotriazole (HOBT).^[20–22] Samples containing various percentages of azo groups, up to 80 mol%, were obtained by increasing the reaction temperature, reaction duration, and the molar excess of the azo reagent. When the modification reaction was carried out in the presence only of



Scheme 3 Chemical structure of poly(L-glutamic acid) modified with 4-amino-azobenzene (III), and 4-amino-azobenzene-4'-sulfonic acid sodium salt (IV).

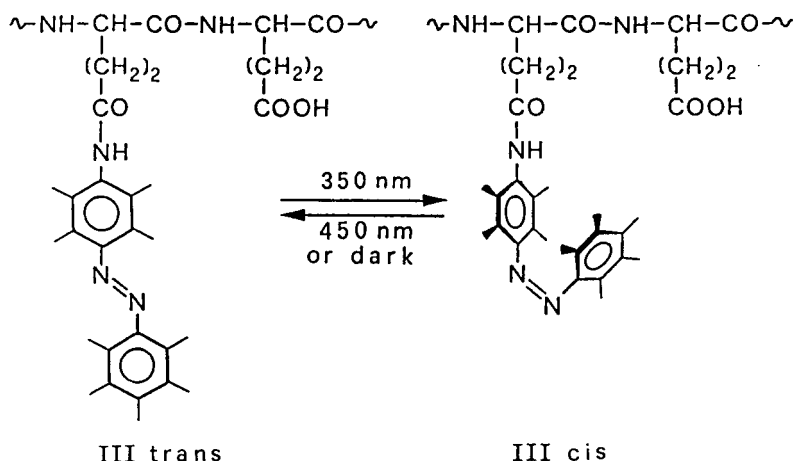


Fig. 3: Photochromic reactions of poly(L-glutamic acid) containing azobenzene units in the side chains (III).

DCCI, the modified polymers were found to contain considerable amounts of *N*-acylureic groups originating from side reactions between DCCI and the γ -carboxylic acid functions. The formation of *N*-acylureic groups was completely suppressed when the modification reactions were carried out in the presence of one equivalent of hydroxy-benzotriazole.^[21,22]

The photochromic reactions are illustrated in Figure 3. At room temperature in the dark, all the azo groups are in the *trans* configuration, which is planar and fully conjugated. Irradiation at 350 nm produces isomerization to the *cis* isomer, which is not planar and is less conjugated, for steric reasons. Indeed, the two benzene rings are forced to occupy skewed planes. The back-reaction to the *trans* form is achieved by irradiation at 450 nm or simply by keeping the samples in darkness.

As a consequence of the different electronic situations of the two isomers, photoisomerization is accompanied by strong variations in the absorption spectra (Figure 4). In particular, the *trans-cis* isomerization is characterized by a strong decrease in the intense band at about 350 nm, associated with a $\pi\text{-}\pi^*$ transition, and a concomitant intensification in the band at 450 nm, associated with the $n\text{-}\pi^*$ transition of the azo chromophore.^[21]

The maximum degree of photoconversion to the *cis* isomer (85%) is achieved by irradiating at 350–370 nm, whereas the maximum yield of the back-reaction from the *cis* to the *trans* isomer (80%) is achieved by irradiating at 450 nm. Using a 200 W lamp, irradiation for 1 or 2 minutes is enough to achieve the photostationary state. The thermal decay in the dark is much slower. At room temperature, it takes more than 200 hours to restore the fully *trans* isomeric composition. The photochromic cycles are completely reversible and can be repeated at will, without any apparent *fatigue*.^[21,22]

In organic solvents such as trimethylphosphate or trifluoroethanol, the azo-modified polymers show the CD pattern of the α -helix structure, with the two typical minima at 208 and 222 nm (Figure 5). In trimethylphosphate, the dark-adapted

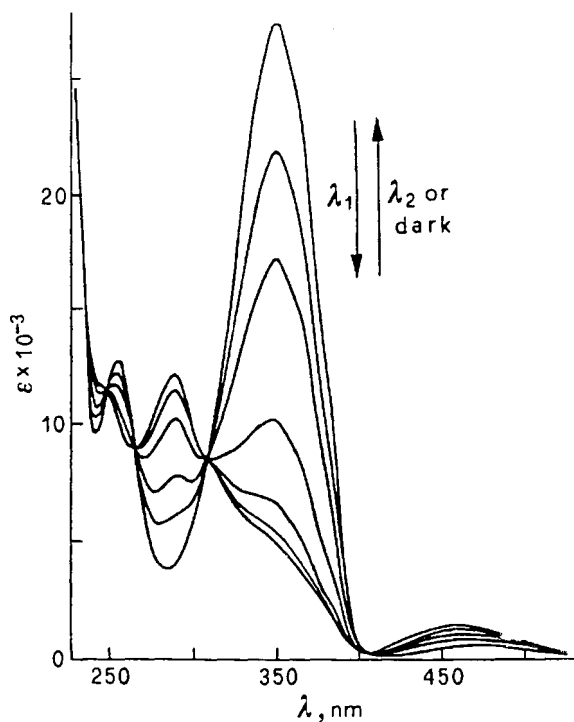


Fig. 4: Reversible light-induced variation in the absorption spectra of azo-modified poly(L-glutamic acid) (III).

samples also exhibit an intense couplet of bands centered at 350 nm, corresponding to the π - π^* transition of the azo chromophore in the *trans* configuration. This couplet of bands, associated with dipole-dipole interactions between azo side chains within the α -helix structure, is not observed in trifluoroethanol. Irradiation, and the consequent *trans*→*cis* photoisomerization, completely abolishes the side chain CD bands in the 250–450 nm region, but does not modify at all the CD spectra in the peptide region (below 250 nm). This indicates that, in these solvents, light induces the *trans*-*cis* isomerization of the azo side chains, but such isomerization does not result in any variation of the main chain structure.^[21] The typical pattern of the α -helix and the lack of any change below 250 nm upon *trans*-*cis* isomerization provide evidence that the azo chromophores do not give rise to any contribution to the CD spectra in the peptide region.

Similar findings have been reported by Sisido et al. for various sequential polypeptides containing *p*-phenylazo-L-phenylalanine residues (II).^[23,24] Upon irradiation, the polypeptides displayed a reversible change of optical rotation at 589 nm, associated with the *trans*-*cis* photoisomerization of the azo units, even though the photoisomerization of the side chains did not induce any change in the α -helical main chain conformation. Sisido et. al. have proposed the photoreversible change of optical rotation as an useful tool to achieve chiroptical photorecording, in which a digital record written as a photoisomerized state (*trans*-*cis*), may be read out by means of the change of optical rotation at a wavelength longer than the wavelength

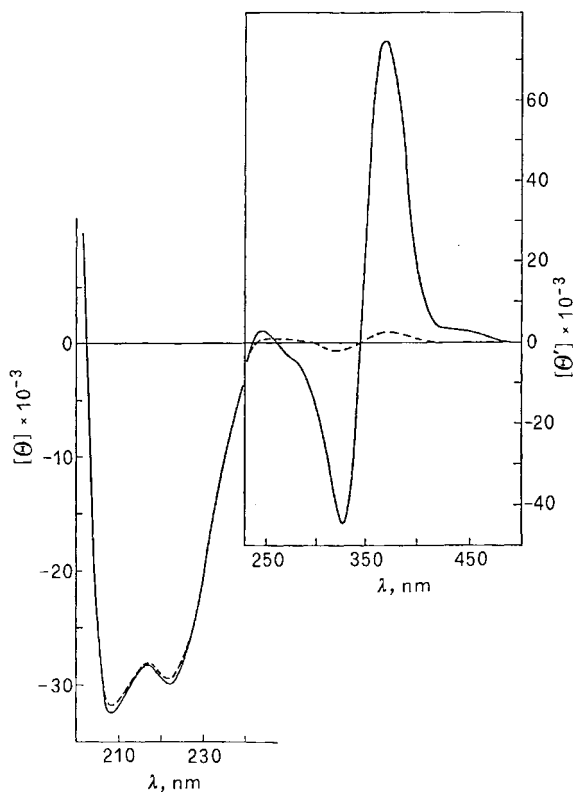


Fig. 5: Poly(L-glutamic acid) containing 56 mol% azobenzene units in the side chains (III). CD spectra in trimethylphosphate before (continuous line) and after (dashed line) irradiation at 360 nm. Below 250 nm, molar ellipticity is based on the mean residue weight; above 250 nm, the ellipticity is referred to one azo-Glu residue.

used for the recording. This should avoid the possibility of the read-out process destroying the original record.^[23,24]

The conformational behavior can be quite different in aqueous solution. Below pH 5, a sample of poly(L-glutamic acid) containing about 30 mol% azobenzene units adopts a β -structure that is not affected by light. Above pH 7, the polypeptide is random coil and the conformation is, once more, not affected by the photoisomerization of the azo side chains. However, at pH values in the range 5–7 (close to the pK of the conformational transition), irradiation causes a remarkable diminishing of the ordered structure, which is completely reversed in the dark.^[20,22]

The mechanism of the photoresponse was explained as follows. The primary event is the *trans-cis* photoisomerization of the azo side chains. However the simple change in geometry of the azo units does not seem to be sufficient to induce appreciable conformational changes in the macromolecules (indeed, no effect was observed in organic solvents). The key factor responsible for the photoinduced conformational transition is likely to result from a polarity change in the environment around the macromolecules, as a consequence of the differences in polarity and hydrophobicity between the *trans* and *cis* azo isomers. In fact, the apparent pK value for the ionization of the unmodified COOH groups is higher when the neighboring

azo units are in the hydrophobic *trans* configuration ($pK_a = 6.8$) than when they are in the polar *cis* configuration ($pK_a = 6.3$). As a result, the *trans*→*cis* photoisomerization of the azo units is accompanied by a higher degree of dissociation of the neighboring COOH side chains, thus increasing the ionic interactions among side chains and causing the unfolding of the polypeptide.

Analogous polypeptides prepared by treatment of poly(L-glutamic acid) with 4-amino-azobenzene-4'-sulfonic acid sodium salt (Scheme 3, Structure IV) exhibited conformational and photoresponsive behavior depending on pH and azo content.^[25] A polypeptide containing a very low proportion (1.9 %) of azobenzene sulfonate units displayed a pH-dependent α -helix/coil transition, while a polypeptide containing 46 mol% azo units was random coil at any pH. Irradiation with UV light and the consequent *trans*→*cis* isomerization of the azo units did not induce any conformational changes for either polypeptide at any pH. In contrast, a polypeptide containing 9.3 mol% azobenzene sulfonate units exhibited remarkable conformational changes upon UV irradiation at appropriate pH values. At pH 4.3, irradiation produced a variation of the CD spectrum corresponding to a decline in the α -helical structure from 96 to 45 %.

The effect was explained on the basis that the change in geometry of the azo moieties, caused by their *trans*-*cis* photoisomerization, might produce an increase in the local charge density of the environment around the helical backbone, thus destabilizing the ordered structure.^[25] Unfortunately, the photoinduced conformational change was not reversible and the original structure could be not restored by irradiation at $\lambda > 390$ nm or upon dark-adaptation.

Cationic surfactants are known to affect the conformation of poly(L-glutamic acid). This suggested that it might be possible to combine the isomerization of the photochromic side chains with the surfactant effect to obtain an amplification of the photoresponse.^[26] This expectation was indeed substantiated upon irradiating 20% azo-modified poly(L-glutamic acid) (III) in the presence of the surfactant dodecyl ammonium chloride (DAC). CD spectra indicated that at pH 7.6, in the absence of surfactant, the polymer is completely random coil and not affected by irradiation. At the same pH, but in the presence of DAC below its critical micellar concentration, both the dark-adapted and the irradiated samples are α -helical. In the presence of surfactant at its critical micellar concentration, irradiation at 350 nm (*trans*→*cis* isomerization) induced an evident random coil→helix transition. The change was completely reversed when the sample was dark-adapted or irradiated at 450 nm (*cis*→*trans* isomerization). So, in the presence of DAC micelles, it is possible to photomodulate the polypeptide conformation by means of alternate exposure to light and darkness, or irradiation at two suitable different wavelengths.^[26]

The mechanism of the photoresponse was tentatively explained as follows. When azo units are in the planar, apolar, *trans* configuration, they merge into the hydrophobic core of the micelles, forcing the polypeptide chains to assume a coil conformation. Isomerization of the azo units to the skewed, polar, *cis* configuration inhibits hydrophobic interactions and causes the azo units to retreat from of the micelles, thus allowing the polypeptide chains to adopt the α -helix structure favored in the absence of micelles. In other words, the primary photochemical event is the *trans*-*cis* isomerization of the azobenzene

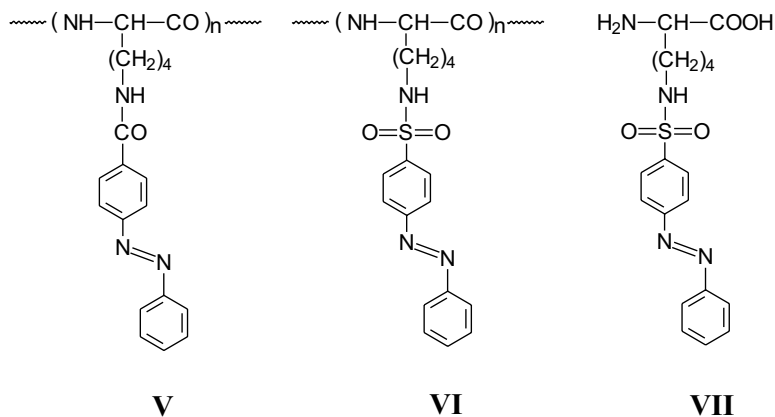
units, but the driving force of the coil/helix transition might be the different location of the macromolecules relative to the micelles.

An interesting analogous photoresponse effect has been reported for a partially esterified poly(L-glutamate) containing 13 mol% of azobenzene units in the side chains.^[27] The polypeptide was incorporated into the bilayer membrane of vesicles composed of distearyl dimethyl ammonium chloride. UV irradiation of the vesicles, and the consequent *trans-cis* isomerization of the azo units, caused a transfer of the polypeptide molecules from the hydrophobic interior to the hydrophilic surface of the bilayer membrane. This synthetic system mimics some biological photoreceptors, such as frog retinal membrane photopigments, which shift their location between the aqueous interface and the hydrocarbon core of the membrane, depending on whether the photopigment is experiencing irradiation or is in darkness.^[28]

13.2.1.3 Azobenzene-containing Poly(L-lysine)

The introduction of azobenzene units into the side chains of poly(L-lysine) has been achieved by means of various procedures and different azo reagents. The polymers described initially contained azobenzene units linked to the lysine side chains by means of an amide moiety^[29–31] (Scheme 4, Structure V). More recently, Fissi et al.^[32] have described azo-modified poly(L-lysine) in which the azobenzene units are linked to the Lys side chains by means of a sulfonamide function (Scheme 4, Structure VI). The two families of azo-modified poly(L-lysine) have been found to exhibit completely different conformational and photoresponsive behavior.

Polymers with various contents (20–90 mol%) of azobenzoyl-L-lysine residues (V) are soluble in hexafluoro-2-propanol (HFP), in which they exhibit very similar CD spectra, independent of their azo content. The dark-adapted samples (azo groups in *trans* configuration) display the α -helix CD pattern below 250 nm. Weak bands are also present in the range of wavelengths between 250 and 500 nm, arising from



Scheme 4 Chemical structures of poly(N ϵ -p-phenylazobenzoyl-L-lysine) (V), poly(N ϵ -p-phenylazobenzenesulfonyl-L-lysine) (VI), and N ϵ -p-phenylazobenzenesulfonyl-L-lysine (VII).

dissymmetric perturbation of the azo chromophores by the polypeptide chains. Alternating irradiation at 340 nm and 450 nm resulted in reversible changes in the CD bands above 250 nm, but did not produce any modification of the CD spectra in the peptide region (below 250 nm).^[29] When using a poly(L-lysine) containing 97 mol% azo moieties, Yamamoto and Nishida observed a decrease in the peptide region CD signal after long irradiation times (up to 4 hours) with a 400 W mercury lamp at 360 nm, but the CD signal change was not reversible.^[30] It may be concluded that, in HFP, light causes the *trans-cis* isomerization of the azo side chains, and hence reversible variation in the CD spectra above 250 nm, but that such isomerization does not produce any changes in the conformation of the macromolecular backbone.

Poly(L-lysine) containing azobenzene units linked to the side chains by means of a sulfonamide function (Scheme 4, Structure VI), was obtained by treating poly(L-lysine) with *p*-phenylazobenzenesulfonyl chloride. The poly(α -amino acid) was modified quantitatively; conversion to the azo-lysine units of VI was effectively 100%. The azo-modified polypeptide was soluble in HFP, in which it exhibited an intense photochromism attributed to the *trans-cis* photoisomerization of the azobenzene units. Like other sulfonated azobenzene compounds,^[33] azosulfonyl-modified polymers of L-lysine were found to be very stable in their *cis* form, and no thermal decay was observed at room temperature over periods of times as long as several weeks. Interconversion between the two forms at room temperature could only be effected by irradiation at appropriate wavelengths. This behavior allowed the authors to purify the *trans* and *cis* forms of the model compound N^E-azobenzenesulfonyl-L-lysine (VII) by chromatography, and to measure the absorption spectra of the two pure photoisomers.

Since the absorbance values of the pure *trans* and the pure *cis* isomers are known, the *trans-cis* isomeric composition at the photostationary state can be determined on the basis of the equations:

$$\text{trans isomer, \%} = \frac{A_{st} - A_{cis}}{A_{trans} - A_{cis}} \times 100 \quad (1)$$

$$\text{cis isomer, \%} = (1 - f_{trans}) \times 100 \quad (2)$$

where A_{st} is the absorbance of the sample at the photostationary state, A_{trans} and A_{cis} are the absorbances of the pure *trans* and the pure *cis* isomers, respectively, and f_{trans} and f_{cis} their molar fractions. In HFP, irradiation at 340 nm gave rise to the maximum degree of *trans*→*cis* photoconversion, the isomeric composition at the photostationary state containing 82% of the *cis* isomer. Irradiation at 417 nm produced the maximum yield for the opposite *cis*→*trans* back-reaction, the isomeric composition at the photostationary state containing 85% of the *trans* isomer. The photochromic cycles obtained by irradiating alternately at 340 and 417 nm were completely reversible.^[32]

Poly(L-lysine) containing azobenzenesulfonyl groups in the side chains (VI) was random coil in pure HFP, and the disordered conformation was not affected by

trans-cis photoisomerization of the azo side chains. However, when appropriate amounts of cosolvents such as methanol (MeOH) or 1,2-dichloroethane (DCE) were added to the HFP solution, the system was able to respond to light, giving rise to reversible variations of the polypeptide conformation. Figure 6 shows the CD spectra of poly(*p*-phenylazobenzenesulfonyl-*L*-lysine) in HFP/MeOH, at various solvent compositions. In pure HFP, the CD spectra are typical of random coil polypeptides both when the sample is irradiated at 340 nm (azo units in *cis* configuration) and when it is irradiated at 417 nm (azo units in *trans* configuration). At methanol concentrations higher than 15%, both samples exhibit the CD pattern of the α -helix. The intensity of the 222 nm CD band corresponds to the value measured in HFP solution for poly(*N*^e-carbobenzoxy-*L*-lysine) ($[\Theta]_{222} = -28,900$), which can be assumed as corresponding to 100% α -helix.^[11] At methanol concentrations in the range between 2 and 15%, alternating illumination at 340 and 417 nm produces photoinduced changes of the helical content, the extent of the photoresponse depending on the solvent composition. Photoinduced changes of helical structure of up to about 80% are observed at 8–10% methanol concentrations.

If the intensity of the CD band at 222 nm, which can be considered a function of the α -helix content, is plotted as a function of methanol concentration, it is observed that addition of methanol induces a coil \rightarrow α -helix transition in the macromolecular conformation (Figure 7). However, the amount of methanol needed to induce the conformational transition is different for the sample irradiated at 340 (*cis* azo units) and that irradiated at 417 nm (*trans* azo units). Therefore, two separate curves are observed for the two samples. At solvent compositions in the range between the two curves, alternating irradiation at 340 and 417 nm gives rise to folding or unfolding of the macromolecular chains. The photoresponse occurs only in a selected and nar-

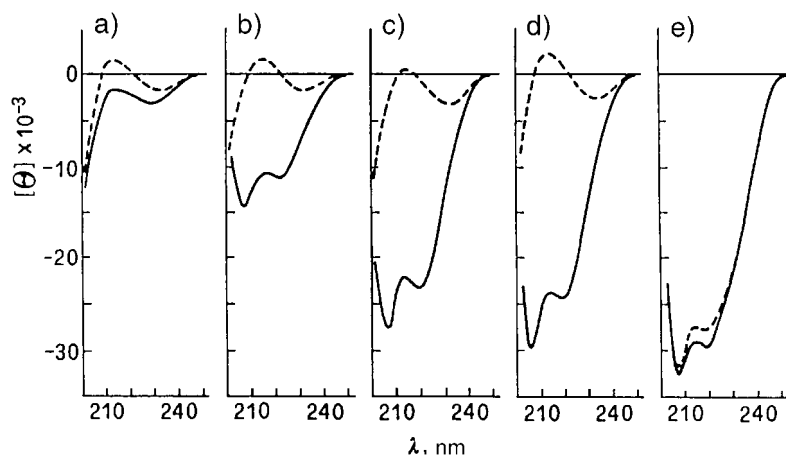


Fig. 6: CD spectra of poly(*N*^e-*p*-phenylazobenzenesulfonyl-*L*-lysine) (VI) in various HFP/MeOH solvent mixtures (v/v): a) 0%; b) 2%; c) 5%; d) 8%; e) 15%. Continuous line: kept in the dark or irradiated at 417 nm; dashed line: irradiated at 340 nm.

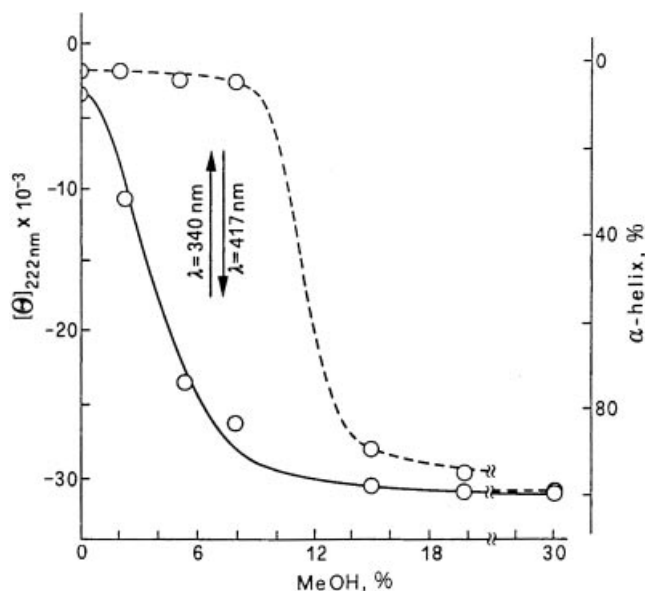


Fig. 7: Poly(N^{ϵ} -*p*-phenylazobenzenesulfonyl-L-lysine) (VI) in HFP/MeOH solvent mixtures: ellipticity at 222 nm and α -helix content percentage, as a function of methanol concentration, for samples irradiated at 417 (continuous line) and at 340 nm (dashed line).

row window of environment conditions, and therefore it can be defined as an example of *gated photoresponse*.^[34,35]

The different conformational behavior of the azobenzoyl- and the azobenzenesulfonyl-L-lysine polymers was explained on the basis that the monomeric units VI may interact with HFP differently than units V do (Scheme 4). The strongly protonating solvent HFP ($pK_a = 9.30$)^[36] is known to form electrostatic complexes with various organic compounds, including amines and dimethylsulfoxide;^[37] on the other hand, sulfonamides are significantly protonated in acid media;^[38] so it may be presumed that protonation and formation of electrostatic complexes can occur for azobenzenesulfonyl-L-lysine residues, as well. In HFP therefore, polypeptides of structure V can adopt the ordered α -helix structure, while polypeptides of structure VI should be forced by the electrostatic interactions arising from complexation with HFP to adopt a disordered conformation.

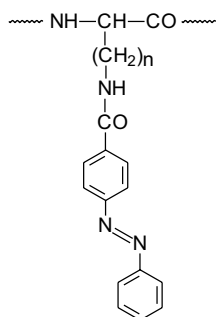
Of course, stability and formation of “HFP·azosulfonyl-Lys” complexes is less favored on going from pure HFP to HFP/MeOH or HFP/DCE solvent mixtures. At appropriate and critical solvent compositions, the formation of the electrostatic complexes described above might be favored or inhibited by the electronic situation of the azo moieties, which differs depending on whether they are in the apolar, conjugated *trans* form, or in the more polar, unconjugated *cis* form. In other words, the *trans-cis* photoisomerization of the azo units, which is the primary photochemical event, does not seem to be sufficient to induce appreciable variations of the back-

bone conformations. Indeed, no photoinduced conformational change is observed in pure HFP or at high MeOH concentrations. Under critical solvent conditions, the *trans-cis* photoisomerization of the azosulfonyl units **VI** should cause the protonation/deprotonation of the sulfonamide function, which should be the key factor responsible for photoregulation of polypeptide conformation.^[32]

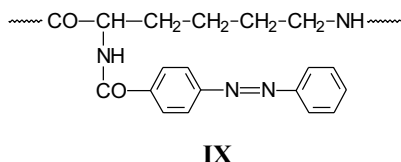
13.2.1.4 Azo-Modified Polypeptide Analogues of Poly(L-lysine)

Yamamoto et al. have investigated a series of photochromic polypeptides obtained by introducing azobenzene units into the side chains of poly(α -amino acid) homologues of poly(L-lysine), such as poly(L-ornithine),^[39,40] poly(L- α,γ -diaminobutanoic acid)^[41] and poly(L- α,β -diaminopropanoic acid)^[42] (Scheme 5, Structures **VIII**, $n = 1, 2, 3,$ and 4). This provided information about the photoresponse of azo-modified polypeptides in which the photochromic units are attached to the macromolecules through spacers of different lengths. The photochromic polymers were prepared by modification of the poly(α -amino acid)s with p-phenylazobenzoic acid in the presence of water-soluble carbodiimide. They were all soluble in hexafluoro-2-propanol (HFP), except for a sample of poly(L-ornithine) containing only a small proportion of azo groups (3%), which was soluble in water.

Polymers of poly(L-ornithine) possessing varying contents of azobenzene groups, from 20% up to almost 100% [Scheme 5, **VIII** ($n = 3$)], were found to be essentially α -helical in HFP when the samples were kept in the dark. The CD spectra also exhibited a couplet of bands centered at about 320 nm, attributed to electronic interactions between the azo side chains in the *trans* configuration. Irradiation at 360 nm and the consequent *trans*→*cis* photoisomerization, abolished the side chain CD



VIII ($n = 1, 2, 3$ and 4)



IX

Scheme 5 Chemical structure of azo-modified polypeptide analogs of poly(L-lysine), **VIII** ($n = 1, 2, 3,$ and 4) and **IX**.

bands and caused a remarkable reduction in helix content to about half of the original value. Irradiation at 460 nm caused a partial reverse photoconversion.^[39,40]

A sample of poly(L-ornithine) containing 48 mol% azo units was found to adopt the α -helix structure in HFP/water = 1/1. In this solvent mixture, however, irradiation at 360 nm followed by irradiation at 460 nm produced the *trans-cis* photoisomerization of the azo moieties, but did not induce any change of the backbone conformation. When the surfactant sodium dodecyl sulfate was added to the HFP/water solvent mixture, the CD spectrum displayed an intense side chain CD couplet and a negative band at about 225 nm which was assigned to the presence of a β -structure. The CD bands were almost completely abolished upon *trans*→*cis* photoisomerization.

A polymer of L- α,γ -diaminobutanoic acid almost quantitatively substituted with azobenzene units in the side chains [Scheme 5, VIII(n = 2)] was not completely soluble in HFP when the sample was kept in the dark. The initial, slightly turbid solution became clear on irradiation at 360 nm and the consequent photoconversion of the azo moieties from their *trans* to the *cis* configuration (for photosolubility effects see Section 13.2.3). The “*cis*” polymer was found to adopt an essentially random coil conformation. Exposure to 460 nm light and the consequent back-isomerization of the azo units to about 70/30 *trans-cis* isomeric composition gave rise to a reversible photoinduced change from random coil to α -helical structure (helix content, about 60%).^[41]

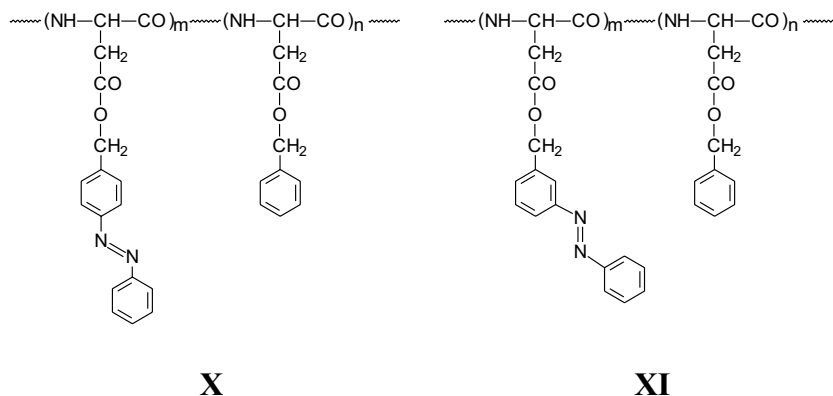
The analogous polymer obtained from L- α,β -diaminopropanoic acid [Scheme 5, VIII(n = 1)] displayed photochromic behavior similar to that observed for the other homologues. In this case, however, irradiation at 360 nm produced variations of the CD spectra in the peptide region, and associated irreversible structural changes in the macromolecules.^[42]

A photochromic polymer containing azobenzene units has also been prepared by modification of a naturally occurring microbial poly(ϵ -L-lysine) (Scheme 5, Structure IX), and investigated by means of absorption and circular dichroism spectroscopy.^[43] The structure of this polymer, however, does not correspond to those of polypeptides, which are poly(amide)s of α -amino acids, and therefore the results cannot be discussed in terms of the typical polypeptide structures (α -helix, β -structure, random coil) and their standard CD spectra.

13.2.1.5 Photoinduced Helix-sense Reversal in Azobenzene-containing

Poly(L-aspartate)s

Poly(L-aspartate)s are able to adopt helical structures of both left-handed and right-handed screw senses, the stability of the two helices depending on the chemical structure of the ester group in the side chains.^[44] Moreover, in poly(β -benzyl-L-aspartate), the presence of substituents such as chloro, methyl, or nitro groups on the benzyl ring results in helical polypeptides that may adopt either the left-handed or right-handed sense, depending on the position of the substituent.^[45] These results suggest that the energy difference between the two helical forms is relatively small. On the basis of these observations, Ueno et al. prepared a series of poly(L-aspartate)s containing azobenzene units in the side chains (Scheme 6), and investigated the



Scheme 6 Chemical structure of poly(β -L-aspartate)s with various contents of *para*- (X) and *meta*-phenylazobenzyl (XI) units in the side chains.

effect of photoisomerization and thermal isomerization of azo side chains on the macromolecular structure.^[46–49]

In 1,2-dichloroethane (DCE), polypeptides containing *para*-phenylazo-L-aspartyl residues (Scheme 6, Structure X) exhibited CD spectra characterized by a positive CD band at about 220 nm, indicative of the presence of a left-handed helical structure. When the azo content was less than 50 mol%, such bands were not affected by irradiation at 320–390 nm. This behavior was found to be quite different for two copolymers containing 59 and 81 mol%, respectively, of *para*-phenylazobenzyl-L-aspartyl residues: before irradiation these too displayed a positive band at 220 nm, but this became negative after irradiation. The change in sign provided evidence for a reversal of the helix sense, induced by the *trans-cis* photoisomerization of the azo units. Analogous polypeptides containing *meta*-phenylazobenzyl-L-aspartyl residues (Scheme 6, Structure XI) did not exhibit reversal of the 220 nm band upon irradiation, but merely a decrease in the intensity of the band, thus suggesting formation of appreciable amount of random coil structure.^[46–48]

Large photoresponse effects could be observed in solvent mixtures, provided that the irradiation was carried out at appropriate solvent compositions. A copolypeptide composed of 33 mol% β -benzyl-L-aspartate and 67 mol% *para*-phenylazo-L-aspartate (X) was found to give different kinds of photoresponse, depending on the composition of the solvent in which irradiation was carried out. In dichloroethane (DCE)/hexafluoropropanol (HFP) = 95/5, irradiation at 320–390 nm produced an increase in right-handed helix content; in DCE/HFP = 54/26, a light-induced conformational change from left-handed helix to random coil was observed; while, finally, reversal of the helix sense occurred in DCE/HFP = 65/35.^[50,51]

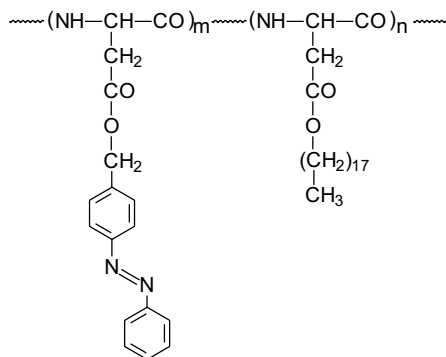
Two polymers respectively containing 8 and 10 mol% of *meta*-phenylazo-L-aspartyl residues (XI) were found to be left-handed helices in pure DCE, while existing as right-handed helices in pure trimethylphosphate (TMP). The inversion of the helix occurred at solvent compositions corresponding to 20–50% TMP concentration;

however the dependence of the helix sense on TMP concentration was different for the samples kept in the dark (azo units in *trans* configuration) and their irradiated counterparts (azo units in *cis* configuration). Accordingly, remarkable effects on CD spectra were observed when irradiation was carried out in the 20–50% TMP concentration range. Particularly in mixed solvent containing 25–30% TMP, irradiation produced an inversion of the CD band at 222 nm, indicating a drastic conformational change from left-handed to right-handed helix, even for polypeptides containing only small proportions of photochromic units.^[52–54]

More recently, Ueno et al. have prepared and investigated a new series of copolymers containing *p*-phenylazobenzyl-L-aspartate and *n*-octadecyl-L-aspartate residues (Scheme 7, Structure XII).^[55,56] In the case of copolymers containing less than 50 mol% azo residues, the CD spectra at 25 °C were consistent with the presence of right-handed helical conformations, which were not affected by irradiation at 320 nm. In contrast, in the case of copolymers containing 68 and 89 mol% azobenzene groups, irradiation caused the reversal of helix sense from the left-handed to the right-handed form.

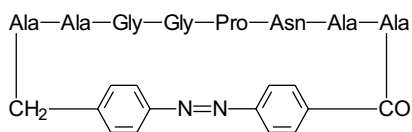
The conformations of these polypeptides were strongly dependent on temperature, so more remarkable photoresponse effects could be obtained if irradiation was carried out at appropriate azo contents and temperature conditions. A copolymer containing 47 mol% azo units, which was not affected by light at 25 °C, was found to undergo a photoinduced helix reversal when irradiation was carried out at 60–70 °C. The authors concluded that octadecyl side chains are likely to change the orientation of their array simultaneously with the photoinduced structural changes of the main chains, so the system provides an example of environmental change induced by light.

Investigation of light-induced conformational changes has also been extended to solid films of azobenzene-containing poly(L-aspartate)s, but no conformational change was induced by photoisomerization of the azobenzene units. This was probably due to the limited mobility of the polypeptide chains in the films.^[57]



XII

Scheme 7 Chemical structure of copolymers containing *p*-phenylazobenzyl-L-aspartate and *n*-octadecyl-L-aspartate residues (XII).^[55,56]



XIII

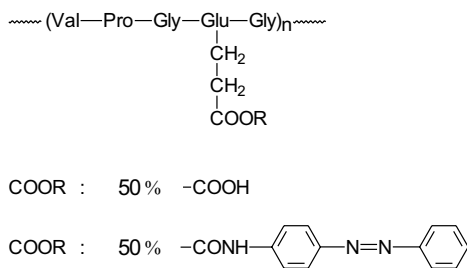
Scheme 8 Chemical structure of the photochromic cyclic peptide XIII.^[58]

13.2.1.6 Other Photochromic Polypeptide Systems

Other photochromic polypeptide systems have been described, in which the ability to photocontrol the specific conformation of polypeptides is an essential feature in the design of biomaterials for devices that can be photoswitched.

Photoregulation of conformation has been reported to occur in the cyclic peptide XIII, which incorporates an azobenzene moiety as an internal switch (Scheme 8).^[58] When the azobenzene linkage was in the *trans* configuration (samples kept in the dark), the peptide exhibited an elongated, even though cyclic, configuration. When the azo linkage was photoisomerized to the *cis* form (samples irradiated at 310–410 nm), the peptide adopted a “ β -turn” structure characterized by a strongly reduced area of the cycle.

The azo-modified, elastin-like polypeptide XIV illustrated in Scheme 9 exhibits a so-called “inverse temperature transition”: that is, the compound gives cross-linked gels that remain swollen in water at temperature below 25 °C but deswell and contract upon a rise of temperature. The *trans-cis* photoisomerization of the azo units, obtained through alternating irradiation at 350 and 450 nm, permits photomodulation of the inverse temperature transition.^[59] The result indicates that attachment of a small proportion of azobenzene chromophores is sufficient to render inverse temperature transition of elastin-like polypeptides photoresponsive, and provides a route to protein-based polymeric materials capable of photomechanical transduction.



XIV

Scheme 9 Chemical structure of the modified, elastin-like poly (pentapeptide) XIV, found to exhibit photomodulated inverse temperature transition.^[59]

13.2.2

Sunlight-induced Conformational Transitions in Spiropyran-containing Polypeptides

13.2.2.1 Spiropyran-modified Poly(L-glutamate)s

As mentioned in Section 13.1 (see Figure 1), photochromism of spiropyran compounds involves two photoisomers, the neutral spiro form and the zwitterionic merocyanine form, characterized by large differences in geometry and polarity. Their interconversion was consequently found to cause large structural changes in attached macromolecules. In polypeptides containing azobenzene units, the generation of *cis* and *trans* isomers, and thus photoregulation of conformation, required artificial UV light sources. Spiropyran compounds, in contrast, respond to visible light, so their introduction into polypeptide macromolecules has allowed the obtainment of photoresponsive polymers with macromolecular structures that can be modulated upon exposure just to sunlight.

Poly(L-glutamate)s containing various molar percentages of spiropyran units in the side chains (XV) have been prepared by treating poly(L-glutamic acid) with *N*-(2-hydroxyethyl)-spiropyran in the presence of dicyclohexylcarbodiimide and 4-pyrrolidino-pyridine.^[60-62] The structure and photochromic behavior of the modified polymers are shown in Figure 8.

The polymers are soluble in hexafluoro-2-propanol (HFP), in which they exhibit reverse photochromism: photochromic behavior opposite to that usually observed in most common organic solvents (see Figure 1). At room temperature in the dark, they give colored solutions, due to the presence of the merocyanine form. Irradiation with visible light, or simple exposure to sunlight, causes the complete bleaching of the solutions, because of formation of the colorless spiro form. The back-reaction occurs in the dark and the original color is reversibly recovered. The reverse photochromism is likely to be due to the very polar solvent HFP, which stabilizes the charged merocyanine form more than it does the apolar spiro form.

Figure 9 shows the effect of light on the absorption spectra of a poly(L-glutamate) containing 85 mol% photochromic units in the side chains. The spectrum of the

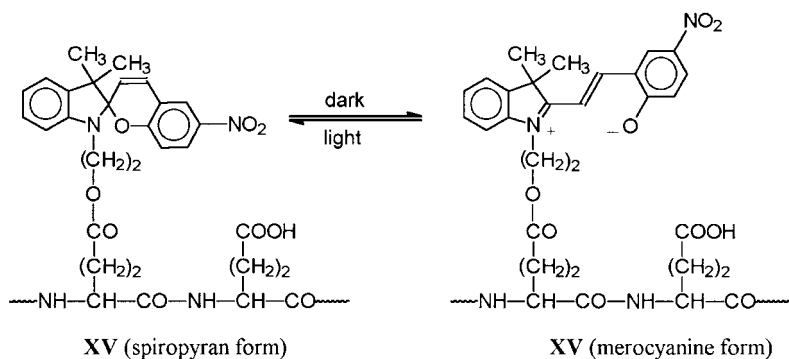


Fig. 8: Structure and reverse photochromic reactions (in hexafluoro-2-propanol) of poly(L-glutamic acid) containing spiropyran units in its side chains (XV).

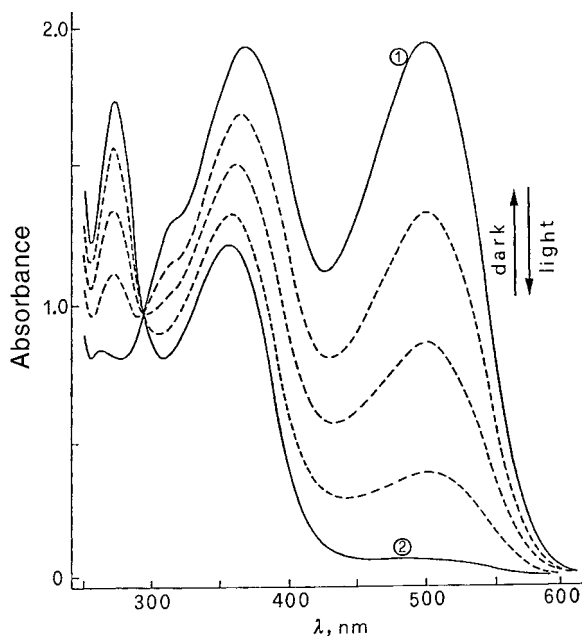


Fig. 9: Absorption spectra of poly(L-glutamic acid) containing 85% spiropyran units, in HFP: 1) sample kept in the dark; 2) exposed to sunlight; dashed lines: intermediate spectra during decay in the dark.

colored solution kept in the dark exhibits two intense bands at 500 and 370 nm, due to the presence of the merocyanine species. Irradiation with visible light (500–550 nm) or exposure to sunlight cancels the intense band in the visible region and produces the spectrum corresponding to the spiro form, characterized by absorption maxima at 355 and 272 nm. On dark-adaptation, the original spectrum is progressively restored, the spectra monitored over time passing through an isobestic point at 295 nm.

The photochemical reaction is very fast: indeed, exposure to sunlight for a few seconds is enough to produce the full conversion of the merocyanine to the spiro form. The back-reaction in the dark is much slower: it takes about 150–250 minutes for the various polymers to regain half of the original absorbance.^[60,61] The photochromic cycles seem to be completely reversible. It is likely that irradiation with low-energy visible light (reverse photochromism) instead of high-energy UV light (normal photochromism) would limit unwanted photochemical side reactions and consequent *fatigue* phenomena.

The structures of spiropyran-modified poly(L-glutamate)s are strongly affected by light or dark conditions, as demonstrated by the CD spectra in Figure 10. Before irradiation, the colored solutions show the CD spectrum of a random coil conformation. After exposure to sunlight, the colorless solutions display the typical CD pattern of the α -helix, thus indicating that the isomerization of the side chains causes a transition from coil to helix in the polypeptide chains. The photoinduced conforma-

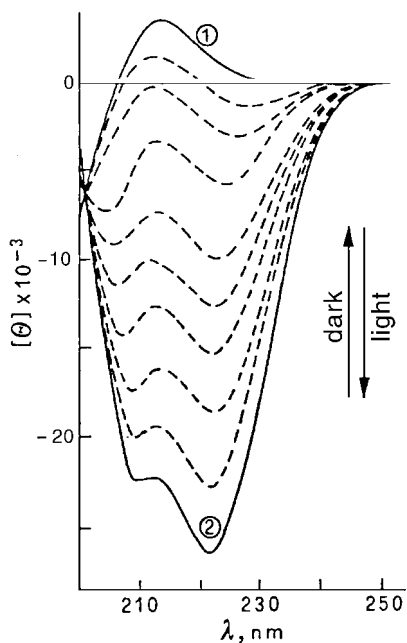


Fig. 10: Effect of irradiation and dark-adaptation on CD spectra of poly(L-glutamic acid) containing 85 mol% spiropyran units, in HFP: **1**) Kept in the dark; **2**) exposed to sunlight; dashed lines: intermediate spectra during decay in the dark over 8 h.

tional variations are fully reversible: on dark-adaptation, the helix content progressively decreases and the original disordered conformation is restored.

On the basis of fluorescence measurements, the driving force responsible for the photoinduced conformational change was attributed to interactions between the photochromic side chains, which differ depending on whether they are in the zwitterionic merocyanine form or the apolar spiro form. In the dark, the merocyanine units have a strong tendency to give dimeric species; as a result the macromolecules are forced to adopt a disordered structure. When the side chains are photoisomerized to the spiro form, such dimers are destroyed, and the macromolecules assume the helical structure.^[63]

Cooper et al. have investigated the kinetics of the helix-to-coil reaction in the dark for a polypeptide containing 33 mol% spiropyran units. CD and FTIR were used, together with molecular dynamics simulation.^[62,64] The polypeptide was found to undergo a slow transition according to the mechanism “helix / solvated-helix / coil”. During the “helix / solvated-helix” step, approximately 25% of the α -helix hydrogen bonding broke and new hydrogen bonds formed between the unmodified carboxylic and the merocyanine groups. No changes in carboxylate hydrogen bonding were observed during the “solvated-helix / coil” step and the breakup of the helix.^[62]

13.2.2.2 Photoresponsiveness of Poly(spiropyran-L-glutamate) under Acidic Conditions

Quite interesting photoresponsive behavior was observed when spiropyran-modified poly(L-glutamate) was dissolved in HFP and a small amount of trifluoroacetic acid

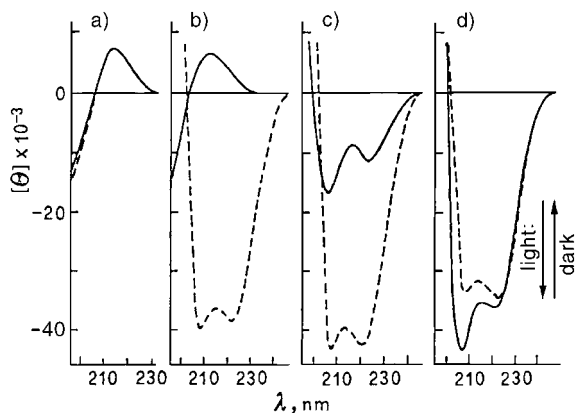


Fig. 11: Poly(L-glutamic acid) incorporating 85 mol% spiropyran units in the side chains. Effect of irradiation on CD spectra in various HFP/MeOH solvent mixtures in the presence

of trifluoroacetic acid (TFA, $c = 5 \times 10^{-4}$ g/ml). MeOH: a) 0–5%; b) 10%; c) 20%; d) 40%. Continuous line: dark-adapted; dashed line: irradiated samples.

(TFA, $c = 5 \times 10^{-4}$ g/ml) added.^[61] In the presence of acid, photoisomerization of the photochromic side chains did not result in any conformational change in the macromolecular main chains, and CD spectra showed that the macromolecules were random coils both in the dark and after light exposure. However, when appropriate amounts of methanol were added as a cosolvent, the system again responded to light, giving random coil \rightarrow α -helix transitions.

The effect of light on CD spectra at various solvent compositions, for a polymer containing 85 mol% spiropyran units, is shown in Figure 11. When methanol concentration is below 5%, both the dark-adapted and the irradiated samples show the typical CD pattern of disordered polypeptides. In HFP/MeOH = 90/10, the sample kept in the dark is random coil, whereas the sample exposed to light displays the standard CD pattern of the α -helix. The intensity of the bands indicates that under these conditions light causes the full conversion from random coil to 100% α -helix. With increasing methanol con-

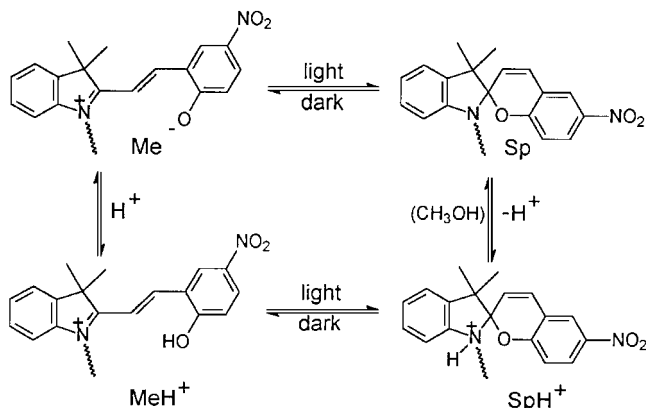


Fig. 12: Photochromic reactions of spiropyrans under acidic conditions.

centration, the dark-adapted sample also becomes partially helical, and finally, when the proportion of methanol is higher than 40%, both the dark-adapted and the irradiated samples are fully helical. It clearly appears that the photoinduced structural changes depend on solvent composition, and thus that photoresponse can be modulated by combined action of light and chemical environment.

The mechanism of photoresponse has been interpreted on the basis of the chemical reactions illustrated in Figure 12.^[61] In HFP acidified by addition of TFA, spiro-*pyran* compounds are present as protonated merocyanine MeH^+ . Exposure to light converts the species MeH^+ into the ring-closed spiro species SpH^+ . In the presence of acid, therefore, the photochromic side chains are present as cationic species both in the dark and in light. In both cases, the repulsive electrostatic interactions among the charged side chains force the macromolecules to adopt an extended random coil structure, and so no photoinduced conformational change resulting from photoisomerization is observed.

When appropriate amounts of methanol are added to the HFP solution, the protonated dark-adapted species MeH^+ is not altered, but the equilibrium between protonated and unprotonated spiro units present in the irradiated solution is shifted toward the neutral form. Under these conditions, the photochromic species in the side chains are charged in the dark-adapted form but neutral in the light, so irradiation induces α -helix formation, as it does in acid-free HFP. The formation of α -helices even in the dark-adapted samples at high methanol concentrations may be due to the same effect as observed with other poly(α -amino acid)s with ionic side chains, such as poly(sodium L-glutamate)^[65] and poly(L-lysine hydrochloride),^[66] which are random coils in water but becomes helical upon addition of excess methanol. Such an effect seems to be due to the ability of methanol to favor “contact ion pairs” between polymer charges and counterions, thus providing a shielding effect among the charged side chains and stabilizing the helical structure.^[65,66]

13.2.2.3 Spiropyran-modified Poly(L-lysine)

Polymers of L-lysine containing spiro-*pyran* units in the side chains (**XVI**) (Figure 13) were found to show photochromic behavior in HFP analogous to that already

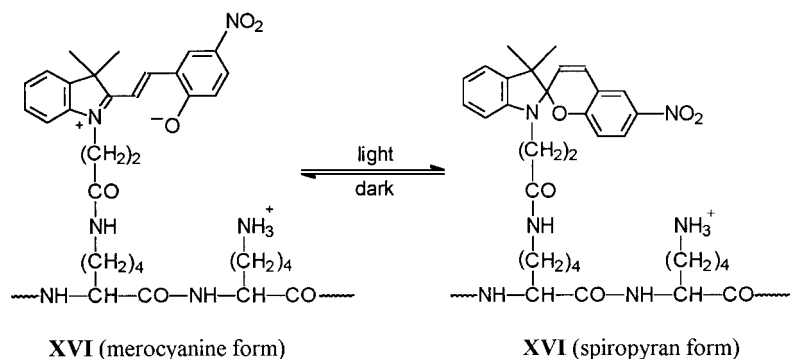


Fig. 13: Reverse photochromic reactions of spiro-*pyran*-modified poly(L-lysine) (**XVI**) in hexafluoro-2-propanol.

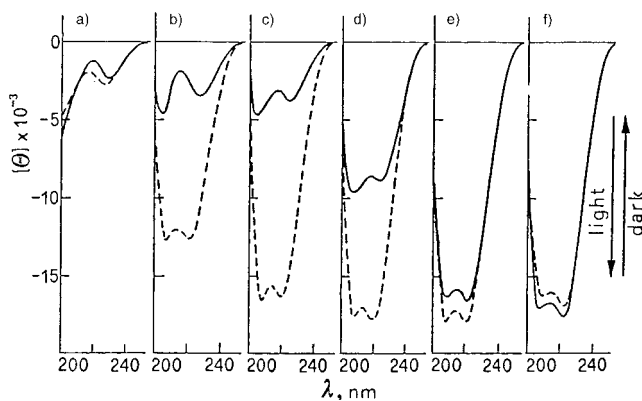


Fig. 14: Poly(L-lysine) containing 46 mol% spiropyran units (**XVI**). Effect of irradiation on CD spectra in various HFP/ NEt_3 solvent mixtures. NEt_3 : a) 3%; b) 6%; c) 8%; d) 10%; e) 13% and f) 16%. Continuous line: dark-adapted; dashed line: irradiated samples.

described for spiropyran-modified poly(L-glutamates). Conformational and photoresponsive behavior was quite different, however.^[67,68]

In fact, while spiropyran-modified polymers of L-glutamic acid undergo coil \rightarrow α -helix transitions upon exposure to light, analogous L-lysine polymers do not produce light-induced conformational changes in pure HFP; their structure is always random coil, whether the samples are kept in the dark or exposed to light. This different conformational behavior is likely to be due to the unmodified lysine side chains, which are probably protonated by the acidic HFP solvent. As a result, the macromolecules are essentially polycations, which adopt extended coil conformations not affected by the photoisomerization of their photochromic units. However, when appropriate amounts of triethylamine (NEt_3) are added to the HFP solutions, the system again shows a response to light, giving coil \rightarrow α -helix conformational changes.^[67,68]

Figure 14 shows the effect of light on CD spectra of poly(L-lysine) modified with 46 mol% spiropyran side chains, in various HFP/ NEt_3 solvent mixtures. When the triethylamine concentration is lower than 3%, both the dark-adapted and the irradiated samples are essentially random coils. At NEt_3 concentrations higher than 16%, both the samples exhibit the CD pattern of the α -helix. At NEt_3 concentrations in the range between 3% and 16%, alternate exposure to light or dark conditions produces reversible variation of the helix content, the extent of the photoresponse depending on triethylamine concentration. The intensities of the CD bands correspond to photoinduced variation of helical structure of up to about 60%.^[11,13]

When the intensity of the 222 nm CD band, also a parameter of the helix content, is plotted as a function of triethylamine concentration, it can be observed that triethylamine induces a transition from coil to helix in the polypeptide chains (Figure 15). The most remarkable aspect is that the amount of NEt_3 needed to induce the transition is different for the dark-adapted sample and the illuminated one. Two separate curves are hence observed: exposure to light and darkness conditions at solvent compositions in the range between the two curves produces reversible

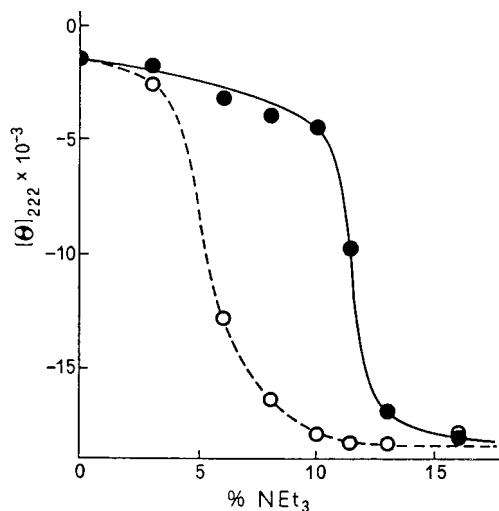
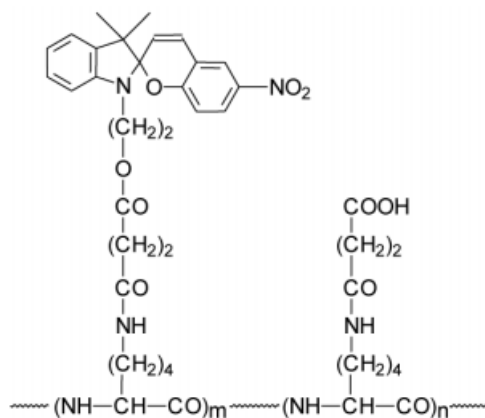


Fig. 15: Poly(L-lysine) containing 46 mol% spiropyran units (XVI) in HFP/NEt₃. Variation of ellipticity at 222 nm as a function of triethylamine concentration for the sample kept in the dark (continuous line) and after irradiation (dashed line).

photoinduced conformational changes. The system described is an example of a photoresponsive system displaying a *gated photoresponse*,^[34,35] in the sense that the photoisomerization of the side chains is able to trigger the macromolecular chain coil→helix transition only in a narrow “window” of environmental conditions.

The role of triethylamine is not clear. One possible effect could be the removal of protons from the unmodified amino side chains. Under these conditions the macromolecular conformation might be controlled by isomerization of the photochromic groups, as occurs in poly(spiropyran-L-glutamate). Alternatively, the system might behave like other polypeptides that are random coils in pure solvents such as dimethyl sulfoxide or dichloroacetic acid, but become helical in a mixture of the two solvents.^[69] The effect was attributed to the formation of a complex system between the solvent components, somehow decreasing their ability to solvate the polypeptide chain and therefore favoring the coil/α-helix transition. For the system of interest, mixing of HFP and triethylamine was indeed found to be strongly exothermic, and definite evidence for formation of a HFP·NEt₃ salt complex is reported in the literature.^[37] Anyway, the concentration of salt complex, and therefore the amount of triethylamine needed to allow the formation of the α-helix structure should be different for the dark-adapted sample and for the irradiated one, thus explaining the occurrence of two separate curves (Figure 15).

To determine the maximum range of correlation between side chain photochromism and polypeptide conformation change, Cooper et al. modified the carboxylate groups of succinylated poly(L-lysine) with a spiropyran to form the polypeptide XVII, with the structure shown in Scheme 10.^[70] The extent of modification was determined to be 35%. The length of the spacer group between the polypeptide α-carbon atom and the dye molecule was 12 atoms, resulting in minimal polypeptide-dye interaction. Study of the polypeptide demonstrated that the length of the spacer group was a significant factor influencing possible photoinduced conformational



XVII

Scheme 10 Chemical structure of the polypeptide obtained after introducing spiropyran units into the side chains of succinylated poly(L-lysine) (XVII).^[70]

changes. CD measurements carried out in hexafluoro-2-propanol/trifluoroethanol solvent mixtures indicated that light-induced conformational changes occurred only at a critical solvent composition, more specifically, near the midpoint of the solvent-induced transition from helix to coil.^[70]

13.2.3

Photostimulated Aggregation-disaggregation Effects

Azo-modified polypeptides have been reported to undergo reversible aggregation-disaggregation processes upon exposure to or shielding from light.^[71] Samples of azo-modified poly(L-glutamic acid) (Scheme 3, Structure III) stored in the dark or irradiated at 450 nm (azo units in *trans* configuration) showed variations of their CD spectra on aging in trimethylphosphate/water solution. The CD time dependence was characterized by progressive distortions of the α -helix pattern, typical of those produced by formation of aggregates of polypeptide chains. Formation of aggregates was also accompanied by a progressive increase in light-scattering intensity. Irradiation at 360 nm (*trans*→*cis* isomerization) at any aging time resulted in the abolition of light-scattering and the full restoration of the initial CD spectra, thus indicating dissociation of the aggregates. The spectra reverted once more to the distorted forms after irradiation at 450 nm or dark-adaptation of the samples, thus confirming the reversibility of the process.^[71]

Investigation of poly(L-glutamic acid) containing a high proportion of azobenzene side chains (more than 80%) provided confirmation of photoinduced aggregation-disaggregation processes, together with significant photosolubility effects.^[72,73] The dark-adapted polypeptide was soluble in hexafluoro-2-propanol (HFP), in which it assumed the α -helix structure. Addition of a small amount of water (15% by volume) to the HFP solution caused formation of aggregates, followed by the total and quantitative precipitation of the polymer as a yellow material. Irradiation of this

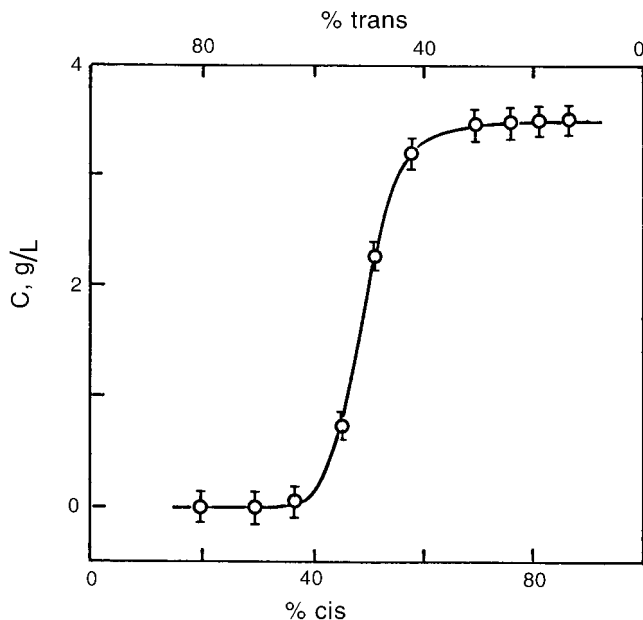


Fig. 16: Poly(L-glutamic acid) containing 85 mol % azobenzene units (III). Change in solubility in HFP/water = 85/15 as a function of the *trans-cis* isomeric composition of the azo side chains.

suspension for a few seconds at 350 nm caused the complete dissolution of the polymer, while irradiation of the solution at 450 nm once more induced polymer precipitation. In this solvent mixture, therefore, the “precipitation-dissolution” cycles were controllable by means of irradiation at the two different wavelengths.

Irradiation experiments carried out with light of various wavelengths permitted the dependence of the polymer solubility on the *cis/trans* isomeric composition of the azobenzene side chains to be measured.^[73] The results are illustrated in Figure 16. Polymer solubility as a function of azobenzene side chain *cis/trans* ratio is described by a sharp sigmoidal curve: the polymer is completely insoluble when more than 60% azo groups are in the *trans* configuration; in contrast, the maximum degree of photosolubilization is achieved when more than 60% of azo groups are in the *cis* configuration. The location of the midpoint of the transition corresponds to 50/50 *trans-cis* isomeric composition.

Similar photosolubility effects have been observed for azo-modified poly(L-ornithine) [Scheme 5, VIII ($n = 3$)]^[39] and poly(L- α,β -diaminopropanoic acid) [Scheme 5, VIII ($n = 1$)]^[42] monitoring transmittance at 650 nm as a function of irradiation time. The initially turbid samples in HFP/water became clear upon irradiation at 360 nm as a consequence of the *trans*→*cis* isomerization. On new irradiation at 460 nm, the clear solutions became turbid once more as a consequence of the reverse *cis*→*trans* isomerization of the azo chromophores.

These photoinduced variations in solubility could in principle be a consequence of the higher polarity of the azobenzene group *cis* isomer, with respect to the *trans* form. Indeed, the dipole moment in azobenzene has been reported to be 3.0–3.1 D for the *cis* isomer, and 0.0–0.5 D for the *trans* isomer.^[74] If the higher polarity of the *cis* isomer were the decisive factor causing the dissolution, polymer solubility should gradually increase with increasing *cis* content. However, the variation in solubility as a function of the *trans-cis* isomeric composition was described by a sharp sigmoidal curve typical of a phase transition.^[73] Therefore, the photosolubility effect was interpreted in terms of supramolecular association, through hydrophobic interactions and stacking of azobenzene side chains. When azobenzene moieties are in the planar *trans* configuration, hydrophobic interactions and stacking between the azo groups are favored, and so aggregation and precipitation occur. When the azo moieties are photoisomerized into the skewed *cis* configuration, interactions and stacking between azo groups are inhibited, so disaggregation of the macromolecules takes place, and polymer dissolution occurs.

Photostimulated polymer precipitation and dissolution may find application in photoresist technology.^[75,76] It may be also relevant to some molecular mechanisms responsible for photoregulated processes in biology. It is interesting here to compare the photostimulated aggregation changes described above with the photobehavior of the natural photoreceptor phytochrome. This photochromic protein exists in two forms – *Pr* (red absorbing phytochrome) and *Pfr* (far red absorbing phytochrome) – which are interconvertible by light. In nonirradiated tissue, phytochrome present as the inactive *Pr* form is uniformly distributed throughout the cytoplasm and the pigment is soluble upon extraction in aqueous buffers. Photoconversion into the active *Pfr* form (irradiation at 660 nm) results in a rapid association of the previously soluble pigment and formation of a pelletable material localized on the membrane. Reconversion into the *Pr* form (irradiation at 730 nm) results in the disaggregation and resolubilization of the pigment molecules.^[77,78]

13.3

Photoeffects in Molecular and Thin Films

13.3.1

Photomechanical Effects in Monolayers

Investigation of photoresponsive systems in the monolayer state formed at water/air interfaces can provide information about photoinduced structural changes of individual molecules, occurring in two-dimensional systems. Reversible photoinduced changes in either surface pressure or surface area of the monolayers have been observed. Therefore, these investigations are of increasing interest in the design of nanostructured systems, and may also be important as energy conversion media, from light to mechanical work. Here we report examples of photoresponsive thin films obtained from polypeptide polymers.

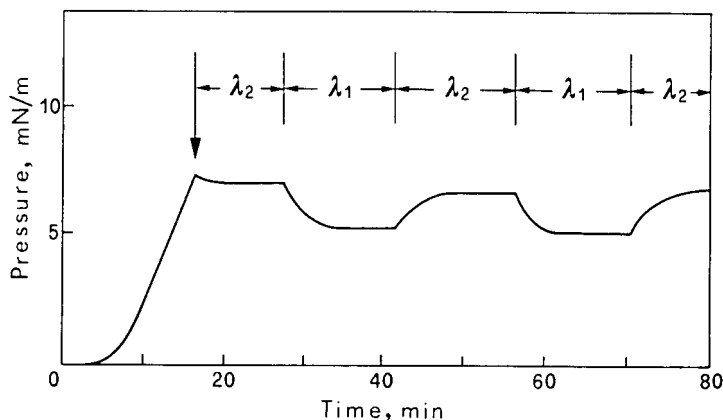
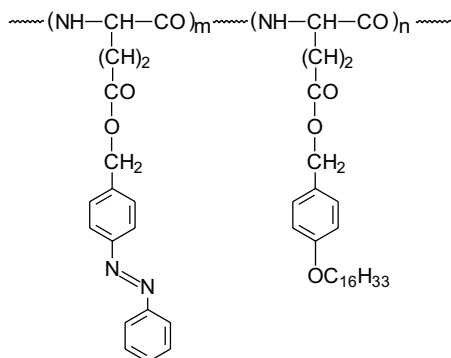


Fig. 17: Reversible surface pressure changes in a monolayer of poly(L-lysine) containing 43 mol% *p*-phenylazobenzoyl units (Scheme 4, structure V). The monolayer at the water/air interface was first compressed to 7 mN m^{-1} , then kept at constant area and illuminated alternately with 365 nm (λ_1) and 450 nm (λ_2) radiation.

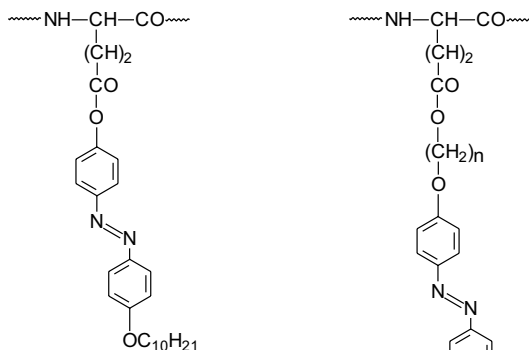
Poly(L-lysine) V, containing about 40 mol% of *p*-phenylazobenzoyl units, was reported to form a stable monolayer at a water/air interface.^[79] When the polypeptide monolayer was kept at a constant area, irradiation at 365 nm produced a decrease in the surface pressure, which reversibly reverted to its original value upon irradiation at 450 nm (Figure 17). At constant pressure, alternating irradiation with 365 and 450 nm light produced reversible changes in the surface area of the monolayer.

IR spectra of specimens prepared from monolayers using the folding frame described by Malcolm^[80] were typical of oriented α -helices, with parallel dichroism of the amide A (3300 cm^{-1}) and amide I (1652 cm^{-1}) bands, and perpendicular dichroism in the amide II band (1545 cm^{-1}). The result was independent of whether the specimen had been prepared from monolayers illuminated with 450 nm light (azo units in *trans* configuration) or with 365 nm light (azo units in *cis* configuration). This evidence suggests that the polymer does not undergo a conformational change upon irradiation in the monolayer state. The photomechanical effects seem simply to be due to *trans-cis* isomerization of the azobenzene groups, which occupy different areas in the interface when in the different configurations. Moreover, the *cis* form is significantly more polar than the *trans* form and should therefore be more attracted to the water phase.

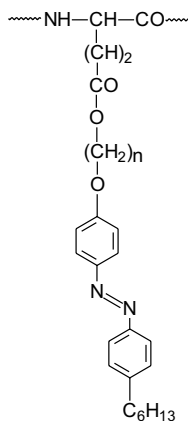
Menzel^[81] more recently described the properties and behavior of monolayers prepared from azobenzene-containing poly(L-glutamate)s possessing the structures XIX and XX ($n=2$) shown in Scheme 11. These monolayers showed photomechanical effects opposite to those described above for azo-modified poly(L-lysine)s. In fact, they expanded when exposed to UV light (*trans*→*cis* isomerization), and shrank when exposed to visible light (*cis*→*trans* isomerization). The expansion was found to be smaller than expected from comparison of the monolayer isotherms obtained from irradiated and nonirradiated solutions. This was attributed to the *trans-cis* photoconversion of the azo units, which occurs with lower yields in monolayers



XVIII



XIX

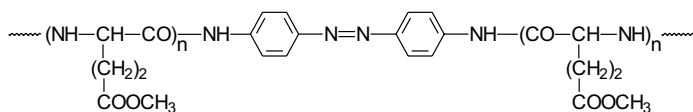


XX(n=2, 4 and 6)

Scheme 11 Chemical structure of “hairy rod” poly(L-glutamate)s used to obtain photochromic monolayers and Langmuir–Blodgett films.^[81,85–91]

than in solution. The nature and extent of photomechanical effects depend strongly on parameters such as subphase temperature and surface pressure, and is also very sensitive to the structure of the polymers.

Higuchi et al.^[82] have prepared an interesting photoresponsive polypeptide consisting of two α -helical chains of poly(L-glutamate) of $M_w = 11,000$, linked by an azobenzene moiety (Scheme 12, **XXI**). Monolayers of the polypeptide were formed at



XXI

Scheme 12 Chemical structure of the polypeptide **XXI**, consisting of two α -helical chains of poly(γ -methyl-L-glutamate) ($M = 11,000$) linked by an azobenzene unit.^[82]

water/air interfaces and the photoresponsive behavior of the monolayer was investigated. The *trans*→*cis* photoisomerization, and the consequent change in geometry of the azobenzene chromophore, produced a bending of the main chain of the molecule. As a result, a contraction in the area of the monolayer was observed. On the basis of the decrease in the limiting area per molecule, it was estimated that the bending angle between the two α -helical rods produced by irradiation with UV light was about 140°.

Photomechanical effects have been also observed in monolayers obtained from poly(L-glutamic acid) modified with carbocyanine^[83] and spiropyran dyes.^[84] In the latter case, irradiation at 254 nm produced changes in the molecular conformation, which in turn caused photomodulation of the surface pressure and surface area of the films. From all these examples, it appears that photoresponsive monolayers are quite fascinating systems, which may eventually come to be regarded as “a machine to transform light into mechanical energy”.^[81]

13.3.2

Photoresponsive LB and Thin Films

Langmuir-Blodgett (LB) films and polymeric liquid crystals have been intensively investigated for applications in optical data storage and the design of photoswitchable devices. In these photoresponsive systems, azobenzene units are usually the working units undergoing *trans-cis* photoisomerization, thus inducing reversible molecular orientation processes.

A wide and in-depth study of LB films of photochromic polypeptides has been carried out by Menzel et al.^[85–91] The authors prepared poly(L-glutamate)s bearing azobenzene units in the side chains, with alkyl spacers as well as tails of different lengths (Scheme 11). The polymers have a so-called “hairy rod” structure – that is, a rigid, rod-like helical backbone with flexible side chains^[92] – and are characterized by a molecular architecture appropriate so as to exhibit liquid-crystalline behavior and surface activity. They can be spread at a water/air interface, to form monomolecular films which can be transferred to substrates using the Langmuir-Blodgett technique. The resulting films were found to be very stable and homogeneous, built up of macromolecules arranged in layers, with the main chains preferentially oriented in the dipping direction, and the photochromic azo side chains preferentially oriented normal to the surface.^[88,91]

Irradiation with UV light ($\lambda = 360$ nm) causes the photoisomerization of the azobenzene chromophores and a concomitant structural change within the LB films. The preferred orientation of the main chains is retained, but the layered structure of the azobenzene moieties between the layers of the stiff poly(L-glutamate) rods is lost, as shown by X-ray reflectivity experiments and absorption spectroscopy. The very good transfer properties and the structural alterations upon irradiation indicate that the described LB films may be promising materials in optical switching and image recording technologies.^[91]

LB films of hairy-rod azo-poly(L-glutamate)s [Scheme 11, compounds XIX and XX ($n = 2$ and 6)] have been used to prepare photoresponsive waveguides.^[93] These

waveguide LB films have a highly optically anisotropic structure when the azo moieties are in the *trans* configuration, while exhibiting an essentially optically isotropic structure when the azo molecules are in the *cis* configuration. Accordingly, it was shown that the refractive index could be reversibly switched by irradiating the films with light of appropriate wavelengths. A perfect “on/off” switching of the optical anisotropy was observed on irradiating alternately at 360 nm (*trans*→*cis* isomerization) and 450 nm (*cis*→*trans* isomerization). The change in optical parameters between the isotropic and anisotropic states was found to be of one order of magnitude.^[93]

Poly(L-glutamate)s with photochromic azobenzene side groups possessing the structure illustrated in Scheme 11 were found to be thermotropic.^[94] They form LB multilayer assemblies in which the rod-like macromolecules are oriented in the dipping direction. The initial LB films have a well defined bilayer structure, in which the rod-like azobenzene moieties are tilted toward the α -helical backbones and form H-aggregates. Aggregation and orientational order of the azobenzene chromophores were found to change upon irradiation and annealing. The lamellar order and in-plane anisotropy of the chromophores were irreversibly lost on UV irradiation. New, ordered structures with a more symmetrical distribution of the side chains around the main chain helix, modified spacing, changed aggregation, and different in-plane anisotropy were established after subsequent visible irradiation or annealing. The system permits photochemical modification of aligned supramolecular structures in liquid crystalline polymers.

Sekkat et al.^[95] have investigated the photobehavior under polarized light of spin-coated films obtained from a hairy-rod poly(L-glutamate) with azobenzene in the side chains (Scheme 11, compound XIX). It is known^[96,97] that, in the presence of a linearly polarized pump light beam, azo molecules experience a cycle of photoisomerization reactions and align themselves perpendicularly to the pump beam polarization direction. For the above polypeptide it was shown that, in the *trans*→*cis* photoisomerization cycle, the created *cis* state is aligned perpendicularly to the polarization of the pump beam.^[95]

Thin films of photochromic polypeptides may have promise as possible nonlinear optical materials.^[98,99] In fact, the alignment of neighboring macromolecules of helical conformations produces a greater opportunity for noncentrosymmetric side chain orientation; a requirement for nonlinear optical materials. The rod-like α -helical conformation of polypeptides is ideal for restraining the orientation of the dye side groups, to a greater extent than in comparably modified synthetic polymers such as poly(methacrylate)s.^[98] Another possible application is as holographic materials. Indeed, Cooper et al.^[100] have prepared spin-coated films from spiropyran-modified poly(L-glutamic acid) (XV, Figure 8) and demonstrated the feasibility of writing gratings onto the films.

The use of photochromic compounds for optical data storage has been proposed. One of the unsolved problems for practical application is the development of techniques that allow nondestructive reading; since the optical data are usually read at the same wavelength as that used in the recording process, the data may fade during the reading process. Sisido et al.^[101–104] have proposed the use of photochromic

polypeptide systems in which a record may be read by measuring the optical rotation or the induced circular dichroism at a wavelength longer than the wavelength used for recording, thus avoiding the read-out process destroying the original record.

A photochromic dye consisting of an anthraquinone covalently linked to an azobenzene moiety was doped in cholesteric liquid-crystalline gels or thermotropic cholesteric films prepared from α -helical polypeptides. The dye showed large induced optical rotations and CD bands in the region of the absorption bands of the anthraquinone moiety, the magnitude of which changed reversibly with the *trans-cis* photoisomerization of the azobenzene moiety. Therefore, the photoisomeric state of the photochromic group could be detected by the large induced anthraquinone dye CD bands, which occur at much longer wavelengths than the wavelengths used to produce the azobenzene moiety's *trans-cis* photoisomerization. This chiroptical system thus provides a tool for a nondestructive read-out technique.^[101–104]

13.4

Photoresponsive Polypeptide Membranes

Photochromic polymers have been used in order to develop artificial membranes with particular physical properties and functions, such as permeability, conductivity, and membrane potential, that can be switched on and off or otherwise controlled in response to light.^[7,105,106] More specifically, photochromic polypeptides have been selected as useful materials due to their ability to undergo photoinduced structural change.

Kinoshita et al.^[107,108] used poly(L-glutamic acid) containing 12–14 mol% azobenzene units in the side chains (Scheme 3, Structure III) to prepare membranes obtained by coating a porous Millipore filter with a 0.2 % chloroform solution of III. Irradiation at 350 nm was found to increase the membrane potential and cross-membrane permeability. The photoinduced alterations of the membrane functions were completely reversible and could be controlled by irradiation and dark-adaptation, in correlation with the *trans-cis* photoisomerization of the azobenzene units.

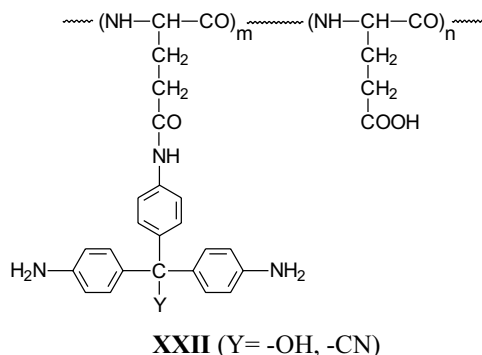
The results were explained on the basis of the observation that the water content of the membrane is increased on irradiation at 350 nm, most probably as a consequence of the different polarities and hydrophobicities of the *trans* and the *cis* isomers. The increase in the degree of hydration of the membrane should be then probably be accompanied by an increase in the degree of dissociation of the unmodified COOH side chains, thus giving rise to an increase in the negative charge of the membrane and enhancing the diffusion of ions. Actually, photoinduced variations of membrane potential and conductivity were observed at an external solution pH of 6.2, but no effect was induced at pH 9.0, thus indicating the important role of the equilibrium between COOH and COO⁻ groups in the photoresponse.

Analogous membranes have been prepared from poly(L-glutamic acid) containing about 14 mol % azobenzene-sulfonate groups in the side chains (Scheme 3, Structure IV).^[25,109] The polypeptide was adsorbed onto a porous support and the hydro-

dynamic permeability of the membrane was investigated as a function of irradiation and pH of the solution. It was found that irradiation with UV light induced membrane permeability changes only at solution pH values in the range 3–7. The photoresponsive behavior of the membrane was explained in terms of a photoinduced transition from helix to coil in the polypeptide structure, caused by the *trans*→*cis* isomerization of the azo chromophores. However, the permeability of a membrane obtained from a polypeptide containing 46 mol% azobenzene-sulfonate units, which was random coil in aqueous solution at all pH values, was not affected by irradiation.^[109]

Insoluble membranes have also been prepared from cross-linked samples of the polypeptide **IV**.^[110] Irradiation of the membranes with UV light at pH values in the range 5–9 induced large variations in hydration and membrane potential. CD measurements showed that such variations were also accompanied by photoinduced conformational changes corresponding to a decrease in α -helix content from 76% to 46%. It was suggested that the *trans*→*cis* isomerization of the azo chromophores might result in a higher degree of dissociation of the unmodified COOH side chains, which should be the key factor responsible for the photoresponse effects. In fact, a shifting of the equilibrium from neutral COOH to ionic COO[−] groups should increase the electrostatic interactions between side chains, thus causing the unfolding of the macromolecules and changing the charge distribution on the membrane. Unfortunately, the photoinduced variations in hydration and membrane potential, and also in macromolecular structure, were found to be nonreversible.^[110]

Photoresponsive membranes have been also prepared from polypeptides chemically modified with triphenylmethane dyes.^[111–114] The photochromic behavior of such compounds involves the ionization of the dye under UV irradiation conditions to give the intensely colored triphenylmethyl cation; the cation thermally recombines with the counteranion in the dark (Figure 1). Poly(L-glutamic acid) was treated with pararosaniline to give a polymer containing about 10 mol% of dye groups in the side chains [Scheme 13, Structure **XXII** (Y = −OH)]. The membrane obtained on casting a dimethyl formamide solution of the polymer was no longer soluble, indicating that a proportion of the dye molecules may act as a cross-linking agent during the casting process



Scheme 13 Chemical structure of poly(L-glutamic acid) containing triphenylmethane dyes in the side chains (**XXII**, Y = −OH and −CN).^[111–114]

Irradiation of the membrane with 250–380 nm light was found to produce photo-induced conformational changes only at critical pH values of the aqueous solution in which irradiation was carried out. In particular, a transition from α -helix to coil was observed at weakly alkaline values (pH 8.6–9.1). The result has been interpreted as follows. Irradiation causes the dissociation of the dye moieties with production of OH^- ions, thus increasing the pH value in the membrane phase. This gives rise to a higher degree of dissociation in the unmodified COOH groups (to COO^-), thus enhancing electrostatic interactions among the side chains and inducing the transition from helix to coil.^[111]

Experiments investigating permeation of substrates across the membrane showed that irradiation with UV light at pH 8.6 induced an increase in permeability, together with an increase in swelling of the membrane. Both permeability and degree of swelling returned to their original values after 100 minutes in the dark. The photoinduced swelling and permeability changes are consistent with the dissociation of the COOH side chains and consequent increase in the hydrophilic nature of the membrane, as discussed above.^[112,113]

Large photoresponse effects have been observed in membranes prepared from poly(L-glutamic acid) containing leucocyanide (triphenylmethyl cyanide) groups in the side chains [Scheme 13, Structure **XXII** ($Y = -\text{CN}$)].^[114] For a membrane prepared at pH 5.3 from a polymer containing 38 mol% of photochromic groups, exposure to UV light induced large variations in the degree of swelling, membrane potential, and the permeation coefficient of KCl through the membrane. All parameters and membrane functions returned to their original values when light was removed and the membrane kept in the dark. These photoinduced changes in membrane function are consistent with the photodissociation of the dye molecules and formation of triphenylmethyl cations in the side chains of the macromolecules (Figure 1), and the consequent polarity change of the membrane.

Inoue et al.^[115,116] synthesized polyvinyl/polypeptide graft copolymers by attaching branches of *p*-phenylazobenzyl/ β -benzyl-L-aspartate (**X**) to poly(hydroxyethyl methacrylate) and poly(butyl methacrylate), and then prepared the corresponding membranes by casting dichloroethane solutions of the polymers. The membranes were stable in trimethylphosphate.

It was observed that the permeability of various substrates across the membranes was enhanced on irradiation with UV light and was suppressed on irradiation with visible light. The photoinduced permeability changes were correlated with the photoinduced and reversible conformational alterations of the polypeptide branches grafted onto the hydrocarbon backbone of the macromolecules, as a consequence of the *trans-cis* isomerization of the azobenzene units. In this case, the photoregulation of permeability across the membrane was achieved by means of photoinduced conformational changes of the polypeptide chains, without any concomitant changes in electrostatic charges in the macromolecules.^[116]

A photoresponsive amphiphilic helical polypeptide (a helical polypeptide in which all the polar residues are located on one side of the helical cylinder and all the hydrophobic residues on the opposite side) was prepared by Higuchi et al., using a simple and unique technique.^[117–121] The polypeptide **XXI** was first placed at a

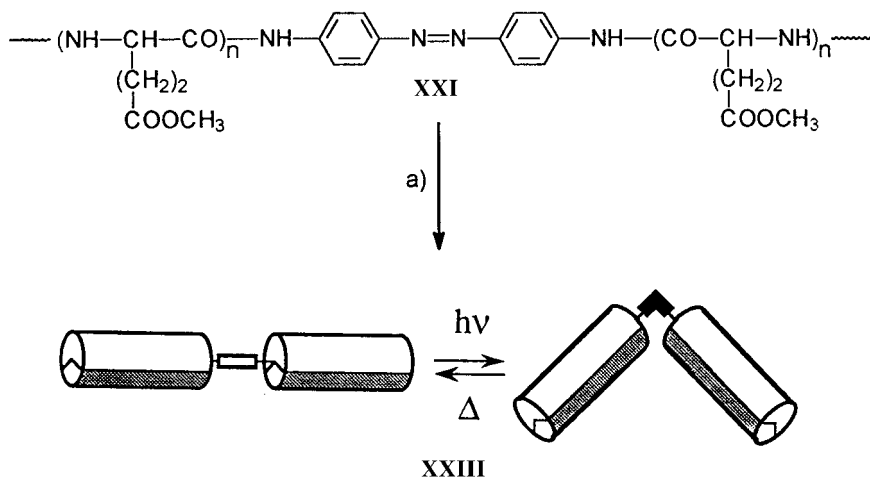


Fig. 18: Schematic illustration of the preparation and photoresponsive behavior of the polypeptide **XXIII**, consisting of two amphiphilic helical rods linked by an azobenzene unit.

a) Selective saponification of COOCH_3 side

chains in the monolayer state. Shaded and unshaded surfaces represent locations of hydrophilic (COOH) and hydrophobic (COOCH_3) side chains, respectively.

water/air interface and a monolayer formed; then NaOH was injected into the water phase beneath the solid condensed monolayer. This resulted in selective saponification of the ester methyl groups on the water side of the monolayer only, so that the final polypeptide **XXIII** consisted of helical rods with COOH side chains on one side (hydrophilic face) and COOCH_3 side chains on the other (hydrophobic face) (Figure 18).^[117–121]

The compound **XXIII**, consisting of two amphiphilic helical rods linked by an azobenzene moiety, was found to form micelles and ordered aggregates in aqueous solution in the dark, when the azo moiety is in the *trans* configuration. Photoisomerization of the azo linkage into the *cis* configuration, and the consequent bending in the structure of the molecules, induced disaggregation and disruption of the micelles.^[118,119]

In nature, polypeptides with amphiphilic structures are known to form transmembrane channels formed by an assembly of several helices, so as to present their polar faces inward and their apolar faces outward. In view of such behavior, the photochromic amphiphilic polypeptide was incorporated into a cationic bilayer membrane composed of dipalmitoyl phosphatidyl choline.^[120] Fluorescence and microscopic measurements provided evidence that the polypeptide was able to form bundles of helical molecules analogous to their natural counterparts, which acted as transmembrane channels for K^+ ions. Irradiation, and the consequent *trans*→*cis* isomerization of the azobenzene link, caused a bending of the molecular structure and a destabilization of the transmembrane bundles. Therefore, formation of ion permeable channels would be favored or inhibited depending on whether the azo moiety

was in the *trans* or the *cis* configuration, thus enabling photoregulation of membrane permeability.^[120]

The investigation was then extended to a monolayer formed from dipalmitoyl phosphatidyl choline and the same amphiphilic photochromic polypeptide **XXIII**.^[121] When the monolayer was kept in the dark, the polypeptide molecules arranged themselves perpendicularly to the membrane (the water/air interface) and formed a bundle of helices which could be observed by atomic force microscopy as a transmembranous particle of about 4 nm in diameter. Irradiation with UV light and the consequent *trans*→*cis* isomerization of the azobenzene moiety caused a bending of the molecular main chain, which in turn produced a destabilization and denaturation of the bundle of helices in the monolayer. After removal of the light, the polypeptide molecules reverted to their original bundle structure.^[121]

13.5

Summary and Future Prospects

As discussed in Section 13.1, organic photochromic compounds such as azobenzene and spiropyran derivatives can exist in two different states that can be reversibly switched from one to another by means of a light stimulus of appropriate wavelength. When such photochromic molecules are incorporated into macromolecular compounds, the interconversion between the two photoisomers may induce structural changes in the attached macromolecules, which in turn may be accompanied by changes in the physical and chemical properties of these materials. Accordingly, the photochromic units actually work as photochemical molecular switches, and photochromic polymers may provide the basis for constructing light-driven switching systems to control spectral properties, optical rotation, refraction index, viscosity, membrane functions, and so forth.

It should be said, however, that the initial light signal associated with the photoisomerization of the photochromic moiety is usually a weak effect, and requires “amplification” in order to construct photoswitchable devices. The greater the amplification factor, the greater is the sensitivity of the system. Substantial amplification can be achieved when the primary photochemical reaction is coupled with a subsequent event that occurs after absorption of light.

From this point of view, polypeptides containing photochromic units in the side chains are quite special polymers. They can exist in ordered or disordered conformations, and photoisomerization of their photochromic side chains can produce “order ⇌ disorder” conformational changes. These photostimulated structural variations, such as random coil ⇌ α -helix, take place as highly cooperative transitions; therefore photochromic polypeptides actually work as amplifiers and transducers of the primary photochemical events occurring in the photosensitive side chains.

Similar behavior has been observed in polyisocyanates, which have been shown to possess a helical structure. Unlike polypeptides, polyisocyanates have no stereocenter in their backbone; they therefore form a racemic mixture of left-handed and right-handed helices.^[122] Incorporation of chiral azobenzene dyes into the side

chains allows an optical switch to be created, in which the equilibrium between the left-handed and right-handed helices is controlled by photoisomerization of the photochromic groups.^[123,124] Because of the high cooperativity along the main chain,^[125,126] the helical twist sense can be triggered by a small quantity of photochromic units. In this case the helical structure also acts as an amplifying element for the photochemical reactions in the side chains.^[124]

Thus far, photoresponsive polymers have been intensively investigated and significant advances have been made on fundamental aspects and strategies. However, it is fair to say that they have found only limited practical application.

A crucial point that must be addressed concerns the thermal stability and the “*fatigue*” phenomenon observed in the chromophores. It is a fact that many photochromic compounds are irreversibly degraded upon long exposure to light, thus limiting their use for various applications. Major advances in the preparation and performance of photochromic materials have been made in the past five years. Irie et al.^[127] have recently developed new photochromic compounds, 1,2-diarylethenes, which display photochromic behavior with unchanged intensity even after 10^4 “coloration \rightleftharpoons decoloration” cycles.

Even though photochromic polymers still require further research and, particularly, technological advances for possible applications, they are likely to become important in the future. A rapidly expanding field concerns the incorporation of photochromic dyes into supramolecular assemblies. Combination of the architecture of supramolecular aggregates or activity of biological systems with the photo-behavior of organic dyes could provide new photoswitchable materials that could find application in a wide variety of uses, ranging from molecular scale computing to photochemical biosensors for medical application.

References

- 1 M. Irie, *Adv. Polym. Sci.* **1990**, *94*, 27.
- 2 V.A. Kongrauz in *Photochromism: molecules and systems* (Eds.: H. H. Durr and H. Bouas-Laurents), Elsevier, Amsterdam, **1990**, pp 793–821.
- 3 C. B. McArdle, *Applied Photochromic Polymer Systems*, Blackie, Glasgow, **1992**.
- 4 M. Sisido, *Prog. Polym. Sci.* **1992**, *17*, 699.
- 5 T.M. Cooper, L.V. Natarajan, and R.L. Crane, *Trends Polym. Sci.* **1993**, *1*, 400 .
- 6 O. Pieroni and F. Ciardelli, *Trends Polym. Sci.* **1995**, *3*, 282.
- 7 T. Kinoshita, *Prog. Polym. Sci.* **1995**, *20*, 527.
- 8 I. Willner and S. Rubin, *Angew. Chem. Ed. Engl.* **1996**, *35*, 367.
- 9 O. Pieroni, A. Fissi, and G. Popova, *Progress Polym. Sci.* **1998**, *23*, 81.
- 10 N. Greenfield and G.D. Fasman, *Biochemistry* **1969**, *8*, 4108.
- 11 R.W. Woody, *J. Polym. Sci.: Macromol. Rev.* **1977**, *12*, 181.
- 12 R.W. Woody, *J. Chem. Phys.* **1968**, *49*, 4797.
- 13 J.R. Parrish and E.R. Blout, *Biopolymers* **1971**, *10*, 1491.
- 14 V. Madison and J. Schellman, *Biopolymers* **1972**, *11*, 1041.
- 15 W.L. Mattice, J.T. Lo and L. Mandelkern, *Macromolecules* **1972**, *5*, 729.
- 16 D.G. Deaborn and D.B. Wetlaufer, *Biochem. Biophys. Res. Commun.* **1970**, *39*, 314.
- 17 R.W. Woody in *The Peptides*, Vol. 7 (Eds.: S. Udenfriend and J. Meienhofer), Academic Press, Orlando, Florida, **1985**, p. 16.
- 18 M. Goodman and A. Kossoy, *J. Am. Chem. Soc.* **1966**, *88*, 5010.
- 19 M. Goodman and M. L. Falxa, *J. Am. Chem. Soc.* **1967**, *89*, 3863.
- 20 O. Pieroni, J. L. Houben, A. Fissi, P. Costantino and F. Ciardelli, *J. Am. Chem. Soc.* **1980**, *102*, 5913.
- 21 J. L. Houben, A. Fissi, D. Bacciola, N. Rosato, O. Pieroni, and F. Ciardelli, *Int. J. Biol. Macromol.* **1983**, *5*, 94.
- 22 F. Ciardelli, O. Pieroni, A. Fissi, and J. L. Houben, *Biopolymers* **1984**, *23*, 1423.
- 23 M. Sisido, Y. Ishikawa, K. Itoh, and S. Tazuke, *Macromolecules* **1991**, *24*, 3993.
- 24 M. Sisido, Y. Ishikawa, M. Harada, and K. Itoh, *Macromolecules* **1991**, *24*, 3999.
- 25 M. Sato, T. Kinoshita, A. Takizawa, and Y. Tsujita, *Macromolecules* **1988**, *21*, 1612.
- 26 Pieroni, D. Fabbri, A. Fissi, and F. Ciardelli, *Makromol. Chem.: Rapid. Commun.* **1988**, *9*, 637.
- 27 M. Higuchi, A. Takizawa, T. Kinoshita, and Y. Tsujita, *Macromolecules* **1987**, *20*, 2888.
- 28 J. K. Blasie, *Biophys. J.* **1972**, *12*, 191.
- 29 A. Fissi, O. Pieroni, and F. Ciardelli, *Biopolymers* **1987**, *26*, 1993.
- 30 H. Yamamoto and A. Nishida, *Macromolecules* **1986**, *19*, 943.
- 31 H. Yamamoto, *Macromolecules* **1986**, *19*, 2472.
- 32 A. Fissi, O. Pieroni, E. Balestreri, and C. Amato, *Macromolecules* **1996**, *29*, 4680.
- 33 M. N. Inscoe, J. H. Gould, and W. R. Brode, *J. Am. Chem. Soc.* **1959**, *81*, 5634.
- 34 M. Irie, O. Miyatake, and K. Uchida, *J. Am. Chem. Soc.* **1992**, *114*, 8715.
- 35 M. Irie, O. Miyatake, K. Uchida, and T. Eriguchi, *J. Am. Chem. Soc.* **1994**, *116*, 9894.
- 36 W. J. Middletown and R. V. Lindsey Jr, *J. Am. Chem. Soc.* **1964**, *86*, 4948.
- 37 K. F. Purcell, J. A. Stikeleather, and S. D. Brunk, *J. Am. Chem. Soc.* **1969**, *91*, 4019.
- 38 J. F. King in *The Chemistry of Sulfonic Acids, Esters and their Derivatives* (Eds.: S. Patai and Z. Rappoport), Wiley, Chichester, **1991**, p. 249.
- 39 H. Yamamoto, A. Nishida, T. Takimoto, and A. Nagai, *J. Polym. Sci.: Polym. Chem.* **1990**, *28*, 67.
- 40 H. Yamamoto, K. Ikeda, and A. Nishida, *Polym. Intern.* **1992**, *27*, 67.
- 41 H. Yamamoto and A. Nishida, *Polym. Intern.* **1991**, *24*, 145.
- 42 H. Yamamoto, A. Nishida, and T. Kawaura, *Int. J. Biol. Macromol.* **1990**, *12*, 257.
- 43 H. Yamamoto, Y. Miyagi, A. Nishida, T. Takagishi, and S. Shima, *J. Photochem.* **1987**, *39*, 343.
- 44 V. Giancotti, F. Quadrifoglio, and V. Crescenzi, *J. Am. Chem. Soc.* **1972**, *94*, 297.
- 45 E. H. Frenrich, R. H. Andreatta, and H. A. Scheraga *J. Am. Chem. Soc.* **1970**, *92*, 1116.
- 46 A. Ueno, J. Anzai, T. Osa, and Y. Kadoma, *J. Polym. Sci.; Polym. Letters* **1977**, *15*, 407.
- 47 A. Ueno, J. Anzai, T. Osa, and Y. Kadoma, *Bull. Chem. Soc. Jpn.* **1977**, *50*, 2995.
- 48 A. Ueno, J. Anzai, T. Osa, and Y. Kadoma, *Bull. Chem. Soc. Jpn.* **1979**, *52*, 549.
- 49 A. Ueno, J. Anzai, and T. Osa, *J. Polym. Sci.: Polym. Letters* **1979**, *17*, 155.

- 50 A. Ueno, K. Takahashi, J. Anzai, and T. Osa, *Macromolecules* **1980**, *13*, 459.
- 51 A. Ueno, K. Takahashi, J. Anzai, and T. Osa, *Bull. Chem. Soc. Jpn.* **1980**, *53*, 1988.
- 52 A. Ueno, K. Takahashi, J. Anzai, and T. Osa, *Chem. Letters* **1981**, 113.
- 53 A. Ueno, K. Takahashi, J. Anzai, and T. Osa, *Makromol. Chem.* **1981**, *182*, 693.
- 54 A. Ueno, K. Takahashi, J. Anzai, and T. Osa, *J. Am. Chem. Soc.* **1981**, *103*, 6410.
- 55 A. Ueno, J. Nakamura, K. Adachi, and T. Osa, *Makromol. Chem., Rapid Commun.* **1989**, *10*, 687.
- 56 A. Ueno, K. Adachi, J. Nakamura, and T. Osa, *J. Polymer Sci.: Polymer Chem.* **1990**, *28*, 1161.
- 57 A. Ueno, K. Takahashi, J. Anzai, and T. Osa, *Makromol. Chem., Rapid Commun.* **1984**, *5*, 639–642.
- 58 L. Ulysse, J. Cubillos, and J. Chmielwski, *J. Am. Chem. Soc.* **1995**, *117*, 8466.
- 59 L. A. Strzegowski, M. B. Martinez, D. C. Gowda, D. W. Urry, and D. A. Tirrell, *J. Am. Chem. Soc.* **1994**, *116*, 813.
- 60 F. Ciardelli, D. Fabbri, O. Pieroni, and A. Fissi, *J. Am. Chem. Soc.* **1989**, *111*, 3470.
- 61 A. Fissi, O. Pieroni, F. Ciardelli, D. Fabbri, G. Ruggeri, and K. Umezawa, *Biopolymers* **1993**, *33*, 1505.
- 62 T. M. Cooper, K. A. Obermeier, L. V. Natarajan, and R. L. Crane, *Photochem. Photobiol.* **1992**, *55*, 1.
- 63 N. Angelini, B. Corrias, A. Fissi, O. Pieroni, and F. Lenci, *Biophys. J.* **1998**, *74*, 2601.
- 64 R. Pachter, T. M. Cooper, L. V. Natarajan, K. A. Obermeier, R. L. Crane, *Biopolymers* **1992**, *32*, 1129.
- 65 M. Satoh, Y. Fujii, F. Kato, and J. Komiyama, *Biopolymers* **1991**, *31*, 1.
- 66 M. Satoh, T. Hirose, and J. Komiyama, *Polymer* **1993**, *34*, 4762.
- 67 O. Pieroni, A. Fissi, A. Viegi, D. Fabbri, and F. Ciardelli, *J. Am. Chem. Soc.* **1992**, *114*, 2734.
- 68 A. Fissi, O. Pieroni, G. Ruggeri, and F. Ciardelli, *Macromolecules* **1995**, *28*, 302.
- 69 K. J. Wen and R. W. Woody, *Biopolymers* **1975**, *14*, 1827.
- 70 T.M. Cooper, M.O. Stone, L.V. Natarajan, and R.L. Crane, *Photochem. Photobiol.* **1995**, *62*, 258.
- 71 O. Pieroni, A. Fissi, J. L. Houben, and F. Ciardelli, *J. Am. Chem. Soc.* **1985**, *107*, 2990.
- 72 F. Ciardelli, O. Pieroni, and A. Fissi, *J. Chem. Soc.: Chem. Commun.* **1986**, 264.
- 73 A. Fissi and O. Pieroni, *Macromolecules* **1989**, *22*, 1115.
- 74 D. J. W. Bullock, C. W. N. Cumper, and A. I. Vogel, *J. Chem. Soc.* **1965**, 5316.
- 75 M. Irie, T. Iwayanagi, and Y. Taniguchi, *Macromolecules* **1985**, *18*, 2418.
- 76 K. Ichimura in *Photochromism, Molecular and Systems*, (Eds.: H. Dürr and H. Bouas-Laurent), Elsevier, Amsterdam, **1990**, Chapter 26.
- 77 P. H. Quail in *Trends in Photobiology* (Eds.: C. Helene, M. Charlier, Th. Monterray-Garestier, G. Laustriat), Plenum Press, New York, **1982**, p. 485.
- 78 L. H. Pratt, *Photochem. Photobiol.* **1978**, *27*, 81.
- 79 B. R. Malcolm and O. Pieroni, *Biopolymers* **1990**, *29*, 1121.
- 80 B. R. Malcolm, *Thin Solid Films* **1989**, *178*, 17.
- 81 H. Menzel, *Macromol. Chem. Phys.* **1994**, *195*, 3747.
- 82 M. Higuchi, N. Minoura and T. Kinoshita, *Colloid Polym. Sci.* **1995**, *273*, 1022.
- 83 H. Menzel and G.V. Popova, *The 7th Int. Conference on Organized Molecular Films*, p. 99, Ancona, Italy (1995).
- 84 G. Munger, G.V. Popova, O.Yu. Fedorovsky, and C. Salesse, *The 7th Int. Conference on Organized Molecular Films*, , Ancona, Italy, **1995**, p. 102.
- 85 M.L. Hallensleben and H. Menzel, *British Polym. J.* **1990**, *23*, 199.
- 86 H. Menzel and M.L. Hallensleben, *Polym. Bull.* **1991**, *27*, 89.
- 87 H. Menzel, B. Weichart and M.L. Hallensleben, *Polym. Bull.* **1992**, *27*, 637.
- 88 H. Menzel, B. Weichart, and M. L. Hallensleben, *Thin Solid Films* **1993**, *223*, 181.
- 89 H. Menzel, M. L. Hallensleben, A. Schmidt, W. Knoll, T. Fischer, and J. Stumpe, *Macromolecules* **1993**, *26*, 3644.
- 90 H. Menzel, *Macromolecules* **1993**, *26*, 6226.
- 91 H. Menzel, B. Weichart, A. Schmidt, S. Paul, W. Knoll, J. Stumpe, and T. Fischer, *Langmuir* **1994**, *10*, 1926.
- 92 G. Wegner, *Thin Solid Films* **1992**, *216*, 105.
- 93 M. Büchel, Z. Sekkat, S. Paul, B. Weichart, H. Menzel, and W. Knoll, *Langmuir* **1995**, *11*, 4460.
- 94 J. Stumpe, T. Fischer, and H. Menzel, *Macromolecules* **1996**, *29*, 2831.

- 95 Z. Sekkat, M. Büchel, H. Orendi, H. Menzel and W. Knoll, *Chem. Phys. Letters* **1994**, *220*, 497.
- 96 A. M. Makushenko, B. S. Neporent, and O. V. Stolbova, *Opt. Spectr.* **1971**, *31*, 295.
- 97 T. Todorov, L. Nicolova, and N. Tomova, *Appl. Opt.* **1984**, *23*, 4309.
- 98 T.M. Cooper, K.L. Hussong, T.M. Grinstead, and W.W. Adams, *Chem. Mater.* **1994**, *6*, 2063.
- 99 T.M. Cooper, A.L. Campbell, and R.L. Crane, *Langmuir* **1995**, *11*, 2713.
- 100 T. M. Cooper, V. Tondiglia, L. V. Natarajan, M. Shapiro, K. A. Obermeier, and R. L. Crane, *Appl. Optics* **1993**, *32*, 674.
- 101 R. Kishi and M. Sisido, *Makromol. Chem.* **1991**, *192*, 2723.
- 102 M. Sisido, H. Narisawa, R. Kishi and J. Watanabe, *Macromolecules* **1993**, *26*, 1424.
- 103 M. Sisido in *Photoreactive Materials for Ultrahigh Density Optical Memory* (Ed.: M. Irie), Elsevier, Amsterdam, **1994**, p. 13.
- 104 H. Narisawa, R. Kishi, and M. Sisido, *Macromol. Chem. Phys.* **1995**, *196*, 1419.
- 105 J. Anzai and T. Osa, *Tetrahedron* **1994**, *50*, 4039.
- 106 T. Kinoshita, *J. Photochem. Photobiol. B: Biology* **1998**, *42*, 12.
- 107 T. Kinoshita, M. Sato, A. Takizawa, and Y. Tsujita, *J. Chem. Soc.: Chem. Commun.* **1984**, 929.
- 108 Kinoshita, M. Sato, A. Takizawa, and Y. Tsujita, *Macromolecules* **1986**, *19*, 51.
- 109 M. Sato, T. Kinoshita, A. Takizawa, Y. Tsujita, and R. Ito, *Polymer J.* **1988**, *20*, 761.
- 110 M. Sato, T. Kinoshita, A. Takizawa, Y. Tsujita, and T. Osada, *Polymer J.* **1989**, *21*, 533.
- 111 T. Kinoshita, M. Sato, A. Takizawa, and Y. Tsujita, *J. Am. Chem. Soc.* **1986**, *108*, 6399.
- 112 M. Sato, T. Kinoshita, A. Takizawa, and Y. Tsujita, *Polymer J.* **1988**, *20*, 729.
- 113 M. Sato, T. Kinoshita, A. Takizawa, and Y. Tsujita, *Macromolecules* **1988**, *21*, 3419.
- 114 M. Sato, T. Kinoshita, A. Takizawa, and Y. Tsujita, *Polymer J.* **1989**, *21*, 369.
- 115 M. Aoyama, A. Youda, J. Watanabe, and S. Inoue, *Macromolecules* **1990**, *23*, 1458.
- 116 M. Aoyama, J. Watanabe, and S. Inoue, *J. Am. Chem. Soc.* **1990**, *112*, 5542.
- 117 M. Higuchi, A. Takizawa, T. Kinoshita, Y. Tsujita, and K. Okochi, *Macromolecules* **1990**, *23*, 361.
- 118 M. Higuchi, N. Monoura, and T. Kinoshita, *Chem Letters* **1994**, 227.
- 119 M. Higuchi and T. Kinoshita, *J. Photochem. Photobiol. B: Biology* **1998**, *42*, 143.
- 120 M. Higuchi, N. Minoura, and T. Kinoshita, *Macromolecules* **1995**, *28*, 4981.
- 121 M. Higuchi, N. Minoura, and T. Kinoshita, *Langmuir* **1997**, *13*, 1616.
- 122 S. Lifson, G. E. Felder, M. M. Green, *Macromolecules* **1992**, *25*, 4142.
- 123 M. Muller and R. Zentel, *Macromolecules* **1994**, *27*, 4404.
- 124 S. Mayer, R. Zentel, *Macromol. Chem. Phys.* **1998**, *199*, 1675.
- 125 M. M. Green, N. C. Peterson, T. Sato, A. Teramoto, R. Cook, and S. Lifson, *Science* **1995**, *268*, 1860.
- 126 M. M. Green, M. P. Reidy, R. J. Johnson, G. Darling, D. J. O'leary, and G. Wilson, *J. Am. Chem. Soc.* **1989**, *111*, 6452.
- 127 M. Irie, O. Miyatake, K. Uchida, and T. Eriguchi, *J. Am. Chem. Soc.* **1994**, *116*, 9894 .